

**The formation and the geochemical and thermal evolution
of the lithospheric mantle beneath the Kaapvaal craton
recorded by subcalcic garnets from harzburgites
and by pristine eclogites and garnet-pyroxenites**

**Dissertation
zur Erlangung des Doktorgrades
der Naturwissenschaften**



**von
Qiao Shu
aus Zhejiang
(China)
Frankfurt (November, 2012)**

**The formation and the geochemical and thermal evolution
of the lithospheric mantle beneath the Kaapvaal craton
recorded by subcalcic garnets from harzburgites
and by pristine eclogites and garnet-pyroxenites**

**Dissertation
zur Erlangung des Doktorgrades
der Naturwissenschaften**

**Vorgelegt beim Fachbereich Geowissenschaften/Geographie
der Johann Wolfgang Goethe-Universität
in Frankfurt am Main**

**von
Qiao Shu
aus Zhejiang
(China)**

Frankfurt (November, 2012)

**Vom Fachbereich Geowissenschaften (FB: Mineralogie) der
Johann Wolfgang Goethe-Universität als Dissertation angenommen.**

Dekan: Prof. Dr. Andreas Junge

Gutachter: Prof. Gerhard Peter Brey, PhD, Dr. h.c.

Prof. Dr. Stefan Weyer

Prof. Dr. Graham Pearson

Datum der Disputation:

Table of contents

Zusammenfassung	I
Summary	XIX
Chapter 1 - Introduction	
1. Significance of studying xenoliths/xenocrysts from SCLM underneath the Archean cratons	1
2. Previous work on peridotites and ways to extract multiple information	2
3. A study on eclogites and garnet pyroxenites to enhance the understanding of the evolution of the SCLM viewed from a different angle	6
4. Aims of this project	7
References	8
Chapter 2 – Geochronological and geochemical constraints on the formation and evolution of the mantle underneath the Kaapvaal craton: Lu-Hf and Sm-Nd systematics of subcalcic garnets from highly depleted peridotites	
Abstract	11
1. Introduction	13
2. Localities, samples, depth of origin and geological background	14
3. Analytical methods (details in the supplementary file- method description)	16
3.1 Major element analysis	
3.2 Trace element analysis	
3.3 Sample preparation and isotope analysis	
4. Results	17
4.1 Major elements	
4.2 Trace elements	
4.2.1 Roberts Victor	18
4.2.2 Lace	19
4.3 Isotope systematics	20
4.3.1 General remarks	
4.3.2 Samarium-neodymium from Roberts Victor and Lace	21
4.3.3 Lutetium-hafnium from Roberts Victor	22
4.3.4 Lutetium-hafnium from Lace	23
4.3.5 A reexamination of lutetium-hafnium isotope data from Finsch	24
5. Discussion	
5.1 Partial melting regimes and enrichment processes from trace element systematics	25
5.1.1 Roberts Victor mine	27
5.1.2 Lace mine	28
5.2 Sm-Nd and Lu-Hf isotope systems – dating enrichment and partial melting	28
5.2.1 Errorchrons from the Sm-Nd system	28
5.2.2 Isochrons from the Lu-Hf system	28
6. Summary and conclusions	30
References	33
Appendix	38

Chapter 3 – Subcalcic garnets, Mantle metasomatism and Diamonds

1. Introduction	57
2. Geological background of the Kaapvaal craton and sample localities	59
3. Results	59
3.1 Major elements	59
3.2 Trace elements	62
3.2.1 Garnets from Roberts Victor (East Block)	63
3.2.2 Garnets from Lace (East Block)	64
3.2.3 Garnets from Bellsbank (West Block)	65
3.2.4 Garnets from Kimberley (West Block)	66
3.2.5 Garnets from Finsch (West Block)	66
3.3 Sm-Nd and Lu-Hf Isotopes	67
3.3.1 Sm-Nd and Lu-Hf isotope compositions from the West Block (Bellsbank, Kimberley and Finsch)	
3.3.2 Nd and Hf isotope compositions from the East Block (Roberts Victor and Lace)	
4. Discussion	
4.1 The enrichment agents and processes	68
4.2 Enrichment events in the East Block	79
4.3 Enrichment events in the West Block	80
4.4 The subcalcic garnets and the affinity to diamond	81
5. Summary	82
References	83
Appendix	87

Chapter 4 – The origin of eclogites and garnet pyroxenites from Bellsbank, Kaapvaal

1. Introduction	116
2. Geological setting and previous work	117
3. Analytical Methods	119
3.1 Major element analysis	
3.2 Trace element analysis	
3.3 Radiogenic Isotope analysis	120
3.3.1 Sample preparation	
3.3.2 Dissolution	
3.3.3 Column chemistry	
3.3.4 Lu and Hf collection	
3.3.5 LREE and Rb-Sr collection	
3.3.6 Sm-Nd collection	
3.4 Analysis	121
3.4.1 Lu-Hf, Sm-Nd, Rb-Sr	122
3.4.2 Oxygen isotopes	123
4. Sample description	123
5. Results	
5.1 Major element composition of garnets and clinopyroxenes	124
5.2 Calculated bulk rock major element compositions	125
5.3 Geothermobarometry	127
5.4 Trace elements	128
5.4.1 Garnets	128

5.4.2 Clinopyroxenes	129
5.4.3 REE element partitioning	130
5.5 Bulk rock trace element composition	132
5.6 The Sm-Nd, Lu-Hf and Sr isotopic systems	
5.6.1 The Lu-Hf isotope system	133
5.6.2 The Sm-Nd isotope system	134
5.6.3 The Sr isotope composition	135
5.7 Oxygen isotopes	137
6. Discussion	
6.1 The nature of the protoliths of the Bellsbank eclogites and garnet pyroxenites, their origin and subsequent modifications	
6.1.1 Group A' and B2 eclogites	138
6.1.2 Group A and B1 eclogites	141
6.2 Age of the Bellsbank eclogites	143
6.2.1 Age of group A' and B2 eclogite	145
6.2.2 Age of group A and B2 eclogites	149
7. Summary, further aspects and thoughts	149
References	152
Appendix	159

Chapter 5 – Mantle eclogites and garnet pyroxenites - The meaning of two-point isochrons, Sm-Nd and Lu-Hf closure temperatures and the cooling of the subcratonic mantle

1. Introduction	179
2. The frame	180
3. Analytical Methods	181
4. Sample description, chemical composition of grt and cpx and geothermobarometry	
4.1 Sample description	183
4.2 Major element mineral composition	183
4.3 Garnet-clinopyroxene geothermobarometry	184
4.4 Trace elements	185
5. Isotopic results	
5.1 The Sm-Nd isotope system	186
5.2 The Lu-Hf isotope system	187
6. Discussion	
6.1 The meaning of the two-point isochrones and closure temperatures	190
6.2 Constraints on the cooling of the subcratonic mantle- inference from the two isotopic systems	192
References	195

Chapter 6 – Future perspectives

1. Perspectives for eclogite studies	198
2. Closure temperatures for Lu/Hf and Sm/Nd in peridotite and cooling of the mantle	200
3. A note on mineral separation and contamination	202

Acknowledgements 205

Curriculum Vitae 207

Zusammenfassung

1. Bildung und Modifizierung des Erdmantels unterhalb des Kaapvaal Kratons erarbeitet aus der Zusammensetzung subkalzischer Granate

Erdmantelxenolithe aus Kimberliten zeigen, dass der Erdmantel unterhalb einer archaischen Kruste hauptsächlich aus residualen Gesteinen mit hohen Graden der partiellen Aufschmelzung besteht, die in ihrer späteren Geschichte wieder angereichert wurden. Die meisten Xenolithe zeigen kryptische Metasomatose, sehr viel weniger auch modale Metasomatose.

Es gibt bereits sehr viele Arbeiten, die sich mit Mantelmetasomatose unter verschiedenen Aspekten beschäftigen. Wir benutzen hier den Spurenelementgehalt und die isotopische Zusammensetzung von subkalzischen Granaten, die von cpx-freien Harzburgiten und Duniten stammen. Die subkalzischen Granate, meist mit einem sinusoidalen SEE Muster, beinhalten fast den gesamten Spurenelementhaushalt dieser Gesteine, so dass die Analyse eines einzigen, genügend großen Korns, z.B. aus einem Schwerminerkonzentrat, fast alle wichtigen Informationen eines Gesteins enthält. Unser Ziel ist es, hauptsächlich Informationen zur Art der Metasomatose und zu ihrer Zeitlichkeit aus diesen Granaten zu gewinnen.

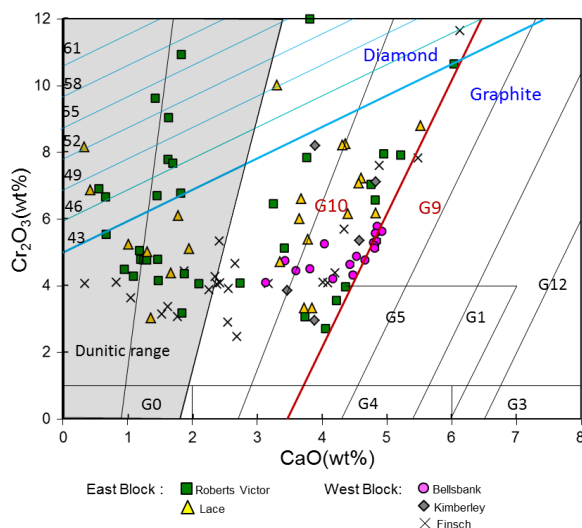


Fig. 1: Cr_2O_3 vs. CaO in subkalzischen Granaten von 5 Lokalitäten des Kaapvaal Kratons; $\text{CaO}-\text{Cr}_2\text{O}_3$ und $\text{Cr}/(\text{Cr}+\text{Al})$ Konturen von Gruetter et al. (2004); Daten für Finsch von Lazarov et al. (2009).

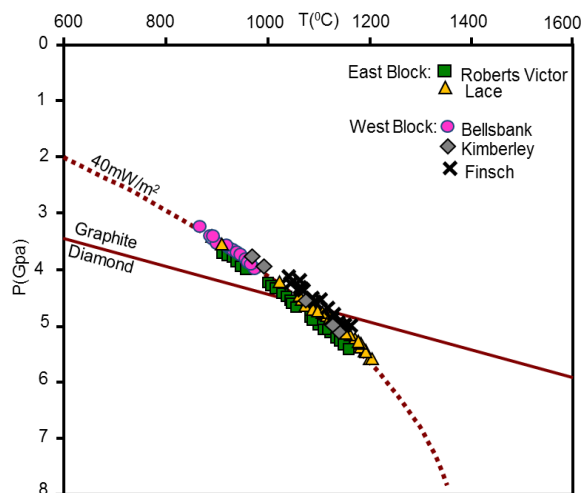


Fig.2: Durchschnitte der Ni-in-Granat Temperaturen von Canil (1999) und Griffin et al. (1989) projiziert auf einen 40 mW/m^2 geothermischen Gradienten zur Abschätzung der Herkunftstiefe der subkalzischen grt

1.1 Ergebnisse

Ungefähr 700 purpur- bis violettfarbene Granate wurden aus den Schwermineralkonzentraten von 4 Diamantminen des Kaapvaalkratons gesammelt: von Bellsbank und Kimberley auf dem Westblock und Lace und Roberts Victor auf dem Ostblock. Ungefähr 500 wurden mit der Elektronenstrahlmikrosonde analysiert. Neunundsiebzig fallen in das Harzburgitfeld in einem Cr_2O_3 gegen CaO Diagramm (Fig.1). Die Anwendung des Ni-in-Granat Thermometers (Durchschnitt aus Griffin et al. 1989 und Canil, 1999) und eine Projektion der Temperatur auf einen 40 mW/m^2 geothermischen Gradienten (Fig. 2) ergibt Drücke für Bellsbank von 3.2-4.0 Gpa und 3.5-5.6 Gpa für Lace, Kimberley und Roberts Victor.

Anschließend wurden die Spurenelemente der Granate mit LA ICP MS analysiert und die Isotopenverhältnisse für Lu-Hf und Sm-Nd aus der Lösung mit MC ICP MS bestimmt. Auf der Basis der Spurenelementhäufigkeiten und –muster wurden die Granate in zwei bis drei Gruppen 1 bis 3 eingeteilt. Der Grad der Wiederanreicherung von inkompatiblen Elementen steigt von 1 nach 3. Als Beispiel werden in Fig. 3 die Spurenelementmuster von Granaten von Roberts Victor gezeigt.

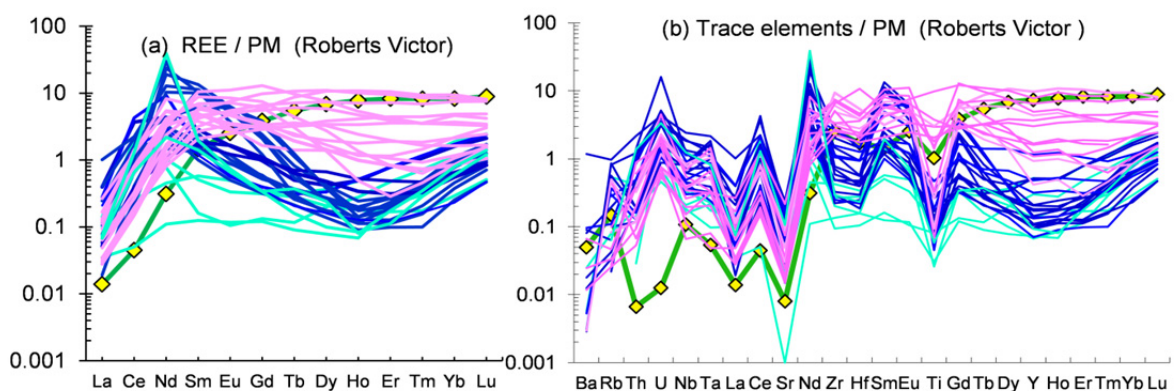


Fig.3: Auf den primitiven Mantel (McDonough and Sun, 1995) normierte SEE (a) und "spider" Diagramme (b) der subkalzischen Granate von Roberts Victor: Drei Gruppen werden unterschieden, die am wenigsten angereicherte Gruppe RV1 (hellblau), eine intermediäre RV2 (dunkelblau) und die am stärksten angereicherte Gruppe RV3 (pink). Die grünen Muster mit gelben Diamanten sind die SEE- und Spurenelementmuster eines Granats aus einem primitiven Granatperidotit 313-105 von Vitim in Siberien (Ionov et al. 2004).

Die Sm-Nd und Lu-Hf Isotopenzusammensetzung der subkalzischen Granate des West blocks (Bellsbank, Kimberley and Finsch) sind in Fig. 4a als ϵHf gegen ϵNd dargestellt und in Fig. 4d diejenigen des Ostblocks (Roberts Victor and Lace). Die Granatgruppen mit einem ausgeprägten sinusoidalen SEE Muster von Finsch (F1), von Bellsbank (B1), Roberts Victor (RV1 und RV2) und L1 von Lace fallen fast ausschließlich in den Quadranten I dieser Figuren. Sie haben teilweise extrem radiogene ϵHf Werte von +16 bis fast + 1000, aber auch ein sehr unradiogenes ϵNd mit Werten bis zu - 40. Das zeigt, dass die Sm-Nd und Lu-Hf Systeme bereits für eine lange Zeit entkoppelt waren. Die stärker angereicherten Gruppen F2 von Finsch und B2 von Bellsbank (weniger ausgeprägtes oder kein sigmoidales SEE Muster), die Granate von Kimberley und die Gruppen RV3 von Roberts Victor und L2 und L3 von Lace fallen in alle vier Quadranten und sind näher oder weiter entfernt von der ozeanischen Korrelationslinie.

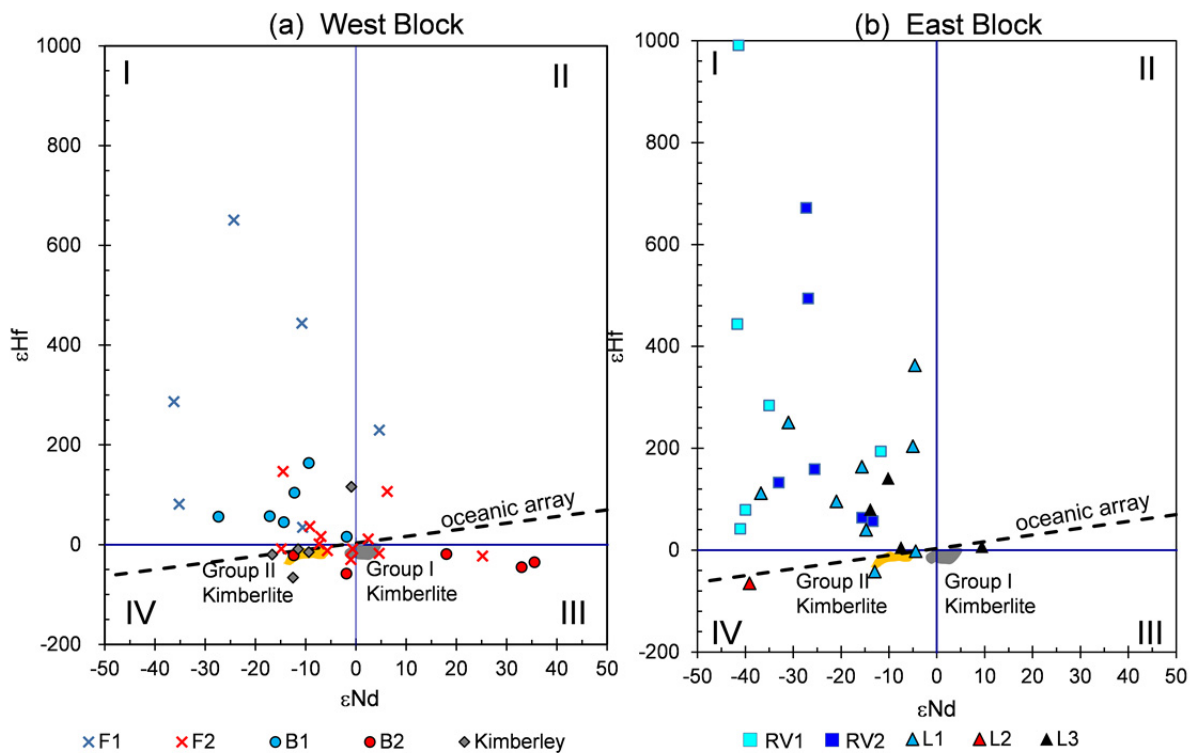


Fig.4: **a)** Die ϵ_{Nd} und ϵ_{Hf} der subkalzischen Granate vom Westblock (Bellsbank: blaue Kreise = B1; rote Kreise = B2; Kimberley = graue Diamanten; Finsch: blaue Kreuze = F1; rote Kreuze = F2) und **b)** vom Ostblock (Lace: blaue Dreiecke = L1; rote = L2; schwarze = L3; Roberts Victor: hellblaue Diamanten = RV1 und dunkelblaue = RV2). Die schwarz gestrichelte Linie ist der heutige ozeanische Trend, der der Gleichung $\epsilon_{Hf} = 1.33 \times \epsilon_{Nd} + 3.19$ entspricht (Vervoort et al., 1999). Zum Vergleich sind die Felder für Gruppe I Kimberlite (hellgrau) und Gruppe II Kimberlite (gelb) ebenfalls dargestellt.

Ein Yttrium gegen Zirkon Diagramm (Griffin et al., 1992) wird oft benutzt, um den Verarmungs- und Wiederanreicherungsgrad und die Art des metasomatischen Agens in Erdmantelgesteinen anzuzeigen. Die von uns in Gruppen 1 bis 3 unterteilten Granate entsprechen in ihrem Charakter den Feldern von Griffin et al. (1992). Diese Y-Zr petrogenetischen Diagramme sind gut geeignet, um die Art des metasomatischen Agens bei starken metasomatischen Prozessen zu erkennen, die selbst noch die stärker kompatiblen Elemente wie Hf und Zr und Y und die schweren SEE überprägen. Aber sie lassen nicht die Details von weniger angereicherten Proben erkennen.

Deshalb wurden für jede Probe die Spurenelementzusammensetzung von Schmelzen und Fluiden berechnet, die potentiell mit den Granaten im Gleichgewicht waren. Um zwischen Silikat- und Karbonatschmelzen zu unterscheiden, wurden zum einen die Spurenelementverteilungskoeffizienten zwischen basaltischer Schmelze und Mantelmineralen von Green et al. (2000) benutzt und zum anderen die von Girniss et al. (2012; revised version submitted to Lithos) mit siliko-karbonatitischen Schmelzen. Die Ergebnisse schließen silikatische Schmelzen aus und zeigen deutlich, dass karbonatitische Schmelzen die Metasomatose verursachen (siehe Fig. 5 als Beispiel für Roberts Victor). Die berechneten Spurenelementmuster liegen innerhalb der Variationsbreite von "Flüssigkeitseinschlüssen" von "fibrous" Diamanten.

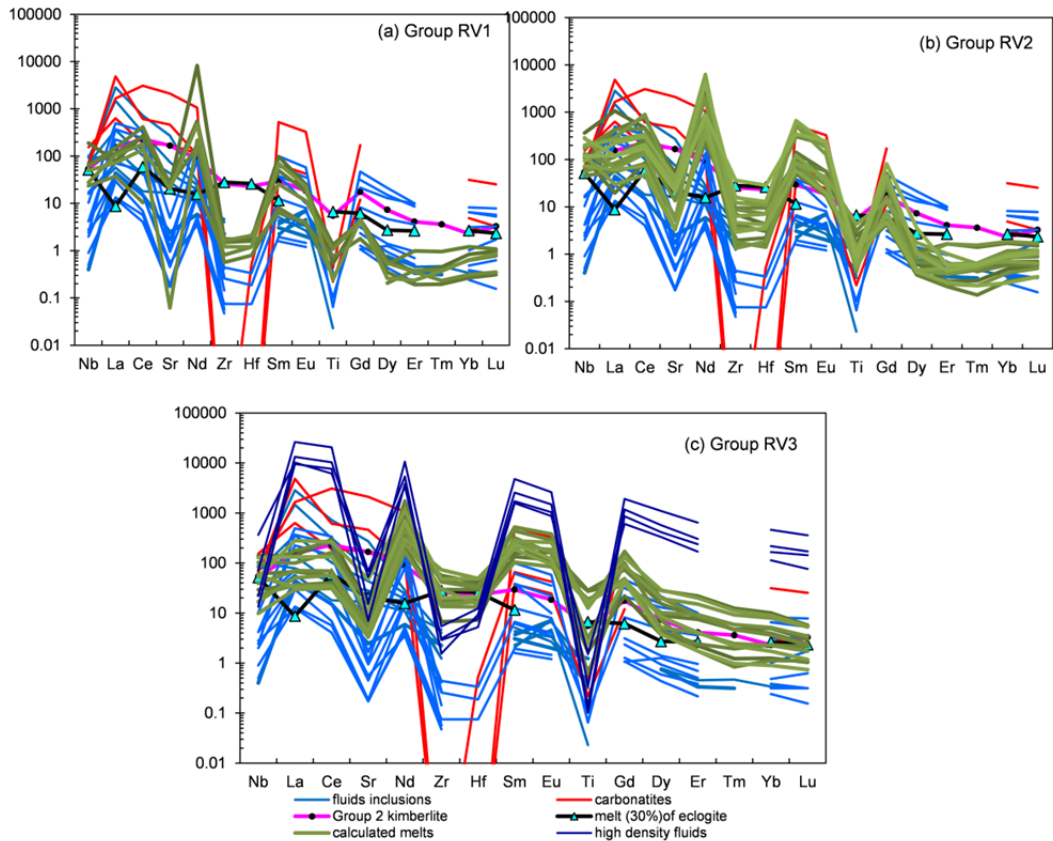


Fig.5: Gerechnete SEE Muster von silico-carbonatitischen Schmelzen (grün) als mögliche Kandidaten für die Metasomatose von subkalzischen Granaten: **a)** für Gruppe RV1, **b)** Gruppe RV2 und **c)** Gruppe RV3. Die Verteilungskoeffizienten stammen aus der Arbeit von Girnis et al. (2012; revised version submitted to Lithos). Die Spurenelementzusammensetzungen für Gruppe II Kimberlite stammen von Nowell und Pearson (2004), die von natürlichen Karbonatiten aus Uganda von Nelson (1988), von Flüssigkeitseinschlüssen (carbonate-K-chloride-H₂O) in „fibrous“ diamonds von Tomlinson et al. (2009) und von karbonatitischen bis kimberlitischen Schmelzen in „fibrous“ Diamanten von Klein-BenDavid et al. (2010). Die Spurenelemente der Silikatschmelze eines Eklogitschmelzexperimentes (30% partielle Schmelze) sind von Rapp et al. (1999).

Ein beeindruckendes Argument für die bestimmende Rolle einer karbonatitischen Metasomatose liefert die Beziehung von Ti/Eu vs. Zr/Hf (Fig.6). Sehr niedrige Ti/Eu und sehr hohe Zr/Hf Verhältnisse in den meisten Granaten führen eindeutig zu diesem Schluss. Granate im Gleichgewicht mit einer karbonatitischen Schmelze fraktionieren Zr von Hf und Ti von Eu, wie die experimentellen Arbeiten von Sweeney et al. (1992) und Grinis et al. (2012) gezeigt haben. Mehr als 90% unserer Proben (93 von 103 Granaten) haben ein Ti/Eu niedriger als 2500 und erhöhte und superchondritische Zr/Hf Verhältnisse (hauptsächlich von 40 bis 110).

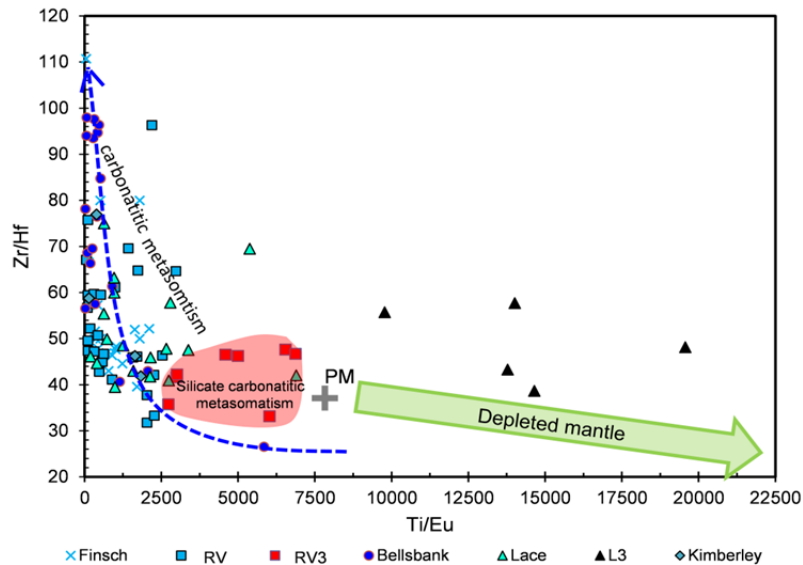


Fig.6: Ein Zr/Hf vs. Ti/Eu Diagramm; drei Granatpopulationen werden unterschieden: Granate mit blauen Symbolen interagierten mit karbonatitischen Schmelze; dies ergab niedrige, subchondritische Ti/Eu und hohe, superchondritische Zr/Hf Verhältnisse. Das rote Feld umfasst Proben, die wahrscheinlich von mehr silizischen Schmelzen betroffen waren. Grüner Pfeil: Trend für residuale Granate. Die Granate mit superchondritischem Ti/Eu (schwarze Dreiecke) sind möglicherweise subkalzische Megakristalle.

1.2 Spurenelemente als Fingerabdruck für das partielle Schmelzregime

Eine Reihe von Elementen, die in Granat kompatibel sind, wie z.B. Cr und die SSEE werden benutzt, um auf das partielle Schmelzregime Rückschlüsse zu ziehen. Voraussetzung ist, dass sie nach dem Schmelzprozess nicht durch Metasomatose verändert wurden.

Zwei Hauptmodelle existieren zur Entstehung der residualen Peridotite des SCLM:

a) Das "plume" Modell, bei dem das partielle Schmelzen bei hohen Drücken im Granatstabilitätsfeld in einem aufsteigenden "plume" stattfindet. Granat und opx sind die residualen Phasen, doch würde Granat bei extrem hohen Schmelzgraden verloren gehen. Die SSEE sind kompatibel in Granat und werden deshalb im Residuum zurückgehalten, solange er vorhanden ist. Nur wenn Granat verschwindet, werden auch die SSEE in den Residuen deutlich abnehmen. .

b) ein Modell mit passiv aufsteigendem Mantel wie an mittelozeanischen Rücken, bei dem der Schmelzprozess in geringen Tiefen im Spinellstabilitätsfeld stattfindet und nur noch ol, cpx und sp als residuale Phasen vorhanden sind. Während der folgenden Subduktion entsteht Granat durch Entmischung aus dem Orthopyroxen. Da alle SEE inkompatibel sind, werden sie im Residuum kontinuierlich während des partiellen Schmelzprozesses verarmt.

Die Cr/Al Verteilungskoeffizienten zwischen Mantelmineralen und Schmelzen sind bei niedrigen Drücken hoch und nur noch 1 bei hohen Drücken (Stachel et al. 1998). Deshalb können Cr-reiche Granate, die sehr häufig sind, nur durch Metamorphose aus Residuen wachsen, die bei niedrigen Drücken entstanden sind. Dafür sprechen auch die häufig sehr stark positiven Steigungen der SSEE, die partielles Schmelzen in Abwesenheit von Granat anzeigen.

Der größere Anteil der Granatperidotite des Kaapvaal Kratons besteht deshalb aus subduzierten Residuen, die durch partielles Schmelzen bei niedrigen Drücken entstanden sind. Ein geringerer Anteil besitzt jedoch chemische Signaturen, die partielles Schmelzen bei hohen Drücken anzeigen.

1.3 Datierung von Anreicherung und partiellem Schmelzen mit Sm-Nd and Lu-Hf

Errorchronen mit dem Sm-Nd System

Die inkompatiblen Elemente überprägen die chemische Zusammensetzung der Granate je nach Grad der Metasomatose und nach der modalen Häufigkeit mehr oder weniger stark. Von den SEE werden Sm und Nd am leichtesten beeinflusst. Da metasomatische Prozesse auch multiple Ereignisse sein können, ist auch die Wahrscheinlichkeit geringer, dass signifikante Korrelationen für das Sm-Nd System gefunden werden, die einer Isochrone entsprechen. Dennoch entspricht die Steigung von sechs RV2, zwei RV1 und sechs Lace Granaten der einer Steigung einer 900 Ma Referenzlinie (hier nicht gezeigt). Die weiteren Proben dieser Lokalitäten sind parallel einer zweiten Referenzlinie mit ebenfalls 900 Ma, jedoch bei niedrigeren $^{143}\text{Nd}/^{144}\text{Nd}$ Verhältnissen. Dieses Alter entspricht dem Ende der Namaqua-Natal Orogenese (0.9 to 1.3 Ga), während der Material unter den Kraton subduziert wurde. Dies könnte eine weit verbreitete Metasomatose verursacht haben, die letzte vor der kretazischen Kimberlitaktivität. Die extrem niedrigen Nd Isotopenverhältnisse (bis $\epsilon\text{Nd} = -40$) der Granate mit den niedrigsten Sm/Nd Verhältnissen zeigen an, dass die metasomatische Schmelze aus einem reaktivierten Reservoir stammen muss, das dem einer alten Erdkruste entspricht

Isochronen des Lu-Hf Systems

Durch die Evaluation der Haupt-, Spurenelement- und Isotopenzusammensetzung konnten wir die subkalzischen Granate identifizieren, die noch eindeutige chemische Merkmale aus der Zeit der Bildung der Protolith und von Wiederanreicherungsprozessen besitzen. Dies ermöglichte es uns, mehrere Isochronen von drei Kimberlitlokalitäten des Kaapvaal Kratons zu erstellen, nämlich von Finsch an der westlichen Grenze des W-block mit dem 1.85 bis 2.0 Ga alten Kheis-Magondi belt, von Roberts Victor an der westlichen Grenze des E-Blocks und von Lace, mehr oder weniger in der Mitte des E-Blocks.

Finsch: Frühere Arbeiten an subkalzischen Granaten von Finsch von Lazarov et al. (2009) hatten Alter von zwei Schmelzepisoden ergeben, einmal ein Granatmodellalter von 3.6 Ga und ein zweites um 2.62 Ga, das als das finale Schmelzereignis betrachtet wurde. Unsere jetzige Interpretation ist, dass es sich dabei eher um einen Wiederanreicherungsprozess eines bereits extrem verarmten Erdmantels mit $\epsilon\text{Hf} = +25$ handelt, der jedoch zugleich einen Schmelzprozess mit geringen Graden der partiellen Schmelze getriggert hat. Ein verarmter Erdmantel sollte $\epsilon\text{Hf} = +8$ vor 2.62 Ga haben. Unser sehr hoher ϵHf Wert zeigt einen extremen Verarmungsprozess noch vor dem 2.62 Ga Ereignis an, doch kann dessen Alter nicht genau bestimmt werden. Es könnte vor 3.6 Ga gewesen sein, doch beträgt das älteste T_{RD} Alter des W-Blocks nur 3.2 Ga. Ein erster Schmelzprozess zu dieser Zeit mit

25% partieller Schmelze (non-modal fractional melting) im Spinellstabilitätsfeld ergibt $\text{Lu}/\text{Hf} = 0.7$, wodurch ϵHf auf +25 vor 2.62 Ga wachsen würde. Nur 50 bis 100 Ma würden benötigt, wenn der partielle Schmelzprozess in Granatstabilitätsfeld stattfinden würde. Bei Durchsicht der publizierten Finschdaten fiel auf, dass noch eine weitere Isochrone mit einem Alter von 1.907 ± 0.19 Ga in dem F2 (Hf-enriched) Datensatz verborgen war (Fig. 7c). Dieses Alter fällt mit dem Alter des Kheis-Magondi belts (1.85 - 2,0 Ga) zusammen, der unmittelbar westlich von Finsch gelegen ist und durch Kompression and „eastward thrusting“ gebildet wurde (e.g. Jacobs et al., 2008).

Roberts Victor und Lacey: Zwei Isochronen wurden in Roberts Victor unterschieden (Fig. 7a): eine mit 2.95 ± 0.06 Ga und $\epsilon\text{Hf} = 2.7 \pm 1.4$ und eine zweite mit 3.27 ± 0.15 Ga und einem $\epsilon\text{Hf} = 17.6 \pm 3.6$. Das 2.95 Ga Alter wird als partieller Schmelzprozess eines fast primitiven Erdmantels interpretiert und das um 3.27 Ga als das eines Wiederanreicherungsprozesses.

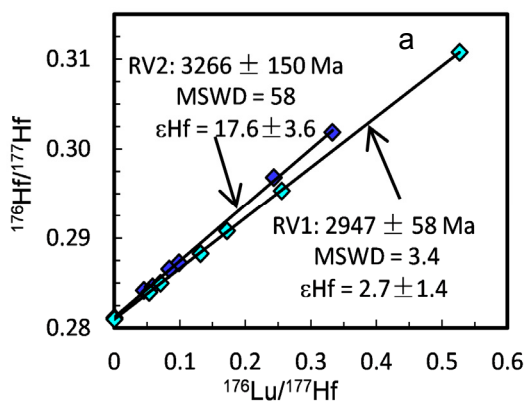


Fig.7a: Isochronen subkalzischer Granate von Roberts Victor: Gruppe RV1 (hellblaue Linie) ergibt 2.95 Ga; Gruppe RV2 (dunkelblau) ergibt 3.27 Ga.

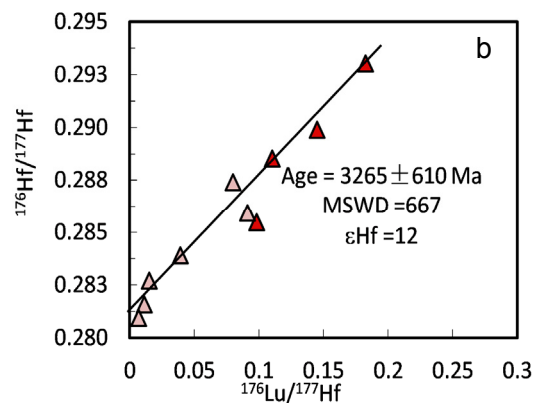


Fig.7b: Subkalzische Granate von Lacey ergeben Errorchrone von 3.27 Ga mit $\epsilon\text{Hf} = +12$. Sie fällt mit der 3.3 Ga Isochrone von Roberts Victor zusammen. Rote Dreiecke: L1 Granate; pink: L2 Granate.

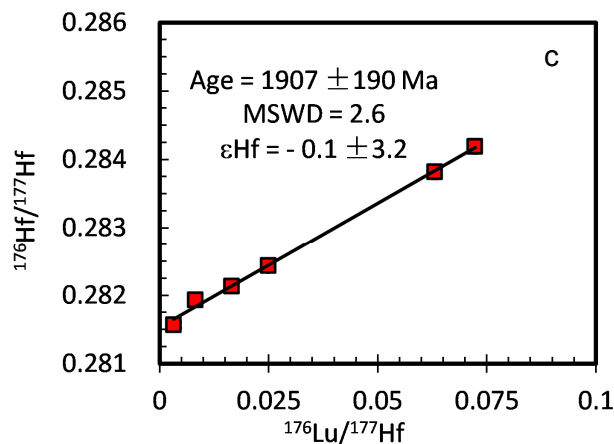


Fig. 7c: Eine Lu/Hf Isochrone von sechs subkalzischen Finsch Granate, die ein gemeinsames Modelalter von 1.9 Ga besitzen und konsequenterweise ein Isochronenalter von 1.9 Ga als die Zeit einer Metasomatose.

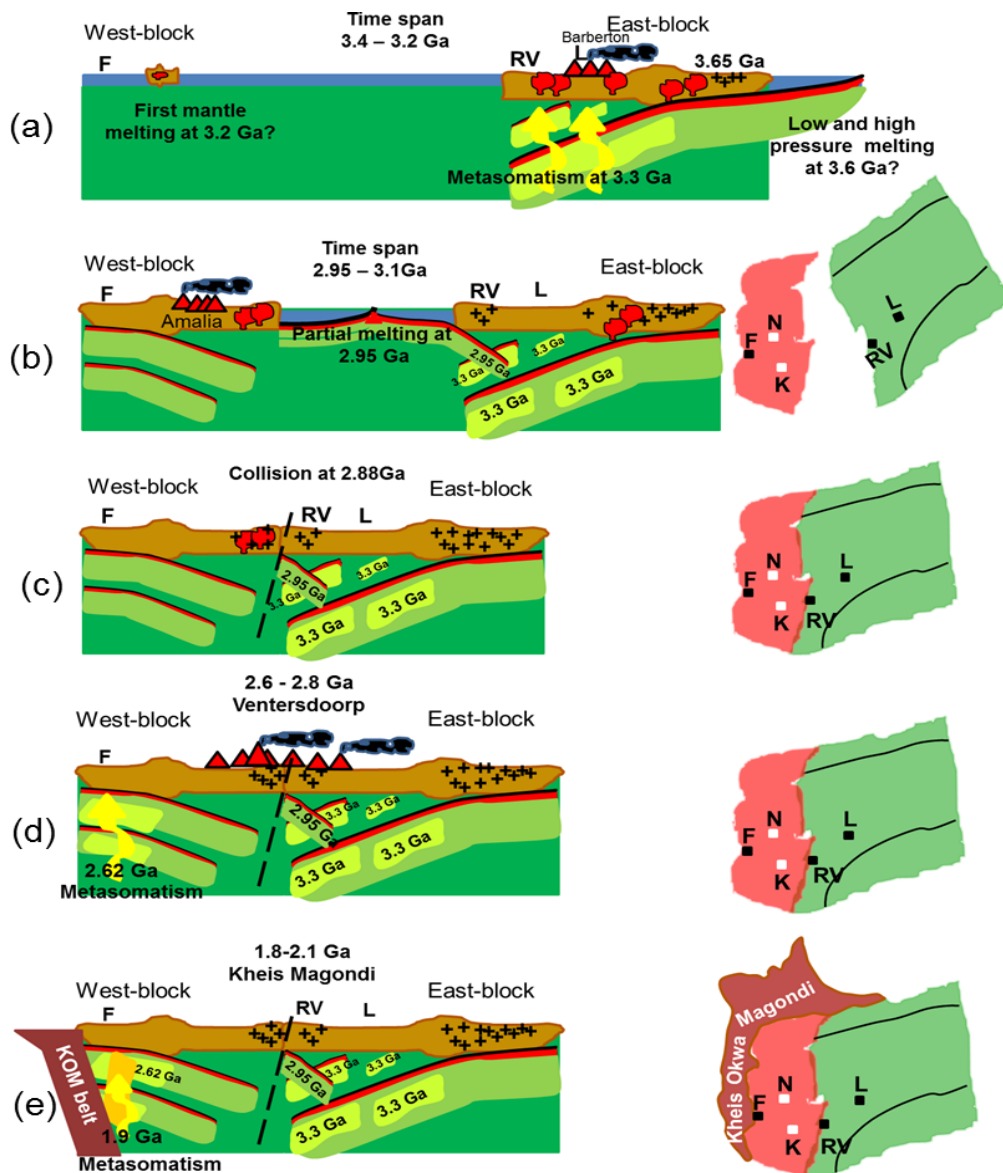


Fig. 8: Modell für die Bildung und Entwicklung des lithospherischen Mantels unterhalb des Kaapvaal Kratons. Partielles Schmelzen im Erdmantel und die Bildung der Kruste geschieht hauptsächlich an mittelozeanischen Rücken und durch subduktionsbezogene Prozesse. **a)** Periode zwischen 3.2 und 3.4 Ga: Der größte Teil der kontinentalen Kruste des E-Blocks existiert bereits. Unter der Kruste gibt es einen bereits stark verarmten Mantel, der vor 3.3 Ga metasomatisch überprägt wird (Lu-Hf Alter der Granate von Roberts Victor and Lacey). Die Existenz und Größe des W-Blocks ist unbekannt bis vor 3.2 Ga (älteste T_{RD} Alter des Erdmantels und U-Pb Alter von kristallinen Zirkonen). **b)** Die Zeitspanne von 3.1 bis 2.95 Ga ist die Zeit der Intrusion von TTG's und der Platznahme von Grünsteingürteln auf dem W-Block. Neue ozeanische Kruste und entsprechender verarmter Mantel entstanden zwischen den beiden Blöcken aus passiv aufströmendem Erdmantel vor 2.95 Ga (partielles Schmelzalter von Roberts Victor Granaten) Diese wurden unter den E-Block subduziert (Begründung: gleiches Metasomatosealter von Roberts Viktor und Lacey). **c)** Die beiden Blöcke kollidierten vor 2.9 Ga entlang des Colesberg lineaments. **d)** Die Ventersdoorp Laven bedeckten zwischen 2.6 und 2.8 Ga große Teile beider Blöcke. Das 2.62 Ga Alter von Finsch fällt in diese Periode und mag eine großräumige Metasomatose in Verbindung mit dem Ventersdoorp Magmatismus datieren. **e)** In der Zeitspanne von 1.8 to 2.1 Ga wurde der Kraton durch die Intrusion des Bushveld Komplexes und vom Westrand durch Subduktionsprozesse modifiziert, die mit der Bildung des Kheis-Magondi belts verknüpft waren. Das 1.9 Ga Anreicherungsalter von Finsch Granaten datiert wahrscheinlich einen solchen Prozess. (N: Newlands; F: Finsch; K: Kimberley; RV: Roberts Victor; L: Lacey)

Der Schmelzprozess fand an einem mittelozeanischen Rücken statt, der sich zwischen dem E- und W-Block befand, gefolgt von Subduktion unter den E-Block (Fig.8). Die RV1 Harzburgite stellen die subduzierte und verarmte Lithosphäre dar und die Eklogite von Roberts Victor möglicherweise die mafische ozeanische Kruste. Die Kollision des W- und E-Blocks fand wenig später um 2.9 Ga entlang des Colesberg lineament statt (Schmitz et al. 2004).

Die 3.27 Ga Isochrone mit $\epsilon_{\text{Hf}} = +17.6$ wird als die Zeit der Metasomatose eines bereits stark verarmten Mantelanteils interpretiert. Die Protolithen waren Spinellharzburgite, die bereits in das Granatstabilitätsfeld vor der Zeit der Metasomatose subduziert worden waren. Der partielle Schmelzprozess im Spinellperidotitstabilitätsfeld sollte in Analogie zur Begründung von Finsch bereits mehrere hundert Mio. Jahre vorher stattgefunden haben. Die zehn Proben von der Lace Mine ergaben eine Isochrone von 3.27 ± 0.6 Ga (Fig. 7b), ein Alter wie die Isochrone von Roberts Viktor. Wir nehmen an, dass derselbe Anreicherungsprozess um 3.27 Ga (oder rein zeitgleicher Prozess) denselben verarmten Mantel unterhalb des E-Block überprägte.

Die Altersinformation über den Erdmantel unterhalb des Kaapvaal Kratons, die durch diese Studie erhalten wurde, die publizierten Re-Os Alter und die kristallinen Altersdaten sind in Fig. 8 als Kartoon von Abfolgen von Schmelzprozessen im Erdmantel, Anreicherungsprozessen und Krustenwachstum dargestellt. Der Kartoon ist eine Modifikation von früheren Arbeiten verschiedener Autoren, z.B. Schmitz et al. (2004) und Shirey et al. (2004).

2. Der Ursprung und das Alter von Eklogiten und Granatpyroxeniten und die Abkühlung des Erdmantels

Eklogite werden im allgemeinen als die metamorphen Äquivalente von basaltischen Gesteinen betrachtet, doch zeigt die Variationsbreite der Mineralogie und der chemischen und isotopischen Zusammensetzung von Eklogit- und Granatpyroxenitxenolithen aus Kimberliten, dass ihre Protolithen sehr unterschiedlicher Natur sein können und dass diese nach ihrer Entstehung sehr unterschiedlichen Prozessen unterworfen werden können wie zum Beispiel Tieftemperaturalteration, Entwässerungsreaktionen bei prograder Metamorphose, partielles Schmelzen und Wiederanreicherungsprozesse. Im folgenden wird das Wort Eklogit oft mit einer breiten Bedeutung benutzt. Dabei kann es Eklogite im engeren Sinn einschließen (auch mit Coesit, Disthen oder Korund) und Granatpyroxenite. In der Hauptsache werden zwei Modelle für die Entstehung von Eklogiten vertreten: (1) eine Entstehung im Erdmantel als Hochdruckkumulate von (ultra-)mafischen Schmelzen und (2) als metamorphe Produkte von subduzierter ozeanischer Kruste. Da sie nach ihrer Metamorphose zu Eklogit noch einen partiellen Schmelzprozess und Metasomatose durchlaufen haben können, kann es schwierig sein, die Protolithen zu entziffern und Alter, die durch Isotopenuntersuchungen gewonnen werden, den jeweiligen Prozessen zuzuordnen.

2.1 Ergebnisse

Um diese Probleme und Fragestellungen weiter zu untersuchen analysierten wir 11 Eklogitxenolithe von Bellsbank mit außerordentlich frischen Granaten und Klinopyroxenen auf ihre Haupt- und Spurenelementgeochemie und ihre Sm-Nd and Lu-Hf Isotopie. Die Xenolithe gehören zu den Gruppen A und B der Eklogitklassifikation von Coleman et al. (1965; siehe Fig. 9 a,b). Sie stammen von Temperaturen zwischen 820 and fast 1200°C (Fig. 9c). Basierend auf ihren Spurenelementen und den Isotopenverhältnissen wurden sie in die Gruppen A' + B2 and A + B1 unterteilt (Figs. 10 und 11 a,b).

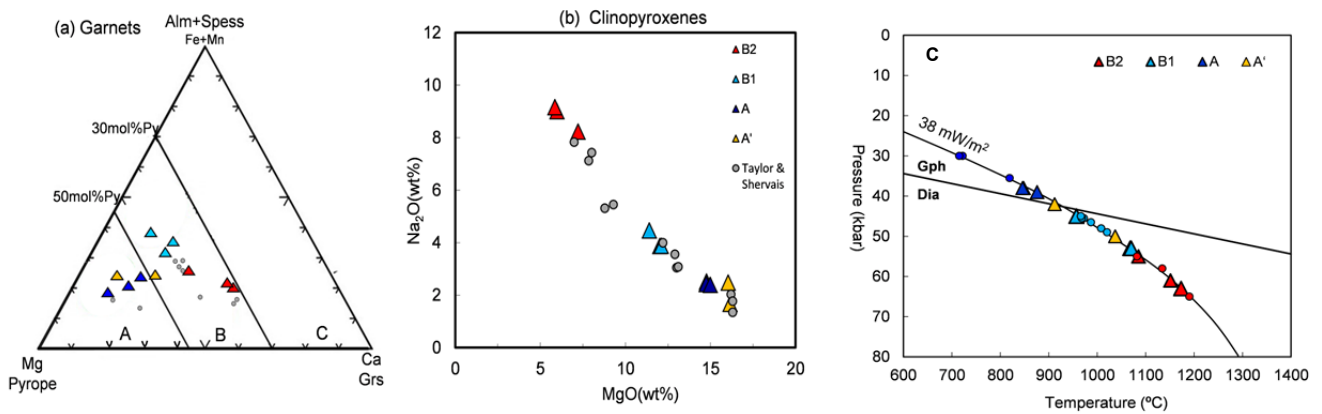


Fig. 9 a,b: Hauptelementzusammensetzung der Granate und Klinopyroxene. Die kleinen grauen Punkte sind Daten aus früheren Arbeiten von Bellsbank (Taylor und Neal, 1989 und Shervais et al., 1988).

Fig.9 c: Temperaturen, berechnet mit Krogh (1988) und auf einen 38 mW/m² konduktiven geothermischen Gradienten projiziert

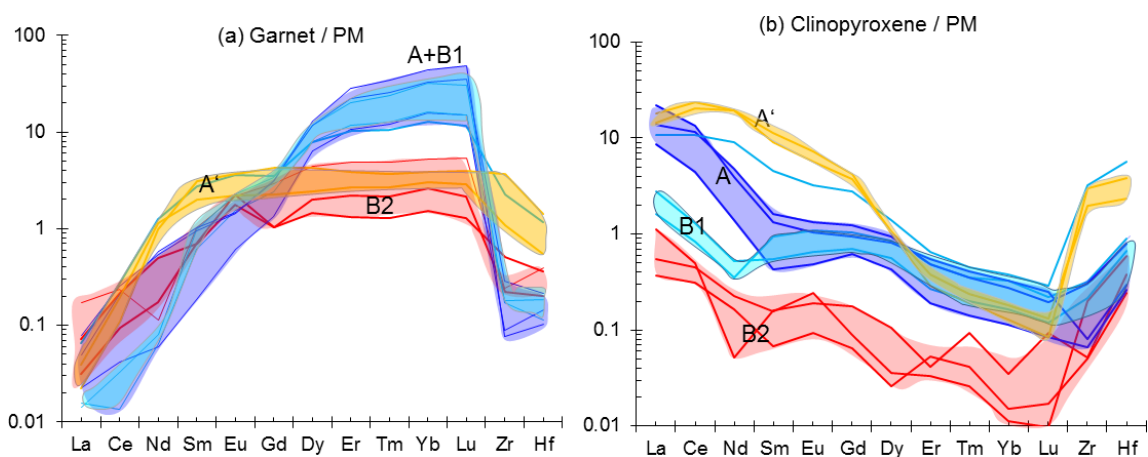


Fig.10: Auf einen primitive Erdmantel (McDonough & Sun 1995.) normierte SEE + Zr + Hf Muster (a) von Granaten und (b) Klinopyroxenen von Bellsbank Eklogiten. Die bunten Bänder zeigen den Zusammensetzungsbereich der vier Gruppen, die aufgrund von petrographischen und geochemischen Merkmalen unterschieden wurden. Die SEE betonen die Verwandtschaft zwischen den Gruppen A + B1 und den Gruppen A' + B2.

Die SEE Muster der Granate der Gruppen A (dunkelblauer Bereich in Fig. 10a) and B1 (hellblau) sind sich ähnlich mit steilen, positiven Steigungen von den leichten zu den schweren SEE und mit extrem hohen SSEE Häufigkeiten ($(\text{Lu})_{\text{PM}}$ up to 50). Nur die Probe BE4 von Gruppe B1 ist stark in den leichten und mittleren SEE angereichert. In den anderen A und B1 Proben sind nur La, Ce und eventuell Nd leicht angereichert. Die Klinopyroxene der Gruppen A and B1 haben ebenfalls ähnliche Spurenelementmuster. Ihre SEE Muster (Fig. 10b) haben negative Steigungen von La bis Nd oder Sm, steigen positiv von Nd bis Gd und nehmen dann wieder zu der SSEE ab.

Die Granate der Gruppen A' und B2 sind sich ebenfalls ähnlich mit flachen mittleren und schweren SEE Mustern und niedrigen SEE Gehalten (Fig. 10a). Die B2 Granate haben schwache bis kräftige positive Eu Anomalien (Eu/Eu^* : 1.1 to 2.7), ebenso die Pyroxene. Die B2 Klinopyroxene haben die niedrigsten SEE Gehalte, die A' Klinopyroxene die höchsten.

Die Lu-Hf und Sm-Nd Isotope zeigen die gleiche Aufteilung in vier Gruppen wie die Spurenelemente, also eine Verwandtschaft zwischen den Gruppen A+B1 und den Gruppen A'+B2 (Figs. 11 und 12). Die Sr isotope (keine Abbildung) variieren von $^{87}\text{Sr}/^{86}\text{Sr} \sim 0.704$ to 0.712 ohne eine Korrelation mit den verschiedenen Gruppen. Die $\delta^{18}\text{O}$ Verhältnisse (2.5 – 5.3) sind alle niedriger als der Mantelwert außer einem $\delta^{18}\text{O} \sim 6.5$ in der Probe BE4, die sehr hoch an inkompatiblen Elementen angereichert ist.

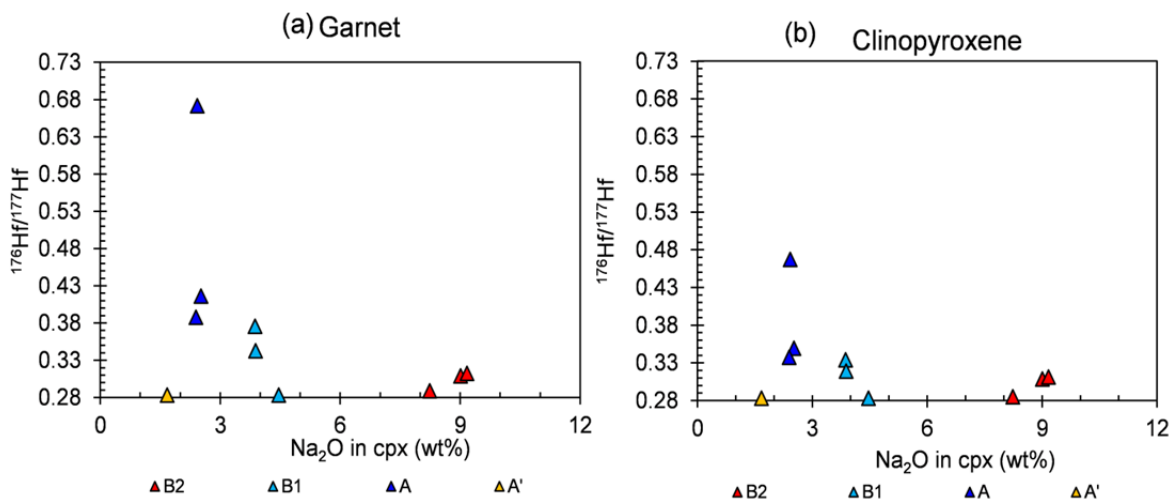


Fig.11 a,b: Die gemessenen $^{177}\text{Hf}/^{176}\text{Hf}$ isotonenverhältnisse von a) Granaten und b) Klinopyroxenen aufgetragen gegen den Natrium-Gehalt in Klinopyroxenen als Indikator der Eklogitgruppen. Die meisten Isotonenverhältnisse sind extrem hoch (zum Vergleich: der heutige primitive Erdmantel hat $^{177}\text{Hf}/^{176}\text{Hf} = 0.282772$ und der MORB-Mantel 0.283250). Die Abfolge der Datenpunkte von hohen zu niedrigen Isotonenverhältnissen für grt und cpx jeder Gruppe der Eklogite entspricht der Probennummer, d.h. hohe Werte in grt gehören zu hohen Werten in cpx usw. Koexistierende grt-cpx Paare können so mit dem Auge verknüpft werden.

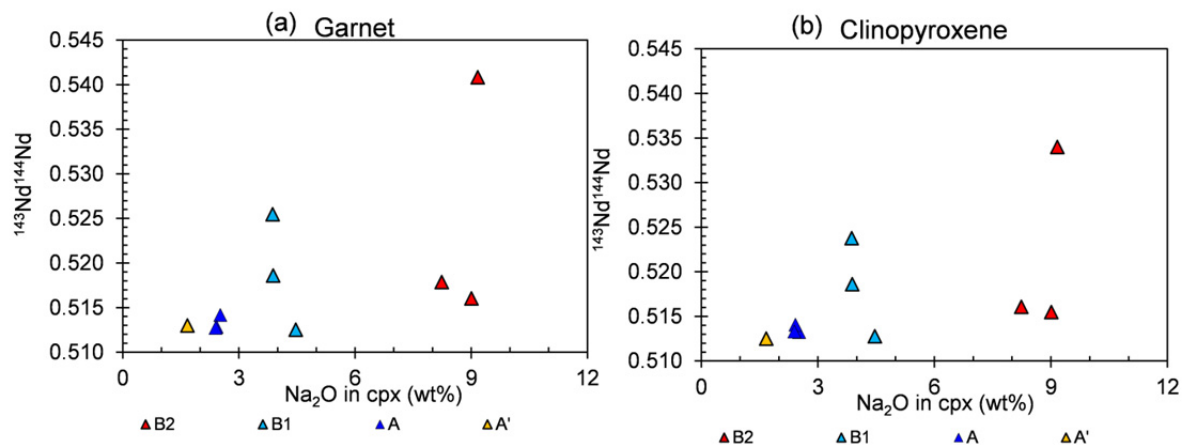


Fig. 12 a,b: Die gemessenen $^{143}\text{Nd}/^{144}\text{Nd}$ Isotopenverhältnisse für **a)** Granat und **b)** Klinopyroxen aufgetragen gegen den Natrium-Gehalt in Klinopyroxen als Indikator der Eklogitgruppen. Die Isotopenverhältnisse sind teilweise extrem hoch.

Die $^{177}\text{Hf}/^{176}\text{Hf}$ resp. die $^{143}\text{Nd}/^{144}\text{Nd}$ wurden in Figs. 11 a,b und 12 a,b gegen den Natriumgehalt in den Klinopyroxenen geplottet. Die Isotopenverhältnisse sind extrem hoch in der Mehrheit der Proben, erreichen aber auch den Wert für den heutigen Erdmantel. Extreme Werte sind $\epsilon\text{Hf} = +13724$ für einen Granat und $\epsilon\text{Hf} = +6552$ für seinen koexistierenden Klinopyroxen. In einer anderen Probe ist $\epsilon\text{Nd} = +553$ in Granat und $\epsilon\text{Nd} = +420$ in cpx. Konsequenterweise ergeben die berechneten Gesamtgesteinszusammensetzungen ebenfalls eine große Spannbreite für ϵHf von mehr als +10000 bis herunter zu +13 für eine A' Probe und für ϵNd von mehr als +550 to +3. Die Sequenz von ϵHf der verschiedenen Gruppen entspricht jedoch nicht der von ϵNd , da das Sm-Nd Isotopensystem teilweise metasomatisch überprägt wurde. Deshalb sind die Hf und Nd isotope Verhältnisse teilweise entkoppelt wie sie es auch in den subkalzischen Granaten sind.

2.2 Der Ursprung und das Alter der Eklogite und Granatpyroxenite

Die rekonstruierte Gesamtgesteinszusammensetzung für die Hauptelemente für die Gruppen A'+B2 und B1+A überlappen mit der von modernen gabbroiden Gesteinen, sind jedoch fast völlig getrennt von archaischen Basalten und Boniniten. Im Gegensatz dazu überlappen die rekonstruierten Spurenelementzusammensetzungen von A'+B2 völlig mit denen von modernen gabbroiden Gesteinen in ihren N-MORB normalisierten Mustern (Fig. 13 b). Besonders die mittleren und schweren SEE sind flach und haben den gleichen Zusammensetzungsbereich wie N-MORBs, während die inkompatibleren Elemente meist niedriger sind. Eine positive Eu Anomalie in den B2 Proben, die niedrigen mittleren und schweren SEE Gehalte und die sehr Al-reiche Gesamtgesteinszusammensetzung zeigen, dass Plagioklas eine dominierende Rolle bei den Protolithen einnahm. Es waren niedrigdruck, Plagioklas-reiche Kumulate einer MORB-ähnlichen Zusammensetzung. Die B2 Probe mit einer nur sehr schwachen Eu Anomalie könnte eine fast unmodifizierte Schmelzzusammensetzung darstellen, die ursprünglich als Gabbro kristallisierte. A' Eklogite haben erhöhte mittlere bis schwere SEE im Vergleich zu den zwei B2 Proben mit einer Eu Anomalie, sind aber niedriger als die B2

Probe ohne Eu Anomalie. Sie sind wahrscheinlich Klinopyroxen-reiche Kumulate desselben Magmas wie das für die Plagioklas-Kumulate.

Die SEE Muster der Gruppen A+B1 (Fig. 13 a) sind extrem fraktioniert. Darin zeigt sich eine zentrale Rolle von Granat in der Genese dieser Eklogite. Eine Entstehung bei hohen Drücken als granatreiches Kumulate einer Schmelze ist vorstellbar, doch liegen die Sauerstoffisotope unterhalb der des Erdmantels, was zunächst einmal ein solches Modell ausschließt. Eine andere Möglichkeit ist, dass diese Gesteine Residuen eines partiellen Schmelzprozesses sind, bei dem Granat eine dominante Rolle spielte. Mögliche Kandidaten sind eklogitfaziell metamorphisierte Protolithen archaische Basalte oder Boninite. Partielles Schmelzen eines eklogitfaziellen, MORB-ähnlichen archaischen Basalts mit flachen SEE müßte bis zu 80 % erfolgen, damit das Residuum den extrem fraktionierten SEE Mustern und den hohen SSEE Gehalten der Gruppe A ähnelt. Archaische Boninite, ein zweistufiges Schmelzprodukt des Erdmantels, haben bereits fraktionierte SEE Muster mit unterschiedlichen Häufigkeiten, was den Grad der partiellen Schmelze erniedrigt, um die SEE Muster der A und B Proben als Residuen zu reproduzieren. Die Schmelzgrade liegen zwischen 20 und 60 %. Die niedrigen Sauerstoffisotope aller Eklogittypen stammen von der Tieftemperaturalteration ihrer Protolithen am Ozeanboden. Möglicherweise gilt dies auch für die hohen und variablen Sr-Isotope.

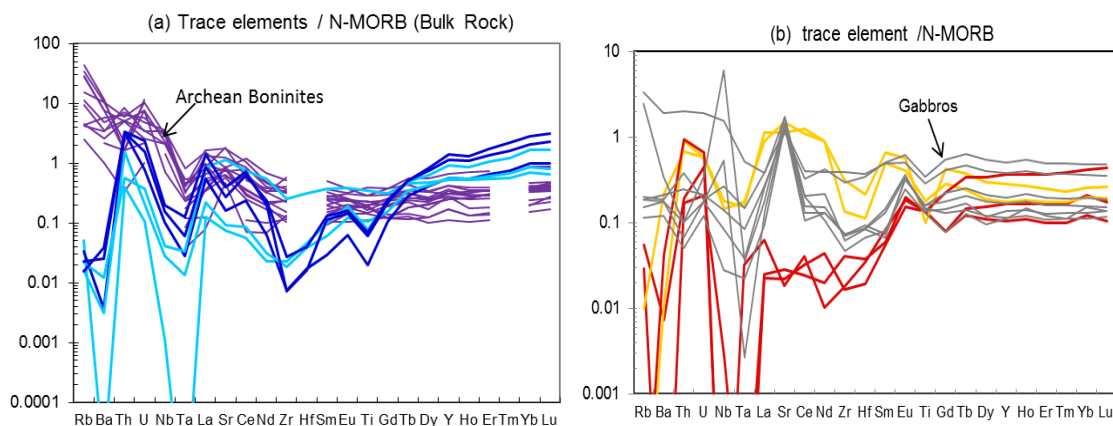


Fig 13: Die N-MORB normierten (Sun & McDonough, 1989) Spurenelementmuster der rekonstruierten Gesamtgesteine. Diagramm (a) zeigt die Spurenelementmuster der Gruppe A (dunkelblau) and B1 (hellblau) und die Spurenelementmuster von archaischen Boniniten (Smithies, 2002). Diagramm (b) zeigt die Spurenelementmuster der Gruppen A' (yellow) and B2 (red lines) und die von modernen gabbroischen Gesteinen (SE Indian Ridge, Hart et al., 1999; Bach et al. 2001).

Potentiell kann eine Reihe unterschiedlicher Alter für Eklogite bestimmt werden: das Alter der Protolithen, das der Eklogitisierung (das sehr nahe an dem des Protolithen liegen kann) und auch die Alter von späterem partiellen Schmelzen und Metasomatose. Protolithalter können theoretisch aus (rekonstruierten) Gesamtgesteinszusammensetzungen oder von Modellaltern erhalten werden. Zweipunktisochronen (grt-cpx) könnten das Eklogitisierungsalter ergeben, was der Fall wäre, wenn die Temperaturen der Eklogite unterhalb der Schließungstemperaturen bleiben. Schließungstemperaturen werden weiter unten diskutiert.

Die Eklogite von Bellsbank sind fast alle nur gering von hoch inkompatiblen Elementen überprägt (siehe Figs. 11 a,b) so dass ihre ursprüngliche chemische Zusammensetzung nach dem

partiellen Schmelzprozess (Gruppen A and B1) oder die des Protoliths (Gruppen A' and B2) generell erhalten geblieben ist. Der geringe Grad der Metasomatose beeinflusste nur die leichten SEE und nicht die mittleren und schweren SEE und Hf. Der größte Teil von Nd und teilweise Sm in den stark SEE fraktionierten Proben wird deswegen von der Metasomatose stammen. Mit dem Sm-Nd Isotopensystem kann deshalb eventuell ein Metasomatosealter bestimmt werden. Wir haben unsere berechneten Gesamtgesteinsdaten für Sm-Nd mit denen von Taylor and Neal (1990) and Shervais, et al. (1988) kombiniert und erhalten eine 2.08 ± 0.38 Ga Errorchrone mit $\epsilon_{Nd} = +28$ (Fig. 14). Die Proben BE11 and BE2 wurden nicht miteinbezogen, da sie praktisch keine Nd Anreicherung in ihren Spurenelementmustern zeigen. Interessanterweise fällt das 2.08 Ga Alter einerseits mit dem Alter des Bushveld Komplex zusammen, andererseits auch mit dem Altersbereich 1.8 bis 2.1 Ga für den Kheis-Magondi belt.

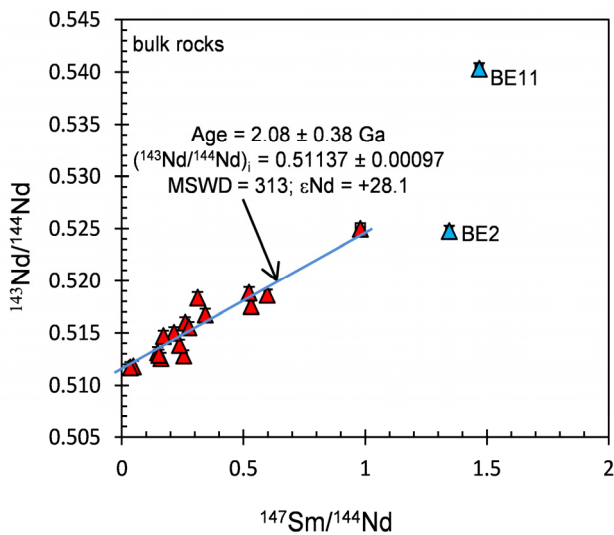


Fig.14: Sm-Nd Isochronendiagramm für Bellsbank Eklogite (eigene und Literaturdaten). Die roten Dreiecke ergeben eine Errochrone mit 2.08 Ga und $\epsilon_{Nd} = +28$.

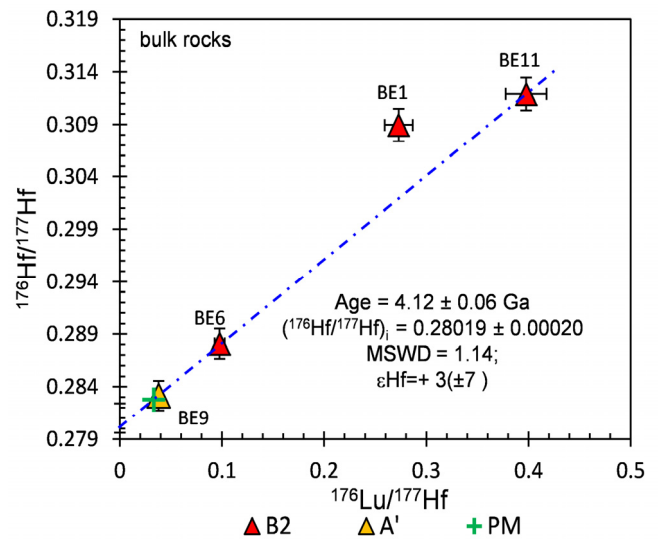


Fig.15: Lu-Hf Isochronendiagramm aus berechneten Gesamtgesteinszusammensetzungen der Eklogitgruppen A' and B2.

Eine gemeinsame Sm-Nd Isochrone durch die Gesamtgesteinszusammensetzungen aller Gruppen ist vernünftig, da der Anreicherungsprozess nach der Stabilisierung des Kaapvaal Kratons erfolgte. Das Lu-Hf System war dagegen praktisch davon nicht betroffen und sollte deshalb Informationen über die frühere Geschichte der Gesteine liefern. Für die Erstellung einer Gesamtgesteinsisochrone ist es jedoch notwendig ist zu zeigen, dass die Gesteine kogenetisch sind. Dies scheint für die Gruppen A' and B2 der Fall zu sein, die als fast unveränderte metamorphe Anteile einer subduzierten ozeanischen Kruste betrachtet werden. Drei der vier Proben bilden eine Isochrone (Fig. 15) mit einem Alter von 4.12 ± 0.06 Ga mit $\epsilon_{Hf} = 3 (\pm 7)$ d.h. der initiale Wert entspricht dem des Erdmantels zu dieser Zeit. Die Probe BE1 liegt nicht auf dieser Isochrone. Ihr Granat scheint kontaminiert zu sein, da er ein zu hohes Modellalter von 5,5 Ga ergibt. Ein Alter von 4,12 Ga erscheint

hoch. Bisher wurde noch von keinem so hohen Alter in Kruste oder Mantel des südlichen Afrika berichtet. Nur eine Re-Os Errorchrone von Eklogiten von Newlands ergab dasselbe Alter.

Dennoch erscheint dieses Alter zuverlässig, da die drei Proben auf der Isochrone jeweils ein Modellalter ergeben, das dem der Isochrone entspricht. Dies muss natürlich so sein, wenn das Initial der Isochrone dem des primitiven Erdmantels entspricht. Unabhängig von dieser Isochrone liefert die Probe BE11 (Gruppe B2) ein Hf-Modellalter von 4.12 ± 0.29 Ga (Fig. 16), das zuverlässig und reell erscheint. Das SEE Muster ist kontinuierlich verarmt bis Nd; eine Hf Anomalie ist nicht erkennbar. Granat und Klinopyroxen haben dasselbe ϵ_{Hf} zum Zeitpunkt der Kimberliteruption (120 Ma) of +1005 und damit auch das Gesamtgestein. Damit die Hf-Isotope bis zu einem so hohen Wert anwachsen, wird sehr viel Zeit benötigt, auch mit einem relativ hohen $^{176}\text{Lu}/^{177}\text{Hf}$ von 0.398. Das Modellalter von 3.51 Ga des Granats dieser Probe ist ein Minimumalter.

Alle A' and B2 ergeben hohe Modellalter für die Gesamtgesteine und Granate, während A und B1 wegen ihrer komplexen Geschichte nur jüngere Alter ergeben (Fig. 16).

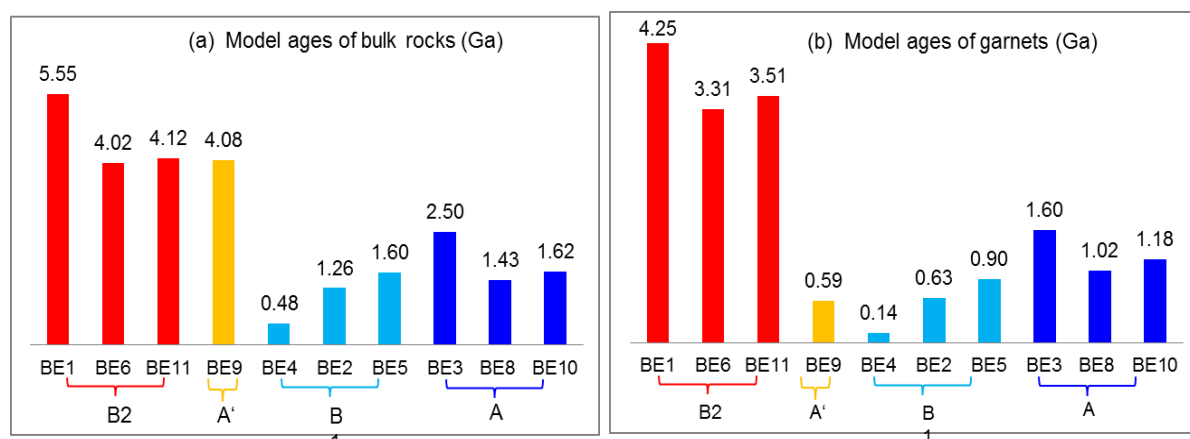


Fig.16: Modellalter von Gesamtgesteinen (linkes Diagramm) und Modellalter von Granaten (rechtes Diagramm). Die verschiedenen Gruppen sind als farbige vertikale Balken dargestellt. Die Alter in Ga sind oberhalb der Balken notiert, Probenamen und -gruppen unterhalb (B2 = rot; A' = gelb; B1 = hellblau und B2 = dunkelblau)

2.3 Die Bedeutung von Zwei-punkt-Isochronen, Schließungstemperaturen für Sm-Nd und Lu-Hf und das Abkühlen des subkratonischen Mantels

Der Erdmantel ist ein riesiger metamorpher Komplex der wegen der Plattentektonik ständigen Änderungen unterliegt. Es gibt jedoch Enklaven unterhalb archaischer Kruste, die vom konvektierenden Erdmantel seit 2,5 Ga getrennt sind. In diesem Teil entwickelte sich ein stabiler thermischer Zustand, seit er entweder durch „plume“ Aktivität oder Subduktion entstand. Thermische Relaxation des subkratonischen Mantels findet bis zur endgültigen Stabilisierung im Archaikum statt. Seitdem sollte der Mantel langsam kühlen durch den Verlust einer remanenten Wärme und eventuell durch Denudation. Zweipunktisochronen (grt-cpx) von Mantelxenolithen (Peridotite oder Eklogite) sollten entweder Abkühlalter oder Eruptionsalter ergeben, abhängig davon, ob die Proben aus einem Mantelteil stammen, der unterhalb oder oberhalb der Schließungstemperatur des betrachteten isotopischen Systems liegt. Eine weitere Art Alter entsteht, wenn das eine oder andere der beiden

Minerale bevorzugt chemisch gestört ist. Da dies meist Klinopyroxen ist, entstehen künstlich hohe Alter.

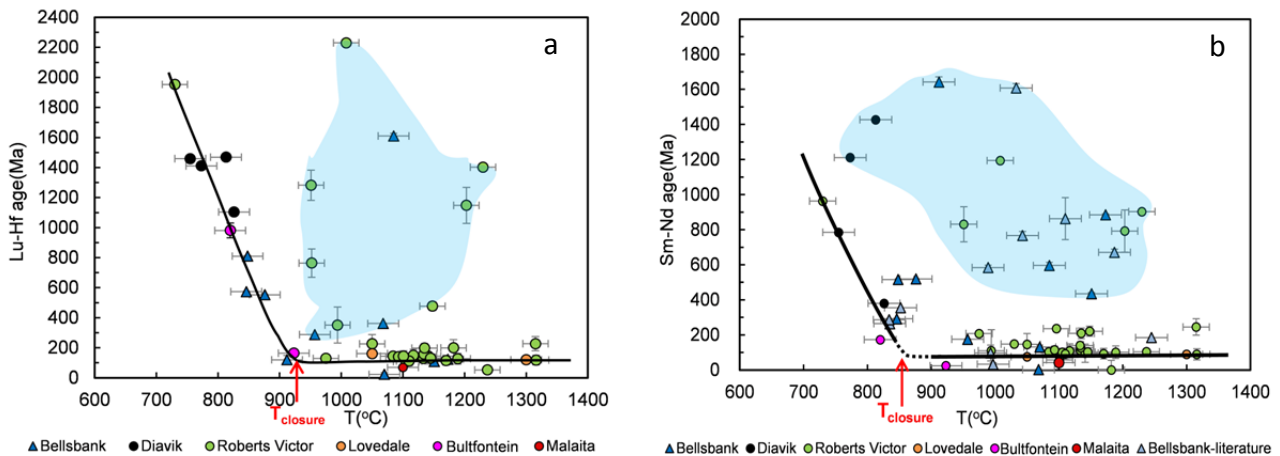


Fig. 17 a,b: Eine Korrelation von Lu-Hf und Sm-Nd Zweipunktisochronenalter und der berechneten Temperaturen von unseren Proben und Proben aus der Literatur. Für eine Population von Tieftemperaturproben werden die Alter mit zunehmender Temperatur niedriger bis 920 °C (Lu-Hf) (a) bzw. 850°C (Sm-Nd) (b) gefolgt von einer großen Anzahl von Proben mit Eruptionsaltern. Die Schließungstemperaturen liegen im Schnittbereich des Tieftemperaturastes der schwarzen Linie mit dem Hochtemperaturast. Die Schließungstemperatur für das Lu-Hf System sollte daher bei 920 °C und für Sm-Nd bei 840°C liegen (rote Pfeile). Das blau schattierte Feld umfaßt die Hochtemperaturproben mit hohen, aber bedeutungslosen Altern, da sie wahrscheinlich durch eine rezente Überprägung verursacht ist, die hauptsächlich den Klinopyroxen betraf.

Die Schließungstemperatur eines Isotopensystems kann für eine angenommene Abkühlrate aus den Diffusionseigenschaften eines Elements in den betrachteten Mineralen und den geometrischen Eigenschaften der Minerale bestimmt werden (Dodson, 1986; Ganguly and Tirone, 1998, 2001). Eine Schließungstemperatur ist ein Mitglied eines Temperaturintervalls, innerhalb dessen die Volumendiffusion während des Kühlprozesses endet. Für ein Mineralpaar bestimmt das Mineral mit der langsameren Diffusionsrate die Schließungstemperatur. Unter Annahme von geometrischen Faktoren und von sinnvollen Diffusionskoeffizienten für das Sm-Nd-System bestimmten Bedini et al. (2004) Abkühlraten für den lithosphärischen Mantel des Kaapvaal Kratons zwischen 40-105 °C/Ga.

Eine Möglichkeit, die Schließungstemperatur eines Isotopensystems für ein Mineralpaar ohne Annahmen über die Diffusivität oder geometrische Faktoren zu bestimmen, besteht darin, ähnliche Gesteinstypen aus einer einheitlichen geologischen Umgebung zu nutzen, die sich nur im Temperaturgefälle unterscheidet. Eine solche Umgebung ist der subkratonische Erdmantel, in dem die Temperaturen je nach Tiefe unterhalb oder oberhalb der Schließungstemperatur liegen. Die Tieftemperaturproben bewahren ihren isotopischen Gradienten zwischen den Mineralen und ergeben Abkühlalter, während die Hochtemperaturproben in einem kontinuierlichen isotopischen Austausch zwischen den Mineralen stehen und identische Alter (Eruptionsalter) ergeben. Deshalb sollte es mit Proben aus einem langsam abkühlenden Erdmantel möglich sein, die Schließungstemperatur eines Isotopensystems mit Hilfe von Zweipunktisochronen zu bestimmen. Zweipunktisochronen verschiedener Isotopensysteme sollten verschiedene Alter entsprechend ihrer Schließungstemperatur

ergeben. Unterhalb der Schließungstemperatur sollte sich eine Anreicherung von ansteigendem Alter (Abkühlalter) mit abnehmender Temperatur bilden; oberhalb der Schließungstemperatur sollten die Zweipunktalter konstant und mit dem Eruptionsalter identisch sein. Der Schnittpunkt dieser beiden Äste sollte die Schließungstemperatur ergeben. Es sollte auch möglich sein, aus der Differenz der Schließungstemperaturen von zwei Isotopensystemen und aus der Temperaturabhängigkeit der Abkühlalter die Abkühlraten des Erdmantels zu bestimmen.

In den Figuren 17 a,b sind die Alter der Zweipunktisochronen gegen die Kristallisationstemperatur für die Lu-Hf und Sm-Nd Isotopensysteme für unsere Daten und Daten aus der Literatur aufgetragen. Es existieren ein Tieftemperaturast aus ansteigendem Alter mit abnehmender Temperatur und eine Linie mit einem konstanten Alter, dem Eruptionsalter der Kimberlite. Der Schnittpunkt ergibt die Schließungstemperaturen, die für das Lu-Hf System etwa 920°C und das Sm-Nd System 840°C ergeben.

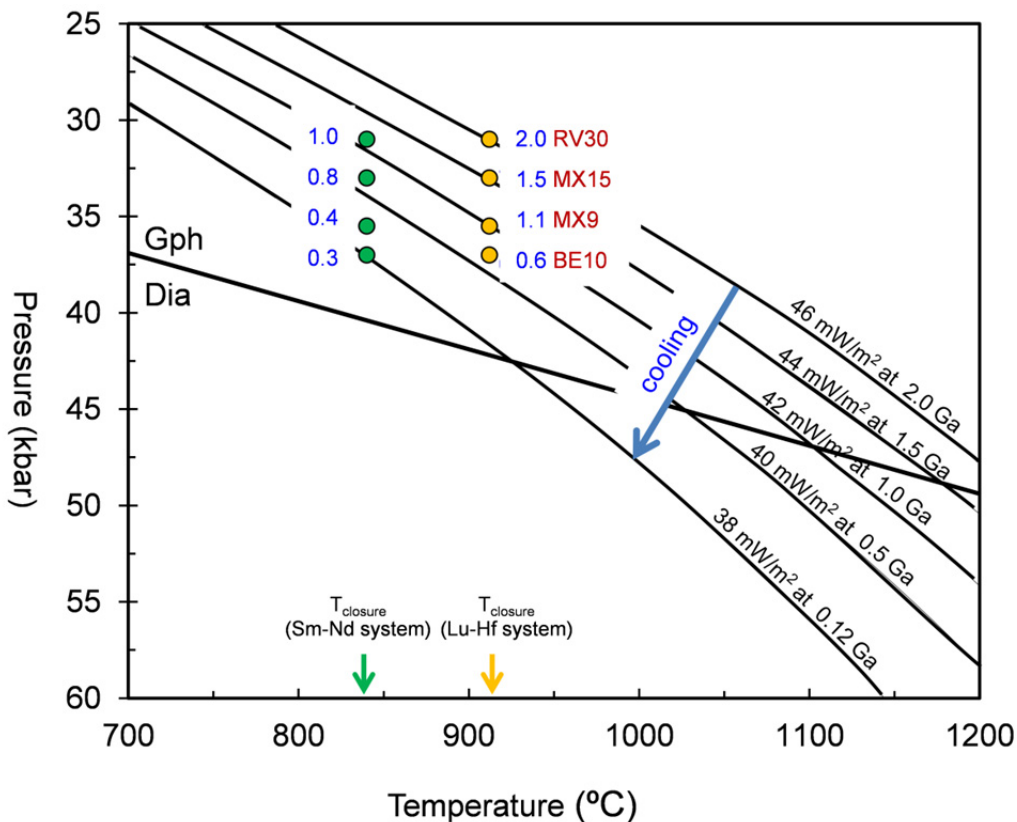


Fig.18: Die Abkühlung des subkratonischen Erdmantels seit dem Proterozoikum. Die Abkühlung entspricht einer Abnahme des geothermischen Gradienten von 46 mW/m² vor 2 Ga auf 38 mW/m² vor 120 Ma und einer Abkühlrate zwischen 80 to 110 °C/Ga.

Der Unterschied der Abkühlalter jeder Probe in den beiden Isotopensystemen kann benutzt werden, um Abkühlraten des subkratonischen Erdmantels vom Proterozoikum bis heute zu bestimmen. Es wird zunächst angenommen, dass die archaische Kruste und ihr Erdmantel seit 2,5 Ga stabil sind und dass die Tiefe, aus der die Eklogite stamen, seit 2,5 Ga dieselbe ist. Betrachtet man nun zum Beispiel die Probe RV30 mit einem Lu-Hf-Abkühlalter von 2 Ga und 0,96 Ga für Sm-Nd und einer

Temperatur von etwa 700°C entlang eines 38 mW/m² geothermischen Gradienten, dann findet man, dass ihre Temperatur 920°C vor 2 Ga (the closure temperature for the Lu-Hf system) war and 840 °C (the closure temperature for Sm-Nd) vor 1 Ga. Das heißt, dass dieser Erdmantelteil innerhalb von einer Milliarde Jahren um etwa 80 °C abgekühlt ist. Dies kann noch auf drei weitere Proben angewandt werden (Fig. 18). Wenn diesen Punkten in Fig. 18 konduktive geothermische von Chapman und Pollack (1977) überlagert werden, so findet man, dass der 2 Ga alte Punkt auf einem 46 mW/m² geothermischen Gradienten liegt, die Punkte mit etwa ~1 Ga nahe an 42 mW/m² and die Probe mit Eruptionsalter für Sm-Nd auf 38 mW/m². Daraus schließen wir, dass der subkratonische Erdmantel seit 2 Ga von einem geothermischen Gradienten entsprechend 46 mW/m² auf 38 mW/m² vor 120 Ma abgekühlt ist. Aus dem Altersunterschied für Lu-Hf and Sm-Nd von jeder Probe und dem Unterschied in der Schließungstemperatur erhalten wir Abkühlraten zwischen 80 und 110 °C/Ga. Dieser Bereich ist konsistent mit Abschätzungen von Michaut et al. (2007) basierend auf Betrachtungen zur Wärmeproduktion durch radiogene Elemente in einem verarmten Mantel und einer archaischen Kruste und dem Wärmeabbau durch Konduktion in einem verarmten Mantel.

Summary

1. Formation and modification of the mantle underneath the Kaapvaal craton from subcalcic garnets

The mantle xenoliths collected by kimberlites indicate that the subcratonic mantle underneath the Archean crust is mostly a residue of high degrees of partial melting which was subsequently re-enriched. The majority of the xenoliths show cryptic metasomatism and only few modal metasomatism.

Much effort has been put into deciphering different kinds of enrichment processes within the mantle. Here, we take the approach to look into the inventory of subcalcic garnets which stem from cpx-free harzburgites and dunites. These subcalcic garnets, commonly with sinusoidal REE patterns, carry the major budget of the trace elements of their host rock. Thus, they are promising objects to study both depletion and enrichment. Most importantly, the analysis of a single grain subcalcic garnet will provide almost all important information of the bulk rock. Our aim is to gain detailed information mainly on metasomatism on a craton wide scale by combining major, trace elements and Lu-Hf and Sm-Nd isotopic signatures from subcalcic garnets. Eventually, we will summarize the metasomatic agent(s) and processes and possibly the timing of the enrichment within the lithospheric mantle underneath the Kaapvaal craton.

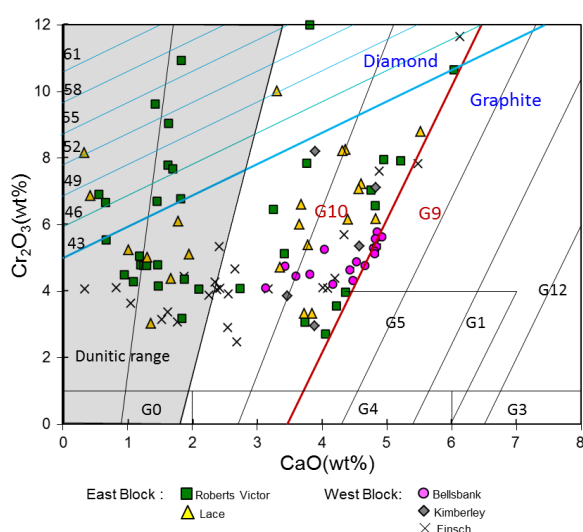


Fig. 1: A plot of Cr_2O_3 vs. CaO with the $\text{CaO}-\text{Cr}_2\text{O}_3$ and $\text{Cr}/(\text{Cr}+\text{Al})$ contours from Gruetter et al. (2004) of subcalcic garnets from 5 localities on the Kaapvaal craton (see legend). Data from Finsch are from Lazarov et al. (2009).

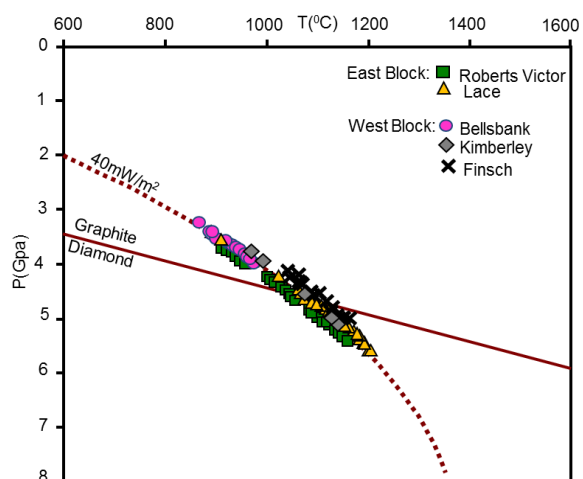


Fig.2 Averages of the Ni-in-garnet temperatures of Canil (1999) and Griffin et al. (1989) projected onto a 40 mW/m^2 geothermal gradient to estimate the depth of derivation of the subcalcic garnets.

1.1 Results

About 700 purple to violet garnets were collected from the heavy mineral concentrate dumps of 4 different localities (Bellsbank and Kimberley mines on the west block and Lace and Roberts Victor mines on the East block) of the Kaapvaal craton, South Africa. About 500 of them were analyzed by electron microprobe. Seventy nine of them plot into the harzburgitic garnet field in a Cr_2O_3 vs. CaO diagram (Fig.1). The application of the Ni-in-garnet thermometer (average of Griffin and Canil) and the projection onto a 40 mW/m^2 geothermal gradient (Fig. 2) yields pressures for Bellsbank garnets of 3.2-4.0 Gpa and a range from 3.5-5.6 Gpa for Lace, Kimberley and Roberts Victor.

They were further analyzed by LA ICP MS for their trace elements and a selection was used for Lu-Hf and Sm-Nd isotope analysis. On the basis of trace element abundances and patterns, the garnets were divided into two to three groups with the degree of reenrichment increasing from 1 to 3. As an example, the REE and trace element patterns from Roberts Victor are shown in Fig. 3.

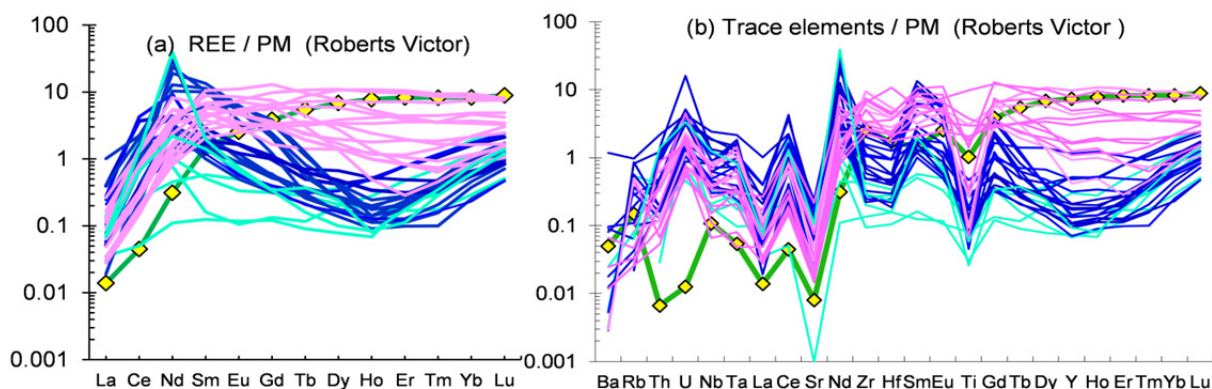


Fig.3: Primitive mantle (McDonough and Sun, 1995) normalized REE and spider diagram of the subcalcic garnets from Roberts Victor: Three types are distinguished, the least enriched group RV1 (light blue patterns), the intermediately enriched group RV2 (dark blue patterns) and the most enriched group RV3 (pink patterns). The green pattern with yellow diamonds is the trace element composition of a garnet from a primitive garnet peridotite 313-105 from Vitim in Siberia(Ionov et al. 2004). It will also be shown in all further similar diagrams.

The Sm-Nd and Lu-Hf isotope compositions of the subcalcic garnets from the West block (Bellsbank, Kimberley and Finsch) are shown in Fig. 4a as present day ϵHf values plotted against ϵNd and in Fig. 4d for those from the East block (Roberts Victor and Lace). The garnet groups with pronounced sinusoidal REE patterns (less enriched) from Finsch (F1), from Bellsbank (B1), groups RV1 and RV2 from Roberts Victor and L1 from Lace almost exclusively plot in quadrant I of these figures. They give extreme radiogenic ϵHf values ranging from +16 to almost + 1000, but give very unradiogenic ϵNd values down to -40. This shows that the Sm-Nd and Lu-Hf systems were decoupled for a long time. The more enriched groups F2 from Finsch and B2 from Bellsbank (less pronounced to no sigmoidal REE patterns), the Kimberley garnets and groups RV3 from Roberts Victor and L2 and L3 from Lace plot in all four quadrants and closer to the present day oceanic array, but partly with extreme deviations to either side.

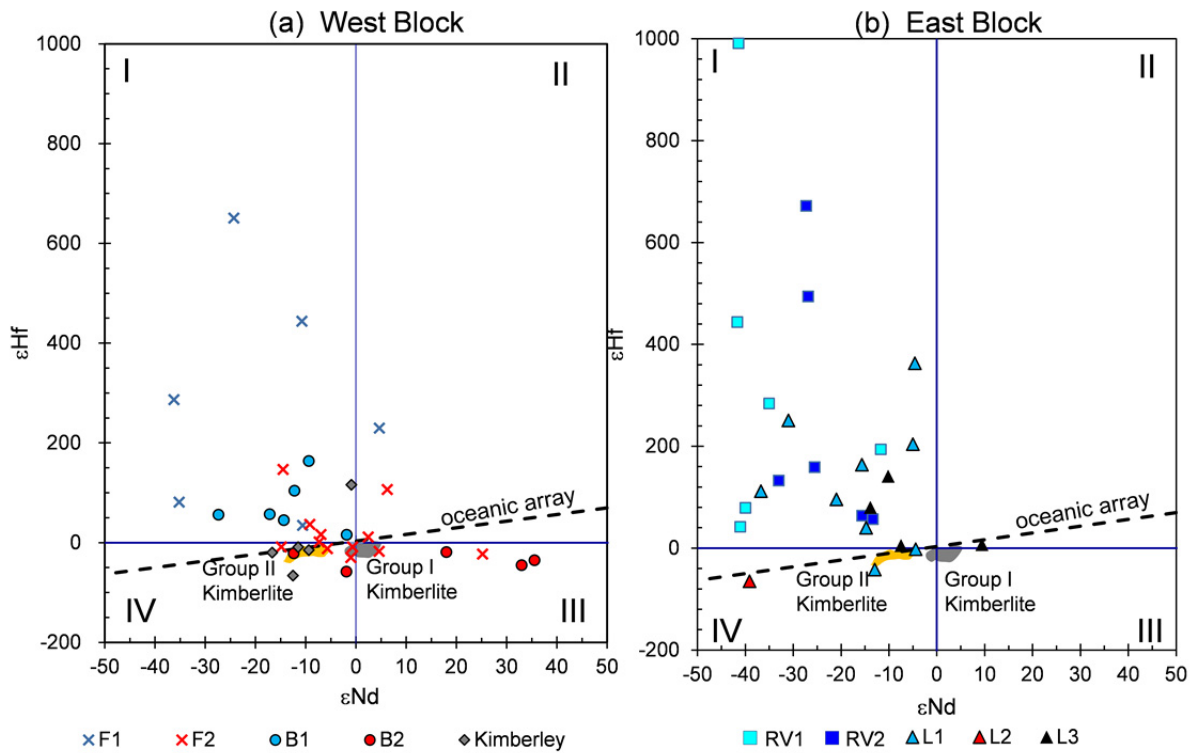


Fig.4: Present day ϵ_{Nd} vs. ϵ_{Hf} diagram of subcalcic garnets from the West Block (Bellsbank: blue circles = B1; red circles = B2; Kimberley = grey diamond; Finsch: blue crosses = F1; red crosses = F2; Figure a), and from the East Block (Lace: blue triangles = L1; red triangle = L2; black triangles = L3; Roberts Victor: light blue diamonds = RV1 and dark blue diamonds = RV2 in Figure b). The present day oceanic array is shown by the black dashed line which is defined as $\epsilon_{\text{Hf}} = 1.33 \times \epsilon_{\text{Nd}} + 3.19$ (Vervoort et al., 1999). The group I kimberlite fields (grey shaded) and group II kimberlite field (yellow shaded) are also shown for comparison.

A widely used diagram to visualize the depleted and enriched character of peridotitic mantle samples is in a diagram of Y versus Zr in garnet with fields which Griffin et al. (1992) designated to depleted and undepleted mantle and fields for metasomatic agents. Our groups 1 to 3 divided on the basis of their trace element contents and patterns correspond in their character to these various fields. These Y-Zr petrogenetic fields provide quite a powerful tool to identify the agents that caused severe enrichment in HFSE and more compatible elements, like Y and the HREE. But they cannot make the fine distinctions for less enriched samples. These are expressed in the more incompatible elements.

For this purpose we calculated the trace element composition of the potential melt or fluid which had been in equilibrium with garnet from each sample. We distinguished between a silicate melt as metasomatizing agent by using the trace element partition coefficients from the experimental work of Green et al. (2000) between basaltic melts and garnet and a silico-carbonatitic agent by using the partition coefficients between mantle minerals and silico-carbonatitic melts of Girniss et al. (2012; revised version submitted to Lithos). The results of the calculations exclude a silicate agent but strongly favour carbonatitic melts (see Fig. 5 as an example for the Roberts Victor samples. The calculated trace element patterns compare very favourably with those measured for “fluid inclusions” in fibrous diamonds.

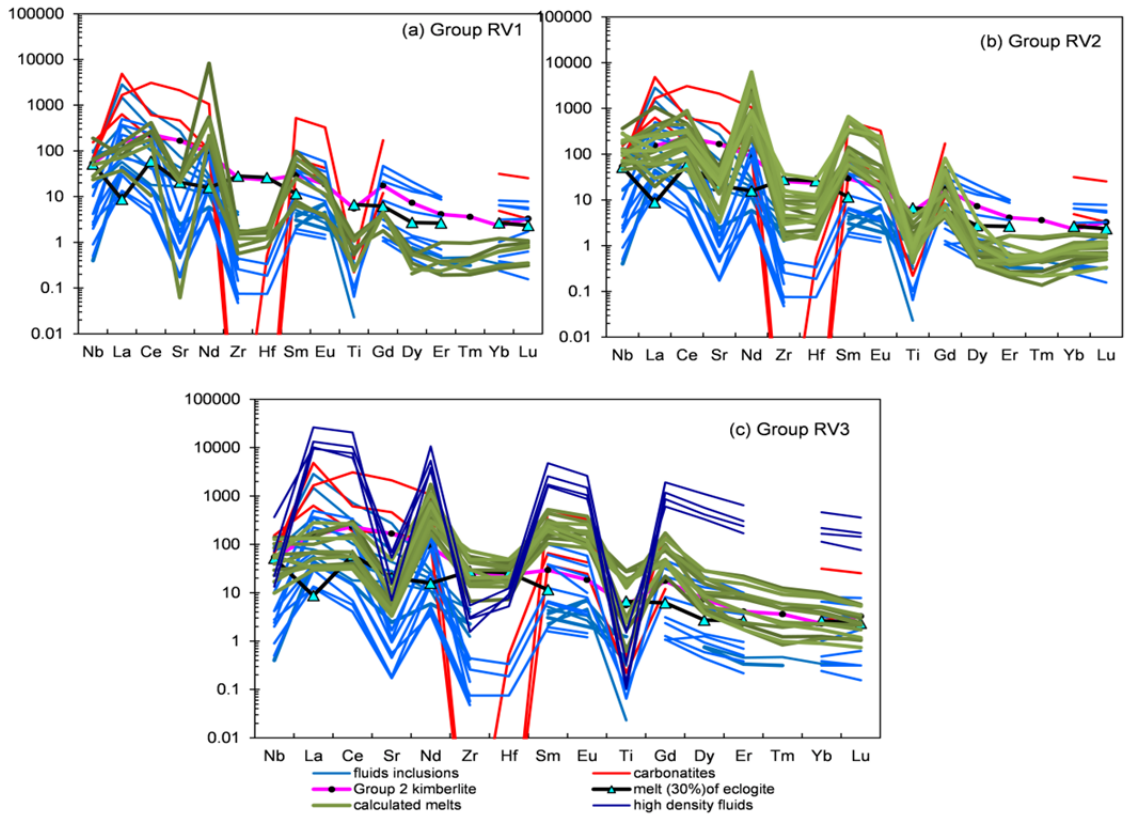


Fig.5: Calculated rare element compositions and patterns of silico-carbonatitic melts (green patterns) as potential metasomatizing agents in subcalcic garnets in separate diagrams for **a)** group RV1, **b)** group RV2 and **c)** group RV3 garnets. The partition coefficients were taken from the work of Grinis et al. (2012; revised version submitted to Lithos). The trace element compositions of group II kimberlites were taken from Nowell and Pearson (2004), of natural carbonatites from Uganda from Nelson, (1988), of fluid inclusions (carbonate-K-chloride-H₂O) in fibrous diamonds from Tomlinson et al. (2009) and of carbonatitic to kimberlitic melts in fibrous diamonds of Klein-BenDavid et al. (2010). The trace elements of 30% experimental melting of eclogites were taken from Rapp et al. (1999).

An impressive argument for the dominating role of carbonatitic agents comes from the Ti/Eu vs. Zr/Hf covariation in the subcalcic garnets (Fig.6). The very low Ti/Eu and very high and superchondritic Zr/Hf ratios in most garnets lead to this inevitable conclusion. Garnets in equilibrium with carbonatitic melt fractionate Zr from Hf and Ti from Eu as shown by experimental work (Sweeney et al. 1992; Grinis et al. 2012). More than 90% of our samples (93 out of 103 garnets) have Ti/Eu ratios lower than 2500 and have elevated and superchondritic Zr/Hf ratios (mostly from 40 to 110).

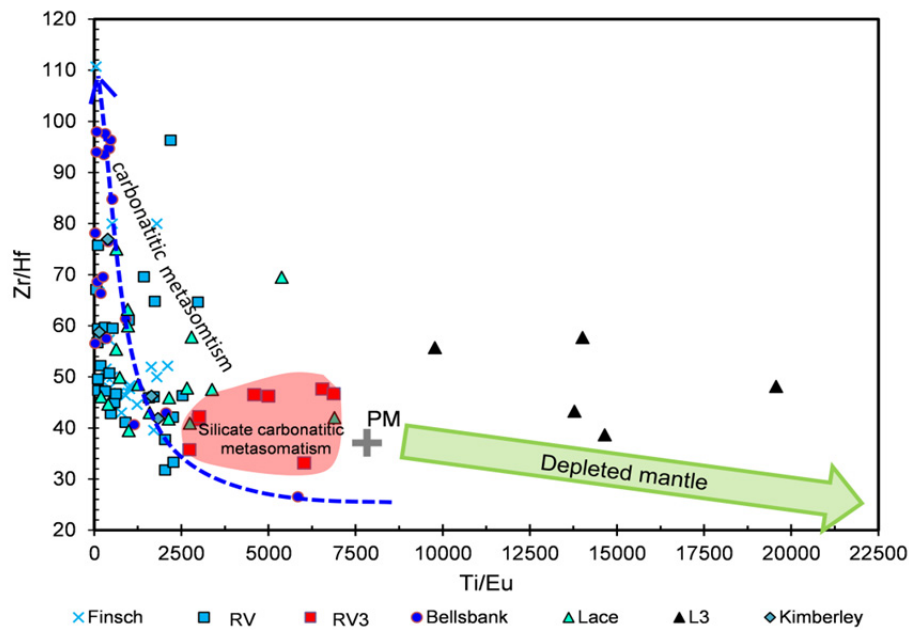


Fig.6: Zr/Hf vs. Ti/Eu diagram: Three garnet populations can be distinguished: The garnets with blueish symbols interacted with a carbonatitic melt which resulted in low and subchondritic Ti/Eu ratios and high and superchondritic Zr/Hf ratios. The red shaded area comprises samples which were affected by more silicic melts. The green arrow indicates the depletion trend for residual garnets. The garnets with superchondritic Ti/Eu ratios shown by black triangles are possibly subcalcic megacrysts.

1.2 Partial melting regimes from trace element systematics

A number of elements which are compatible in garnets like Cr and the HREE are useful to infer melting regimes of the protoliths (Klein-Ben David and Pearson, 2009). The prerequisite is that they are not or were only negligibly modified by metasomatism subsequent to partial melting.

Two models (with modifications) exist for the origin of residual subcratonic mantle:

a) The plume model, where partial melting occurred at high pressures in the garnet stability field in an uprising plume. Garnet and opx generally are residual phases but garnet may be lost at extremely high degrees of partial melting. The HREE are compatible in garnet, are retained in the residue and remain high as long as garnet is present. Only when garnet is exhausted at very high degrees of partial melting, the HREE contents will also decrease.

b) an upwelling mantle model, where partial melting occurred at shallow depths in the spinel stability field beyond the exhaustion of cpx in a setting similar to mid ocean ridges. This is followed by subduction which generates rich garnets by exsolution from opx. Because all REE are incompatible they decrease in the residue from the onset of low-pressure melting i.e. all REE will be depleted in the residue.

The Cr/Al partition coefficients between minerals and melt are high at low pressures and around 1 at high pressures (e.g. Stachel et al. 1998) so that high Cr-garnets, as they commonly occur amongst the subcalcic garnets, can only grow from peridotite residues which were generated at low

pressures. The positively sloped HREE patterns of the sinusoidal garnets also reflect the original signature of partial melting in a garnet-absent melting regime.

The major proportion of the garnet peridotites from the Kaapvaal craton must therefore be subducted residues of partial melting at low pressures, but a smaller proportion also bears the signs of high pressure melting. Melting may occur successively, first at low pressures and a second time at high pressures after subduction.

1.3 Sm-Nd and Lu-Hf isotope systems – dating enrichment and partial melting

Errorchrons from the Sm-Nd system

Incompatible trace elements indicate a two to many fold metasomatic overprint of most samples by different agents. The imprint on the garnets varies with the nature and the amount of the metasomatizing agent and the modal abundance of garnet in the rock (garnets of lower modal abundances are more affected by the same amount of metasomatizing agent). Sm and Nd will always be affected by each metasomatic event. Probably because of such multiplicities, no significant correlation could be found which would correspond to an isochron. However, the slope of six RV2 garnets, two RV1 samples and six of the Lace garnets is roughly parallel to a 900 Ma reference line (not shown). The other samples from both localities also plot parallel to a 900 Ma reference line but at lower $^{143}\text{Nd}/^{144}\text{Nd}$ ratios. Such an age corresponds to the last stages of the Namaqua-Natal orogeny (0.9 to 1.3 Ga) which subducted material underneath the craton. It may have caused the last widespread metasomatism in this area of the subcratonic mantle before the Mesozoic kimberlite activity. The extremely low Nd isotope ratios (down to $\epsilon\text{Nd} = -40$) of the lowest Sm/Nd samples show that the enriching agents stem from a reactivated reservoir with long time low Sm/Nd ratios such as old crust.

Isochrons from the Lu-Hf system

By using single grain subcalcic garnets as proxies of the bulk rock composition and by the combined evaluation of their major, trace element and isotope compositions we have been able to select those samples which still contain unequivocal evidence of the formation of their protoliths and the timing of depletion and re-enrichment. We were able to retrieve several isochrons from three kimberlite localities from the Kaapvaal craton, namely from Finsch on the western border of the W-block with the 1.85 to 2.0 Ga Kheis-Magondi belt, from Roberts Victor at the western edge of the E-block and at the border to the W-block and from Lace, roughly in the middle of the E-block.

Finsch: The previous work on subcalcic garnets from Finsch by Lazarov et al. (2009) had concluded that these are products of two melting episodes, the first with high to very high degrees of partial melting at around 3.6 Ga (model age of one subcalcic garnet) and the second, final depletion at 2.62 Ga and enrichment in between. We modify this interpretation somewhat by considering the latter age as dating the re-enrichment of an ultra depleted mantle with $\epsilon\text{Hf} = +25$ by a carbonatitic melt which simultaneously may have triggered some small degrees of partial melting. Depleted upper mantle is assumed to have $\epsilon\text{Hf} = +8$ at 2.62 Ga. The unusual, very high ϵHf for our samples shows high

depletion prior to 2.62 Ga but the timing of partial melting cannot strictly be fixed. If we take the oldest 3.2 Ga T_{RD} age from the west block as the time of the first melting event, we estimate that 25% non-modal fractional melting in the spinel stability field gives a Lu/Hf ratio of 0.7 which would yield the high ϵ_{Hf} of +25 at 2.62 Ga, i.e. within 600 Ma. The time span would be only 50 to 100 Ma, if melting occurred in the garnet stability field because of the high Lu/Hf ratio in the residue. Our scrutiny of the published Finsch data revealed a further isochron with an age of 1.907 ± 0.19 Ga hidden in the F2 (Hf-enriched) garnet data set (Fig. 7c). This age coincides with the age range reported from the 1.85 - 2.0 Ga old Kheis-Magondi belt immediately to the west of Finsch which was formed by compression and eastward thrusting (e.g. Jacobs et al., 2008).

Roberts Victor and Lace: Two isochrons could be distinguished amongst the subcalcic garnets from Roberts Viktor (Fig. 7a): first a 2.95 ± 0.06 Ga isochron with $\epsilon_{Hf} = 2.7 \pm 1.4$ and second a 3.27 ± 0.15 Ga isochron with $\epsilon_{Hf} = 17.6 \pm 3.6$. The age of 2.95 Ga is interpreted as dating the partial melting of a close to primitive mantle at shallow pressures in an upwelling mantle setting.

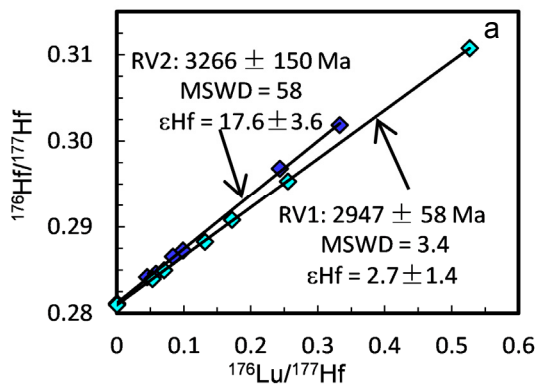


Fig. 7a: Isochrons from subcalcic garnets from Roberts Victor: group RV1 (light blue line) give 2.947 Ga; group RV2 (dark blue line) give 3.266 Ga.

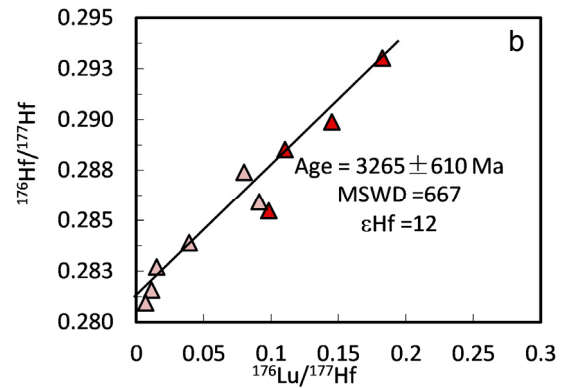


Fig. 7b: Diagram of the lace samples define an errorchron of 3.265 ± 0.61 Ga with $\epsilon_{Hf} = +12$ coincident with the 3.3 Ga isochron from Roberts Victor. Red triangles are group L1 garnets and purple triangles are L2 garnets.

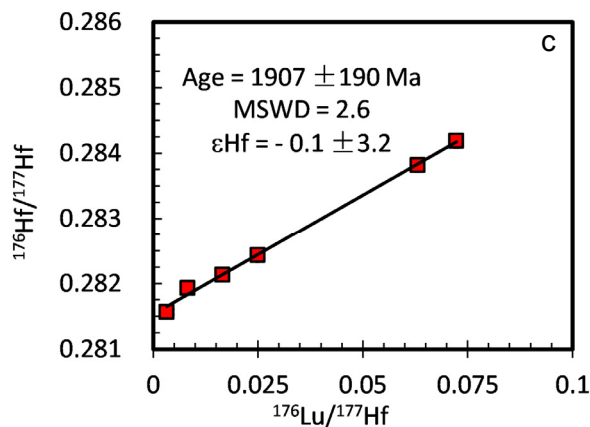


Fig. 7c: A Lu/Hf isochron from six Finsch garnets which all give a model age of 1.9 Ga and consequently an isochron age of 1.9 Ga as the date of an enrichment process.

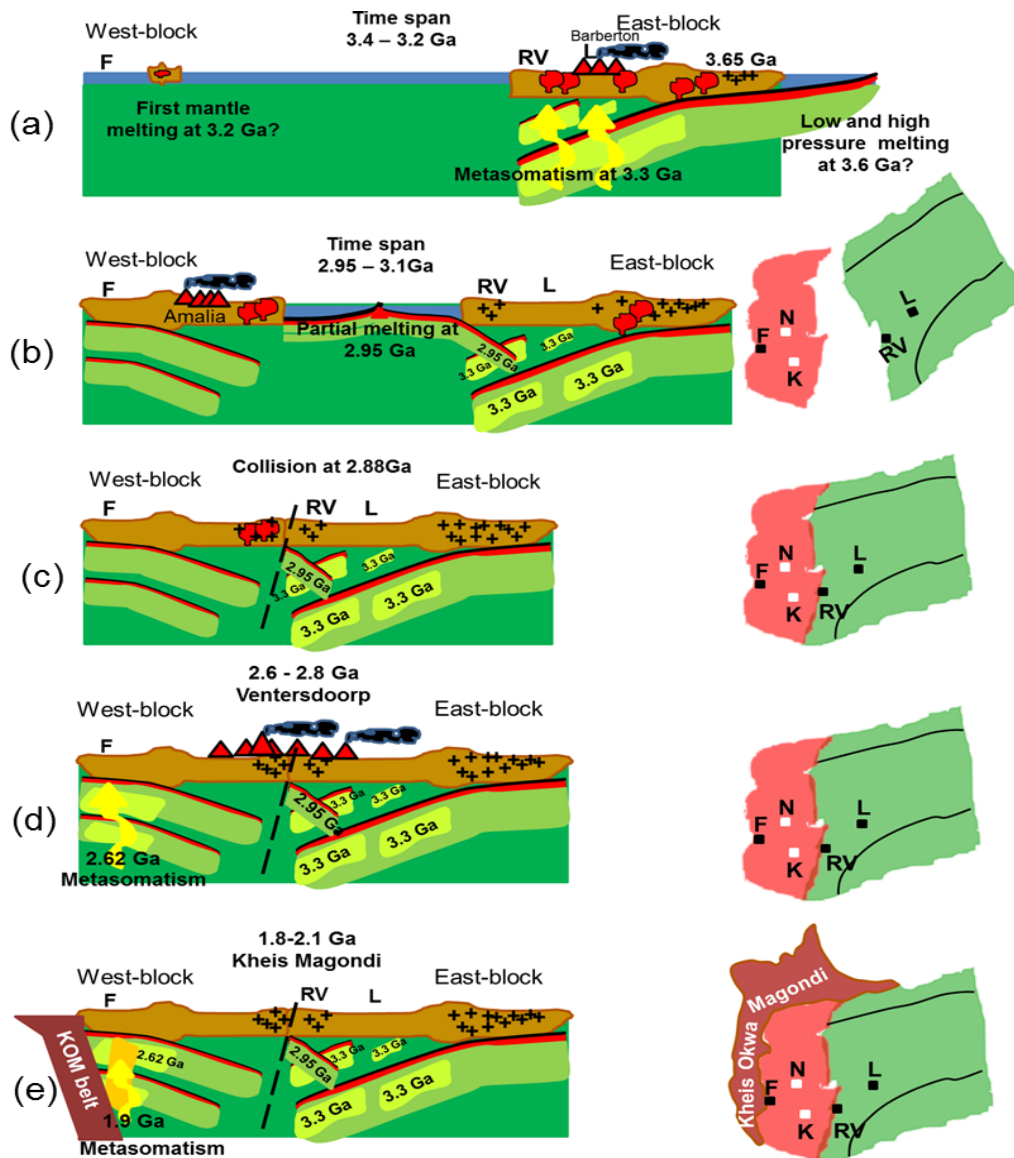


Fig. 8: Proposed model for the formation and evolution of the lithospheric mantle beneath the Kaapvaal craton. Mantle melting and crust formation is taken as being caused mainly by passive upwelling and subduction related processes. **a)** The period between 3.2 and 3.4 Ga: The major part of the continental crust of the E-block already existed. The crust rested on a highly depleted mantle which was metasomatized 3.3 Ga ago (Lu-Hf age from subcalcic garnets from the Roberts Victor and Lace mines). The existence and size of the W-block is enigmatic until 3.2 Ga, from when the oldest mantle T_{RD} ages from Newlands and crustal zircon ages are reported. **b)** During the time span between 3.1 and 2.95 Ga igneous activity increased on the W-block with TTG's and the emplacement of greenstone belts. Oceanic crust and depleted mantle was created in between the two blocks in a passively upwelling mantle setting at 2.95 Ga (partial melting age from Roberts Victor subcalcic garnets) and subducted underneath the E-block. **c)** At around 2.9 Ga, the two blocks collided along the Colesberg lineament. **d)** Between 2.6 and 2.8 Ga, the voluminous Ventersdoorp volcanics poured out over a major part of the then unified Kaapvaal craton. The 2.62 Ga enrichment event at Finsch falls within this period and may record pervasive metasomatism in connection with the Ventersdoorp magmatism. **e)** During 1.8 to 2.1 Ga, the craton was subjected chiefly to modification from the margins by subduction which caused metasomatism in the SLCM. The 1.9 Ga enrichment age from Finsch garnets lies within the period of the attachment of the Kheis-Magondi belt to the Kaapvaal craton. Abbreviations: (N: Newlands; F: Finsch; K: Kimberley; RV: Roberts Victor; L: lace)

Melting occurred in some kind of mid ocean ridge setting in between the E- and W-block followed by subduction under the E-block (see Fig.8). The RV1 harzburgites represent the subducted, depleted lithosphere and, possibly, the ubiquitous eclogites from Roberts Victor the mafic oceanic crust. Collision of the W- and E-block with westward subduction of the E-block occurred at around 2.9 Ga along the Colesberg lineament (Schmitz et al. 2004).

The 3.27 Ga isochron with its high ϵ_{Hf} of +17.6 is interpreted as the time of enrichment of an already strongly depleted mantle portion. Its protolith were spinel harzburgites which were already subducted into the garnet stability field by the time of enrichment. The age of partial melting in the spinel peridotite field can be placed several hundred million years earlier by a similar reasoning as for Finsch. The ten samples from the Lace mine yield an errorchron of the 3.27 ± 0.6 Ga which overlaps with the enrichment age from Roberts Victor (Fig. 7b). We take it that the same enrichment event around 3.27 Ga (or a simultaneous event) overprinted the same depleted mantle underneath the E-block.

The age information for the mantle underneath the Kaapvaal craton from this study, from the published Re-Os age data and the age data of crustal events is summarized in Fig. 8 in a cartoon of successions of mantle melting, modification and crustal growth. It modifies work from various authors, e.g. that of Schmitz et al. (2004) and Shirey et al. (2004). The description of the successive events is given in the figure caption.

2. The origin and age of eclogites and garnet pyroxenites and the cooling of the mantle

Eclogite, the high-pressure equivalent to basalt or picrite makes up a small but petrologically significant portion of the subcontinental lithospheric mantle. Eclogitic xenoliths from kimberlites show a wide variation in mineralogy, isotopic and chemical composition. The word eclogite is used here in a wide sense and includes eclogites *sensu strictu* (possibly with coesite, kyanite or corundum) and garnet pyroxenites. Two main models are proposed for eclogite petrogenesis: (1) a mantle origin: eclogites are re-equilibrated high-pressure igneous cumulates of (ultra-)mafic melts within the upper mantle and (2) a subduction origin: eclogites are the metamorphic products of subducted oceanic crust. They may have experienced subsequent partial melting and metasomatism. Conclusive age constraints are difficult to obtain from these rocks because of the wide variability in petrological and geochemical character as a result of very different protoliths and differing subsequent history of metamorphism, melting and re-enrichment.

2.1 Results

In order to investigate these problems and questions further we studied 11 eclogite xenoliths from Bellsbank with exceptionally fresh garnets and clinopyroxenes for their major and trace elements

Summary

and their Sm-Nd and Lu-Hf systematics. They belong to groups A and B in the eclogite classification scheme of Coleman et al. (1965; see Fig. 9 a,b). They are derived from a temperature interval between 820 and almost 1200°C (Fig. 9c). On the basis of their trace elements and isotope ratios we had to divide them into groups A' and B2 and groups A and B1 (Fig. 10 a,b).

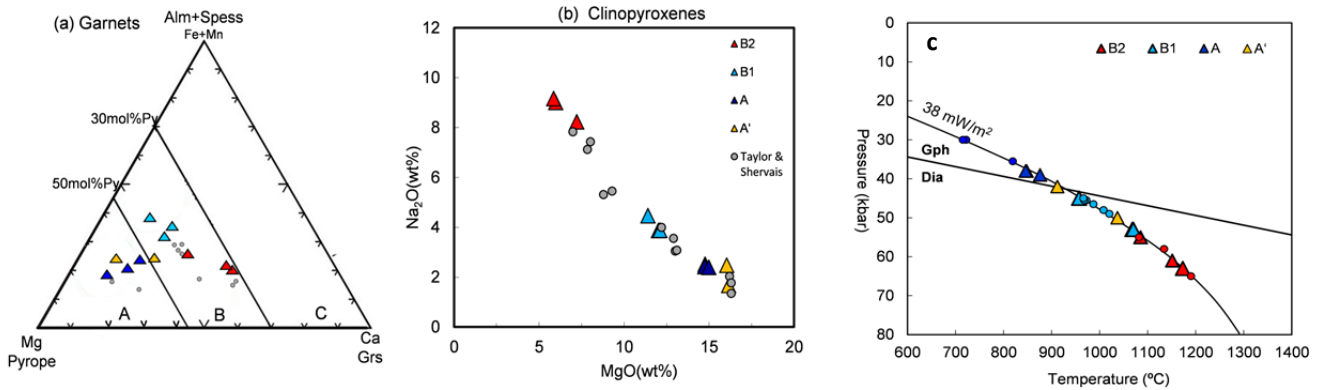


Fig.9a,b: Major element composition of garnets and clinopyroxenes. The small grey dots are data from previous work from Bellsbank (Taylor and Neal, 1989 and Shervais, 1988).

Fig.9c: Temperatures calculated with Krogh (1988) and projected onto a 38 mW/m² conductive geothermal gradient

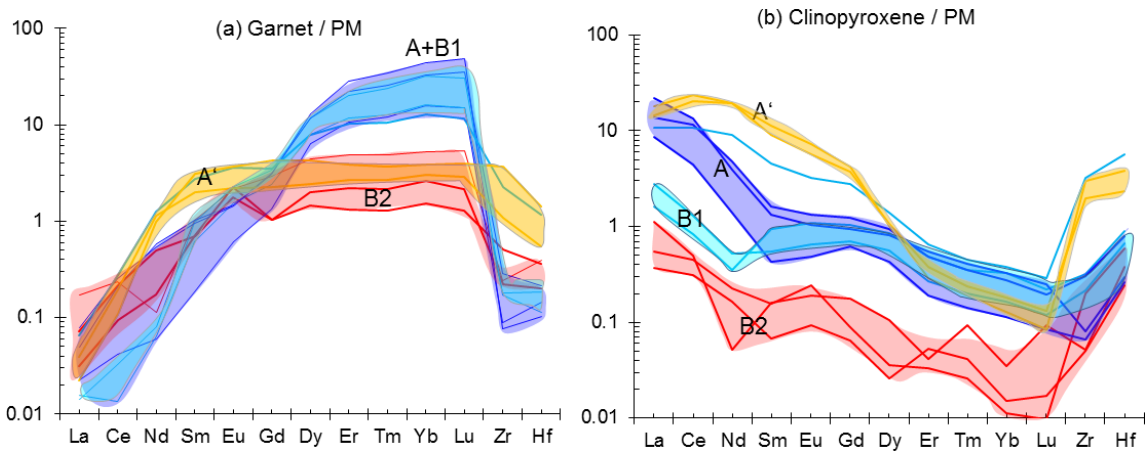


Fig. 10: Primitive mantle (McDonough & Sun 1995.) normalized trace element patterns + Zr and Hf of (a) garnets and (b) clinopyroxenes from Bellsbank eclogites. The coloured bands highlight the range of each of the four types which were distinguished from their petrography and major and trace element abundances. The REE patterns indicate similarities between groups A (dark blue shaded) and B1 (light blue shaded) and groups B2 (red shaded in red) and A' (yellow shaded).

The garnet REE patterns of groups A (dark blue field in Fig. 10a) and B1 (light blue field) are similar with steep positive slopes from light to the heavy REE and with extremely high HREE abundances ((Lu)_{PM} up to 50). Sample BE4 from group B1 is severely enriched in the light to middle REE. In the other samples only La, Ce and possibly also Nd appear very slightly enriched. Group A and B1 clinopyroxenes also have similar trace element patterns. The REE patterns (Fig. 10b) have

Summary

negative slopes from La to Nd or Sm, increase positively from Nd to Gd and again turn negative towards the HREE.

Group A' and B2 garnets also show similarities with flat heavy to middle REE patterns and low REE contents (Fig. 10a). Group B2 garnets have slight to strong positive Eu anomalies (Eu/Eu^* : 1.1 to 2.7). Group B2 clinopyroxenes (red lines) have the lowest REE contents while group A' pyroxenes have the overall highest trace elements.

The Lu-Hf and Sm-Nd isotope ratios show the same division into the four groups but also show the kinship between groups A+B1 and groups A'+B2 (Figs. 11 and 12). The Sr isotope ratios (not shown) vary from $^{87}\text{Sr}/^{86}\text{Sr} \sim 0.704$ to 0.712 without a correlation with the various groups. The $\delta^{18}\text{O}$ ratios (2.5 – 5.3) are all lower than the mantle value except for one sample with very high incompatible trace element contents with $\delta^{18}\text{O} \sim 6.5$.

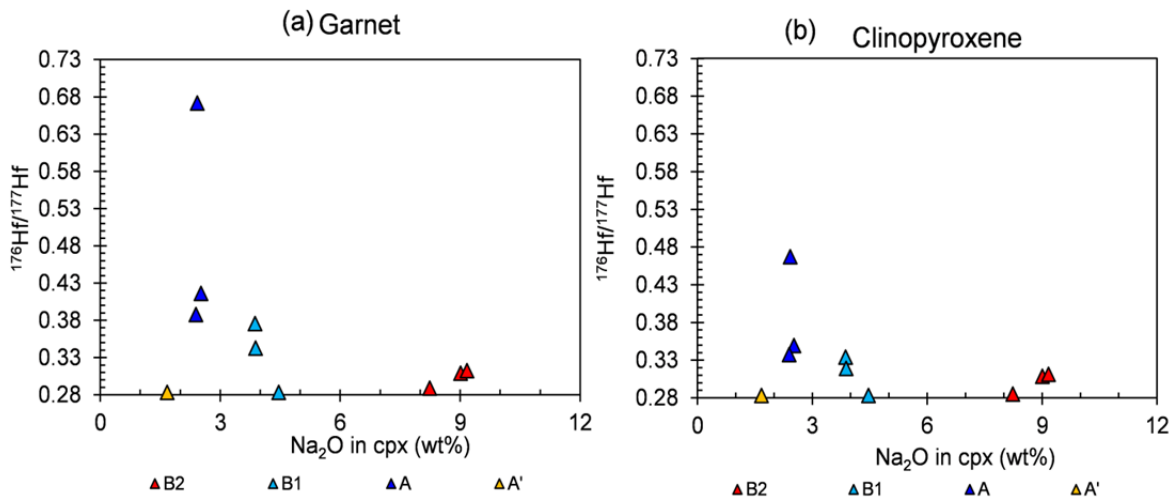


Fig.11 a,b: The measured $^{177}\text{Hf}/^{176}\text{Hf}$ isotope ratios for **a)** garnet and **b)** clinopyroxene plotted against the sodium content in clinopyroxene an indicator of the type of eclogite. Most isotope ratios are extremely high (for comparison: the present day primitive mantle has $^{177}\text{Hf}/^{176}\text{Hf} = 0.282772$ and the depleted MORB mantle has 0.283250). The sequence of the data points from high to low isotope ratios for garnets and clinopyroxenes for each group of eclogites also corresponds to sample numbers i.e. high garnet belongs to high cpx. Coexisting grt-cpx pairs can thus be connected by eye.

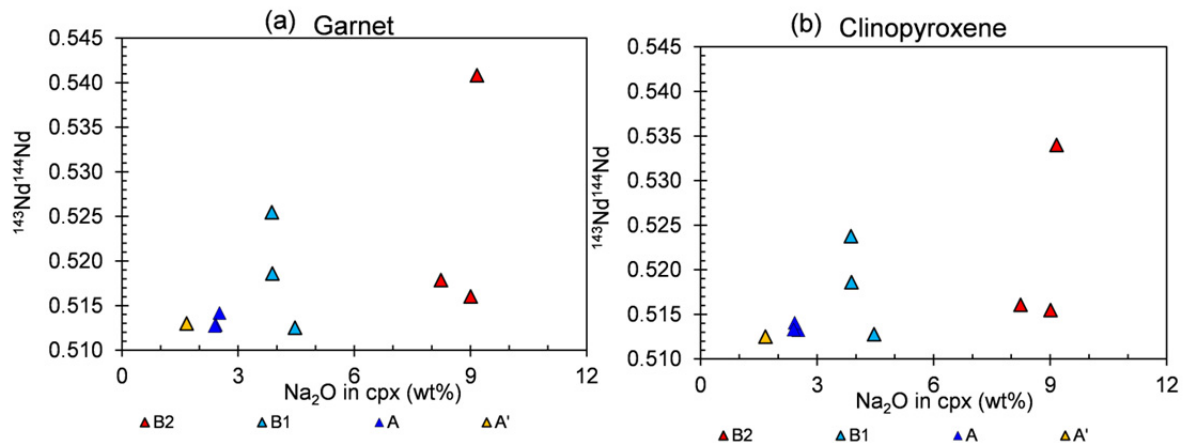


Fig.12 a,b: The measured $^{143}\text{Nd}/^{144}\text{Nd}$ isotope ratios determined for **a)** garnet and **b)** clinopyroxene plotted against the sodium content in clinopyroxene as indicator of the type of eclogite. The isotope ratios partly are extremely high.

The $^{177}\text{Hf}/^{176}\text{Hf}$ resp. the $^{143}\text{Nd}/^{144}\text{Nd}$ ratios are plotted in Figs. 11 a,b and 12 a,b against the sodium content in clinopyroxene as an indicator of the type of eclogite. The isotope ratios are extremely high in the majority of the samples but also fall in the range of the present day mantle. Extreme values are $\epsilon\text{Hf} = +13724$ for a garnet and $\epsilon\text{Hf} = +6552$ for its coexisting clinopyroxene and, in another sample, $\epsilon\text{Nd} = +553$ in garnet and $\epsilon\text{Nd} = +420$ in cpx. Consequently, calculated bulk rock compositions also give a huge range for ϵHf from more than +10000 down to +13 for one group A' sample and for ϵNd from more than +550 to +3. The sequence in ϵHf of the groups is, however, not the same as for ϵNd because the Sm-Nd isotope system is much more prone to metasomatism than the Lu-Hf system i.e. the Hf and Nd isotope ratios are partly decoupled as in the subcalcic garnets.

2.2 The origin and age of the eclogites and garnet pyroxenites

The reconstructed bulk rock major element compositions (not shown) of groups A' + B2 and groups B1 + A overlap with modern gabbroic rocks, but are mostly separated from Archean basalts and Archean boninitic rocks. Contrary, the reconstructed bulk rock trace element compositions of groups A' + B2 fully overlap with modern gabbroic rocks as shown in Fig. 13 b in N-MORB normalized patterns. Especially the middle to heavy REE patterns are flat and show the same compositional range as N-MORB while the more incompatible elements are mostly lower. A positive Eu anomaly in group B2, the low middle to heavy REE abundances and the very aluminous bulk composition indicate a dominant role of plagioclase in the precursors of these rocks. These must have been low pressure, plagioclase rich cumulates from MORB-like compositions. One B2 sample has only a slight Eu anomaly and may actually represent an almost unmodified melt composition which had originally crystallized to a gabbro. Group A' eclogites have more elevated middle to heavy REE compared to the two group B2 samples with a Eu anomaly but lower compared to the one with almost no anomaly. They are also much lower in Na_2O and have higher Mg-values. They may be clinopyroxene rich cumulates from the magma as the plagioclase cumulates of group B2.

The groups A + B1 REE patterns (Fig. 13 a) are extremely fractionated in the REE with very high contents of HREE and a strong decrease in abundances towards the LREE (but an increase again of the LREE beginning from Sm or Nd). A central role of garnet in the genesis of these eclogites is suggested by the REE patterns. A high pressure origin as garnet rich cumulates from a melt could be feasible but oxygen isotope ratios below the mantle values a priori preclude such a model. Another possibility is that the rocks are residues of partial melting in which garnet plays the dominant role. Candidates for eclogite facies metamorphosed protoliths are Archean basaltic or boninitic precursors. The partial melting of eclogite facies, MORB-like Archean basalts with flat middle to heavy REE patterns would require more than 80 % partial melting to match the extremely fractionated REE patterns of group A garnet pyroxenites as residues. Archean boninites, a second stage melting product of a depleted mantle, already have fractionated REE patterns which will reduce the degrees of partial melting necessary to match A and B1 samples as residues. Model calculations with two Archean boninites with different REE abundances show that the range in composition of the A and B1 eclogites can be explained by 20 to 60 % partial melting of boninitic precursors. The low oxygen isotope ratios of the eclogites (also groups A'+B2) would be inherited from the precursors from low temperature alteration in an ocean floor. This is possibly also the case for the high and variable Sr isotope ratios.

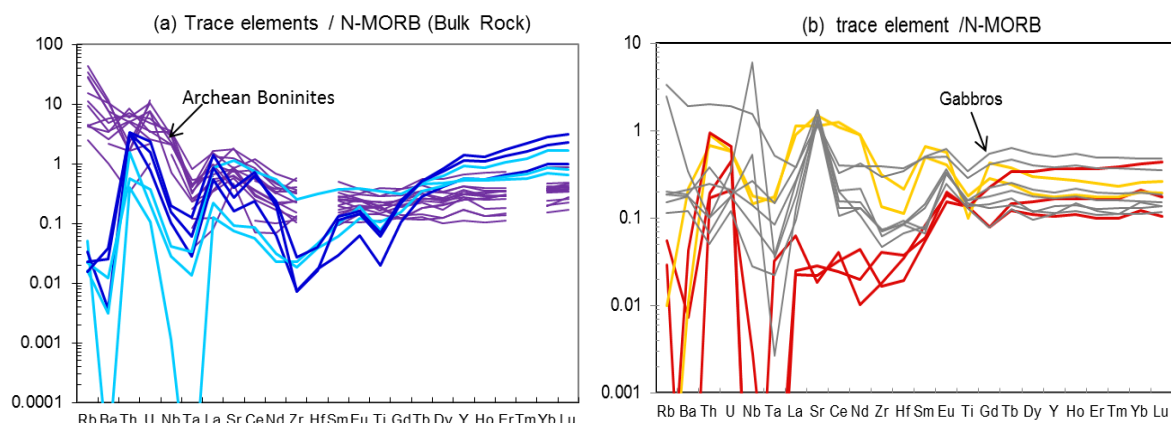


Fig 13: The trace element patterns of reconstructed bulk rocks. The diagram (a) shows the trace element patterns of group A (dark blue lines) and B1 (light blue lines) and the trace element of Archean boninites (Smithies, 2002). The diagram (b) shows trace element patterns of group A' (yellow) and B2 (red lines) and modern gabbroic rocks (SE Indian Ridge, Hart et al., 1999; Bach et al. 2001), Normalized to N-MORB of Sun & McDonough (1989).

Age information potentially obtainable from eclogitic rocks from the mantle is the age of their protolith, of eclogitisation (which may be very close to that of the protolith) and possibly also the age(s) of subsequent partial melting and metasomatic events. In theory, protolith ages may be obtained from (reconstructed) bulk rock isochrons or from model ages. Two-point grt-cpx isochrons could give the age of eclogitisation which would be the case, if the eclogite temperatures were always below the closure temperature of the isotope system under consideration. Closure temperatures will be discussed below.

The eclogitic rocks from the Bellsbank diamond mine show very little to almost no chemical overprint of highly incompatible elements (compare Figs. 11 a,b) so that their original chemistry after

melt extraction (groups A and B1 except for BE4) or from the protoliths (Groups A' and B2) is largely kept. The small degrees of enrichment affected only the LREE and not the middle to heavy REE and Hf. Most of the Nd and partly also Sm will therefore stem from the enriching agents and an enrichment age may be obtained from the Sm-Nd isotope system. We combined our own data with the Sm-Nd data of Neal et al. (1990) and Shervais, et al. (1988) and obtained a 2.08 ± 0.38 Ga errorchron with $\epsilon_{Nd} = +28$ (Fig. 14). We excluded the samples BE11 and BE2 from this correlation because they show practically no Nd enrichment in their trace element patterns. It is interesting to note that the 2.08 Ga age coincides with the age of the Bushveld Complex on the one hand and with the range of ages between 1.8 to 2.1 Ga for the Kheis-Magondi belt.

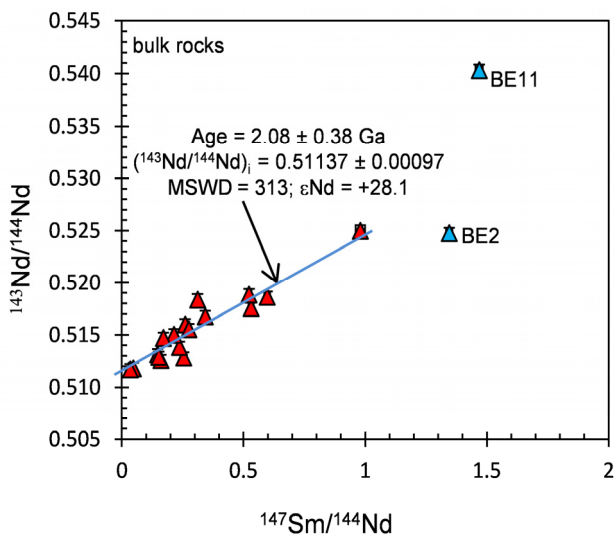


Fig. 14: Sm-Nd isochron diagram for Bellsbank eclogites (own and literature data). The red triangles yield an errorchron age of 2.08 Ga with $\epsilon_{Nd} = +28$.

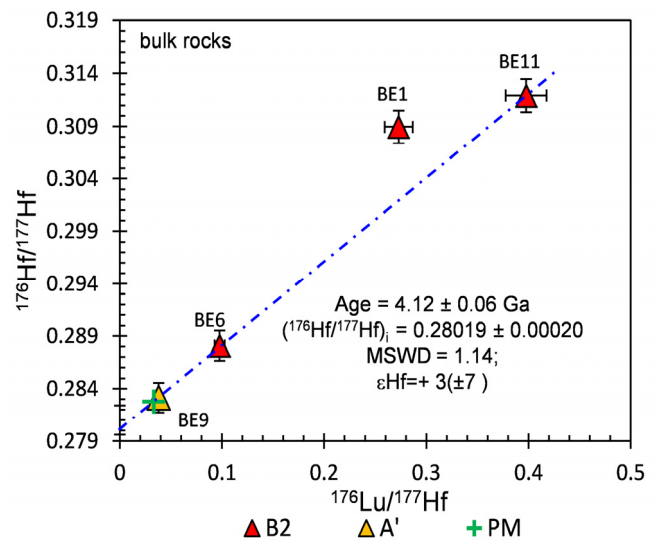


Fig. 15: Lu-Hf isochron diagram for calculated bulk rocks from group A' and B2 eclogites. (PM: present-day primitive mantle value)

A common Sm-Nd isochron through the bulk rock isotopic compositions of all groups is permissible since enrichment occurred after the assembly and stabilization of the Kaapvaal craton. The Lu-Hf system, however, was practically not affected by the enrichment process and may therefore give information of the more original history of the rocks. But then, only cogenetic rock suites are comparable. We have suggested that the protoliths of groups A' and B2 are cogenetic and metamorphosed portions of a subducted oceanic crust. The reconstructed bulk rocks should therefore linearly align in an isochron diagram. It can be seen in Fig. 15 that three samples give an age of 4.12 ± 0.06 Ga with $\epsilon_{Hf} = 3 (\pm 7)$ i.e. the initial is that of the primitive mantle at that time, but sample BE1 lies off the supposed isochron. Such an old age is not directly matched by any crustal ages from the Kaapvaal craton nor by Re-depletion ages from its lithospheric mantle. Only a Re-Os errorchron from Newlands eclogites yields the same age.

Nevertheless, this old age appears quite reliable, because the members of the isochron give an identical model age (which must be the case if the initial of the isochron is that of the primitive mantle). Sample BE11 (group B2) is most convincing that it gives a meaningful and accurate model age: its REE pattern is continuously depleted until Nd with no Hf anomaly (= no Hf addition). Garnet and clinopyroxene have the same ϵ_{Hf} at the time of eruption (120 Ma) of ~ 1005 each and therefore, the bulk rock had the same very radiogenic ϵ_{Hf} at that time. Such high values require a long-time evolution even with the relatively high $^{176}\text{Lu}/^{177}\text{Hf}$ of 0.398. Consequently, the Hf model age is 4.12 ± 0.29 Ga (Fig. 16). The model ages from garnet alone is a minimum ages but is already 3.51 Ga for this sample.

All A' and B2 samples give high model ages for bulk rocks and garnets whereas groups A and B1 give young to very young ages (Figs. 16). The reason lies in the multistage history of these rocks for which the primitive mantle is not a reference line anymore.

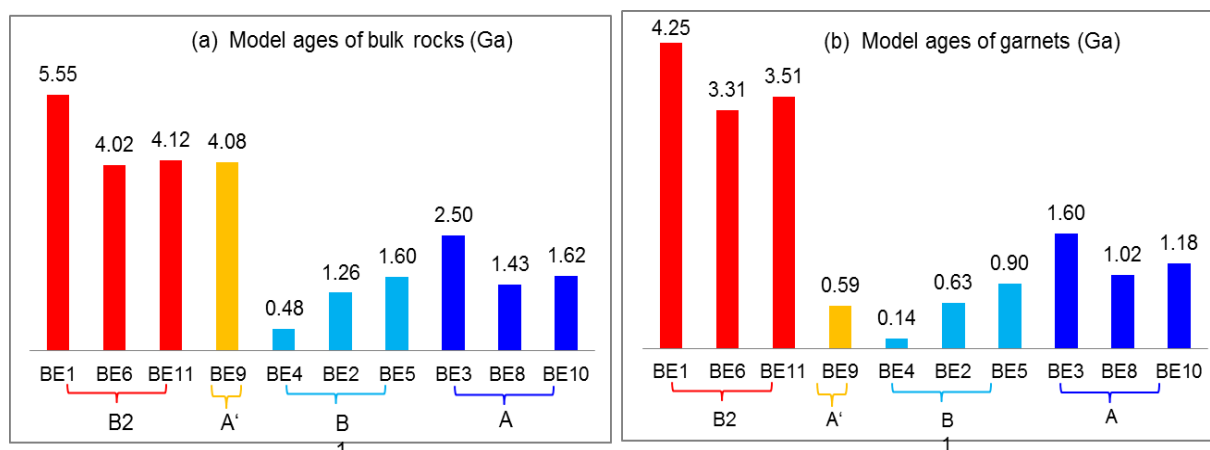


Fig.16: Model ages of bulk rocks (a) and model ages of garnets (b). Different groups present as bar with colors. The ages are noted on the top of the bars (in Ga). Sample names and group names are noted under the bars (group B2: red, group A': yellow, group B1: light blue, group B2: dark blue)

2.3 The meaning of two-point isochrons, Sm-Nd and Lu-Hf closure temperatures and the cooling of the subcratonic mantle

The Earth's mantle is a huge metamorphic complex which undergoes permanent changes ruled by plate tectonics but which also has enclaves underneath Archean crust which are exempt from the convecting mantle since at least 2.5 Ga. This part has evolved towards a steady thermal state since it originated either by plume accretion or subduction. Thermal relaxation after the assembly of the subcratonic mantle has to occur until the final stabilization in the Archean. Since then, the mantle may cool slowly because of the decay of remanent heat aided by denudation. Under such circumstances, two point garnet-clinopyroxene isochrons from mantle xenoliths (peridotites or eclogites) should give either cooling ages or eruption ages depending on whether the mantle portion under consideration was below or above the closure temperature of a radiogenic system. A further kind of "age" is obtained if either of the two mineral phases is preferentially disturbed by a more recent event. The phase to be disturbed is generally cpx with the effect that artificially old ages are obtained.

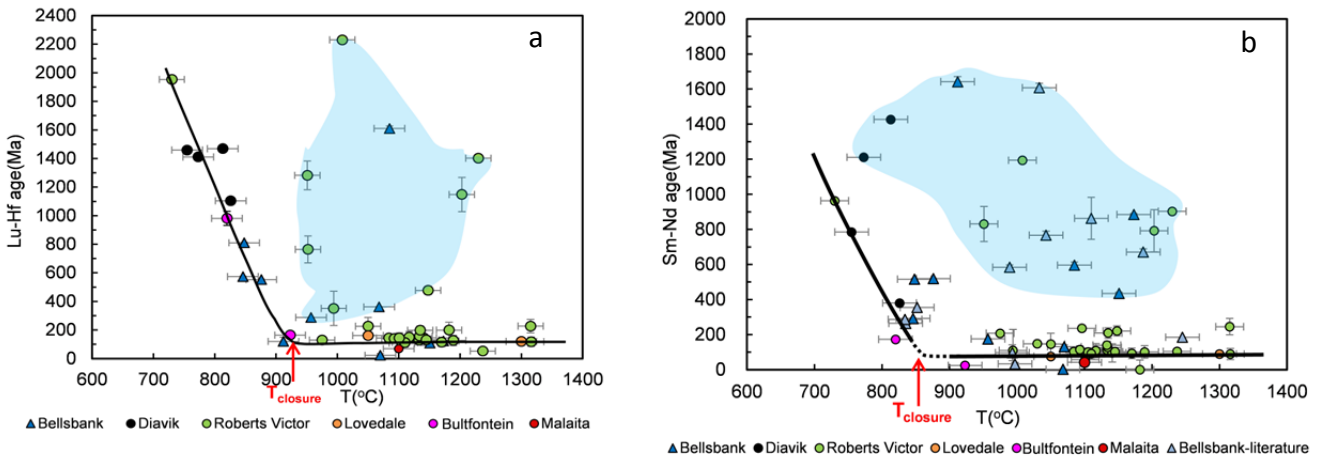


Fig.17 a,b: Correlation of Lu-Hf (a) and Sm-Nd (b) two point isochrone ages and the calculated temperature of our samples and sample from the literature. One population of low-T samples show ages decreasing with increasing temperature until 920 °C followed by a substantial number of samples which give constant ages close to the eruption age at higher temperatures as indicated by the black line. We propose a closure temperature for the Lu-Hf system around 920 °C resp. 840°C at the bend of the black line (indicated by the red arrows). The field shaded in blue comprises high-T samples with old, but meaningless ages which were probably caused by a recent preferred enrichment of clinopyroxene.

Principally, closure temperatures of a system at an assumed cooling rate can be determined from the diffusion properties of the element (or pair) in the constituent minerals and the geometric properties of the minerals (Dodson, 1986 and later work e.g. by Ganguly and Tirone, 1998, 2001). A closure temperature is defined as a member of a temperature interval, where volume diffusion ceases upon cooling. For a mineral pair, it is determined by the mineral with the slower diffusion rate. With assumptions on the size of the geometric factors and of reasonable diffusion coefficients cooling rates for the Kaapvaal lithospheric mantle were determined e.g. by Bedini et al. (2004) between 40-105 °C/Ga.

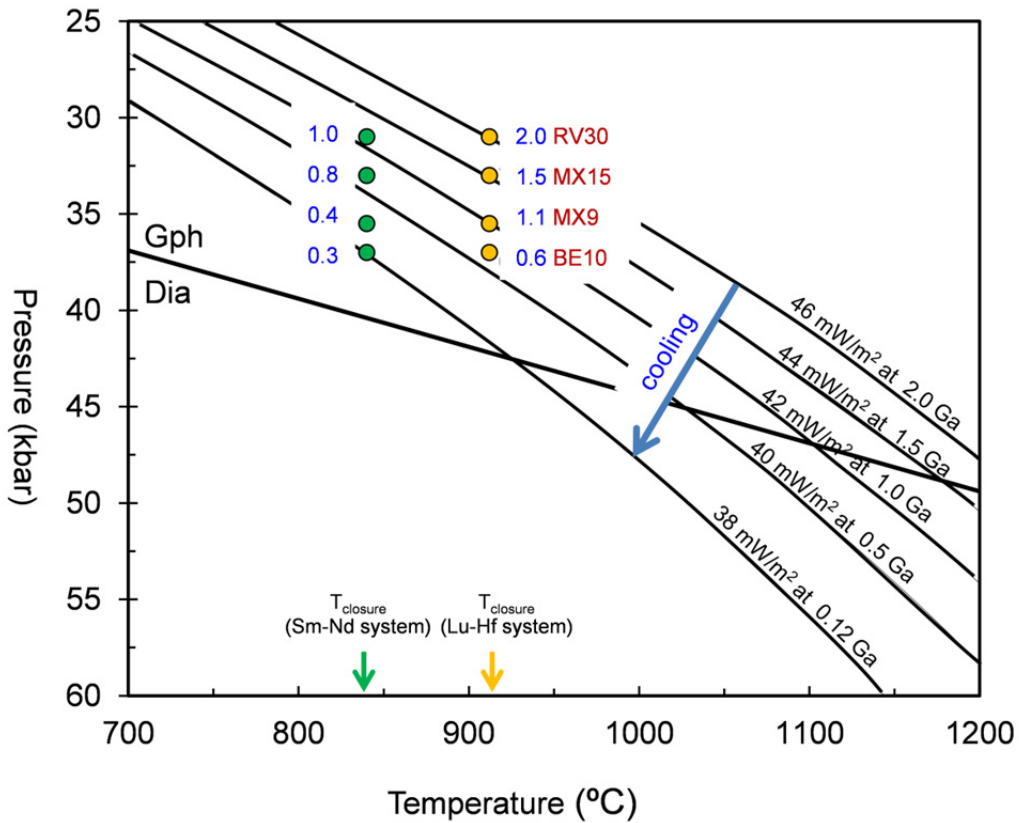


Fig.18: The cooling of the subcratonic mantle since the Proterozoic. The cooling corresponds to a decrease of a geothermal gradient from 46 mW/m² at around 2 Ga to 38 mW/m² at 120 Ma ago and a cooling rate between 75 to 110 °C/Ga). ($T_{closure}$: closure temperature; green arrow indicates the closure temperature of Sm-Nd system at 840°C; yellow arrow: 920°C for Lu-Hf system)

A way to evaluate the closure temperature of an isotopic system for mineral pairs independent of assumptions on diffusivity and geometric factors is to investigate similar rock types from similar geologic setting but from temperatures which cover the range from below and above the closure temperatures. The low temperature samples will develop and keep the isotopic gradient between minerals while the high temperature samples continue to be in isotopic mineral exchange and give identical ages. In a slowly cooling subcratonic mantle it should be possible to obtain an estimate of the closure temperature from grt-cpx two-point ages. Two point isochrons from different isotopic systems should give different ages depending the closure temperatures of the isotopic systems. They should give an alignment of increasing age (cooling ages) with decreasing temperature below the closure temperature and kimberlite eruption age above. The intersect should be the closure temperature. It should also be possible to estimate the cooling rate of the mantle from the difference in the closure temperatures and the temperature dependence of the cooling ages.

Figures 17 a,b are a compilation of our own data and those from the literature, where two-point isochron data are available for the Sm-Nd and Lu-Hf system or both. There is a low temperature alignment for both systems of increasing age with decreasing temperatures, of kimberlite eruption ages at high temperatures and also of unsystematic ages at high temperatures. We interpret the intersect between the low temperature limb and the kimberlite eruption age as closure temperature which gives around 920°C for the Lu-Hf system and 840°C for the Sm-Nd system.

The difference for each sample in the cooling ages of the two isotopic systems can be used to make deductions about the cooling of the subcratonic mantle from the Proterozoic until today. We assume in a first step that Archean cratons and their mantle were a stable assembly since 2.5 Ga and that the depth from which the eclogites were derived by the kimberlites is the same as 2.5 Ga ago. If we take, e.g. sample RV30 with a 2 Ga Lu-Hf and a 0.96 Ga Sm-Nd cooling age and a present day temperature of around 700 °C along a 38 mW/m² geothermal gradient we must deduce that its temperature was 920°C two Ga ago (the closure temperature for the Lu-Hf system) and 840 °C (the closure temperature for Sm-Nd) 1 Ga ago, i.e. that this part of the mantle cooled by 80°C within 1 Ga. We can extend this approach to three further samples along the cooling limbs in Figs. 17 and plot them into Fig. 18. If we then superimpose the conductive geothermal gradients as given by Chapman and Pollack (1977) onto these points, we find that the 2 Ga age point lies on the 46 mW/m² geothermal gradient, the ~1 Ga age points close to 42 mW/m² and that with an eruption age for Sm-Nd on the 38 mW/m². From this, we infer that the subcratonic mantle cooled since 2 Ga from a geothermal gradient corresponding to 46 mW/m² to 38 mW/m² at 120 Ma ago. By using the age differences for Lu-Hf and Sm-Nd of each sample and the difference between the closure temperatures, we derive cooling rates between 80 to 110 °C/Ga. This range is consistent with estimates by Michaut et al. (2007) based on considerations of the heat production by radiogenic elements in a depleted mantle and an Archean crust and the heat decay by conduction in a depleted mantle.

Chapter 1

Introduction

1. Significance of studying xenoliths/xenocrysts from SCLM underneath the Archean cratons

The Archean crust is studied today in more and more detail in the search of an understanding of the early history of the Earth. The subcontinental lithospheric mantle (SCLM) underneath the Archean cratons equally well draws the attention of scientists to study its early history because it stabilizes the overlying crust since at least 2.5 Ga. Numerous geophysical studies of these mantle portions show that deep roots maintain this stability (e.g. Jordan, 1975 as the foremost proponent of very deep roots). Because of its long time isolation from the convecting mantle a variety of chemical and isotopic specialities and diversities could develop (e.g. Kramers, 1983; Menzies and Murthy 1980; Richardson, 1985; Walker, et al., 1989; Carlson et al., 1999; Pearson et al., 1998; Irvine et al., 2001; Simon et al., 2007; Lazarov et al., 2009). These will help to reconstruct early processes (depletion and re-enrichment) and their timing hidden in these witnesses of the Earth's early history.

The source for these information is hidden in the xenoliths, xenocrysts and inclusions in diamonds brought by kimberlites to the Earth's surface. Two main types of fragments are the aim of the investigations - peridotites and eclogites. The peridotites are the primary constituents of the Earth's mantle. Peridotites from the subcontinental root of Archean cratons are especially known for their highly depleted but also severely re-enriched character. They are generally derived from the depth range between 100 to 240 km deep into the diamond stability field. A smaller component of the SCLM derived from the same depth range is eclogites and garnet pyroxenites of roughly basaltic composition. Yet, an understanding of their time and depth of origin and that of their protoliths will be crucial for an understanding of the early geodynamic history of the Earth. Peridotites and eclogites will give information on various parts of the puzzle on how the Earth worked in the early days, and, considered together, may even augment the information from each other. This thesis makes the attempt to achieve this from the combination of the two lithologies.

2. Previous work on peridotites and ways to extract multiple information (age dating and geochemical development) from a single mineral (subcalcic garnets)

The timing of growth and amalgamation of Archean continental nuclei, and the temporal and spatial relationships between processes recorded in the present day subcratonic mantle and its overlying crust are fundamental questions concerning stabilization of long-lived cratonic blocks by buoyant underlying lithospheric mantle (lithospheric keel). A fundamental question is the origin of the residual subcratonic mantle for which two contrasting models (with modifications) exist:

a) The plume model (1) where high degrees of partial melting occurred at high pressures in the garnet stability field in an uprising plume. Olivine, garnet and opx are residual phases and only extreme degrees of partial melting would exhaust garnet as a residual phase.

b) An upwelling mantle model (2), where partial melting occurred at shallow depths in the spinel stability field beyond the exhaustion of cpx in a setting similar to mid ocean ridges. This was followed by subduction to generate the subcratonic mantle.

A number of chemical indicators in the subcratonic peridotites (e.g. very depleted HREE abundances, very Cr-rich garnets) favour the hypothesis that the major part of the subcontinental lithospheric mantle (SCLM) are restites of partial melting at shallow pressures with subsequent subduction. Intimately connected with the solution and distinction of these models is the origin and age of eclogites and garnet pyroxenites which also occur in the SCLM (e.g. Stachel et al., 1998; Lazarov et al., 2009; Wittig et al., 2008; Pearson and Wittig, 2008). Combining genetic evidence from eclogites with the information from residual peridotites will give answers to the origin of the subcratonic lithospheric mantle from a different angle.

Most of the evidence for the timing of crustal evolution comes from U-Pb zircon ages and for mantle evolution from the Re-Os system (T_{RD} =Re depletion and T_{MA} =Re model ages) (Walker et al., 1989). The Re depletion age is usually taken as indicating most closely the time of partial melting from a primitive mantle. These methods were the major tools to obtain information on the development of the Kaapvaal craton and its underlying mantle. The two major building units of the Kaapvaal craton are the West- and the East-block (Fig.1). These blocks themselves consist of a number of individual terranes (the most important ones are also shown in Fig. 1) which amalgamated at around 2.9 Ga (Schmitz et al., 2004). The T_{RD} 's of peridotite xenoliths from the W- and E-block completely overlap and form a scewed continuum between less than 2.5 and 3.2 Ga with a peak at 2.8 to 2.9 Ga (Fig.2 a,b). The frequency distribution is a summary of data from Pearson et al. (1995), Carlson et al.(1999), Menzies et al.(1999), Irvine et al.(2001), Carlson and Moore, (2004), Griffin et al. (2004) and O'Reilly et al., (2008). Re depletion model ages are minimum ages because it is assumed **i**) that Re was partitioned quantitatively into the melt because of high degrees of partial melting and **ii**) that only recent to subrecent secondary Re enrichment may have occurred. In contrast to the continua of the Re model ages, crustal ages report episodic events. On the W-block, these episodes fall mainly between 3.25 to 2.8 Ga (Drennan et al., 1990; Thomas et al., 1993; Robb et al., 1990; Poujol et al., 2002; Schmitz et al., 2004) and overlap between crust and mantle ages exists (Fig. 2a). Quite differently, crustal ages on the E-block are older (up to 3.65 Ga) and episodic (see Fig. 2b);

summaries are given by de Wit et al. 1992; Armstrong, 1991; Eglington and Armstrong 2004) while the oldest T_{RD} ages of mantle peridotites from Northern Lesotho and the Monastery mine in the south of the E-block reach only 3.25 and 3.02 Ga respectively (Carlson and Moore, 2004). The existence of older crustal rocks on the E-block led to suggestions that the subcontinental lithospheric mantle (SCLM) was formed after the crust or an older SCLM was replaced during younger events or completely reset by metasomatism (Carlson et al., 2004; Irvine et al., 2001; Shirey et al., 2004; Gao et al., 2002, Griffin et al., 2004). However, the disparity on the E-block of crustal and mantle ages may also be due to a sampling problem in that age-dated crustal rocks stem from different terranes than the kimberlites in which the peridotites were brought to the surface: on the E-block, crust is dated mainly from the NE Witwatersrand and adjacent northerly terranes, but good xenoliths localities are lacking there. Good mantle xenoliths localities exist in the SW of the E-block and the Re-Os model ages stem from there, but basement outcrops do not occur. These drawbacks are inherent to the geological situation. A way out of this dilemma is to make use of the ubiquitous mantle debris, i.e. of the minerals from disintegrated mantle xenoliths which is available from every kimberlite locality. The same kimberlites also often contain basement xenoliths and their disintegrated minerals, esp. zircons. Single mineral grains could give the necessary answers if the analytical techniques are sensitive enough for their analysis and if they give information of the bulk rock. This requirement is obviously fulfilled for zircons and also for single grain subcalcic garnets (= garnets from harzburgites which do not contain clinopyroxene) as representatives of strongly depleted upper mantle. The latter are proxies of the bulk rock composition for many elements and also for the Sm-Nd and Lu-Hf isotope systems. Their analysis allows to characterize and to date mantle processes (Lazarov et al., 2009, 2012). These authors analyzed single grain subcalcic garnets from heavy mineral concentrates and also cpx and grt separates from peridotite xenoliths from Finsch (a 118 Ma old group 2 kimberlite) and derived isochrons and errorchrons which date depletion and enrichment events.

Xenoliths or xenocrysts from group 2 kimberlites i.e. generally from the older group of the cretaceous kimberlites (between 115 and 150 Ma) in southern Africa have the better potential to provide more pristine information on early processes than those from the younger group 1 kimberlites. The mantle brought up by xenoliths of these kimberlites was probably chemically overprinted by the earlier kimberlite magmas and the more pristine information contained within them partly erased. Therefore, mantle samples and especially single grain subcalcic garnets from disintegrated garnet harzburgites from group 2 kimberlites were the targets of this study. We wanted to extend previous work on the Lu-Hf and Sm-Nd isotope systems of such from the Finsch mine on the W-Block of the Kaapvaal craton to further localities, also from the E-block. Finsch is located on the western edge of the Kimberly (W-) block (Fig. 1). We collected further garnets from the Bellsbank mine and from the Boshof road dump in Kimberly (a group 1 kimberlite). Previous work on rare garnet peridotites from Bellsbank gave a highest Re depletion age (T_{RD}) of 2.81 ± 0.06 Ga, and a highest T_{RD} from spinel peridotites of 3.2 and 3.4 Ga (Garden et al., 2003, extended abstract 8th IKC). The Roberts Victor diamond mine lies close to the Colesberg lineament on the E-block. This was an excellent locality for collecting subcalcic garnets as well as the Lace mine close the center of the East block. After a selection process guided by the major element composition from EPMA we ended up with 79

subcalcic garnets which were analyzed by LA ICP MS and 42 of them were analyzed for their Lu-Hf and Sm-Nd isotopes. These data are the basis for a discussion on the origin, the subsequent processes which occurred in the SCLM of the Kaapvaal craton and of their ages.

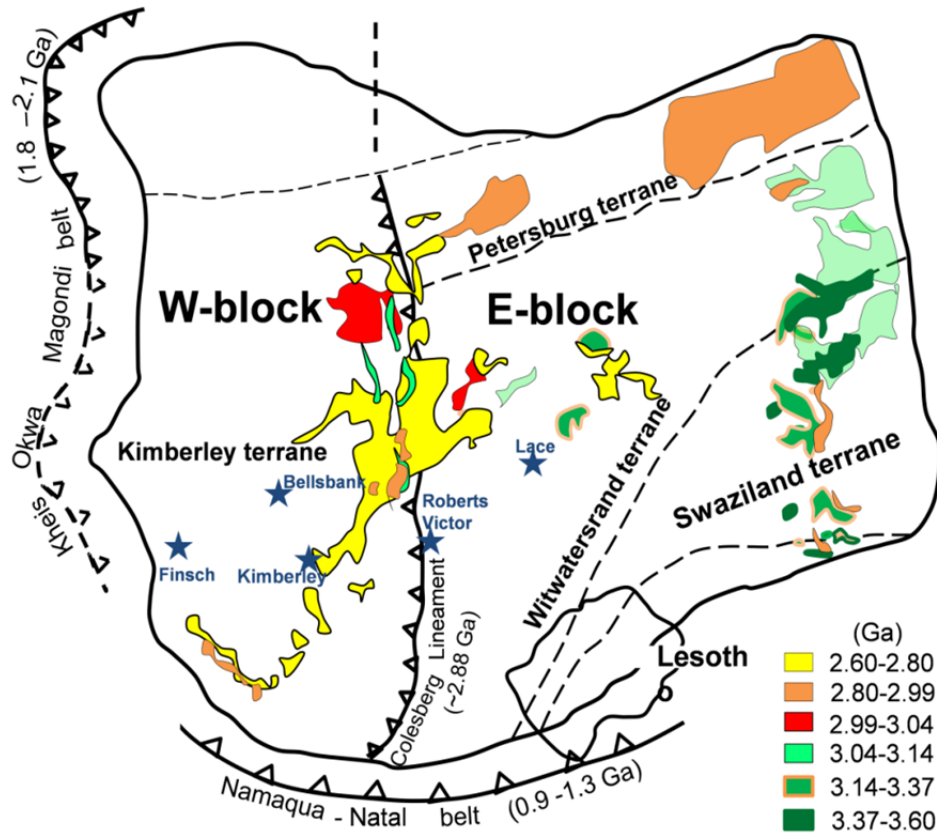


Fig.1 A simplified map of the structural units of the Kaapvaal craton and color coded areas according to age of exposed Paleo- to Neo-Archean crystalline basement and volcano sedimentary basin remnants throughout the Kaapvaal craton. Blue stars show the localities from which subcalcic garnets and eclogites were studied.

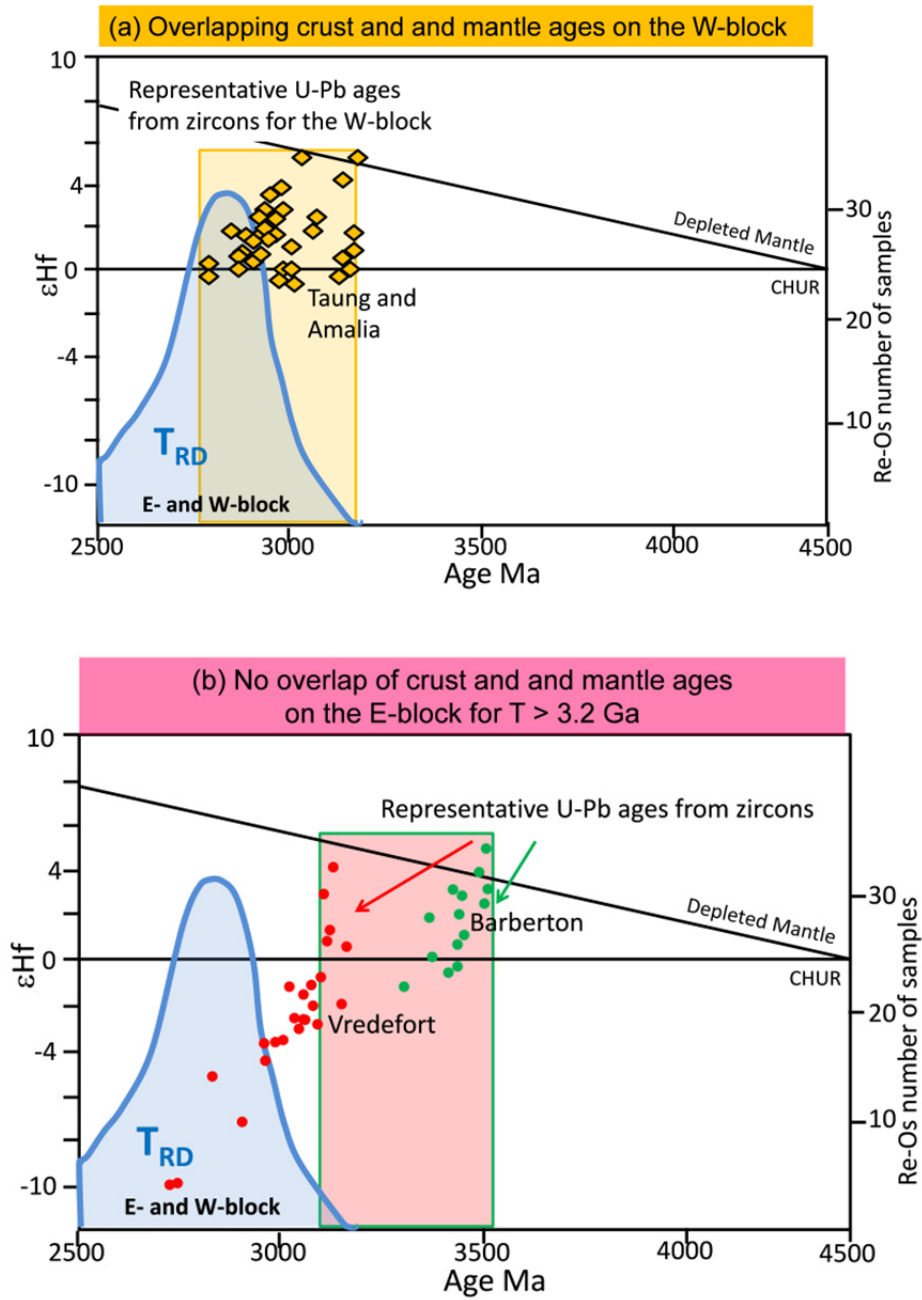


Fig.2 The comparison of the age distribution from the crust (U-Pb ages from crustal zircons) and the mantle (T_{RD} ages) in the Kaapvaal craton. **(a)** Kimberley terreane (west block), **(b)** Witwatersrand terrane (East block) summarized various literature sources (see respective chapters).

3. A study on eclogites and garnet pyroxenites to enhance the understanding of the evolution of the SCLM viewed from a different angle

The study of subcalcic garnets gives information on the origin and fate of the depleted reservoir and the study of eclogites and garnet pyroxenites information on the melts derived from such depleted eclogites, their origin and their later history. Two main hypotheses exist for eclogites: (a) subduction origin where eclogites are metamorphosed oceanic crust and its assemblies via subduction and possibly experienced melt loss (e.g. Jagoutz et al., 1984; MacGregor and Manton, 1986; Shervais et al., 1988; Taylor and Neal, 1989; Neal et al., 1990; Schulze et al., 2000; Barth et al., 2001; Schmickler et al., 2004; Jacob et al., 2005 and 2009; Aulbach et al., 2007; Smart et al., 2009.); (b) mantle origin where eclogites originated as high pressure cumulates from mantle-derived melts (O'Hara and Yoder, 1967; O'Hara, 1969; O'Hara et al., 1975; Hatton and Gurney, 1987; Caporuscio and Smyth, 1990; Griffin and O'Reilly, 2007; Huang et al., 2012). The correct interpretation of their origin, the determination of the age of their protoliths and of subsequent processes which altered their original composition provide important constraints for the reconstruction of ancient geodynamic processes and the determination of the beginning of plate tectonics. Potentially, eclogites and related rocks transferred large amounts of a basaltic component back into the Earth's mantle and added to mantle heterogeneity.

Eclogites and garnet pyroxenites are in themselves heterogeneous which is the result of multiple origins of their protoliths and potential chemical changes before and after eclogitisation. Therefore, age dating of mantle eclogites and the interpretation of these ages poses a substantial challenge. Many attempts have been made with many different methods e.g. Kramers, 1979; Jagoutz et al., 1984; Pearson et al., 1995; Schmidberger et al., 2002; Shirey et al., 2004; Jacob et al., 2005; Aulbach et al., 2007; Gonzaga et al., 2010 and Tappe et al., 2011).

We selected 11 eclogites from the Bellsbank mine on the W-block of the Kaapvaal craton (see Fig. 1). Eclogites and garnet pyroxenites from there are known for their least enriched character in incompatible trace elements compared to many other localities (Shervais et al., 1988; Neal et al., 1990). This enhances the chance to decipher the original signatures of potential protoliths and to obtain ages which can be attributed to particular processes.

4. Aims of this project

In this project, there are several aspects which will be investigated by combining the information from eclogites and from subcalcic garnets as members of the depleted mantle. Special questions to be addressed are:

- (a) When, where and how did the mantle start to differentiate? How is the connection to early crust formation? When did plate tectonics or some precursor scenario start?
- (b) Which processes caused the heterogeneity observed in the subcontinental mantle today? When did metasomatism occur on the depleted mantle? By which kind of enrichment agent and what was its source? Which processes initiate the enrichment events?
- (c) What were the thermal conditions during the assembly of the subcratonic mantle? How did the geothermal condition change with time?

References

- Aulbach S., Pearson N.J., O'Reilly S.Y. and Doyle B.J., 2007, Origins of xenolithic eclogites and pyroxenites from the central Slave Craton, Canada. *Journal of Petrology* **48**, 1843-1873.
- Armstrong, R.A., Compston, W., Retief, E.A. and Welker, H.J., 1991, Zircon ion microprobe studies bearing on the age and evolution of the Witwatersrand triad. *Precambrian Research* **53**, 243-266.
- Barth M., Rudnick R.L., Horn I., McDonough W.F., Spicuzza M, Valley J.W., and Haggerty S.E., 2002, Geochemistry of xenolithic eclogites from West Africa, part II: origins of the high MgO eclogites. *Geochim Cosmochim Acta* **66**, 4325–4345.
- Caporuscio, F.A. and Smyth, J.R., 1990, Trace element crystal chemistry of mantle eclogites. *Contrib. Mineral. Petrol.* **105**, 550–561.
- Carlson, R.W., Pearson, D.G., Boyd, F.R., Shirey, S.B., Irvine, G., Menzies, A.H. and Carlson, R.W. and Moore, R.O., 2004, Age of the Eastern Kaapvaal mantle: Re-Os isotope data for peridotite xenoliths from the Monastery kimberlite. *South African Journal of Geology* **107**, 81-90.
- Carlson, R.W., Irving, A.J., Schulze, D.J. and Carter Hearn B, 2004, Timing of Precambrian melt depletion and Phanerozoic refertilization events in the lithospheric mantle of the Wyoming Craton and adjacent Central Plains Orogen. *Lithos* **77**, 453– 472.
- Gurney, J.J., 1999, Re-Os systematics of lithospheric peridotites: implications for lithosphere formation and preservation. *Proceedings of the 7th International Kimberlite Conference Red Roof Design, CapeTown, South Africa*, 99-108.
- Eglington, B.M. and Armstrong, R.A., 2004, The Kaapvaal Craton and adjacent orogens, Southern Africa: a geochronological database and overview of the geological development of the craton: *South African Journal of Geology* **107**, 13-32.
- Drennan, G.R., Robb, L.J., Meyer, F.M., Armstrong, R.A. and de Bruijn, H., 1990, The nature of the Archaean basement in the hinterland of the Witwatersrand Basin: II. A crustal profile west of the Welkom Goldfield and comparison with the Vredefort crustal profile. *South African Journal of Geology* **93**, 41-53.
- de Wit, M.J., de Ronde, C.E.J., Tredoux, M., Roering, C., Hart, R.J., Armstrong, R.A., Green, R.W.E., Peberdy, E. and Hart, R.A., 1992, Formation of an Archaean continent. *Nature* **357**, 553-562.
- Gao, S., Rudnick R.L., Carlson R.W. McDonough F.W., Liu Y.S., 2002, Re-Os evidence for replacement of ancient mantle lithosphere beneath the North China craton **198**, 307-322.
- Garden, P.B., Carlson, W.R., Shirey B.S. and Gurney J.J., 2003, Re-Os systematics of lithospheric peridotites and eclogites from the Bobbejaan and Bellsbank Dykes, Kaapvaal Craton. 8th International Kimberlite Conference.
- Gonzaga, R.G., Menzies M.A., Thirlwall M.F., Jacob D.E. and Leroex A., 2010, Eclogites and Garnet Pyroxenites: Problems Resolving Provenance Using Lu-Hf, Sm-Nd and Rb-Sr Isotope Systems **51**, 513-535.
- Griffin, W.L., Graham, S., O'Reilly, S.Y. and Pearson, N.J., 2004, Lithosphere evolution beneath the Kaapvaal Craton: Re-Os systematics of sulfides in mantle-derived peridotites. *Chemical Geology* **208**, 89–118.
- Griffin, W.L. and O'Reilly, S.Y., 2007, Cratonic lithospheric mantle: is anything subducted? *Episodes* **30 (1)**, 43–53.
- Hatton, C.J. and Gurney, J.J., 1987, Roberts Victor eclogites and their relation to the mantle. In: Nixon, P.H. (Ed.), *Mantle Xenoliths*. Wiley, London, pp. 453– 463.
- Huang J.X., Gréau Y., Griffin, W.L., O'Reilly, S.Y., and Pearson N. J., 2012, Multi-stage origin of Roberts Victor eclogites: Progressive metasomatism and its isotopic effects, *Lithos* **142–143**, 161–181.
- Irvine, G.J., Pearson, D.G. and Carlson, R.W., 2001, Lithospheric mantle evolution of the Kaapvaal Craton: A Re-Os isotope study of peridotite xenoliths from Lesotho kimberlites. *Geophysical Research Letters* **28**, 2505-2508.
- Jacob, D.E., Bizimis, M., Salters, V.J.M., 2005, Lu/Hf and geochemical systematics of recycled ancient oceanic crust: evidence from Roberts Victor eclogites. *Contributions to Mineralogy and Petrology* **148 (6)**, 707–720.
- Jacob, D.E., Viljoen, K.S. and Grassineau, N.V., 2009, Eclogite xenoliths from Kimberley, South Africa - a case study of mantle metasomatism in eclogites. *Lithos* **112 (Suppl. 2)**, 1002–1013.
- Jagoutz, E., Dawson, J.B., Hoernes, S., Spettel, B., Waenke, H., 1984. Anorthositic oceanic crust in the Archean Earth. 15th Lunar Planet. Sci. Conf., pp. 395–396. Abs.
- Jordan, T.H., 1978, Composition and development of continental tectosphere. *Nature* **257**, 745-750.

- Jordan, T.H., 1988, Structure and formation of the continental tectosphere. In: M.A. Menzies and K.G. Cox (Editors), *Oceanic and continental lithosphere: Similarities and differences*. Oxford University Press, Oxford.
- Kramers, J.D., 1979, Lead, uranium, strontium, potassium and rubidium in inclusion-bearing diamonds and mantle-derived xenoliths from Southern Africa. *Earth Planet. Sci. Lett.* **42**, 58–70.
- Kramers, J.D., Roddick, J.C.M. and Dawson, J.B., 1983, Trace-element and isotope studies on veined, metasomatic and MARID xenoliths from Bultfontain, South-Africa. *Earth and Planetary Science Letters* **65**, 90-106.
- Klama, K.O., 2008, U-Pb geochronology, Hf isotope and trace element geochemistry of detrital zircons from recent sediment of the Orange and Vaal river system in South Africa. Unpublished PhD, university Frankfurt am Main, Germany, 179pp.
- Lazarov, M., Brey, G.P. and Weyer, S., 2009. Time steps of depletion and enrichment in the Kaapvaal craton as recorded by subcalcic garnets from Finsch (SA). *Earth and Planetary Science Letters*, **279 (1-2)**, 1-10.
- Lazarov, M., Brey, G.P. and Weyer, S., 2012, evolution of the South African mantle a case study of garnet peridotite from the Finsch diamond mine (Kaapvaal craton), part 2: Multiple depletion and re-enrichment processes, *Lithos*, 2012.
- Menzies, M.A. and Murthy, R., 1980, Enriched mantle: Nd and Sr isotopes in diopsides from kimberlite nodules. *Nature* **283**, 634-636
- Menzies, A.H., Carlson, R.W., Shirey, S.B. and Gurney, J.J., 1999, Re–Os systematics of Newlands peridotite xenoliths: implications for diamond and lithosphere formation. *Proceedings of the 7th International Kimberlite Conference*, Cape Town, 1998. Red Roof Design, Cape Town, South Africa, 566–573.
- MacGregor, I.D. and Manton, W.I., 1986, Roberts Victor eclogites: ancient oceanic crust. *J. Geophys. Res.* **91 (B14)**, 14063-14079.
- Neal C. R., Taylor A. L., Davidson P. J., Holden P., Halliday N. A., Nixon H. P., Paces B. J., Clayton R. N., and Mayeda K. T., 1990, Eclogites with oceanic crustal and mantle signatures from the Bellsbank kimberlite, South Africa, part 2: Sr, Nd, and O isotope geochemistry. *Earth and Planetary Science Letters* **99**, 362-379.
- O'Reilly, S.Y., Griffin, W.L., Pearson, N.J., Jackson, S.E., Belousova, E.A., Alard, O. and Saeed, A., 2008, Taking the pulse of the Earth: linking crustal and mantle events. *Australian Journal of Earth Sciences* **55**, 983 – 995.
- O'Hara, M.J., Yoder, H.S., 1967, Formation and fractionation of basic magmas at high pressure. *Scott. J. Geol.* **3**, 67-117.
- O'Hara, M., 1969., and Rb-Sr isotope evidence for thick Archean lithospheric mantle beneath the Siberian Craton modified by multistage metasomatism. *Geochimica et Cosmochimica Acta* **59**, 959-977.
- Pearson, D.G., Shirey, S.B., Bulanova, G.P., Carlson, R.W. and Milledge, H.J., 1999, Re–Os isotope measurements of single sulfide inclusions in a Siberian diamond and its nitrogen aggregation systematics. *Geochim. Cosmochim. Acta* **63**, 703–711.
- Pearson, D.G. and Wittig, N. (2008) Formation of Archaean continental lithosphere and its diamonds: the root of the problem. *Journal of the Geological Society* **165**, 895-914.
- Robb, L.R., Davis, D.W. and Kamo, S.L., 1990, U-Pb ages on single detrital zircon grains from the Witwatersrand Basin: constraints on the age of sedimentation and on the evolution of granite adjacent to the basin. *Journal of Geology* **T98**, 311-328.
- Richardson, S.H., Erlank, A.J., Hart, S.R., 1985, Kimberlite-borne garnet peridotite xenoliths from old enriched subcontinental lithosphere. *Earth and Planetary Science Letters* **75**, 116-128.
- Shirey, S.B., Richardson, S.H. and Harris, J.W., 2004, Integrated model of diamond formation and craton evolution. *Lithos* **77**, 923-944.
- Shervais, J.W., Taylor, L.A., G. Lugmair, R.N. Clayton, Mayeda, T.K. and Korotev, R., 1988, Archean oceanic crust and the evolution of sub-continental mantle: Eclogites from southern Africa, southern Africa. *Geological Society of America Bulletin* **100**, 411-423.
- Schulze, D.J., Valley, J.W. and Spicuzza, M., 2000, Coesite eclogites from the Roberts Victor kimberlite, South Africa. *Lithos* **54**, 23– 32.
- Schmickler, B., Jacob, D.E. and Foley, S.F., 2004, Eclogite xenoliths from the Kuruman kimberlites, South Africa: geochemical fingerprinting of deep subduction and cumulate processes. *Lithos* **75 (1–2)**, 173–207.
- Smart, K.A., et al., 2009, The origin of high-MgO diamond eclogites from the Jericho Kimberlite, Canada. *Earth and Planetary Science Letters* **284 (3–4)**, 527–537.

- Schmidberger S. S., Simonetti A., Heaman M. L., Creaser A. R. and Whiteford S., 2007, Lu–Hf, in-situ Sr and Pb isotope and trace element systematics from mantle eclogites from the Diavik diamond mine: Evidence for Paleoproterozoic subduction beneath the Slave craton, Canada, *Earth and Planetary Science Letters* **254**, 55–68.
- Schmitz, M.D., Bowring, S.A., de Wit, M.J. and Gartz, V., 2004, Subduction and terrane collision stabilize the western Kaapvaal craton tectosphere 2.9 billion years ago. *Earth and Planetary Science Letters* **222**, 363-376.
- Stachel, T., Viljoen, K.S., Brey, G., and Harris, J.W., 1998, Metasomatic processes in lherzolitic and harzburgitic domains of diamondiferous lithospheric mantle: REE in garnets from xenoliths and inclusions in diamonds. *Earth and Planetary Science Letters* **159**, 1-12.
- Simon, N.S.C., Carlson, R.W., Pearson, D.G., Davies, G.R., 2007, The Origin and Evolution of the Kaapvaal Cratonic Lithospheric Mantle. *Journal of Petrology* **48**, 589-625.
- Tappe S., Smart A. K., Pearson D. G., Steenfelt A. and Simonetti An., 2011, Craton formation in Late Archean subduction zones revealed by first Greenland eclogites **39**, 1103-1106.
- Thomas, R.J., von Veh, M.W. and McCourt, S., 1993, The tectonic evolution of southern Africa: an overview. *Journal of African Earth Sciences* **16**, 5-24.
- Taylor, L.A. and Neal, C.R., 1989, Eclogites with oceanic crustal and mantle signatures from the Bellsbank kimberlite, South Africa, Part 1: Mineralogy, petrography, and whole-rock chemistry, *J. Geol.* **97**, 551-567.
- Walker, R.J., Carlson, R.W., Shirey, S.B. and Boyd, F.R., 1989, Os, Sr, Nd and Pb isotope systematics of southern African peridotite xenoliths: Implications for the chemical evolution of subcontinental mantle. *Geochimica Et Cosmochimica Acta* **53**, 1583-1595.
- Wittig, N., Pearson, D.G., Webb, M., Ottley, C.J., Irvine, G.J., Kopylova, M., Jensen, S.M. and Nowell, G.M., 2008, Origin of cratonic lithospheric mantle roots: A geochemical study of peridotites from the North Atlantic Craton, West Greenland. *Earth Planet. Sci. Lett.* **274**, 24-33.

Chapter 2

Geochronological and geochemical constraints on the formation and evolution of the mantle underneath the Kaapvaal craton: Lu-Hf and Sm-Nd systematics of subcalcic garnets from highly depleted peridotites

Qiao Shu, Gerhard P. Brey, Axel Gerdes, Heidi Hoefler

Manuscript submitted to *Geochimica et Cosmochimica Acta*, June 2012

Abstract

Subcalcic garnets carry the major inventory of most trace elements of their host harzburgites and are thus proxies of bulk composition. We used single garnet grains from heavy mineral concentrates from the East-block of the Kaapvaal craton (Roberts Victor and Lace mine) to determine the major and trace elements and the Sm-Nd and Lu-Hf isotope systematics of these highly depleted members of the peridotitic suite. The Lu-Hf isotope systematics of subcalcic garnets from Roberts Victor date the enrichment of a previously highly depleted mantle portion at 3.27 ± 0.15 Ga ($\epsilon_{\text{Hf}} = +17.6$) and define the age for partial melting of another mantle portion with a close to primitive composition ($\epsilon_{\text{Hf}} = 2.7 \pm 1.4$) at 2.95 ± 0.06 Ga. The 3.27 Ga enrichment event appears to be wide spread underneath the East-block (Witwatersrand terrane) because it is also seen in a Lu/Hf errorchron from the Lace mine garnets. We compared our results from the East-Block with previous work on subcalcic garnets from the Finsch mine on the West-block (Lazarov et al., 2009). Our re-evaluation of their Lu/Hf isotope data confirmed an old metasomatic age (corrected now to 2.62 ± 0.11 Ga) and yielded a further enrichment at 1.90 ± 0.19 Ga.

Several lines of evidence on major and trace elements from this study suggest in agreement with previous work that mantle melting was mainly at shallow pressures followed by subduction into the garnet stability field. The 3.27 Ga metasomatic event underneath the East-block must have occurred in a previously depleted mantle (very high ϵ_{Hf}) which was sufficiently stabilized by that time to preserve the record of metasomatism and to hold a crust with tonalite–trondhjemite–granodiorite

(TTG's) and greenstone belts. Oceanic lithosphere between W- and E-block was created around 2.95 Ga (recorded in Roberts Victor samples) and subducted underneath the East-block. The creation of a cratonic nucleus for the West-block is unknown until 3.2 Ga when the oldest T_{RD} ages were reported from Newlands and Kimberley and also oldest crustal zircons from there. Such ages were not obtained with our isotope systems but the high positive ϵ_{Hf} of the 2.62 Ga Lu/Hf enrichment age from Finsch indicates depletion several hundred million years earlier. This enrichment may be linked to the 2.6 to 2.8 Ga old voluminous Ventersdoorp volcanics which poured over a major part of then unified Kaapvaal craton. Further metasomatism at Finsch around 1.90 Ga can be easily brought in connection with the attachment of the Kheis-Magondi belt to the Kaapvaal craton. The present study and previous work on subcalcic garnets show that they can be excellent recorders of multiple mantle events which can be correlated with the tectonomagmatic evolution of the craton.

1. Introduction

The timing of growth and amalgamation of Archean continental nuclei, and the temporal relationships between processes in the mantle and the overlying crust are fundamental questions concerning stabilization of long-lived cratonic blocks by buoyant underlying lithospheric mantle (lithospheric keel). Most of the evidence for crustal evolution comes from U-Pb zircon ages and for the mantle from the Re-Os system (Re depletion T_{RD} and Re model ages T_{MA}) (Walker et al., 1989). For the Kaapvaal craton with the West-block (W-block) and the East-block (E-block) as the two major building units (Fig.1a) there is broad overlap of the timing of crustal building events and mantle Re depletion (T_{RD}) (Pearson et al., 1995; Carlson et al., 1999; Menzies et al., 1999; Irvine, et al., 2001; Carlson and Moore, 2004; Griffin et al., 2004; Pearson and Nowell, 2004; O'Reilly et al., 2008). The amalgamation between the two blocks occurred at around 2.9 Ga whereby the E-block was subducted underneath the W-block in a modern style subduction zone scenario (Schmitz et al., 2004). The T_{RD} 's from both the W- and E-block form a continuum between 2.5 and 3.2 Ga with a peak at 2.8 to 2.9 Ga. In contrast crustal growth is episodic. On the W-block, these episodes fall mainly between 3.25 to 2.8 Ga (Drennan et al., 1990; Thomas et al., 1993; Robb et al., 1990; Poujol et al., 2002; Schmitz et al., 2004) and overlap between crust and mantle ages exists. Quite differently, crustal ages on the E-block are older than the T_{RD} 's of the underlying mantle and episodic between 3.65 to 3.1 Ga (summaries by de Wit et al., 1992; Armstrong, 1990; Eglington and Armstrong, 2004). The oldest T_{RD} ages of mantle peridotites from Northern Lesotho and the Monastery mine in the south of the E-block reach only 3.25 and 3.02 Ga respectively (Carlson and Moore, 2004). The existence of older crustal rocks led to suggestions that the subcontinental lithospheric mantle (SCLM) was formed after the crust or an older SCLM was replaced during younger events or completely reset by metasomatism (Carlson et al., 2001; Irvine et al., 2001; Shirey et al., 2004; Gao et al., 2002, Griffin et al., 2004).

The disparity on the E-block of crustal and mantle ages may be due to a sampling problem: **i)** sampling localities for mantle and crustal material often do not coincide especially on the E-block. **ii)** the crust is sampled laterally while the mantle is sampled vertically **iii)** the mantle is sampled more comprehensively on the W-block with its numerous xenoliths bearing kimberlite diatremes than on the E-block; and **iv)** the Archean crust is much better exposed on the E-block than on the W-block. These drawbacks are inherent to the geological situation and they may be overcome only in special cases, e.g. where crustal and mantle xenoliths are sampled together by the kimberlite. Insight into whether the continuous Re-Os age spectra reflect prolonged craton formation or metasomatic overprinting and whether the lack of Re-Os ages corresponding to the old crustal ages of the E-block is due to extensive metasomatism or mantle replacement may be reflected in isochron information from other isotopic systems, such as the Lu-Hf system. Isochrons have the advantage of providing both age and initial ratios, which can indicate the sources and the petrogenetic history. The Lu-Hf system has emerged as very promising in that respect (Blichert-Toft *et al.*, 1999; Scherer et al., 1997; Ionov and Weiss., 2002; Schmidberger et al., 2002; Carlson et al., 2004; Pearson et al., 2004; Wittig et al., 2007; Lazarov et al., 2009). These authors used Lu-Hf isotopic compositions from measured or calculated bulk rocks or single grain subcalcic garnets (as representative of a bulk rock) to derive isochrons

which date depletion or enrichment events. The correct interpretation of enrichment or depletion can only be derived from a joint consideration of the isotope ratios and trace element abundances (see discussion below).

Subcalcic garnets (often presented in CaO-Cr₂O₃ correlation diagrams like Fig.1b) stem from clinopyroxene-free harzburgites and are found in such xenoliths, as inclusions in diamonds and in heavy mineral concentrates from kimberlites. In the absence of clinopyroxenes, such garnets carry the major proportion of the incompatible lithophile elements of the bulk rock and potentially record melting and enrichment events of the lithospheric mantle. Error- and isochrons from subcalcic garnets and reconstructed bulk rocks were successfully used to unravel multiple depletion and enrichment events at Finsch mine, South Africa, by the combined use of the Lu-Hf and Sm-Nd isotope systems (Lazarov et al., 2009). The present study aims to extend this approach to other localities on the E-block in the Kaapvaal craton (Roberts Victor and Lace mine) to test whether (1) these results can be representative for the craton-wide Kaapvaal lithospheric mantle, (2) mantle processes can be dated more precisely and (3) there are age differences in processes between and within the cratonic blocks. We have concentrated on mantle samples from the older group II kimberlite generation because those from the younger group I kimberlites appear to have been metasomatized by the preceding kimberlite generation as their isotopic compositions were heavily disturbed and time was not sufficient to reach full re-equilibration within these mantle portions (Simon et al., 2007).

2. Localities, samples, depth of origin and geological background

The Finsch mine is located close to the western border of the W-block with the Kheis-Okwa-Magondi belt (Fig.1a). Lazarov et al. (2009) studied the trace element and isotope geochemistry of the subcalcic garnets there and derived a Lu-Hf isochron and Sm-Nd errorchrons. In this study, we have used their data set for further evaluation (see below).

The Roberts Victor mine is located fairly central in the Kaapvaal craton very close to the Colesberg lineament, i.e. close to the collision zone between the E- and W-blocks. Jelsma et al. (2004) place it to the east of the Colesberg lineament, i.e. on the westernmost border of the E-block. It lies in the Witwatersrand terrane within this block. The Lace mine is situated slightly to the west of the centre of the E-block (Fig.1a). About 100 purple to violet garnets with grain sizes > 2 mm in diameter were preselected from heavy mineral concentrates from the Lace mine and about 300 were preselected from the Roberts Victor mine. Eighteen subcalcic garnets were identified from Lace by electron probe micro analysis from their CaO-Cr₂O₃ relationships and 36 from Roberts Victor (Fig.1b; **Tables A.1** in the appendix). Depths of origin were estimated from the average temperatures of the Ni in garnet thermometers of Griffin et al. (1989) and Canil (1999) which were projected onto a conductive geothermal gradient of 40 mW/m² (Chapman and Pollack, 1977) (Fig.1c). The subcalcic garnets from Lace mine give a depth range from 140-185 km (only one sample from 120 km) and those from Roberts Victor from 125 to 175 km. The samples from the Finsch mine come from a restricted depth range of 150 to 180 km. The empirical Cr-barometer of Gruetter et al. (2006) gives only minimum pressures in the absence of spinel. This information is missing for our garnets but about half of the

higher pressure samples as projected on the conductive geotherm (Fig.1c) from Finsch and Roberts Victor give similar high pressures with the Cr-barometer. These could be spinel saturated. Trace elements were measured in all selected garnets by Laser Ablation Inductively Coupled Plasma Mass Spectrometry (LA ICP MS). With a few exceptions only garnets plotting in quadrant I on a $(Lu/Hf)_{C1}$ versus $(Lu/Er)_{C1}$ diagram (Fig.1d) were analysed for Sm-Nd and Lu-Hf isotope compositions. Quadrant I corresponds to the field of residues of partial melting of a peridotitic mantle (further discussed in section 5.1). The degree of chemical overprint of these garnets by re-enrichment processes should be low compared to garnets in the other quadrants. They should provide the best opportunity to date partial melting or re-enrichment processes or both in the mantle. Seven samples from Lace and 25 from Roberts Victor plot into quadrant I. Twelve of the 25 samples from Roberts Victor (representative for the spread of Lu/Hf and Lu/Er ratios) were analyzed for their isotopic compositions and also the seven Lace samples from quadrant I and 3 Lace samples from quadrant II.

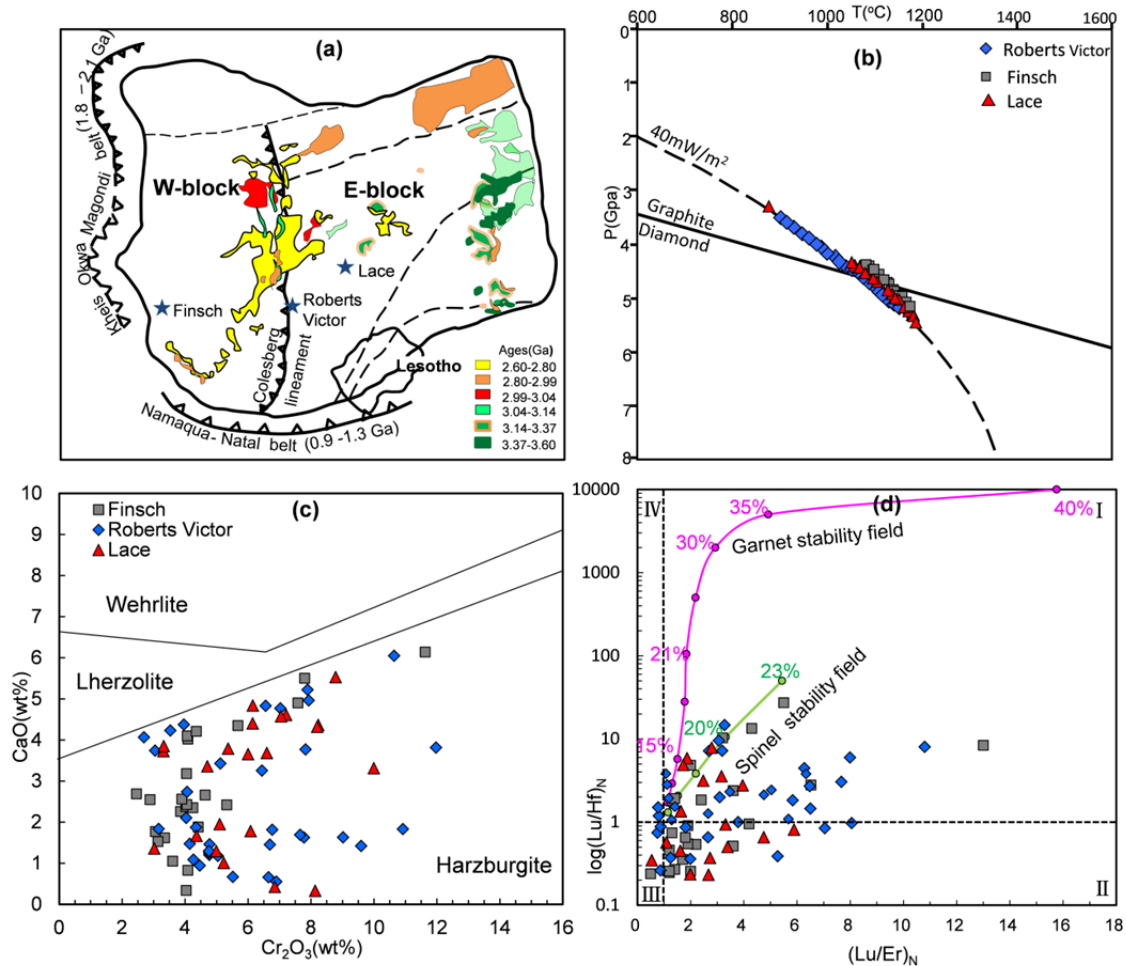


Fig.1 **a)** Structural units of the Kaapvaal craton and colour coded fields of exposed Paleo- to Neo-archean crystalline basement, volcanic and magmatic rocks with age division schematic after Eglington and Armstrong (2004), Anhaeusser (2006) with interpretations after Jacob et al. (2008). Also shown are the locations of the Newlands, Kimberley, Finsch, Roberts Victor and Lace mines. The conditions of origin and chemical parameters of the subcalcic garnets studied from these three localities are shown in the following diagrams as grey squares, blue diamonds and red triangles respectively. **b)** Conditions of crystallization of the subcalcic garnets calculated as the averages of the Ni-in-garnet thermometers of Canil (1994) and Griffin (1989) and projected onto a 40 mW/m² conductive geothermal gradient of Chapman and Pollack (1977). **c)** CaO-Cr₂O₃ correlation diagram of the

subcalcic garnets. **d)** Subcalcic garnets plotted into a $\log(\text{Lu}/\text{Hf})_{\text{C1}} - (\text{Lu}/\text{Er})_{\text{C1}}$ diagram. These ratios are equal to those of the bulk host rock. Both ratios increase in partial melting residues and plot in quadrant I. Garnets from this quadrant were selected for isotopic work because they record the nature of the partial melting process most closely. Model calculations for non-modal fractional melting in the garnet (5 GPa; pink line) and spinel (1.5 GPa; green line) stability are shown for comparison.

3. Analytical methods (details in the supplementary file- method description)

3.1 Major element analysis

Analyses of the major and trace elements and the Sm-Nd and Lu-Hf isotopic systems were carried out as described by Lazarov et al. (2009); detailed information is also supplied in the supplementary file of the present paper). Major elements were measured in wave length dispersive mode (WDS) with a JEOL JXA 8900RL electronprobe microanalyser. Three to 6 spots on each of several pieces of the crushed garnet grains were mounted in epoxy, polished and analyzed to establish compositional homogeneity. For details and accuracy see electronic appendix).

3.2 Trace element analysis

The trace elements were analyzed by Laser ablation ICP MS using a New Wave Research LUV213™ ultraviolet Nd-YAG laser coupled with a Finnigan Element 2 at the Goethe University in Frankfurt. The laser was used at a pulse frequency of 10 Hz and an energy pulse of 0.6 -0.8 mJ (corresponding to 60%-80% laser power) with spot sizes of 60-95 μm . NIST 612 glass was used as a calibration standard. USGS BIR-1 glass (concentrations from Eggins et al.1997) was the external and Ca from microprobe analysis of the minerals the internal standard. BIR-1 glass and one in-house garnet standard (PN2b) were measured several times within each sequence. The raw data were processed on-line using the GLITTER software.

3.3 Sample preparation and isotope analysis

For analysis of the Lu-Hf and Sm-Nd isotopic systems the crushed garnet grains were first leached at room temperature in 6 M HCl or HNO_3 in an ultrasonic bath for about half an hour. The dried down fragments were hand-picked to optical purity and, if necessary, the acid ultrasonication repeated and the grains re-picked. Finally, 30 to 150 mg of garnet separates were ultrasonicated with MQ H_2O and dried prior to spiking with ^{176}Lu - ^{180}Hf and ^{149}Sm - ^{150}Nd tracers before dissolution. Our total procedural Hf blank measured for our methods were from 25 ± 5 pg for repeat measurements by isotope dilution (ID) ICP MS, which is necessary for measurement of the very low Hf concentrations. For those samples with Hf lower than 5 ng, blank corrections were carefully applied. Our total procedural Lu blank were from 5 ± 2 pg. The isotope ratios were analysed in a static mode with a multi collector ICP-MS (Finnigan Neptune). The sample amounts of Hf were always more than 3 ng. With our instrumental set up we are able to measure such low concentrations of Hf (3 ng result in a signal of ~ 90 mV on ^{176}Hf) with a precision of around 1ϵ (on $^{176}\text{Hf}/^{177}\text{Hf}$). Repeated measurements of the Hf standard JMC475 produced $^{176}\text{Hf}/^{177}\text{Hf}$ of 0.282153 ± 0.000014 (2σ), which is in good agreement with the literature (Blichert-Toft et al. 1997; Chu et al. 2002). Replicate digestion and analysis of BHVO-1

gave $^{176}\text{Hf}/^{177}\text{Hf} = 0.283107 \pm 0.000013$ (2σ) which is in good agreement with the values reported by Blichert-Toft et al. (2001) and Bizzarro et al. (2003). Nd-isotope and Sm-ID measurements were also performed by MC ICP-MS. The Nd aliquots always contained more than 10 ng Nd. Such amounts could be measured with a precision of better than 0.5ϵ as determined by replicate standard measurements. Procedure blanks were lower than 70 pg for Nd and 25 pg for Sm. Repeated measurements of Nd isotope standards yielded $^{143}\text{Nd}/^{144}\text{Nd} = 0.511725 \pm 0.000068$ (2σ) for Merck Nd_2O_3 and 0.5119538 ± 0.000026 for Ames-Nd. This is in good agreement with literature values (Deckart et al., 2005; Caro et al., 2006). Replicate digestion and analysis of BHVO-1 yielded $^{143}\text{Nd}/^{144}\text{Nd} = 0.512938 \pm 0.000017$ (2σ). Uncertainties of Lu–Hf and Sm–Nd ratios and isotope compositions are based on replicate BHVO-1 standard solutions measurements are within 2ϵ for $^{176}\text{Hf}/^{177}\text{Hf}$ and $^{143}\text{Nd}/^{144}\text{Nd}$, and 0.33% for $^{176}\text{Lu}/^{177}\text{Hf}$ and 0.54% for $^{147}\text{Sm}/^{144}\text{Nd}$.

4. Results

4.1 Major elements

The major element compositions of the garnets are given in **Tables A.1a-b** in the appendix and shown in Fig.1b in a $\text{CaO}-\text{Cr}_2\text{O}_3$ diagram. Our larger-sized garnets (>2 mm) from all three localities give similar ranges in Cr_2O_3 (2 - 12 wt%) with a mean at around 4 wt% and high and low CaO contents (from 0.3 wt% to 4.3 wt%). It seems that the large-sized garnets are restricted in composition compared to those found in heavy mineral concentrates used in diamond exploration (selected grain size usually < 1 mm) and as inclusions in diamonds which range up to 20 wt% Cr_2O_3 with low to very low CaO in the most Cr-rich samples. The Mg#s from Roberts Victor vary from 83 to 89 while garnets from Lace mine vary from 85-91. The higher average Mg# from Lace (88) indicates higher average degree of partial melting compared to Roberts Victor (86).

4.2 Trace elements

Trace elements of subcalcic garnets from Roberts Victor and Lace are given in **Tables A.2** in the appendix and shown in chondrite (McDonough and Sun, 1995) and Vitim garnet (Ionov et al., 2005) normalized REE diagrams and in Primitive Mantle (Hofmann et al., 1988) normalized spider diagrams in Figs.2 and 3. The sequence of elements for the spider diagrams is taken from the order derived by Hofmann (1988) for decreasing incompatibility except for Zr and Hf. The Hofmann sequence reflects the nature of the residual phases for low pressure melting with olivine, orthopyroxene, \pm clinopyroxene and spinel as residual phases. If one of these phases is exhausted or if another phase like garnet appears in the residue, this order will change. Garnet harzburgites from the subcratonic lithosphere are recrystallised residua of high to very high degrees of partial melting. The phases present during the partial melting process were either ol + high-T opx + Cr-rich spinel (low pressure melting) or ol + high-T opx + low-Cr grt (high pressure melting). For both kinds of residua Zr and Hf will behave more compatible than indicated in the Hofmann et al. (1988) sequence. They have their place between the REE heavier than Sm and Eu. We chose to place them between Gd and Tb since the relative partition coefficients of garnet/ silicate melt and of orthopyroxene/silicate melt for Zr and Hf are such that they

fall somewhere between Gd and Dy (e.g. Irving and Frey, 1978; Green et al., 2000; van Kan Parker et al., 2010). In addition to our own data, the REE and trace element pattern of a garnet from a primitive garnet peridotite xenolith (313-105) from Vitim near Lake Baikal (Ionov et al., 2005) is also shown in Figs. 2 a,c and 3 a,c and we have normalized our garnet REE data to the REE of the Vitim garnet. Sample 313-105 has coexisting ol, opx, cpx, grt and probably small amounts of spinel and a major and trace element composition close to a primitive mantle. It is used here to visualize the differences in composition of our subcalcic garnets to the primitive mantle.

4.2.1 Roberts Victor

The chondrite normalized REE patterns of garnets from Roberts Victor are typically sinusoidal as they are well known e.g. from subcalcic inclusions in diamonds (Stachel et al. 2004). However, there are significant variations in the extent of LREE-MREE enrichment and HFSE contents. The REE and trace element patterns in the spider diagram of the garnets selected from Roberts Victor (Fig. 2c) can be divided into 2 groups (RV1- light blue lines; RV2 dark blue lines). All garnets have strongly fractionated HREE and minima in the M-HREE segments of the patterns which vary between Ho and Tb. The RV1 garnets (light blue lines) show on average a lower degree of enrichment in LREE and MREE than RV2 garnets (dark blue lines). The RV2 samples (and two RV-1) also are characterized by a pronounced peak at Nd with up to 100 times chondritic contents. This Nd peak is not an analytical artifact because LA ICP MS and isotope dilution data are in agreement (see Fig.A.1 in the Appendix). The garnets have therefore very low $(\text{Sm}/\text{Nd})_{c1}$ ratios, down to 0.05. Most RV1 garnets are more depleted in LREE and Zr-Hf compared to group RV2 except RV24 which is enriched in LREE but not Zr-Hf. The normalization of the REE to Vitim garnet (Fig. 2b) shows that the HREE of the Roberts Victor garnets are strongly depleted and the MREE and LREE enriched in two segments as indicated in the two black lines.

The primitive mantle normalized spider diagrams show that the garnets are enriched in most incompatible elements, like LREE, U, Nb and Sr compared to Vitim garnet (Fig.2c). All samples show high U contents and negative Sr anomalies. Zirconium and Hf have similar abundance levels in RV1 with respect to their neighbouring elements Gd and Tb, but there is a negative slope from Dy, Tb, Hf, Zr to Gd in RV2 garnets. Overall, the more incompatible elements of group RV2 sample are more enriched than group RV1.

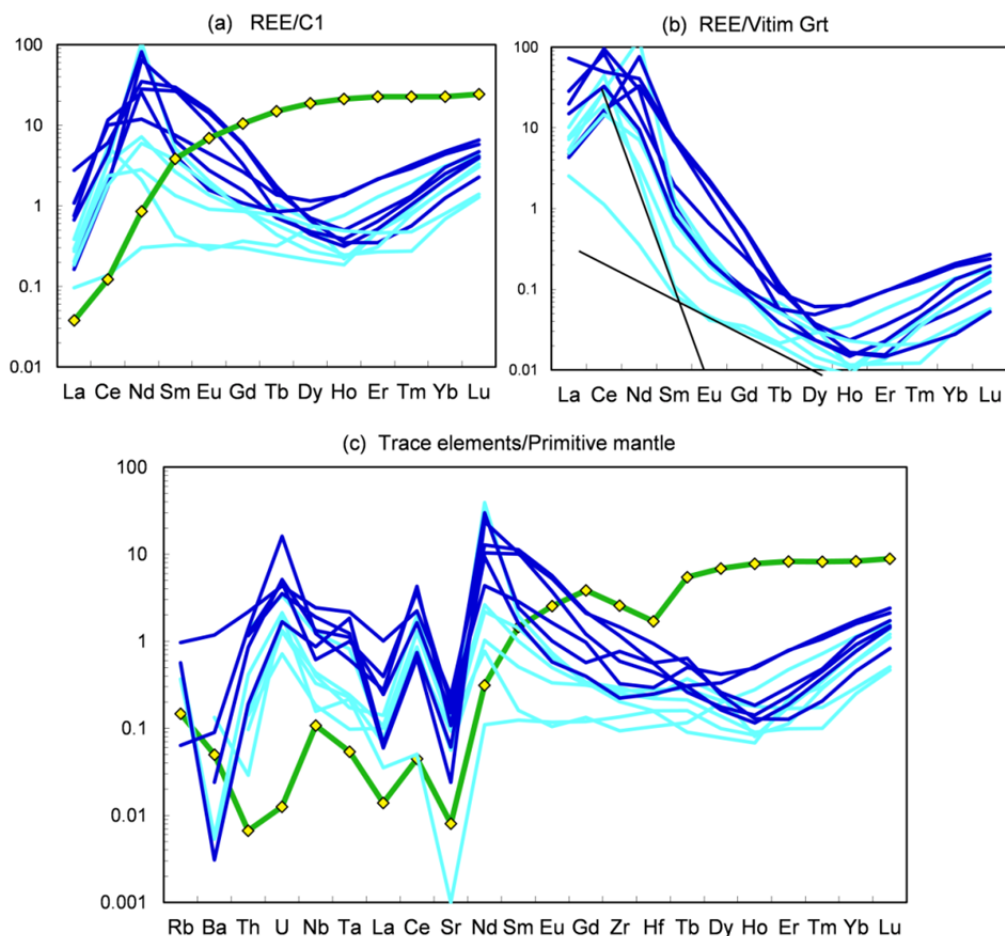


Fig.2 Subcalcic garnets from Roberts Victor: **a)** C1 Chondrite normalized REE patterns. Light blue patterns are RV1, dark blue patterns are RV2 garnets. The green pattern with yellow diamonds is that of a garnet from a primitive garnet peridotite 313-105 from Vitim in Siberia (see text); **b)** Vitim garnet normalized REE patterns; note the depleted HREE which are taken as the signature left from partial melting and the enrichment of the middle and LREE in two steps as indicated by the black lines; **c)** Primitive mantle normalized spider diagrams of the subcalcic garnets.

4.2.2 Lace

The REE and trace element patterns of the garnets from Lace allowed us to divide them into two groups L1 (red lines) and L2 (pink lines; Figs.3). The four group L1 garnets with the highest $(Lu/Hf)_{C1}$ ratios (red patterns in Fig.3) plot into quadrant I of Fig.1d. Two of these (L12 and L32) show only a weak sinusoidal pattern and high HREE contents (only 3 times below Vitim garnet). The other two have strong sinusoidal patterns and low HREE and both have negative Zr and Hf anomalies in primitive mantle normalized patterns (Fig.3c). The six L2 garnets (pink lines; 3 garnets from quadrant I and 3 garnets from quadrant II in Fig. 1d) have low HREE (4 to 73 times below Vitim garnet), are higher in LREE and have much more pronounced sinusoidal patterns with peaks at NdC1 or SmC1 and minima around ErC1 (Fig. 3a). The normalization to primitive mantle shows positive Zr and Hf anomalies (Fig. 3c). The normalization of REE to Vitim garnet shows that all samples are depleted in HREE and that the MREE and LREE are divided in two segments as indicated by the two black lines in Fig. 3b. All Lace samples are higher than the Vitim garnet in the highly incompatible elements from Sm onwards except for the most incompatible elements Ba and Rb.

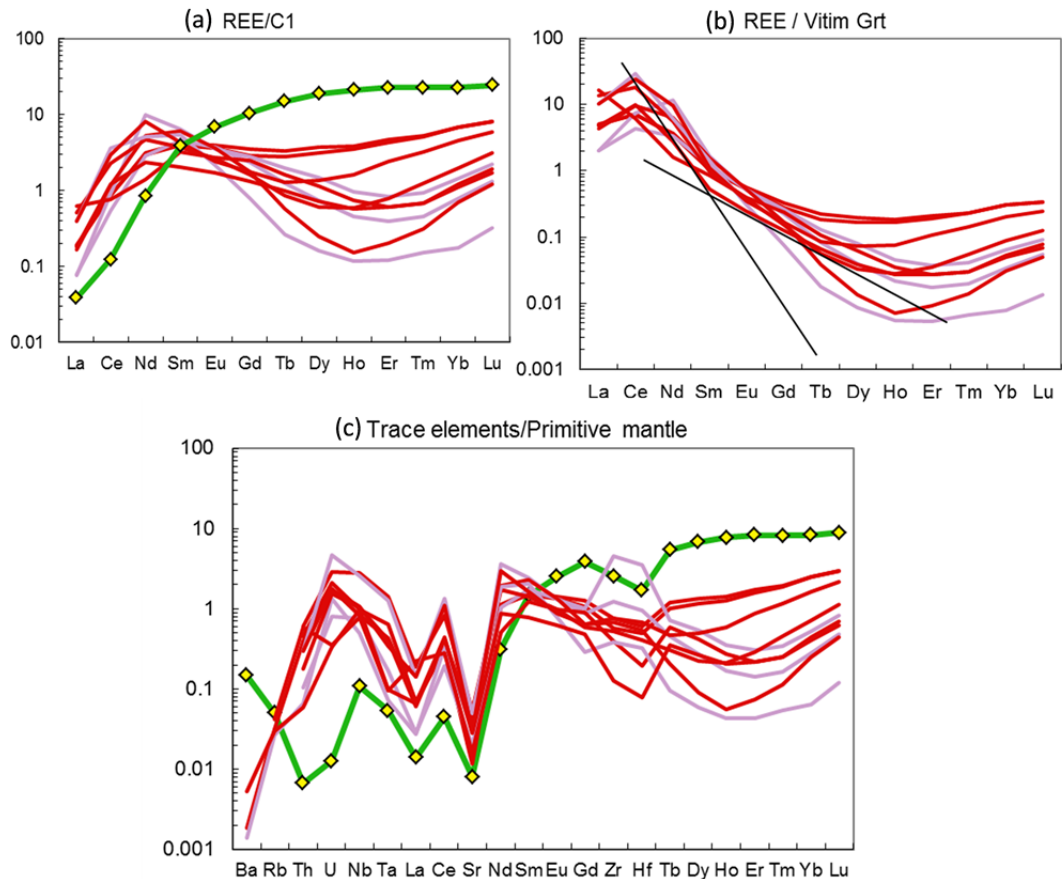


Fig.3 Subcalcic garnets from Lace: **a)** C1 Chondrite normalized REE patterns; **b)** Vitim garnet normalized REE patterns; note the depleted HREE which are taken as the signature left from partial melting and the enrichment of the middle and LREE in two steps as indicated by the black lines; **c)** Primitive mantle normalized spider diagrams. Red lines are L1 and purple are L2 garnets; primitive Vitim garnet is in green.

4.3 Isotope systematics

4.3.1 General remarks

A reliable isochron is a regression line with a statistically meaningful number of data points and a resulting MSWD value of around one. The initial characterizes the source common to all members along the isochron. Due to the special sampling process of mantle xenoliths through vertical melt channels, working on mantle samples generally means that we deal with material from a huge depth range resp. a huge rock volume. Portions of this may have different origins and histories. It may become problematic to identify those members amongst the xenoliths or xenocrysts with a common genetic origin. However, the antique nature of Archean peridotites brings two distinct advantages: a) The antiquity ascertains sufficient time for the isotopic systems to develop into significant correlations for any kind of event and b) the peridotitic mantle samples are a priori residues of medium to very high degrees of partial melting which will provide a good spread in mother/daughter ratios of a radiogenic system in the residue. Subsequent metasomatism and possibly second stage melting appears to be inevitable in Archean mantle samples. If an afflicted rock volume is not completely homogenized by the second event the initials will vary outside the analytical uncertainties for a resulting correlation in

an isochron diagram. The MSWD value can be much higher than one but the correlation will nevertheless have an age significance for old events. Dealing with Archean samples has the advantage that high MSWD can be tolerated.

The interpretation of an isochron as monitoring an enrichment or a partial melting event can be decided upon from the relative abundances of the incompatible elements and especially from the mother/daughter relationships of the isotopic systems. We introduce the relationship between the isochron age and calculated model age of each data point as a tool to decide whether an isochron reflects partial melting of a primitive source, second stage depletion or re-enrichment. We show this for Lu/Hf in diagrams of model ages (calculated with respect to Primitive Mantle) versus $^{176}\text{Hf}/^{177}\text{Hf}$ ratios. The model age of each data point along an isochron will be identical to the isochron age for partial melting of a primitive mantle. Model ages will be younger than the isochron age for second stage partial melting. They will be older than the isochron age and will increase with decreasing $^{176}\text{Hf}/^{177}\text{Hf}$ isotope ratios for an event which enriches Hf in depleted mantle samples. This increase will become exponential when the chondritic Lu/Hf ratio is approached and ages far in excess of the Earth's age are obtained and errors are also very high. For $^{176}\text{Lu}/^{177}\text{Hf}$ lower than the chondritic value (high degrees of re-enrichment) model ages will decrease again and eventually become negative. The initial ratio of the isochrons will provide information on the prehistory of the residues (primitive vs. depleted vs. re-enriched mantle) and on the value to which the residues were reset by an enrichment process.

The results of our isotope measurements for Sm-Nd and Lu-Hf are given in **Tables A.3b** and **Tables A.3a** in the appendix and shown in Figs. 4, 5, 6 and 7 as isochron diagrams and, for Lu-Hf, in diagrams of model ages (calculated with respect to Primitive Mantle for each point along the isochron) versus $^{176}\text{Hf}/^{177}\text{Hf}$ ratios.

4.3.2 Samarium-neodymium from Roberts Victor and Lace (**Data are shown in Tables A.3b in the appendix**)

There is no significant correlation of the Nd isotope with the $^{147}\text{Sm}/^{143}\text{Nd}$ ratios for both localities (Fig. 4; two 900 Ma reference lines are given in this figure). The Roberts Victor samples mostly have lower Sm/Nd ratios than the Lace samples but overlap exists. The six RV2 garnets (with very pronounced Nd-peaks in their REE patterns - Fig. 2a) have high $^{143}\text{Nd}/^{144}\text{Nd}$ ratios (dark blue diamonds in Fig. 4) compared to most RV1 garnets. Their $^{143}\text{Nd}/^{144}\text{Nd}$ ratios increase with Sm/Nd and overlap with and are followed by six Lace samples. The group RV2 and 6 Lace garnets scatter around a 900 Ma reference line (blue dashed line in Fig. 4). One RV1 (RV24) sample which plots with the RV2 garnets also has a very pronounced Nd peak and thus the lowest Sm/Nd ratio. Its present-day ϵNd value is -35. One further RV1 garnet (RV93) with the least overprint on LREE (and therefore the highest Sm/Nd and $^{143}\text{Nd}/^{144}\text{Nd}$ ratios amongst the RV1 garnets) also lies close to the blue dashed reference line. The remaining four RV1 garnets have nearly constant and very low $^{143}\text{Nd}/^{144}\text{Nd}$ ratios but variable $^{147}\text{Sm}/^{144}\text{Nd}$ (0.03-0.10). There are four more garnets from Lace which plot close to another 900 Ma reference line at lower $^{143}\text{Nd}/^{144}\text{Nd}$ ratios.

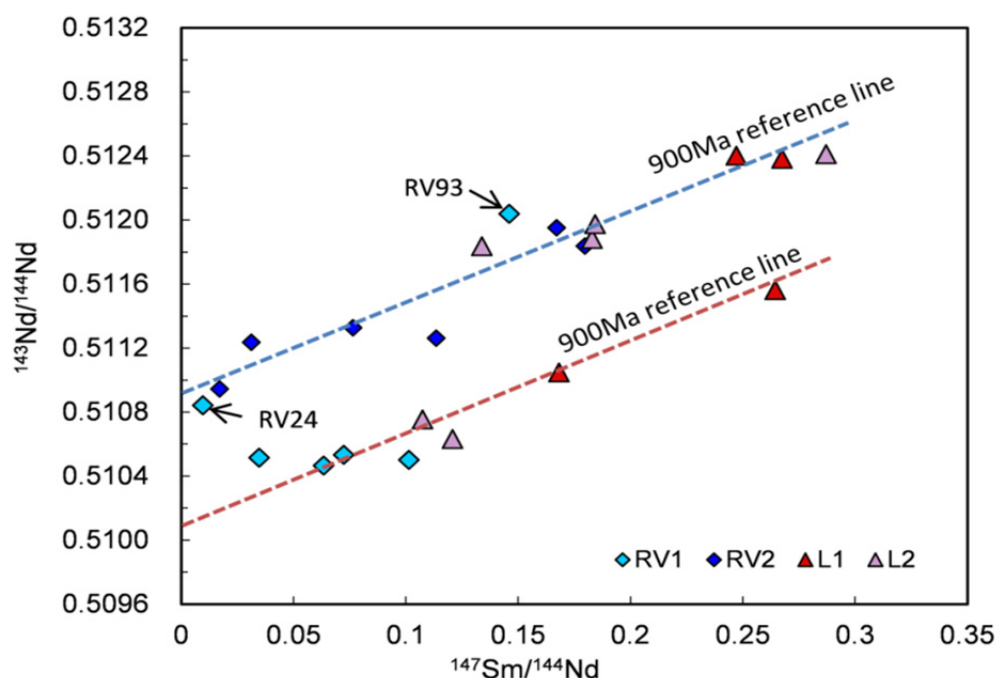


Fig.4 The combined data from Lace and Roberts Victor for the Sm-Nd system with two 900 Ma reference lines: There is no correlation of the Nd isotope with the $^{147}\text{Sm}/^{143}\text{Nd}$ ratios for both localities. However, the six RV2 garnets with very pronounced Nd-peaks in their REE patterns correlate at high $^{143}\text{Nd}/^{144}\text{Nd}$ ratios with Sm/Nd parallel with a 900 Ma reference isochron, overlapped and followed by six Lace samples (with a maximum at Nd). Sample RV24 from the RV1 garnets also has a very pronounced Nd peak and plots with the RV2 garnets and RV1 garnet RV93 with the least LREE overprint on also lies close to the upper correlation trend. The remaining four RV2 garnets have constant, but very low $^{143}\text{Nd}/^{144}\text{Nd}$ ratios with variable Sm/Nd. There are four more garnets from Lace which plot close to a 900 Ma reference line at lower $^{143}\text{Nd}/^{144}\text{Nd}$ ratios. The errors are smaller than the symbols.

4.3.3 Lutetium-hafnium from Roberts Victor (Data are shown in Table A.3a-1 in the appendix)

The subcalcic garnets from Roberts Victor are highly correlated in a $^{176}\text{Hf}/^{177}\text{Hf}$ versus $^{176}\text{Lu}/^{177}\text{Hf}$ diagram (Fig. 5a). On close inspection two correlation lines can be distinguished: i) a line from the RV1 garnets (low MREE and low Hf) which yields an isochron of 2.947 ± 0.058 Ga (MSWD = 3.4) with $\epsilon_{\text{Hf}} = 2.7 \pm 1.4$; ii) a second line from the RV2 garnets giving an age of 3.266 ± 0.15 Ga (MSWD = 58) with $\epsilon_{\text{Hf}} = 17.6 \pm 3.6$. In Fig. 5b, we have plotted the model ages, calculated with respect to a primitive mantle, against the $^{176}\text{Hf}/^{177}\text{Hf}$ ratios. Four of the six RV1 data points from the 2.947 Ga isochron have model ages close to 2.95 Ga in agreement with the isochron age; the two samples with the lowest Lu/Hf ratios have around 3.10 ± 0.02 Ga. The closeness of the model and isochron ages and the ϵ_{Hf} close to zero lead us to interpret this isochron as dating the partial melting of a near primitive mantle. The model ages of data points from the 3.266 Ga isochron are older than 3.31 Ga and increase with decreasing $^{176}\text{Hf}/^{177}\text{Hf}$. This increase becomes exponential when the chondritic $^{176}\text{Lu}/^{177}\text{Hf}$ ratio is approached. The 3.266 Ga isochron with its high $\epsilon_{\text{Hf}} = +17.6$ is therefore interpreted as dating an enrichment process of an already depleted mantle.

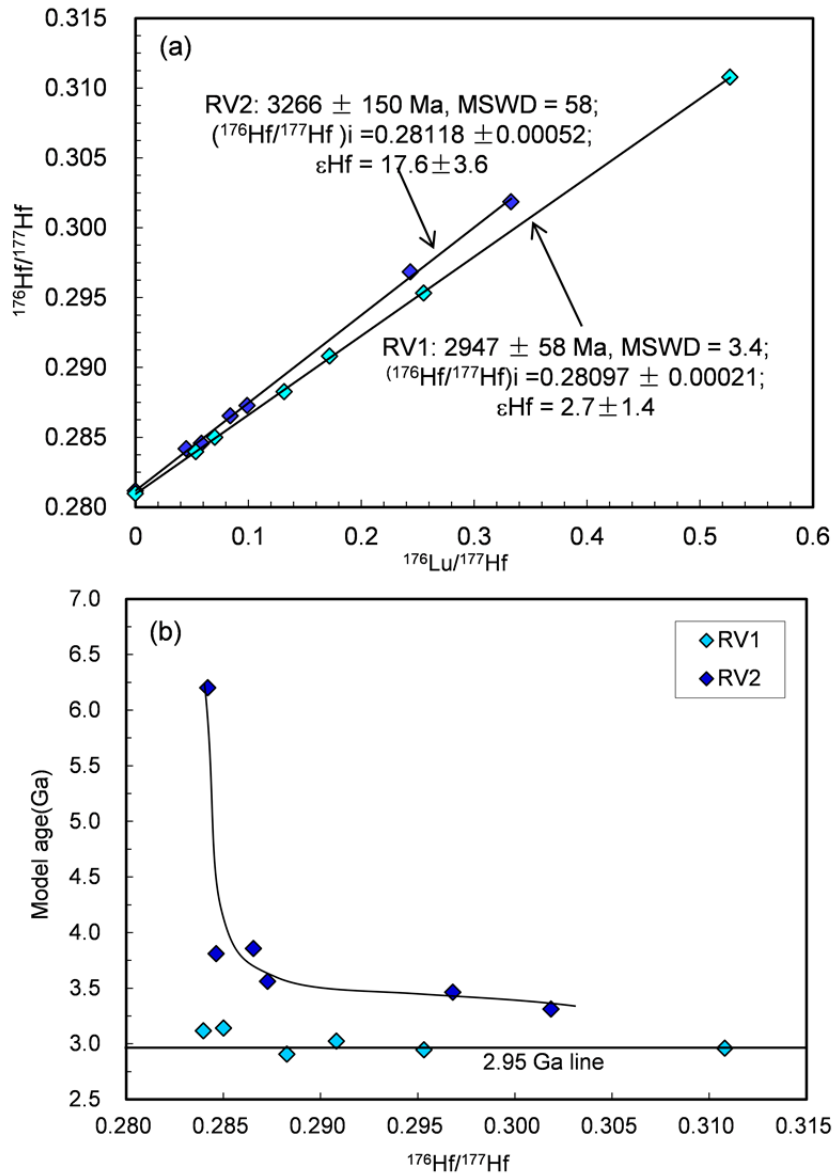


Fig.5 **a**). Isochrons from subcalcic garnets from Roberts Victor: group RV1 (light blue line) give 2.947 Ga; group RV2 (dark blue line) give 3.266 Ga; **b**). The Hf-model ages of the RV1 garnets are around 2.95 Ga and the same as the isochron age (light blue diamonds connected by black horizontal line). All six RV2 garnets have higher model ages than their isochron age (= 3.266 Ga); the model ages increase with decreasing $^{176}\text{Hf}/^{177}\text{Hf}$ (Lu/Hf). The errors are smaller than the symbols.

4.3.4 Lutetium-hafnium from Lace (Data are shown in Table A.3a-2 in the appendix)

The Lace garnets (Fig. 6a) give a Lu-Hf errorchron age of 3.265 ± 0.61 Ga with a high initial of $\epsilon_{\text{Hf}} = +12$. In the model age vs. $^{176}\text{Hf}/^{177}\text{Hf}$ diagram those garnets with high $^{176}\text{Hf}/^{177}\text{Hf}$ (which are also those with $^{176}\text{Lu}/^{177}\text{Hf}$ ratios higher than the primitive mantle) show a broad correlation of increasing model ages with decreasing $^{176}\text{Hf}/^{177}\text{Hf}$. Three L2 garnets (purple triangles) with strong positive Zr-Hf anomalies and with low $^{176}\text{Hf}/^{177}\text{Hf}$ isotope ratios plot to the left and below this correlation (Fig. 6b). The similarity of the $^{176}\text{Hf}/^{177}\text{Hf}$ - $^{176}\text{Lu}/^{177}\text{Hf}$ relationships from Roberts Victor and Lace points to a common, widespread enrichment event at around 3.27 Ga of a depleted mantle underneath the E-block.

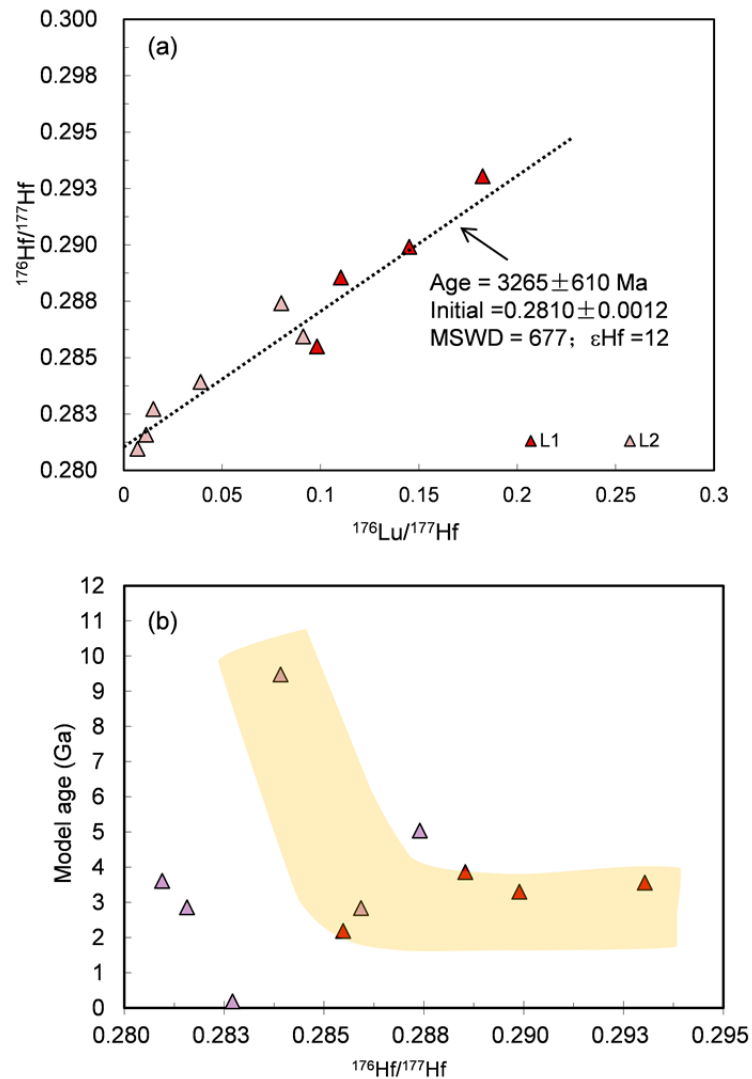


Fig.6 **a)** Isochron diagram for Lace subcalcic garnets: the lace samples form an errorchron of 3.265 ± 0.61 Ga isochron with $\epsilon\text{Hf} = +12$. Red triangles are L1 and purple triangles are L2 garnets. **b)** In a model age versus $^{176}\text{Hf}/^{177}\text{Hf}$ diagram, the garnets with high $^{176}\text{Hf}/^{177}\text{Hf}$ (which are also those with $^{176}\text{Lu}/^{177}\text{Hf}$ ratios higher than the primitive mantle) show a broad correlation of increasing model ages with decreasing $^{176}\text{Hf}/^{177}\text{Hf}$. Three L2 garnets (purple triangles) with strong positive Zr-Hf anomalies and with low $^{176}\text{Hf}/^{177}\text{Hf}$ isotope ratios plot to the left and below this correlation. The errors are smaller than the symbols.

4.3.5 A reexamination of lutetium-hafnium isotope data from Finsch (Lazarov et al., 2009)

We have re-examined the Lu-Hf-isotope data of the subcalcic garnets from Finsch (group F1 and F2 distinguished by Lazarov et al., 2009). Six group F1 garnets define an isochron of 2.62 Ga which is about 100 Ma older reported due to the use of the newer Lu decay constant. (Fig.7a). It can be seen in Fig.7c that all F1 data points have model ages older than 2.62 Ga. The model ages increase with decreasing $^{176}\text{Hf}/^{177}\text{Hf}$ first linearly and then exponentially, when the Lu/Hf ratios come close to the chondritic value. Accordingly, this isochron is interpreted as an enrichment age. Our attention was further drawn in Fig. 7b to the fact that six F2 garnets give a constant model age close to 1.9 Ga. When these samples are plotted into an isochron diagram they give an age of 1.90 ± 0.19 Ga and, out of necessity (agreement of isochron and model ages), an initial ϵHf of zero (-0.1 ± 3.2 ; Fig.

7c). The $^{176}\text{Lu}/^{177}\text{Hf}$ ratios of these samples spread from subchondritic (4 garnets) to superchondritic (2 garnets) which indicates that the Lu-Hf system dates a 1.9 Ga enrichment event rather than a partial melting event.

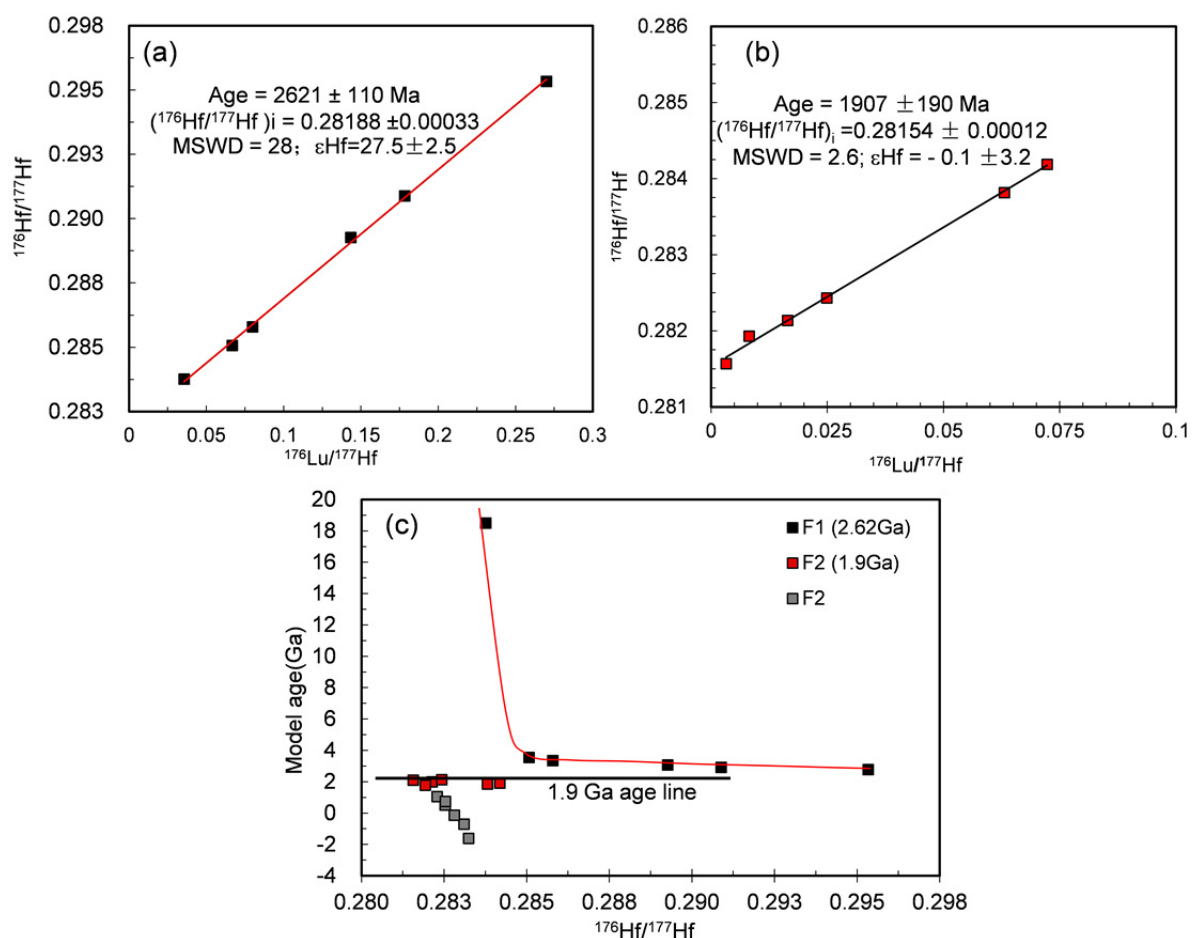


Fig.7 The Lu-Hf isotopic systematics for subcalcic garnets from Finsch (data from Lazarov et al., 2009). **a)** Six F1 garnets from quadrant I in Fig. 1d define an isochron of 2.621 Ga; **b)** The model ages for these garnets (black squares) are all older than the isochron age and increase with decreasing $^{176}\text{Hf}/^{177}\text{Hf}$. Six F2 garnets (red squares) from quadrant II in Fig. 1d give constant model age of 1.9 Ga; **c)** These define an isochron of 1.907 Ga. The errors are smaller than the symbols.

5. Discussion

5.1 Partial melting regimes and enrichment processes from trace element systematics

The low-Ca garnets from Roberts Victor (0.55 to 3.7 wt% CaO) in quadrant I (Fig.1.d) show a large range of Cr# from 8 to 28 [Cr# = $100 \text{ Cr}/(\text{Cr} + \text{Al})$], low to extremely low HREE contents and a high fractionation of the HREE with (Lu/Er)_{C1} up to 11. A similar range exists in the subcalcic garnets from Lace and is also described for those from Finsch (Lazarov et al., 2009). Subcalcic garnets are the compositional proxies for many elements of their host rocks and protoliths and some of these compatible elements in garnets like Cr and the HREE are useful to infer melting regimes of the

protoliths (Pearson and Wittig, 2008; Klein-Ben David and Pearson, 2009). The prerequisite is that they are not or were only negligibly modified by metasomatism subsequent to partial melting. This is valid for chromium. Klein-Ben David et al. (2011) found that it may be mobilized and transported under mantle conditions by saline solutions but without significantly affecting the comparatively high Cr-contents of the bulk rocks. The positively sloped HREE patterns of sinusoidal garnets also reflect the original signature of the partial melting residue since they can only be generated in a garnet-absent melting regime. Also, metasomatizing agents in the mantle have steep REE patterns with low to very low HREE contents.

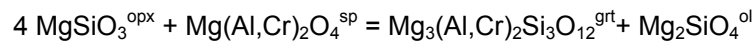
Two models (with modifications) exist for the origin of residual subcratonic mantle:

a) The plume model, where partial melting occurred at high pressures in the garnet stability field in an uprising plume. Garnet and opx are residual phases but partial melting may have reached the extent that only high temperature opx is left as a residual phase besides olivine (Boyd, 1989). Garnets grow upon cooling by exsolution from opx via the reaction:



The HREE are compatible in garnet. They diminish only slightly with increasing degree of partial melting and are retained in the residue as long as garnet is present. Only when garnet is exhausted at very high degrees of partial melting, the HREE contents will also decrease.

b) an upwelling mantle model, where partial melting occurred at shallow depths in the spinel stability field beyond the exhaustion of cpx in a setting similar to mid ocean ridges (Kesson and Ringwood, 1989). This was followed by subduction to generate Cr-rich garnets by the reactions



and



Because all REE are incompatible they decrease in the residue from the onset of low-pressure melting i.e. all REE will be much more strongly depleted in the residue than in a residue from the garnet stability field. The Cr/Al partition coefficient ratios of $(D^{\text{Cr}}/D^{\text{Al}})_{\text{grt/melt}}$ and $(D^{\text{Cr}}/D^{\text{Al}})_{\text{opx/melt}}$ are about 1.0 and 2.0, respectively, at pressures of 5 GPa and more (Bulatov et al. 1991; Canil and Wei, 1992; Stachel et al. 1998). Residual garnets and orthopyroxenes will have low Cr/Al ratios i.e. Cr-rich garnets cannot be generated as residual phases at high pressure and also not by exsolution from residual opx. At low pressures in the spinel peridotite stability field, the Cr/Al partition coefficient ratios of $(D^{\text{Cr}}/D^{\text{Al}})_{\text{spinel/melt}}$ and $(D^{\text{Cr}}/D^{\text{Al}})_{\text{opx/melt}}$ are about 40 and 10 resp. (see refs. above) and residual harzburgites would have very high Cr/Al ratios. Very Cr-rich garnets grow from such compositions upon subduction into the garnet stability field.

The boundary conditions placed by the partition coefficients and resulting element ratios and abundances have been used previously to deduce that a major proportion of the garnet peridotites from the Kaapvaal craton are subducted residues of partial melting at low pressures (e.g. Ringwood, et al., 1977; Kesson and Ringwood, 1989; Stachel et al., 1998; Pearson and Nowell, 2002; Wittig et al., 2008; Pearson and Wittig, 2008) but that a smaller proportion also bears the signs of high pressure

melting including multiple depletions (Lazarov et al., 2009). Our new data are in full accord with the conclusions of all these authors. A small population of our subcalcic garnets with low Cr_2O_3 (< 4 wt%) may have a partial melting origin at high pressures and possibly in a rising and hot plume as envisaged by (Aulbach, 2012).

Partial melting increases the Lu/Hf and Lu/Er ratios in the residues to various extents depending on the melting regime, the degree of melting and the melting mode. Partial melting model calculations were carried out using partition coefficients D_i (for element i) from Green et al. (2000) for the garnet stability field and for the spinel stability field from Kelemen et al. (1993) and Suhr et al. (1998). Melting modes were taken from Kinzler (1997) for spinel peridotite and Walter (1998) for garnet peridotite melting. The results for non-modal fractional melting are shown in Fig.1d. Batch melting (not shown in Fig. 1d) would yield the smallest range of these ratios compared to a somewhat higher range for non-modal batch melting. Non-modal fractional melting at high pressures in the presence of ol, opx and grt and, on further melting, of ol and opx only yields much higher Lu/Hf ratios in comparison with the ratios from the same degree of melting in the spinel stability field. Low pressure melting fractionates HREE (higher Lu/Er ratios) at high degrees of melting and dramatically diminishes the HREE contents in the residue compared to garnet present melting. The comparison of the model calculation with the element ratios of our subcalcic garnets (= those of the bulk rock) shows that single stage non-modal fractional melting of primitive mantle component in the garnet stability field is not a viable scenario for the majority of our samples, but that a number of samples from Lace, Roberts Victor and Finsch follow the trend for melting in the spinel stability field. A number of Roberts Victor garnets also form a parallel alignment to the calculated spinel melting trend at lower Lu/Hf (Fig.1d). This trend would be a possible melting trend, if the bulk Hf partition coefficients were similar to Ho or Er. Lower $(\text{Lu}/\text{Hf})_{\text{C1}}$ ratios in quadrant I off the modeling melting trend are caused by small amounts of metasomatic overprint. Samples which plot in the other quadrants were more severely overprinted and possibly several times.

5.1.1 Roberts Victor mine

The REE patterns of the Roberts Victor garnets, normalized to the Vitim garnet have a positive slope from Ho or Er to Lu, a shallow increase from Ho to Ce for four RV1 garnets and a negative slope in two increments from Ho to Nd or Ce for the RV2 and two RV1 garnets (Fig. 2b). An increase in two steps indicates at least a two-fold overprint by metasomatizing agents. The agents which equilibrated with group RV2 garnets were rich in LREE, MREE, Sr, Zr-Hf and U, depleted in Nb and had extremely high LREE/HREE ratios. Based on low HFSE/LREE ratios, high U contents and high Zr/Hf and Nb/Ta ratios we conclude that the RV2 samples were metasomatized mostly by a carbonatitic melt (Yaxley et al., 1991; Ionov et al., 1993; Rudnick et al., 1993; Brey et al., 2008). The overprint of the four RV1 samples with a shallow increase to the LREE seemed to occur by an agent with lower incompatible trace element contents than carbonatitic or kimberlitic melts. It may have been fluids from reactivated old crust as indicated by the very negative $\epsilon\text{Nd} = -35$. These overprints were inflicted upon the host rocks of the subcalcic garnets which were residues of high degrees of partial melting with only ol, opx

and spinel left and in which Hf and Zr behaved similar to or were even more compatible than Gd (Girnis et al. 2012, submitted to *Lithos* and references therein).

5. 1.2 Lace mine

Group L1 samples (red lines in Fig. 6) show higher HREE contents than group L2 samples (pink lines in Fig. 6) but both groups are re-enriched in the more incompatible elements. Group L2 garnets have strongly positive Zr-Hf anomalies. Group L1 samples are characterized by negative Zr-Hf anomalies compared to the neighbouring Gd and Tb which are similar to the trace element features of the RV2 garnets. As described already in the “Results” section the Roberts Victor and Lace samples seem to form a continuum and record the enrichment at similar times but with varying agents.

5.2 Sm-Nd and Lu-Hf isotope systems – dating enrichment and partial melting

5.2.1 Errorchrons from the Sm-Nd system

Incompatible trace elements indicate a two to many fold metasomatic overprint of most samples by different agents. The imprint on the garnets varies with the nature and the amount of the metasomatizing agent and the modal abundance of garnet in the rock (garnets of lower modal abundances are more affected by the same amount of metasomatizing agent). Sm and Nd will always be affected by each metasomatic event. Because of this multiplicity, no significant correlation could be found in this study which would correspond to an isochron. However, the slope of six RV2 garnets, two RV1 samples and six of the Lace garnets is roughly parallel to a 900 Ma reference line with low initial with ϵ_{Nd} of -13 (red dashed line in Fig. 4). The other samples from both localities also plot parallel to a 900 Ma reference line but with much lower initial with ϵ_{Nd} of -29 (blue dashed line in Fig. 4). Such an age corresponds to the last stages of the Namaqua-Natal orogeny (0.9 to 1.3 Ga; see Fig. 1) which subducted material underneath the craton (Thomas et al. 1993, Schmitz and Bowring, 2003, Hopp, et al., 2008). It may have caused the last widespread metasomatism in this area of the subcratonic mantle before the Mesozoic kimberlite activity. The extremely low Nd isotope ratios (down to $\epsilon_{\text{Nd}} = -40$) of the lowest Sm/Nd samples show that the enriching agents stem from a reactivated reservoir with long term low Sm/Nd ratios such as old crust.

5.2.2 Isochrons from the Lu-Hf system

By using single grain subcalcic garnets as proxies of the bulk rock composition and by the combined evaluation of their major, trace element and isotope compositions we have been able to select those samples which still contain unequivocal evidence of the formation of their protoliths and the timing of depletion and re-enrichment. We were able to retrieve several isochrons from three kimberlite localities from the Kaapvaal craton, namely from Finsch on the western border of the W-block with the 1.85 to 2.0 Ga Kheis-Magondi belt, from Roberts Victor at the western edge of the E-block and at the border to the W-block and from Lace, roughly in the middle of the E-block.

Finsch:

The previous work on subcalcic garnets from Finsch by Lazarov et al. (2009) had concluded that these are products of two melting episodes, the first with high to very high degrees of partial melting at around 3.6 Ga (model age of one subcalcic garnet) and the second, final depletion at 2.62 Ga and enrichment in between.

The criteria described in the “Results” section lead us to the re-interpretation of this age as dating the re-enrichment of an ultra depleted mantle with $\epsilon\text{Hf} = +25$ by a metasomatizing agent (fluid phase) which simultaneously may have triggered some small degrees of partial melting and nearly re-homogenized this mantle portion. Depleted upper mantle is assumed to have $\epsilon\text{Hf} = +8$ at 2.62 Ga. The unusual, very high ϵHf shows high depletion prior to 2.62 Ga but the timing of partial melting cannot strictly be fixed. Four published rhenium depletion ages from Finsch peridotites lie at 2.0, 2.0, 2.6 and 2.8 Ga (Carlson and Moore, 2004) and T_{RD} ages from sulfides in Finsch peridotites give 1.1 to 2.4 Ga (Griffin et al. 2004). However, the rhenium depletion ages from Finsch do not reflect the age of primary melting; they are not depletion ages but rather the results of later re-enrichment (Griffin et al. 2004). If we take the oldest 3.2 Ga T_{RD} age from the west block as the time of the first melting event (Menzies et al., 1999), we estimate that 25% non-modal fractional melting in the spinel stability field gives a Lu/Hf ratio of 0.7 which would yield the high ϵHf of +25 at 2.62 Ga, i.e. within 600 Ma. The time span would be only 50 to 100 Ma, if melting occurred in the garnet stability field.

Lu-Hf ages derived from subcalcic garnets alone are systematically low because of the coexistence of opx (Lazarov et al. 2009) in the rocks. Considering the contents and Lu/Hf ratios of orthopyroxene these authors concluded that the age would increase by about 30 Ma at most. This lies within the error of the isochron but it would bring up the Finsch age up to 2.65 Ga. Already the garnet age alone overlaps with the late period of the extensive Ventersdoorp volcanism which lasted from 2.8 to 2.6 Ga and covered a major portion of the Kaapvaal craton. The ultra depleted Finsch peridotites could not have been the source rocks for these volcanics. Nevertheless, they may witness this major event because they were overprinted by the fluids, which possibly triggered partial melting in the Ventersdoorp magma source region. These may have been pervasive throughout the Kaapvaal lithosphere.

Our scrutiny of the “Lu-Hf model age versus $^{176}\text{Hf}/^{177}\text{Hf}$ ” relationship from the Finsch data (Fig. 7b) revealed a further isochron hidden in the F2 (Hf-enriched) garnet data set with an age of 1.907 ± 0.19 Ga and $\epsilon\text{Hf} \sim 0$ (Fig. 7c). This age can be interpreted as dating the re-enrichment of parts of the SCLM underneath the Finsch mine by an agent which stems from the asthenosphere. The age coincides with the age range reported from the 1.85 – 2.0 Ga old Kheis-Magondi belt immediately to the west of Finsch which was formed by compression and eastward thrusting (Cornell et al., 1998; Griffin et al., 2003; Eglinton, 2006; Jacobs et al., 2008).

Roberts Victor:

Two isochrons could be distinguished amongst the subcalcic garnets which plot into quadrant I of Fig. 1d:

- a) a 2.95 ± 0.06 Ga isochron with $\epsilon\text{Hf} = 2.7 \pm 1.4$ and
- b) a 3.27 ± 0.15 Ga isochron with $\epsilon\text{Hf} = 17.6 \pm 3.6$

The age of 2.95 Ga is interpreted as dating the partial melting of a close to primitive mantle at shallow pressures in an upwelling mantle setting. Reasons are i) that the isochron and the model ages of the individual data points agree (see Fig. 5b). ii) that Cr₂O₃ contents in garnets can become very high (Fig.2) and that the abundance levels of the HREE is low to very low. Melting occurred in some kind of mid ocean ridge setting in between the E- and W-block and subduction under the E-block (see Fig.8). The RV1 harzburgites represent the subducted, depleted lithosphere and the ubiquitous eclogites from Roberts Victor the mafic oceanic crust. Collision of the W- and E-block with westward subduction of the E-block occurred at around 2.9 Ga along the Colesberg lineament (Schmitz et al., 2004). The Re-Os age of eclogitic sulfide inclusion in diamonds is about 2.9 Ga in several localities on the W-block (Shirey et al., 2004). They may record this subduction coupled with diamond formation.

Six RV2 garnets define the 3.27 Ga isochron with its high ϵ_{Hf} of +17.6. From the trace element patterns and abundances (Fig. 2), the “model age vs. $^{176}\text{Hf}/^{177}\text{Hf}$ ” relationship (Fig. 5b) and the high positive ϵ_{Hf} we interpret this age as dating an enrichment event of an already strongly depleted mantle. Its protolith were spinel harzburgites which i) originated by high degrees of partial melting at shallow depths as indicated by low HREE abundances and highly variable Cr/Al ratios and ii) were already subducted by the time of enrichment into the garnet stability field underneath the then existing Witwatersrand terrane (part of the E-block). The age of partial melting in the spinel peridotite field can be placed several hundred million years earlier which explains the high positive ϵ_{Hf} by a similar reasoning as for Finsch (see above). Crustal ages on the E-block are periodic from 3.1 Ga onwards up to 3.65 Ga. According to de Wit et al. (1992) the amalgamation of the E-Block from different small terranes occurred at 3.31 Ga. The 3.27 Ga (± 150 Ma) enrichment from some mantle portions underneath Roberts Victor (and Lace) may be connected with this event. Freshly depleted mantle from partial melting at 2.95 Ga at shallow depth was injected into this older, reenriched mantle relatively shortly before the 2.9 Ga collision of the E- and the W-block. These two lithologies were sampled by the Roberts Victor kimberlite.

Lace:

The ten samples from the Lace mine yield an isochron of the 3.27 ± 0.6 Ga which overlaps with the enrichment age from Roberts Victor (Fig. 6a). We take it that the same enrichment event around 3.27 Ga (or a simultaneous event) overprinted the same depleted mantle underneath the E-block. The enriching agent may have been different in composition as judged from the different trace element patterns of the garnets from the two localities.

6. Summary and conclusions

The age information for the mantle underneath the Kaapvaal craton from this study, from the published Re-Os age data and the age data of crustal events is summarized in Fig. 8 in a cartoon of successions of mantle melting, modification and crustal growth. It modifies work from various authors, e.g. that of Schmitz et al. (2004) and Shirey et al. (2004). Mantle melting was mainly at shallow pressures, followed by subduction. Crust formation began for parts of the E-block at about 3.65 Ga

ago (Kröner et al., 1993). A correspondingly old, depleted mantle component of similar age has not been reported yet from underneath the E-block of the Kaapvaal craton. However, the ϵ_{Hf} initial of the 3.27 Ga enrichment isochron is high (+17) and partial melting for the original depletion of this portion should have occurred only several hundred million years earlier. The depleted mantle underneath parts of the E-block which existed at 3.27 Ga must have been sufficiently stabilized to preserve a record of metasomatism and to hold a crust with TTG's and greenstone belts. The existence of the W-block is enigmatic until 3.2 Ga, which is the age of the oldest TRD's and of crustal zircons. In the time span between 3.1 and 2.95 Ga igneous activity increased on the W-block with TTG's and greenstone belts. Oceanic crust was created in between the two blocks in an upwelling mantle setting at 2.95 Ga and subducted underneath the E-block (evidence from the melting age from this study on Roberts Victor samples and the occurrence of abundant eclogites there). At around 2.9 Ga the E-block collided with the W-block and was possibly partly subducted (Schmitt et al., 2004) underneath the W-block. A major period of diamond formation seems to be connected with the time around 2.9 Ga since eclogitic sulfide inclusions in diamonds from Kimberley (DeBeers pool), Koffiefontein but also from far away localities (Jwaneng and Orapa) yield a Re-Os isochron of this age (Shirey et al., 2004 and Shirey and Richardson, 2011). The overlying crust is intruded at that time by abundant granites. Between 2.6 and 2.8 Ga the voluminous Ventersdoorp volcanics covered a major part of the then unified Kaapvaal craton. The 2.62 Ga enrichment event at Finsch mine falls within this period and may record pervasive metasomatism, which was related to the Ventersdoorp magmatism. Metasomatism was renewed at Finsch at 1.9 Ga through subduction processes connected with the attachment of the Kheis-Magondi belt to the Kaapvaal craton. Further metasomatic overprint occurred in the later stages of the combined Archean and Proterozoic crustal blocks through the accretion of the surrounding belts.

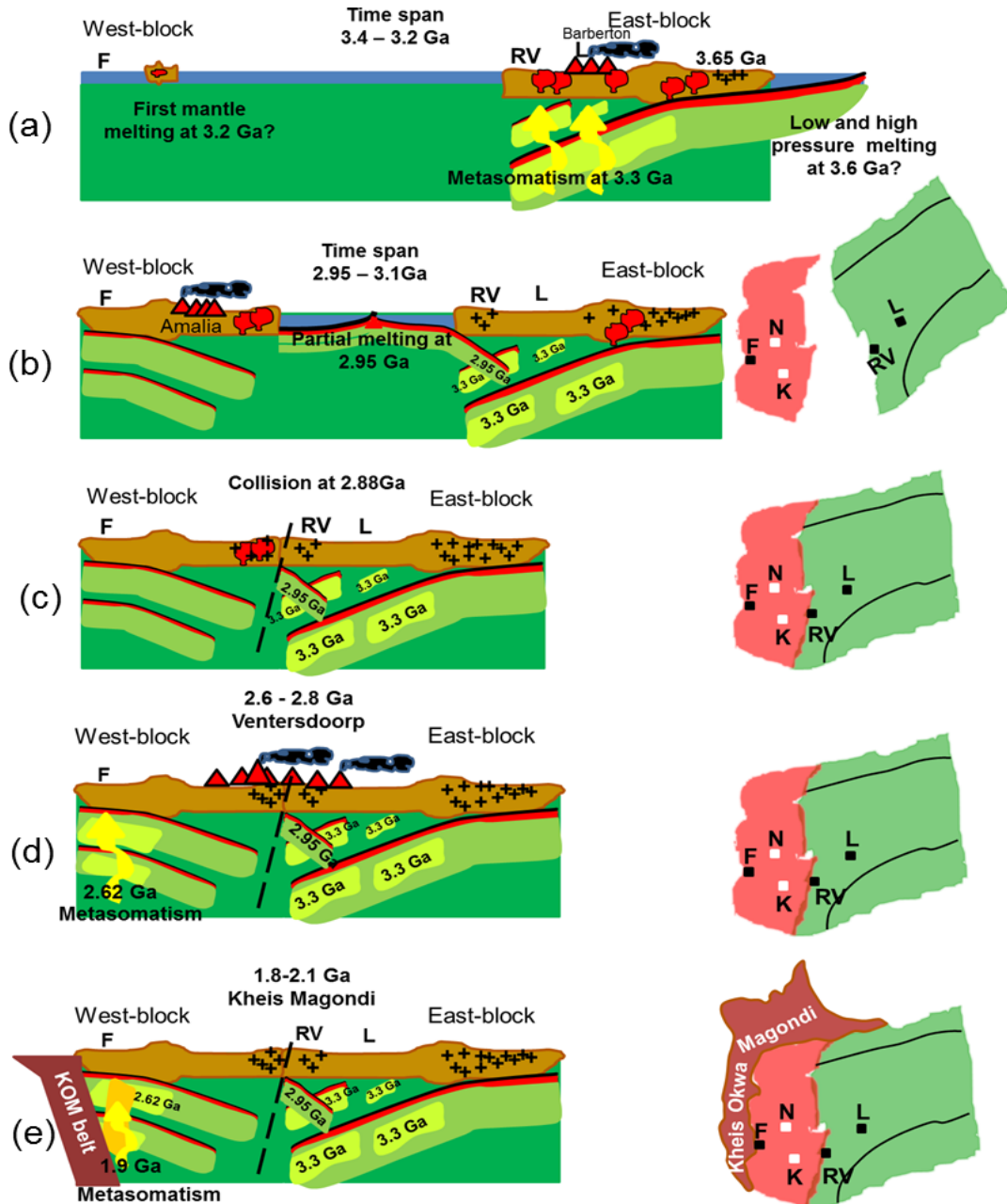


Fig.8 Proposed model for the formation and evolution of the lithospheric mantle beneath the Kaapvaal craton. Mantle melting and crust formation is taken as being caused mainly by passive upwelling and subduction related processes. **a)** The period between 3.2 and 3.4 Ga: The major part of the continental crust of the E-block already existed. The crust rested on a highly depleted mantle which was metasomatized 3.3 Ga ago (Lu-Hf age from subcalcic garnets from the Roberts Victor and Lace mines). The existence and size of the W-block is enigmatic until 3.2 Ga, from when the oldest mantle T_{RD} ages from Newlands and crustal zircon ages are reported. **b)** During the time span between 3.1 and 2.95 Ga igneous activities increased on the W-block with TTG's and the emplacement of greenstone belts. Oceanic crust and depleted mantle was created in between the two blocks in a passively upwelling mantle setting at 2.95 Ga (partial melting age from Roberts Victor subcalcic garnets) and subducted underneath the E-block. **c)** At around 2.9 Ga, the two blocks collided along the Colesberg lineament. **d)** Between 2.6 and 2.8 Ga, the voluminous Ventersdoorp volcanics poured out over a major part of the then unified Kaapvaal craton. The 2.62 Ga enrichment event at Finsch falls within this period and may record pervasive metasomatism in connection with the Ventersdoorp magmatism. **e)** During 1.8 to 2.1 Ga, the craton was subjected chiefly to modification from the margins by subduction which caused metasomatism in the SLCM. The 1.9 Ga enrichment age from Finsch garnets lies within the period of the attachment of the Kheis-Magondi belt to the Kaapvaal craton. Abbreviations: (N: Newlands; F: Finsch; K: Kimberley; RV: Roberts Victor; L: lace)

Acknowledgements

The authors gratefully acknowledge the continuous help and support in the laboratory and through discussions by S. Aulbach, J. Heliosch, F. Kneissl, M. Lazarov, A. Neumann, J. Schastok and H.-M. Seitz. Jeff Harris was fantastic company in the field through his local knowledge, advice, discussions and social skills. Steve West from diamondcorp.plc is thanked for allowing access to the coarse concentrates from the Lace mine. The project was supported by the Deutsche Forschungsgemeinschaft (BR 1012/33-1).

References

- Aulbach, S. (2012) Craton nucleation and formation of thick lithospheric roots, *Lithos* doi:10.1016/j.lithos.2012.02.011
- Anhaeuser, C.R. (2006) A reevaluation of Archean intracratonic terrane boundaries on the Kaapvaal Craton, South Africa: Collisional suture zone? *GSA Special Papers* **405**, 93-210.
- Armstrong, R.A., Compston, W., Retief, E.A. and Welker, H.J. (1991) Zircon ion microprobe studies bearing on the age and evolution of the Witwatersrand triad. *Precambrian Research* **53**, 243-266.
- Becker, H., Shirey, S.B. and Carlson, R.W. (2001) Effects of melt percolation on the Re-Os systematics of peridotites from a Paleozoic convergent plate margin. *Earth Planet. Sci. Lett.* **188**, 107-121.
- Bizzarro, M., Baker, J.A. and Ulfbeck, D. (2003) A new digestion and chemical separation technique for rapid and highly reproducible determination of Lu/Hf and Hf isotope ratios in geological materials by MC-ICP-MS. *Geostandards and Geoanalytical Research* **27**, 133-145.
- Blichert-Toft, J., Chauvel, C. and Albarede, F. (1997) Separation of Hf and Lu for high precision isotope analysis of rock samples by magnetic sector multiple collector ICP MS. *Contributions to Mineralogy and Petrology* **127**, 248-260.
- Blichert-Toft, J., Albarede, F. and Kornprobst, J. (1999) Lu-Hf isotope systematics of garnet pyroxenites from Beni Bousera, Morocco: Implications for basalt origin. *Science* **283**, 1303-1306.
- Blichert-Toft J. (2001) On the Lu-Hf isotope geochemistry of silicates. *Geostandards and Geoanalytical Research* **25**, 41-56.
- Boyd, F.R. (1989) Compositional distinction between oceanic and cratonic lithosphere. *Earth Planet. Sci. Lett.* **96**, 15-26.
- Boyd, F.R., Pearson, D.G., Nixon, P.H. and Mertzman, S.A. (1993) Low-calcium garnet harzburgites from Southern Africa – their relations to craton structure and diamond crystallization. *Contributions to Mineralogy and Petrology* **113**, 352-366.
- Brey, G.P., Bulatov, V.K., Gurnis, A.V. and Lahaye, Y. (2008) Experimental melting of carbonated peridotite at 6-10 GPa. *Journal of Petrology* **49**, 797-821.
- Bulatov, V., Brey, G.P. and Foley, S.F. (1991) Origin of low-Ca, high-Cr garnets by crystallization of low-pressure harzburgites. *Extended Abstract, 5 Int. Kimberlite Conf. Araxa, Brazil. CPRM Special Publication 2/91 Rio de Janeiro, Brazil* 29-31.
- Canil, D. and Wei, K.J. (1992) Constraints on the origin of mantle-derived low-Ca garnets. *Contributions to Mineralogy and Petrology* **109**, 421-430.
- Canil, D. (1999) The Ni-in-garnet geothermometer: calibration at natural abundances. *Contributions to Mineralogy and Petrology* **136**, 240-246.

- Carlson, R.W., Pearson, D.G., Boyd, F.R., Shirey, S.B., Irvine, G., Menzies, A.H. and Gurney, J.J. (1999) Re-Os systematics of lithospheric peridotites: implications for lithosphere formation and preservation. Proceedings of the 7th International Kimberlite Conference Red Roof Design, Cape Town, South Africa, 99-108.
- Carlson, R.W., Irving, A.J., Schulze, D.J. and Carter Hearn B. (2004a) Timing of Precambrian melt depletion and Phanerozoic refertilization events in the lithospheric mantle of the Wyoming Craton and adjacent Central Plains Orogen. *Lithos* **77**, 453– 472.
- Carlson, R.W. and Moore, R.O. (2004b). Age of the Eastern Kaapvaal mantle: Re-Os isotope data for peridotite xenoliths from the Monastery kimberlite. *South African Journal of Geology* **107**, 81-90.
- Caro, G., Bourdon, B. and Birck, J.L. (2006) High-precision $^{142}\text{Nd}/^{144}\text{Nd}$ measurements in terrestrial rocks: Constraints on the early differentiation of the Earth's mantle. *Geochimica et Cosmochimica Acta* **70**, 164-191.
- Cornell, D.H., Armstrong, R.A. and Walraven, F. (1998) Geochronology of the Proterozoic Hartley Basalt Formation, South Africa: constraints on the Kheis tectogenesis and the Kaapvaal Craton's earliest Wilson cycle. *Journal of African Earth Sciences* **26**, 5–27.
- Chapman, D.S. and Pollack, H.N. (1977) Regional geotherms and lithospheric thicknesses. *Geology* **5**, 265–268.
- Chu, N.C., Taylor, R.N., Chavagnac, V., Nesbitt, R.W., Boella, R.M., Milton, J.A., German, C.R., Bayon, G. and Burton, K. (2002) Hf isotope ratio analysis using multi-collector inductively coupled plasma mass spectrometry: an evaluation of isobaric interference corrections. *Journal of Analytical Atomic Spectrometry* **17**, 1567-1574.
- de Wit, M.J., de Ronde, C.E.J., Tredoux, M., Roering, C., Hart, R.J., Armstrong, R.A., Green, R.W.E., Peberdy, E. and Hart, R.A. (1992) Formation of an Archaean continent. *Nature* **357**, 553-562.
- Deckart, K., Bertrand, H. and Liegeois, J.P. (2005) Geochemistry and Sr, Nd, Pb isotopic composition of the Central Atlantic Magmatic Province (CAMP) in Guyana and Guinea. *Lithos* **82**, 289-314.
- Drennan, G.R., Robb, L.J., Meyer, F.M., Armstrong, R.A. and de Bruijn, H. (1990) The nature of the Archaean basement in the hinterland of the Witwatersrand Basin: II. A crustal profile west of the Welkom Goldfield and comparison with the Vredefort crustal profile. *South African Journal of Geology* **93**, 41-53.
- Egginis, S.M., Woodhead, J.D., Kinsley, L.P.J., Mortimer, G.E., Sylvester, P., McCulloch, M.T., Hergt, J.M. and Handler, M.R. (1997) A simple method for the precise determination of >40 trace elements in geological sample by ICP-MS using enriched isotope internal standardization. *Chemical Geology* **134**, 311-326.
- Eglington, B.M. and Armstrong, R.A. (2004) The Kaapvaal Craton and adjacent orogens, southern Africa: a geochronological database and overview of the geological development of the craton: South African. *Journal of Geology* **107**, 13-32.
- Eglington, B.M. (2006) Evolution of the Namaqua-Natal Belt, southern Africa—A geochronological and isotope geochemical review. *Journal of African Earth Sciences* **46**, 93-111.
- Foley, S.F., Buhre, S. and Jacob, D.E. (2003) Evolution of the Archaean crust by delamination and shallow subduction. *Nature* **421**, 249–252.
- Gao, S., Rudnick, R.L., Xu, W.L., Yuan, H.L., Liu, Y.S., Walker, R.J., Puchtel, I.S., Liu, X.M., Huang, H., Wang, X.R. and Yang, J. (2008) Recycling deep cratonic lithosphere and generation of intraplate magmatism in the North China Craton. *Earth Planet. Sci. Lett.* **270**, 41-53.
- Green, T.H., Blundy, J.D., Adam, J. and Yaxley, G.M. (2000) SIMS determination of trace element partition coefficients between garnet, clinopyroxene and hydrous basaltic liquids at 2–7.5 GPa and 1080–1200 °C. *Lithos* **53** 165–187.
- Griffin, W.L., Cousens, D.R., Ryan, C.G., Sie, S.H. and Suter, G.F. (1989) Ni in chrome pyrope garnets – a new geothermometer. *Contributions to Mineralogy and Petrology* **103**, 199-202.

- Griffin WL, SY, O'Reilly, S.Y., Natapov L.M and Ryan C.G. (2003) The evolution of the lithospheric mantle beneath the Kalahari Craton and its margins. *Lithos* **71**, 215–241.
- Griffin, W.L., Graham, S., O'Reilly, S.Y. and Pearson, N.J. (2004) Lithosphere evolution beneath the Kaapvaal Craton: Re–Os systematics of sulfides in mantle-derived peridotites. *Chemical Geology* **208**, 89–118.
- Grütter, H., Latti, D. and Menzies, A. (2006) Cr-Saturation Arrays in Concentrate Garnet Compositions from Kimberlite and their Use in Mantle Barometry. *Journal of Petrology* **47**, 801–820.
- Hofmann, A.W. (1988) Chemical differentiation of the earth – the relationship between mantle, continental-crust, and oceanic-crust. *Earth Planet. Sci. Lett.* **90**, 297-314.
- Hopp, J., Trierloff, M., Brey, G.P., Woodland, A.B., Simon, N.S.C., Wijbrans, J.R., Siebel, W. and Reitter, E. (2008) $^{40}\text{Ar}/^{39}\text{Ar}$ -ages of phlogopite in mantle xenoliths from South African kimberlites: evidence for metasomatic mantle impregnation during the Kibaran orogenic cycle. *Lithos* **106**, 351–364.
- Ionov, D.A., Dupuy, C., O'Reilly, S.Y., Kopylova, M.G. and Genshaft, Y.S. (1993) Carbonated peridotite xenoliths from Spitsbergen: implications for trace element signature of mantle carbonate metasomatism. *Earth Planet. Sci. Lett.* **119**, 283-297.
- Ionov, D. A. and Weiss, D. (2002) Hf isotope composition of mantle peridotites: first results and inferences for the age and evolution of the lithospheric mantle. Abstracts, 4th International Conference on Orogenic Lherzolites and Mantle processes. Japan: Semani, pp. 56–57.
- Ionov, D.A., Blichert-Toft, J. and Weis, D. (2005) Hf isotope compositions and HREE variations in off-craton garnet and spinel peridotite xenoliths from central Asia. *Geochimica et Cosmochimica Acta* **69**, 2399–2418.
- Irvine, G.J., Pearson, D.G. and Carlson, R.W. (2001) Lithospheric mantle evolution of the Kaapvaal Craton: A Re–Os isotope study of peridotite xenoliths from Lesotho kimberlites. *Geophysical Research Letters* **28**, 2505-2508.
- Irving, A.J. and Frey F.A. (1978) Trace element abundances in megacrysts and their host basalts: Constraints on partition coefficients and megacryst genesis. *Geochimica et Cosmochimica Acta.* **48**, 1201-1221.
- Jacobs, J., Pisarevsky, S., Thomas, R.J. and Becker, T. (2008) The Kalahari Craton during the assembly and dispersal of Rodinia. *Precambrian Research* **160**, 142–158.
- Jelsma, H.A., de Wit, M., Thiar, C., Dirks, P.H.G.M., Viola, G., Basson, I.J., and Anckar, E. (2004) Preferential distribution along transcontinental corridors of kimberlites and related rocks of Southern Africa. *South African Journal of Geology* **107**, 301–324.
- Kelemen, P.B., Shimizu, N. and Dunn, T. (1993) Relative depletion of niobium in some arc magmas and the continental crust: partitioning of K, Nb, La and Ce during melt/rock reaction in the upper mantle. *Earth Planet. Sci. Lett.* **120**, 111–134.
- Kesson, S.E. and Ringwood, A.E. (1989) Slab-mantle interactions 2. The formation of diamonds. *Chemical Geology* **78**, 97-118.
- Klein-Ben David, O. and Pearson, D. G. (2009) Origins of subcalcic garnets and their relation to diamond forming fluids-Case studies from Ekati (NWT-Canada) and Murowa (Zimbabwe). *Geochimica et Cosmochimica Acta* **73**, 837–855.
- Klein-Ben David, O., Pettke, T. and Kessel, R. (2011) Chromium mobility in hydrous fluids at upper mantle conditions. *Lithos* **125**, 122–130.
- Kröner, A., Hegner, E., Wendt, J.I. and Byerly, G.R. (1996) The oldest part of the Barberton granitoid greenstone terrain, South Africa: evidence for crust formation at 3.5 and 3.7 Ga. *Precambrian Research* **78**, 105 -124.
- Lazarov, M., Brey G.B. and Weyer S. (2009) Time steps of depletion and enrichment in the Kaapvaal craton as recorded by subcalcic garnets from Finsch (SA). *Earth Planet. Sci. Lett.* **27**, 1–10.
- McDonough, W.F. and Sun, S.S. (1995) The composition of the Earth. *Chemical Geology* **120**, 223–253.

- Menzies, A.H., Carlson, R.W., Shirey, S.B. and Gurney, J.J. (1999) Re–Os systematics of Newlands peridotite xenoliths: implications for diamond and lithosphere formation. Proceedings of the 7th International Kimberlite Conference, Cape Town, Red Roof Design, Cape Town, South Africa, 566–573.
- O'Reilly, S.Y., Griffin, W.L., Pearson, N.J., Jackson, S.E., Belousova, E.A., Alard, O. and Saeed, A. (2008) Taking the pulse of the Earth: linking crustal and mantle events. *Australian Journal of Earth Sciences* **55**, 983–995.
- Pearson, D.G., Shirey, S.B., Carlson, R.W., Boyd, F.R., Pokhilenko, N.P. and Shimizu, N. (1995) Re–Os, Sm–Nd, and Rb–Sr isotope evidence for thick Archean lithospheric mantle beneath the Siberian Craton modified by multistage metasomatism. *Geochimica et Cosmochimica Acta* **59**, 959–977.
- Pearson, D.G., Shirey, S.B., Harris, J.W. and Carlson, R.W. (1998) Sulphide inclusions in diamonds from the Koffiefontein kimberlite, S Africa: constraints on diamond ages and mantle Re–Os systematics. *Earth Planet. Sci. Lett.* **160**, 311–326.
- Pearson, D.G. and Nowell, G.M. (2002) The continental lithospheric mantle: characteristics and significance as a mantle reservoir. *Philosophical Transactions of the Royal Society of London A* **360**, 2383–2410.
- Pearson, D.G. and Nowell, G.M. (2004) Re–Os and Lu–Hf Isotope Constraints on the Origin and Age of Pyroxenites from the Beni Bousera Peridotite Massif: Implications for Mixed Peridotite–Pyroxenite Mantle Sources. *Journal of Petrology* **45**, 439–455.
- Pearson, D.G. and Wittig, N. (2008) Formation of Archean continental lithosphere and its diamonds: the root of the problem. *Journal of the Geological Society* **165**, 895–914.
- Poujol, M., Anhaeusser, C.R. and Armstrong, R.A. (2002) Episodic granitoid emplacement in the Archean Amalia–Kraaipan terrane, South Africa: Confirmation from single zircon U–Pb geochronology. *Journal of African Earth Sciences* **35/1**, 147–161.
- Richardson, S.H., Shirey, S.B., Harris, J.W. and Carlson, R.W. (2001) Archean subduction recorded by Re–Os isotopes in eclogitic sulfide inclusions in Kimberley diamonds. *Earth Planet. Sci. Lett.* **191**, 257–266.
- Shirey, S. B and Richardson, S. H. (2011) Start of the Wilson Cycle at 3 Ga shown by diamonds from subcontinental Mantle. *Science* **333**, 434–436.
- Ringwood, A.E. (1977) Synthesis of pyrope–knorringite solid-solution series. *Earth Planet. Sci. Lett.* **36**, 443–448.
- Robb, L.R., Davis, D.W. and Kamo, S.L. (1990) U–Pb ages on single detrital zircon grains from the Witwatersrand Basin: constraints on the age of sedimentation and on the evolution of granite adjacent to the basin. *Journal of Geology* **T98**, 311–328.
- Rudnick, R.L., McDonough, W.F. and Chappell, B.W. (1993) Carbonatite metasomatism in the northern Tanzanian mantle – petrographic and geochemical characteristics. *Earth Planet. Sci. Lett.* **114**, 463–475.
- Shirey, S.B., Richardson, S.H. and Harris, J.W. (2004) Integrated model of diamond formation and craton evolution. *Lithos* **77**, 923–944.
- Scherer, E.E., Cameron, K.L., Johnson, C.M., Beard, B.L., Barovich, K.M. and Collerson, K.D. (1997) Lu–Hf geochronology applied to dating Cenozoic events affecting lower crustal xenoliths from Kilbourne Hole, New Mexico. *Chemical Geology* **142**, 63–78.
- Schmidberger, S.S., Simonetti, A., Francis, D. and Gariépy, C. (2002) Probing Archean lithosphere using the Lu–Hf isotope systematics of peridotite xenoliths from Somerset Island kimberlites, Canada. *Earth Planet. Sci. Lett.* **197**, 245–259.
- Schmitz, M.D. and Bowring, S.A. (2003) Constraints on the thermal evolution of continental lithosphere from U–Pb accessory mineral thermochronometry of lower crustal xenoliths, southern Africa. *Contributions to Mineralogy and Petrology* **144**, 592–618.

- Schmitz, M.D., Bowring, S.A., de Wit, M.J. and Gartz, V. (2004) Subduction and terrane collision stabilize the western Kaapvaal craton tectosphere 2.9 billion years ago. *Earth Planet. Sci. Lett.* **222**, 363-376.
- Simon, N.S.C., Carlson, R.W., Pearson, D.G. and Davies, G.R. (2007) The origin and evolution of the Kaapvaal cratonic lithospheric mantle. *Journal of Petrology* **48**, 589–625.
- Suhr, G., Seck, H.A., Shimizu, N., Gunther, D. and Jenner, G. (1998) Infiltration of refractory melts into the lower most oceanic crust: evidence from dunite- and gabbro-hosted clinopyroxenes in the Bay of Islands ophiolite. *Contributions to Mineralogy and Petrology* **131**, 136-154.
- Stachel, T., Viljoen, K.S., Brey, G.P. and Harris, J.W. (1998) Metasomatic processes in lherzolitic and harzburgitic domains of diamondiferous lithospheric mantle: REE in garnets from xenoliths and inclusions in diamonds. *Earth Planet. Sci. Lett.* **159**, 1-12.
- Thomas, R.J., von Veh, M.W. and McCourt, S. (1993) The tectonic evolution of southern Africa: an overview. *Journal of African Earth Sciences* **16**, 5-24.
- van Kan Parker, M., Liebscher A., Frei D., van Sijl, J. van Westrenen, W., Blundy, J. and Franz, G. (2010) Experimental and computational study of trace element distribution between orthopyroxene and anhydrous silicate melt: substitution mechanisms and the effect of iron. *Contributions to Mineralogy and Petrology* **159**, 459–473.
- Walker, R.J., Carlson, R.W., Shirey, S.B. and Boyd, F.R. (1989) Os, Sr, Nd and Pb isotope systematics of southern African peridotite xenoliths: Implications for the chemical evolution of subcontinental mantle. *Geochimica et Cosmochimica Acta* **53**, 1583–1595.
- Walter, M.J. (1998) Melting of garnet peridotite and the origin of komatiite and depleted lithosphere. *Journal of Petrology* **39**, 29-60.
- Wittig, N., Baker, J.A. and Downes, H. (2007) U–Th–Pb and Lu–Hf isotopic constraints on the evolution of sub-continental lithospheric mantle, French Massif Central. *Geochimica et Cosmochimica Acta* **71**, 1290–1311.
- Wittig, N., Pearson, D.G., Webb, M., Ottley, C.J., Irvine, G.J., Kopylova, M., Jensen, S.M. and Nowell, G.M. (2008) Origin of cratonic lithospheric mantle roots: A geochemical study of peridotites from the North Atlantic Craton, West Greenland. *Earth Planet. Sci. Lett.* **274**, 24-33.
- Yaxley, G.M., Crawford, A.J. and Green, D.H. (1991) Evidence for carbonatite metasomatism in spinel peridotite xenoliths from western Victoria, Australia. *Earth Planet. Sci. Lett.* **107**, 305-317.

Appendix

Tables A.1 Major elements and structural formulae of subcalcic garnets

Table A.1a : Roberts Victor mine

Table A.1b : Lace mine

Table A.1a Major and minor element compositions (**Table A.1a-1**) and structural formulae (**Table A.1a-2**) of subcalcic garnets from the **Roberts Victor mine**, obtained by EPMA. Values are in wt%. Three to five measurements were performed on each garnet depending on sample size. Relative errors are 1-2% for major elements. Since the variation of the data of each element on individual sample is always smaller than the relative errors. Only averages are shown here.

Table A.1a-1 Subcalcic garnets from Roberts Victor mine - major element (wt%)															
	sample	SiO ₂	Na ₂ O	CaO	MnO	MgO	Cr ₂ O ₃	FeO ^{total}	Al ₂ O ₃	TiO ₂	P ₂ O ₅	Total	Mg#	Cr#	Cr/Al
Group RV1	RV24	43.09	<0.02	1.21	0.40	24.22	4.78	6.61	20.81	<0.03	<0.04	101.20	87	13	0.15
	RV26	43.27	0.02	0.55	0.31	25.24	6.90	5.77	19.18	<0.03	<0.04	101.30	87	13	0.15
	RV31	42.92	<0.02	1.18	0.38	23.90	5.05	7.20	20.63	<0.03	<0.04	101.30	86	14	0.16
	RV93	43.30	0.02	3.74	0.26	22.86	3.05	6.18	21.87	<0.03	<0.04	101.30	87	9	0.09
	RV111	41.64	<0.02	1.42	0.35	23.95	9.60	5.91	16.85	<0.03	<0.04	99.76	88	28	0.38
	RV123	43.07	<0.02	0.67	0.29	25.12	5.52	5.61	19.81	<0.03	<0.04	100.10	89	16	0.19
Group RV2	RV12	43.42	0.03	0.94	0.36	24.88	4.47	6.24	21.15	<0.03	<0.04	101.60	88	12	0.14
	RV23	42.96	0.02	1.45	0.34	24.39	6.70	6.04	19.45	0.03	<0.04	101.40	88	19	0.23
	RV54	42.13	0.04	1.47	0.35	23.52	4.15	6.25	21.30	<0.03	<0.04	99.27	87	12	0.13
	RV94	42.68	0.02	1.82	0.33	23.53	6.77	6.13	18.70	<0.03	<0.04	100.00	89	18	0.22
	RV100	42.82	0.02	1.25	0.37	24.10	4.77	6.52	20.30	<0.03	<0.04	100.20	87	14	0.16
	RV124	42.90	0.02	1.46	0.36	23.77	4.78	6.80	20.33	<0.03	<0.04	100.50	86	14	0.16
	RV17	43.74	0.03	1.09	0.28	25.25	4.27	5.60	21.31	0.04	<0.04	101.60	89	12	0.13
	RV27	43.72	<0.02	1.84	0.28	24.75	3.17	5.77	21.91	<0.03	<0.04	101.50	88	9	0.1
	RV28	43.27	0.02	0.55	0.31	25.24	6.90	5.77	19.18	<0.03	<0.04	101.30	89	19	0.24
	RV37	42.77	0.04	2.11	0.33	23.83	4.04	6.04	21.35	<0.03	<0.04	100.60	88	11	0.13
	RV38	41.85	0.03	3.77	0.43	21.77	7.83	6.55	18.21	<0.03	<0.04	100.50	86	22	0.29
	RV42	42.00	0.08	4.37	0.31	21.30	3.96	6.86	20.58	0.38	<0.04	99.90	85	11	0.13
	RV57	41.68	0.02	3.26	0.40	22.01	6.45	6.13	19.54	<0.03	<0.04	99.52	86	18	0.22
	RV79	43.58	<0.02	0.66	0.29	25.20	6.65	5.81	19.10	<0.03	<0.04	101.30	89	19	0.23
	RV96	42.80	0.07	4.23	0.35	21.58	3.54	7.30	20.49	0.33	<0.04	100.70	84	10	0.12
	RV98	41.67	0.06	4.96	0.31	20.88	7.93	6.57	17.18	0.28	<0.04	99.90	85	24	0.31
RV105	42.14	0.06	4.07	0.40	21.30	2.70	7.56	21.34	0.25	0.05	99.87	83	8	0.08	
RV108	42.24	0.04	1.87	0.36	23.69	4.35	6.50	20.73	<0.03	0.05	99.86	87	12	0.14	
RV130	43.02	0.04	1.30	0.36	24.10	4.76	6.39	20.41	<0.03	0.04	100.50	87	14	0.16	
Group RV3	RV34	43.02	0.03	1.63	0.30	24.35	7.78	5.88	18.48	0.03	<0.04	101.50	88	22	0.28
	RV35	42.12	0.07	4.83	0.41	20.83	6.56	7.01	18.90	0.25	0.08	101.10	84	19	0.23
	RV55	40.52	0.08	6.05	0.34	19.21	10.64	6.77	15.20	0.45	<0.04	99.31	83	32	0.47
	RV84	43.06	0.04	3.45	0.39	22.49	5.12	6.62	20.10	0.04	0.05	101.40	86	15	0.17
	RV90	42.43	0.06	5.22	0.38	20.86	7.89	6.42	17.74	0.21	0.07	101.30	85	23	0.3
	RV110	41.90	0.03	1.69	0.29	24.09	7.66	5.68	18.16	0.07	<0.04	99.59	88	22	0.28
	RV112	41.17	0.07	4.77	0.40	20.88	7.03	6.52	18.17	0.22	0.07	99.30	85	21	0.26
	RV115	40.11	0.07	3.82	0.39	21.33	11.98	6.67	14.43	0.27	0.05	99.15	85	36	0.56
	RV119	42.36	0.04	2.74	0.33	23.25	4.07	6.20	20.94	<0.03	0.05	99.99	87	12	0.13
	RV127	42.19	0.02	1.83	0.32	23.80	10.92	5.47	15.63	0.04	<0.04	100.20	89	32	0.47
RV128	42.55	0.02	1.63	0.33	23.86	9.02	5.93	17.21	<0.03	<0.04	100.60	88	26	0.35	

Table A.1a-2 Subcalcic garnets from Roberts Victor mine - cation												
	sample	Si	Na	Ca	Mn	Mg	Cr	Fe	Al	Ti	P	Total
Group RV1	RV24	3.007	0.002	0.090	0.024	2.519	0.264	0.386	1.712	0.000	0.000	8.005
	RV26	3.019	0.002	0.041	0.018	2.626	0.381	0.337	1.577	0.001	0.000	8.003
	RV31	3.002	0.001	0.088	0.022	2.493	0.279	0.422	1.701	0.001	0.000	8.008
	RV93	3.014	0.003	0.279	0.015	2.372	0.168	0.360	1.794	0.000	0.000	8.007
	RV111	2.993	0.001	0.110	0.021	2.566	0.545	0.356	1.427	0.001	0.001	8.020
	RV123	3.025	0.001	0.050	0.017	2.630	0.307	0.330	1.640	0.000	0.001	8.001
Group RV2	RV12	3.007	0.004	0.070	0.021	2.568	0.245	0.361	1.726	0.000	0.003	8.006
	RV23	3.005	0.003	0.109	0.020	2.543	0.370	0.353	1.603	0.001	0.001	8.009
	RV54	2.989	0.005	0.112	0.021	2.487	0.233	0.371	1.782	0.001	0.002	8.003
	RV94	3.052	0.004	0.132	0.018	2.518	0.353	0.327	1.577	0.001	0.000	7.984
	RV100	3.017	0.003	0.094	0.022	2.531	0.266	0.385	1.686	0.000	0.002	8.006
	RV124	3.020	0.003	0.110	0.022	2.494	0.266	0.400	1.687	0.000	0.001	8.004
	RV17	3.015	0.004	0.080	0.016	2.594	0.233	0.323	1.732	0.002	0.002	8.000
	RV27	3.017	0.002	0.136	0.016	2.547	0.173	0.333	1.782	0.001	0.000	8.005
	RV28	3.019	0.002	0.041	0.018	2.626	0.381	0.337	1.577	0.001	0.000	8.003
	RV37	2.995	0.005	0.158	0.020	2.488	0.224	0.354	1.762	0.000	0.003	8.010
	RV38	2.997	0.005	0.289	0.026	2.324	0.444	0.392	1.537	0.000	0.001	8.015
	RV42	2.996	0.012	0.334	0.019	2.264	0.224	0.409	1.731	0.020	0.002	8.011
	RV57	2.988	0.003	0.250	0.024	2.353	0.365	0.368	1.651	0.001	0.000	8.003
	RV79	3.036	0.002	0.049	0.017	2.618	0.367	0.339	1.568	0.000	0.000	7.997
	RV96	3.026	0.009	0.321	0.021	2.274	0.198	0.431	1.707	0.017	0.002	8.006
	RV98	3.014	0.009	0.385	0.019	2.251	0.454	0.398	1.465	0.015	0.002	8.012
RV105	3.000	0.009	0.311	0.024	2.261	0.152	0.450	1.791	0.013	0.003	8.015	
RV108	2.990	0.005	0.142	0.021	2.500	0.244	0.385	1.730	0.001	0.003	8.021	
RV130	3.021	0.005	0.098	0.022	2.522	0.265	0.375	1.689	0.001	0.003	8.001	
Group RV3	RV34	3.015	0.003	0.122	0.018	2.544	0.431	0.345	1.526	0.002	0.001	8.005
	RV35	3.001	0.009	0.369	0.025	2.212	0.369	0.418	1.587	0.013	0.005	8.006
	RV55	2.993	0.011	0.479	0.021	2.115	0.621	0.418	1.324	0.025	0.002	8.011
	RV84	3.021	0.006	0.258	0.023	2.352	0.284	0.389	1.663	0.002	0.003	8.002
	RV90	3.022	0.008	0.399	0.023	2.214	0.445	0.383	1.489	0.011	0.004	7.999
	RV110	2.995	0.005	0.130	0.017	2.567	0.433	0.340	1.530	0.004	0.001	8.021
	RV112	2.988	0.009	0.371	0.025	2.259	0.403	0.396	1.555	0.012	0.004	8.021
	RV115	2.965	0.010	0.302	0.024	2.350	0.700	0.413	1.258	0.015	0.003	8.042
	RV119	2.994	0.005	0.207	0.020	2.450	0.227	0.367	1.744	0.001	0.003	8.018
	RV127	3.025	0.002	0.141	0.019	2.544	0.619	0.328	1.321	0.002	0.000	8.003
RV128	3.024	0.002	0.124	0.020	2.527	0.507	0.353	1.442	0.001	0.000	8.001	

Table A.1b Major and minor element compositions (**Table A.1b-1**) and structural formulae (**Table A.1b-2**) of subcalcic garnets from the Lace mine, obtained by EPMA. Values are in wt%. Three to five measurements were performed on each garnet depending on sample size. Relative errors are 1-2% for major elements. Since the variation of the data of each element on individual sample is always smaller than the relative errors. Only averages are shown here.

Table A.1b-1 Subcalcic garnets from Lace mine - major element (wt%)															
	sample	SiO ₂	Na ₂ O	CaO	MnO	MgO	Cr ₂ O ₃	FeO ^{total}	Al ₂ O ₃	TiO ₂	P ₂ O ₅	Total	Mg#	Cr#	Cr/Al
Group L1	L12	43.20	0.03	3.73	0.26	23.40	3.31	5.53	21.70	0.06	<0.04	101.00	88	9	0.1
	L14	43.00	0.01	3.36	0.37	22.60	4.71	6.84	20.60	<0.03	<0.04	101.00	85	14	0.16
	L25	42.10	0.06	5.53	0.34	20.90	8.78	6.29	17.10	0.14	<0.04	101.00	86	26	0.35
	L26	42.10	0.05	3.31	0.38	22.30	10.00	6.35	16.70	0.07	<0.04	101.00	86	29	0.4
	L28	43.30	0.02	1.01	0.26	25.40	5.23	5.31	20.50	<0.03	<0.04	101.00	89	15	0.17
	L31	42.30	0.02	4.84	0.37	21.00	6.16	6.86	19.40	<0.03	<0.04	101.00	85	18	0.21
	L32	43.10	0.03	3.85	0.26	23.10	3.33	5.41	21.70	0.06	<0.04	101.00	88	9	0.1
	L33	42.60	0.02	4.41	0.36	21.60	6.15	6.58	19.40	<0.03	<0.04	101.00	85	18	0.21
L36	43.00	0.03	1.78	0.29	24.40	6.08	5.46	19.80	0.05	<0.04	101.00	89	17	0.21	
Group L2	L2	43.00	0.03	1.36	0.33	24.50	3.02	6.18	22.20	0.03	<0.04	101.00	88	8	0.09
	L4	42.90	0.04	1.67	0.26	24.80	4.37	5.39	21.00	0.06	<0.04	100.00	89	12	0.14
	L7	43.00	0.03	1.30	0.24	25.00	4.99	5.28	20.60	0.05	<0.04	101.00	89	14	0.16
	L8	42.10	0.07	3.65	0.35	22.30	6.00	6.17	19.50	0.16	0.06	100.00	87	17	0.21
	L16	42.80	0.06	3.68	0.34	22.90	6.60	5.54	19.20	0.05	0.13	101.00	88	19	0.23
	L20	43.30	0.05	1.95	0.25	24.50	5.10	5.34	20.20	0.16	<0.04	101.00	89	14	0.17
	L30	43.10	0.01	0.33	0.25	26.30	8.14	4.56	18.50	<0.03	<0.04	101.00	91	23	0.29
	L38	43.40	0.01	0.43	0.24	26.10	6.85	4.43	19.30	<0.03	<0.04	101.00	91	19	0.24
L39	42.40	0.05	4.58	0.35	22.00	7.05	5.82	18.80	0.08	0.13	101.00	87	20	0.25	

Table A.1b-2 Subcalcic garnets from Lace mine - cation												
	sample	Si	Na	Ca	Mn	Mg	Cr	Fe	Al	Ti	P	Total
Group L1	L12	3.005	0.005	0.278	0.015	2.420	0.182	0.321	1.781	0.003	0.000	8.011
	L14	3.016	0.002	0.265	0.022	2.336	0.265	0.400	1.696	0.000	0.000	8.003
	L25	3.011	0.008	0.424	0.021	2.232	0.497	0.376	1.439	0.007	0.001	8.015
	L26	3.005	0.007	0.254	0.023	2.370	0.565	0.380	1.403	0.004	0.001	8.010
	L28	3.008	0.003	0.075	0.015	2.631	0.288	0.309	1.677	0.000	0.001	8.009
	L31	3.008	0.002	0.369	0.022	2.226	0.346	0.408	1.622	0.001	0.001	8.007
	L32	3.007	0.004	0.288	0.015	2.404	0.184	0.316	1.784	0.003	0.002	8.007
	L33	3.013	0.003	0.334	0.022	2.274	0.344	0.389	1.620	0.001	0.002	8.003
L36	3.012	0.003	0.134	0.017	2.549	0.337	0.319	1.629	0.002	0.001	8.003	
Group L2	L2	2.994	0.005	0.101	0.020	2.543	0.166	0.360	1.820	0.001	0.002	8.011
	L4	2.999	0.006	0.128	0.016	2.580	0.242	0.315	1.723	0.004	0.002	8.015
	L7	3.003	0.005	0.097	0.014	2.601	0.276	0.308	1.698	0.003	0.002	8.007
	L8	2.993	0.010	0.278	0.021	2.359	0.337	0.366	1.634	0.009	0.004	8.012
	L16	3.008	0.008	0.278	0.020	2.399	0.367	0.325	1.590	0.003	0.008	8.005
	L20	3.022	0.006	0.155	0.015	2.537	0.279	0.313	1.661	0.009	0.001	8.000
	L30	3.005	0.002	0.025	0.015	2.728	0.449	0.266	1.521	0.000	0.000	8.011
	L38	3.020	0.001	0.032	0.014	2.712	0.377	0.258	1.583	0.000	0.001	7.999
L39	3.000	0.007	0.347	0.021	2.318	0.395	0.345	1.564	0.004	0.008	8.008	

Tables A.2 Trace elements of subcalcic garnets

Table A.2a : Roberts Victor mine

Table A.2b : Lace mine

Table A.2c : Standards(BIR-1 Basalt glass and in house garnet standard- PN2b)

Table A.2a LA-ICP-MS analyses of trace element concentrations of subcalcic garnets from the Roberts Victor. The $(Lu/Er)_{c1}$ and $(Lu/Hf)_{c1}$ ratios are normalized to C1 chondrite (McDonough and Sun, 1995). Abbreviations: n – number of spot analyses; <d.l. – below detection limit; T (°C) Canil – temperatures calculated by Ni in garnet thermometer (Canil 1999); T (°C) Griffin – temperatures calculated by Ni in garnet thermometer (Griffin et al., 1989).

Table A.2a Trace element concentrations of subcalcic garnets from the Roberts victor mine (in ppm)													
n	Group RV1						Group RV2						
	5	4	5	5	6	5	3	5	7	5	5	5	5
sample	RV24	RV26	RV31	RV93	RV111	RV123	RV12	RV23	RV54	RV94	RV100	RV124	RV17
Sc	110	100	93	140	193	122	77	136	100	175	122	133	70
V	178	220	221	161	282	230	177	185	176	286	236	257	188
Cr	27474	50053	40660	24318	77369	42663	36236	34849	23726	57256	37004	36306	27557
Mn	3136	2938	4048	2364	2966	2247	3562	2579	2976	2858	2870	2956	2465
Co	40	49	59	54	51	50	53	35	38	50	50	51	39
Ni	27	51	40	39	45	60	41	26	27	41	40	43	40
Ga	1.955	2.57	4.537	1.66	1.761	3.137	3.968	2.375	1.912	4.296	2.92	2.918	4.15
Rb	0.038	0.22	0.324	<d.l.	<d.l.	<d.l.	0.582	0.492	0.339	0.038	0.013	<d.l.	0.06
Sr	2.12	2.51	2.19	<d.l.	1.113	1.849	4.728	3.789	1.214	2.14	0.478	3.006	0.295
Y	0.401	0.3	1.289	0.313	0.582	0.288	0.473	2.204	0.78	2.214	0.452	0.574	0.737
Zr	3.077	2.62	0.985	1.415	2.815	2.117	12.165	3.423	15.29	2.336	6.21	8.048	7.407
Nb	0.82	0.29	0.264	0.103	0.121	0.216	1.596	0.405	0.571	0.808	1.251	0.877	0.471
Ba	<d.l.	0.04	0.038	0.88	<d.l.	<d.l.	7.785	<d.l.	0.02	0.591	<d.l.	0.158	<d.l.
La	0.048	0.07	0.091	0.023	0.065	0.044	0.654	0.256	0.043	0.178	0.039	0.159	0.012
Ce	2.176	2.1	3.327	0.084	1.445	1.101	3.728	6.2	1.24	7.152	1.078	2.737	0.686
Pr	2.385	0.57	0.445	0.027	0.344	0.411	1.4	1.28	0.839	2.86	1.428	2.478	0.46
Nd	48.827	3.28	0.959	0.138	1.286	2.747	15.95	5.45	12.91	11.612	29.616	37.39	3.82
Sm	0.763	0.39	0.063	0.049	0.199	0.551	4.395	1.112	3.923	0.623	4.032	0.949	0.761
Eu	0.114	0.08	0.016	0.018	0.051	0.102	0.872	0.251	0.809	0.089	0.575	0.155	0.181
Gd	0.185	0.17	0.073	<d.l.	0.171	0.183	1.185	0.53	1.141	0.216	0.656	0.31	0.312
Tb	0.037	0.02	0.012	<d.l.	0.028	0.016	0.063	0.049	0.054	0.031	0.03	0.026	0.035
Dy	0.163	0.09	0.133	0.053	0.14	0.067	0.163	0.282	0.175	0.225	0.109	0.118	0.166
Ho	0.012	0.01	0.042	0.01	0.027	0.012	0.019	0.073	0.027	0.076	0.017	0.021	0.026
Er	0.076	0.04	0.207	0.08	0.074	0.049	0.056	0.344	0.129	0.341	0.082	0.103	0.086
Tm	0.023	0.01	0.049	0.02	0.012	0.019	0.014	0.072	0.033	0.079	0.026	0.031	0.024
Yb	0.348	0.11	0.502	0.259	0.129	0.265	0.201	0.705	0.485	0.761	0.338	0.403	0.283
Lu	0.094	0.03	0.104	0.075	0.034	0.082	0.056	0.143	0.116	0.162	0.097	0.101	0.067
Hf	0.066	0.06	0.03	0.045	0.079	0.045	0.161	0.083	0.265	0.07	0.125	0.159	0.114
Ta	0.03	0.01	0.006	0.008	0.004	0.008	0.08	0.037	0.068	0.023	0.045	0.041	0.027
Pb	0.02	0.06	0.02	0.199	0.026	0.252	0.31	0.05	0.026	1.408	0.071	0.26	0.024
Th	0.11	0.01	0.033	0.002	0.011	0.008	0.173	0.097	0.015	0.111	0.092	0.068	0.009
U	0.068	0.03	0.043	0.041	0.015	0.027	0.088	0.095	0.034	0.326	0.072	0.104	0.028
Zr/Hf	47	42	33	32	36	47	76	41	58	33	50	51	65
$(Lu/Hf)_{c1}$	6	2.1	14.7	4.4	2	8	1.5	7.2	1.8	9.6	3.1	2.7	2.4
$(Lu/Er)_{c1}$	8	4.8	3.3	6.3	3.1	10.8	6.5	2.7	5.8	3.1	7.3	6.5	5
T (°C) Griffin	908	1098	1015	1008	1052	1151	1026	890	901	1026	1018	1036	1019
T (°C) Canil	950	1068	1018	1014	1041	1099	1025	938	946	1025	1020	1031	1021

Table A.2a continued													
	Group RV2											Group RV3	
n	5	5	5	5	6	5	3	4	5	5	4	5	5
sample	RV28	RV37	RV38	RV42	RV57	RV79	RV96	RV98	RV105	RV108	RV130	RV34	RV35
Sc	100	88	227	76	289	128	111	142	112	120	135	97	168
V	220	167	192	239	171	256	227	396	201	248	239	227	165
Cr	50053	25877	49647	28811	41802	58093	28256	62611	21475	35713	36252	57641	40000
Mn	2938	2803	3498	3095	3640	2671	2864	2641	3514	3023	2794	2942	3476
Co	49	41	38	48	40	53	46	46	49	51	49	47	36
Ni	51	30	25	57	29	63	62	67	37	41	40	54	29
Ga	2.568	2.64	2.011	9.85	0.96	3.451	11.732	9.815	10.292	3.393	2.667	3.183	2.54
Rb	0.221	0.066	0.168	0.279	0.06	0.02	0.015	0.016	<d.l.	<d.l.	0.117	0.179	0.05
Sr	2.505	3.33	1.35	0.326	0.661	2.298	0.298	0.345	0.297	0.296	2.363	0.547	0.33
Y	0.301	0.585	4.955	12.99	4.68	0.399	15.84	6.945	27.882	0.902	0.617	1.367	41.95
Zr	2.622	28.163	11.695	28.753	32.19	3.13	23.736	26.558	53.458	21.277	27.417	16.48	98.89
Nb	0.288	0.743	0.608	0.128	0.366	0.245	0.1	0.074	0.043	0.527	1.207	0.198	0.244
Ba	0.035	0.638	<d.l.	<d.l.	<d.l.	0.082	0.078	<d.l.	0.067	1.776	0.531	<d.l.	<d.l.
La	0.07	0.263	0.086	0.022	0.108	0.051	0.022	0.031	0.018	0.018	0.074	0.034	0.019
Ce	2.103	3.557	2.393	0.324	2.166	1.271	0.288	0.455	0.249	0.38	1.682	0.653	0.27
Pr	0.57	0.827	1.123	0.11	1.056	0.502	0.1	0.231	0.116	0.254	1.421	0.204	0.109
Nd	3.283	5.297	6.835	1.187	10.323	4.124	1.013	2.962	1.465	3.597	23.893	1.364	1.232
Sm	0.39	2.408	1.937	1.046	2.498	0.598	0.815	2.259	1.642	4.41	5.21	0.722	1.234
Eu	0.077	0.938	0.458	0.52	0.712	0.134	0.379	0.725	0.844	0.868	0.97	0.255	0.734
Gd	0.174	2.084	0.897	1.632	1.809	0.324	1.566	1.98	3.608	1.308	1.83	0.594	3.223
Tb	0.021	0.123	0.139	0.316	0.245	0.027	0.324	0.229	0.707	0.082	0.111	0.063	0.862
Dy	0.093	0.256	0.941	2.289	1.14	0.114	2.592	1.323	4.992	0.281	0.269	0.321	7.23
Ho	0.013	0.021	0.184	0.504	0.173	0.017	0.614	0.266	1.058	0.036	0.026	0.051	1.609
Er	0.043	0.078	0.462	1.568	0.502	0.049	1.936	0.829	3.154	0.122	0.093	0.138	4.587
Tm	0.007	0.024	0.063	0.243	0.099	0.011	0.302	0.125	0.47	0.033	0.029	0.022	0.638
Yb	0.111	0.347	0.517	2.045	0.957	0.166	2.134	0.937	3.306	0.423	0.393	0.244	4.167
Lu	0.032	0.085	0.1	0.284	0.205	0.048	0.331	0.165	0.51	0.107	0.113	0.056	0.548
Hf	0.062	0.42	0.273	0.615	0.68	0.053	0.498	0.629	0.555	0.408	0.484	0.359	1.53
Ta	0.009	0.042	0.032	0.008	0.012	0.012	0.012	0.002	0.003	0.061	0.054	0.012	0.02
Pb	0.062	0.011	0.012	0.026	0.046	0.199	0.139	0.078	0.069	0.063	0.68	0.01	0.004
Th	0.013	0.081	0.039	0.005	0.031	0.015	0.004	0.07	0.008	0.009	0.039	0.01	0.009
U	0.027	0.069	0.085	0.011	0.091	0.022	0.012	0.032	0.015	0.018	0.064	0.022	0.014
Zr/Hf	42	67	43	47	47	60	48	42	96	52	57	46	65
(Lu/Hf) _{c1}	2.1	0.8	1.5	1.9	1.3	3.8	2.8	1.1	3.8	1.1	1	0.7	1.5
(Lu/Er) _{c1}	4.8	7	1.4	1.2	2.7	6.3	1.1	1.3	1.1	5.7	8.1	2.7	0.8
T (°C) Griffin	1098	929	885	1135	923	1172	1169	1194	991	1025	1018	1115	926
T (°C) Canil	1068	964	935	1089	960	1111	1109	1123	1004	1024	1020	1078	962

Table A.2a continued									
	Group RV3								
n	5	6	5	4	5	6	5	5	5
sample	RV55	RV84	RV90	RV110	RV112	RV115	RV119	RV127	RV128
Sc	106	141	190	146	193	227	113	419	179
V	201	251	217	314	292	340	246	226	304
Cr	55565	38856	61265	60242	55801	96340	31183	87700	72776
Mn	2604	3195	3308	2309	3276	3215	2695	2550	2717
Co	33	48	43	44	45	48	47	47	52
Ni	42	41	38	42	40	61	39	60	63
Ga	8.167	2.948	6.288	5.276	4.245	5.082	3.256	1.808	2.095
Rb	0.3	0.028	<d.l.	<d.l.	0.02	0.017	<d.l.	<d.l.	0.025
Sr	0.598	1.479	0.474	0.3	0.379	4.312	1.874	0.967	3.778
Y	18.73	5.348	21.204	2.066	39.793	10.23	1.8	3.982	0.41
Zr	51.107	78.328	73.832	11.058	127.91	84.598	63.752	35.46	5.105
Nb	0.264	0.447	0.171	0.32	0.246	0.227	0.512	0.556	0.41
Ba	0.019	0.437	0.214	<d.l.	0.162	<d.l.	0.122	<d.l.	0.118
La	0.041	0.061	0.043	0.037	0.02	0.172	0.073	0.081	0.135
Ce	0.443	1.307	0.555	0.592	0.274	2.113	1.363	1.06	2.46
Pr	0.19	0.612	0.286	0.228	0.135	0.775	0.544	0.448	0.82
Nd	2.124	4.536	4.016	2.075	1.808	6.685	5.174	4.118	3.725
Sm	1.81	3.422	4.096	0.655	2.182	1.471	2.7	1.878	0.462
Eu	0.799	1.301	1.712	0.189	1.156	0.427	1.099	0.541	0.086
Gd	3.023	4.074	7.01	0.539	5.327	1.82	3.328	1.68	0.193
Tb	0.598	0.439	0.962	0.07	1.059	0.357	0.303	0.192	0.02
Dy	3.937	1.854	5.122	0.449	7.408	2.188	0.912	0.967	0.108
Ho	0.705	0.203	0.796	0.078	1.503	0.359	0.074	0.148	0.019
Er	1.716	0.364	1.85	0.214	4.173	0.859	0.125	0.363	0.053
Tm	0.237	0.043	0.24	0.032	0.576	0.113	0.031	0.05	0.011
Yb	1.637	0.468	1.506	0.288	3.687	0.717	0.374	0.372	0.102
Lu	0.231	0.106	0.219	0.062	0.525	0.113	0.1	0.071	0.032
Hf	1.099	1.312	1.208	0.266	1.838	1.83	1.073	0.788	0.135
Ta	0.019	0.054	0.012	0.028	0.024	0.012	0.039	0.044	0.019
Pb	0.008	0.415	0.195	0.032	0.032	0.114	0.12	0.06	0.115
Th	0.01	0.031	0.048	0.03	0.007	0.016	0.032	0.026	0.04
U	0.024	0.043	0.037	0.027	0.015	0.042	0.047	0.038	0.065
Zr/Hf	47	60	61	42	70	46	59	45	38
(Lu/Hf) _{c1}	0.9	0.4	0.7	0.9	1.2	0.3	0.4	0.4	1
(Lu/Er) _{c1}	0.9	2	0.8	1.8	0.8	0.9	5.3	1.2	3.8
T (°C) Griffin	1031	1022	996	1032	1015	1162	1007	1151	1171
T (°C) Canil	1028	1023	1006	1029	1018	1105	1013	1099	1110

Table A.2b Trace element concentrations of subcalcic garnets from the Lace mine (in ppm)									
	Group L1								
n	4	5	5	5	6	5	7	6	5
sample	L12	L14	L25	L26	L31	L32	L33	L36	L28
Sc	82	117	126	162	128	82	117	122	100
V	264	293	377	361	329	242	316	326	274
Cr	26454	35428	67794	76007	48290	25487	45603	46825	41758
Mn	2282	2873	2785	3184	3349	2202	3024	2467	2293
Co	50	53	49	53	55	48	53	52	52
Ni	52	50	73	56	54	51	55	71	72
Ga	5.706	2.431	7.608	4.422	4.158	5.52	3.267	3.028	3.926
Rb	<d.l.	0.025	<d.l.	<d.l.	0.018	0.019	<d.l.	<d.l.	<d.l.
Sr	0.262	0.322	0.899	1.077	0.557	0.232	0.418	0.579	0.771
Y	5.438	1.016	4.738	0.857	0.917	6.052	1.014	2.541	0.226
Zr	5.928	4.143	19.53	5.494	1.327	7.932	2.939	7.952	7.064
Nb	0.652	0.515	1.053	1.822	0.653	0.547	0.805	0.704	0.691
Ba	<d.l.	<d.l.	0.008	0.391	0.035	0.012	0.08	0.01	1.777
La	0.044	0.147	0.062	0.122	0.042	0.045	0.218	0.092	0.039
Ce	0.545	0.466	0.711	1.38	0.751	0.523	2.6	1.827	0.71
Pr	0.184	0.119	0.254	0.353	0.202	0.185	0.473	0.624	0.278
Nd	1.363	0.633	2.355	2.163	1.085	1.415	2.235	3.762	2.437
Sm	0.582	0.476	1.734	0.556	0.304	0.623	0.446	0.63	0.899
Eu	0.206	0.152	0.669	0.15	0.095	0.22	0.115	0.135	0.205
Gd	0.58	0.49	1.923	0.319	0.262	0.692	0.326	0.349	0.354
Tb	0.1	0.058	0.217	0.031	0.035	0.119	0.041	0.047	0.021
Dy	0.775	0.283	1.008	0.149	0.179	0.904	0.221	0.334	0.062
Ho	0.191	0.04	0.181	0.032	0.031	0.212	0.038	0.087	0.008
Er	0.692	0.096	0.581	0.125	0.097	0.757	0.096	0.383	0.033
Tm	0.128	0.017	0.098	0.031	0.017	0.13	0.013	0.08	0.008
Yb	1.103	0.195	0.848	0.321	0.18	1.113	0.11	0.729	0.111
Lu	0.199	0.047	0.146	0.076	0.042	0.201	0.024	0.146	0.03
Hf	0.142	0.055	0.454	0.116	0.022	0.173	0.074	0.194	0.153
Ta	0.024	0.004	0.024	0.053	0.004	0.016	0.007	0.013	0.015
Pb	0.04	0.047	0.036	0.01	0.023	0.039	0.02	0.024	0.025
Th	0.037	0.047	0.021	0.048	0.005	0.031	0.616	0.023	0.014
U	0.043	0.007	0.046	0.058	0.007	0.036	0.054	0.035	0.032
Zr/Hf	42	75	43	48	60	46	39	41	46
(Lu/Hf) _{ct}	5.9	3.6	1.3	2.8	7.9	4.9	1.3	3.1	0.8
(Lu/Er) _{ct}	1.9	3.2	1.6	4	2.8	1.7	1.6	2.5	5.9
T (°C) Griffin	1104	1086	1234	1131	1116	1097	1123	1222	1226
T (°C) Canil	1072	1061	1145	1087	1079	1067	1083	1138	1141

Table A.2b continued									
	Group L2								
n	4	5	5	3	5	6	5	5	5
sample	L2	L4	L7	L8	L16	L20	L30	L38	L39
Sc	99	91	94	121	122	96	103	99	137
V	144	257	324	185	245	281	188	190	238
Cr	24000	33679	37132	45627	54095	44595	60515	53123	54403
Mn	2691	2201	2048	2948	2792	2341	1918	1918	2842
Co	53	51	49	50	51	52	45	48	48
Ni	23	67	69	48	55	74	63	71	47
Ga	2.153	5.017	3.776	2.908	3.186	4.678	2.303	3.294	3.023
Rb	0.016	0.087	<d.l.	<d.l.	0.019	0.02	<d.l.	0.046	0.017
Sr	0.615	0.496	0.387	0.312	0.718	0.398	0.986	0.714	0.587
Y	1.371	0.57	0.577	3.05	2.23	1.003	0.133	0.293	11.94
Zr	48.17	12.76	12.96	25.84	29.85	20.96	4.044	4.074	58.04
Nb	0.323	0.464	0.503	0.713	0.834	0.617	1.716	0.98	0.95
Ba	0.009	0.228	0.055	<d.l.	0.513	0.005	0.054	0.021	0.032
La	0.018	0.011	0.018	0.022	0.049	0.01	0.093	0.059	0.038
Ce	0.559	0.211	0.327	0.219	0.551	0.207	2.227	0.674	0.562
Pr	0.404	0.153	0.146	0.082	0.318	0.092	0.47	0.286	0.261
Nd	4.52	1.672	1.308	0.893	3.284	1.085	2.369	1.747	3.13
Sm	0.944	0.824	0.682	0.515	1.667	0.607	0.797	0.277	1.769
Eu	0.2	0.221	0.207	0.234	0.576	0.197	0.12	0.055	0.639
Gd	0.551	0.56	0.47	0.852	1.288	0.432	0.158	0.141	2.477
Tb	0.071	0.046	0.045	0.148	0.134	0.052	0.01	0.016	0.479
Dy	0.367	0.188	0.182	0.779	0.589	0.261	0.039	0.07	2.985
Ho	0.052	0.022	0.025	0.122	0.088	0.039	0.006	0.013	0.45
Er	0.134	0.047	0.062	0.3	0.234	0.092	0.019	0.036	0.921
Tm	0.023	0.006	0.011	0.042	0.036	0.012	0.004	0.006	0.092
Yb	0.232	0.125	0.125	0.307	0.307	0.124	0.028	0.065	0.502
Lu	0.055	0.035	0.033	0.05	0.058	0.028	0.008	0.018	0.076
Hf	0.993	0.221	0.271	0.372	0.539	0.499	0.091	0.082	0.918
Ta	0.003	0.006	0.006	0.011	0.018	0.011	0.047	0.014	0.069
Pb	0.113	0.01	0.022	0.019	0.518	0.168	0.024	0.028	0.015
Th	0.005	0.005	0.008	0.006	0.011	0.003	0.024	0.041	0.015
U	0.027	0.013	0.016	0.012	0.045	0.013	0.095	0.042	0.053
Zr/Hf	49	58	48	70	55	42	45	50	63
(Lu/Hf) _{c1}	0.2	0.7	0.5	0.6	0.5	0.2	0.4	0.9	0.3
(Lu/Er) _{c1}	2.7	4.7	3.4	1.1	1.6	2	2.7	3.3	0.5
T (°C) Griffin	861	1197	1211	1071	1121	1239	1174	1222	1070
T (°C) Canil	919	1125	1132	1052	1082	1148	1112	1139	1052

Table A.2c Trace elements of BIR-1 Basalt glass and in house garnet standard- PN2b (in ppm)

n	13			34				
standard	PN2b	relative stdev(%) (1 σ)	std Err(%) (1 σ)	BIR-1 basalt glass standard	relative stdev(%) (1 σ)	std Err(%) (1 σ)	Deletion limite average(ppm)	Eggins et al. (1997)
Sc	78	6.4	1.8	42	13	2.2	0.053	44
V	121	4.1	1.1	310	21.8	3.7	0.03	310
Cr	112	5.3	1.5	416	32.8	5.6	0.912	382
Mn	2910	6.2	1.7	1446	15.8	2.7	0.265	1417
Co	71	4.4	1.2	51	17.6	3	0.027	52
Ni	41	5	1.4	159	11.9	3.8	0.356	166
Ga	6.362	3.3	0.9	12.84	18.7	3.2	0.052	16
Rb	0.029	32.1	9.7	0.18	30.1	5.2	0.09	0.24
Sr	0.276	27.4	7.9	108	10.6	1.8	0.047	110
Y	55.883	8.5	2.3	13.25	12.2	2.1	0.009	16.5
Zr	44.242	8.4	2.3	14.26	11.2	1.9	0.026	14.5
Nb	0.045	21	8	0.518	10.1	1.7	0.012	0.55
Ba	b.d.l			6.33	10.2	1.7	0.033	6.4
La	0.016	33.5	10.1	0.6	9.9	1.7	0.004	0.58
Ce	0.19	20.2	6.1	1.834	12.5	2.1	0.008	1.85
Pr	0.086	8.9	2.5	0.363	10.4	1.8	0.004	0.37
Nd	1.057	7.5	2.1	2.357	9.8	1.7	0.013	2.35
Sm	1.268	7.2	2	1.062	10.2	1.7	0.033	1.1
Eu	0.772	4.6	1.3	0.509	10.3	1.8	0.006	0.52
Gd	3.875	8	2.2	1.606	13.7	2.4	0.034	1.97
Tb	0.962	7.5	2.1	0.314	11.2	1.9	0.005	0.38
Dy	8.762	7.9	2.2	2.354	12.3	2.1	0.013	2.5
Ho	2.123	8.3	2.3	0.509	12.1	2.1	0.003	0.57
Er	6.68	7.9	2.2	1.512	12.4	2.1	0.012	1.7
Tm	0.982	9.1	2.5	0.222	12.6	2.2	0.005	0.27
Yb	6.562	8.4	2.3	1.59	11.8	2	0.003	1.6
Lu	0.926	9.5	2.6	0.227	13.2	2.3	0.005	0.25
Hf	0.838	10.5	2.9	0.557	13.3	2.3	0.008	0.56
Ta	0.005	35.7	13.5	0.037	11.8	2	0.009	0.04
Pb	0.922	59.1	17.1	4.043	12.3	14.5	0.01	3.2
Th	0.004	46.5	15.5	0.03	10.1	1.7	0.007	0.03
U	0.004	21.6	6.8	0.015	16.5	3.8	0.007	0.01

Tables A.3 Lu-Hf and Sm-Nd isotope compositions of subcalcic garnets

Tables A.3a for Lu-Hf isotope: Table A.3a-1: Roberts Victor mine

Table A.3a-2: Lace mine

Table A.3a-3: in house garnet standard (PN3b)

Table A.3a-3: BHVO-1 standard

Table A.3b for Sm-Nd isotope: Table A.3b-1: Roberts Victor mine

Table A.3b-2: Lace mine

Table A.3b-3: in house garnet standard (PN3b)

Table A.3b-3: BHVO-1 standard

Table A.3a Lu-Hf isotope compositions of subcalcic garnets from the Roberts Victor (**Table A.3a-1**) and Lace mine (**Table A.3a-2**); Lu-Hf isotope data for repeated digestion of in house garnet standard (PN3b) (**Table A.3a-3**) and BHVO-1 Basalt (**Table A.3a-4**). The internal precisions for all the Hf runs are less than the external error of the standards. Abbreviations: ID – isotope dilution ; Laser- in situ measurement by Laser Ablation ICP-MS.

Table A.3a-1 Lu-Hf isotope compositions of subcalcic garnets from the Roberts Victor mine								
	sample	ID-Lu(ppm)	ID-Hf(ppm)	$^{176}\text{Lu}/^{177}\text{Hf}$	$^{176}\text{Hf}/^{177}\text{Hf}$	Error (2s)	$\epsilon\text{Hf}(0)$	T CHUR(Ga)
Group RV1	RV 24	0.092	0.075	0.1719	0.290817	0.000006	284	3.02
	RV26	0.037	0.073	0.0703	0.285001	0.000012	79	3.11
	RV 31	0.135	0.036	0.5266	0.310794	0.000015	991	2.96
	RV 93	0.062	0.065	0.1318	0.288261	0.000018	194	2.89
	RV111	0.027	0.071	0.0534	0.283971	0.000006	42	3.06
	RV 123	0.07	0.038	0.2553	0.295319	0.000013	444	2.94
Group RV2	RV12	0.075	0.196	0.0451	0.284192	0.000005	57	6
	RV23	0.141	0.081	0.2435	0.296838	0.000008	494	3.47
	RV54	0.121	0.256	0.0585	0.284582	0.000008	64	3.67
	RV 94	0.16	0.067	0.3327	0.301857	0.000009	672	3.31
	RV 100	0.091	0.127	0.099	0.287279	0.000008	159	3.54
	RV 124	0.094	0.155	0.084	0.286545	0.000005	133	3.83

Table A.3a-2 Lu-Hf isotope compositions of subcalcic garnets from the Lace mine								
	sample	ID-Lu(ppm)	ID-Hf(ppm)	$^{176}\text{Lu}/^{177}\text{Hf}$	$^{176}\text{Hf}/^{177}\text{Hf}$	Error (2s)	$\epsilon\text{Hf}(0)$	TCHUR(Ga)
Group L1	L12	0.201	0.157	0.1825	0.293031	0.000005	363	3.56
	L14	0.039	0.057	0.0982	0.28548	0.000009	96	2.19
	L26	0.07	0.124	0.0801	0.2874	0.000006	164	5.04
	L28	0.028	0.103	0.0391	0.283912	0.000007	40	9.48
	L31	0.039	0.038	0.1451	0.289892	0.000005	251	3.3
	L32	0.198	0.255	0.1103	0.288539	0.000004	204	3.86
	L36	0.137	0.213	0.0912	0.285929	0.000004	112	2.84
Group L2	L2	0.05	1.006	0.007	0.280946	0.000004	-65	3.61
	L7	0.032	0.303	0.0151	0.282708	0.000002	-2	0.19
	L30	0.008	0.096	0.0113	0.281572	0.000005	-42	2.86

Table A.3a-3 Lu-Hf isotope data of PN3b in house standard						
sample	$^{176}\text{Hf}/^{177}\text{Hf}$	$^{176}\text{Lu}/^{177}\text{Hf}$	ID-Lu [ppm]	ID-Hf [ppm]	laser-Lu [ppm]	laser-Hf [ppm]
PN3b-1	0.283022	0.0890	0.49	0.79		
PN3b-2	0.283061	0.0901	0.51	0.81		
PN3b-3	0.283057	0.0883	0.48	0.76		
PN3b-4	0.283087	0.0897	0.42	0.67		
mean	0.283057	0.0893	0.48	0.76	0.52	0.77
std.Err (abs) (2 σ)	0.00002	0.0007				
std.Err (%) (2 σ)	0.007	0.8				

sample	$^{176}\text{Hf}/^{177}\text{Hf}$	$^{176}\text{Lu}/^{177}\text{Hf}$	ID-Lu [ppm]	ID-Hf [ppm]
BHVO-1-1	0.283095	0.00874	0.28	4.50
BHVO-1-2	0.283080	0.00876	0.30	4.90
BHVO-1-3	0.283126	0.00873	0.26	4.19
BHVO-1-4	0.283119	0.00872	0.28	4.50
BHVO-1-5	0.283098	0.00880	0.28	4.59
mean	0.283107	0.00875	0.28	4.53
std.Err(abs) (2 σ)	0.000013	0.00003		
std.Err(% (2 σ)	0.005	0.33		
Blicher-Toft et al.2001	0.283108 \pm 5	0.00876	0.29	4.48
Bizzarro et al. 2003	0.283108 \pm 8	0.00877		

Table A.3b Sm-Nd isotope compositions of subcalcic garnets from the Roberts Victor (**Table A.3b-1**) and Lace mine (**Table A.3b-2**); Lu-Hf isotope data for repeated digestion of in house garnet standard (PN3b) (**Table A.3b-3**) and BHVO-1 Basalt (**Table A.3b-4**). The internal precisions for all the Hf runs are less than the external error of the standards. Abbreviations: **ID** – isotope dilution ; **Laser**- in situ measurement by Laser Ablation ICP-MS.

		ID-Sm (ppm)	ID-Nd (ppm)	$^{147}\text{Sm}/^{144}\text{Nd}$	$^{143}\text{Nd}/^{144}\text{Nd}$	Error (2 σ)	$\epsilon\text{Nd}(0)$	T CHUR(Ga)
Group RV1	RV24	0.78	48.48	0.00974	0.510841	0.000006	-35	1.46
	RV26	0.41	3.92	0.06352	0.510466	0.000012	-40	2.47
	RV31	0.07	1.26	0.03468	0.510515	0.000006	-41	1.99
	RV93	0.04	0.15	0.14609	0.512038	0.000065	-12	1.79
	RV111	0.18	1.53	0.07242	0.510533	0.000011	-41	2.57
	RV123	0.44	2.75	0.10147	0.510501	0.000007	-42	3.39
Group RV2	RV12	4.49	18.1	0.16712	0.511952	0.000008	-13	3.49
	RV23	1.03	5.84	0.11363	0.511261	0.000007	-27	2.51
	RV54	3.75	12.6	0.17981	0.511837	0.000008	-16	7.06
	RV94	0.61	11.76	0.03132	0.511237	0.000007	-27	1.29
	RV100	3.85	30.44	0.07643	0.511328	0.000004	-26	1.65
	RV124	0.95	34.09	0.0171	0.510945	0.000006	-33	1.43

		ID-Sm (ppm)	ID-Nd (ppm)	$^{147}\text{Sm}/^{144}\text{Nd}$	$^{143}\text{Nd}/^{144}\text{Nd}$	Error (2 σ)	$\epsilon\text{Nd}(0)$	T CHUR(Ga)
Group L1	L12	0.57	1.4	0.2471	0.512401	0.000008	-5	-0.71
	L14	0.44	0.75	0.2645	0.511561	0.00001	-21	-2.44
	L26	0.55	2.47	0.1339	0.511835	0.000008	-16	1.94
	L28	0.88	2.18	0.183	0.511881	0.000008	-15	8.21
	L31	0.34	1.2	0.1683	0.511047	0.000007	-31	3.99
	L32	0.69	1.56	0.2675	0.51238	0.000006	-6	-0.55
	L36	0.67	3.75	0.1075	0.510753	0.000008	-37	8.32
Group L2	L2	0.9	4.48	0.1209	0.510631	0.000013	-39	3.19
	L7	0.66	1.38	0.2872	0.512411	0.000007	-4	7.97
	L30	0.79	2.61	0.1843	0.511973	0.000008	-13	-0.38

Table A.3b-3 Sm-Nd isotope data of PN3b in house standard						
sample	$^{143}\text{Nd}/^{144}\text{Nd}$	$^{147}\text{Sm}/^{144}\text{Nd}$	ID-Sm	ID-Nd	laser-Sm	laser-Nd
			(ppm)	(ppm)	(ppm)	(ppm)
PN3b-1	0.7196	0.512876	1.52	1.2		
PN3b-2	0.7227	0.512962	1.54	1.21		
PN3b-3	0.7198	0.512913	1.6	1.29		
PN3b-4	0.719	0.512913	1.51	1.19		
mean	0.7203	0.512916	1.54	1.22	1.53	1.17
std Err(abs) (2 σ)	0.0016	0.000035				
std Err(%) (2 σ)	0.23	0.00692				

Table A.3b-4 Sm-Nd isotope data of BHVO -1 standard				
sample	$^{143}\text{Nd}/^{144}\text{Nd}$	$^{147}\text{Sm}/^{144}\text{Nd}$	ID-Sm (ppm)	ID-Nd (ppm)
BHVO-1-1	0.512937	0.1482	6.4	25.5
BHVO-1-2	0.51292	0.1461	5.9	24.1
BHVO-1-3	0.512929	0.1467	5.9	24.6
BHVO-1-4	0.512971	0.1479	6.4	25.3
BHVO-1-5	0.512934	0.147	6.3	25.1
mean	0.512938	0.1472	6.2	24.9
std.Err(abs) (2 σ)	0.000017	0.0008	0.2	0.4
std.Err(%) (2 σ)	0.0034	0.54		
Raczek et al. 2003; 2001	0.512957 \pm 8		6.2	25

Appendices of figures:

Fig. A.1 Comparison of Lu-Hf ;Sm-Nd concentrations obtained by “in situ” LA-ICP-MS and by isotope dilution (ID) MC-ICP-MS of garnets from the Roberts Victor mine

Fig. A.2 Comparison of Lu-Hf ;Sm-Nd concentrations obtained by “in situ” LA-ICP-MS and by isotope dilution (ID) MC-ICP-MS of garnets from the Lace mine

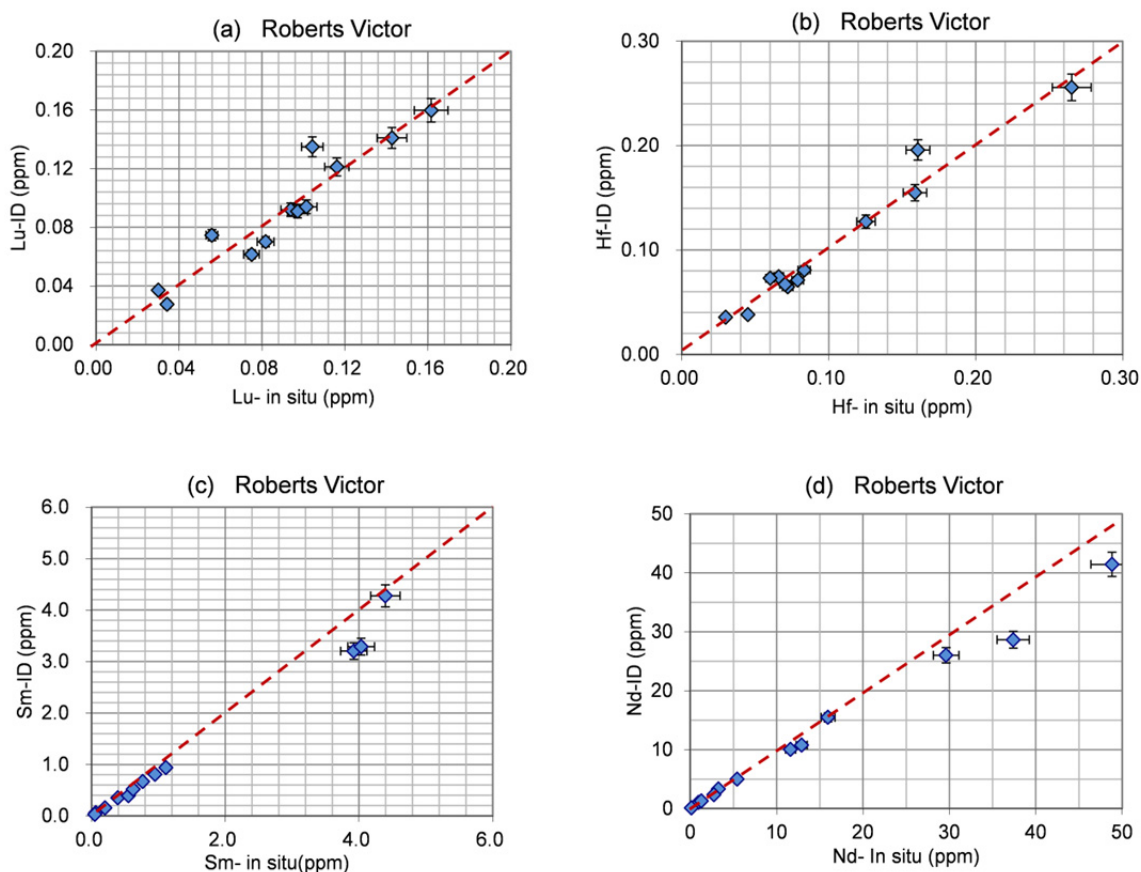


Fig. A.1 Comparison of Lu-Hf ;Sm-Nd concentrations obtained by “in situ” LA-ICP-MS (Table A.2.1 and Table A.2.2) and by isotope dilution (ID) MC-ICP-MS measurements (Tables A.3a-1 and Table A.3b-1) of garnets from Roberts Victor mine . Error bars for the LA-ICP-MS are: around 10% for Lu and Hf in garnets. Error bars for the ID measurements are taken from the errors calculated from the BHVO-1 and PN3b standards (Tables A.3a-3.4 and Table A.3b-3.4). The dash line in each diagram is 1:1 line.

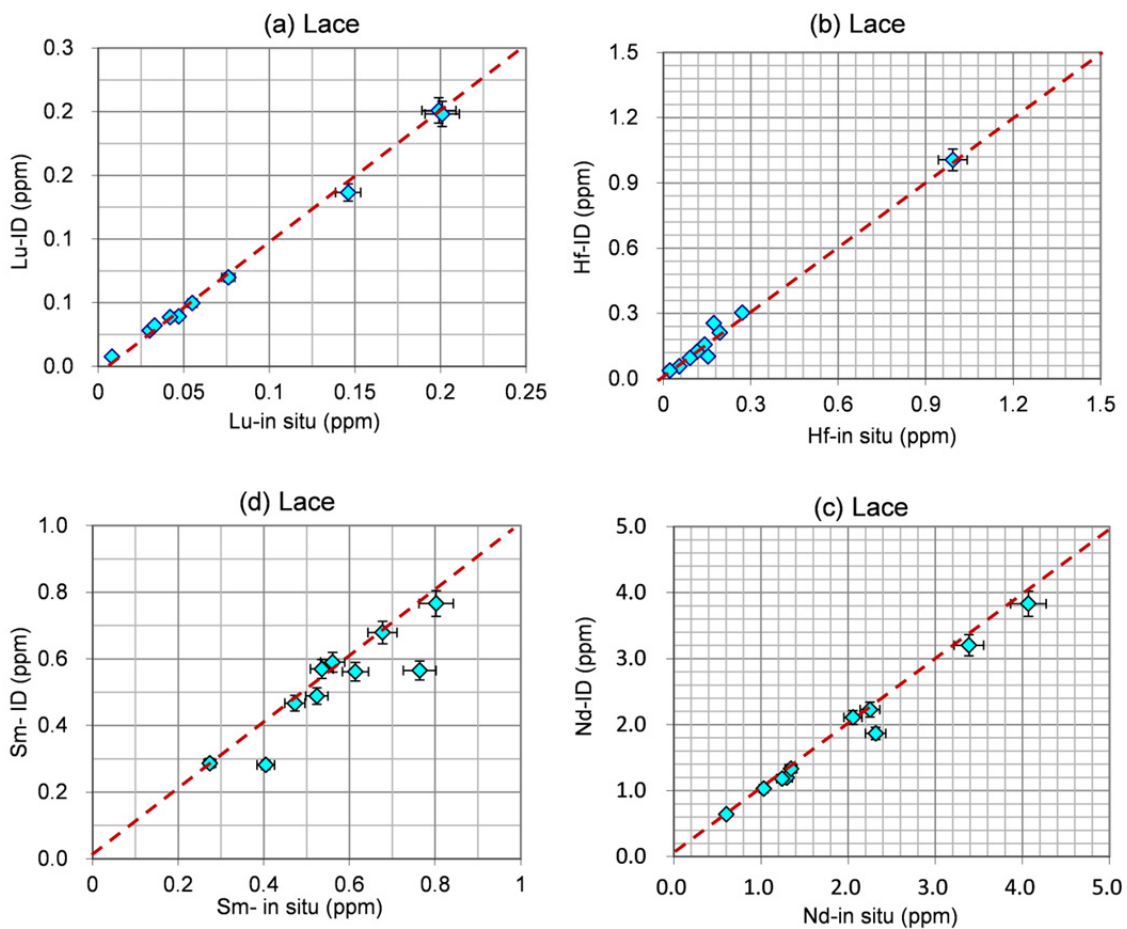


Fig. A.2 Comparison of Lu-Hf ;Sm-Nd concentrations obtained by “in situ” LA-ICP-MS (Table A.2.1 and Table A.2.2) and by isotope dilution (ID) MC-ICP-MS measurements (Tables A.3a-2 and Table A.3b-2.) of garnets from Lace mine . Error bars for the LA-ICP-MS are: around 10% for Lu and Hf in garnets. Error bars for the ID measurements are taken from the errors calculated from the BHVO-1 and PN3b standards (Tables A.3a-3.4 and Table A.3b-3.4). The dash line in each diagram is 1:1 line.

Methods

Major element analysis

A few pieces of each garnet grain were mounted in epoxy and polished for detailed major element analysis by Electron Probe Micro Analyser (EPMA) were carried out in a wavelength-dispersive mode (WDS) with a JEOL JXA 8900RL at Geoth University in Frankfurt. Analyses were performed using an acceleration voltage of 15 kV, a beam current of 20 nA and a spot size of 3 μm . Each grain was randomly analysed on 5-10 spots (depending on the grain size) to ascertain compositional homogeneity to test for compositional homogeneity (the average compositions are given in appendix Table1.). For Al, Cr, Fe, Ti and Ni integration time of 30 s on peak was used and 20 s for Si, Mg, Ca, Na, K, Mn and P. Back ground measurement were run with an integration time of 10 to 30 s at different distances from the peak depending on which element was measured. Standards were natural minerals and pure oxides and metals. The ZAF algorithm method was used for matrix correction. Relative errors are usually 1-2% for major elements. Detection limits for EPM analyses are given in Table A below.

deletion limit	wt%
SiO ₂	0.0426
Al ₂ O ₃	0.0153
CaO	0.0177
MgO	0.0239
Na ₂ O	0.0255
Cr ₂ O ₃	0.0276
TiO ₂	0.0399
FeO ^{tot}	0.0734
MnO	0.0203
K ₂ O	0.0100
NiO	0.0256
P ₂ O ₅	0.0456

Trace element analysis

The trace elements were analysed by Laser ablation -ICP-MS using a New Wave Research LUV213™ ultraviolet Nd-YAG laser coupled with a Finnigan Element 2 at the Goethe University in Frankfurt. The laser was used at a pulse frequency of 10 Hz and an energy pulse of around 0.6 -0.8 mJ (corresponding to 60%-80% laser power). For garnets spot sizes of 60-95 µm was used depending on the sample size. NIST 612 glass was used as a calibration standard with the preferred concentration values of Pearce et al. (1997) and using ⁴⁴Ca as an internal standard isotope. Calcium contents in the minerals had been previously determined by EPMA. The first few seconds ablated at the surface of the sample were discarded when calculating concentrations to avoid surface contamination from preparation and polishing. The presence of inclusions or zoning or cracks within minerals was easily observed and avoided or taken into account when calculating concentrations. Accuracy was within 10% of the recommended values for most elements for BIR 1 basaltic glass reference materials were taken from Eggins et al. (1997) and one in-house garnet standard (PN2b). Aluminium cones were used for garnet analysis to avoid instrumental Ni background from the cones. Accurate Ni values are applied for "Ni in garnet thermometry" of Griffin et al., 1989 and Canil, 1994, 1999. The values, especially for Ni, were checked against one international standard (BIR 1-Glass) and one in-house garnet standard (PN2b), which were always measured several times within the sequence. An analytical accuracy of around 4-5% (2 sigma) on Ni is indicated by multiple analyse on the BIR 1-Glass standards. The average compositions of trace elements are given in appendix Tables A.2 .

Isotope analysis

1). Sample preparation

Our garnets were collected from the heavy mineral concentration from Roberts Victor and Lace mine in the Kaapvaal craton. Each garnet was crushed to small pieces in a Jaw crusher and a hand mortar and sieved. Mineral separates were hand-picked to optical purity. To remove possible grain surface impurities, the separated grains were leached at room temperature in 6 M HCl in an ultrasonic bath for 30 min, afterwards ultrasoniced three times in MQ H₂O and finally dried down. Where necessary the leaching procedure was repeated. Previous work from (DeWolf et al., 1996; Wittig et al., 2007) proved that leaching even at high temperatures (up to 120 °C) with 6 M HCl does not fractionate Lu, Hf, Sm and Nd in silicates. After each leaching procedure the grains were re-picked to optical purity. Finally, 30 to 150 mg of garnet separates was ultrasoniced in MQ H₂O and dried down prior to spiking.

2). Dissolution

Twelve samples from Roberts Victor mine and 10 samples from Lace mine were performed for Lu-Hf and Sm-Nd isotope work. Knowledge of the exact parent-daughter element ratios for low-Hf and Nd in minerals is essential for precise age constrains and therefore all samples were spiked with solutions contain ¹⁵⁰Nd-¹⁴⁹Sm and ¹⁷⁶Lu-¹⁸⁰Hf prior to dissolution. The sample digestion and chromatographic separation of Lu-Hf and Sm-Nd were performed by combining existing protocols for REE, Lu-Hf and Sm-Nd separation (Maboko and Nakamura, 1995; Münker et al., 2001; Pin and Zalduequi, 1997). Samples were dissolved in a Teflon vial in a 3-5 ml mixture high concentrated acids of HF(29N)-HNO₃(15N) (3:1) on a hot plate around 120 °C for three days. After drying down the fluorides, 3-5 ml 6 M HCl was added to remove remaining HF and dissolve the fluorides. If necessary, some samples will be repeatedly treated with 6 N HNO₃ and 6N HCl to remove all remaining fluorides and ensure the complete dissolution.

3). Column chemistry

We used small-size (2-5mm) and Hf-poor samples which make it difficult to duplicate for our subcalcic garnets. Therefore, we used one garnet megacryst (PN3b) as a duplicate. Repeated result from different batches chemistry of this garnet is shown in appendix Tables 3.C and 4.C. As we have very low Hf concentration in samples, mostly 3 to 15 ng, the low Hf blank is crucial for the accuracy of the Hf analyses. Our total procedural Hf blank measured for our methods were from 25 ± 5 pg. For those samples with Hf lower than 5ng, blank corrections were carefully applied.

Therefore, chromatography was always started with the purification of Lu and Hf from the samples matrix, to keep the Hf blank as low as possible. The separation was based on the procedure of Münker et al. (2001) using Eichrom Ln spec resin. However, in contrast to the protocol described in their study, separation of Zr from Hf was omitted, because this may lead to a loss of about 10% Hf during this step. The separation of Zr is not necessary, since it does not affect the precision of the Hf isotope measurement when applied on the multiple collector ICP-MS (Blichert-Toft et al., 1997).

3.1) Lu collection

Lu was separated from the HREE fraction using the column (filled with 1ml Ln-spec resin, inner diameter ~ 5.5mm). The sample was loaded in 1ml 2N HCl, and washed the matrix with 12 ml of 3N HCl and the Lu eluted in 10 ml of 6N HCl afterwards Hf was collected in 12ml of 2N HF. The Hf and Lu cuts were dried down and taken up in an appropriate volume of 2% HNO₃ for mass spectrometry measurements.

3.2) LREE collection

The matrix(from Lu collection step), including the light and middle REE, was dried down and re-dissolved in 1 ml 2 M HCl and the REE were separated using a column filled with a cation exchange resin (Bio Rad 50Wx8). Most important step was the separation of the REE from Fe to avoid overloading the Ln-spec resin, which was used for the Sm–Nd separation (Pin and Zalduequi, 1997). Based on the knowledge from Lazarov et al, 2009, it was possible to reduce the conventional column size (5-10 ml) to 1.5 ml because of our low sample amounts (30-150 mg). After loading the samples on the 1.5ml column, the matrix was separated with 14 ml of 2.2 M HCl prior to eluting the REE with 10 ml of 6 M HCl (Fig. 2.1 from Lazarov, 2009). With this procedure it was possible to separate more than 90% of the Fe from the REE without losing more than 10% of Sm and Nd.

3.3) Sm-Nd collection

Chromatographic separation of Sm and Nd was performed on the same column that was previously used for Lu-Hf purification (with 1 ml Eichrom Ln-spec resin), following the procedure of Pin and Zalduequi (1997). The samples were loaded with 1ml of 0.18N HCl. Then first collect the Nd with 6-7ml 0.25N HCl and Sm were collected separately by the following 3.5 ml of 0.75N HCl. The Nd and Sm cuts were dried down and taken up in an appropriate volume of 2% HNO₃ for mass spectrometry measurements.

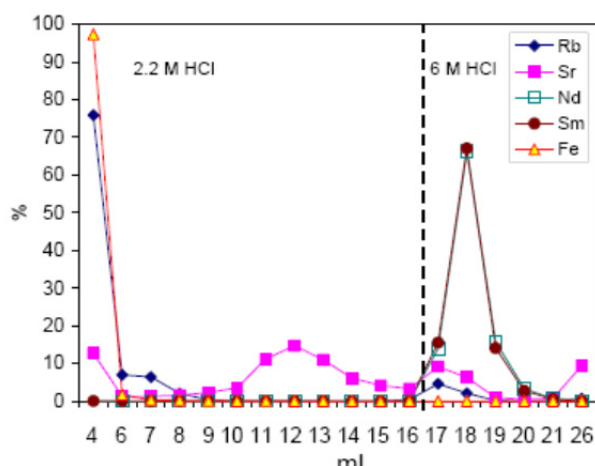


Fig. 2.1. Abundance (in %) of elements eluted with the acid (ml). Separation of REE from matrix on 1.5 ml Bio Rad 50Wx8 column 2. The 2.5 ml of dissolved garnet was loaded on a column, followed by matrix elution with 14 ml 2.2 M HCl and REE were collected with the next 10 ml of 6 M HCl. Dashed line indicate acid change.

4). Analysis

All isotopic composition were analysed in static mode on MC-ICP-MS (Finnigan Neptune) at the Goethe University in Frankfurt. Sample aspiration for Hf and Lu was performed using a Cetac-Aridus desolvating nebulizer, whereas Sm and Nd analyses were performed using a dual spray chamber (wet plasma). Hafnium measurements were performed with the cup configuration, mass bias and interference corrections as described by Blichert-Toft et al. (1997). During our Lu-Hf separation we always collect 30-50% of Yb together with Lu. Therefore, we had to correct for the large mass interference of ^{176}Yb on ^{176}Lu . This was possible with high precision by monitoring the mass bias using the interference free Yb isotopes ^{173}Yb and ^{171}Yb (and assuming a natural $^{173}\text{Yb}/^{171}\text{Yb} = 1.1248$, Blichert-Toft et al., 1997). The amounts of Hf in our samples were always more than 5 ng, except for 4 samples that contained only around 3 ng. With our instrumental set up we were able to measure such low concentrations of Hf (3 ng result in a signal of ~ 90 mV on ^{176}Hf) with a precision of around 1ϵ (on $^{176}\text{Hf}/^{177}\text{Hf}$). The total blank for Hf was always lower than 30 pg, and also was lower than 7 pg for Lu. Blank correction was only significant for some extremely low Hf samples (total Hf is lower than 5 ng). Repeated measurements of the Hf standard JMC475 produced $^{176}\text{Hf}/^{177}\text{Hf}$ of 0.282153 ± 0.000014 (2σ), which is in good agreement with the literature (Blichert-Toft et al., 1997; Chu et al., 2002). Replicate digestion and analyses of BHVO-1 yielded $^{176}\text{Lu}/^{177}\text{Hf} = 0.00875 \pm 0.00003$ (2σ) and $^{176}\text{Hf}/^{177}\text{Hf} = 0.283107 \pm 0.000013$ (2σ). These data are in good agreement with those reported Blichert-Toft et al. (2001) and Bizzarro et al. (2003). The Nd aliquots always contained more than 20 ng, which was measured with a precision of around 0.5 to 1 ϵ , as determined by replicate standard measurements. Our procedural blanks were lower than 70 pg for Nd and 30 pg for Sm. Repeated measurements of Nd isotope standards yielded $^{143}\text{Nd}/^{144}\text{Nd} = 0.511725 \pm 0.000068$ (2σ) (for the Merck Nd_2O_3) and are in a good agreement with literature values (Deckart et al., 2005; Caro et al., 2006). Replicate digestion and analysis of BHVO-1 yielded $^{143}\text{Nd}/^{144}\text{Nd} = 0.512976 \pm 0.000008$ (2σ) that is in a good agreement with the literature values (Raczek, et al., 2001, 2007). Uncertainties of Lu-Hf and Sm-Nd ratios and isotope compositions are based on replicate standard measurements and are 1-2 ϵ for $^{176}\text{Hf}/^{177}\text{Hf}$ and $^{143}\text{Nd}/^{144}\text{Nd}$, and around 0.32% for $^{176}\text{Lu}/^{177}\text{Hf}$ and 0.54% for $^{147}\text{Sm}/^{144}\text{Nd}$.

Chapter 3

Subcalic garnets, mantle metasomatism and diamonds

1. Introduction

The mantle xenoliths collected by kimberlites indicate that the subcratonic mantle underneath the Archean crust is mostly a residue of high degrees of partial melting which was subsequently re-enriched as documented by a depleted major element composition and elevated incompatible element contents when compared to the primitive mantle. (e.g. Boyd and Merzhan, 1987; McDonough and Sun, 1995; Walter, 1998; Kesson and Ringwood, 1989; Herzberg, 1993; Rudnick et al., 1994; Kelemen et al., 1998; Walter 1998; Boyd et al., 1997; Herzberg, 1999; Simon et al., 2007; Pearson and Wittig, 2008; Lazarov et al., 2012). The majority of the xenoliths show either modal metasomatism by introduced mineral phases, such as cpx, rutile, phlogopite (Harte, 1983; Erlank et al., 1987; Gregoire et al., 2002) or cryptic metasomatism (Dawson, 1984) as seen in high abundances of incompatible elements and high compatible elements (e.g. Kesson and Ringwood, 1989; Herzberg, 1993; Rudnick et al., 1994; Kelemen et al., 1998; Walter 1998; Boyd et al., 1997; Herzberg, 1999; Simon et al., 2007; Downes and Dupuy, 1987; Downes et al., 1992; O'Reilly et al., 1991; Neumann, 1991; Neumann et al., 1995; Carignan et al., 1996; Zangana et al., 1997). A major debate is the origin of the overabundance of opx in a substantial number of peridotites from the Kaapvaal and Siberia craton compared to residues from oceanic melting trends and experimental partial melting of peridotites. Boyd et al. (1997) proposed that cumulative processes were responsible for the opx overabundance or metamorphic differentiation. A presently more widely accepted model is that the high opx content is the result of addition of a silica-rich melt from subducted slabs to the mantle (e.g. Kesson and Ringwood, 1989; Kelemen et al., 1992; Rudnick et al., 1994; Kelemen et al., 1998; Bell et al., 2005; Simon et al., 2007; Pearson and Wittig, 2008; Wash et al., 2009). Another model considers the opx-rich mantle portions as metamorphosed serpentinites where Si-enrichment occurs via the serpentinisation process (Schulze et al., 1986; Zhang et al., 2001; Bell et al., 2005; Simon et al., 2007). In recent work by Lazarov et al. (2012) a new model is proposed where opx is enriched as a residual phase of partial melting of carbonated peridotite. Re-enrichment of the depleted mantle is ubiquitous (Dawson, 1984, 1987, 1992; Haggerty, 1987; Menzies et al., 1987; Hoal et al., 1994; Griffin et al.,

1999a; Gregoire et al., 2002; Gregoire et al., 2003). It may be related to process early in the Earth's history as indicated by isotopic data (e.g. Harte et al., 1993; Klein-Ben David and Pearson, 2009 and Lazarov et al., 2009, 2012). However, work from Zhang et al. (2000) or Simon et al. (2003) shows that enrichment also occurred subrecent by kimberlite magmatism.

Much effort has been put into deciphering different kinds of enrichment processes within the mantle (e.g. Dawson, 1982; Menzies and Hawkesworth, 1987; Hoal, 1994; Griffin et al., 1992, 1999(b); Simon et al., 2003; Lazarov et al., 2009, 2012). Bulk rock analytical work on mantle xenoliths from kimberlites cannot avoid contamination from the kimberlite magma and at least 5% kimberlite material can be expected in the bulk rocks which overwhelms the original trace element abundances and isotope composition (e.g. Jacob et al., 2005; Barth et al., 2001, 2002; Simon et al., 2003). Therefore, reconstructed bulk rock compositions from the constituent minerals are favored (Jacob et al., 2005; Barth et al., 2001, 2002; Simon et al., 2003; Lazarov et al., 2012). However, it is difficult to obtain accurate reconstructed bulk compositions, since the modal mineral amounts have to be known precisely

Here, we take a different approach and look into the inventory of subcalctic garnets which stem from cpx-free harzburgites and dunites (Gurney and Switzer, 1973; Sobolev et al., 1973) and are common as inclusions in diamonds (Dawson and Stephens, 1975; Gurney et al., 1984). These subcalctic garnets, commonly with sinusoidal REE patterns, carry the major budget of the trace elements of their host rock. Thus, they are promising objects to study both depletion and enrichment (Lazarov et al., 2012). Most importantly, the analysis of a single grain subcalctic garnet will provide almost all important information of the bulk rock. The low modal abundances (lower than 10%) of subcalctic garnets in the depleted peridotites and their overall low contents of incompatible trace elements make them very susceptible to the subsequent metasomatic overprint as seen in the ubiquitous, but also very variable sinusoidal patterns in the subcalctic garnets. By looking at a sufficiently large number of garnets and using constraints from petrological and geochemical facts this variability provides the opportunity to investigate different kinds of enrichment processes within the subcratonic mantle and to study primary melting processes. The unbeatable advantage of using single garnets or clean garnet separates instead of a bulk rock is that the potential contamination from the kimberlite host magma and the errors in reconstructing bulk rock compositions are avoided.

In this chapter, our aim is to gain detailed information mainly on metasomatism on a craton scale and finally make a tomography of the enrichment agents and their origin within the deep mantle by combining major, trace elements and Lu-Hf and Sm-Nd isotopic signatures from subcalctic garnets. Eventually, we will summarize the metasomatic agent(s) and processes and possibly the timing of the enrichment within the lithospheric mantle underneath the Kaapvaal craton. Also, we will look into the affinity of the episodes of enrichment of these sinusoidal garnets and of diamond formation. The data of subcalctic garnets include 5 different localities on the Kaapvaal craton which cover both West block (Bellsbank, Kimberly and Finsch mine) and east Block (Roberts Victor, and Lace mine). The data from Finsch mine used here are from Lazarov et al. (2009).

2. Geological background of the Kaapvaal craton and sampling localities

The Archean Kaapvaal craton is the continental nucleus of southern Africa. It consists of ca. 3.6-3.7 Ga eastern domain and a younger ca 3.2 Ga western domain (e.g. de Wit, 1990; Eglington and Armstrong, 2004). These two domains amalgamated of by collision at around 2.88 Ga ago along the Colseberg magnetic lineament (Schmitz et al., 2004). The latest major magmatic event was the 2.6 to 2.7 Ga old Ventersdorp magmatic activity which may coincide with the final cratonization of the Kaapvaal craton. Later margin accretion and intra-cratonic igneous activity caused the modifications within the craton, like the 2.05 Ga old Buschveld Complex, the ca. 2 Ga Eburnian orogenic event, followed by the 1.75 Ga Kheis orogeny which reworked the Archean in the west-southwest margin of the Kaapvaal craton (Beukes and Smit, 1987; Alterman and Hoelbich, 1991). The Kibaran event occurred at around 1.2 Ga and formed the Namaqualand by the accretion of the Namaqua and Natal terrains (e.g. Schmitz and Bowring, 2003). The end of the Namaqual-Natal orogenesis is marked by a 950-900 Ma mineral cooling age (Thomas et al., 1993).

The subcalic garnets studied here were collected from the heavy mineral concentration dumps from 4 different diamond mines on the Kaapvaal craton. Data from the Finsch samples are from Lazarov et al. (2009). Purple and violet garnets with diameter larger than 2 mm are used because they generally are sufficiently large to provide the required amounts of elements for wet chemistry. Three sample locations are situated on the west block (Bellsbank, Kimberley and Finsch mine), the Lace mine is situated roughly in the middle of the east block and the Roberts Victor mine is on the western most margin of the East block close to the Colesberg lineament (see Fig. 1 in chapter 2). Except for Kimberley which is a 85 Ma old group I kimberlite), all other kimberlites belong to the older group II kimberlites with eruption around 120 Ma (Smith et al., 1985). To investigate the ancient and possibly multiple metasomatic events, samples from older group II kimberlites are preferred. It appears that this older magmatism had once again overprinted the mantle so that xenoliths and xenocrysts from group I kimberlites are from such recently overprinted mantle portion which are out of internal mineral equilibrium and in which signatures of previous events are erased or falsified as seen from the few samples of this study and was shown earlier by Simon et al. (2007).

3. Results

The analytical techniques used in this study are already described in Chapter 2. They follow closely the procedures already published by Lazarov et al. (2009).

3.1 Major elements

The major element compositions of the subcalic garnets are given in the supplementary **Tables A.1a-e**. A few hundred purple to violet garnets were collected from the heavy mineral

concentrate dumps of 4 different localities (Bellsbank and Kimberley mines on the west block and Lace and Roberts Victor mines on the East block) of the Kaapvaal craton, South Africa. About 500 of them were analyzed by electron microprobe. Seventy nine of them plot into the harzburgitic garnet field in a Cr_2O_3 vs. CaO diagram (Fig.1). These 79 garnets (35 from Roberts Victor, 21 from Lace, 18 from Bellsbank, and 5 from Kimberley) are the objects of this study. They were further analyzed by LA ICP MS for their trace elements and a selection was used for Lu-Hf and Sm-Nd isotope analysis (see Chapter 2). We also combine the data on subcalcic garnets (Lazarov et al., 2009) from the Finsch mine which is located on the western margin of the west block. The subcalcic garnets of our study show a wide range in Cr_2O_3 (2.2-12 wt%) and a wide variation of CaO (0.2-5.5 wt%). Some of them overlap with the main field of garnet inclusions in diamonds which are high in Cr and low in Ca. A substantial number of the garnets has higher CaO contents than these inclusions in diamonds but a similar range in Cr_2O_3 . Garnets from the Finsch mine were divided into two populations (Lazarov et al., 2009): Group I (samples F1) have restricted and low Cr_2O_3 (2-4 wt%) and low, CaO contents (0.2-3wt%); group II (samples F2) are characterized by high CaO (2-5.5 wt%) and high and variable Cr_2O_3 contents (4-12 wt%). The garnets from Roberts Victor mine can also be divided into two populations with a similar range as the Finsch samples: group RV1 has a low and restricted range in Cr_2O_3 and CaO; group RV2 has high CaO and variable and high Cr_2O_3 . The high Cr_2O_3 garnets also overlap with the main garnet inclusion field in diamonds. The subcalcic garnets from the Lace mine are also in a similar range as the Roberts Victor samples. Garnets from Bellsbank have a much restricted compositional range with high CaO (3-5 wt%) and intermediate Cr_2O_3 (4-6 wt%). The five Kimberley garnets overlap with the Bellsbank garnets. The application of the CaO- Cr_2O_3 barometer of Gruetter et al. (2006) using a the 40 mW/m^2 conductive geothermal gradient, gives the minimum pressures because there is no information on coexisting spinel from the single grain garnets. Garnets from Bellsbank yield a tight and low-pressure cluster of 3.2-4.0 Gpa, the Finsch samples equilibrated at higher pressures of 4.2-5.5 Gpa. The garnets from Lace, Kimberley and Roberts Victor broadly yield a similar pressure range from 3.5-5.6 Gpa. The deepest samples are from the Lace mine. A very similar information can be obtained from a projection the Ni-in-garnet thermometer onto the 40 mW/m^2 geothermal gradient (Fig. 2) provided that the averages of the two thermometer version as published by Griffin et al. (1989) and Canil et al. (1999) are used.

The Mg#s of the garnets vary between different localities. On the west block, Bellsbank samples have the lowest average Mg# of 85 and the Kimberley samples yield a similar average Mg# of 86. Finsch garnets have a relatively high Mg# of 88. On the east block, Roberts Victor samples give an average Mg# of 87, ranging from 83 to 89 and the garnets from the Lace mine have on average Mg# =88, from 82-91. These ranges probably reflect more the temperature differences of these depleted rocks and not so much differences in the degrees of depletion.

CaO generally seems positively correlated with TiO_2 (not shown). The Ca and Ti richest samples straddle along the harzburgite-Iherzolite boundary. A positive correlation generally seems to exist with quite a number of further incompatible trace elements which is the expression of enrichment processes.

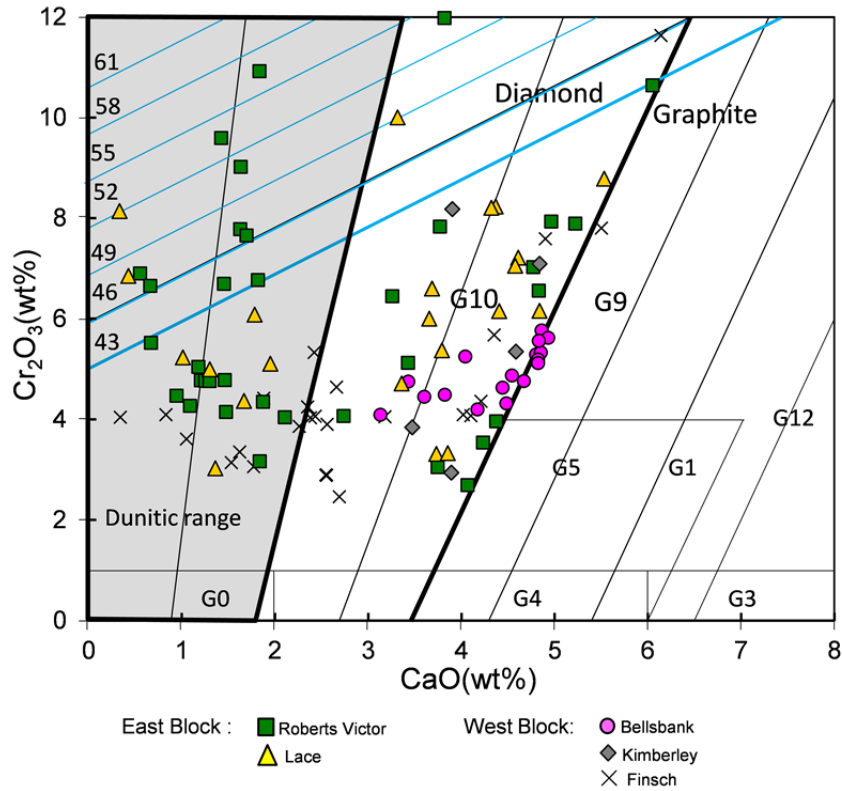


Fig.1 A plot of Cr_2O_3 vs. CaO with the $\text{CaO}-\text{Cr}_2\text{O}_3$ and $\text{Cr}/(\text{Cr}+\text{Al})$ contours from Gruetter et al. (2004) of subcalcic garnets from 5 localities on the Kaapvaal craton (see legend). Data from Finsch are from Lazarov et al. (2009).

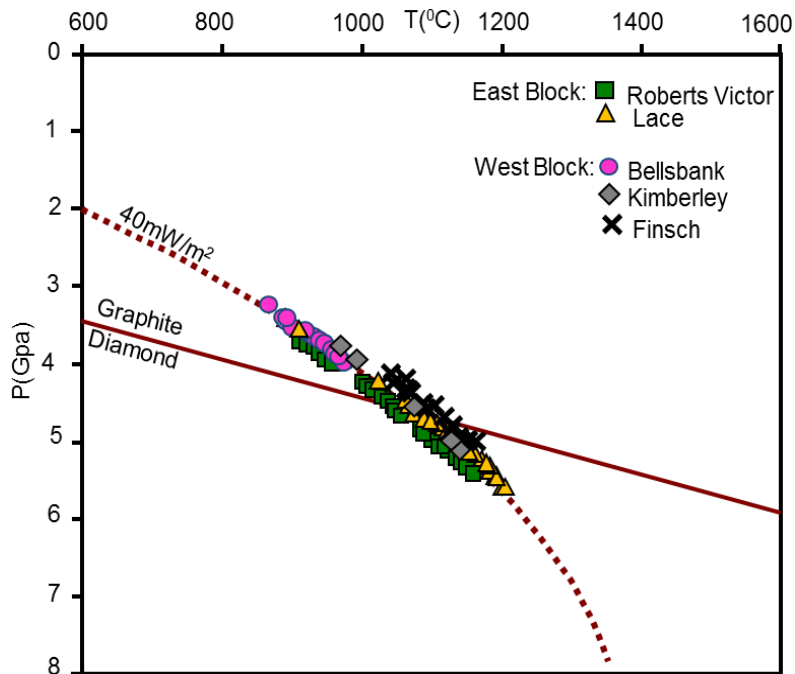


Fig.2 Averages of the Ni-in-garnet temperatures of Canil (1999) and Griffin et al (1989) projected onto a $40\text{mW}/\text{m}^2$ geothermal gradient to estimate the depth of derivation of the subcalcic garnets.

3.2 Trace elements

Few points have to be taken into consideration, before we try to explore the enrichment agents based only on the composition of single garnet grains from depleted and reenriched harzburgites. The first is which other minerals may have equilibrated with garnet. The two main phases are opx and olivine. Because of the extremely small contribution to the bulk budget which can come from olivine for many elements, only opx can be a competitor for garnet due its potential high modal abundance in the Kaapvaal peridotites. Garnet and opx partition coefficients are shown in Fig.3. The high Ti and Sr partition coefficients in opx and high abundance relative to garnet are the cause that more than 80% of Sr will reside in opx, and more than 50% of Ti. This may cause the negative anomalies as they are observed in most subcalic garnets trace element patterns. Therefore, such anomalies may not be taken to characterize an enrichment agent. Garnet, opx and olivine all have fractionated REE patterns in their partition coefficients. Therefore, fractionated REE patterns in a residue can be produced during melting either by the presence of garnet or in the absence of garnet by high degrees of melting leaving opx and ol alone in the residue. But a residue with high HREE contents can only be left, if garnet was a residual phase during melting.

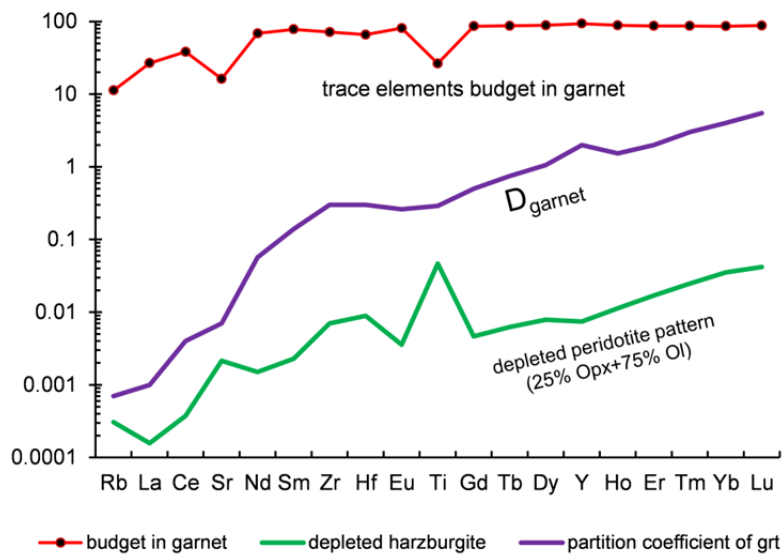


Fig.3 The potential distribution of trace elements in a cpx-free garnet harzburgite calculated from experimental partition coefficients and assumed modal olivine and opx abundances. The partition coefficients for garnet, opx and olivine are a compilation of experimental work (Beattie P., 1994; Hauri et al., 1998; Johnson K.T.M.,1998; Green et al., 2000; Adam and Green, 2006; Tuff and Giboson, 2007). The compilation is given in the appendix **Table A.4**. The green pattern corresponds to that of the abundances of a depleted peridotite with 25% opx and 75% olivine (i.e. the y-axis is used as a scale like a chondrite normalized pattern). The second use of the y-axis is as a scale for the partition coefficients of garnet. And for the third purpose it is used to demonstrate in % how much of a trace element budget resides in a garnet, which crystallized from the depleted peridotite by subduction or cooling. This is the red pattern with black circles. It shows for a garnet harzburgite with 5% garnet, 25 % opx and 70% olivine how much of the trace element inventory is sitting in the garnet. Most trace elements shown here partition into garnet varying from 80 to 96% except for the most incompatible elements, like Rb, La and Sr. Strontium resides in opx and causes low Sr in garnet. Titanium is partitioned into opx to a lesser extent but may still cause an anomaly in garnet.

The trace elements were measured by Laser ablation-ICP-MS. There is no zonation observed within each garnet. Therefore, the average concentrations of 3 to 10 analyses from random pieces of each garnet are presented in **Tables A.2 a-e** in the appendix. All garnets show minor to very significant enrichments in incompatible elements, such as the LREE, or even the MREE, and depleted and non-depleted HREE. The majority are sinusoidal patterns which are similar to those observed by Stachel et al. (1998) and Stachel et al. (2008) for subcalic garnet inclusions in diamonds. It appears, however, that the subcalic garnet xenocrysts generally have much higher Sr abundances than the inclusions in diamonds. A number of subcalic garnets have distinguished primitive mantle normalized garnet patterns, which are flat in HREE and depleted in LREE and MREE. Such patterns are commonly described from lherzolitic garnets. There is no clear connection between the trace element patterns with the major elements of the garnets. However, generally, the extent of incompatible element enrichment appears to have a positive correlation with CaO and TiO₂ and negative correlation with Mg numbers.

3.2.1 Garnets from the Roberts Victor (East Block)

Both the trace element concentrations and patterns display extreme variations in the garnets (Fig.4a and b). The concentrations of incompatible elements in subcalic garnets show minor to extensive enrichment and low and fractionated HREE. The concentrations of some elements, like Zr, Hf, and certain trace element ratios are used to diagnose the subsequent enrichment agents. The diversity of the trace element patterns of Roberts Victor garnets allows us to divide them into three extreme groups: a) a group RV1 with the least enrichment (light blue patterns in Fig. 4), b) a group RV2 with intermediate enrichment (dark blue patterns) and c) a group RV3 with the most enrichment (pink patterns)). In the following we use the subscript N to express that an element content is normalized to primitive mantle.

Group RV1 garnets (light blue patterns) have weak sinusoidal patterns are characterized by least enrichments in the MREE [(Eu)_N=0.11 to 0.66], a peak at Nd [(Nd)_N is mostly between 0.01 and 2.2, but one has an extreme value of 39] and low HREE abundances, but strongly fractionated HREE patterns. The HREE continuously and smoothly decrease from Lu to Gd or Y which we take as the original pattern left from the partial melting process.

Most of the incompatible elements contents in group RV2 garnets (dark blue patterns) are enriched and show peaks at Nd, [(Nd)_N is up to 40], and humped MREE, but depleted and fractionated HREE patterns. Both group RV1 and RV2 garnets have similar sinusoidal. In a spider diagram (Fig. 4b), most of the RV1 and RV2 garnets show positive Nb-Ta and LILE, but negative Zr-Hf and Ti anomalies. The Zr/Hf ratios are superchondritic and both RV1 and RV2 show positive U anomalies

Group RV3 garnets (pink patterns) are overall enriched in all trace elements and have maxima at the MREE as their common feature. Most of the group RV3 garnets show high and flat HREE to MREE patterns, but a few have pronounced sinusoidal patterns. There seems to be a complete transition from these to those with flat middle and heavy REE. They have minor or no negative Zr-Hf anomalies with superchondritic Zr/Hf ratios. They also show Ti negative anomalies but with higher Ti

abundances compared to the other two groups. A strong Sr anomaly is universal in all sample which may be because of coexisting opx.

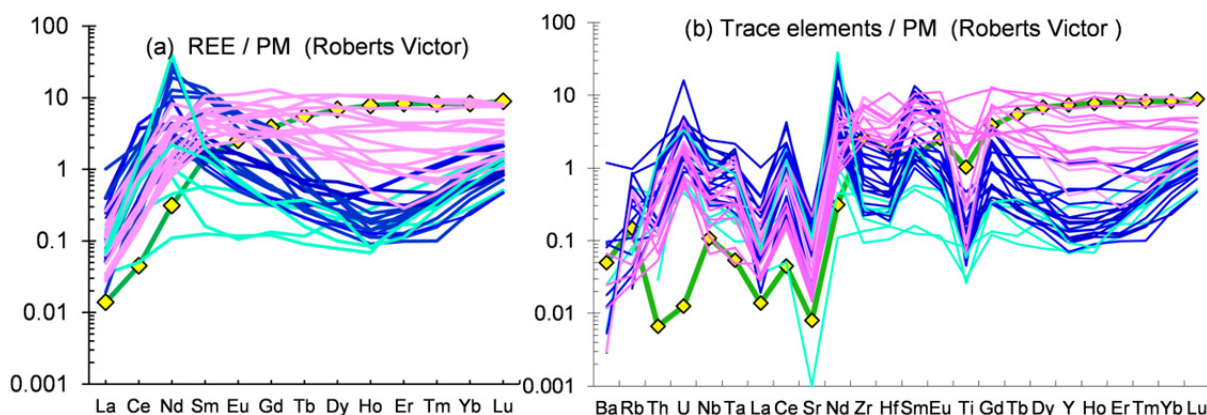


Fig.4 Primitive mantle (McDonough and Sun, 1995) normalized REE **(a)** and spider diagram **(b)** of the subcalcic garnets from Roberts Victor: Three types are distinguished, the least enriched group RV1 (light blue patterns), the intermediately enriched group RV2 (dark blue patterns) and the most enriched group RV3 (pink patterns). The green pattern with yellow diamonds is the trace element composition of a garnet from a primitive garnet peridotite 313-105 from Vitim in Siberia (Ionov et al., 2005). It will also be shown in all further similar diagrams.

3.2.2 Garnets from Lace (East Block)

The primitive mantle normalized trace element patterns of Lace garnets (Fig. 5) show enrichment in most incompatible elements (except Rb, Sr and Ba) and fractionated and depleted HREE patterns compared to the primitive Vitim garnet. Three groups can be identified based on the trace element patterns (groups L1, L2, L3). Group L1 garnets (blue patterns) are characterized by pronounced to weakly expressed sinusoidal REE patterns with peaks at $(Nd)_N$ or $(Sm)_N$. Their common features are steeply sloped HREE from Ho, Er or Tm to Lu and a compressed range of LREE abundances. Samples L12 and L32 are shown separately in Fig. 5c and to emphasize their positively sloping middle to heavy REE, their overall higher HREE abundances and their sinusoidal character which is only weakly pronounced. The more incompatible elements are enriched in group L1 with positive Th-U and Nb-Ta and negative Zr-Hf and Ti anomalies. Group L2 garnets (pink patterns) also are sinusoidal but their maxima lie at the MREE which are overall higher than for L1 and L3. A further distinguishing feature is that they are highest in the HFSE (Nb, Ta, Zr and Hf). Group L3 (black patterns) have the highest LREE to HREE abundances with slopes parallel to the two L1 samples (L12 and L32). The LREE seem slightly elevated (Fig. 5c). They do have positive Zr-Hf and Ti anomalies like the L2 samples but at lower abundance levels. Like all other groups they do have strongly positive U and Th anomalies.

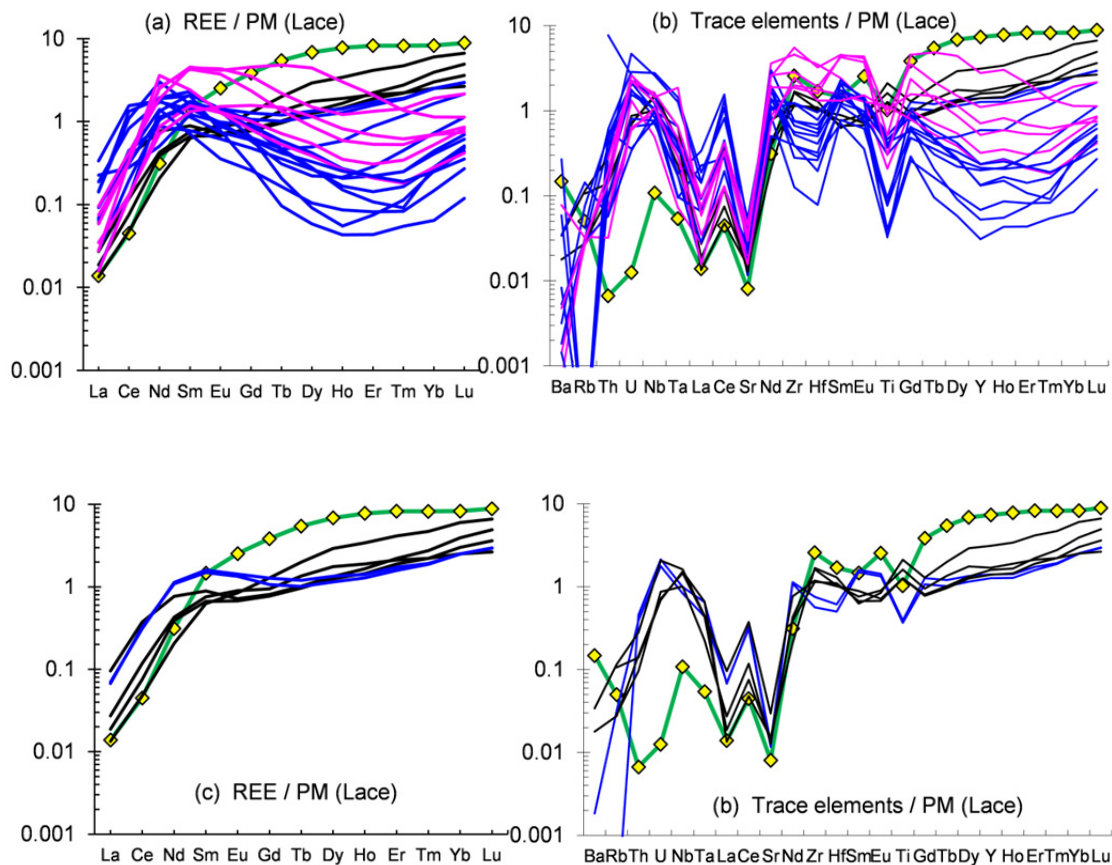


Fig.5 Primitive mantle (McDonough and Sun, 1995) normalized REE **(a)** and spider diagrams **(b)** of subcalctic garnets from Lace. Three garnet groups are distinguished: groups L1 (blue patterns), L2 (pink patterns) and L3 (black patterns) Diagrams **(c)** and **(d)** show the REE and trace element patterns group L3 (black patterns) and the two least enriched garnets (blue patterns) from group L1 for a better comparison.

3.2.3 Garnets from Bellsbank (West Block)

The majority of the subcalctic garnets from Bellsbank show sinusoidal primitive mantle normalized REE patterns (Fig.6a). They are divided into two groups Group B1 garnets (blue patterns) have low HREE ($(Lu)_N = 0.2 - 1$), and MREE abundances which are positively sloped from Dy to Lu. The maxima of the sinusoidal patterns lie at $(Ce)_N$ or $(Nd)_N$. The spider diagram (Fig. 6a) shows the low concentrations of Zr and Hf and Nb and Ta of group B1 garnets. Group B2 garnets have much higher MREE and Zr and Hf contents. Their maxima in the REE patterns lie at $(Sm)_N$ or $(Eu)_N$ with decrease to $(Er)_N$ or $(Tm)_N$ or $(Lu)_N$. Two of the group B2 garnets are not sinusoidal at all but have negative Zr/Hf and Nb/Ta anomalies.

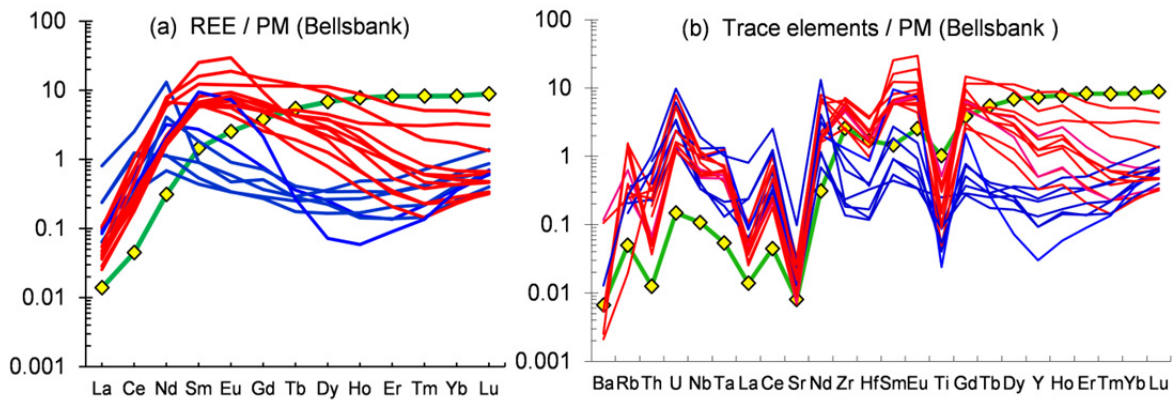


Fig.6 Primitive mantle (McDonough and Sun, 1995) normalized REE **(a)** and spider diagrams**(b)** of the subcalcic garnets from Bellsbank mine: Two types of garnets can be distinguished from their minor element patterns, the less enriched group, here inferred to group B1 (blue patterns) and the more enriched group here noted as group B2 (red patterns). The green pattern with yellow diamonds is that of a garnet from a primitive garnet peridotite 313-105 from Vitim in Siberia.

3.2.4 Garnets from Kimberley (West Block)

The primitive mantle normalized REE patterns of the garnets from Kimberley also have sinusoidal REE patterns. The REE patterns of the two distinguishable groups K1 (blue patterns) and K2 (red patterns) (Fig. 7) are very similar to those of the Bellsbank B1 resp. B2 groups. $(REE)_N$ maxima also lie at Nd resp. Sm+Eu.

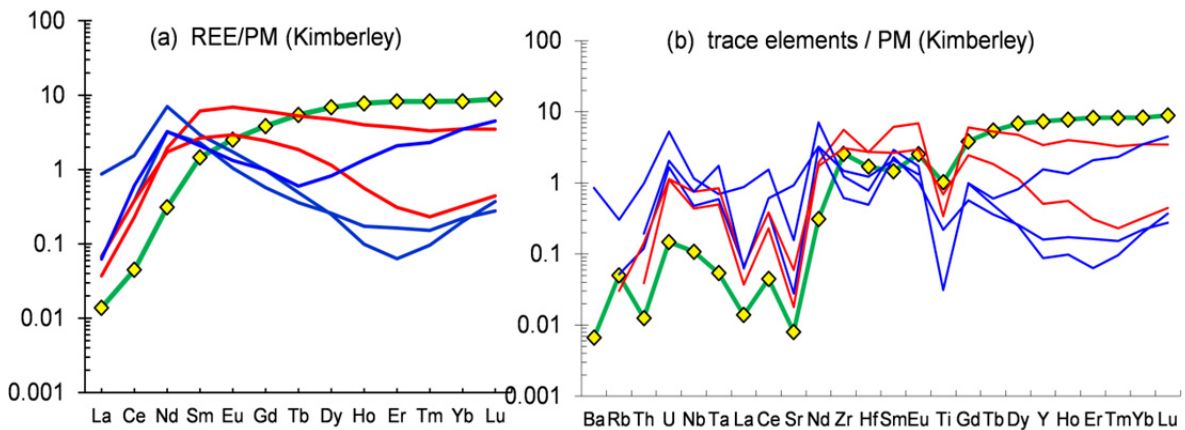


Fig.7 Primitive mantle normalized REE **(a)** and spider diagrams **(b)** of the subcalcic garnets from Kimberley: Two types of garnets K1 (blue patterns) and K2 (red patterns) are distinguished.

3.2.5 Garnets from Finsch (West Block)

The trace element data of Finsch garnets are taken from Lazarov et al. (2009) and their PM-normalized trace element patterns reproduced here (Fig. 8). They are similar in shape to those of garnets from the other localities. Two groups were distinguished: the blue patterns represent group F1 and the red group F2. The overall trace element abundances of group F1 are lower than for group F2. They have their maxima at the MREE (Sm or Eu) while group F1 have a spike at Nd.

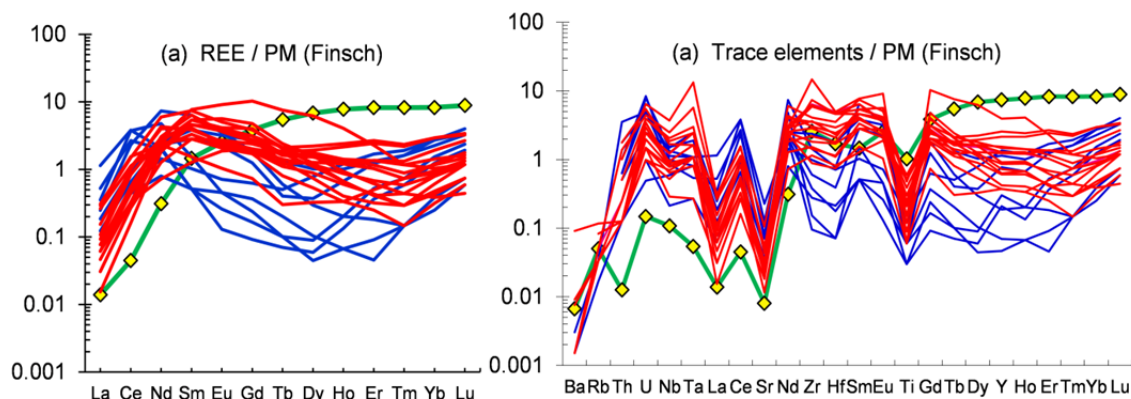


Fig.8 Subcalcic garnets from Finsch (data form Lazarov et al., 2009): Two garnet groups were distinguished: group F1 (blue patterns) and the more enriched group F2 (red patterns) shown as REE (a) and spider diagrams (b).

3.3 Sm-Nd and Lu-Hf Isotopes

Isotope analyses were performed only on a reduced number of garnets which were selected according to criteria given in Chapter 2 (e.g. superchondritic Lu/Hf and Lu/Er ratios which indicate the least degree of metasomatism). Detailed information of the analytical methods is also given in chapter 2. The Lu-Hf and Sm-Nd isotopic results will include two further localities, Bellsbank and Kimberley, are given in **Table A.3a-e** in the appendix and shown in Fig. 9.

3.3.1 Sm-Nd and Lu-Hf isotope compositions from the West Block (Bellsbank, Kimberley and Finsch)

The data are shown in Fig. 9a as present day ϵ_{Hf} values plotted against ϵ_{Nd} . The two garnet groups with pronounced sinusoidal REE patterns (less enriched) from Finsch (F1) and from Bellsbank (B1) almost exclusively plot in quadrant I of this figure. They give extreme radiogenic ϵ_{Hf} values ranging from +35 to +630 for Finsch and +16 to +164 for Bellsbank. But they also give very unradiogenic ϵ_{Nd} values from -36 to -11 for Finsch and from -27 to -2 for Bellsbank. This shows that the Sm-Nd and Lu-Hf systems were decoupled for a long time. The more enriched groups F2 from Finsch and B2 from Bellsbank (less pronounced to no sigmoidal REE patterns) and the Kimberley garnets plot in all four quadrants and closer to the present day oceanic array but partly with extreme deviations to either side.

3.3.2 Nd and Hf isotope compositions from the East Block (Roberts Victor and Lace)

The isotope data from Lace and Roberts Victor were already reported in Chapter 2. Here, we show only their ϵ_{Hf} and ϵ_{Nd} values in Fig. 9b. Both groups RV1 and RV2 have more or less pronounced sinusoidal REE patterns and were distinguished only by lower incompatible trace element abundances in RV1 compared to RV2. The third group RV3 with overall very high REE contents and flat middle to heavy REE was not analysed for isotopes. Both groups RV1 and 2 plot into quadrant I in

Fig.9b, the field with radiogenic Hf and unradiogenic Nd. This is coincident with groups F1 from Finsch and B1 from Bellsbank. The L1 samples from Lace also plot mostly in this quadrant, but L2 plots into quadrant IV, the quadrant with unradiogenic Hf and Nd. Two group L3 samples also plot in Quadrant I and the other two plot close to the present day oceanic array.

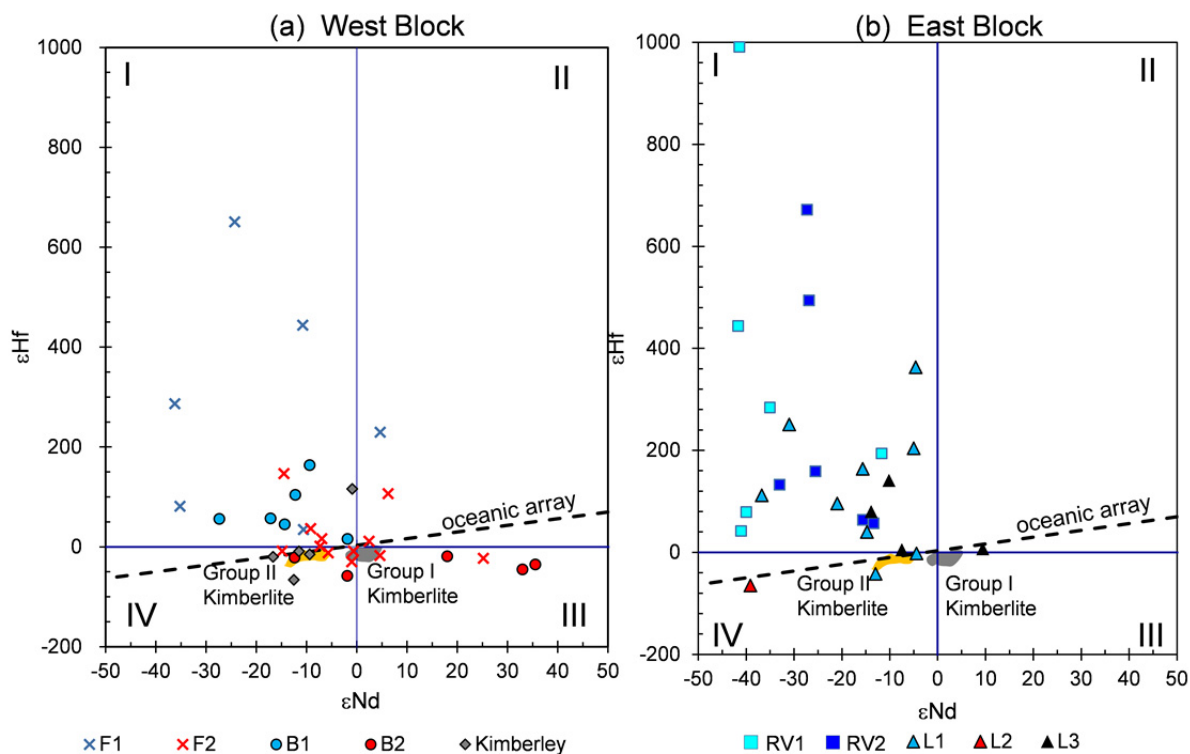


Fig.9 Present day ϵ_{Nd} vs. ϵ_{Hf} diagram of subcalpic garnets from the West Block (a) (Bellsbank: blue circles = B1; red circles = B2; Kimberley = grey diamond; Finsch: blue crosses = F1; red crosses = F2; Figure a), and from the East Block (b) (Lace: blue triangles = L1; red triangle = L2; black triangles = L3; Roberts Victor: light blue diamonds = RV1 and dark blue diamonds = RV2 in Figure b). The present day oceanic array is shown by the black dashed line which is defined as $\epsilon_{Hf} = 1.33 \times \epsilon_{Nd} + 3.19$ (Vervoort et al., 1999). The group I kimberlite fields (grey shaded) and group II kimberlite field (yellow shaded) are also shown for comparison (Nowell et al., 2004).

4. Discussion

4.1 The enrichment agents and processes

We divided the subcalpic garnets from each locality into two or three groups according to the trace element abundances and patterns and the Nd and Hf isotope ratios. The less enriched groups were noted as groups 1 and the more enriched as groups 2 and, for Roberts Victor and Lace, further, most enriched group 3. However, the most incompatible elements show similar abundances and patterns in all groups. The differences are mostly displayed in the middle REE and HFSE abundances and their ratios. They can be used to identify the enrichment agents and possible processes. A widely

used diagram for that purpose is a plot of Y versus Zr in garnet for which Griffin et al. (1999b) provided fields of depleted and undepleted mantle and fields for metasomatic agents (see Fig. 10 and 11).

The almost non-enriched group RV1 garnets (light blue squares) are restricted to the bottom left corner of the depleted garnet field with 1-3.1 ppm Zr and 0.3 -1.3 ppm Y. Group RV2 garnets (dark blue diamonds) also plot in the depleted area, but with higher Zr from 2 to 28 ppm, and restricted Y from 0.3 to 2.2 ppm. Group RV3 garnets fall in- and outside the metasomatic fields. Garnet compositions from Lace are more restricted: both L1 (blue triangles) and L2 (red triangles) garnets fall in the depleted area except for two, which plot in the phlogopite and melt metasomatism field. The L3 garnets (black triangles) plot on the border between the depleted and silicate enriched field. B2 garnets (red circles) from Bellsbank also fall into the metasomatic fields and group B1 (blue circles) into the depleted area (Fig.11a). All group-F1 garnets (blue crosses) from Finsch are restricted to the depleted field (Fig.11.b) and Finsch F2 garnets (red crosses) show a trend from the depleted to the fluid enrichment field. The three group-K1 garnets (blue diamonds) are in the depleted garnet field and the two group K2 (red diamonds) in the low-temperature fluid enrichment field (Fig.11.c).

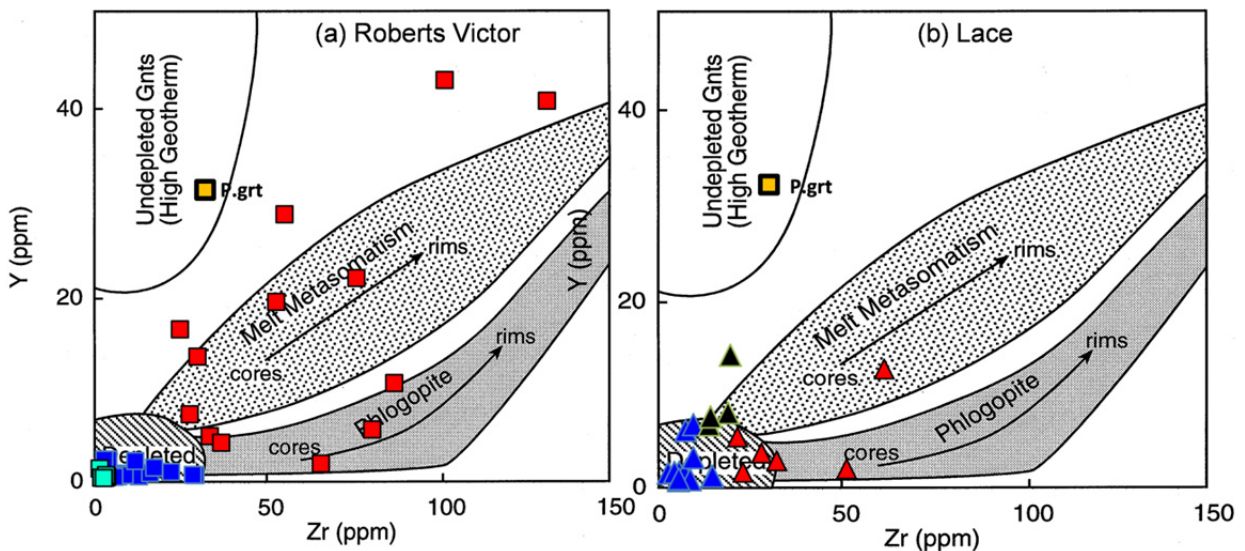


Fig.10 Diagram of Zr versus Y of the subcalcic garnets from Roberts Victor and Lace on the East block. Griffin et al. (1999b) designated compositional fields for depleted and undepleted and enriched mantle. These “drawers” probably hold for the relatively compatible elements but not for the more incompatible elements because most of the samples in the “depleted field” are re-enriched in LREE. According to Griffin et al. (1999b) the phlogopite field stands for intense fluid metasomatism at relatively low temperature with enrichment in Zr but negligible addition of Y. The melt metasomatism field with addition of both Zr and Y stands for high-temperature silicate melt metasomatism. The yellow square stands is the composition of garnet from a primitive garnet peridotite from Vitim. (Roberts Victor (a): light blue squares = RV1; dark blue squares = RV2; red squares = RV3), (Lace (b): blue triangles = L1; red triangles = L2; black triangles = L3)

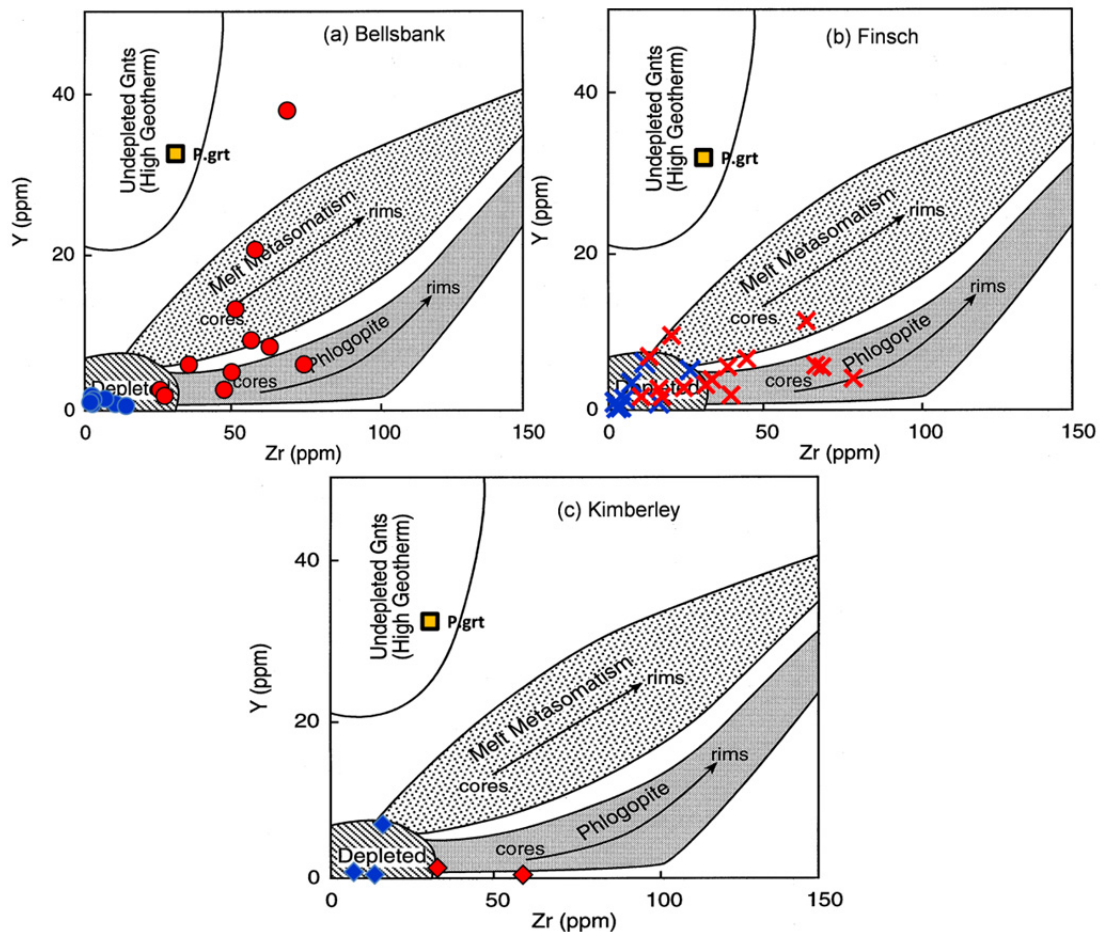


Fig.11 Diagram of Zr versus Y of the subcalcic garnets from the in West block: (Bellsbank (a): Blue circles = B1; red circles = B2; Finsch (b): Blue crosses = F1; red crosses = F2; Kimberley (c): -blue diamonds = K1; red diamonds = K2

Clearly, these Zr-Y petrogenetic fields provide quite a powerful tool to identify the agents that caused severe enrichment in HFSE and more compatible elements, like Y and the HREE. But they cannot make the fine distinctions for less enriched samples which are expressed in the more incompatible elements. Because the modal abundance of subcalcic garnets in a harzburgite is low and because garnet is the only phase in these depleted rocks with relatively (to opx and ol) high partition coefficients for the generally incompatible elements it will sensitively react to infiltrating metasomatic agents. Looking at those garnets with relatively little chemical overprint (those in the “depleted” fields in Figs. 10 and 11) the fingerprint of the metasomatizing agent should be better identifiable.

For this purpose we calculated the trace element composition of the potential melt or fluid which had been in equilibrium with garnet from each sample. At first, we assumed that the garnets were last in equilibrium with a silicate melt and used the trace element partition coefficients from the experimental work of Green et al. (2000) between basaltic melts and garnet. These results are not shown because a melt in equilibrium with garnets with very steep negative slopes in the HREE (as is the case for all group 1 and 2 garnets) has to be very depleted in these elements. The calculations with the silicate partition coefficients lead then to very high abundances of the more incompatible

elements. The trace element patterns of such a melt would have very steep negative slopes with extreme LREE abundances higher than kimberlitic magmas.

Basaltic compositions or compositions corresponding to TTGs [an example for such compositions was taken from the experimental work of Rapp et al. (1999) and is shown in Figs. 12 to 16 as “melt (30%) of eclogite”] cannot be the metasomatizing agents of these garnets. They were rather equilibrated with an agent which had extremely fractionated trace element patterns like carbonatitic to silico-carbonatitic melts. Giris et al. (2012; revised version submitted to *Lithos*) provide a very comprehensive set of trace element partition coefficients between mantle minerals and silico-carbonatitic melts which they derived from high pressure experiments. The results of these calculations are shown in Figs. 12 to 16 as PM-normalized trace element patterns calculated for each sample (green patterns). Also shown in these figures are the compositions of three carbonatites from Uganda (red patterns; Nelson et al., 1988), the trace element compositions of fluid inclusions in fibrous diamonds (light blue patterns; Tomlinson et al., 2009) and high density fluids also in fibrous diamonds (dark blue patterns; Klein-BenDavid et al., 2009).

Most calculated melt patterns from each locality show extremely high LREE and strong negative Zr-Hf anomalies and very low middle to heavy REE. The HREE calculated for melts in equilibrium with group 1 and group 2 garnets from Roberts Victor, Lace and Finsch and for group 1 from Bellsbank appear unusual at first because they still show positively sloped patterns beginning either at Er (RV1 and F1) or Tm (RV2, L1, L2, F2, B1). This only reflects the fact that the HREE contents and patterns in these garnets are still mostly those of the protoliths which were left as residua from the partial process. Both the amount of the interacting fluids and their HREE contents were too low to seriously affect the HREE in the garnet. Groups RV3, L3, B2 and K1 and K2 were more seriously overprinted and lost their original signature. The calculated melt compositions show many similarities with the natural carbonatites from Uganda (Nelson et al., 1988) although these are not directly derived from the mantle. The calculated melt compositions are sandwiched between the (carbonate–K–chloride–H₂O) fluid inclusions in fibrous diamonds given by Tomlinson et al. (2009) and the high density (carbonatitic to kimberlitic) inclusions in other fibrous diamonds (Klein-BenDavid et al., 2010). Melt compositions with continuously negative, but less steep sloping trace element patterns and much smaller Zr/Hf and Ti anomalies were only calculated for the very enriched RV3, B2 and K1 and K2 garnets. Group L3 garnets potentially are direct precipitates from a melt. Their metasomatizing agents most have been different and more akin to silicate melts.

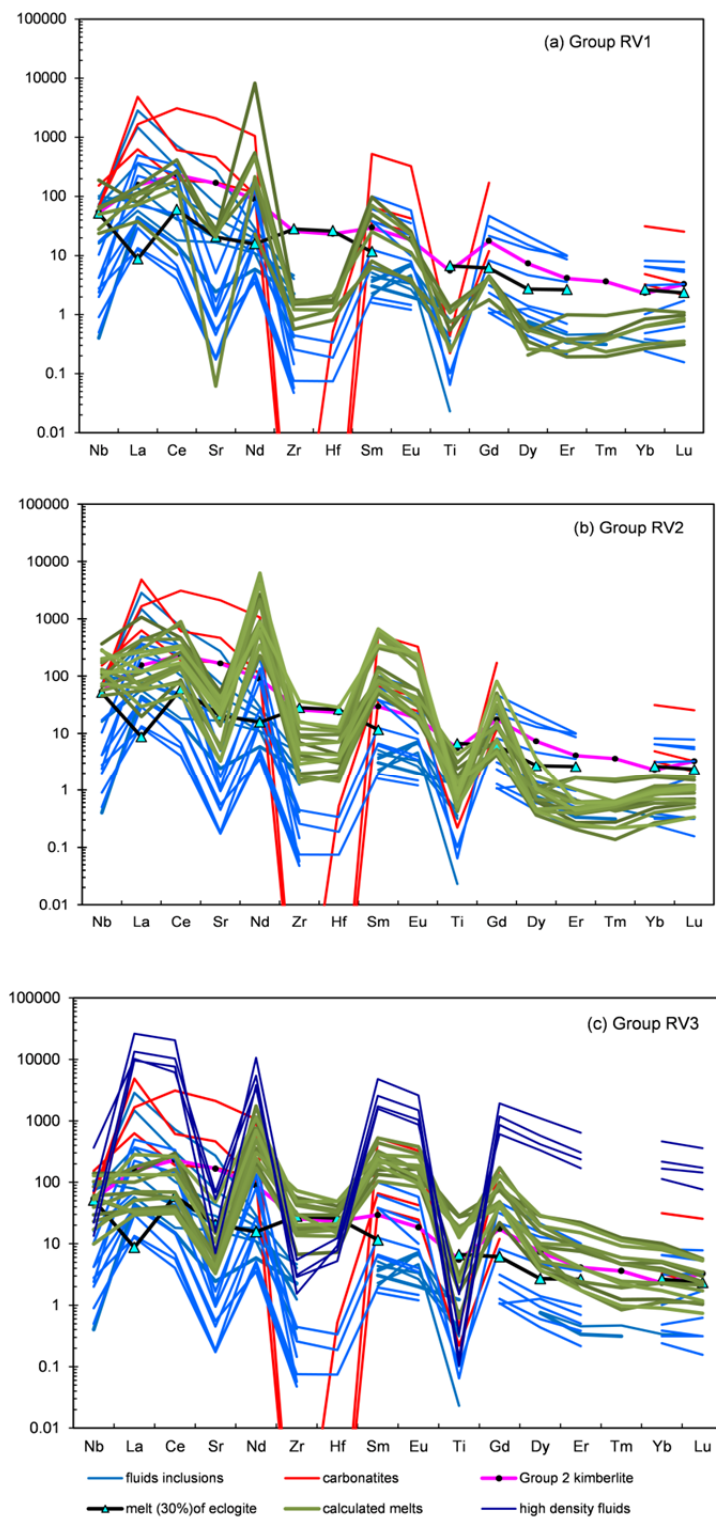


Fig.12 Calculated trace element compositions and patterns of silico-carbonatitic melts (green patterns) as potential metasomatizing agents in subcalciic garnets from **Roberts Victor** mine in separate diagrams for **a)** group RV1, **b)** group RV2 and **c)** group RV3 garnets. The partition coefficients were taken from the work of Girmis et al. (2012; revised version submitted to Lithos. The trace element compositions of group II kimberlites were taken from Nowell et al. (2004), of natural carbonatites are from Uganda from Nelson et al. (1988), of fluid inclusions (carbonate-K-chloride-H₂O) in fibrous diamonds from Tomlinson et al. (2009) and of carbonatitic ro kimberlitic melts in fibrous diamonds of Klein-BenDavid et al. (2009). The trace elements of 30% experimental melting of eclogites were taken from Rapp et al. (1999).

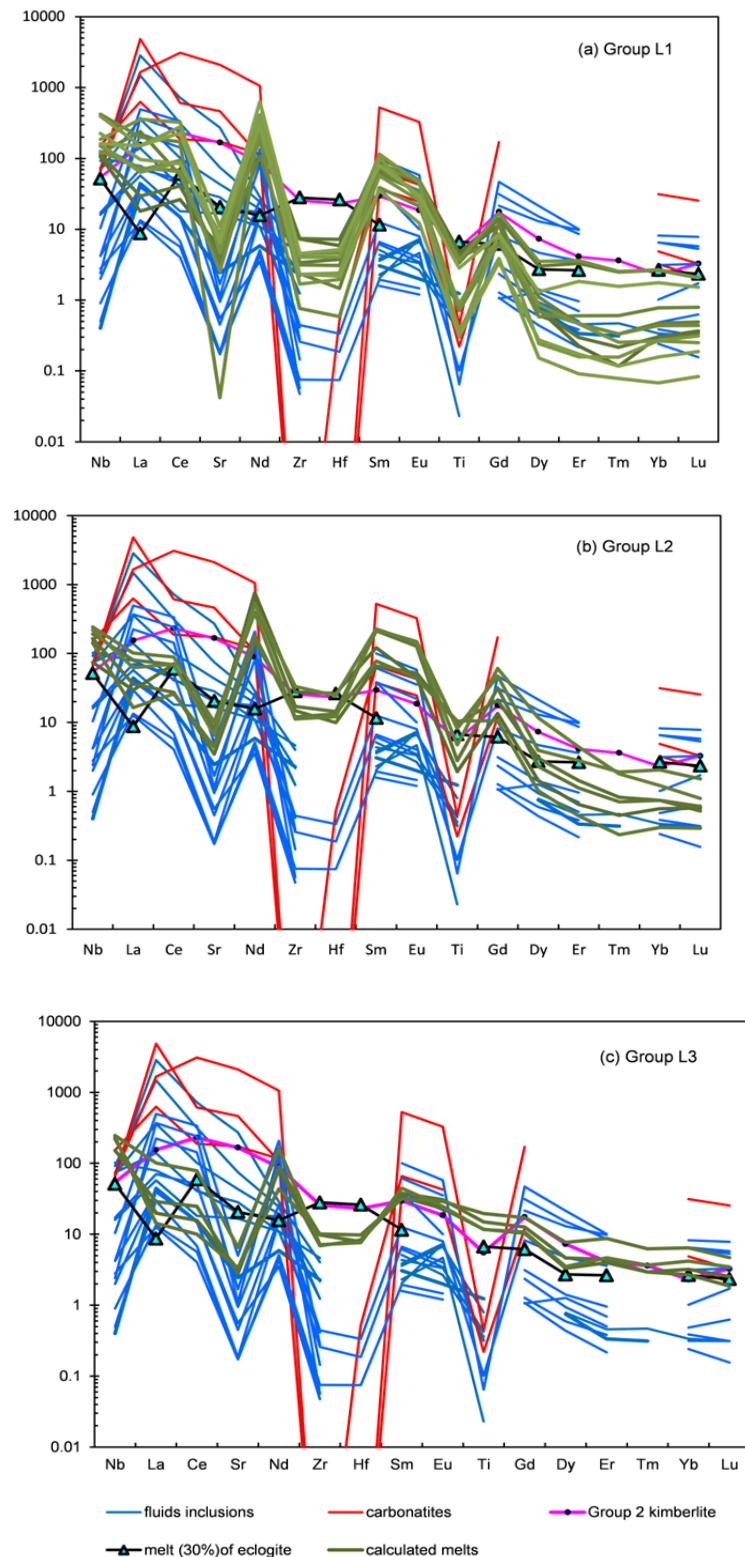


Fig.13 Calculated trace element compositions and patterns of silico-carbonatitic melts (green patterns) as potential metasomatizing agents in subcalic garnets from **Lace** mine in separate diagrams for **a)** group L1, **b)** group L2 and **c)** group L3 garnets. The partition coefficients were taken from the work of Girnis et al. (2012; revised version submitted to Lithos). The trace element compositions of group II kimberlites were taken from Nowell et al. (2004), of natural carbonatites from Uganda from Nelson et al. (1988), of fluid inclusions (carbonate-K-chloride-H₂O) in fibrous diamonds from Tomlinson et al. (2009) and of carbonatitic ro kimberlitic melts in fibrous diamonds of Klein-BenDavid et al. (2009). The trace elements of 30% experimental melting of eclogites were taken from Rapp et al. (1999).

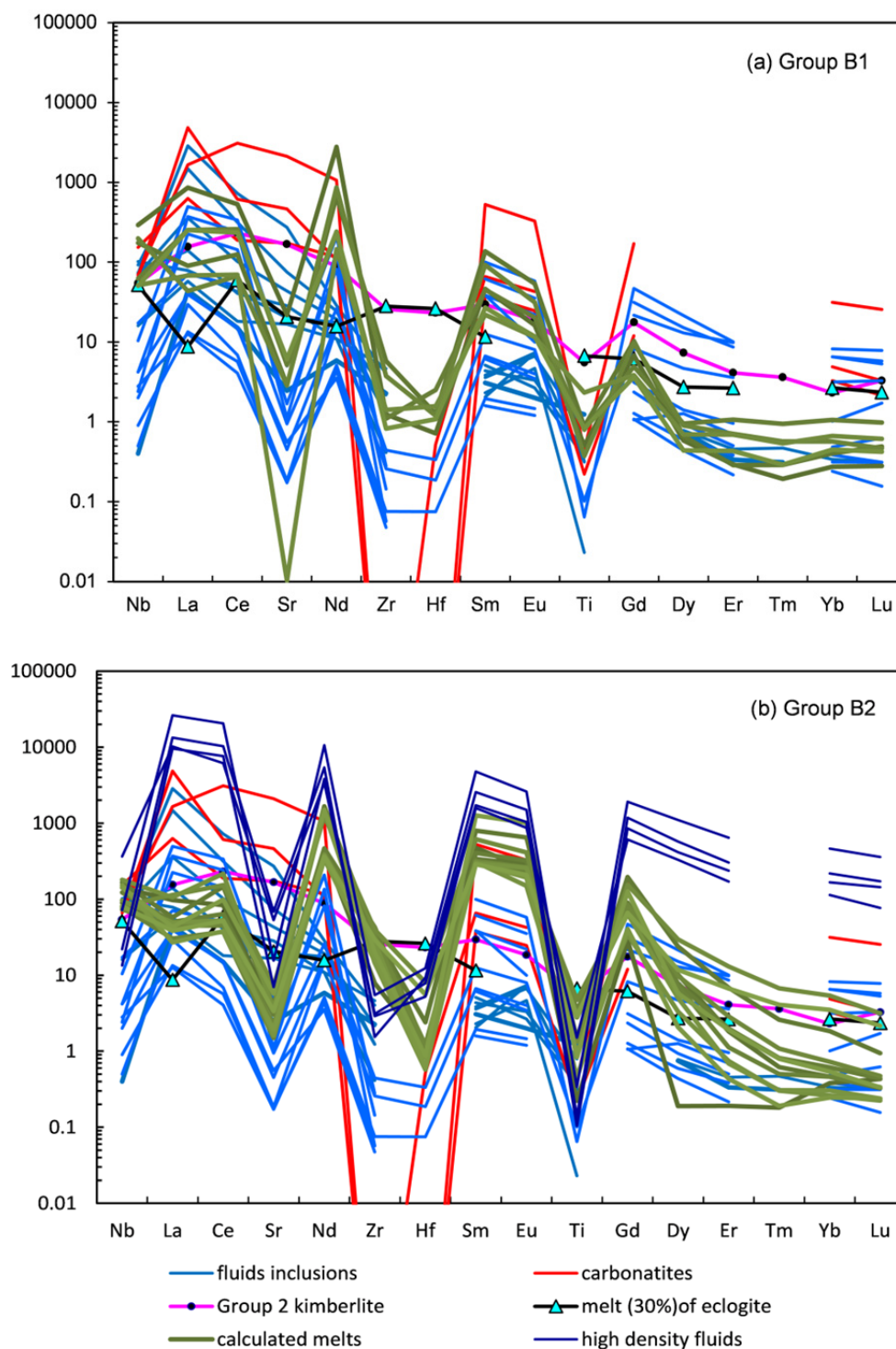


Fig.14 Calculated trace element compositions and patterns of silico-carbonatitic melts (green patterns) as potential metasomatizing agents in subcalic garnets from **Bellsbank** mine in separate diagrams for **a)** group B1 and **b)** group B2 garnets. The partition coefficients were taken from the work of Girnis et al. (2012; revised version submitted to Lithos). The trace element compositions of group II kimberlites were taken from Nowell et al. (2004) of natural carbonatites from Uganda from Nelson et al. (1988), of fluid inclusions (carbonate-K-chloride-H₂O) in fibrous diamonds from Tomlinson et al. (2009) and of carbonatitic ro kimberlitic melts in fibrous diamonds of Klein-BenDavid et al. (2009). The trace elements of 30% experimental melting of eclogites were taken from Rapp et al. (1999).

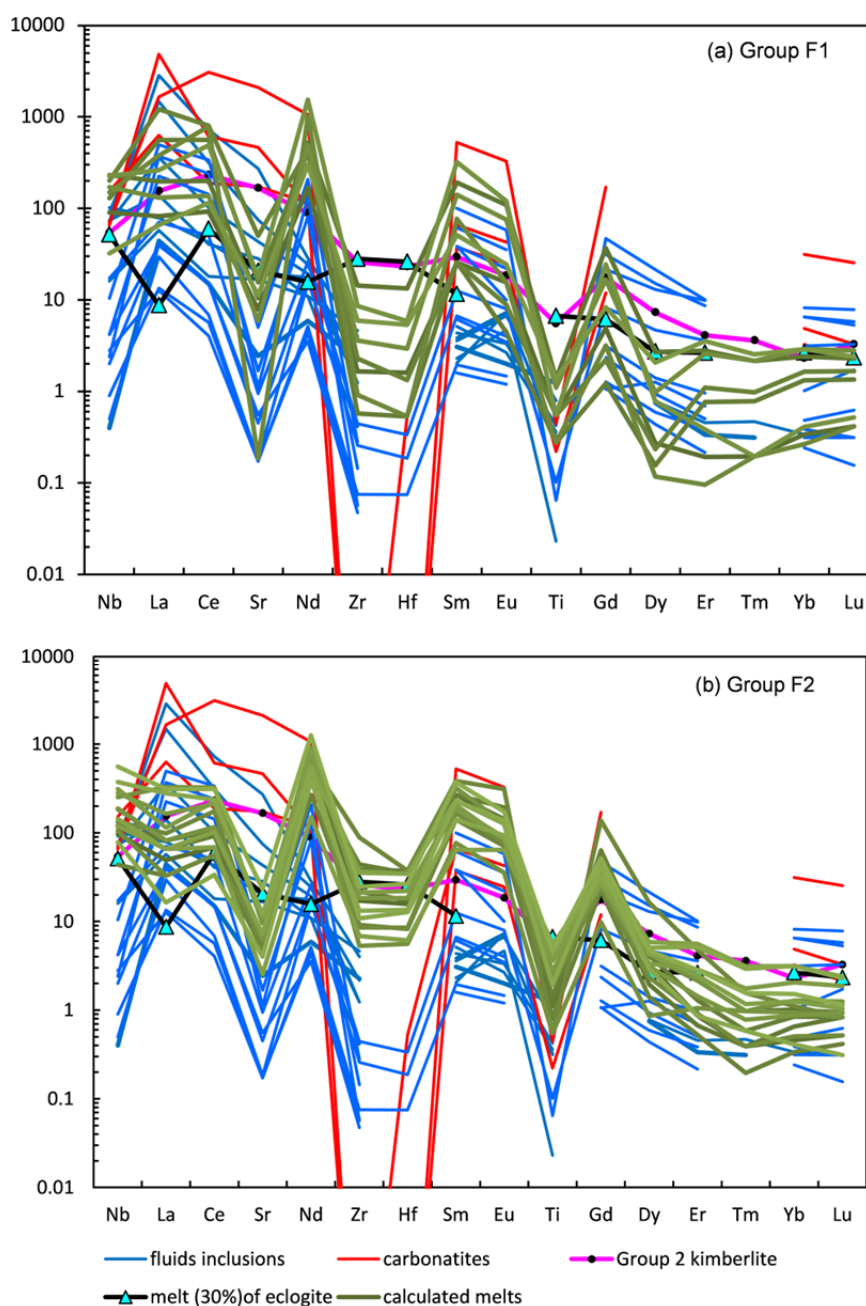


Fig.15 Calculated trace element compositions and patterns of silico-carbonatitic melts (green patterns) as potential metasomatizing agents in subcalic garnets from **Finsch** mine in separate diagrams for **a)** group F1 and **b)** group F2 garnets. The partition coefficients were taken from the work of Girnis et al. (2012; revised version submitted to Lithos). The trace element compositions of group II kimberlites were taken from Nowell et al. (2004) of natural carbonatites from Uganda from Nelson et al. (1988), of fluid inclusions (carbonate-K-chloride-H₂O) in fibrous diamonds from Tomlinson et al. (2009) and of carbonatitic ro kimberlitic melts in fibrous diamonds of Klein-BenDavid et al. (2009). The trace elements of 30% experimental melting of eclogites were taken from Rapp et al. (1999).

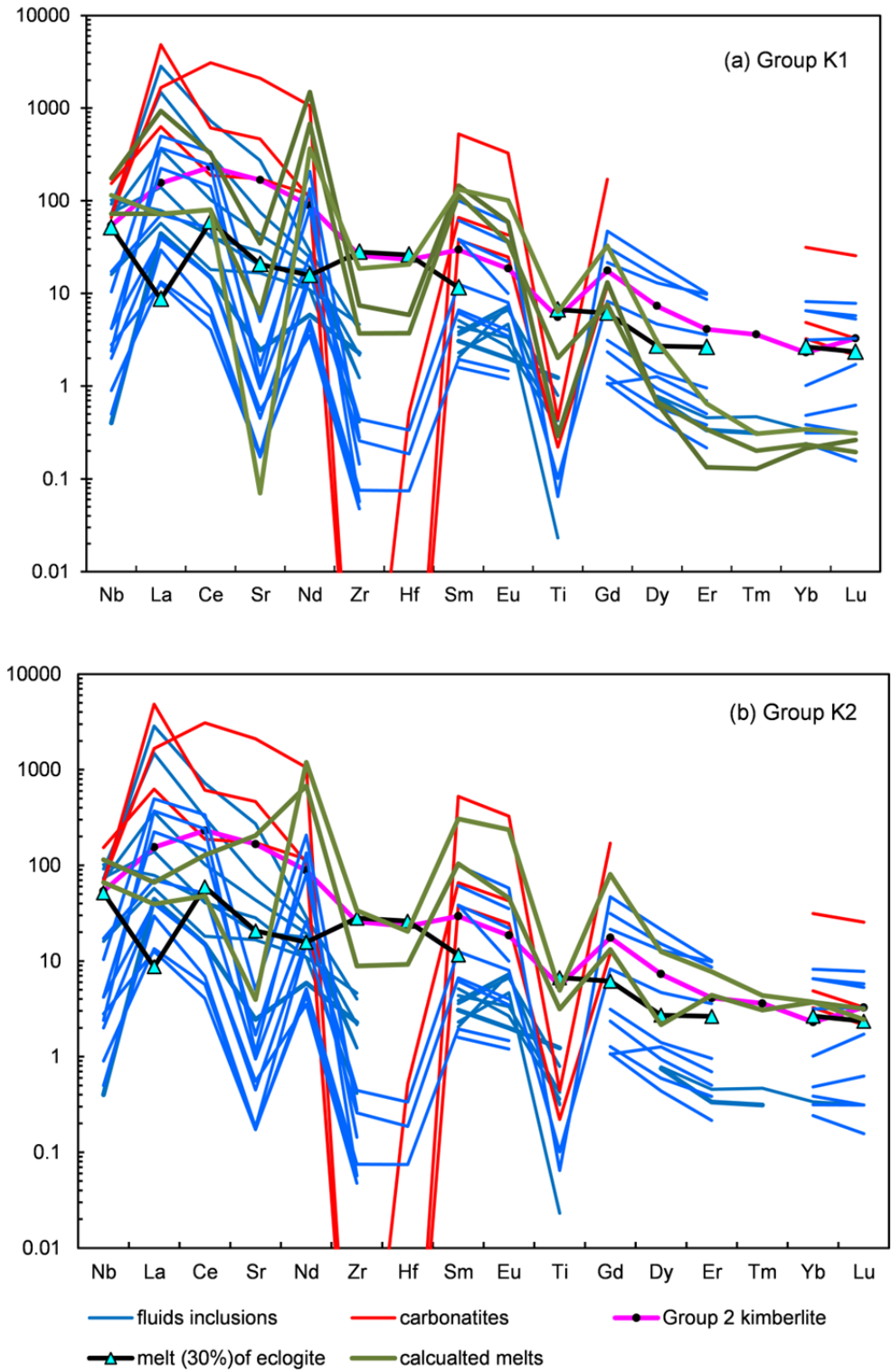


Fig.16 Calculated trace element compositions and patterns of silico-carbonatitic melts (green patterns) as potential metasomatizing agents in subcalic garnets from **Kimberley** mine in separate diagrams for **a)** group K1 and **b)** group K2 garnets. The partition coefficients were taken from the work of Girnis et al. (2012; revised version submitted to Lithos). The trace element compositions of group II kimberlites were taken from Nowell et al. (2004) of natural carbonatites from Uganda from Nelson et al. (1988), of fluid inclusions (carbonate-K-chloride-H₂O) in fibrous diamonds from Tomlinson et al. (2009) and of carbonatitic ro kimberlitic melts in fibrous diamonds of Klein-BenDavid et al. (2009). The trace elements of 30% experimental melting of eclogites were taken from Rapp et al. (1999).

The Ti/Eu vs. Zr/Hf correlation of subcalic garnets also argue for the inevitable carbonatitic metasomatism in most samples (Fig.17). The very low Ti/Eu and very high and superchondritic Zr/Hf ratios in most garnets require this conclusion. Garnets in equilibrium with carbonatitic melt fractionates Zr from Hf and Ti from Eu. Experimental work showed that that the partition coefficients of Zr between garnet and carbonatitic melts is higher than for garn-silicate melt and vice versa for Hf (Sweeney et al. 1992; Grinis et al., 2012). Also, Ti is relatively more compatible in silicate than in carbonatitic melts. Therefore, the negative correlation of these two ratios (Ti/Eu vs. Zr/Hf) shows carbonatite as an enrichment agent. More than 90% of our samples (93 out of 103 garnets) have Ti/Eu ratios lower than 2500 and have elevated and superchondritic Zr/Hf ratios (mostly from 40 to 110). A small number of samples have the Ti/Eu ratio higher than 2500 up to 7300 but still lower than the mantle values (7800). These samples, mostly group RV3, are interpreted as a result of garnets exchanging with more silicic melts. There is, however, also the possibility of multiple enrichments by different agents, first by a carbonatitic agent followed by a silicate rich agent.

Group L3 (black triangles) in Fig.17, have Ti/Eu ratios higher than the mantle, but not a subchondritic Zr/Hf ratio. They cannot be the residues from partial melting because this would lead to an increase of the Ti/Eu ratios and a decrease of Zr/Hf. The L3 garnets have positively sloped REE pattern from LREE to HREE, high HREE abundances and positive Zr-Hf and Ti anomalies. Our interpretation is that these garnets may actually be megacrysts precipitated from a melt with high Ti/Eu ratios. The calculated melt compositions are close to group II kimberlite. These may have acquired the high Ti, Zr and Hf from a previous dissolution of rutile and ilmenite as was described from a polymict breccias by Lazarov (PhD thesis).

Group L3 samples from Lace mine fall below the 3.3 Ga enrichment age line (Fig.18a, black triangles) and their trace element patterns are quite different from all others (Fig. 5 c,d; black patterns). They have positively sloped patterns from LREE to HREE, high HREE abundances and only a minor enrichment in most incompatible elements. The most apparent differences are their positive Ti and Zr-Hf anomalies while all other garnets have negative anomalies. These features indicate that L3 garnets are not products of intense metasomatic overprint of depleted garnets and, because of the positive Zr-Hf and Ti anomalies they can also not be residues of partial melting. They have high Cr# (15 to 25) and relatively low Mg# (82 to 86). These garnets are similar to overgrowths on preexisting subcalic garnets found in the Wesselton kimberlite mine in Kimberley described by Griffin et al. (1999b) and multiple grain overgrowths on garnets of any garnet composition in a polymict breccia from the Boshof road dump in Kimberley as described by Lazarov (PhD thesis, 2009; freely available in the internet). Lazarov (2009) interpreted that these garnets as precipitates from a kimberlite-like melt which possibly was the carrier of the inventory of the polymict breccias and which had reacted with and dissolved ilmenite to achieve the positive Ti and Z-Hf anomalies. The calculated melts from group L3 garnets are similar to group II kimberlites. The L3 garnets from Lace are several mm sized broken pieces of larger crystals and may actually be subcalic megacrysts of percolating kimberlitic melts.

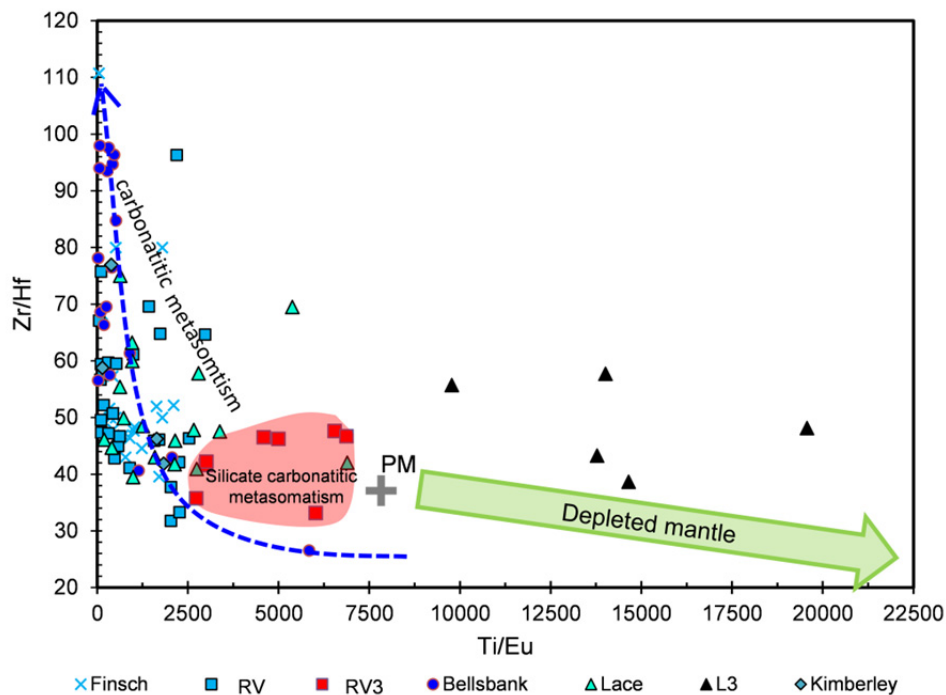


Fig.17 Zr/Hf vs. Ti/Eu diagram: Three garnet populations can be distinguished: The garnets with blueish symbols interacted with a carbonatitic melt which resulted in low and subchondritic Ti/Eu ratios and high and superchondritic Zr/Hf ratios. The red shaded area comprises samples which were affected by more silicic melts. The green arrow shows the depletion trend for residual garnets. The garnets with superchondritic Ti/Eu ratios shown by black triangles are possibly subcalic megacrysts.

The significance of carbonatitic metasomatism for the refertilization of the depleted mantle has been emphasized first by Frey and Green (1973) and experimentally demonstrated by Wallace and Green (1988). It was shown by further work like Yaxley et al. (1991), Baker and Wyllie (1988), Rudnick et al. (1993), Dupuy et al.(1992), Sweeney et al. (1992) and Griffin et al. (1992 ,1999b). The extreme mobility of carbonatite melts allows them to metasomatize the depleted mantle on a large scale. The present study very significantly increases the cases where evidence for pervasive carbonatite metasomatism comes directly from the rocks like very low Ti/Eu, very high Zr/Hf and depleted HFSE. Also, the decoupled Nd and Hf isotope data seen in this study and earlier work (Nowell et al., 2004; Simon et al., 2007; Lazarov et al., 2009 and 2012,) are explicable in terms of carbonatite metasomatism as carbonatitic melts will bring insignificant amounts of Hf but sufficient Nd or Sm to erase the depleted nature of mantle peridotites.

The evidence for carbonatitic melts as metasomatizing agent appears to be overwhelming. We do not see any significant evidence for silicate melt metasomatism at least not in the garnets with sinusoidal REE patterns. This contradicts the currently popular model that tonalitic melts, which had originated from subducted slabs, were responsible for the opx enrichment seen in many peridotites from the Kaapvaal craton and from Siberia (Kesson and Ringwood, 1989; Rudnick et al., 1994; Kelemen, 1998; Bell et al., 2005; Simon et al., 2007). An alternative may be a model recently put forward by Lazarov et al. (2012) who suggested that the high modal abundances of opx in many peridotites are the result of melting of carbonated peridotite which leaves opx as a residual phase in

increased abundance over olivine. This model needs a source for carbon which may be in old subducted material.

4.2 Enrichment events in the East Block

On the East block, RV2 and L1 garnets from Lace and Roberts Victor share a 3.3 Ga Lu/Hf age of enrichment of an already depleted mantle (ϵ_{Hf} is +17; see Chapter 2 and the reproduction of the isochron in Fig.18 a). The metasomatizing agent was carbonatitic from the criteria above. The garnets plotting along this 3.3 Ga enrichment age line have very variable ϵ_{Hf} values from -65 to +679 as well as ϵ_{Nd} from -4 to -39. Such huge variations are the result of the addition of varying amounts of Hf and Nd to the samples and a decay of the systems over a very long time. One sample from Lace (L2) lied at the lowest end of the 3.3 Ga errorchron with $\epsilon_{\text{Hf}} = -65$ and $\epsilon_{\text{Nd}} = -39$ (Fig.18, pink triangle and its isotope data shown in **Table A.3b-1 and -2**). Such low ϵ_{Hf} and ϵ_{Nd} values require an early enrichment of LREE and Hf in a depleted mantle. The enriching agent must come from an older crustal material, if the 3.3 Ga are the correct age for enrichment. The age of the crust must lie between 3.65 to 3.99 Ga as indicated by the Hf and Nd model ages of this sample. The old model ages are due to the extremely low $^{176}\text{Lu}/^{177}\text{Hf}$ of 0.0070 and subchondritic $^{43}\text{Nd}/^{144}\text{Nd}$ of 0.1209 and the high Hf (1.01 ppm) and Nd (4.48 ppm) contents. It can be deduced from the position on the isochron close to the origin that the isotope ratios of this sample closely characterize the initial of the enriching agent.

The Sm/Nd isotopes do not yield any isochron age. Eight garnets (triangles) from Lace together with seven garnets (squares) from the Roberts Victor mine lie along a 900 Ma reference line with ϵ_{Nd} of -11 (see previous chapter and Fig. 18b). Four further samples from Lace plot close to another 900 Ma reference line with an ϵ_{Hf} of -29. The four garnets shaded in pink, one from Lace and three from Roberts Victor, have nearly constant Nd isotope with ϵ_{Nd} around -41. There may a widespread enrichment in the East Kaapvaal craton around 900 Ma. These four samples with the lowest Nd isotope may not be affected by the 900 Ma enrichment in LREE.

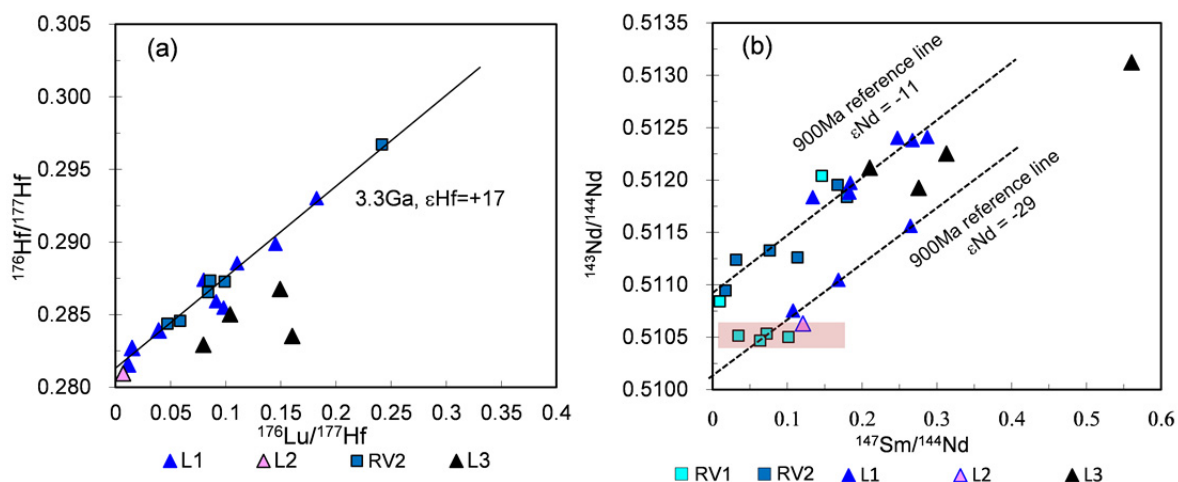


Fig.18 The Lu-Hf isochron shown in **a)** was derived in the previous chapter only from the RV2 samples The L1 samples plot along this isochron. The group L3 garnets (black triangles) from Lace lie below this line The Sm/Nd

isotope variation diagram in **b**) is also reproduced from chapter 2 including the two 900 Ma reference lines. One population of the samples lies close to the 900 Ma reference line with a $\epsilon_{\text{Nd}} = -11$, the other close to second 900 Ma reference line with a $\epsilon_{\text{Nd}} = -29$. A third sample group has nearly constant $^{143}\text{Nd}/^{144}\text{Nd}$ ratios of $\epsilon_{\text{Nd}}(0)$ of -41 (shaded in pink).

4.3 Enrichment events in the West Block

On the West block, two Lu/Hf isochrons were derived from a) subcalcic garnets and b) calculated bulk rock compositions of grt and cpx bearing peridotites date the same event at 2.62 Ga which was interpreted by Lazarov et al. (2009 and 2012) as the age of second stage melting paired with re-enrichment. In the data set of the more strongly metasomatized F2 subcalcic garnets we discovered that there was a further enrichment age recorded at 1.9 Ga (see chapter 2). Younger enrichment events at around 1.3 Ga are indicated in Sm-Nd a errorchron from Finsch (Lazarov et al., 2009) and 1.2 Ga Lu/Hf errorchron from Bellsbank and Kimberley (see Fig.19a) poorly defined by both Lu/Hf isotope in Bellsbank (B1) and Kimberley garnets. The Sm/Nd isotope data from Bellsbank and Kimberley are too scattered to define a confident age. They plot along a 989 Ma and a 812 Ma regression lines (Fig.19b). The youngest enrichment age reported is around 390 ± 120 Ma Sm/Nd errorchron age from Finsch garnets (Lazarov et al., 2009).

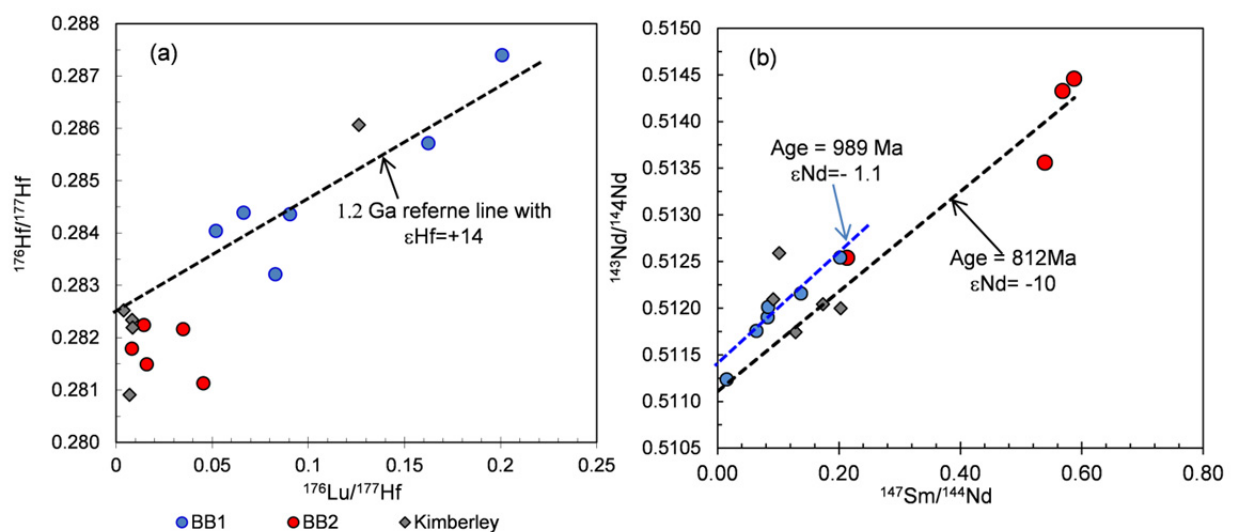


Fig.19 **a**) The $^{176}\text{Lu}/^{177}\text{Hf}$ data from Bellsbank and Kimberley plotted into an isochron diagram. No isochron can be obtained. The group B1 garnets (light blue circles) together with one sample from Kimberley (grey diamonds) lie close to a 1.2 Ga reference line with $\epsilon_{\text{Hf}} = +14$. The B2 (red circles) and the other Kimberley samples lie below this age line and plot on the area with lower $^{176}\text{Hf}/^{177}\text{Hf}$ which may indicate different enrichment processes at different times. **b**) The Sm/Nd isotope data are also shown in an isochron diagram. No isochron can be obtained. One set of garnets lies along the 989 Ma age line as indicated as the blue dashed line. The others set of garnets lie close to the 812 Ma age line shown as the black dashed line.

4.4 The subcalic garnet and the affinity to diamond

The similarity between garnet inclusions in diamonds and the compositions of garnets from xenoliths was already discussed at length by Stachel et al. (1998). The subcalic garnets studied here have many geochemical features in common with the subcalic garnet inclusions in diamonds. Strong negative Zr-Hf and Ti anomalies and high LREE/HREE ratios are observed in both. They have similar high, $^{87}\text{Sr}/^{86}\text{Sr}$ ratios which are not supported by corresponding low Rb/Sr ratios (Richardson et al., 1984; Richardson and Harris, 1997; Pearson et al., 1995; Jacob et al., 1998; Ofra Klein-BenDavid and Pearson, 2009). Also and more general, the calculated trace element patterns of silicate-carbonatitic melts in equilibrium with the subcalic garnet xenocrysts resemble the compositions of fluid inclusions in fibrous diamonds (see above). All these features indicate that the agents involved in diamond formation and metasomatism of depleted peridotites are very similar and genetically related. The source for the carbonatitic metasomatic agents must reactivated old crustal components like sedimentary components of subducted material. The time of diamond formation for peridotitic diamonds is difficult to constrain (see overview by Stachel and Harris, 2008). They are mostly Pb-Pb/U-Pb, Sm-Nd and Re-Os model ages derived from the inclusions in diamonds. Richardson et al. (1988) were the first to provide a Sm-Nd model age of pooled peridotitic garnet inclusions in diamond which gave 3.2 Ga. It cannot be shown with complete certainty that this is the age of diamond growth or that it is the isotopic fingerprint of a metasomatizing agent. Tighter constraints on diamond formation ages come from isochrons for eclogitic diamonds. If diamond growth and metasomatism of the mantle occur in parallel, periods of diamond growth could be inferred from the determination of enrichment ages in the peridotites.

The results given in chapter 2 on enrichment ages obtained from subcalic garnets and the work from Lazarov et al. (2009, 2012) show a sequence of enrichment events in the mantle which appear parallel to major tectonic events during crust formation and also periods of diamond formation.

We have seen the oldest enrichment event in the depleted mantle at around 3.3 Ga on the East block from a Lu-Hf isochron from Roberts Victor. It coincides with widespread pluses of igneous activity in the crust around 3.2 to 3.3 Ga. The 3.2 Ga “diamond growth” age of Richardson et al. (1984) coincides with these ages but is derived from Finsch and Kimberley on the W-block. Growth of peridotitic diamonds are reported again from around 2.0 Ga from Venetia in the Limpopo belt and the Premier mine on the East block. Closest to these ages is the 1.9 Ga enrichment age seen in the Finsch subcalic garnets (see previous chapter). This age coincides with the age range of the Kheis-Magondi belt. All other diamond growth ages in southern Africa were obtained from eclogitic diamonds. The most prominent are ages around 2.95 Ga (Richardson et al., 2001 and 2004; De Beers Pool and Jwaneng). We do not see an enrichment in the subcalic garnets, but rather see the generation of subcalic garnets by partial melting at 2.95 Ga recorded in the RV1 garnets from Roberts Victor (see previous chapter). Younger enrichment events are possibly recorded in Sm-Nd errorchrons from the subcalic garnets at 1.3 Ga (Finsch; Lazarov et al., 2009) and 900 Ma from Lace, Roberts Victor, Bellsbank and Kimberley. These ages can be related to crustal events but not to younger diamond growth ages derived from eclogitic inclusions except for a 1 Ga year age from Koffiefontein (Pearson et al., 1998). Otherwise, the eclogitic ages lay at 1.5–1.6 Ga in Finsch and Jwaneng (summarized by

Shirey et al., 2004) and at Jagersfontein (Aulbach et al., 2009). Contemporaneous formation of diamonds and mantle metasomatism is indicated from the available data and in our opinion very probably but the spotty information in time and space on diamond growth, mantle metasomatism and crustal events leave a degree of uncertainty. The enrichment ages from the subcalic garnets are connected to the major tectonic events for building the present state of the Kaapvaal craton. These major tectonic events can be the force to reactivate the subducted material existing in the mantle from early subduction by bringing heat and generating carbonatitic melts or kimberlitic melts and consequently continuously refertilized the depleted mantle. If the diamond formation is related to the carbonatitic metasomatism recorded in subcalic garnets, then there will be episodes of diamond formation throughout the Earth's evolution.

5. Summary

(1) The prominent agents for metasomatism and refertilization of the depleted mantle are low-viscosity carbonatitic to kimberlitic melts. The ultimate source material for these carbonatitic melts is subducted oceanic crustal material which reacted with peridotite to form silico-carbonatitic melts. Episodic remobilization through major geotectonic events of the subducted material and the reaction products with peridotite leads to episodic metasomatism and diamond growth.

(2) The preferred model for the origin of sinusoidal low-Ca garnets involves a three stage process. The protoliths were low pressure melting residues at middle ocean ridge like settings which were subsequently subducted into a preexisting mantle which may or may not have been already depleted. Garnet was ultimately exsolved from the very depleted harzburgites from orthopyroxene. Oceanic crust basalts, more mafic lithologies and sediments were subducted together with the depleted peridotites. They are the ultimate source of the metasomatizing agents but also can be the source of large amounts of carbon. In the process of thermal and compositional equilibration of the lithospheric mantle mélange, the carbon may be the source for carbonation of the peridotitic mantle by redox reactions. Carbonated peridotite will melt form silic-carbonatitic melts and, if sufficient CO₂ is present (sufficient carbonate was formed), it will leave an opx-rich residue. Orthopyroxene-rich peridotites are formed this way by partial melting rather than by enrichment with silicate melts.

(3) The non-sinusoidal subcalic L3 garnets with flat middle to heavy REE from Lace appear more as phases which precipitated from percolating melts within the mantle. Contrary, the RV3 garnets from Roberts Victor, a number of them also with flat middle to heavy REE, appear to represent a series of more and more metasomatized garnets, which show the transition from sinusoidal to "normal" LREE depleted garnets. An isotopic study of these garnets may yield a pure signal of the metasomatizing agent.

References

- Adam, J. and Green, T., 2006, Trace element partitioning between mica- and amphibole-bearing garnet lherzolite and hydrous basanitic melt: 1. Experimental results and the investigation of controls on partitioning behavior. *Contributions to Mineralogy and Petrology* **152**: 1-17.
- Alterman, W. and Höllich, I.W., 1991, Structural history of the southwestern corner of the Kaapvaal craton and the adjacent Namaqua realm: new observations and a reappraisal. *Precambrian Research* **52**: 133-166.
- Aulbach S., Shirey B.S., Stachel T., Creighton S., Muehlenbachs K. and Harris W.J., 2009, Diamond formation episodes at the southern margin of the Kaapvaal Craton: Re–Os systematics of sulfide inclusions from the Jagersfontein Mine, *Contrib Mineral Petrol* **157**: 525–540.
- Barth M., Rudnick R.L., Horn I., McDonough W.F., Spicuzza M., Valley J.W. and Haggerty S.E., 2001, Geochemistry of xenolithic eclogites from West Africa, part I: a link between low MgO eclogites and Archean crust formation. *Geochim Cosmochim Acta* **65**: 1499–1527.
- Barth M., Rudnick R.L., Horn I., and McDonough W.F., Spicuzza M., Valley J.W., Haggerty S.E., 2002, Geochemistry of xenolithic eclogites from West Africa, part II: origins of the high MgO eclogites. *Geochim Cosmochim Acta* **66**: 4325–4345.
- Baker M.B. and Wyllie P.J., 1990, An liquid immiscibility in a nephelinite–carbonate system at 25 kbar and implications for carbonatite origin. *Nature*, **346**: 168-170.
- Beattie, P., 1994, Systematics and energetics of trace-element partitioning between olivine and silicate melts: Implications for the nature of mineral/melt partitioning. *Chemical Geology* **117**: 57-71.
- Bell, D.R., Gregoire, M., Grove, T.L., Chatterjee, N., Carlson, R.W., Buseck, P.R., 2005, Silica and volatile element metasomatism of Archean mantle: a xenolith-scale example from the Kaapvaal Craton. *Contributions to Mineralogy and Petrology* **150**: 251-267.
- Beukes, N.J., Smit, C.A., 1987, New evidence for thrust faulting in Griqualand West South Africa: implications for stratigraphy and the age of red beds. *South African Journal of Geology* **90**: 378-387.
- Boyd, F.R., Merzman, S.A., 1987, Composition and structure of the Kaapvaal lithosphere, southern Africa. In: B.O. Masen (Editor), *Magmatic processes: physicochemical principles*. The Special Publications, pp.13-24. geochemical Society.
- Boyd, F.R., Pokhilenko, N.P., Pearson, D.G., Mertzman, S.A., Sobolev, N.V., Finger, L.W., 1997, Composition of the Siberian cratonic mantle: evidence from Udachnaya peridotite xenoliths. *Contributions to Mineralogy and Petrology* **128 (2–3)**: 228–246.
- C. Dupuy, J.M. Liotard and Dostal J., 1992, Zr/Hf fractionation in intraplate basaltic rocks: Carbonate metasomatism in the mantle source. *Geochim. Cosmochim. Acta* **56**: 2417-2424.
- Canil, D., 1999, The Ni-in-garnet geothermometer: calibration at natural abundances. *Contributions to Mineralogy and Petrology* **136**: 240-246.
- Dawson J. B. and Stephens W. E., 1975, Statistical classification of garnets from kimberlite and associated xenoliths. *J. Geol.* **83**: 589–607.
- Dawson, J.B., 1982, *Kimberlites and their xenoliths*. Springer-Verlag, Berlin, 159 pp.
- Dawson, J.B., 1984, Constraining types of upper-mantle metasomatism? In: J. Kornprobst (Editor), *Kimberlites II: The mantle and the crust-mantle relationships*. Elsevier, pp. 282-331.
- de Wit, M.J., de Ronde, C.E.J., Tredoux, M., Roering, C., Hart, R.J., Armstrong, R.A., Green, R.W.E., Peberdy, E. and Hart, R.A., 1992, Formation of an Archaean continent. *Nature* **357**: 553-562.
- Downes, H. and Dupuy, C., 1987, Textural, Isotopic and REE Variations in Spinel Peridotite Xenoliths, Massif-Central, France. *Earth and Planetary Science Letters* **82(1-2)**: 121-135.
- Downes, H., Embey-Isztin, A. & Thirlwall, M. F., 1992, Petrology and geochemistry of spinel peridotite xenoliths from the western Panonian Basin (Hungary): evidence for an association between enrichment and texture in the upper mantle. *Contributions to Mineralogy and Petrology* **109**: 340-354.
- Eglington, B.M. and Armstrong, R.A., 2004, The Kaapvaal Craton and adjacent orogens, southern Africa: a geochronological database and overview of the geological development of the craton: *South African Journal of Geology* **107**: 13-32.
- Erlank, A.J., Waters, F.G., Hawkesworth, C.J., Haggerty, S.E., Allsopp, H.L., Rickard, R.S., Menzies, M., 1987, Evidence for mantle metasomatism in peridotite nodules from the Kimberley pipes, South Africa. In: M.A. Menzies, C.J. Hawkesworth (Editors), *Mantle Metasomatism*, Academic Press, London. pp. 221-309.
- F.A. Frey and D.H. Green, 1974, The mineralogy, geochemistry and origin of lherzolite inclusions in Victorian basanites, *Geochim. Cosmochim. Acta* **38**: 1023-1059.

- Gibson, S.A., Malarkey, J., Day, J.A., 2008, Melt depletion and enrichment beneath the Western Kaapvaal craton: evidence from Finsch peridotite xenoliths. *J. Petrol.* **49**:1817–1852.
- Girnis A., Bulatov V. K., Brey P.G., Gerdas A., Höfer E.H., 2012, Trace element partitioning between mantle minerals and silicate-carbonate melts at 6-12 GPa and applications to mantle metasomatism and kimberlite genesis. submitted to *Lithos*.
- Green, T.H., Blundy, J.D., Adam, J. and Yaxley, G.M., 2000, SIMS determination of trace element partition coefficients between garnet, clinopyroxene and hydrous basaltic liquids at 2–7.5 GPa and 1080–1200 °C. *Lithos* **53**: 165–187.
- Gregoire, M., Bell, D.R., Le Roex, A.P., 2002, Trace element geochemistry of phlogopite-rich mafic mantle xenoliths: their classification and their relationship to phlogopite-bearing peridotites and kimberlites revisited. *Contributions to Mineralogy and Petrology* **142**: 603-625.
- Gregoire, M., Bell, D.R., Le Roex, A.P., 2003, Garnet Iherzolites from the Kaapvaal craton (South Africa): Trace element evidence for a metasomatic history. *Journal of Petrology* **44**: 629-657.
- Griffin, W.L., Cousens, D.R., Ryan, C.G., Sie, S.H., Suter, G.F., 1989, Ni in chrome pyrope garnets – a new geothermometer. *Contributions to Mineralogy and Petrology* **103**: 199-202.
- Griffin, W.L., Gurney, J.J., Ryan, C.G., 1992, Variation in trapping temperatures and trace-elements in peridotite-suite inclusions from African diamonds – evidence for 2 inclusion suites, and implications for lithosphere stratigraphy. *Contributions to Mineralogy and Petrology* **110**: 1-15.
- Griffin, W.L., O'Reilly, S.Y., Ryan, C.G., 1999a, The composition and origin of subcontinental lithospheric mantle. In: Y. Fei, C.M. Bertka and Mysen (Editors), *Mantle petrology: Field experimentation*. Spec Pub No. The Geochemical Society, Washington, pp.13-45.
- Griffin, W.L., Shee, S.R., Ryan, C.G., Win, T.T. and Wyatt, B.A., 1999b, Harzburgite to Iherzolite and back again: metasomatic processes in ultramafic xenoliths from the Wesselton kimberlite, Kimberley, South Africa. *Contributions to Mineralogy and Petrology* **134**: 232-250.
- Grueter H. S., Gurney J. J., Menzies A. H. and Winter F. ,2004, An updated classification scheme for mantle-derived garnet, for use by diamond explorers. *Lithos* **77(1–4)**: 841–857.
- Grueter H., Latti D. and Menzies A., 2006, Cr-saturation arrays in concentrate garnet compositions from kimberlite and their use in mantle barometry. *J. Petrol.* **47(4)**: 801–820.
- Gurney J. J. and Switzer G. S. ,1973, The discovery of garnets closely related to diamonds in the Finsch pipe, South Africa. *Contrib. Mineral. Petrol.* **39(2)**: 103–116.
- Gurney J., Harris J. and Rickard R., 1984, Silicate and oxide inclusions in diamonds from the Orapa Mine, Botswana. In *Kimberlites II: The Mantle and Crust–mantle relationships* (ed. J. Kornprobst). Elsevier, pp. 1–9.
- Haggerty, S.E., 1987, Mantle metasomes and the kinship between carbonatites and kimberlites. In: K. Bell (Editor) *Carbonatites: genesis and Evolution*, Uniwinn Hyman, London, pp. 546-560.
- Harte, B., 1983, Mantle peridotites and processes – the kimberlite samples. In: C.J. Hawkesworth and M.J. Norry (Editors) *Continental Basalts and Mantle xenoliths*. Shiva, UK, pp. 46-91.
- Hauri, E.H., Wagner, T.P. and Grove, T.L., 1994, Experimental and natural partitioning of Th, U, Pb and other trace elements between garnet, clinopyroxene and basaltic melts. *Chemical Geology* **117**: 149-166.
- Herzberg, C., 1993, Lithosphere peridotites of the Kaapvaal craton. *Earth and Planetary Science Letters* **120**: 13-29.
- Herzberg, C., 1999, Phase equilibrium constraints on the formation of cratonic mantle. In: Y. Fei, C.M. Bertka and Mysen (Editors), *Mantle petrology: Field observation and high- pressure experimentation*. Spec Pub No.6, The Geochemical Society, Washington, pp. 241-257.
- Hoal, K.E.O., Hoal, B.G., Erlank, A.J., Shimizu, N., 1994, Metasomatism of the mantle lithosphere recorded by rare earth elements in garnets. *Earth and Planetary Science Letters* **126**: 303-313.
- Ionov, D.A., Blichert-Toft, J. and Weis, D., 2005, Hf isotope compositions and HREE variations in off-craton garnet and spinel peridotite xenoliths from central Asia. *Geochimica et Cosmochimica Acta* **69**: 2399–2418
- Jacob D. E., Jagoutz E. and Sobolev N. V. (1998) Neodymium and strontium isotopic measurements on single subcalic garnet grains from Yakutian kimberlites. *Neues Jahrbuch Fur Mineralogie-Abhandlungen* **172(2–3)**: 357–379.
- Jacob, D.E., Bizimis, M. and Salters, V.J.M., 2005, Lu/Hf and geochemical systematics of recycled ancient oceanic crust: evidence from Roberts Victor eclogites. *Contributions to Mineralogy and Petrology* **148 (6)**: 707–720.

- Johnson, K.T.M. ,1998, Experimental determination of partition coefficients for rare earth and high-field-strength elements between clinopyroxene, garnet, and basaltic melt at high pressures. *Contributions to Mineralogy and Petrology* **133(1-2)**: 60-68.
- Kelemen, P.B., Dick, H.J.B., Quick, J.E., 1992, Formation of harzburgite by pervasive melt/rock reaction in the upper mantle. *Nature* **358**: 635-641.
- Kelemen, P.B., Hart, S.R., Bernstein, S., 1998, Silica enrichment in the continental upper mantle via melt/rock reaction. *Earth and Planetary Science Letters* **164**: 387-406
- Kesson, S.E., Ringwood, A.E., 1989, Slab-mantle interactions 2. The formation of diamonds. *Chemical Geology* **78**: 97-118.
- Lazarov, M., Brey G.B. and Weyer S., 2009, Time steps of depletion and enrichment in the Kaapvaal craton as recorded by subcalic garnets from Finsch (SA). *Earth Planet. Sci. Lett.* **27**: 1–10.
- Lazarov, M., Brey G.B. and Weyer S., 2012, Evolution of the South African mantle—a case study of garnet peridotites from the Finsch diamond mine (Kaapvaal craton); Part 2: Multiple depletion and re-enrichment processes. *Lithos*.
- Lazarov, Marina , PhD thesis, 2009, Archean to present day evolution of the lithospheric mantle beneath the Kaapvaal craton -Processes recorded in subcalic garnets, peridotites and polymict breccia.
- McDonough, W.F. and Sun, S.S. ,1995, The composition of the Earth. *Chemical Geology* **120**: 223–253.
- Menzies, M.A. and Hawkesworth, C., 1987, Upper mantle processes and composition. In: P.H. Nixon (Editor), *Mantle Xenoliths*. John Wiley, Chichester, pp. 725-738.
- Nelson, D.R., Chivas, A.R., Chappell, B.W. and McCulloch, M.T.,1988, Geochemical and isotope systematics in carbonatites and implications for the evolution of ocean-island sources. *Geochimica et Cosmochimica Acta*, **52(1)**: 1-17.
- Nowell, G.M., Pearson, D.G., Bell, D.R., Carlson, R.W., Smith, C.B., Kempton, P.D., Noble, S.R., 2004, Hf Isotope Systematics of Kimberlites and their Megacrysts: New Constraints on their Source Regions. *Journal of Petrology* **45**: 1583-1612.
- Ofra Klein-BenDavid and Pearson, D. G. ,2009, Origins of subcalic garnets and their relation to diamond forming fluids-Case studies from Ekati (NWT-Canada) and Murowa (Zimbabwe). *Geochimica et Cosmochimica Acta* **73**: 837–855
- Ofra Klein-BenDavid, Graham P., Nowell M. G. Ottley, C. McNeill C.R. J., and Cartigny P., 2009, Mixed fluid sources involved in diamond growth constrained by Sr–Nd–Pb–C–N isotopes and trace elements, *Earth and Planetary Science Letters* **289**: 123–133.
- Pearson D. G., Shirey S. B., Carlson R. W., Boyd F. R., Pokhilenko N. P. and Shimizu N., 1995, Re–Os, Sm–Nd, and Rb–Sr isotope evidence for thick archaic lithospheric mantle beneath the Siberian Craton modified by multistage metasomatism. *Geochim. Cosmochim. Acta* **59(5)**: 959–977.
- Pearson, D.G., Shirey, S.B., Harris, J.W., Carlson, R.W.,1998, Sulphide inclusions in diamonds from the Koffiefontein kimberlite, South Africa: constraints on diamond ages and mantle Re–Os systematics. *Earth and Planetary Science Letters* **160**: 311–326.
- Pearson, D.G. and Wittig, N., 2008, Formation of Archaean continental lithosphere and its diamonds: the root of the problem. *Journal of the Geological Society* **165**, 895-914.
- Rapp, R.P., Watson, E.B., 1995, Dehydration melting of metabasalt at 8– 32 kbar. Implications for continental growth and crust – mantle recycling. *J. Petrol.* **36**: 891– 931.
- Richardson S. H. and Harris J. W. ,1997, Antiquity of peridotitic diamonds from the Siberian craton. *Earth Planet. Sci. Lett.* **151**:271–277.
- Richardson S., Gurney J., Erlank A. and Harris J.,1984, Origin of diamonds in old enriched mantle. *Nature* **310(5974)**: 198–202
- Richardson SH, Shirey SB and Harris JW ,2004, Episodic diamond genesis at Jwaneng, Botswana, and implications for Kaapvaal craton evolution. *Lithos* **77**: 143–154.
- Richardson S.H., Shirey S.B., Harris J.W. and Carlson R.W. ,2001, Archean subduction recorded by Re–Os isotopes in eclogitic sulfide inclusions in Kimberley diamonds. *Earth Planet Sci Lett* **191**: 257–266.
- Rudnick, R.L., McDonough, W.F., Chappell, B.W., 1993, Carbonatite metasomatism in the northern Tanzanian mantle – petrographic and geochemical characteristics. *Earth and Planetary Science Letters* **114**: 463-475.
- Rudnick, R.L., McDonough, W.F., Orpin, A., 1994, Northern Tanzanian xenoliths: a composition with Kaapvaal peridotites and inferences on metasomatic interactions. In: L.O. Meyer HOA (Editor), *Kimberlites, related rocks and mantle xenoliths*. CPRM Spec Pub Jan/94, Brazilia, pp.336-353.

- Schmitz, M.D., Bowring, S.A., 2003, Constraints on the thermal evolution of continental lithosphere from U-Pb accessory mineral thermochronometry of lower crustal xenoliths, southern Africa. *Contributions to Mineralogy and Petrology* **144**: 592-618.
- Schmitz, M.D., Bowring, S.A., de Wit, M.J., Gartz, V., 2004, Subduction and terrane collision stabilize the western Kaapvaal craton tectosphere 2.9 billion years ago. *Earth and Planetary Science Letters* **222**: 363-376.
- Schulze, D.J., 1986, Calcium anomalies in the mantle and a subducted metaserpentinite origin for diamonds. *Nature* **319**, 483-485.
- Shirey S.B., Richardson S.H. and Harris J.W., 2004, Integrated models of diamond formation and craton evolution. *Lithos* **77**: 923–944.
- Simon, N.S.C., Carlson, R.W., Pearson, D.G., Davies, G.R., 2007, The Origin and Evolution of the Kaapvaal Cratonic Lithospheric Mantle. *Journal of Petrology* **48**: 589-625.
- Simon, N.S.C., Irvine, G.J., Davies, G.R., Pearson, D.G., Carlson, R.W., 2003, The origin of garnet and clinopyroxene in "depleted" Kaapvaal peridotites. *Lithos* **71**: 289-322.
- Smith C.B., Allsopp, H.L., Kramers, J.D., Hutchinson, G., Roddick, J.C., 1985, Emplacement ages of Jurassic-Cretaceous South African kimberlites by the Rb-Sr method on phlogopite and whole rock samples. *Trans. of the Geol. Soc. South Africa* **88**, pp 249-287.
- Sobolev N. V., Lavrente Y. g., Pokhilen N. p. and Usova L. V., 1973, Chrome-Rich Garnets from kimberlites of Yakutia and their Parageneses. *Contrib Mineral. Petrol.* **40(1)**: 39–52.
- Stachel T. and Harris J., 2008, The origin of cratonic diamonds – constraints from mineral inclusions. *Ore Geology Reviews* **34**: 5-32.
- Stachel, T., Viljoen, K.S., Brey, G.P. and Harris, J.W., 1998, Metasomatic processes in Iherzolitic and harzburgitic domains of diamondiferous lithospheric mantle: REE in garnets from xenoliths and inclusions in diamonds. *Earth Planet. Sci. Lett.* **159**: 1-12
- Sweeney R.J., Green D.H. and Sie S.H., 1992, trace element partitioning between garnet and amphibole and carbonatitic melt, *Earth Planetary Science Letter* **113**:1-14.
- Thomas, R.J., von Veh, M.W., McCourt, S., 1993, The tectonic evolution of southern Africa: an overview. *Journal of African Earth Sciences* **16**: 5-24.
- Tomlinson E.L., Müller W. and EIMF, 2009, a snapshot of mantle metasomatism: trace element analysis of coexisting fluid (LA-ICP-MS) and silicate (SIMS) inclusions in fibrous diamonds. *Earth and Planetary Science letters* **279**: 362-372.
- Tuff J. and Gibson A., 2007, Trace-element partitioning between garnet, clinopyroxene and Fe-rich picritic melts at 3 to 7 GPa, *Contrib Mineral Petrol.* **153**: 369–387.
- Vervoort, J.D., Patchett, P.J., Blichert-Toft, J., Albarède, F., 1999, Relationships between Lu-Hf and Sm-Nd isotopic systems in the global sedimentary system. *Earth and Planetary Science Letters* **168**: 79-99.
- Walter, M.J. 1998, Melting of garnet peridotite and the origin of komatiite and depleted lithosphere. *Journal of Petrology* **39**: 29-60.
- Wasch, L.J., van der Zwan, F.M., Nebel O. Morel M.L.A. Hellebrand E.W.G., Pearson D.G. and G.R. Davies, 2009, An alternative model for silica enrichment in the Kaapvaal subcontinental lithospheric mantle. *Geochimica et Cosmochimica Acta* **73**: 6894–6917
- Wallace M. and Green D.H., 1988, An experimental determination of primary carbonatite magma composition. *Letters to Nature* **25**: 343-346.
- Yaxley, G.M., Crawford, A.J., Green, D.H., 1991. Evidence for carbonatite metasomatism in spinel peridotite xenoliths from western Victoria, Australia. *Earth and Planetary Science Letters* **107**: 305-317.
- Zhang, H. F., Matthey, D. P., Grassineau, N., Lowry, D., Brownless, M., Gurney, J. J., Menzies, M. A., 2000, Recent fluid processes in the Kaapvaal Craton, South Africa: coupled oxygen isotope and trace element disequilibrium in polymict peridotites. *Earth and Planetary Science Letters* **176**: 57-72.
- Zhang, H.F., Menzies, M.A., Gurney, J.J., Zhou, X.H., 2001, Cratonic peridotites and silica-rich melts: Diopside-enstatite relationships in polymict xenoliths, Kaapvaal, South Africa. *Geochimica Et Cosmochimica Acta* **65**: 3365-3377.

Appendix

Tables A.1: major element compositions and structural formulae from subcalcic garnets

Table A.1a: Roberts Victor mine,

Table A.1b: Lace mine,

Table A.1c: Bellsbank mine,

Table A.1d: Kimberley mine,

Table A.1e: Finsch mine

Table A.1a: Major and minor element compositions (**Table A.1a-1**) and structural formulae (**Table A.1a-2**) of subcalcic garnets from the **Roberts Victor mine**, obtained by EPMA. Values are in wt%. Three to five measurements were performed on each garnet depending on sample size. Relative errors are 1-2% for major elements. Since the variation of the data of each element on individual sample is always smaller than the relative errors. Only averages are shown here.

Table A.1a-1 Subcalcic garnets from the Roberts Victor mine - major element (wt%)															
group	sample	SiO ₂	Na ₂ O	CaO	MnO	MgO	Cr ₂ O ₃	FeO ^{total}	Al ₂ O ₃	TiO ₂	P ₂ O ₅	Total	Mg#	Cr#	Cr/Al
	RV24	43.09	<0.02	1.21	0.4	24.22	4.78	6.61	20.81	<0.03	<0.04	101.2	87	13	0.15
	RV26	43.27	0.02	0.55	0.31	25.24	6.9	5.77	19.18	<0.03	<0.04	101.3	87	13	0.15
Group	RV31	42.92	<0.02	1.18	0.38	23.9	5.05	7.2	20.63	<0.03	<0.04	101.3	86	14	0.16
RV1	RV93	43.3	0.02	3.74	0.26	22.86	3.05	6.18	21.87	<0.03	<0.04	101.3	87	9	0.09
	RV111	41.64	<0.02	1.42	0.35	23.95	9.6	5.91	16.85	<0.03	<0.04	99.76	88	28	0.38
	RV123	43.07	<0.02	0.67	0.29	25.12	5.52	5.61	19.81	<0.03	<0.04	100.1	89	16	0.19
	RV12	43.42	0.03	0.94	0.36	24.88	4.47	6.24	21.15	<0.03	<0.04	101.6	88	12	0.14
	RV17	43.74	0.03	1.09	0.28	25.25	4.27	5.6	21.31	0.04	<0.04	101.6	89	12	0.13
	RV23	42.96	0.02	1.45	0.34	24.39	6.7	6.04	19.45	0.03	<0.04	101.4	88	19	0.23
	RV28	43.27	0.02	0.55	0.31	25.24	6.9	5.77	19.18	<0.03	<0.04	101.3	89	19	0.24
	RV37	42.77	0.04	2.11	0.33	23.83	4.04	6.04	21.35	<0.03	<0.04	100.6	88	11	0.13
	RV34	43.02	0.03	1.63	0.3	24.35	7.78	5.88	18.48	0.03	<0.04	101.5	88	22	0.28
Group	RV54	42.13	0.04	1.47	0.35	23.52	4.15	6.25	21.3	<0.03	<0.04	99.27	87	12	0.13
RV2	RV79	43.58	<0.02	0.66	0.29	25.2	6.65	5.81	19.1	<0.03	<0.04	101.3	89	19	0.23
	RV94	42.68	0.02	1.82	0.33	23.53	6.77	6.13	18.7	<0.03	<0.04	100	89	18	0.22
	RV100	42.82	0.02	1.25	0.37	24.1	4.77	6.52	20.3	<0.03	<0.04	100.2	87	14	0.16
	RV108	42.24	0.04	1.87	0.36	23.69	4.35	6.5	20.73	<0.03	0.049	99.86	87	12	0.14
	RV110	41.9	0.03	1.69	0.29	24.09	7.66	5.68	18.16	0.07	<0.04	99.59	88	22	0.28
	RV124	42.9	0.02	1.46	0.36	23.77	4.78	6.8	20.33	<0.03	<0.04	100.5	86	14	0.16
	RV128	42.55	0.02	1.63	0.33	23.86	9.02	5.93	17.21	<0.03	<0.04	100.6	88	26	0.35
	RV130	43.02	0.04	1.3	0.36	24.1	4.76	6.39	20.41	<0.03	0.042	100.5	87	14	0.16
	RV35	42.12	0.07	4.83	0.41	20.83	6.56	7.01	18.9	0.25	0.076	101.1	84	19	0.23
	RV38	41.85	0.03	3.77	0.43	21.77	7.83	6.55	18.21	<0.03	<0.04	100.5	86	22	0.29
	RV42	42	0.08	4.37	0.31	21.3	3.96	6.86	20.58	0.38	<0.04	99.9	85	11	0.13
	RV55	40.52	0.08	6.05	0.34	19.21	10.64	6.77	15.2	0.45	<0.04	99.31	83	32	0.47
	RV57	41.68	0.02	3.26	0.4	22.01	6.45	6.13	19.54	<0.03	<0.04	99.52	86	18	0.22
	RV84	43.06	0.04	3.45	0.39	22.49	5.12	6.62	20.1	0.04	0.05	101.4	86	15	0.17
Group	RV90	42.43	0.06	5.22	0.38	20.86	7.89	6.42	17.74	0.21	0.07	101.3	85	23	0.3
RV3	RV96	42.8	0.07	4.23	0.35	21.58	3.54	7.3	20.49	0.33	<0.04	100.7	84	10	0.12
	RV98	41.67	0.06	4.96	0.31	20.88	7.93	6.57	17.18	0.28	<0.04	99.9	85	24	0.31
	RV105	42.14	0.06	4.07	0.4	21.3	2.7	7.56	21.34	0.25	0.047	99.87	83	8	0.08
	RV112	41.17	0.07	4.77	0.4	20.88	7.03	6.52	18.17	0.22	0.07	99.3	85	21	0.26
	RV115	40.11	0.07	3.82	0.39	21.33	11.98	6.67	14.43	0.27	0.05	99.15	85	36	0.56
	RV119	42.36	0.04	2.74	0.33	23.25	4.07	6.2	20.94	<0.03	0.05	99.99	87	12	0.13
	RV127	42.19	0.02	1.83	0.32	23.8	10.92	5.47	15.63	0.04	<0.04	100.2	89	32	0.47

Table A.4a-2 Subcalcic garnets from the Roberts Victor mine - cation												
group	sample	Si	Na	Ca	Mn	Mg	Cr	Fe	Al	Ti	P	Total
	RV24	3.007	0.002	0.090	0.024	2.519	0.264	0.386	1.712	0.000	0.000	8.005
	RV26	3.019	0.002	0.041	0.018	2.626	0.381	0.337	1.577	0.001	0.000	8.003
Group	RV31	3.002	0.001	0.088	0.022	2.493	0.279	0.422	1.701	0.001	0.000	8.008
RV1	RV93	3.014	0.003	0.279	0.015	2.372	0.168	0.360	1.794	0.000	0.000	8.007
	RV111	2.993	0.001	0.110	0.021	2.566	0.545	0.356	1.427	0.001	0.001	8.020
	RV123	3.025	0.001	0.050	0.017	2.630	0.307	0.330	1.640	0.000	0.001	8.001
	RV12	3.007	0.004	0.070	0.021	2.568	0.245	0.361	1.726	0.000	0.003	8.006
	RV17	3.015	0.004	0.080	0.016	2.594	0.233	0.323	1.732	0.002	0.002	8.000
	RV23	3.005	0.003	0.109	0.020	2.543	0.370	0.353	1.603	0.001	0.001	8.009
	RV28	3.019	0.002	0.041	0.018	2.626	0.381	0.337	1.577	0.001	0.000	8.003
	RV34	3.015	0.003	0.122	0.018	2.544	0.431	0.345	1.526	0.002	0.001	8.005
	RV37	2.995	0.005	0.158	0.020	2.488	0.224	0.354	1.762	0.000	0.003	8.010
Group	RV54	2.989	0.005	0.112	0.021	2.487	0.233	0.371	1.782	0.001	0.002	8.003
RV2	RV79	3.036	0.002	0.049	0.017	2.618	0.367	0.339	1.568	0.000	0.000	7.997
	RV94	3.052	0.004	0.132	0.018	2.518	0.353	0.327	1.577	0.001	0.000	7.984
	RV100	3.017	0.003	0.094	0.022	2.531	0.266	0.385	1.686	0.000	0.002	8.006
	RV108	2.990	0.005	0.142	0.021	2.500	0.244	0.385	1.730	0.001	0.003	8.021
	RV110	2.995	0.005	0.130	0.017	2.567	0.433	0.340	1.530	0.004	0.001	8.021
	RV124	3.020	0.003	0.110	0.022	2.494	0.266	0.400	1.687	0.000	0.001	8.004
	RV128	3.024	0.002	0.124	0.020	2.527	0.507	0.353	1.442	0.001	0.000	8.001
	RV130	3.021	0.005	0.098	0.022	2.522	0.265	0.375	1.689	0.001	0.003	8.001
	RV35	3.001	0.009	0.369	0.025	2.212	0.369	0.418	1.587	0.013	0.005	8.006
	RV38	2.997	0.005	0.289	0.026	2.324	0.444	0.392	1.537	0.000	0.001	8.015
	RV42	2.996	0.012	0.334	0.019	2.264	0.224	0.409	1.731	0.020	0.002	8.011
	RV55	2.993	0.011	0.479	0.021	2.115	0.621	0.418	1.324	0.025	0.002	8.011
	RV57	2.988	0.003	0.250	0.024	2.353	0.365	0.368	1.651	0.001	0.000	8.003
	RV84	3.021	0.006	0.258	0.023	2.352	0.284	0.389	1.663	0.002	0.003	8.002
Group	RV90	3.022	0.008	0.399	0.023	2.214	0.445	0.383	1.489	0.011	0.004	7.999
RV3	RV96	3.026	0.009	0.321	0.021	2.274	0.198	0.431	1.707	0.017	0.002	8.006
	RV98	3.014	0.009	0.385	0.019	2.251	0.454	0.398	1.465	0.015	0.002	8.012
	RV105	3.000	0.009	0.311	0.024	2.261	0.152	0.450	1.791	0.013	0.003	8.015
	RV112	2.988	0.009	0.371	0.025	2.259	0.403	0.396	1.555	0.012	0.004	8.021
	RV115	2.965	0.010	0.302	0.024	2.350	0.700	0.413	1.258	0.015	0.003	8.042
	RV119	2.994	0.005	0.207	0.020	2.450	0.227	0.367	1.744	0.001	0.003	8.018
	RV127	3.025	0.002	0.141	0.019	2.544	0.619	0.328	1.321	0.002	0.000	8.003

Chapter 3: Subcalcic garnets, Mantle metasomatism and Diamonds

Table A.1b: Major and minor element compositions (**Table A.1b-1**) and structural formulae (**Table A.1b-2**) of subcalcic garnets from the Lace mine obtained by EPMA. Values are in wt%. Three to five measurements were performed on each garnet depending on sample size. Relative errors are 1-2% for major elements. Since the variation of the data of each element on individual sample is always smaller than the relative errors. Only averages are shown here.

Table A.1b-1 Subcalcic garnets from the Lace mine - major element (wt%)															
	sample	SiO ₂	Na ₂ O	CaO	MnO	MgO	Cr ₂ O ₃	FeO ^{total}	Al ₂ O ₃	TiO ₂	P ₂ O ₅	Total	Mg#	Cr#	Cr/Al
	L4	42.86	0.04	1.67	0.26	24.83	4.37	5.39	20.97	0.06	<0.04	100.49	89	12	0.14
	L7	43.03	0.03	1.30	0.24	25.00	4.99	5.28	20.64	0.05	<0.04	100.62	89	14	0.16
	L12	43.22	0.03	3.73	0.26	23.35	3.31	5.53	21.73	0.06	<0.04	101.24	88	9	0.10
	L14	43.03	0.01	3.36	0.37	22.55	4.71	6.84	20.6	<0.03	<0.04	101.48	85	14	0.16
	L26	42.08	0.05	3.31	0.38	22.26	10.00	6.35	16.67	0.07	<0.04	101.18	86	29	0.40
Group	L28	43.25	0.02	1.01	0.26	25.37	5.23	5.31	20.45	<0.03	<0.04	100.94	89	15	0.17
L1	L30	43.12	0.01	0.33	0.25	26.27	8.14	4.56	18.52	<0.03	<0.04	101.23	91	23	0.29
	L31	42.32	0.02	4.84	0.37	21.01	6.16	6.86	19.37	<0.03	<0.04	101.02	85	18	0.21
	L32	43.09	0.03	3.85	0.26	23.12	3.33	5.41	21.7	0.06	<0.04	100.88	88	9	0.10
	L33	42.61	0.02	4.41	0.36	21.56	6.15	6.58	19.43	<0.03	<0.04	101.19	85	18	0.21
	L36	43.03	0.03	1.78	0.29	24.44	6.08	5.46	19.75	0.05	<0.04	100.93	89	17	0.21
	L38	43.36	0.01	0.43	0.24	26.12	6.85	4.43	19.28	<0.03	<0.04	100.75	91	19	0.24
	L2	43.02	0.03	1.36	0.33	24.52	3.02	6.18	22.18	0.03	<0.04	100.71	88	8	0.09
	L8	42.14	0.07	3.65	0.35	22.28	6.00	6.17	19.52	0.16	0.063	100.43	87	17	0.21
Group	L16	42.77	0.06	3.68	0.34	22.88	6.6	5.54	19.18	0.05	0.132	101.23	88	19	0.23
L2	L20	43.34	0.05	1.95	0.25	24.51	5.10	5.34	20.22	0.16	<0.04	100.94	89	14	0.17
	L25	42.09	0.06	5.53	0.34	20.93	8.78	6.29	17.06	0.14	<0.04	101.24	86	26	0.35
	L39	42.41	0.05	4.58	0.35	21.98	7.05	5.82	18.76	0.08	0.131	101.22	87	20	0.25
	L19	42.29	0.09	4.37	0.38	21.26	8.23	6.64	17.52	0.19	0.03	100.99	85	24	0.32
Group	L21	42.62	0.07	3.79	0.36	22.17	5.37	6.58	19.83	0.23	0.05	101.08	86	15	0.18
L3	L27	41.82	0.09	4.61	0.37	20.38	7.21	8.08	18.07	0.34	0.05	101.02	82	21	0.27
	L37	41.96	0.07	4.32	0.44	20.95	8.20	7.00	17.50	0.19	0.03	100.66	84	24	0.31

Table A.1b-2 Subcalcic garnets from the Lace mine - cation												
	sample	Si	Na	Ca	Mn	Mg	Cr	Fe	Al	Ti	P	Total
	L4	2.999	0.006	0.128	0.016	2.580	0.242	0.315	1.723	0.004	0.002	8.015
	L7	3.003	0.005	0.097	0.014	2.601	0.276	0.308	1.698	0.003	0.002	8.007
	L12	3.005	0.005	0.278	0.015	2.420	0.182	0.321	1.781	0.003	0.000	8.011
	L14	3.016	0.002	0.265	0.022	2.336	0.265	0.400	1.696	0.000	0.000	8.003
	L26	3.005	0.007	0.254	0.023	2.370	0.565	0.380	1.403	0.004	0.001	8.010
Group	L31	3.008	0.002	0.369	0.022	2.226	0.346	0.408	1.622	0.001	0.001	8.007
L1	L32	3.007	0.004	0.288	0.015	2.404	0.184	0.316	1.784	0.003	0.002	8.007
	L33	3.013	0.003	0.334	0.022	2.274	0.344	0.389	1.620	0.001	0.002	8.003
	L36	3.012	0.003	0.134	0.017	2.549	0.337	0.319	1.629	0.002	0.001	8.003
	L28	3.008	0.003	0.075	0.015	2.631	0.288	0.309	1.677	0.000	0.001	8.009
	L30	3.005	0.002	0.025	0.015	2.728	0.449	0.266	1.521	0.000	0.000	8.011
	L38	3.020	0.001	0.032	0.014	2.712	0.377	0.258	1.583	0.000	0.001	7.999
	L2	2.994	0.005	0.101	0.020	2.543	0.166	0.360	1.820	0.001	0.002	8.011
	L8	2.993	0.010	0.278	0.021	2.359	0.337	0.366	1.634	0.009	0.004	8.012
Group	L16	3.008	0.008	0.278	0.020	2.399	0.367	0.325	1.590	0.003	0.008	8.005
L2	L20	3.022	0.006	0.155	0.015	2.537	0.279	0.313	1.661	0.009	0.001	8.000
	L25	3.011	0.008	0.424	0.021	2.232	0.497	0.376	1.439	0.007	0.001	8.015
	L39	3.000	0.007	0.347	0.021	2.318	0.395	0.345	1.564	0.004	0.008	8.008
	L19	3.020	0.012	0.334	0.023	2.264	0.465	0.397	1.475	0.010	0.002	8.002
Group	L21	3.007	0.010	0.287	0.022	2.331	0.300	0.388	1.649	0.012	0.003	8.007
L3	L27	3.001	0.012	0.355	0.023	2.180	0.409	0.485	1.528	0.018	0.003	8.014
	L37	3.014	0.010	0.333	0.027	2.243	0.466	0.420	1.481	0.010	0.002	8.005

Chapter 3: Subcalcic garnets, Mantle metasomatism and Diamonds

Table A.1c: Major and minor element compositions (**Table A.1c-1**) and structural formulae (**Table A.1c-2**) of subcalcic garnets from the **Bellsbank mine** obtained by EPMA. Values are in wt%. Three to five measurements were performed on each garnet depending on sample size. Relative errors are 1-2% for major elements. Since the variation of the data of each element on individual sample is always smaller than the relative errors. Only averages are shown here.

group	sample	SiO ₂	Na ₂ O	CaO	MnO	MgO	Cr ₂ O ₃	FeO ^{total}	Al ₂ O ₃	TiO ₂	P ₂ O ₅	Total	Mg#	Cr#	Cr/Al
	BB7	42.33	0.02	4.86	0.41	21.01	5.77	6.84	19.46	0.02	0.01	100.72	85	17	0.20
	BB14	43.00	0.03	4.44	0.39	21.51	4.63	6.76	20.42	0.02	0.02	101.19	85	13	0.15
group	BB19	43.26	0.02	3.13	0.37	22.59	4.09	6.99	20.82	0.03	0.01	101.30	85	12	0.13
B1	BB20	42.59	0.02	4.67	0.40	21.26	4.76	6.92	20.32	0.01	0.04	100.96	85	14	0.16
	BB22	42.22	0.03	3.43	0.37	22.31	4.75	6.93	20.45	0.03	0.00	100.51	85	13	0.16
	BB27	42.62	0.03	3.82	0.38	22.20	4.49	6.68	20.50	0.01	0.01	100.72	86	13	0.15
	BB4	42.60	0.03	4.93	0.41	21.07	5.62	6.83	19.60	0.04	0.06	101.14	85	16	0.19
	BB5	42.46	0.02	4.04	0.37	22.18	5.25	6.40	20.17	0.02	0.05	100.91	86	15	0.17
	BB13	42.58	0.04	4.48	0.43	21.27	4.32	6.96	20.55	0.03	0.06	100.66	84	12	0.14
	BB17	42.45	0.04	4.80	0.38	21.21	5.29	6.68	19.74	0.04	0.07	100.62	85	15	0.18
group	BB18	42.55	0.04	4.85	0.39	21.35	5.33	6.62	19.87	0.08	0.06	101.07	85	15	0.18
B2	BB21	42.36	0.05	4.82	0.39	21.65	5.19	6.16	19.97	0.02	0.05	100.62	85	13	0.16
	BB24	42.65	0.03	4.54	0.41	21.46	4.87	6.66	20.15	0.00	0.05	100.77	85	14	0.16
	BB25	42.15	0.03	4.83	0.38	21.15	5.56	6.75	19.72	0.04	0.06	100.62	85	16	0.19
	BB26	42.24	0.03	4.82	0.38	21.26	5.12	6.75	19.96	0.02	0.07	100.56	85	15	0.17
	BB28	42.42	0.02	4.17	0.36	22.07	4.20	6.55	20.91	0.00	0.07	100.70	86	12	0.13
	BB30	42.31	0.03	3.60	0.40	22.21	4.45	6.78	20.66	0.02	0.06	100.47	85	13	0.14
	BB32	42.41	0.04	5.05	0.46	20.70	5.73	7.26	19.46	0.07	0.05	101.18	84	16	0.20

group	sample	Si	Na	Ca	Mn	Mg	Cr	Fe	Al	Ti	P	Total
	BB7	3.013	0.003	0.371	0.025	2.229	0.325	0.407	1.633	0.001	0.001	8.008
	BB14	3.026	0.004	0.334	0.023	2.256	0.258	0.398	1.694	0.001	0.002	7.996
group	BB19	3.027	0.003	0.235	0.022	2.357	0.226	0.410	1.718	0.001	0.000	8.000
B1	BB20	3.011	0.003	0.353	0.024	2.241	0.266	0.409	1.694	0.001	0.002	8.005
	BB22	2.992	0.003	0.260	0.022	2.356	0.266	0.411	1.708	0.001	0.000	8.021
	BB27	3.009	0.004	0.289	0.022	2.336	0.251	0.395	1.706	0.001	0.001	8.013
	BB4	3.016	0.004	0.374	0.024	2.224	0.315	0.405	1.636	0.002	0.003	8.004
	BB5	2.997	0.003	0.306	0.022	2.333	0.293	0.378	1.678	0.001	0.003	8.014
	BB13	3.014	0.005	0.340	0.026	2.245	0.242	0.412	1.714	0.002	0.003	8.004
	BB17	3.014	0.005	0.365	0.023	2.245	0.297	0.397	1.652	0.002	0.004	8.006
group	BB18	3.008	0.006	0.368	0.023	2.250	0.298	0.392	1.656	0.004	0.004	8.008
B2	BB21	3.024	0.006	0.370	0.022	2.266	0.292	0.369	1.648	0.001	0.003	8.003
	BB24	3.017	0.004	0.345	0.025	2.263	0.273	0.394	1.680	0.000	0.003	8.004
	BB25	2.999	0.005	0.368	0.023	2.243	0.313	0.402	1.654	0.002	0.004	8.012
	BB26	3.002	0.004	0.367	0.023	2.252	0.288	0.401	1.672	0.001	0.004	8.014
	BB28	2.992	0.003	0.315	0.022	2.320	0.234	0.386	1.738	0.000	0.004	8.016
	BB30	2.993	0.004	0.273	0.024	2.343	0.249	0.402	1.723	0.001	0.003	8.017
	BB32	3.011	0.005	0.385	0.028	2.191	0.322	0.431	1.629	0.004	0.003	8.009

Table A.1d: Major and minor element compositions (**Table A.1d-1**) and structural formulae (**Table A.1d-2**) of subcalcic garnets from the **Kimberley mine** obtained by EPMA. Values are in wt%. Three to five measurements were performed on each garnet depending on sample size. Relative errors are 1-2% for major elements. Since the variation of the data of each element on individual sample is always smaller than the relative errors. Only averages are shown here.

Table A.1d-1 Subcalcic garnets from the Kimberley mine - major element (wt%)															
group	sample	SiO ₂	Na ₂ O	CaO	MnO	MgO	Cr ₂ O ₃	FeO ^{total}	Al ₂ O ₃	TiO ₂	P ₂ O ₅	Total	Mg#	Cr#	Cr/Al
group K1	ken1	42.66	0.02	3.47	0.33	22.77	3.84	6.31	21.20	0.02	0.02	100.67	87	15	0.18
	ken2	42.34	0.02	4.84	0.30	21.60	7.09	6.29	18.42	0.04	0.01	100.96	86	11	0.12
	bosh7	42.80	0.05	3.89	0.27	22.77	2.94	5.91	21.84	0.13	0.03	100.65	87	24	0.31
group	bosh11	42.51	0.01	4.58	0.36	21.74	5.34	6.26	20.23	0.00	0.05	101.10	86	8	0.09
	ken5	42.26	0.03	3.90	0.29	22.17	8.18	6.37	17.59	0.11	0.02	100.93	86	21	0.26

Table A.1d-2 Subcalcic garnets from the Kimberley mine - cation												
group	sample	Si	Na	Ca	Mn	Mg	Cr	Fe	Al	Ti	P	Total
group K1	Ken1	2.999	0.003	0.262	0.020	2.386	0.213	0.371	1.757	0.001	0.002	8.015
	Ken2	3.012	0.003	0.368	0.018	2.290	0.399	0.374	1.545	0.002	0.001	8.014
	bosh7	2.999	0.006	0.292	0.016	2.378	0.163	0.346	1.803	0.007	0.001	8.012
group k2	Bosh11	2.999	0.002	0.346	0.021	2.286	0.298	0.369	1.682	0.000	0.003	8.007
	Ken5	3.012	0.004	0.298	0.018	2.355	0.461	0.380	1.478	0.006	0.001	8.014

Table A.1e: Major and minor element compositions of subcalic garnets from **the Finsch mine** obtained by EPMA. Values are in wt% (**Data are from Lazarov et al., 2009**).

Table A.1e Major and minor element compositions of subcalic garnets from the Finsch mine														
	Sample	SiO ₂	Na ₂ O	CaO	MnO	MgO	Cr ₂ O ₃	FeO	Al ₂ O ₃	TiO ₂	Total	Mg#	Ca#	Cr#
group F1	HMCF-grt 12	43.03	0.02	0.83	0.24	25.4	4.09	5.05	21.22	0.02	99.92	90	2.3	11.4
	HMCF-grt 20	42.97	0.04	2.55	0.24	23.85	2.89	5.52	21.84	0.05	100	89	7.2	8.1
	HMCF-grt 28	43.01	0.02	1.62	0.27	24.23	3.35	5.86	21.54	0.01	99.93	87	4.6	9.5
	HMCF-grt 29	43.03	0.02	1.53	0.27	24.28	3.14	5.82	21.73	0.02	99.86	88	4.3	8.8
	HMCF-grt 35	43.14	0.02	0.34	0.24	25.87	4.04	4.98	21.26	0.01	99.91	90	0.9	11.3
	HMCF-grt 38	43.19	0.04	1.77	0.23	24.81	3.06	5.02	21.96	0.04	100.1	90	4.9	8.5
	HMCF-grt 43	43.1	0.05	1.05	0.25	25.32	3.61	5.09	21.72	0.02	100.3	90	2.9	10
	HMCF-grt 58	43.11	0.04	2.69	0.25	23.71	2.46	5.57	22.12	0.05	100	88	7.7	6.9
group F2	HMCF-grt 3	42.42	0.03	2.42	0.28	23.61	5.33	5.66	20.11	0.08	100	88	6.9	15.1
	HMCF-grt 11	42.65	0.04	2.38	0.28	23.88	4.03	5.55	21.25	0.07	100.2	89	6.7	11.3
	HMCF-grt 13	42.63	0.04	2.66	0.27	23.43	4.64	5.64	20.64	0.04	100.1	88	7.5	13.1
	HMCF-grt 14	42.62	0.05	3.18	0.29	23.15	4.05	5.65	21.06	0.05	100.2	88	9	11.5
	HMCF-grt 18	42.28	0.02	4.35	0.28	21.9	5.68	6.05	19.48	0.03	100.1	87	12.5	16.4
	HMCF-grt 30	42.36	0.04	4.02	0.36	21.62	4.09	6.61	20.86	0.02	100.1	88	11.8	11.6
	HMCF-grt 32	42.78	0.02	2.35	0.29	23.78	4.25	5.77	20.77	0.07	100.1	89	6.6	12.1
	HMCF-grt 33	42.8	0.03	2.26	0.27	23.76	3.86	5.8	21.2	0.02	100	88	6.4	10.9
	HMCF-grt 37	42.77	0.05	2.43	0.26	23.73	4.06	5.59	21.05	0.08	100.1	91	6.8	11.5
	HMCF-grt 39	42.95	0.05	1.88	0.23	24.53	4.42	4.94	20.91	0.10	100.1	90	5.2	12.4
	HMCF-grt 67	42.86	0.04	2.56	0.27	23.59	3.9	5.6	21.02	0.13	100	92	7.2	11.1
	HMCF-grt 82	42.33	0.05	4.1	0.31	21.53	4.07	6.82	20.67	0.17	100.1	85	12	11.7
	HMCF-grt 85	42.28	0.05	4.21	0.35	21.69	4.36	6.36	20.51	0.16	100	86	12.2	12.5
	F2-grt	41.99	0.04	5.5	0.32	20.97	7.8	6.17	17.8	0.20	100.9	85	15.9	22.7
	F7-grt	41.99	0.02	4.9	0.31	21.7	7.59	6.13	18.16	0.07	100.9	86	14	21.9
882-grt	40.93	0	6.14	0.33	20.22	11.63	5.59	14.96	0.17	99.97	87	17.9	34.3	

Tables A.2: trace element compositions of garnets

Table A.2a: Roberts Victor mine

Table A.2b: Lace mine

Table A.2c: Bellsbank mine

Table A.2d: Kimberley mine

Table A.2e: Finsch mine

Table A.2f: in house garnet standard PN2b and BIR-1 Basalt glass

Table A.2a LA-ICP-MS analyses of trace element concentrations of subcalcic garnets from the Roberts victor mine. Values (in ppm) are averages of several spot analyses. The $(Lu/Er)_{c1}$ and $(Lu/Hf)_{c1}$ ratios are normalized to C1 chondrite (McDonough and Sun, 1995). Abbreviations: n – number of spot analyses; b.d.l.– below detection limit; T (°C) Canil – temperatures calculated by Ni in garnet thermometer (Canil, 1999); T (°C) Griffin – temperatures calculated by Ni in garnet thermometer (Griffin et al. 1989).

Table A.2a Trace element concentrations of subcalcic garnets from the Roberts victor mine (in ppm)													
	Group RV1						Group RV2						
n	3	3	3	3	6	4	4	4	3	3	3	3	3
isotope	done	done	done	done	done	done	done	done	done	done	done	done	done
sample	RV24	RV26	RV31	RV93	RV111	RV123	RV12	RV17	RV23	RV28	RV34	RV37	RV54
Sc	110	100	93	140	193	122	77	70	136	100	97	88	100
Ti	70	174	98	37	140	31	94	314	224	130	401	55	121
V	178	220	221	161	282	230	177	188	185	220	227	167	176
Cr	27474	50053	40660	24318	77369	42663	36236	27557	34849	50053	57641	25877	23726
Mn	3136	2938	4048	2364	2966	2247	3562	2465	2579	2938	2942	2803	2976
Co	40	49	59	54	51	50	53	39	35	49	47	41	38
Ni	27	51	40	39	45	60	41	40	26	51	54	30	27
Ga	1.955	2.57	4.537	1.66	1.761	3.137	3.968	4.15	2.375	2.568	3.183	2.64	1.912
Rb	0.038	0.22	0.324	b.d.l.	b.d.l.	b.d.l.	0.582	0.06	0.492	0.221	0.179	0.066	0.339
Sr	2.12	2.51	2.19	b.d.l.	1.113	1.849	4.728	0.295	3.789	2.505	0.547	3.33	1.214
Y	0.401	0.3	1.289	0.313	0.582	0.288	0.473	0.737	2.204	0.301	1.367	0.585	0.78
Zr	3.077	2.62	0.985	1.415	2.815	2.117	12.165	7.407	3.423	2.622	16.48	28.163	15.29
Nb	0.82	0.29	0.264	0.103	0.121	0.216	1.596	0.471	0.405	0.288	0.198	0.743	0.571
Ba	b.d.l.	0.04	0.038	0.88	b.d.l.	b.d.l.	7.785	b.d.l.	b.d.l.	0.035	b.d.l.	0.638	0.02
La	0.048	0.07	0.091	0.023	0.065	0.044	0.654	0.012	0.256	0.07	0.034	0.263	0.043
Ce	2.176	2.1	3.327	0.084	1.445	1.101	3.728	0.686	6.2	2.103	0.653	3.557	1.24
Pr	2.385	0.57	0.445	0.027	0.344	0.411	1.4	0.46	1.28	0.57	0.204	0.827	0.839
Nd	48.827	3.28	0.959	0.138	1.286	2.747	15.95	3.82	5.45	3.283	1.364	5.297	12.91
Sm	0.763	0.39	0.063	0.049	0.199	0.551	4.395	0.761	1.112	0.39	0.722	2.408	3.923
Eu	0.114	0.08	0.016	0.018	0.051	0.102	0.872	0.181	0.251	0.077	0.255	0.938	0.809
Gd	0.185	0.17	0.073	<d.l.	0.171	0.183	1.185	0.312	0.53	0.174	0.594	2.084	1.141
Tb	0.037	0.02	0.012	<d.l.	0.028	0.016	0.063	0.035	0.049	0.021	0.063	0.123	0.054
Dy	0.163	0.09	0.133	0.053	0.14	0.067	0.163	0.166	0.282	0.093	0.321	0.256	0.175
Ho	0.012	0.01	0.042	0.01	0.027	0.012	0.019	0.026	0.073	0.013	0.051	0.021	0.027
Er	0.076	0.04	0.207	0.08	0.074	0.049	0.056	0.086	0.344	0.043	0.138	0.078	0.129
Tm	0.023	0.01	0.049	0.02	0.012	0.019	0.014	0.024	0.072	0.007	0.022	0.024	0.033
Yb	0.348	0.11	0.502	0.259	0.129	0.265	0.201	0.283	0.705	0.111	0.244	0.347	0.485
Lu	0.094	0.03	0.104	0.075	0.034	0.082	0.056	0.067	0.143	0.032	0.056	0.085	0.116
Hf	0.066	0.06	0.03	0.045	0.079	0.045	0.161	0.114	0.083	0.062	0.359	0.42	0.265
Ta	0.03	0.01	0.006	0.008	0.004	0.008	0.08	0.027	0.037	0.009	0.012	0.042	0.068
Pb	0.02	0.06	0.02	0.199	0.026	0.252	0.31	0.024	0.05	0.062	0.01	0.011	0.026
Th	0.11	0.01	0.033	0.002	0.011	0.008	0.173	0.009	0.097	0.013	0.01	0.081	0.015
U	0.068	0.03	0.043	0.041	0.015	0.027	0.088	0.028	0.095	0.027	0.022	0.069	0.034
T (°C) Griffin	908	1098	1015	1008	1052	1151	1026	1019	890	1098	1115	929	901
T (°C) Canil	950	1068	1018	1014	1041	1099	1025	1021	938	1068	1078	964	946
T (°C) average	929	1083	1017	1011	1047	1125	1026	1020	914	1083	1097	947	924

Chapter 3: Subcalcic garnets, Mantle metasomatism and Diamonds

Table A.2a continued													
	Group RV2								Group RV3				
n	3	4	6	6	5	5	6	4	3	3	3	3	3
isotope	done		done	done									
sample	RV79	RV94	RV100	RV108	RV110	RV124	RV12 8	RV130	RV38	RV35	RV42	RV55	RV57
Sc	128	175	122	120	146	133	179	135	227	168	76	106	289
Ti	71	203	61	153	565	67	175	92	219	2184	3574	3663	81
V	256	286	236	248	314	257	304	239	192	165	239	201	171
Cr	58093	57256	37004	35713	60242	36306	6	36252	49647	40000	28811	55565	41802
Mn	2671	2858	2870	3023	2309	2956	2717	2794	3498	3476	3095	2604	3640
Co	53	50	50	51	44	51	52	49	38	36	48	33	40
Ni	63	41	40	41	42	43	63	40	25	29	57	42	29
Ga	3.451	4.296	2.92	3.393	5.276	2.918	2.095	2.667	2.011	2.54	9.85	8.167	0.96
Rb	0.02	0.038	0.013	<d.l.	<d.l.	<d.l.	0.025	0.117	0.168	0.05	0.279	0.3	0.06
Sr	2.298	2.14	0.478	0.296	0.3	3.006	3.778	2.363	1.35	0.33	0.326	0.598	0.661
Y	0.399	2.214	0.452	0.902	2.066	0.574	0.41	0.617	4.955	41.95	12.99	18.73	4.68
Zr	3.13	2.336	6.21	21.277	11.058	8.048	5.105	27.417	11.695	98.89	28.753	51.107	32.19
Nb	0.245	0.808	1.251	0.527	0.32	0.877	0.41	1.207	0.608	0.244	0.128	0.264	0.366
Ba	0.082	0.591	b.d.l.	1.776	b.d.l.	0.158	0.118	0.531	b.d.l.	b.d.l.	b.d.l.	0.019	<d.l.
La	0.051	0.178	0.039	0.018	0.037	0.159	0.135	0.074	0.086	0.019	0.022	0.041	0.108
Ce	1.271	7.152	1.078	0.38	0.592	2.737	2.46	1.682	2.393	0.27	0.324	0.443	2.166
Pr	0.502	2.86	1.428	0.254	0.228	2.478	0.82	1.421	1.123	0.109	0.11	0.19	1.056
Nd	4.124	11.612	29.616	3.597	2.075	37.39	3.725	23.893	6.835	1.232	1.187	2.124	10.323
Sm	0.598	0.623	4.032	4.41	0.655	0.949	0.462	5.21	1.937	1.234	1.046	1.81	2.498
Eu	0.134	0.089	0.575	0.868	0.189	0.155	0.086	0.97	0.458	0.734	0.52	0.799	0.712
Gd	0.324	0.216	0.656	1.308	0.539	0.31	0.193	1.83	0.897	3.223	1.632	3.023	1.809
Tb	0.027	0.031	0.03	0.082	0.07	0.026	0.02	0.111	0.139	0.862	0.316	0.598	0.245
Dy	0.114	0.225	0.109	0.281	0.449	0.118	0.108	0.269	0.941	7.23	2.289	3.937	1.14
Ho	0.017	0.076	0.017	0.036	0.078	0.021	0.019	0.026	0.184	1.609	0.504	0.705	0.173
Er	0.049	0.341	0.082	0.122	0.214	0.103	0.053	0.093	0.462	4.587	1.568	1.716	0.502
Tm	0.011	0.079	0.026	0.033	0.032	0.031	0.011	0.029	0.063	0.638	0.243	0.237	0.099
Yb	0.166	0.761	0.338	0.423	0.288	0.403	0.102	0.393	0.517	4.167	2.045	1.637	0.957
Lu	0.048	0.162	0.097	0.107	0.062	0.101	0.032	0.113	0.1	0.548	0.284	0.231	0.205
Hf	0.053	0.07	0.125	0.408	0.266	0.159	0.135	0.484	0.273	1.53	0.615	1.099	0.68
Ta	0.012	0.023	0.045	0.061	0.028	0.041	0.019	0.054	0.032	0.02	0.008	0.019	0.012
Pb	0.199	1.408	0.071	0.063	0.032	0.26	0.115	0.68	0.012	0.004	0.026	0.008	0.046
Th	0.015	0.111	0.092	0.009	0.03	0.068	0.04	0.039	0.039	0.009	0.005	0.01	0.031
U	0.022	0.0326	0.072	0.018	0.027	0.104	0.065	0.064	0.085	0.014	0.011	0.024	0.091
T (°C) Griffin	1172	1026	1018	1025	1032	1036	1171	1018	885	926	1135	1031	923
T (°C) Canil	1111	1025	1020	1024	1029	1031	1110	1020	935	962	1089	1028	960
T (°C) average	1142	1026	1019	1025	1031	1034	1141	1019	910	944	1112	1030	942

Table A.2a continued									
	Group RV3								
n	5	4	5	6	6	6	5	4	5
isotope									
sample	RV84	RV90	RV96	RV98	RV105	RV112	RV115	RV119	RV127
Sc	141	190	111	142	112	193	227	113	419
Ti	391	1693	2480	2179	1848	1643	2131	114	311
V	251	217	227	396	201	292	340	246	226
Cr	38856	61265	28256	62611	21475	55801	96340	31183	87700
Mn	3195	3308	2864	2641	3514	3276	3215	2695	2550
Co	48	43	46	46	49	45	48	47	47
Ni	41	38	62	67	37	40	61	39	60
Ga	2.948	6.288	11.732	9.815	10.292	4.245	5.082	3.256	1.808
Rb	0.028	b.d.l.	0.015	0.016	b.d.l.	0.02	0.017	b.d.l.	b.d.l.
Sr	1.479	0.474	0.298	0.345	0.297	0.379	4.312	1.874	0.967
Y	5.348	21.204	15.84	6.945	27.882	39.793	10.23	1.8	3.982
Zr	78.328	73.832	23.736	26.558	53.458	127.91	84.598	63.752	35.46
Nb	0.447	0.171	0.1	0.074	0.043	0.246	0.227	0.512	0.556
Ba	0.437	0.214	0.078	b.d.l.	0.067	0.162	b.d.l.	0.122	b.d.l.
La	0.061	0.043	0.022	0.031	0.018	0.02	0.172	0.073	0.081
Ce	1.307	0.555	0.288	0.455	0.249	0.274	2.113	1.363	1.06
Pr	0.612	0.286	0.1	0.231	0.116	0.135	0.775	0.544	0.448
Nd	4.536	4.016	1.013	2.962	1.465	1.808	6.685	5.174	4.118
Sm	3.422	4.096	0.815	2.259	1.642	2.182	1.471	2.7	1.878
Eu	1.301	1.712	0.379	0.725	0.844	1.156	0.427	1.099	0.541
Gd	4.074	7.01	1.566	1.98	3.608	5.327	1.82	3.328	1.68
Tb	0.439	0.962	0.324	0.229	0.707	1.059	0.357	0.303	0.192
Dy	1.854	5.122	2.592	1.323	4.992	7.408	2.188	0.912	0.967
Ho	0.203	0.796	0.614	0.266	1.058	1.503	0.359	0.074	0.148
Er	0.364	1.85	1.936	0.829	3.154	4.173	0.859	0.125	0.363
Tm	0.043	0.24	0.302	0.125	0.47	0.576	0.113	0.031	0.05
Yb	0.468	1.506	2.134	0.937	3.306	3.687	0.717	0.374	0.372
Lu	0.106	0.219	0.331	0.165	0.51	0.525	0.113	0.1	0.071
Hf	1.312	1.208	0.498	0.629	0.555	1.838	1.83	1.073	0.788
Ta	0.054	0.012	0.012	0.002	0.003	0.024	0.012	0.039	0.044
Pb	0.415	0.195	0.139	0.078	0.069	0.032	0.114	0.12	0.06
Th	0.031	0.048	0.004	0.07	0.008	0.007	0.016	0.032	0.026
U	0.043	0.037	0.012	0.032	0.015	0.015	0.042	0.047	0.038
T (°C) Griffin	1022	996	1169	1194	991	1015	1162	1007	1151
T (C°) Canil	1023	1006	1109	1123	1004	1018	1105	1013	1099
T (C°)average	1023	1001	1139	1159	998	1017	1134	1010	1125

Table A.2b LA-ICP-MS analyses of trace element concentrations of subcalcic garnets from the **Lace mine**. Values (in ppm) are averages of several spot analyses. The (Lu/Er)_{c1} and (Lu/Hf)_{c1} ratios are normalized to C1 chondrite (McDonough and Sun, 1995). Abbreviations: n – number of spot analyses; b.d.l. – below detection limit; T (°C) Canil – temperatures calculated by Ni in garnet thermometer(Canil .1999); T (°C) Griffin – temperatures calculated by Ni in garnet thermometer(Griffin et al. 1989).

Table A.2b Trace element concentrations of subcalcic garnets from the Lace mine (in ppm)												
	group L1											
n	5	5	5	5	5	5	5	5	5	5	5	5
isotope	done	done	done	done	done	done	done	done	done	4	done	done
sample	L4	L7	L12	L14	L26	L31	L32	L33	L28	L30	L38	L36
Sc	91	94	82	117	162	128	82	117	100	103	99	122
Ti	618	552	441	97	507	92	473	114	39	49	40	370
V	257	324	264	293	361	329	242	316	274	188	190	326
Cr	33679	37132	26454	35428	76007	48290	25487	45603	41758	60515	53123	46825
Mn	2201	2048	2282	2873	3184	3349	2202	3024	2293	1918	1918	2467
Co	51	49	50	53	53	55	48	53	52	45	48	52
Ni	67	69	52	50	56	54	51	55	72	63	71	71
Ga	5.017	3.776	5.706	2.431	4.422	4.158	5.520	3.267	3.926	2.303	3.294	3.028
Rb	0.087	b.d.l.	b.d.l.	0.025	b.d.l.	0.018	0.019	<d.l.	b.d.l.	b.d.l.	0.046	<d.l.
Sr	0.496	0.387	0.262	0.322	1.077	0.557	0.232	0.418	0.771	0.986	0.714	0.579
Y	0.570	0.577	5.438	1.016	0.857	0.917	6.052	1.014	0.226	0.133	0.293	2.541
Zr	12.757	12.960	5.928	4.143	5.494	1.327	7.932	2.939	7.064	4.044	4.074	7.952
Nb	0.464	0.503	0.652	0.515	1.822	0.653	0.547	0.805	0.691	1.716	0.980	0.704
Ba	0.228	0.055	<d.l.	<d.l.	0.391	0.035	0.012	0.080	1.777	0.054	0.021	0.010
La	0.011	0.018	0.044	0.147	0.122	0.042	0.045	0.218	0.039	0.093	0.059	0.092
Ce	0.211	0.327	0.545	0.466	1.380	0.751	0.523	2.600	0.710	2.227	0.674	1.827
Pr	0.153	0.146	0.184	0.119	0.353	0.202	0.185	0.473	0.278	0.470	0.286	0.624
Nd	1.672	1.308	1.363	0.633	2.163	1.085	1.415	2.235	2.437	2.369	1.747	3.762
Sm	0.824	0.682	0.582	0.476	0.556	0.304	0.623	0.446	0.899	0.797	0.277	0.630
Eu	0.221	0.207	0.206	0.152	0.150	0.095	0.220	0.115	0.205	0.120	0.055	0.135
Gd	0.560	0.470	0.580	0.490	0.319	0.262	0.692	0.326	0.354	0.158	0.141	0.349
Tb	0.046	0.045	0.100	0.058	0.031	0.035	0.119	0.041	0.021	0.010	0.016	0.047
Dy	0.188	0.182	0.775	0.283	0.149	0.179	0.904	0.221	0.062	0.039	0.070	0.334
Ho	0.022	0.025	0.191	0.040	0.032	0.031	0.212	0.038	0.008	0.006	0.013	0.087
Er	0.047	0.062	0.692	0.096	0.125	0.097	0.757	0.096	0.033	0.019	0.036	0.383
Tm	0.006	0.011	0.128	0.017	0.031	0.017	0.130	0.013	0.008	0.004	0.006	0.080
Yb	0.125	0.125	1.103	0.195	0.321	0.180	1.113	0.110	0.111	0.028	0.065	0.729
Lu	0.035	0.033	0.199	0.047	0.076	0.042	0.201	0.024	0.030	0.008	0.018	0.146
Hf	0.221	0.271	0.142	0.055	0.116	0.022	0.173	0.074	0.153	0.091	0.082	0.194
Ta	0.006	0.006	0.024	0.004	0.053	0.004	0.016	0.007	0.015	0.047	0.014	0.013
Pb	0.010	0.022	0.040	0.047	0.010	0.023	0.039	0.020	0.025	0.024	0.028	0.024
Th	0.005	0.008	0.037	0.047	0.048	0.005	0.031	0.616	0.014	0.024	0.041	0.023
U	0.013	0.016	0.043	0.007	0.058	0.007	0.036	0.054	0.032	0.095	0.042	0.035
T (°C) Griffin	1197	1211	1104	1086	1131	1116	1097	1123	1226	1174	1222	1222
T (°C) Canil	1125	1132	1072	1061	1087	1079	1067	1083	1141	1112	1139	1138
T (°C) average	1161	1172	1088	1074	1109	1098	1082	1103	1184	1143	1181	1180

Table A.2b continued										
	group L2						group L3			
n	5	5	5	5	5	5	5	5	5	5
isotope	done						done	done	done	done
sample	L2	L8	L16	L20	L25	L39	L19	L21	L27	L37
Sc	99	121	122	96	126	137	196.03	115.11	198.51	238.68
Ti	251	1260	363	1359	1063	615	1527	1942	2548	1522
V	144	185	245	281	377	238	285.07	194.91	219.84	275.24
Cr	24000	45627	54095	44595	67794	54403	61706	43169	53721	65023
Mn	2691	2948	2792	2341	2785	2842	2972.3	3210.9	3165.4	3623.3
Co	53	50	51	52	49	48	51.702	53.172	56.918	52.756
Ni	23	48	55	74	73	47	49.316	51.22	39.648	49.596
Ga	2.153	2.908	3.186	4.678	7.608	3.023	5.428	5.104	6.282	6.732
Rb	0.016	b.d.l.	0.019	0.020	b.d.l.	0.017	0.017	0.017	0.064	0.069
Sr	0.615	0.312	0.718	0.398	0.899	0.587	0.291	0.253	0.301	0.588
Y	1.371	3.050	2.230	1.003	4.738	11.935	6.020	7.286	13.382	6.850
Zr	48.172	25.844	29.848	20.963	19.532	58.038	12.044	17.014	17.646	12.432
Nb	0.323	0.713	0.834	0.617	1.053	0.950	0.959	0.662	1.008	1.068
Ba	0.009	b.d.l.	0.513	0.005	0.008	0.032	0.118	b.d.l.	b.d.l.	0.225
La	0.018	0.022	0.049	0.010	0.062	0.038	0.012	0.018	0.009	0.062
Ce	0.559	0.219	0.551	0.207	0.711	0.562	0.126	0.198	0.080	0.627
Pr	0.404	0.082	0.318	0.092	0.254	0.261	0.052	0.067	0.026	0.149
Nd	4.520	0.893	3.284	1.085	2.355	3.130	0.488	0.534	0.258	0.959
Sm	0.944	0.515	1.667	0.607	1.734	1.769	0.260	0.296	0.245	0.347
Eu	0.200	0.234	0.576	0.197	0.669	0.639	0.104	0.139	0.130	0.110
Gd	0.551	0.852	1.288	0.432	1.923	2.477	0.422	0.515	0.701	0.439
Tb	0.071	0.148	0.134	0.052	0.217	0.479	0.096	0.134	0.198	0.101
Dy	0.367	0.779	0.589	0.261	1.008	2.985	0.849	1.183	1.972	0.896
Ho	0.052	0.122	0.088	0.039	0.181	0.450	0.217	0.283	0.509	0.247
Er	0.134	0.300	0.234	0.092	0.581	0.921	0.829	0.926	1.822	0.971
Tm	0.023	0.042	0.036	0.012	0.098	0.092	0.150	0.151	0.320	0.188
Yb	0.232	0.307	0.307	0.124	0.848	0.502	1.329	1.112	2.662	1.735
Lu	0.055	0.050	0.058	0.028	0.146	0.076	0.244	0.179	0.450	0.333
Hf	0.993	0.372	0.539	0.499	0.454	0.918	0.312	0.295	0.367	0.287
Ta	0.003	0.011	0.018	0.011	0.024	0.069	0.016	0.008	0.024	0.016
Pb	0.113	0.019	0.518	0.168	0.036	0.015	0.068	0.085	0.021	0.041
Th	0.005	0.006	0.011	0.003	0.021	0.015	0.012	0.008	0.011	0.022
U	0.027	0.012	0.045	0.013	0.046	0.053	0.014	0.018	0.014	0.042
T (°C) Griffin	861	1071	1121	1239	1234	1070	1065	1077	996	1066
T (C°) Canil	919	1052	1082	1148	1145	1052	1048	1056	1006	1050
T (C°) average	890	1062	1102	1194	1190	1061	1057	1067	1001	1058

Table A.2c LA-ICP-MS analyses of trace element concentrations of subcalcic garnets from **the Bellsbank mine**. Values (in ppm) are averages of several spot analyses. The $(Lu/Er)_{c1}$ and $(Lu/Hf)_{c1}$ ratios are normalized to C1 chondrite (McDonough and Sun, 1995). Abbreviations: n – number of spot analyses; T (°C) Canil – temperatures calculated by Ni in garnet thermometer(Canil .1999); T (°C) Griffin – temperatures calculated by Ni in garnet thermometer(Griffin et al. 1989).

Table A.2c Trace element concentrations of subcalcic garnets from the Bellsbank mine (in ppm)						
Bellsbank	group B1					
n	3	3	3	3	3	3
sample	BB7	BB14	BB19	BB20	BB22	BB27
Sc	84	101	99	78	92	86
Ti	66	114	104	49	304	108
Cr	54936	42933	36833	40324	34281	34225
Co	45	46	50	42	41	35
Ni	32	31	35	27	31	26
Ga	1.975	2.160	1.735	2.010	2.103	1.744
Sr	1.963	0.259	0.465	0.256	0.185	0.549
Y	0.400	0.399	1.415	1.032	0.934	0.569
Zr	2.169	10.080	1.924	6.530	2.471	1.437
Nb	1.266	0.754	0.269	0.860	0.222	0.220
La	0.523	0.055	0.155	0.027	0.041	0.154
Ce	4.250	1.000	2.074	0.535	0.558	1.871
Nd	16.490	4.010	1.395	5.135	0.864	1.441
Sm	0.359	1.068	0.353	0.717	0.171	0.211
Eu	0.073	0.243	0.091	0.141	0.052	0.053
Gd	0.278	0.420	0.201	0.394	0.156	0.148
Tb	0.028	0.036	0.029	0.041	0.025	0.017
Dy	0.150	0.170	0.244	0.231	0.178	0.112
Ho	0.021	0.023	0.073	0.051	0.040	0.025
Er	0.061	0.060	0.223	0.148	0.144	0.090
Tm	0.010	0.015	0.048	0.029	0.028	0.015
Yb	0.114	0.167	0.437	0.236	0.275	0.186
Lu	0.027	0.047	0.094	0.045	0.059	0.041
Hf	0.035	0.105	0.047	0.114	0.093	0.033
Ta	0.038	0.025	0.005	0.049	0.007	0.008
Pb	0.044	0.013	0.016	b.d.l.	b.d.l.	0.006
Th	0.083	0.045	0.051	0.019	0.018	0.067
U	0.200	0.125	0.069	0.049	0.027	0.066
T (°C) Griffin	953	940	975	908	944	895
T (C°) Canil	979	971	994	950	973	941
T (C°) average	966	955	985	929	959	918

Table A.2c. continued												
Bellsbank	group B2											
n	3	3	3	3	3	3	3	3	3	3	3	3
sample	BB28	BB4	BB5	BB13	BB17	BB18	BB21	BB24	BB25	BB26	BB30	BB32
Sc	77	87	133	105	82	91	302	86	73	77	85	125
Ti	29	362	190	363	457	615	175	126	364	59	109	379
Cr	34811	45381	55463	39632	44464	49500	39118	43711	52748	35640	36835	33177
Co	41	48	56	47	41	46	31	47	51	36	42	35
Ni	23	35	34	27	30	33	21	28	36	26	24	23
Ga	1.988	1.859	0.997	2.040	1.695	2.050	0.518	1.528	2.054	1.689	1.501	1.877
Sr	0.283	0.193	0.354	0.272	0.135	0.199	0.646	0.325	0.144	0.172	0.516	0.305
Y	0.130	7.583	19.753	5.370	4.360	8.397	37.240	2.152	2.159	1.402	5.310	12.267
Zr	13.750	63.233	58.180	75.040	50.090	56.820	69.230	25.460	47.520	27.023	35.327	51.430
Nb	0.618	0.389	0.720	0.531	0.340	0.318	0.352	0.783	0.420	0.664	0.620	0.350
La	0.059	0.025	0.035	0.031	0.018	0.027	0.069	0.065	0.030	0.016	0.026	0.023
Ce	0.670	0.424	1.169	0.511	0.298	0.358	1.225	1.730	0.422	0.303	0.792	0.416
Nd	2.584	2.395	9.900	2.780	2.145	2.330	7.420	8.480	2.282	2.012	8.917	2.156
Sm	3.700	2.627	6.230	3.170	2.315	2.507	4.780	2.405	2.328	2.298	9.910	2.241
Eu	1.132	1.284	2.913	1.450	1.077	1.177	1.850	0.673	1.160	0.865	4.563	0.937
Gd	1.164	3.127	7.990	3.690	2.780	3.447	6.320	1.406	2.631	1.657	5.160	2.707
Tb	0.026	0.425	1.213	0.431	0.319	0.423	1.140	0.191	0.323	0.142	0.332	0.516
Dy	0.049	2.606	6.133	1.996	1.867	2.507	7.610	0.851	1.287	0.533	1.479	3.028
Ho	0.009	0.304	0.825	0.267	0.197	0.398	1.319	0.100	0.103	0.057	0.214	0.499
Er	0.040	0.381	1.426	0.415	0.235	0.598	2.710	0.155	0.143	0.091	0.400	1.392
Tm	0.009	0.032	0.133	0.042	0.026	0.056	0.346	0.016	0.016	0.010	0.041	0.210
Yb	0.158	0.191	0.759	0.255	0.192	0.302	2.240	0.108	0.126	0.102	0.222	1.451
Lu	0.041	0.031	0.091	0.042	0.032	0.045	0.302	0.022	0.023	0.023	0.032	0.208
Hf	0.243	0.676	0.619	1.079	0.529	0.670	1.009	0.384	0.487	0.276	0.452	0.673
Ta	0.044	0.022	0.026	0.016	0.020	0.017	0.022	0.025	0.019	0.046	0.027	0.024
Pb	0.011	b.d.l.	b.d.l.	b.d.l.	0.011	0.010	0.011	b.d.l.	b.d.l.	b.d.l.	0.010	b.d.l.
Th	0.032	0.004	0.019	0.025	0.004	0.005	0.025	0.038	0.005	0.011	0.015	0.003
U	0.048	0.031	0.109	0.106	0.024	0.025	0.109	0.160	0.029	0.033	0.049	0.025
T (°C) Griffin	869	975	963	901	929	960	839	914	986	891	872	868
T (C°) Canil	924	993	986	946	964	984	904	954	1001	939	926	924
T (C°) average	897	984	975	923	946	972	872	934	993	915	899	896

Table A.2d LA-ICP-MS analyses of trace element concentrations of subcalcic garnets from **the kimberley mine**. Values (in ppm) are averages of several spot analyses. The $(Lu/Er)_{c1}$ and $(Lu/Hf)_{c1}$ ratios are normalized to C1 chondrite (McDonough and Sun, 1995). Abbreviations: n – number of spot analyses; b.d.l. – below detection limit; n.m.- not measured. T (°C) Canil – temperatures calculated by Ni in garnet thermometer(Canil,1999); T (°C) Griffin – temperatures calculated by Ni in garnet thermometer(Griffin et al., 1989).

Table A.2d Trace element concentrations of subcalcic garnets from the kimberley mine (in ppm)					
	group K1			group K2	
n	6	7	10	5	7
isotope	done	done	done	done	done
sample	ken01	ken02	bosh7	bosh11	ken05
Sc	70	101	n.d.	134	113
Ti	38	264	410	643	830
V	186	301	n.m.	156	255
Cr	31407	60188	n.m.	79344	67640
Mn	2702	2512	n.m.	3979	2490
Co	43	41	n.m.	42	42
Ni	37	67	55	34	66
Ga	1.978	2.566	n.m.	2.426	2.710
Rb	0.183	0.031	n.m.	b.d.l.	0.018
Sr	3.122	0.554	18.397	0.357	1.190
Y	0.377	0.688	6.692	14.683	2.188
Zr	12.955	6.455	15.485	58.880	32.420
Nb	0.759	0.314	0.497	0.288	0.497
Ba	5.597	b.d.l.	n.m.	b.d.l.	b.d.l.
La	0.567	0.044	0.040	0.024	0.043
Ce	2.585	0.639	1.024	0.384	0.643
Pr	1.056	0.303	0.408	0.171	0.241
Nd	8.835	4.020	4.039	7.126	2.164
Sm	1.141	0.898	0.813	2.388	1.031
Eu	0.266	0.161	0.204	1.061	0.453
Gd	0.536	0.311	0.540	3.297	1.335
Tb	0.048	0.036	0.060	0.523	0.184
Dy	0.168	0.174	0.553	3.200	0.772
Ho	0.015	0.026	0.201	0.594	0.084
Er	0.028	0.072	0.913	1.614	0.136
Tm	0.007	0.010	0.157	0.224	0.016
Yb	0.089	0.097	1.537	1.547	0.142
Lu	0.025	0.019	0.304	0.235	0.030
Hf	0.220	0.140	0.346	0.765	0.775
Ta	0.026	0.022	0.064	0.018	0.031
Pb	0.062	0.044	0.089	0.020	0.030
Th	0.078	0.010	0.015	0.003	0.011
U	0.107	0.034	0.042	0.023	0.023
T (°C) Griffin	990	1196	1099	968	1188
T (C°) Canil	1003	1124	1069	989	1120
T (C°) average	996	1160	1084	978	1154

Table A.2e LA-ICP-MS analyses of trace element concentrations of subcalcic garnets from **the Finsch mine**. Values (in ppm) are averages of several spot analyses. The $(Lu/Er)_{c1}$ and $(Lu/Hf)_{c1}$ ratios are normalized to C1 chondrite (McDonough and Sun, 1995). Abbreviations: n – number of spot analyses; b.d.l. – below detection limit; T (°C) Canil – temperatures calculated by Ni in garnet thermometer(Canil .1999); T(°C) Griffin – temperatures calculated by Ni in garnet thermometer(Griffin et al. 1989).

Table A.2e. Trace element concentrations of subcalcic garnets from Finsch (in ppm); Lazarov et al. 2009											
n	group-1								group-2		
	2	4	2	3	2	3	2	3	2	2	2
sample	HMCF-Gt12	HMCF-Gt20	HMCF-Gt28	HMCF-Gt29	HMCF-Gt35	HMCF-Gt38	HMCF-Gt43	HMCF-Gt58	HMCF-gtr 3	HMCF-gtr11	HMCF-gtr13
B	0.28	0.32	0.29	0.32	0.3	0.35	0.27	0.55	0.32	0.24	0.34
Ti	72	180	36	72	36	144	72	180	287	251	144
V	174	186	253	278	187	177	185	192	211	261	259
Co	44	47	46	52	44	56	43	42	51	54	46
Ni	56	55	48	54	50	65	43	52	69	59	49
Cu	b.d.l.	0.12	b.d.l.	b.d.l.	b.d.l.	0.08	b.d.l.	0.06	0.12	b.d.l.	b.d.l.
Zn	9.5	9.6	9.6	10.4	8.7	11.3	8.5	9.5	12.1	10.7	9
Rb	b.d.l.	b.d.l.	0.02	b.d.l.	b.d.l.	b.d.l.	b.d.l.	0.01	b.d.l.	0.03	b.d.l.
Sr	0.71	0.94	1.40	4.50	2.51	0.53	1.58	1.01	0.52	0.58	0.41
Y	0.30	4.90	0.90	1.30	0.20	3.30	0.80	5.80	3.10	5.30	1.80
Zr	2.90	25.00	1.00	4.00	1.60	6.30	15.00	10.40	30.00	67.00	38.00
Nb	0.39	1.00	0.56	0.87	0.65	0.74	0.98	0.14	0.42	0.80	0.53
Mo	0.16	0.40	0.39	0.44	0.23	0.39	0.19	0.26	0.34	0.33	0.33
Ba	0.01	0.03	0.02	0.03	0.03	0.01	0.02	0.01	b.d.l.	0.01	0.02
La	0.05	0.12	0.34	0.74	0.23	0.08	0.16	0.04	0.03	0.05	0.05
Ce	0.74	1.60	4.50	6.40	6.30	1.10	3.90	0.92	0.55	0.93	0.85
Nd	1.00	3.10	2.50	2.60	6.00	2.90	9.20	1.80	3.20	3.80	3.60
Sm	0.20	1.50	0.20	0.20	0.60	1.10	2.50	0.40	2.10	2.50	1.80
Eu	0.07	0.49	0.02	0.04	0.07	0.34	0.54	0.11	0.64	0.57	0.59
Gd	0.20	1.50	0.05	0.09	0.13	0.68	1.00	0.34	2.20	1.50	1.50
Tb	0.02	0.13	0.00	0.01	0.01	0.04	0.06	0.05	0.20	0.16	0.13
Dy	0.07	0.69	0.04	0.06	0.03	0.25	0.20	0.53	0.84	1.03	0.50
Ho	0.01	0.15	0.02	0.03	0.01	0.10	0.03	0.18	0.10	0.18	0.06
Er	0.04	0.58	0.16	0.23	0.02	0.54	0.08	0.74	0.18	0.45	0.14
Tm	0.01	0.11	0.04	0.05	0.01	0.11	0.01	0.13	0.02	0.05	0.02
Yb	0.14	1.00	0.55	0.68	0.11	1.20	0.17	1.20	0.19	0.42	0.27
Lu	0.04	0.22	0.13	0.16	0.04	0.27	0.05	0.23	0.05	0.09	0.08
Hf	0.06	0.50	0.02	0.05	0.02	0.11	0.22	0.20	0.59	1.40	0.65
Ta	0.03	0.07	0.02	0.04	0.03	0.04	0.09	0.01	0.03	0.09	0.04
W	0.01	b.d.l.	0.01	b.d.l.	b.d.l.	0.01	0.92	0.01	0.56	b.d.l.	0.01
Pb	0.01	0.21	0.01	0.01	0.01	0.01	0.02	0.01	0.01	0.01	0.02
Th	0.01	0.04	0.28	0.14	0.08	0.05	0.05	0.01	0.01	0.02	0.01
U	0.01	0.05	0.10	0.10	0.17	0.11	0.16	0.02	0.03	0.05	0.06
T (°C) Griffin	1142	1123	1077	1113	1088	1195	1041	1133	1213	1165	1095
T (°C) Canil	1075	1070	1042	1065	1050	1107	1023	1067	1119	1086	1047
Average	1109	1097	1060	1089	1069	1151	1032	1100	1166	1126	1071

Table A.2e continued													
n	group-2												
	3	2	3	2	2	3	2	2	3	3	4	5	3
sample	HMCF-grt14	HMCF-grt18	HMCF-grt30	HMCF-grt32	HMCF-grt33	HMCF-grt37	HMCF-grt39	HMCF-grt67	HMCF-grt82	HMCF-grt85	F2-grt	F7-grt	882-grt
B	0.3	0.15	0.28	0.3	0.29	0.32	0.29	0.29	0.28	0.3	0.51	1.95	0.46
Ti	180	108	72	251	72	287	359	467	611	575	718	251	611
V	226	185	161	188	248	253	192	201	203	259	375	303	288
Co	45	28	50	49	44	52	51	47	50	44	46	40	38
Ni	49	44	41	69	46	57	59	55	61	50	74	59	61
Cu	0.07	0.04	b.d.l.	0.08	b.d.l.	0.06	0.07	0.11	0.16	0.07	0.14	b.d.l.	b.d.l.
Zn	8.1	5.5	9.2	12.9	9.1	10.1	10.4	10.9	11.3	9.5	11.3	8.8	10.7
Rb	0.02	b.d.l.	0.07	0.02	b.d.l.	0.02	b.d.l.	0.02	0.02	0.02	0.03	0.05	b.d.l.
Sr	0.47	0.44	0.4	0.62	0.86	0.56	1.02	0.99	0.23	0.65	1.08	0.36	2.09
Y	3.9	1.6	17	2.6	1.6	5.5	3.7	5.3	6.6	11	9.2	2.7	6.3
Zr	77	16	155	15	9.3	65	32	37	12	62	19	23	43
Nb	0.51	0.19	0.58	0.46	1.1	0.82	1.22	1.35	0.52	0.62	1.63	0.34	2.43
Mo	0.45	0.19	0.51	0.45	0.35	0.35	0.33	0.35	0.45	0.55	0.41	b.d.l.	0.51
Ba	0.01	b.d.l.	0.6	0.01	0.01	0.05	0.01	0.01	0.01	0.06	0.01	b.d.l.	0.02
La	0.04	0.02	0.06	0.02	0.2	0.05	0.1	0.07	0.04	0.04	0.17	0.01	0.19
Ce	0.74	0.45	1.4	0.45	2.6	0.93	1.7	1.8	0.55	0.82	1.9	0.27	2.5
Nd	2.5	1.6	3.7	2.7	2.9	3.8	5.4	5	0.9	3.4	3.1	2.3	7.5
Sm	2.1	1.1	3	1.3	0.6	2.5	1.5	1.6	0.5	1.8	1.1	1.8	2.9
Eu	0.87	0.32	1.4	0.35	0.16	0.56	0.4	0.38	0.29	0.57	0.42	0.62	0.78
Gd	2.6	0.93	5.6	1	0.4	1.4	1.1	1.1	1.1	1.7	1.3	1.7	2.1
Tb	0.24	0.08	0.75	0.11	0.03	0.16	0.14	0.12	0.17	0.21	0.18	0.17	0.21
Dy	1.06	0.36	4.2	0.6	0.22	1.1	0.8	0.86	1.1	1.5	1.3	0.75	1.2
Ho	0.14	0.05	0.61	0.09	0.05	0.19	0.13	0.18	0.21	0.36	0.32	0.1	0.21
Er	0.27	0.11	1	0.19	0.22	0.45	0.3	0.6	0.51	1.17	1.07	0.18	0.59
Tm	0.03	0.01	0.08	0.02	0.05	0.05	0.04	0.09	0.06	0.16	0.15	0.03	0.08
Yb	0.35	0.14	0.46	0.21	0.53	0.39	0.36	0.85	0.52	1.3	1.3	0.17	0.63
Lu	0.08	0.04	0.08	0.05	0.12	0.08	0.09	0.18	0.1	0.23	0.22	0.03	0.11
Hf	1.31	0.31	1.4	0.32	0.21	1.3	0.69	0.83	0.23	1.3	0.48	0.51	1
Ta	0.04	0.01	0.04	0.04	0.06	0.09	0.09	0.11	0.04	0.06	0.21	0.04	0.49
W	0.01	b.d.l.	0.02	b.d.l.	3.9	b.d.l.	0.01	b.d.l.	b.d.l.	b.d.l.	0.03	b.d.l.	0.02
Pb	0.01	b.d.l.	0.01	0.03	0.01	0.01	0.02	0.02	0.01	b.d.l.	0.03	0.25	0.01
Th	0.01	b.d.l.	0.01	0.01	0.14	0.02	0.04	0.02	0.01	0.01	0.11	0.01	0.08
U	0.030	0.030	0.070	0.020	0.110	0.050	0.080	0.080	0.040	0.050	0.090	0.020	0.130
T (°C) Griffin	1079	1047	1022	1218	1061	1141	1152	1126	1170	1090			
T (°C) Canil	1047	1024	1013	1118	1034	1079	1086	1069	1092	1053			
Average	1063	1036	1018	1168	1048	1110	1119	1098	1131	1072			

Table A.2f LA-ICP-MS analyses of trace element concentrations of results on the international standard BIR Basalt glass and the in house garnet standard PN2b. The trace elements data of BIR-1 from Eggins et al. (1997) are shown for comparison. Abbreviations: n – number of analyses; b.d.l. – below detection limit.

Table A.2f Trace elements of BIR-1 Basalt glass and in house garnet standard- PN2b (in ppm)								
n	35			54				
standard	PN2b	relative stdev(%)	std Err(%)	BIR-1 basalt glass standard	relative stdev(%)	std Err(%)	dl average(ppm)	Eggins et al. (1997),
		(1σ)	(1σ)		(1σ)	(1σ)		
Sc	78	6.4	1.8	42	13	2.2	0.053	44
V	121	4.1	1.1	310	21.8	3.7	0.03	310
Cr	112	5.3	1.5	416	32.8	5.6	0.912	382
Mn	2910	6.2	1.7	1446	15.8	2.7	0.265	1417
Co	71	4.4	1.2	51	17.6	3	0.027	52
Ni	41	5	1.4	159	11.9	3.8	0.356	166
Ga	6.362	3.3	0.9	12.84	18.7	3.2	0.052	16
Rb	0.029	32.1	9.7	0.18	30.1	5.2	0.09	0.24
Sr	0.276	27.4	7.9	108	10.6	1.8	0.047	110
Y	55.883	8.5	2.3	13.25	12.2	2.1	0.009	16.5
Zr	44.242	8.4	2.3	14.26	11.2	1.9	0.026	14.5
Nb	0.045	21	8	0.518	10.1	1.7	0.012	0.55
Ba	b.d.l			6.33	10.2	1.7	0.033	6.4
La	0.016	33.5	10.1	0.6	9.9	1.7	0.004	0.58
Ce	0.19	20.2	6.1	1.834	12.5	2.1	0.008	1.85
Pr	0.086	8.9	2.5	0.363	10.4	1.8	0.004	0.37
Nd	1.057	7.5	2.1	2.357	9.8	1.7	0.013	2.35
Sm	1.268	7.2	2	1.062	10.2	1.7	0.033	1.1
Eu	0.772	4.6	1.3	0.509	10.3	1.8	0.006	0.52
Gd	3.875	8	2.2	1.606	13.7	2.4	0.034	1.97
Tb	0.962	7.5	2.1	0.314	11.2	1.9	0.005	0.38
Dy	8.762	7.9	2.2	2.354	12.3	2.1	0.013	2.5
Ho	2.123	8.3	2.3	0.509	12.1	2.1	0.003	0.57
Er	6.68	7.9	2.2	1.512	12.4	2.1	0.012	1.7
Tm	0.982	9.1	2.5	0.222	12.6	2.2	0.005	0.27
Yb	6.562	8.4	2.3	1.59	11.8	2	0.003	1.6
Lu	0.926	9.5	2.6	0.227	13.2	2.3	0.005	0.25
Hf	0.838	10.5	2.9	0.557	13.3	2.3	0.008	0.56
Ta	0.005	35.7	13.5	0.037	11.8	2	0.009	0.04
Pb	0.922	59.1	17.1	4.043	12.3	14.5	0.01	3.2
Th	0.004	46.5	15.5	0.03	10.1	1.7	0.007	0.03
U	0.004	21.6	6.8	0.015	16.5	3.8	0.007	0.01

Tables A.3: Lu-Hf and Sm-Nd isotope compositions of garnets

Table A.3a: Roberts Victor mine

Table A.3b: Lace mine

Table A.3c: Bellsbank mine

Table A.3d: Kimebrley mine

Table A.3e: Finsch mine

Table A.3e: Lu –Hf isotope data of standards(in house garnet standard PN3b and BHVO-1 Basalt)

Table A.3f: Sm –Nd isotope data of standards(in house garnet standard PN3b and BHVO-1 Basalt)

Tables A.3a Lu-Hf isotope compositions (**Table A.3a-1**) and Sm-Nd isotope (**Table A.3a-2**) of subcalic garnets from the **Roberts Victor mine**. The internal precisions for all the Hf runs are less than the external error of the standards. Abbreviations: ID – isotope dilution

Table A.3a-1 Lu-Hf isotope compositions of subcalic garnets from the Roberts Victor mine								
	sample	ID-Lu (ppm)	ID-Hf (ppm)	$^{176}\text{Lu}/^{177}\text{Hf}$	$^{176}\text{Hf}/^{177}\text{Hf}$	Error (2s)	$\epsilon_{\text{Hf}}(0)$	T CHUR(Ga)
Group RV1	RV 24	0.092	0.075	0.1719	0.290817	0.000006	284	3.02
	RV26	0.037	0.073	0.0703	0.285001	0.000012	79	3.11
	RV 31	0.135	0.036	0.5266	0.310794	0.000015	991	2.96
	RV 93	0.062	0.065	0.1318	0.288261	0.000018	194	2.89
	RV111	0.027	0.071	0.0534	0.283971	0.000006	42	3.06
	RV 123	0.07	0.038	0.2553	0.295319	0.000013	444	2.94
Group RV2	RV12	0.075	0.196	0.0451	0.284192	0.000005	57	6.00
	RV23	0.141	0.081	0.2435	0.296838	0.000008	494	3.47
	RV54	0.121	0.256	0.0585	0.284582	0.000008	64	3.67
	RV 94	0.16	0.067	0.3327	0.301857	0.000009	672	3.31
	RV 100	0.091	0.127	0.099	0.287279	0.000008	159	3.54
	RV 124	0.094	0.155	0.084	0.286545	0.000005	133	3.83

Table A.3a-2 Sm-Nd isotope compositions of subcalic garnets from the Roberts Victor mine								
	sample	ID-Sm (ppm)	ID-Nd (ppm)	$^{147}\text{Sm}/^{144}\text{Nd}$	$^{143}\text{Nd}/^{144}\text{Nd}$	Error (2s)	$\epsilon_{\text{Nd}}(0)$	T CHUR(Ga)
Group RV1	RV24	0.78	48.48	0.00974	0.510841	0.000006	-35	1.46
	RV26	0.41	3.92	0.06352	0.510466	0.000012	-40	2.47
	RV31	0.07	1.26	0.03468	0.510515	0.000006	-41	1.99
	RV93	0.04	0.15	0.14609	0.512038	0.000065	-12	1.79
	RV111	0.18	1.53	0.07242	0.510533	0.000011	-41	2.57
	RV123	0.44	2.75	0.10147	0.510501	0.000007	-42	3.39
Group RV2	RV12	4.49	18.1	0.16712	0.511952	0.000008	-13	3.49
	RV23	1.03	5.84	0.11363	0.511261	0.000007	-27	2.51
	RV54	3.75	12.6	0.17981	0.511837	0.000008	-16	7.06
	RV94	0.61	11.76	0.03132	0.511237	0.000007	-27	1.29
	RV100	3.85	30.44	0.07643	0.511328	0.000004	-26	1.65
	RV124	0.95	34.09	0.0171	0.510945	0.000006	-33	1.43

Chapter 3: Subcalic garnets, Mantle metasomatism and Diamonds

Tables A.3b Lu-Hf isotope compositions (**Table A.3b-1**) and Sm-Nd isotope (**Table A.3b-2**) of subcalic garnets from the **Lace mine**. The internal precisions for all the Hf runs are less than the external error of the standards. Abbreviations: **ID** – isotope dilution.

Table A.3b-1 Lu-Hf isotope compositions of subcalic garnets from the Lace mine								
Group	sample	ID-Lu (ppm)	ID-Hf (ppm)	$^{176}\text{Lu}/^{177}\text{Hf}$	$^{176}\text{Hf}/^{177}\text{Hf}$	Error	$\epsilon\text{Hf}(0)$	T CHUR(Ga)
Group L1	L7	0.03	0.30	0.0151	0.282708	0.000002	-2.0	0.19
	L12	0.20	0.16	0.1825	0.293031	0.000005	363	3.56
	L14	0.04	0.06	0.0982	0.28548	0.000009	96	2.19
	L26	0.07	0.12	0.0801	0.2874	0.000006	164	5.04
	L28	0.03	0.10	0.0391	0.283912	0.000007	40	9.48
	L30	0.01	0.10	0.0113	0.281572	0.000005	-42	2.86
	L31	0.04	0.04	0.1451	0.289892	0.000005	251	3.3
	L32	0.20	0.26	0.1103	0.288539	0.000004	204	3.86
	L36	0.14	0.21	0.0912	0.285929	0.000004	112	2.84
GroupL2	L2	0.05	1.01	0.007	0.280946	0.000004	-65	3.61
Group L3	L19	0.24	0.33	0.1039	0.285022	0.000011	80	1.68
	L21	0.17	0.31	0.0797	0.282925	0.000062	5	0.18
	L27	0.42	0.37	0.1603	0.283527	0.000061	7	0.32
	L37	0.30	0.29	0.1494	0.286767	0.000018	141	1.81

Table A.3b-2 Sm-Nd isotope compositions of subcalic garnets from the Lace mine								
	sample	ID-Sm (ppm)	ID-Nd (ppm)	$^{147}\text{Sm}/^{144}\text{Nd}$	$^{143}\text{Nd}/^{144}\text{Nd}$	Error (2s)	$\epsilon\text{Nd}(0)$	T CHUR(Ga)
Group L1	L7	0.66	1.38	0.2872	0.512411	0.000007	-4	-0.38
	L12	0.57	1.40	0.2471	0.512401	0.000008	-5	-0.71
	L14	0.44	0.75	0.2645	0.511561	0.00001	-21	-2.44
	L26	0.55	2.47	0.1339	0.511835	0.000008	-16	1.94
	L28	0.88	2.18	0.183	0.511881	0.000008	-15	8.21
	L30	0.79	2.61	0.1843	0.511973	0.000008	-13	7.97
	L31	0.34	1.20	0.1683	0.511047	0.000007	-31	8.32
	L32	0.69	1.56	0.2675	0.51238	0.000006	-5	-0.55
	L36	0.67	3.75	0.1075	0.510753	0.000008	-37	3.19
Group L2	L2	0.90	4.48	0.1209	0.510631	0.000013	-39	3.99
Group L3	L19	0.21	0.45	0.2759	0.511924	0.000008	-14	-1.38
	L21	0.23	0.45	0.3128	0.512253	0.000011	-8	-5.06
	L27	0.19	0.21	0.5606	0.513121	0.000010	9	2.04
	L37	0.27	0.77	0.2102	0.512116	0.000010	-10	-6.01

Tables A.3c Lu-Hf isotope compositions (Table A.3c-1) and Sm-Nd isotope (Table A.3c-2) of subcalcic garnets from the Bellsbank mine. The internal precisions for all the Hf runs are less than the external error of the standards. Abbreviations: ID –isotope dilution.

Table A.3c-1 Lu-Hf isotope compositions of subcalcic garnets from the Bellsbank mine								
Group	sample	ID-Lu (ppm)	ID-Hf (ppm)	$^{176}\text{Lu}/^{177}\text{Hf}$	$^{176}\text{Hf}/^{177}\text{Hf}$	Error (2s)	$\epsilon\text{Hf}(0)$	T CHUR(Ga)
Group B1	BB7	0.05	0.07	0.0904	0.284361	0.000015	56	1.47
	BB14	0.10	0.17	0.0828	0.283214	0.000022	16	0.48
	BB19	0.10	0.07	0.2008	0.287399	0.000018	164	1.46
	BB22	0.06	0.13	0.0663	0.284392	0.000021	57	2.56
	BB20	0.06	0.15	0.0519	0.284045	0.000021	45	3.52
	BB27	0.06	0.06	0.1623	0.285717	0.000017	104	1.21
Group B2	BB17	0.05	0.89	0.0081	0.281790	0.000021	-35	2.05
	BB18	0.10	0.92	0.0159	0.281494	0.000022	-45	3.82
	BB21	0.37	1.16	0.0453	0.281130	0.000038	-58	-7.78
	BB28	0.09	0.36	0.0348	0.282164	0.000018	-21	-26.09
	BB30	0.07	0.72	0.0144	0.282241	0.000011	-19	1.49

Table A.3c-2 Sm-Nd isotope compositions of subcalcic garnets from the Bellsbank mine								
	sample	ID-Sm (ppm)	ID-Nd (ppm)	$^{147}\text{Sm}/^{144}\text{Nd}$	$^{143}\text{Nd}/^{144}\text{Nd}$	Error (2s)	ϵNd	T CHUR(Ga)
Group B1	BB7	0.82	32.73	0.0151	0.511236	0.000017	-27	1.17
	BB14	1.26	3.78	0.2020	0.512542	0.000017	-2	-2.71
	BB19	0.34	1.47	0.1375	0.512156	0.000024	-9	1.23
	BB20	0.66	6.27	0.0641	0.511756	0.000022	-17	1.01
	BB22	0.34	2.47	0.0826	0.511902	0.000026	-14	0.98
	BB27	0.23	1.67	0.0835	0.512011	0.000026	-12	0.84
Group B2	BB17	2.22	2.29	0.5875	0.514460	0.000020	36	0.71
	BB18	2.12	2.25	0.5685	0.514327	0.000021	33	0.69
	BB21	3.01	8.52	0.2136	0.512541	0.000019	-2	-0.86
	BB28	3.34	9.59	0.2106	0.512013	0.000020	-12	-7.03
	BB30	1.55	1.74	0.5392	0.513560	0.000022	18	0.41

Tables A.3d Lu-Hf isotope compositions (Table A.3d-1) and Sm-Nd isotope (Table A.3d-2) of subcalic garnets from the Kimberley mine. The internal precisions for all the Hf runs are less than the external error of the standards. Abbreviations: ID –isotope dilution.

Table A. 3d-1 Lu-Hf isotope compositions of subcalic garnets from the Kimberley mine								
Group	sample	ID-Lu (ppm)	ID-Hf (ppm)	$^{176}\text{Lu}/^{177}\text{Hf}$	$^{176}\text{Hf}/^{177}\text{Hf}$	Error (2s)	$\epsilon_{\text{Hf}}(0)$	T CHUR(Ga)
Group K1	ken01	0.02	0.40	0.0084	0.282341	0.000015	-15	0.92
	ken02	0.01	0.18	0.0086	0.282197	0.000031	-20	1.24
	bosh07	0.25	0.28	0.1262	0.286066	0.000023	116	1.86
Group K2	bosh11	0.03	0.93	0.0039	0.282523	0.000035	-9	0.45
	ken05	0.04	0.74	0.0069	0.280911	0.000023	-66	3.67

Table A. 3d-2 Sm-Nd isotope compositions of subcalic garnets from the Kimberley mine								
	sample	ID-Sm (ppm)	ID-Nd (ppm)	$^{147}\text{Sm}/^{144}\text{Nd}$	$^{143}\text{Nd}/^{144}\text{Nd}$	Error (2s)	$\epsilon_{\text{Nd}}(0)$	T CHUR(Ga)
Group K1	ken01	0.77	5.08	0.0918	0.512096	0.000017	-9	0.79
	ken02	1.13	5.33	0.1286	0.511742	0.000020	-17	1.99
	bosh07	0.63	3.74	0.1018	0.512591	0.000020	-1	0.73
Group K2	bosh11	2.11	7.34	0.2030	0.511999	0.000018	-13	-16.40
	ken05	0.84	2.51	0.1739	0.512043	0.000020	-12	3.92

Tables A. 3e Lu-Hf isotope data for repeated digestion of in house garnet standard (PN3b)(Table A. 3e-1) and BHVO-1 Basalt (Table A. 3e-2). Abbreviations: ID –isotope dilution ; Laser- in situ measurement by Laser Ablation ICP-MS.

Table A.3e-1 Lu-Hf isotope data of PN3b in house standard						
sample	$^{176}\text{Hf}/^{177}\text{Hf}$	$^{176}\text{Lu}/^{177}\text{Hf}$	ID-Lu [ppm]	ID-Hf [ppm]	laser-Lu [ppm]	laser-Hf [ppm]
PN3b-1	0.283022	0.089	0.49	0.79		
PN3b-2	0.283061	0.0901	0.51	0.81		
PN3b-3	0.283057	0.0883	0.48	0.76		
PN3b-4	0.283087	0.0897	0.42	0.67		
mean	0.283057	0.0893	0.48	0.76	0.52	0.77
std.Err (abs) (2 σ)	0.00002	0.0007				
std.Err (%) (2 σ)	0.007	0.8				

Table A.3e-2 Lu-Hf isotope data of BHVO-1 standard				
sample	$^{176}\text{Hf}/^{177}\text{Hf}$	$^{176}\text{Lu}/^{177}\text{Hf}$	ID-Lu [ppm]	ID-Hf [ppm]
BHVO-1-1	0.283095	0.00874	0.28	4.5
BHVO-1-2	0.28308	0.00876	0.3	4.9
BHVO-1-3	0.283126	0.00873	0.26	4.19
BHVO-1-4	0.283119	0.00872	0.28	4.5
BHVO-1-5	0.283098	0.0088	0.28	4.59
mean	0.283107	0.00875	0.28	4.53
std.Err(abs) (2 σ)	0.000013	0.00003		
std.Err(%) (2 σ)	0.005	0.33		
Blicher-Toft et al., 2001	0.283108 \pm 5	0.00876	0.29	4.48
Bizzarro et al., 2003	0.283108 \pm 8	0.00877		

Tables A.3f Sm-Nd isotope data for repeated digestion of in house garnet standard (PN3b)(**Table A.3f-1**) and BHVO-1 Basalt (**Table A.3f-2**). The internal precisions for all the Hf runs are less than the external error of the standards. Abbreviations: ID – isotope dilution ; Laser- in situ measurement by Laser Ablation ICP-MS.

Table A. 3f-1 Sm-Nd isotope data of PN3b in house standard						
sample	$^{143}\text{Nd}/^{144}\text{Nd}$	$^{147}\text{Sm}/^{144}\text{Nd}$	ID-Sm (ppm)	ID-Nd (ppm)	laser-Sm (ppm)	laser-Nd(ppm)
PN3b-1	0.7196	0.512876	1.52	1.2		
PN3b-2	0.7227	0.512962	1.54	1.21		
PN3b-3	0.7198	0.512913	1.6	1.29		
PN3b-4	0.7190	0.512913	1.51	1.19		
mean	0.7203	0.512916	1.54	1.22	1.53	1.17
std Err(abs) (2σ)	0.0016	0.000035				
std Err(%) (2σ)	0.23	0.00692				

Table A. 3f-2 Sm-Nd isotope data of BHVO -1 standard				
sample	$^{143}\text{Nd}/^{144}\text{Nd}$	$^{147}\text{Sm}/^{144}\text{Nd}$	ID-Sm (ppm)	ID-Nd (ppm)
BHVO-1-1	0.512937	0.1482	6.4	25.5
BHVO-1-2	0.51292	0.1461	5.9	24.1
BHVO-1-3	0.512929	0.1467	5.9	24.6
BHVO-1-4	0.512971	0.1479	6.4	25.3
BHVO-1-5	0.512934	0.147	6.3	25.1
mean	0.512938	0.1472	6.2	24.9
std.Err(abs) (2σ)	0.000017	0.0008	0.2	0.4
std.Err(%) (2σ)	0.0034	0.54		
Raczek et al., 2003; 2001	0.512957± 8		6.2	25

Table A.4 Partition coefficients of trace elements between ol, grt, opx and silicate melts from experimental data.

Table A.4 Partition Coefficients of ol, grt, opx from experimental work					
				30%opx+70%ol	5%Grt+25%opx+70%ol
	D(ol)	D(opx)	D(grt)	D-(depleted harzburgite)	trace element budget in garnet
La	0.00005	0.0004	0.001	0.0002	27
Ce	0.00011	0.001	0.004	0.0004	38
Sr	0.00015	0.007	0.007	0.023	14
Nd	0.0004	0.004	0.057	0.002	69
Sm	0.0007	0.006	0.140	0.002	78
Zr	0.0010	0.021	0.300	0.007	72
Hf	0.0029	0.023	0.300	0.009	66
Eu	0.0008	0.010	0.260	0.004	81
Ti	0.0150	0.120	0.290	0.035	32
Gd	0.0015	0.012	0.498	0.005	86
Tb	0.0021	0.016	0.750	0.006	87
Dy	0.00270	0.020	1.1	0.008	88
Y	0.007	0.010	2.0	0.007	94
Ho	0.005	0.026	1.5	0.011	88
Er	0.010	0.033	2.0	0.017	87
Tm	0.016	0.045	3.0	0.025	87
Yb	0.027	0.055	4.0	0.035	86
Lu	0.030	0.070	5.5	0.042	88

Data are from Beattie P., Chemical Geology (1994); Hauri, E.H., Chemical Geology (1994); Johnson, K.T.M. Contributions to Mineralogy and Petrology(1998); Adam, J. and Green, T. Contributions to Mineralogy and Petrology(2006), Tuff and Giboson, 2007.
D-(depleted harzburgite) is the calculated bulk partition of trace elements in a depleted peridotite with 30% opx and 70% ol.

Appendices of figures:

Fig. A.1: Comparison of Lu-Hf ;Sm-Nd concentrations obtained by “in situ” LA-ICP-MS and by isotope dilution (ID) of garnets from Bellsabnk mine mine

Fig. A.2: Comparison of Lu-Hf ;Sm-Nd concentrations obtained by “in situ” LA-ICP-MS and by isotope dilution (ID) of garnets from Kimberley mine mine

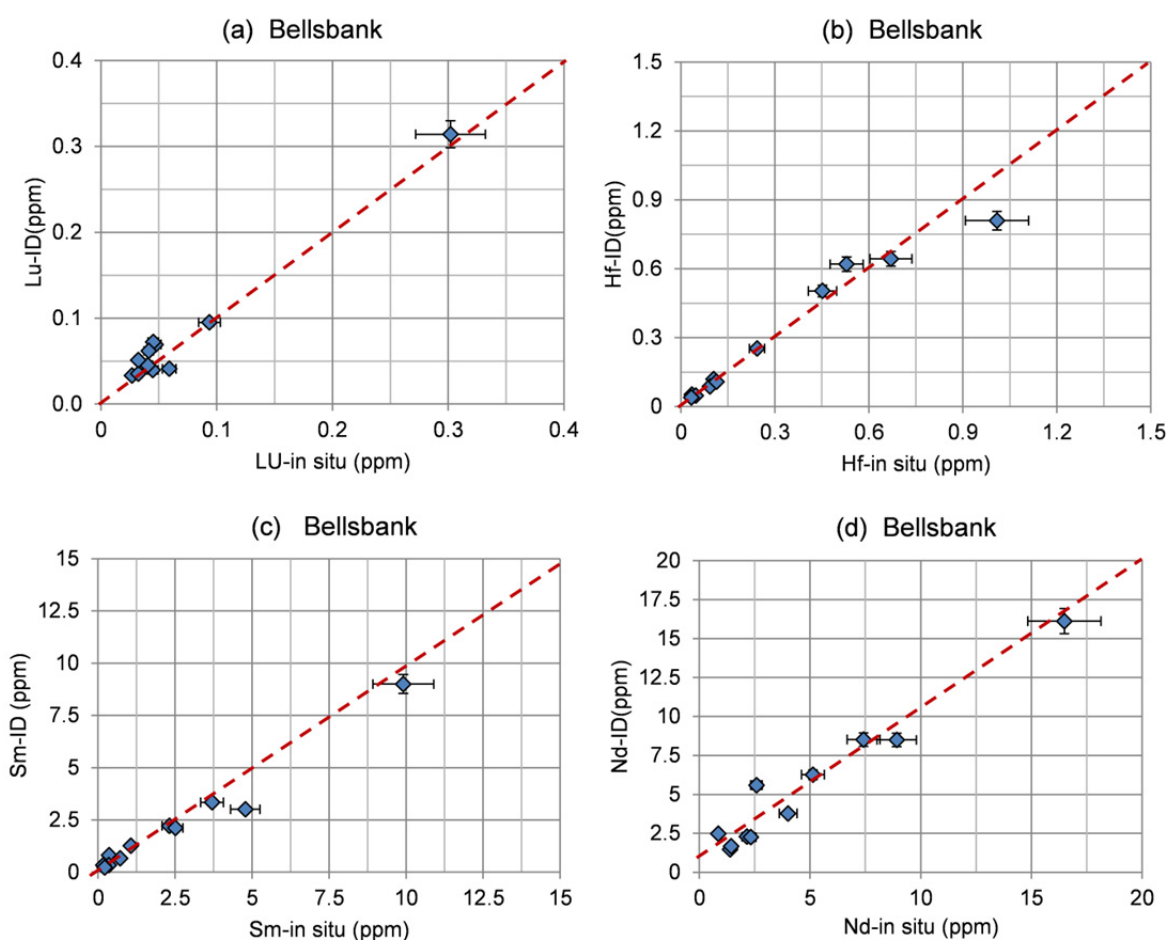


Fig. A.1 Comparison of Lu-Hf ;Sm-Nd concentrations obtained by “in situ” LA-ICP-MS (Table A.2.c) and by isotope dilution (ID) MC-ICP-MS measurements (Tables A.3c) of garnets from Bellsabnk mine mine. Error bars for the LA-ICP-MS are around 10% for Lu and Hf in garnets. Error bars for the ID measurements are taken from the errors calculated from the BHVO-1 and PN3b standards (Table A.3e and Table A.3f). The dash line in each diagram is 1:1 line.

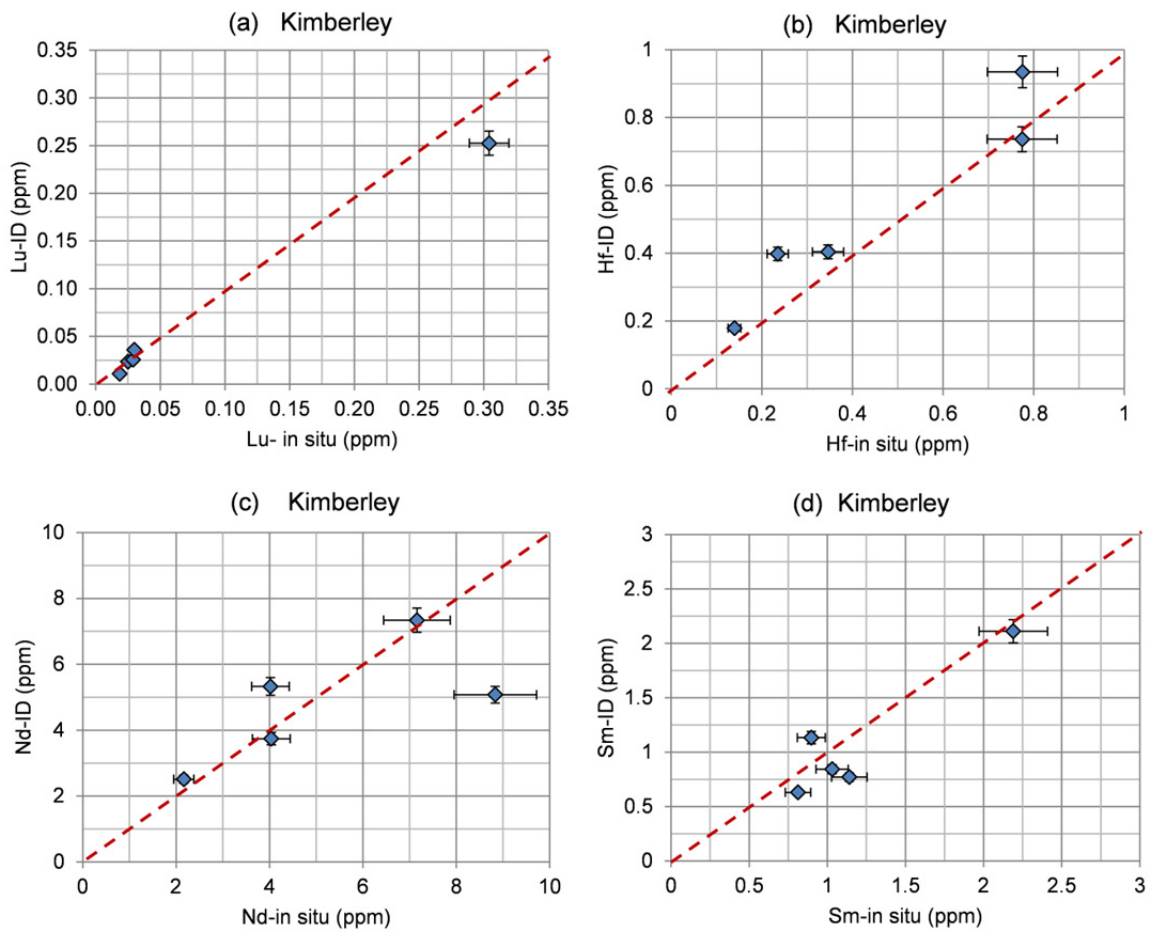


Fig. A.2 Comparison of Lu-Hf ;Sm-Nd concentrations obtained by "in situ" LA-ICP-MS (Table A.2b) and by isotope dilution (ID) MC-ICP-MS measurements (Tables A.3B) of garnets from Roberts Vcitor mine . Error bars for the LA-ICP-MS are around 10% for Lu and Hf in garnets. Error bars for the ID measurements are taken from the errors calculated from the BHVO-1 and PN3b standards (Table A.3e and Table A.3f.). The dash line in each diagram is 1:1 line.

Chapter 4

The origin of eclogites and garnet pyroxenites from Bellsbank, Kaapvaal craton (South Africa)

1. Introduction

Eclogite, the high-pressure equivalent to basalt or picrite makes up a small but petrologically significant portion of the subcontinental lithospheric mantle (Hatton and Gurney, 1987; Schulz, 1989). Eclogitic xenoliths from kimberlites and alkali basalts show a wide variation in mineralogy, isotopic and chemical composition. The word eclogite is used here in a wide sense and includes eclogites *sensu strictu* (possibly with coesite, kyanite or corundum) and garnet pyroxenites. Two main models are proposed for eclogite petrogenesis: (1) a mantle origin: eclogites are re-equilibrated high-pressure igneous cumulates of (ultra-)mafic melts within the upper mantle (O'Hara and Yoder, 1967; O'Hara, 1969; O'Hara et al., 1975; Hatton and Gurney, 1987; Caporuscio and Smyth, 1990; Griffin and O'Reilly, 2007; Huang et al. 2012) or (2) a subduction origin: eclogites are the metamorphic products of subducted oceanic crust. Some of them may have experienced subsequent partial melting and metasomatism (e.g. Jagoutz et al., 1984; MacGregor and Manton, 1986; Shervais, 1988; Taylor and Neal, 1989, 1990; Viljoen, 1995; Schulze et al., 2000; Barth et al., 2001; Schmickler et al., 2004; Jacob et al., 2005 and 2009; Aulbach et al., 2007; Smart et al., 2009.).

If the eclogitic component in the subcontinental lithospheric mantle is the result from the subduction of oceanic slabs, the characterization of these eclogitic materials and their geologic ages provide important constraints on the petrologic processes by which they formed and on the tectonic setting in the Archean and also on the origin of diamonds. A significant fraction of the macro-diamonds formed in the subcontinental lithosphere contains eclogitic sulfides (e.g. Harris and Gurney, 1979). Unravelling the genetic processes in the formation of eclogites will contribute to an understanding of craton stabilization and modification. If eclogites are derived from deep lithospheric magmatism, they will give information on crystallization of magmatic rocks at high pressures and continental growth models. Mantle eclogites and related garnet pyroxenites appear to be highly diverse rock types which seem to be quite different in different localities.

The Bellsbank kimberlite mine provides eclogites and garnet pyroxenites which became known by the work of Shervais et al. (1988); Neal et al. (1990) for their extremely radiogenic Nd isotope composition. Such values are rarely reported from any craton worldwide. On the other hand, the

graphite and diamond bearing eclogites from there give more conventional Nd isotope due to severe overprints (Viljoen, 1995). Neal et al. (1990) proposed that such extremely high Nd isotopic composition originate through melt extraction from eclogites with compositions similar to modern MORB. The extreme Nd isotope values require a long-time development (Nd model ages of 2.3-2.4 Ga) and Sr and oxygen isotopes indicate a complex history of the precursor rocks. Bellsbank eclogites are generally depleted in LREE relative to the MREE and HREE, yet a slight LREE modification (compared to a pattern generated by partial melting) is still seen in the REE patterns. This indicates that the Nd ages are blurred by enrichment. It becomes now more and more accepted that the Lu-Hf system is more robust to metasomatism in mantle rocks than the Sm-Nd system (Schmidberger et al. 2002; Ionov and Weiss, 2002 and Pearson and Nowell, 2004, Lazarov et al. 2009 and 2012). If so the Lu-Hf isotopic system may give more pristine information on the eclogite protolith's formation and on eclogitisation.

2. Geological setting and previous work

The Bellsbank kimberlite fissures are situated approximately 100 km northwest of Kimberley, South Africa on the Kaapvaal craton (Fig.1). The group II kimberlites were emplaced 118 ± 3 Ma (Smith et al., 1985). There are two main diamond-bearing dyke systems (Clement et al., 1973) which contain abundant eclogite xenoliths while peridotite xenoliths are rare. The Archean Kaapvaal Craton in Southern Africa with a one billion year long history (Hartnady et al., 1985) is divided from north to south by the Colesberg lineament into two main blocks, the Kimberley block in the west and the Witwatersrand block in the east. The two blocks amalgamated around 2.88 Ga (Schmitz et al., 2004). Before, they had a separate history in the Archean. The oldest crustal ages on the Witwatersrand (East) block are 3.7-3.6 Ga from rocks which developed from a mid-ocean ridge in a shallow-water environment (see de Wit et al., 1992 and ref. therein). Younger, 3.54 Ga old trondhjemitic - tonalitic rocks are ascribed to an arc-like terrain (Armstrong et al., 1990). Later at around 3.4 to 3.2 Ga, the Natal granite-greenstone terrain developed in the Barberton region which includes boninites and komatiites (see summaries by de Wit et al., 1992 and Thomas et al., 1993). Thrusting connected with igneous activities at 3.3 -3.2 Ga affected both terrains.

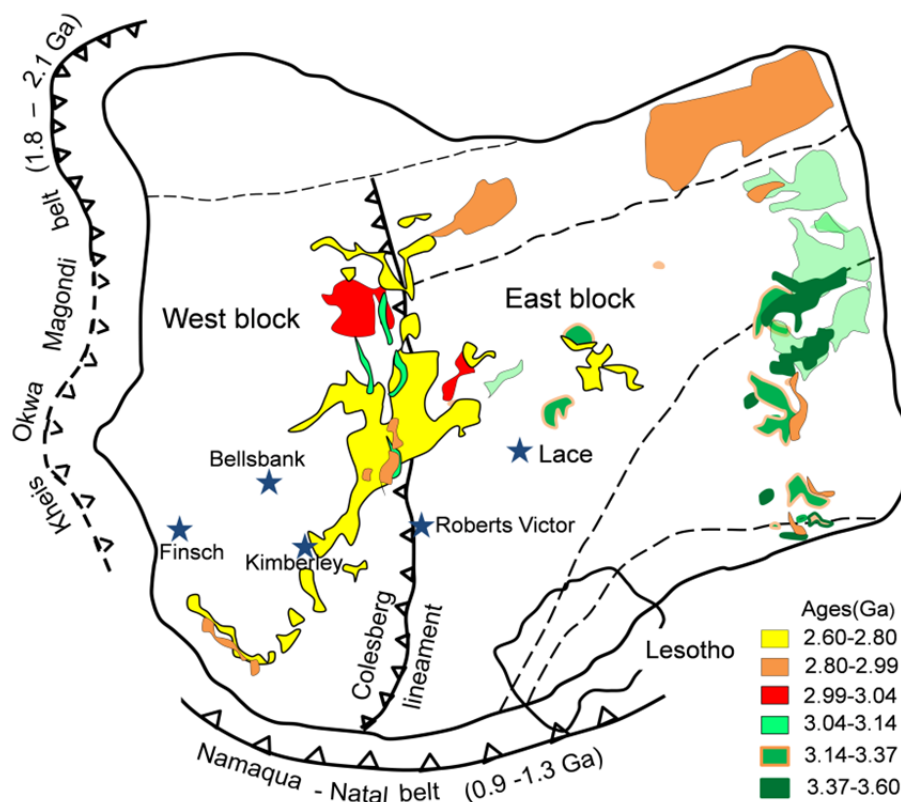


Fig.1 Structural units of the Kaapvaal craton and color coded fields of exposed Paleo- to Neoproterozoic crystalline basement, volcanic and magmatic rocks with age division schematic after Eglington and Armstrong (2004), Anhaeusser (2006) with interpretations after Jacob et al. (2008). Also shown are the locations of the Kimberley, Finsch, Roberts Victor and Lace mines.

Eclogites have been studied from various diamond mines in the Kaapvaal craton (such as Roberts Victor, Kimberley and Bellsbank). Most work has been done on eclogites from Roberts Victor (e.g. Hatton and Gurney, 1987) which is located close to the Colesberg Lineament (Fig.1). Eclogites from there were interpreted e.g. by Jacob et al. (2005) as relics of subducted oceanic crust which may have experienced subsequently partial melting and/or metasomatism. Huang et al. (2012) resurrected the proposal that eclogites from Roberts Victor are high pressure high-Al clinopyroxene cumulates and that garnets are exsolved from them upon cooling. Eclogites from Kimberley are interpreted as seawater-altered oceanic cumulates by Jacob et al. (2009) which were overprinted by mantle-derived metasomatism after eclogitisation. Taylor and Neal (1989, 1990) proposed that eclogites from the Bellsbank mine are both oceanic crustal and mantle derived based on differing chemical and isotopic signatures. A wide variability in major and trace element and isotopic composition requires the consideration of a variety of models for their origin.

Eclogites appear to be old and some evidence suggests that they may be even older than 4 Ga like eclogites from Newlands on the Kimberley block (Menzies et al. 2003). An age of 2.7 Ga was suggested by Jagoutz et al.(1984) and Jacob et al. (2001) for eclogites from Roberts Victor based on the Sm-Nd isotope system and ~2,5 Ga from Pb-Pb isotope systematics (Kramers 1979). The majority of ages stems from two-point garnet-clinopyroxene isochrons. Their meaning is the subject of the next

chapter. Inclusions of eclogitic phases in diamonds can provide information on the age of diamond formation and may or may not provide age information on subduction and eclogitisation. A predominance of eclogitic sulfide inclusions in diamonds from the W-block with an age of about 2.9 Ga may link the subduction-related amalgamation of the western and eastern Kaapvaal along the Colesberg magnetic lineament with subduction of oceanic lithospheric and eclogitic diamond formation (e.g. Shirey et al., 2008). A wide spread of ages (2.0 Ga, 1.7 Ga, 1.5 Ga 1.0-1.2 Ga) of eclogitic inclusions in diamonds may be related to the accretionary processes at the craton margins and may record remobilization of eclogitic components (Rudnick et al., 1993; Pearson et al., 1998,1999; Richardson et al., 2001; Richardson et al. 2004).

We studied eleven eclogites and garnet pyroxenites from the Bellsbank diamond mine with very fresh garnets and clinopyroxenes even in kyanite-bearing samples. A number of them have extremely fractionated incompatible trace element patterns with resultant extreme isotope ratios (Sr, Nd, Hf but also oxygen isotopes). Others have pristine looking trace element patterns which allow unequivocal deductions on their protoliths and the Sm-Nd and Lu-Hf isotopic systems on their formation ages. Most of our samples have more similarity to the eclogite xenoliths reported by Taylor and Neal (1989), Neal et al. (1990) and Shervais et al. (1988) which were mostly classified as type I eclogites, except one sample (BE4) is put into type II variety similar to the graphite- and diamond-bearing eclogites reported by Viljoen (1995).

3. Analytical Methods

3.1 Major element analysis

The major element compositions of garnets and clinopyroxenes were determined by Electron Probe Micro Analysis (EPMA) in the wavelength-dispersive mode (WDS) with a JEOL JXA 8900RL at the Goethe University in Frankfurt. Analyses were performed using an acceleration voltage of 15 kV, a beam current of 20 nA and a spot size of 3 μm . Each garnet was randomly analyzed in 3-10 spots on different pieces to test for compositional homogeneity. Because the variation of the analyses was always within the range of the analytical accuracy, only the average compositions are given in **Tables A.1a-b** in the appendix of the supplement of the supplement of this appendix. For Al, Cr, Fe, Ti and Ni, an integration time of 30 s on peak was used and 20 s for Si, Mg, Ca, Na, K, Mn and P. The background was measured for 10 to 30 s at different distances from the peak depending on the element. Standards were natural minerals and pure oxides and metals. The ZAF algorithm method was used for matrix correction. Relative errors are usually 1-2% for major elements.

3.2 Trace element analysis

The trace elements were analysed by Laser ablation ICP MS using a New Wave Research LUV213TM ultraviolet Nd-YAG laser coupled with a Finnigan Element 2 at the Goethe University in Frankfurt. The laser was used at a pulse frequency of 10 Hz and an energy pulse of 0.6 -0.8 mJ (corresponding to 60%-80% laser power). For garnets, spot sizes of 60-95 μm were used depending

on the sample size. Aluminium cones were used to avoid instrumental Ni background from the cones. NIST 612 glass was used as a calibration standard with the preferred concentration values of Pearce et al. (1997). USGS BIR-1 glass (concentrations from Eggins et al., 1997) was the external and Ca from microprobe analysis of the minerals the internal standard. BIR-1 glass and one in-house garnet standard (PN2b) were measured several times within each sequence.

The raw data were processed on-line using the GLITTER software. The first few seconds of the time resolved spectra and also peaks and minima were discarded in the concentration calculations. This eliminates surface contamination from preparation and signals from inclusions or cracks in the minerals. From our long-time monitoring of international standards and an in-house standard garnet PN2b (**Table A.2c** in the supplement) we estimate that our analyses are accurate to within 10 % for REE and Hf.

3.3 Radiogenic Isotope analysis

3.3.1 Sample preparation

The xenoliths were disintegrated with a SelFrag® fragmentation system using voltages of 90 - 120 kV and a built in sieve of 1 mm mesh size. The garnet and clinopyroxene pieces were hand-picked to optical purity. To remove possible grain surface impurities, the crushed pieces were leached at room temperature in 3-6 M HCl in an ultrasonic bath for 30 min, afterwards ultrasonicated three times in MQ H₂O and finally dried down. When necessary, the leaching procedure was repeated. Previous work from DeWolf et al. (1996) and Wittig et al. (2007) proved that leaching even at high temperatures (up to 120 °C) with 6 M HCl does not fractionate the isotopes of Lu, Hf, Sm and Nd in silicates. After each leaching procedure the grains were re-picked to optical purity. Finally, 30 to 100 mg of clean-picked garnet and clinopyroxene separates were ultrasonicated in MQ H₂O and dried down prior to spiking.

3.3.2 Dissolution

Mineral separates were prepared from ten eclogites for Lu-Hf and Sm-Nd isotope work. Prior to dissolution, all samples were spiked with solutions containing ¹⁵⁰Nd, ¹⁴⁹Sm, ¹⁷⁶Lu and ¹⁸⁰Hf for isotope dilution measurements. The sample digestion and chromatographic separation of Lu-Hf and Sm-Nd were performed by combining existing protocols for REE, Lu-Hf and Sm-Nd separation (Maboko and Nakamura, 1995; Münker et al., 2001; Pin and Zalduequi, 1997). Samples were dissolved in capped Teflon beakers in a 3-5 ml mixture of highly concentrated acid mixtures of HF (29N)-HNO₃ (15N) (3:1) on a hot plate at around 120 °C for three days. After drying down, 3-5 ml 6N HCl were added to dissolve the fluorides. If necessary, some samples were repeatedly treated with 6 N HNO₃ and 6N HCl to remove all remaining fluorides and ensure complete dissolution.

3.3.3 Column chemistry

Besides duplicates of some samples, we also used a garnet megacryst (PN3b) to prepare a duplicate. Results of repeated column chemistry of this garnet are shown in **Table A.5c-1**, **Table A.5d-1** in the appendix. The chromatography is based on the procedure by Münker et al. (2001) using Eichrom Ln spec resin. We started with the collection of Lu and Hf, to keep the Hf blank as low as possible. Our total procedural Hf blank for our methods is 25 ± 5 pg. However, we omitted the separation of Zr from Hf, because this would lead to a loss of about 10% Hf. The separation of Zr is not necessary, since it does not affect the precision of the Hf isotope measurement by MC ICP MS (Blichert-Toft et al., 1997).

3.3.4 Lu and Hf collection

Lu and Hf were separated from the matrix using a column with an inner diameter of ~ 5.5 mm filled with 1ml Ln-spec resin. The sample was loaded in 1ml 2N HCl and the matrix washed out with 12 ml of 3N HCl. Lutetium was eluted with 10 ml of 6N HCl and afterwards Hf with 12ml of 2N HF. The Hf and Lu cuts were dried down and taken up in an appropriate volume of 2% HNO₃ for mass spectrometry measurements.

3.3.5 LREE and Rb-Sr collection

The left over matrix, which includes the light and middle REE, was dried down and re-dissolved in 1 ml 2N HCl. The REE were separated using a column filled with Bio Rad 50Wx8. It is most important to separate the REE from Fe to avoid overloading the Ln-spec resin, which was used for the Sm–Nd separation (Pin and Zalduequi, 1997). Based on the experience of Lazarov et al. (2009), it was possible to reduce the conventional column size (5-10 ml) to 1.5 ml to adjust for our low sample amounts (30-150 mg). After loading the samples on the 1.5ml column, the matrix was separated with 14 ml of 2.2 M HCl prior to eluting Rb with 4 ml of 2.2 M HCl and then eluting Sr with 8 ml of 2.2 M and the REE with 10 ml of 6 M HCl (Lazarov, 2009; PhD thesis available in the internet.). With this procedure it was possible to separate more than 90% of the Fe from the REE without losing more than 10% of Sm and Nd.

3.3.6 Sm-Nd collection

Chromatographic separation of Sm and Nd was performed on the same column that was previously used for Lu-Hf purification (with 1 ml Eichrom Ln-spec resin), following the procedure of Pin and Zalduequi (1997). The samples were loaded with 1ml of 0.18N HCl. Neodymium was first collected with 6-7ml 0.25N HCl and then Sm with 3.5 ml of 0.75N HCl. The Nd and Sm cuts were dried down and taken up in an appropriate volume of 2% HNO₃ for mass spectrometry measurements.

3.4 Analysis

3.4.1 Lu-Hf, Sm-Nd, Rb-Sr

All isotopic compositions were analysed in a static mode with a MC ICP MS (Finnigan Neptune) at the Goethe University in Frankfurt. Sample aspiration for Hf and Lu was performed using a Cetac-Aridus desolvating nebulizer, whereas Sm and Nd analyses were performed using a dual spray chamber (wet plasma). Hafnium measurements were performed with the cup configuration, mass bias and interference corrections as described by Blichert-Toft et al. (1997). During our Lu-Hf separation we always collect 30-50% of Yb together with Lu. Therefore, we had to correct for the large mass interference of ^{176}Yb on ^{176}Lu . This was possible with high precision by monitoring the mass bias using the interference free Yb isotopes ^{173}Yb and ^{171}Yb (and assuming a natural $^{173}\text{Yb}/^{171}\text{Yb} = 1.1248$, Blichert-Toft et al., 1997). The amounts of Hf in our samples were from 4 to 33 n. With our instrumental set up we were able to measure such low concentrations of Hf (3 ng result in a signal of ~90 mV on ^{176}Hf) with a precision of around 1ε (on $^{176}\text{Hf}/^{177}\text{Hf}$). The total blank for Hf was always lower than 30 pg, and also was lower than 7 pg for Lu. Repeated measurements of the Hf standard JMC475 produced $^{176}\text{Hf}/^{177}\text{Hf}$ of 0.282153 ± 0.000014 (2σ), which is in good agreement with the literature (Blichert-Toft et al., 1997; Chu et al., 2002). Replicate digestion and analyses of BHVO-1 yielded $^{176}\text{Lu}/^{177}\text{Hf} = 0.00875 \pm 0.00003$ (2σ) and $^{176}\text{Hf}/^{177}\text{Hf} = 0.283107 \pm 0.000013$ (2σ). These data are in good agreement with those reported by Bizzarro et al. (2003). The Nd aliquots always contained more than 20 ng Nd, which was measured with a precision of 0.5 to 1 ε, as determined by replicate standard measurements. Our procedural blanks were lower than 70 pg for Nd and 30 pg for Sm. Repeated measurements of Nd isotope standards yielded $^{143}\text{Nd}/^{144}\text{Nd} = 0.511725 \pm 0.000068$ (2σ) (for the Merck Nd₂O₃) and are in a good agreement with literature values (Deckart et al., 2005; Caro et al., 2006). Replicate digestion and analysis of BHVO-1 yielded $^{143}\text{Nd}/^{144}\text{Nd} = 0.512938 \pm 0.000017$ (2σ) that is in a good agreement with the literature values (Raczek, et al., 2003). Uncertainties of Lu-Hf and Sm-Nd ratios and isotope compositions are based on replicate standard measurements and are within 2 ε for $^{176}\text{Hf}/^{177}\text{Hf}$ and $^{143}\text{Nd}/^{144}\text{Nd}$, and around 0.33% for $^{176}\text{Lu}/^{177}\text{Hf}$ and 0.54% for $^{147}\text{Sm}/^{144}\text{Nd}$.

Garnets from our sample set has relatively low Sr content, 0.03-0.59 ppm. Also the majority of the clinopyroxenes has low Sr concentrations, from 10 to 76 ppm, except for three samples with 112, 254, 419 ppm. Accordingly, only clinopyroxenes were used to determine the Sr isotopic composition. The low Rb concentrations close to or even below the detection limit allowed us to measure the Sr isotopes in unspiked samples. The Sr isotope ratios were measured on our Neptune MC ICP MS. For each analysis we used around 50 ng in 2% HNO₃. To determine the reproducibility of unspiked Sr solutions, a 50 ppb solution in 0.2% HNO₃ of the NIST isotope standard reference material Sr-carbonate SRM987 was analysed in replicate during all analytical sessions. These replicate analyses (n = 10) carried out over several analytical sessions yielded an average value of $^{87}\text{Sr}/^{86}\text{Sr} = 0.710245 \pm 0.000116$ (2 S.D.). These values and reproducibilities are comparable to those obtainable by high quality TIMS techniques ($^{87}\text{Sr}/^{86}\text{Sr} = 0.710241 \pm 12$, 2 S.D.) (Thirlwall, et al., 1991) and are in good agreement with other Sr isotope data collected by MC-ICPMS (e.g. Ehrlich, et al., 2001, Waight et al., 2002)). The international basalt standard BHVO-1 was also used in the chemical separation procedure together with the clinopyroxenes. Its measured $^{87}\text{Sr}/^{86}\text{Sr}$ ratio is 0.703429 ± 6 (2 S.D.), which is consistent with the reference value from USGS (0.703436 ± 9 , Raczek et al., 2003).

3.4.2 Oxygen isotopes

Oxygen isotopic ratios were measured in the lab of Janz Hebig at Frankfurt University, using the CO₂-laser fluorination technique with a strongly oxidizing BrF₅ reagent and a CO₂ Laser connected to the inlet system of an isotope ratio gas mass spectrometer after Sharp (1990), Rumble and Hoering (1994) and Valley et al. (1995). Optically clean mineral separates with a weight of 1.5-2.0 mg were prepared for analysis. The grains were rinsed with water and ethanol. Oxygen is extracted in the form of O₂ from samples and this O₂ as an analyzing gas for mass spectrometric measurement in order to obtain accurate ¹⁸O/¹⁶O and ¹⁷O/¹⁶O ratios. The average total O₂ yield was higher than 90%. The ¹⁸O/¹⁶O and ¹⁷O/¹⁶O ratios are reported relative to the Vienna Standard Mean Ocean Water (VSMOW) (Coplen, et al., 1995) as a conventional notation i.e. as permil deviations from VSMOW. They are defined as δ (‰) = (R_{sample}/R_{VSMOW}-1) *1000, where R_{sample} and R_{VSMOW} are the ¹⁸O/¹⁶O or ¹⁷O/¹⁶O ratios of the sample and VSMOW, respectively. Two working standards, the quartz standard Lausanne-1 with a reference value of $\delta^{18}\text{O}=+18.15$ ‰ (Allaz, et al 2005; used only for the first three runs) and the garnet standard UWG-2 with a reference value of $\delta^{18}\text{O} = +5.89$ ‰ (Valley, et al. 1995) were used. Each run consists of the analysis of one sample holder with 8 dimples. Each sample was bracketed by standard analyses to allow corrections for systematic errors. Our overall precision (2s) on the UWG-2 garnet standard is ± 0.1 ‰ and on the quartz standard L-1 ± 0.24 ‰. The higher uncertainty of the quartz standard was already observed in previous work (e.g. Kusakabe et al. 2004).

4. Sample description

Eleven eclogite xenoliths with 3-6 cm in diameter from the coarse grained concentrate of the Bellsbank diamond mine were studied here. Photographs of all handspecimens can be found in **Figs. A.1** in the appendix. The primary minerals, garnet and clinopyroxene, are exceptionally fresh with less than 10% alteration products which are restricted to the grain boundaries and cracks. Most samples have secondary spongy rims of cpx around primary cpx cores. Altered areas are composed of fine grained phlogopite, serpentine, calcite and some microcrystalline material with dark and brownish colors. Grain sizes of garnets and clinopyroxenes range between 5 and 7 mm. All but one sample texturally belong to type II eclogites, as defined by MacGregor and Carter (1970) except sample (BE4) which belongs to the type I eclogite similar to graphile- and diamond-bearing eclogites from Bellsbank. (Viljoen, 1995). Phlogopite occurs in all samples with modes between 1-5%. Kyanite, SiO₂ (coesite?) and corundum have been identified in three high-CaO samples (see below). Based on chemical and isotopic criteria (see below) we divided the samples in groups A, A', B1 and B2. In hand specimen, group A eclogites (3 samples) show pinkish garnets and light green clinopyroxenes. The modal abundances are somewhere between 50%:50% to 60%:40%. Group B1 eclogites (3 samples) appear similar to group A but garnets are more orangy and clinopyroxenes dark green. Also, relatively large phlogopites (plates of up to 4 mm) exist which appear primary. Group B2 eclogites (3 samples) have pale-orange garnets, buff-green clinopyroxenes (75:25) and two have kyanite and one corundum. The clinopyroxenes are most strongly altered at their rims compared to the other eclogite types. The two

group A' eclogites have large and roundish orange garnets embedded in a matrix of irregular, smaller pale-green clinopyroxenes.

Group B2 with their jadeitic clinopyroxenes are real eclogites, groups A and A' are garnet pyroxenites and group B1 are transitional.

5. Results

5.1 Major element composition of garnets and clinopyroxenes

The major element compositions of garnet and the primary central parts of the clinopyroxenes were determined by EMPA. Both garnets and clinopyroxenes from the 11 eclogites are very homogeneous within each sample with no core-to-rim or inter-grain variation in garnets and clinopyroxenes. However, the jadeite component in cpx and the grossular content in garnet differ widely between the samples (Table 1 in the appendix and Figs.2a,b). The figures also show the compositional overlap of our samples and those analyzed by Shervais et al. (1988) and Taylor and Neal (1989).

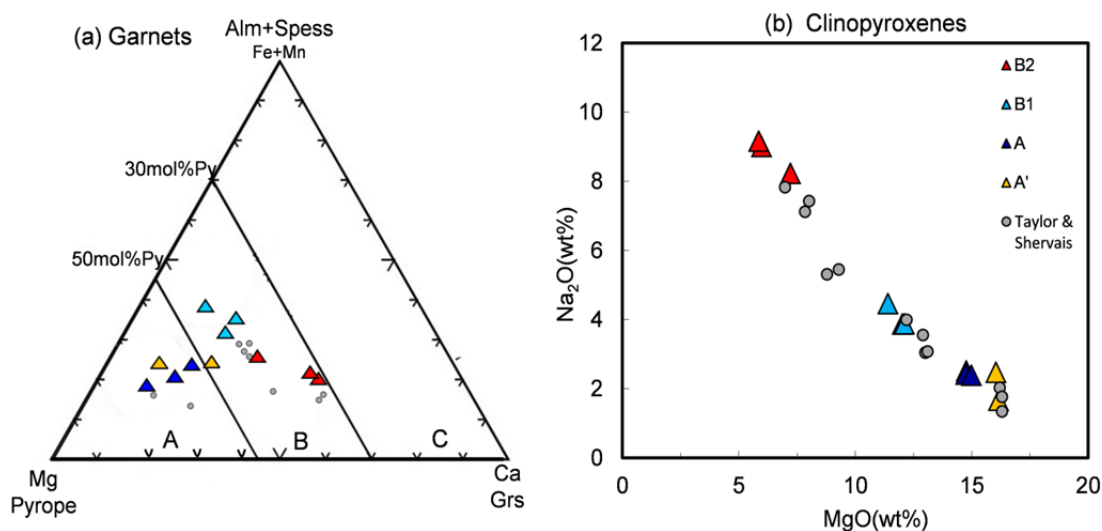


Fig.2 a,b Major element compositions of garnets and clinopyroxenes. The triangles with various colors present the samples from this study divided into 4 groups A, A', B1 and B2 (see legend). The grey dots are data from previous work of Taylor and Neal (1989) and Shervais et al. (1988).

Garnets plot in the eclogite nomenclature scheme of Coleman et al. (1965) into fields A and B (Fig.2a) but are divided into 4 subgroups based on further information from the trace element and isotope compositions: (1) high-Mg group A' with highest MgO (18-21wt%), and lowest CaO contents (4.4-4.7 wt%) in the garnets; (2) high-Mg group A comprises garnets with lower MgO (15-18 wt%) and intermediate CaO (7.4-9.3 wt%) contents; (3) low-Mg group B1 has still lower MgO (12-13 wt%) and intermediate CaO (6.0-9.2 wt%) and (4) a high-Ca group B2 with garnets with the lowest MgO (9-12 wt%) and highest CaO (12.1-17.6 wt%) contents. The latter are kyanite and corundum bearing. Cr₂O₃

contents in the garnets range from 0.06 to 0.25 wt%, TiO₂ from 0.1 to 0.4 wt% and MnO from 0.2 (high T) to 0.5 wt% (low T).

Clinopyroxenes have a corresponding wide compositional variability as shown in Fig.2b in a negative correlation of Na₂O versus MgO. The Cr₂O₃ contents vary from 0.06 to 0.34 wt%, TiO₂ from 0.04 to 0.5 wt% and MnO 0.1 to 0.03 wt%. If they are split into the four groups as shown for the the garnets, we find that (1) group A' has clinopyroxenes with high MgO (~16wt%) and low Na₂O (1.7-2.5wt%) and Al₂O₃ (2.2-3.5wt%); (2) group A has clinopyroxenes with relatively high MgO(14.7-14.9 wt%) and low Na₂O (2.4-2.5wt%) and Al₂O₃ (4.0-4.5wt%); (3) group B1 has clinopyroxenes with low MgO (11.4-12.1wt%) and intermediate Na₂O (3.9-4.5 wt%) and Al₂O₃ (6.2-6.3 wt%) contents and (4) group B2 have clinopyroxenes with lowest MgO (5.9-7.2 wt%) and highest Na₂O (8.2-9.2 wt%) and Al₂O₃ (15-17 wt%). A positive correlation of Na₂O and Al₂O₃ and equal contents of Na and Al in the structural formulae show that Na is present in the clinopyroxenes entirely as a jadeite component. Group B2 samples have the highest jadeite component, followed by B1 and then groups A and A' with the lowest jadeite component. According to the jadeite component group B2 are eclogites *sensu strictu*, groups A and A' are garnet pyroxenites and group B1 are transitional.

5.2 Calculated bulk rock major element compositions

The small size of the xenoliths did not allow bulk rock analysis. Besides, kimberlite-borne xenoliths are often contaminated and overprinted by their host kimberlite sometimes often visible as precipitated secondary carbonate and silicates e.g. amphibole, mica, clinopyroxene as reaction products with the primary eclogite minerals (e.g. Barth et al., 2001,2002; Aulbach et al.,2007 and references therein). To constrain the primary composition of the xenoliths, we calculated bulk rock compositions from the composition and modal abundance of the constituent primary phases. Modal abundances in the small samples were estimated visually in hand specimen and from the relative amounts of the minerals after crushing. The estimated numbers are given in **Table A.1c** in the appendix They range from 50:50 to 60:40 (grt:cpx) for groups A, A' and B1. Group B2 quite apparent have higher grt:cpx ratios of about 75:25. Changing the relative modal abundances of garnet and clinopyroxene markedly influences the calculated major element bulk composition. The patterns of the bulk composition for trace elements are not very sensitive even for a variation by 30%.

The calculated bulk rocks are given in appendix table2 and shown in Figs.3,4 and 5. Group B2 samples are high in CaO, Na₂O and Al₂O₃, and low in MgO and overlap with modern gabbroic rocks from South East Indian Ridge (Hart et al., 1999). The two group A' eclogites also plot in the modern gabbroic field in the Mg[#]-SiO₂ and Mg[#]-CaO diagrams but plot at much lower Na₂O and Al₂O₃ contents than this field in the Na₂O-Al₂O₃ diagram. Compared to fresh and altered Archean basalts they are relatively higher in Al₂O₃ and lower in Na₂O. Groups B1 and A have higher Mg[#] (60-84) and CaO contents (11.5-14.0 wt%), but lower SiO₂ contents (45-47 wt%) compared to Archean basalts and Archean boninitic rocks. In the Na₂O vs. Al₂O₃ diagram they plot in the very low end of Na₂O and slightly higher Al₂O₃ region of Archean basalts and boninitic rocks.

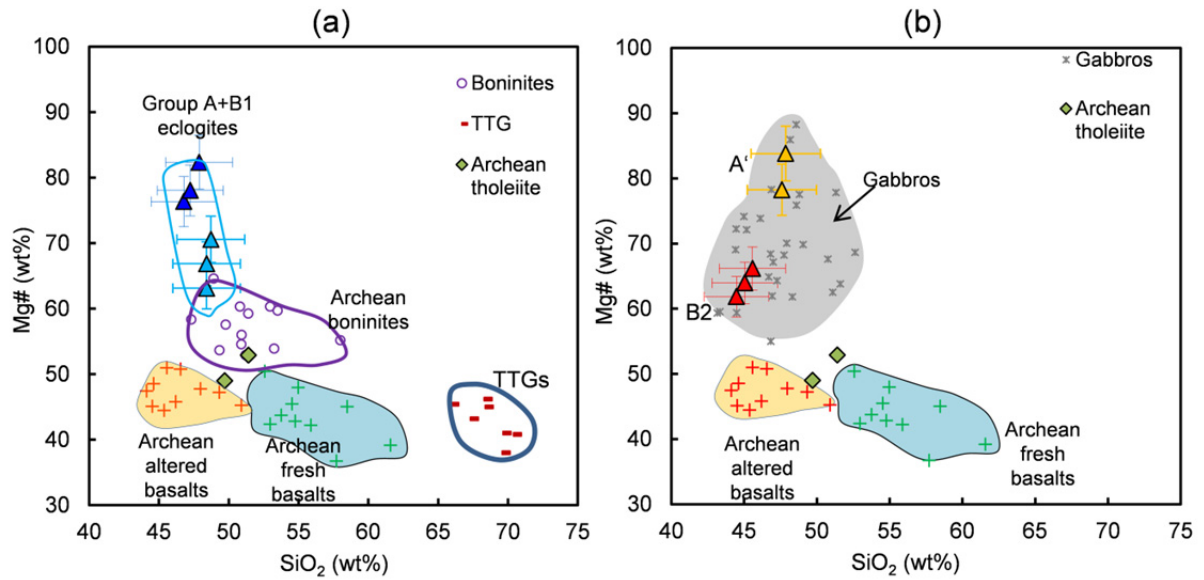


Fig. 3 a,b Calculated major element compositions of bulk rocks from Bellsbank mine shown in Mg# vs. SiO₂ diagrams. Fig.3a shows the comparison of group A (dark blue triangles) and B1 (light blue triangles) eclogites with Archean Basalts (Polat et al., 2003) and boninites (Smithies, 2004). Fig.3b shows group A' (yellow triangles) and B2 (red triangles) eclogites in comparison with Archean Basalts (Polat et al., 2003) and modern gabbroic rocks (SE Indian Ridge, Hart et al., 1999; Bach et al., 2001).

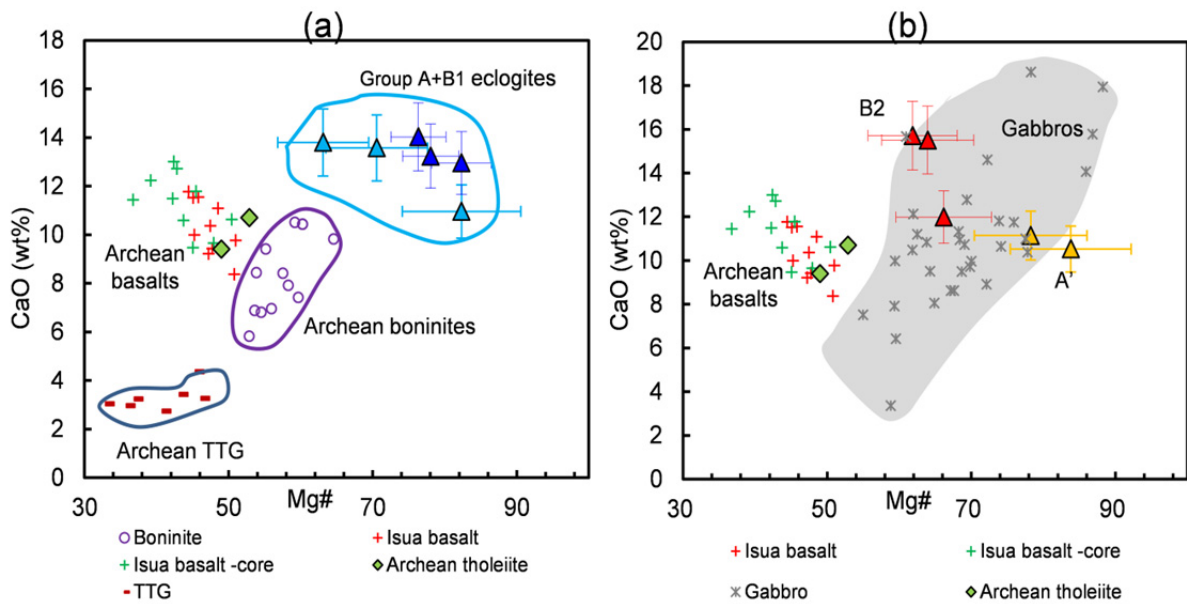


Fig.4 a,b Calculated major element compositions of bulk rocks from Bellsbank mine shown in CaO vs.Mg# diagrams. Fig.4a shows the comparison of group A (dark blue triangles) and B1 (light blue triangles) eclogites with Archean Basalts (Polat et al., 2003) and boninites (Smithies, 2004). Fig.4b shows group A' (yellow triangles) and B2 (red triangles) eclogites in comparison with Archean Basalts (Polat et al., 2003) and modern gabbroic rocks (SE Indian Ridge, Hart et al., 1999; Bach et al., 2001).

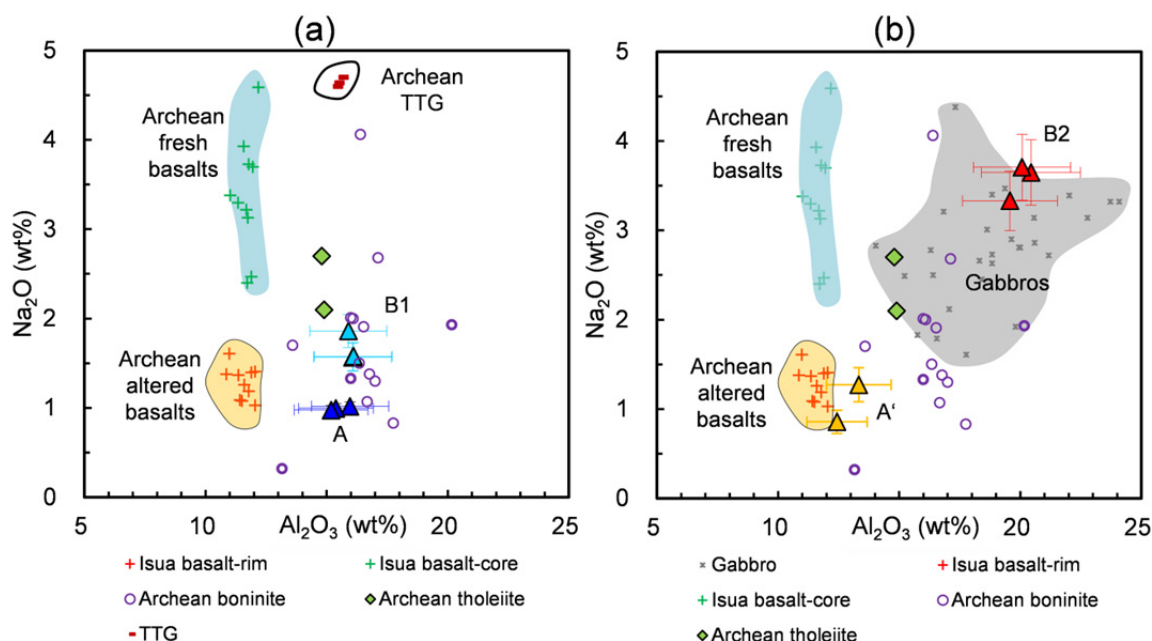


Fig.5 a,b Calculated major element compositions of bulk rocks from Bellsbank mine shown in Na₂O vs. Al₂O₃ diagrams. Fig.5a shows the comparison of group A (dark blue triangles) and B1 (light blue triangles) eclogites with Archean Basalts (Polat et al., 2003) and boninites (Smithies, 2004). Fig.5b shows group A' (yellow triangles) and B2 (red triangles) eclogites in comparison with Archean Basalts (Polat et al., 2003) and modern gabbroic rocks (SE Indian Ridge, Hart et al., 1999; Bach et al., 2001).

5.3 Geothermobarometry

Only the original clinopyroxene cores were combined with the garnet compositions to estimate temperatures with the Fe²⁺-Mg exchange thermometer between garnet and clinopyroxene in the version of Krogh (1988). Uncertainties in the use of this thermometer are the influence of the possible presence of Fe³⁺ and, related to this, the presence of excessive amounts of an acmite (NaFe³⁺Si₂O₆) component. Purwin et al. (2012, accepted for publication in Contributions to Mineralogy and Petrology) showed experimentally in a Na-free system that the influence of Fe³⁺ for this thermometer is negligible because of a partition coefficient of about one for Fe³⁺ between garnet and clinopyroxene. Sodium potentially has an influence if it is incorporated into cpx as acmite component. However, we find from Moessbauer spectroscopy (unpublished data) that Fe³⁺ in both garnet and clinopyroxene is very low. Also, Al is high enough in our clinopyroxenes that all Na present can be incorporated as a jadeite component.

Temperatures were calculated in an iterative way with the help of the in house PTEXTL spreadsheet in the version updated by T. Stachel, U of A, Canada. The pressures were estimated by projecting the Krogh (1988) K_D's onto a 38 mW/m² conductive geothermal gradient (Chapman and Pollack, 1977) which is suggested to be valid for Bellsbank by Garden et al. (8th IKC). The geothermal gradient of Newlands is similar, which is situated 30km to the southeast (Menzies et al., 1999) The results are presented in Table.3 and shown in Fig.6. Group B2 give the highest temperatures between 1050-1150°C between 5.5-6.5 GPa and group A the lowest around 825°C at 3.5-4.0 GPa. Groups B1 and A' give intermediate temperatures between 850-1000°C at intermediate pressures between 4.2-5.2 GPa.

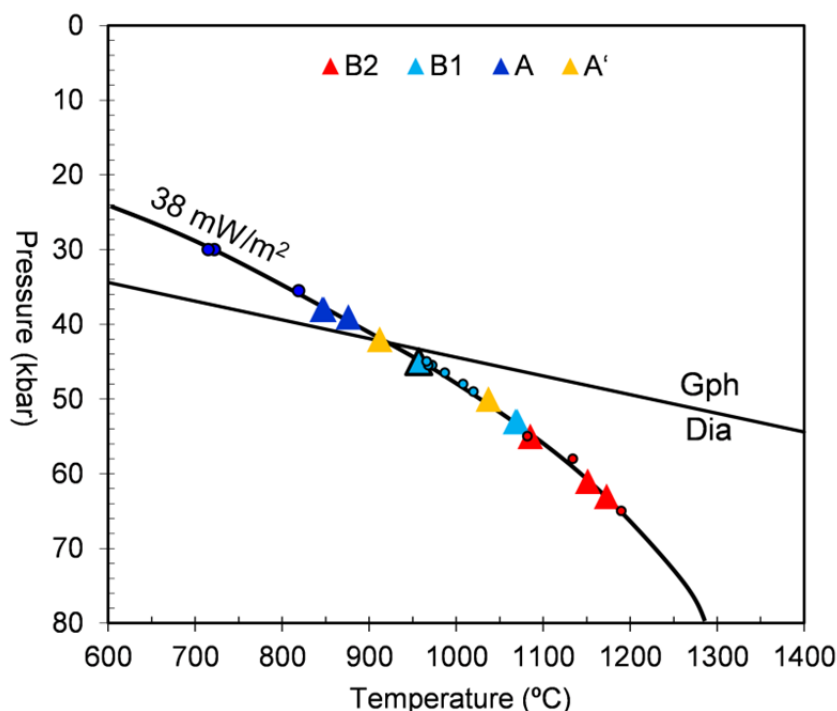


Fig. 6 Temperatures calculated from the exchange of Fe-Mg between garnet and clinopyroxene (Krogh, 1988) projected onto a 38 mW/m² geothermal gradient (Pollack and Chapman, 1977) for our samples and literature data (small circles) from Taylor and Neal (1989) and Shervais et al. (1988).

5.4 Trace elements

5.4.1 Garnets (Figs.7a,b)

Garnet trace element abundances are given in table 2 and shown in primitive mantle normalized (McDonough & Sun, 1995) REE and trace-element patterns in Figs.7a,b. The garnet REE patterns of groups A (dark blue lines) and B1 (light blue lines) are similar with steep negative slopes from heavy to middle REE to the LREE with extremely high HREE abundances ((Lu)PM up to 50). Sample BE4 from group B1 is severely enriched in the light to middle REE. In the other samples only La, Ce and possibly also Nd appear very slightly enriched.

Group A' and B2 garnets also show similarities with flat heavy to middle REE patterns, low REE contents with 1-6 x the primitive mantle value at Lu and with positive Th-U anomalies. Group A' have strongly negative Sr, Ti, Zr and Hf anomalies but not group B2 samples. These have slight to strong positive Eu anomalies (Eu/Eu*: 1.1 to 2.7) and are enriched in U and Th. Niobium and Ta in group B2 garnets are below the detection limit of our routine LA ICP MS setup.

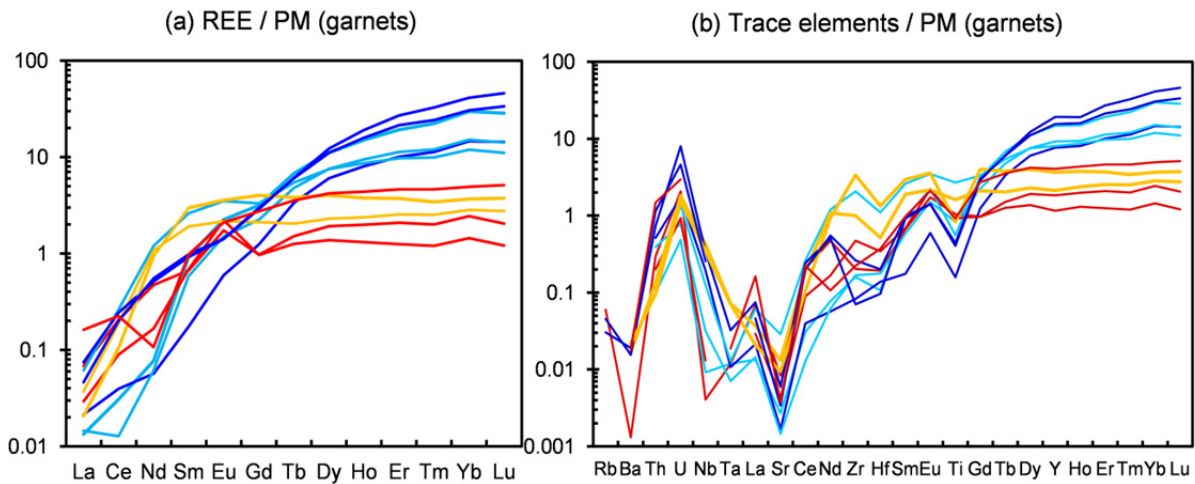


Fig.7a,b REE element and trace element patterns of the garnets from this study normalized to of the primitive mantle of McDonough & Sun (1995). (Group A: dark blue lines; Group B1: light blue lines; Group A': yellow lines; Group B2: red lines.)

5.4.2 Clinopyroxenes (Fig. 8 a,b)

Clinopyroxene trace element abundances are also given in table 2 and shown in Figs. 8 a,b. Group A and B1 clinopyroxenes show similar trace element patterns. The REE patterns have negative slopes from La to Nd or Sm, increase positively from Nd to Gd and again turn negative towards the HREE. Both groups have negative Ti, Zr- Hf and Nb-Ta anomalies and subchondritic Zr/Hf ratios(9-20). Clinopyroxene from sample BE4 also has elevated highly incompatible trace elements like its coexisting garnet. Group A pyroxenes are more enriched in LREE with $(Ce/Lu)_N$ ratios of 65-73 than group B1 with 5 to 46.

Group B2 clinopyroxenes (red lines) have the lowest trace element contents with positive Ti and negative Zr-Hf and Nb-Ta anomalies and enrichment in the most incompatible elements like Th-U , Sr and La-Ce. In contrast and other than for garnet, the group A' (yellow lines) pyroxenes have the overall highest trace elements contents with strongly negative Ti, Zr-Hf and Nb-Ta anomalies.

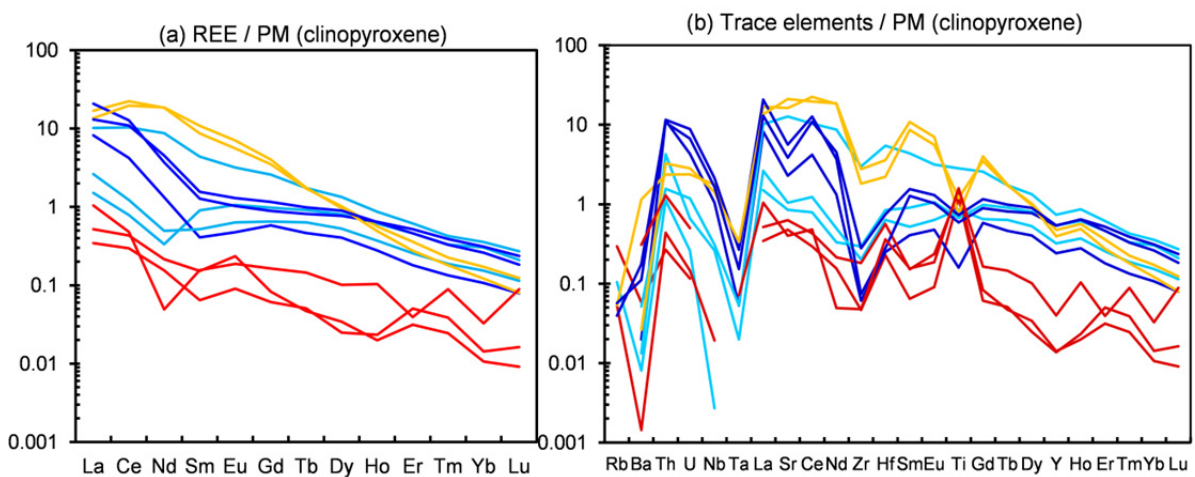


Fig.8a,b REE element and trace element patterns of the clinopyroxenes from this study normalized to of the primitive mantle of McDonough & Sun (1995). (Group A: dark blue lines; Group B1: light blue lines; Group A': yellow lines; Group B2: red lines.)

5.4.3 REE element partitioning

Trace element partitioning can depend on pressure, temperature and chemical composition. Our sample set shows a wide variation in these parameters. They should be suitable to distinguish between these effects in the partitioning e.g. of the REE between garnet and clinopyroxene and enable us to test for equilibrium between cpx and garnet. Recognition of equilibrium or non-equilibrium is a prerequisite before starting to discuss inferences from isotopic work or bulk rock compositions. We focus on the REE for which experimental partition coefficients are available over a range of P and T conditions and composition. We selected partition coefficients which were derived at 3 GPa, 1100 and 1200°C and 4 GPa, 1160°C by Green et al. (2000) for basaltic systems and compared them with our natural data (Fig. 9). The Green et al. (2000) experimental partition coefficients vary within a fairly narrow range. Our natural samples from similar P, T conditions are grouped around this range but vary much wider. Low MgO group B1 samples (light blue lines) and A' samples (yellow lines) with the highest MgO come from a similar temperature range (957-1070 °C and 912-1037 °C, respectively), but group A' have overall higher $D_{\text{cpx/grt}}$ ratios than group B1. The latter are generally more similar in composition to group B1 (light blue lines) but very different in temperature. Their REE partitioning practically shows no difference. Partition coefficients for group B2 samples (red lines) are the lowest and outside the range of the other samples. These samples have the Na-richest clinopyroxenes. It appears therefore that composition is the decisive factor which determines the partitioning behaviour of trace elements between garnet and clinopyroxene. Figures 9 and 10 show that the partitioning of the REE into garnet is favoured when the clinopyroxenes are rich in sodium and the garnets rich in calcium and that these effects are much larger than pressure and temperature effects. This corresponds to similar findings already in 1997 by Harte and Kirkley and to the results of experimental work by Bennett et al. (2004) who found a profound influence of sodium in clinopyroxene on trace element partitioning with melt. It appears from the above that the primary minerals of the eclogites used in this study are in internal mineral equilibrium.

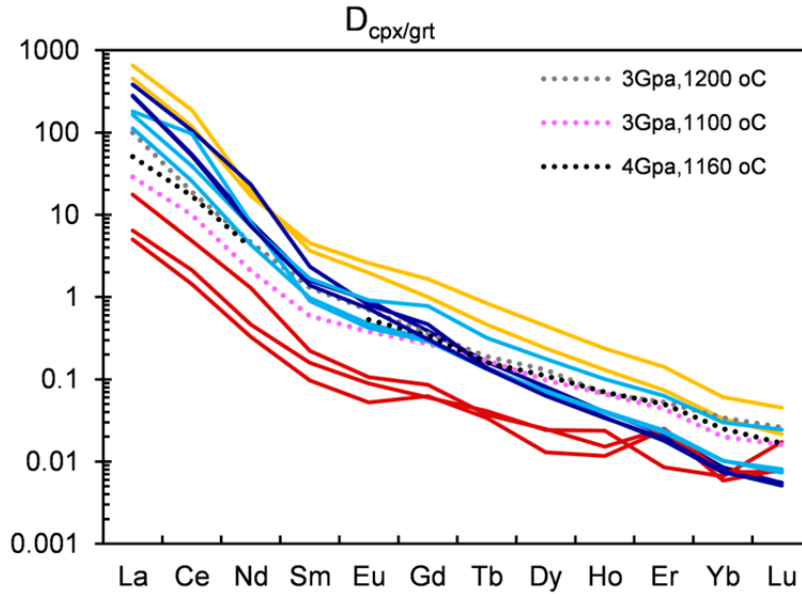


Fig.9 REE partitioning between garnets and clinopyroxenes. Different groups are shown as color-coded lines as in Figs. 7 and 8. (red lines-group B2; yellow lines-group A'; dark blue-group A; light blue- group B1).The experimenta data from different P-T condition from Green et al.(2000) are shown for comparison (dotted lines).

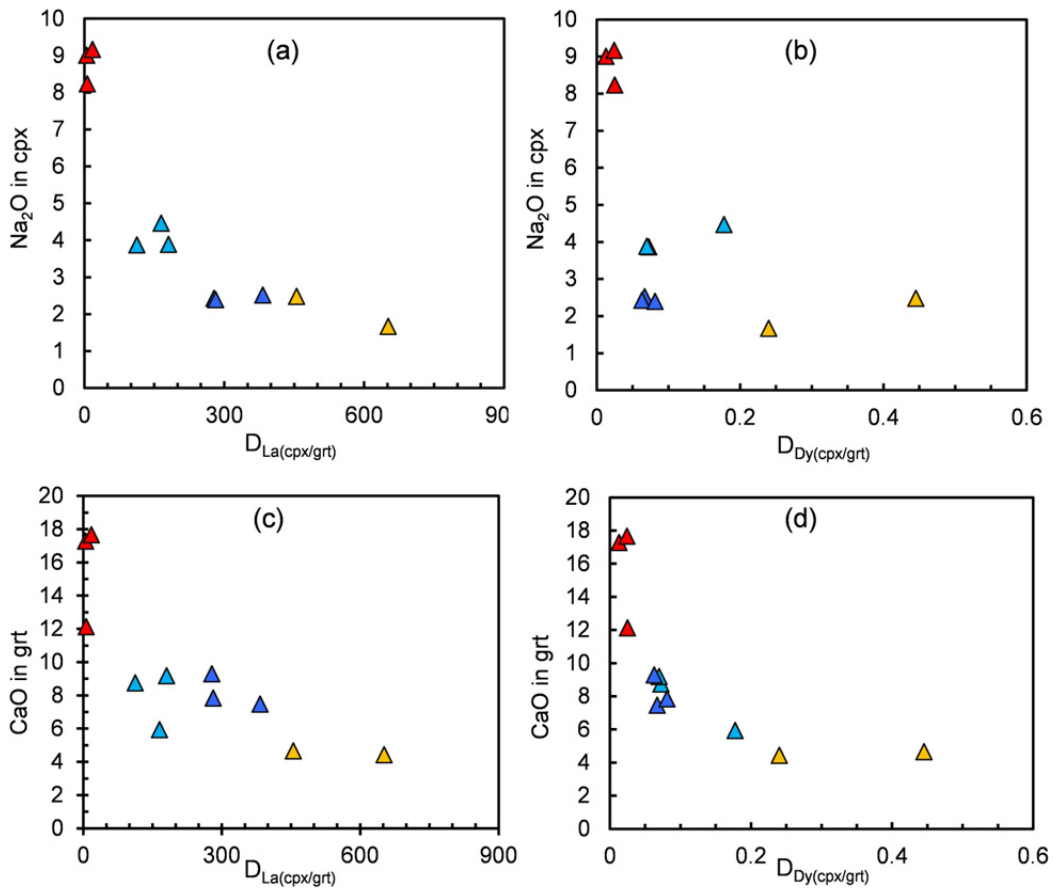


Fig.10 Covariation of Na_2O in cpx and CaO grt with the partitioning of La and Dy between clinopyroxene and garnet.

5.5 Bulk rock trace element composition

The reconstructed bulk rock trace element compositions are given in table 2 and shown in Figs. 11 a,b as primitive mantle normalized patterns.

In their REE patterns groups A (dark blue patterns) and B1 (light blue patterns) show high contents of HREE (7-32 x PM) and a strong decrease in abundances towards the LREE but an increase again of the LREE beginning from Sm or Nd. Groups A' (yellow patterns) and B2 (red patterns) have low HREE contents (1 to 4 x PM) and flat middle to heavy REE patterns. Group A' has an upward REE patterns with enriched LREE ($(Ce/Lu)_N=4.2-6.5$), while group B2 REE patterns continuously decrease (except for positive Eu anomalies) until Sm or Nd with minor enrichment in La, Ce or Nd.

The overall trace element patterns of group B2 samples show incompatible element depletion, including the fluid mobile elements Rb and Ba, but enriched U-Th which, together with the positive Eu anomalies resemble compositions of mid ocean ridge clinopyroxene-plagioclase cumulates which were possibly slightly chemically modified during subduction and/or metamorphism. The group A' samples (yellow patterns) have no Eu anomaly, are otherwise similar to B2 in middle and heavy REE but have much higher contents in the more incompatible trace elements and resemble pure cpx cumulates, but with strongly negative Ti and Zr-Hf and Nb-Ta anomalies.

The reconstructed bulk rock trace element compositions of groups A (dark blue patterns) and B1 (light blue patterns) also show negative Zr-Hf, Nb-Ta and Ti anomalies except sample BE4 which has very high contents in the more incompatible elements. Group A' has superchondritic Zr/Hf ratios (38 to 46) while groups B2, A and B1 have subchondritic Zr/Hf ratios (15 - 32). The negative Ti and Zr-Hf and Nb-Ta anomalies in most eclogites may be due to the non-consideration of a Ti-phase, either ilmenite or rutile, which were not found. Previous studies show a common occurrence of rutile or ilmenite in the mineral assemblage of eclogites. Such phases should therefore be considered in the whole rock reconstruction (e.g. Barth et al., 2001, 2002; Jacob, et al. 2005, Heaman et al., 2006). We did not find any rutile or ilmenite in our samples but this may be due to the small sample size and a low rutile abundance in our rocks. Its abundance must be less than 0.5 vol% as estimated according to a suggestion by Aulbach et al. (2007) who calculated a potential rutile abundance by removing the negative Ti anomaly from the N-MROB normalized pattern.

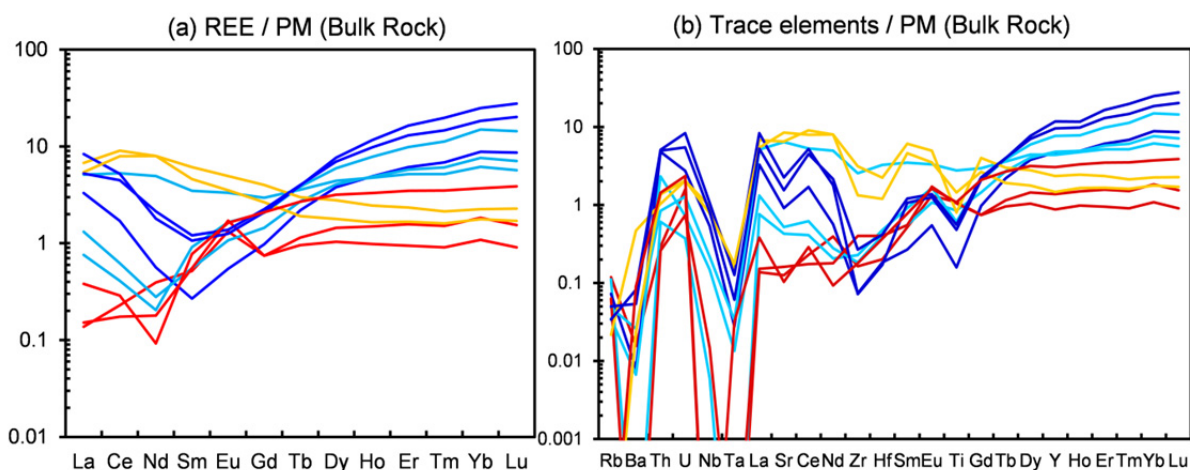


Fig.11.a,b Primitive mantle (McDonough and Sun, 1995) normalized REE and trace element patterns of reconstructed bulk rock. Color-coded lines as in the figures above.

5.6 The Sm-Nd, Lu-Hf and Sr isotopic systems

5.6.1 The Lu-Hf isotope system

The data are given in **Table A.5a** in the appendix and shown in Fig.12 a,b in diagrams of $^{177}\text{Hf}/^{176}\text{Hf}$ against the sodium content in clinopyroxene as an indicator of the type of eclogite. The isotope ratios are extremely high in the majority of the samples. The most extreme values correspond to $\epsilon\text{Hf} = +13724$ for garnet and to $\epsilon\text{Hf} = +6552$ for the coexisting clinopyroxene [high ϵHf values were reported only twice before in previous work on eclogites and only for garnets ($\epsilon\text{Hf} = +2561$ for a garnet from Roberts Victor; Jacob et al., 2006 and $\epsilon\text{Hf} = +2532$ for a garnet from Lac de Gras; Aulbach et al, 2007)]. High $^{177}\text{Hf}/^{176}\text{Hf}$ ratios in grt correspond to high $^{177}\text{Hf}/^{176}\text{Hf}$ in cpx and low correspond to low as may be seen in Table 4 and Figs.12a,b. Consequently, calculated bulk rock compositions (neglecting the possible presence of rutile) also give a huge range in ϵHf from more than +10000 to +13 for the one group A' sample (Fig. 13). Groups A and B1, the lower temperature groups, have the very high isotope ratios (except for the enriched sample BE4). Their clinopyroxenes always have lower Hf isotope ratios than their coexisting garnets. Groups A' and B2 are the higher temperature groups with lower but very similar isotope ratios in garnets and clinopyroxenes. Consequently, the latter give eruption ages from their two-point isochrons and the former older ages (up to 810 Ma). The meaning of two-point isochrones for eclogites is discussed in the following chapter.

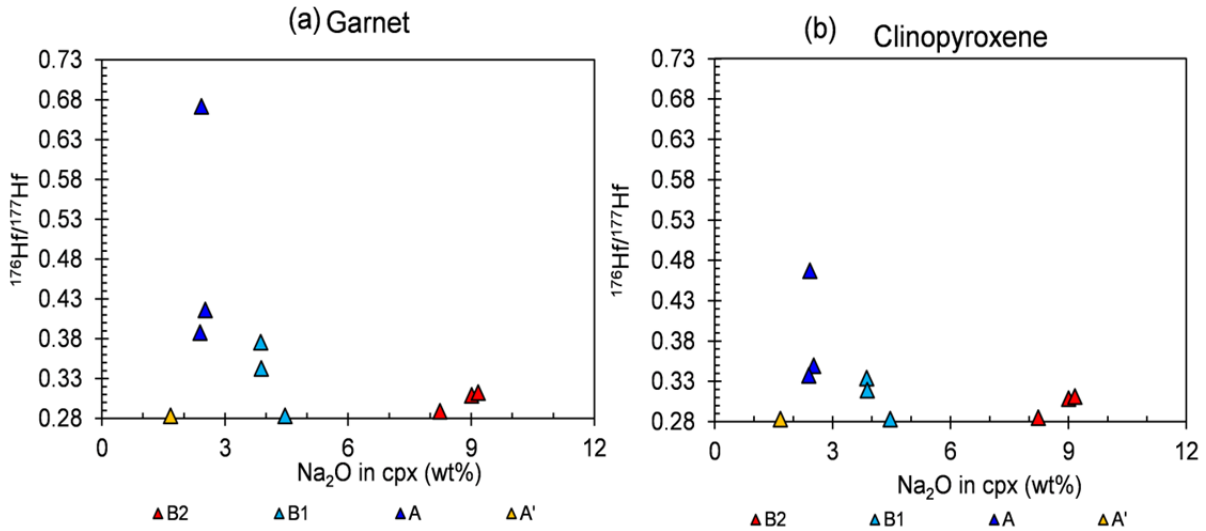


Fig.12 a,b The measured $^{177}\text{Hf}/^{176}\text{Hf}$ isotope ratios for a) garnet and b) clinopyroxene plotted against the sodium content in clinopyroxene an indicator of the type of eclogite. Most isotope ratios are extremely high (for comparison: the present day primitive mantle has $^{177}\text{Hf}/^{176}\text{Hf} = 0.282772$ and the depleted MORB mantle has 0.283250). The sequence of the data points from high to low isotope ratios for garnets and clinopyroxenes for each group of eclogites also corresponds to sample numbers i.e. high garnet belongs to high cpx. Coexisting grt-cpx pairs can thus be connected by eye.

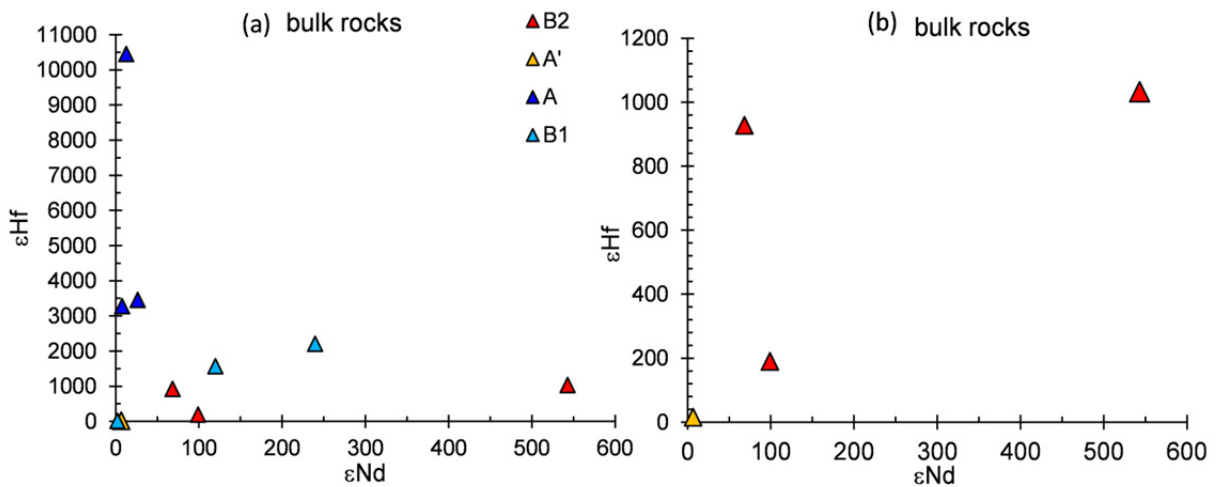


Fig.13 Diagram of ϵ_{Nd} plotted against ϵ_{Hf} for reconstructed bulk eclogites. Fig.13 a shows all data from this study and Fig.3 b shows in more detail the group A' and B2 eclogites. Three of the four samples lie along a line.

5.6.2 The Sm-Nd isotope system

The data are given in **Table A.5b** and shown in Fig.14 a,b in diagrams of $^{143}\text{Nd}/^{144}\text{Nd}$ against the sodium content in clinopyroxene as an indicator of the type of eclogite. The isotope ratios are very high in the majority of the samples as already reported by Shervais et al.(1988) and Neal and Taylor (1990). The most extreme values were found in sample BE11 with $\epsilon_{\text{Nd}} = +553$ in garnet and $\epsilon_{\text{Nd}} = +420$ in cpx. Like for Hf, high $^{143}\text{Nd}/^{144}\text{Nd}$ ratios in grt correspond to high $^{143}\text{Nd}/^{144}\text{Nd}$ in cpx and low ratios in grt to low ratios in cpx (**Table A.5b** in the appendix and Fig.14). Consequently, calculated bulk

rock compositions also give a large range in ϵ_{Nd} from more than +550 to +3 (Fig. 13). The sequence of the various groups is, however, different as for the Hf isotopes because the Sm-Nd isotope system is much more prone to metasomatism than the Lu-Hf system. This is discussed in more detail below and in the next chapter which deals with the meaning of two-point isochron ages. These vary from 2 Ma to 1.6 Ga. Two of the samples give close to eruption ages. One sample yields with 2 Ma younger than eruption age. The rest of the samples give older than eruption ages from 292 to 1642Ma.

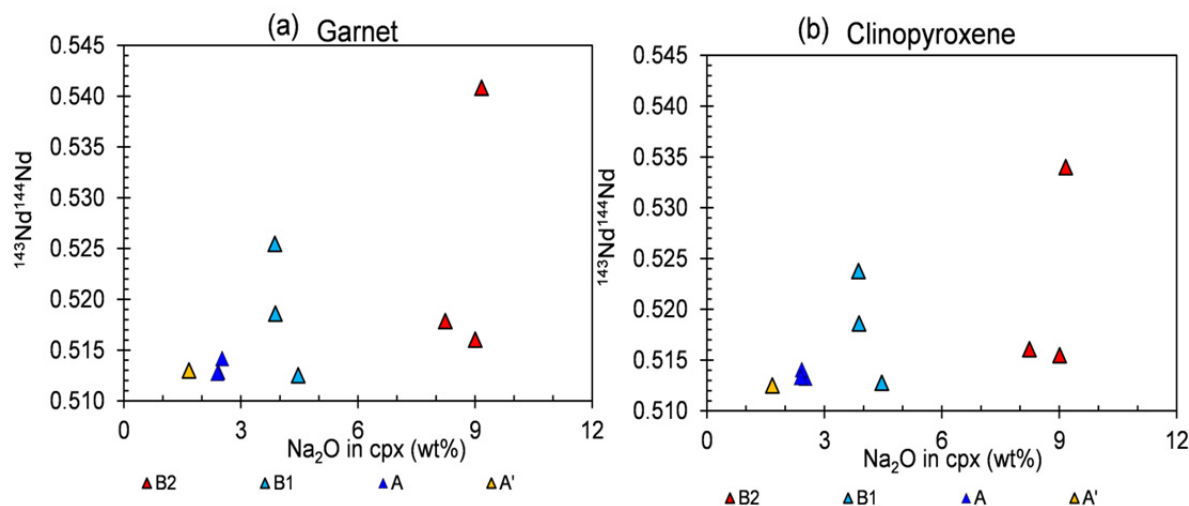


Fig.14 a,b The measured $^{143}\text{Nd}/^{144}\text{Nd}$ isotope ratios determined for a) garnet and b) clinopyroxene plotted against the sodium content in clinopyroxene as indicator of the type of eclogite. The isotope ratios partly are extremely high.

5.6.3 The Sr isotope composition

The Sr isotope ratios were only determined in clinopyroxenes and not in garnet, because the Sr contents in grt are too low and sample sizes too small. The Rb abundances are lower than detection limit of our LA ICP MS set up except in three clinopyroxenes. The Rb and Sr contents from in-situ measurement and the Sr isotope ratios are given in **Table A.6** and shown in Figs. 15 and 16. The low Sr samples (8 to 13 ppm) B1 and B2 have high $^{87}\text{Sr}/^{86}\text{Sr}$ ratios (from 0.7084 to 0.7123), while the group A clinopyroxenes with 21 to 254 ppm have lower $^{87}\text{Sr}/^{86}\text{Sr}$ ratios from 0.7044 to 0.7058. The only exception is the group A' sample which has the highest Sr content of 419 ppm, Rb below the detection limit but a high $^{87}\text{Sr}/^{86}\text{Sr}$ ratio of 0.7123. Our results confirm those of previous work of Taylor and Neal (1990) and Viljoen (1995) which also shows unsupported Sr isotope ratios.

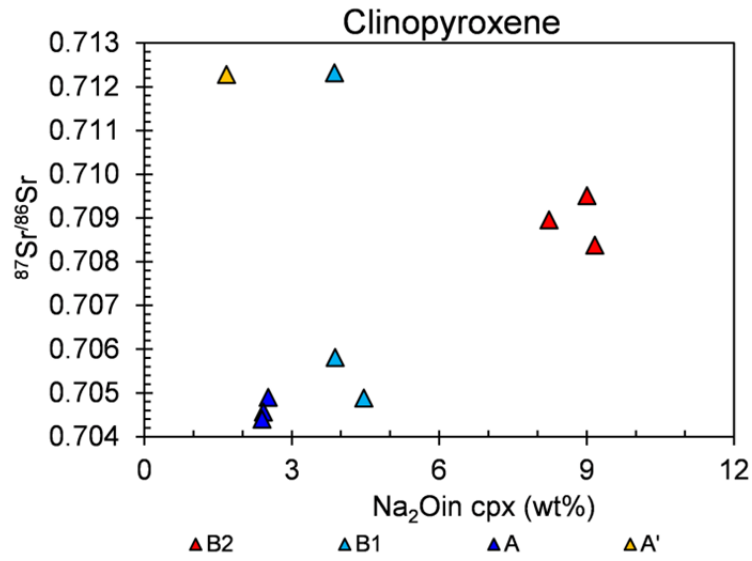


Fig.15 The measured ⁸⁷Sr/⁸⁶Sr isotope ratios for clinopyroxene plotted against the sodium content in clinopyroxene as an indicator of the type of eclogite.

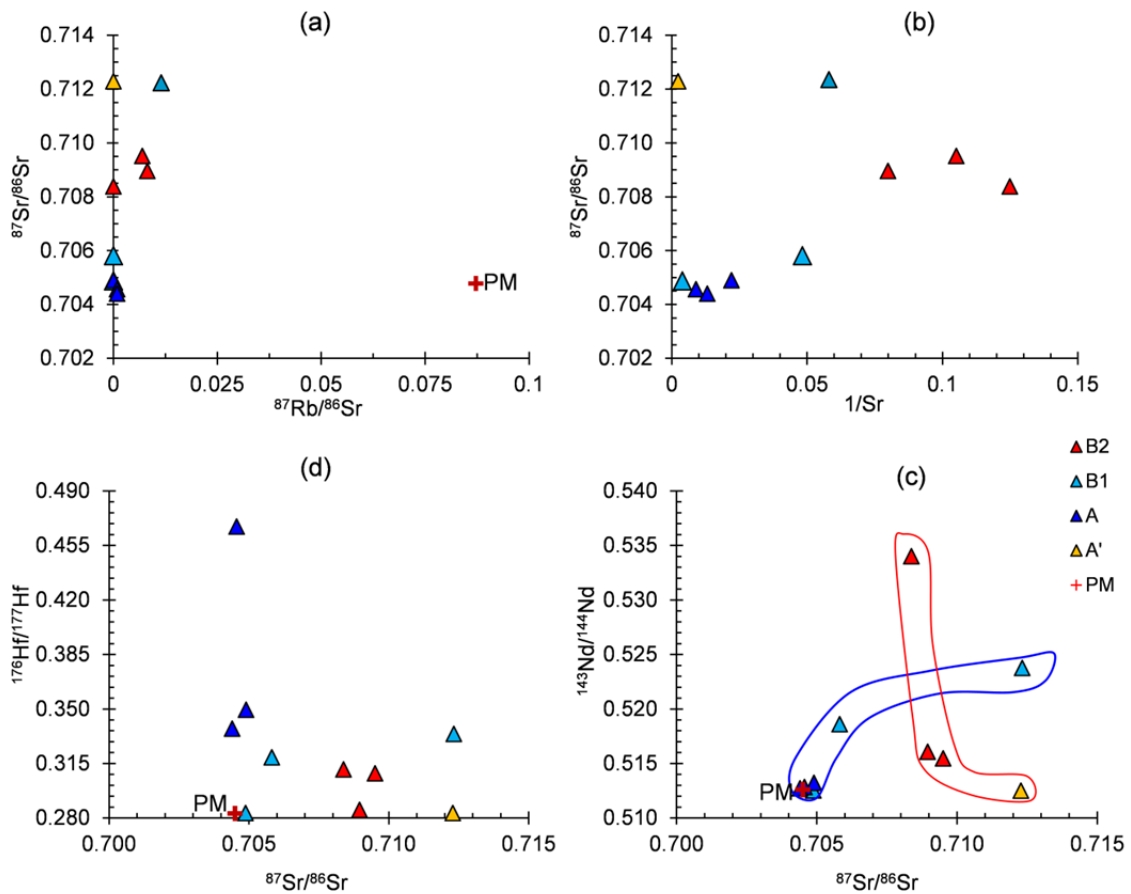


Fig.16 Correlation of Sr, Nd and Hf isotope compositions. The Sr isotope ratios plotted against Rb/Sr (a), 1/Sr (b), the Nd isotope ratios (c) and the hafnium isotope (d)

5.7 Oxygen isotopes

Oxygen isotopes were analyzed in grt and cpx ten out of 11 samples. The results are given in Table 3 and shown in Figs.17 and 18. Garnets and clinopyroxenes from nine out of 10 samples have $\delta^{18}\text{O}$ below the mantle value ($5.5 \pm 0.22 \text{ ‰}$, Harmon and Hoefs, 1995) ranging from 2.5 to 5.3 ‰. The only sample with values higher than the mantle is BE4, which is again the sample with the most enrichment in incompatible elements. Garnets are always lower in $\delta^{18}\text{O}$ by 0.7 ‰ on average but there are somewhat smaller and larger differences. There is no correlation of this difference with temperature.

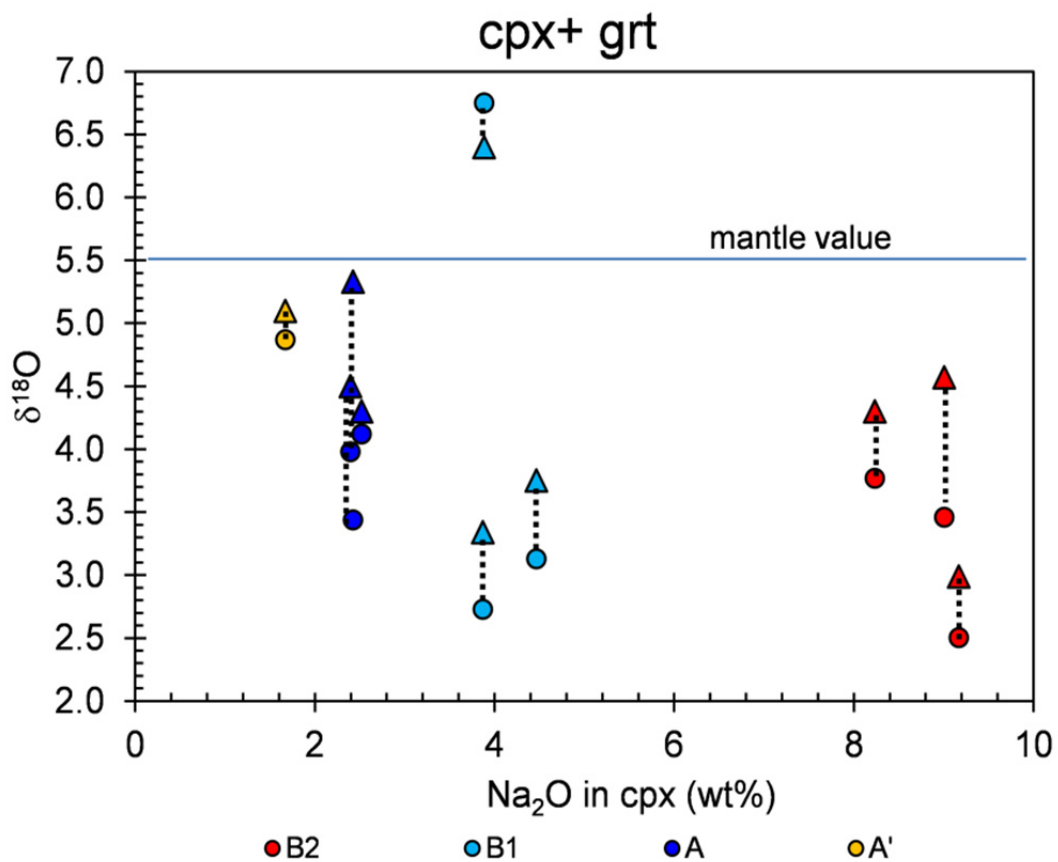


Fig.17 The measured oxygen isotope ratios for garnets (circles) and clinopyroxenes (triangles) plotted against the sodium content in clinopyroxene an indicator of the type of eclogite

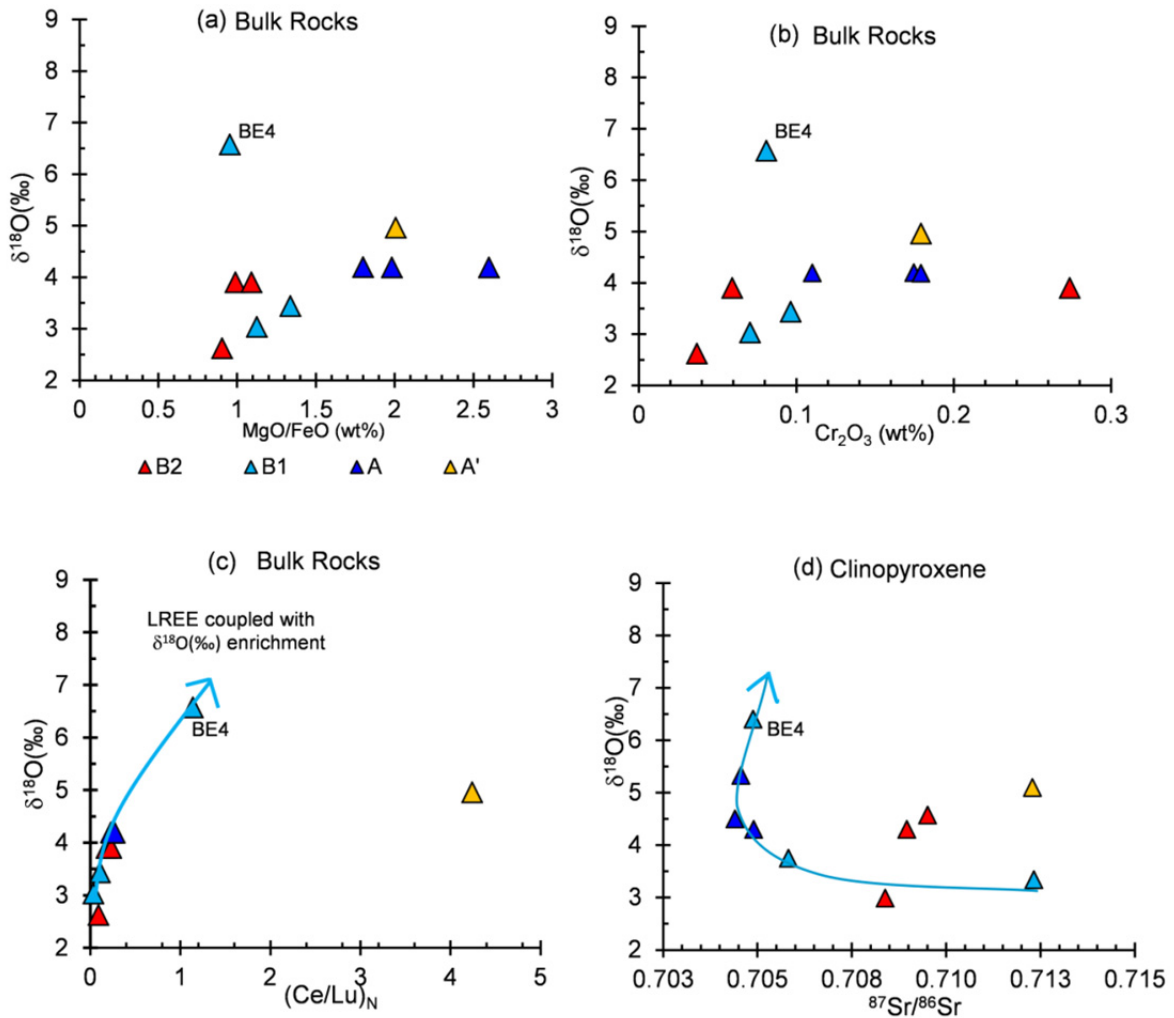


Fig.18 Diagrams of calculated bulk rock $\delta^{18}\text{O}$ against MgO/FeO (a), the Cr_2O_3 -content of calculated bulk rocks (b), the $(\text{Ce/Lu})_N$ of calculated bulk rocks (c) and the $^{87}\text{Sr}/^{86}\text{Sr}$ ratio in clinopyroxenes (d).

6. Discussion

6.1 The nature of the protoliths of the Bellsbank eclogites and garnet pyroxenites, their origin and subsequent modifications

6.1.1 Group A' and B2 eclogites

Protoliths of metamorphic rocks may be recognized from geochemical and isotopic fingerprints. A pronounced Eu anomaly in the REE patterns of a rock is always interpreted as indicating the role of plagioclase in the genesis of that rock, a correct interpretation beyond any reasonable doubt. Two of the B2 eclogites have a positive Eu anomaly and major element compositions of the reconstructed bulk-rocks which coincide with the broad field of modern oceanic gabbroic rocks (Figs.3, 4 and 5). They overlap in their middle to heavy REE patterns with the low concentration end of MOR gabbros (Fig.19b). The positive Eu anomaly, the low middle to heavy REE abundances and the very aluminous

bulk composition all demonstrate the dominant role of former plagioclase in the precursors of these rocks. These must have been low pressure, plagioclase rich cumulates from MORB-like compositions with coprecipitating or intercumulus clinopyroxene and possibly some olivine. The third B2 sample (BE11) shows very similar chemical features but higher middle to heavy REE and no Eu anomaly (Fig. 19b). It may be a cumulate where cpx and plagioclase coprecipitated in appropriate amounts so that there is no Eu-anomaly in the bulk rock or, the preferred interpretation, an almost unmodified melt which had originally crystallized to a gabbro. Group A' eclogites are very similar to group B2, are somewhat elevated in the middle to heavy REE compared to the two group B2 samples with a Eu anomaly but lower compared to the one without an anomaly (Fig.19b). They are also much lower in Na₂O and have higher Mg-values (Figs.3,5). The similarities and differences can be best explained, if group A' eclogites were clinopyroxene rich cumulates (accompanied by some olivine) from the same magma as group B2. The composition of this magma may correspond to that of sample BE11. The protoliths of groups A' and B2 eclogites may therefore have been generated in a mid ocean ridge setting followed by eclogitisation during subduction. Such an origin was already suggested by Neal et al. (1990) for their samples from Bellsbank corresponding to group B2. Jacob et al. (2004) summarize arguments for a subduction origin of many eclogites worldwide and also discuss the role of the oxygen isotopes in this chain of argumentation.

The oxygen isotopes ($\delta^{18}\text{O} = 2.7 - 4.1\text{‰}$ for calculated bulk rocks) for groups A' and B2 are below the mantle value. Lower than the mantle values in basaltic rocks are difficult to obtain except by low temperature sea water alteration. This was taken originally by Jacob et al.(1994) as an important prove for a subduction origin of kimberlite borne eclogites.

Both groups A' and B2 have very high ⁸⁷Sr/⁸⁶Sr and very low Rb/Sr ratios i.e. the Sr isotope ratios are not supported by Rb in todays rocks. This either means that Rb has been lost or that Sr with high ⁸⁷Sr/⁸⁶Sr has been reintroduced some time along the history of the rocks. The latter may be caused for the B2 samples as a contamination by the host kimberlite eruption because of the very low Sr contents of the B2's and because their Sr isotope ratios and those of the kimberlites (0.70990±8; Smith, 1983.) overlap.

Very differently, the group A' sample has a very much higher Sr isotope ratio of 0.7123 than the kimberlite, a high Sr content of 417 ppm and a very low Rb/Sr ratio. Such high values are not possibly derived from contamination by any agent with a reasonable composition. The high Sr content may still be close to the original signature from sea floor alteration since this sample apparently was subjected only to a weak dehydration process as judged from their high incompatible trace elements (see discussion below). Rubidium is removed by dehydration much more easily which leaves a rock with a low Rb/Sr ratio. If the Rb/Sr ratio was very high before dehydration the ⁸⁷Sr/⁸⁶Sr ratio grew very fast and was high before dehydration. High Rb/Sr ratios can be caused by higher temperature sea water alteration as described e.g. from altered Archean pillow basalts from the Isua greenstone belt by Polat et al.(2003). Modern day altered pillow basalts have very high ⁸⁷Rb/⁸⁶Sr ratios of up to 12 by the introduction of chlorite and/or sericite (e.g. Erzinger, 1989; Alt, 1995; Humphris, 1998). Such high ⁸⁷Rb/⁸⁶Sr ratios can generate a Sr isotope of 0.7123 within 65 Ma at 3.8 Ga. Sample A' may be a chemically almost unchanged equivalent of an altered seafloor gabbroic rock.

We had deduced from the HREE abundances and patterns that the protoliths of the group A' and B2 samples were seawater altered members of a suite corresponding to modern gabbroic rocks. However, group B2 eclogites have overall depleted incompatible elements from Sm onwards which indicates additional melt or fluid loss during or after eclogitisation. It may be fluid loss by dehydration during subduction as the very low of fluid mobile elements like K, Rb and Ba indicate or partial melting after eclogitisation as the extremely low LREE/HREE ratios [e.g. $(Ce/Lu)_N = 0.03-0.27$] indicate. Evolved gabbroic rocks have on average a high $(La/Lu)_N$ ratio of about 2.6 (Hart et al., 1999). Very low LREE/HREE ratios can be achieved only by partial melting with garnet as a residual phase. Contrary, group A' garnet pyroxenites have high $(Ce/Lu)_N$ ratios of 5-7, which overlap with gabbroic rocks and which argue against a melt loss. Their highly incompatible element inventory may largely stem still from their protoliths.

Group B2 eclogites do not have negative Ti and HFSE (Zr-Hf, Nb-Ta) anomalies which is in accord with their possible origin as a plagioclase-rich cumulate and their high temperatures of origin where garnet and clinopyroxene can take up all Ti and no rutile is present. However, group A' garnet pyroxenites do have such an anomaly which may be due to non-discovered rutile in the small samples. The amount of rutile is less than 0.5 vol% as calculated from the depth of the Ti-anomaly as suggested by Aulbach et al. (2007). This is reasonable since, at the relatively low temperatures of group A', garnets and and clinopyroxenes may be at their Ti-saturation level (which is largely temperature dependent).

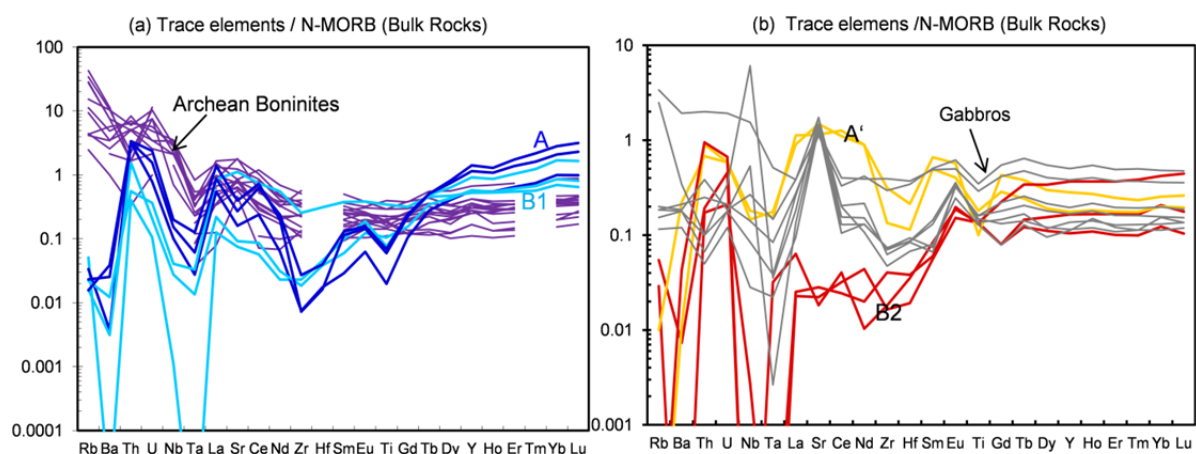


Fig. 19 The trace element patterns of reconstructed bulk rocks. The diagram (a) shows the trace element patterns of group A (dark blue lines) and B1 (light blue lines) and the trace element of Archean boninites (Smithies, 2002). The diagram (b) shows trace element patterns of group A' (yellow) and B2 (red lines) and modern gabbroic rocks (SE Indian Ridge, Hart et al., 1999; Bach et al. 2001), Normalized to N-MORB of Sun & McDonough (1989).

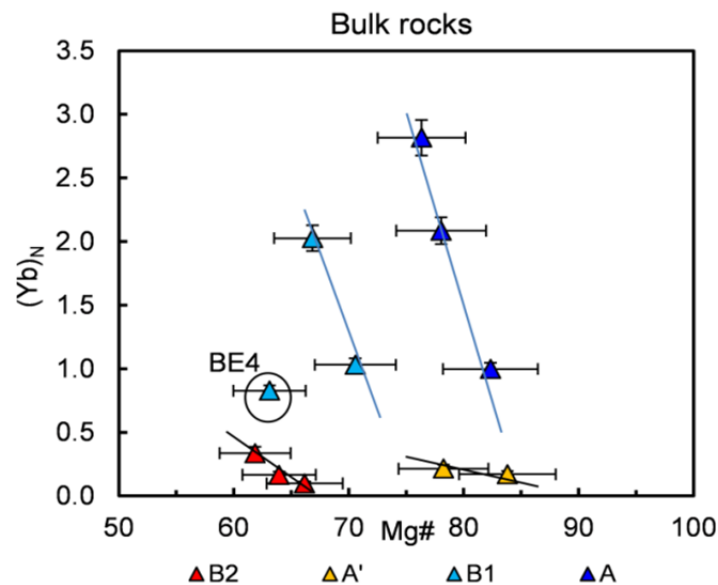


Fig.20 Correlation of Mg# and (Yb)_N. Each group show negative correlation between Mg # and (Yb)_N which can be the olivine fraction origin indicated by the lines. The most enriched sample (BE4). from group B2 eclogites is marked by circle and plot outside of the olivine fraction trend.

6.1.2 Group A and B1 eclogites

Garnets in group A (high-MgO).and B1 (low-MgO) eclogites compositionally overlap with those of group A and B samples (Fig. 2a) reported in previous studies by Taylor and Neal (1989) and Neal et al., (1990). Based on the major- and trace element compositions these authors had proposed that their group A (=group A here) high Mg eclogites originated as high pressure garnet and clinopyroxene cumulates and their group B low Mg eclogites (= our group B1) as basaltic oceanic crust. But such a model cannot be applied to these eclogites, at least not in this simple way. The positive slopes of the middle to heavy REE in the N-MORB normalized REE patterns (Figs.19a) and high HREE abundances show that A and B1 eclogites are genetically related and that the B1 protoliths cannot be simply basaltic oceanic crust. However, a central role of garnet in the genesis of these eclogites is suggested by the REE patterns. A high pressure origin as garnet rich cumulates from a melt could be feasible but oxygen isotope ratios below the mantle values a priori preclude such a model. The mantle, from which the melts stem, would have to be overwhelmed in its oxygen isotope ratio by low-temperature fluids in an arc setting. Pearson et al., (1993) describe garnet pyroxenites from Beni Bousera which are very similar to the group A samples in their major and trace elements and also oxygen isotope ratios. Their tentative model suggests a scenario similar to above; they remain, however, cautious. Another possibility is that the rocks are residues of partial melting in which garnet plays the dominant role. Candidates for eclogites with high and fractionated HREE can be boninites as suggested by Aulbach et al.(2007). The extremely high abundances of HREE in both group A and B1 eclogites argue against the simple metasomatically boninites model. However, Archean basaltic or boninitic precursors can be the candidates for eclogite facies metamorphosed protoliths to be molten. Archean basalts have, like MORB, flat middle to heavy REE patterns and model calculations show that

degrees of eutectic like partial melting of more than 80 % are required for such a source to obtain residues with the extremely high HREE abundances and the extremely fractionated REE patterns as seen in the group B1 samples. Archean boninites, as second stage melting products of a depleted mantle, already have fractionated REE patterns (e.g. summarized by Smithies et al. 2004; see Fig. 21) which will reduce the degrees of partial melting necessary to match A and B1 samples as residues.

Consequently, we used two Archean boninites (sample 462903 and sample NC-33) as starting compositions and the experimental trace element partition coefficients for garnet and cpx from Green et al. (2000) for fractional melting calculations. We assume that initial modal abundance for garnet and cpx is 50% to 50%. Pertermann et al. (2003) stated that both garnet and cpx are equally contributing to the melt composition near the solidus, but that with increasing melting, more cpx contributes to the melt. Therefore, we use a melting model with 60% cpx+40% garnet=100% melt. Sample 462903 is from Isua in Greenland (Polat et al. 2002) and sample NC-33 is from Abitibi in Canada (Kerrick et al. 1998). These two samples have roughly similar shaped REE patterns but very different abundances. Consequently, 20 to 70 % partial melting are required to match the our group B1 samples as residues with the low HREE Isua boninite as starting composition but the group A eclogites are not reached (Fig. 21a). Abitibi boninite NC-33 as another extreme composition has HREE abundances higher than two B1 and one A sample and is not a feasible starting composition for these rocks. However, 60% of partial melting will leave the most extreme group A sample as a residue (Fig. 21b). The compositional range of boninites is large [$(\text{Lu})_{\text{N-MORB}}$ from 0.2 to 1.3; Smithies, 2004] and groups A and B1 samples may be the residues of a range of boninitic parental compositions. However, the elevated incompatible trace elements in these two groups must be the result of later enrichment, whereby group A eclogites are generally more enriched in incompatible elements than group B1, except for sample BE4.

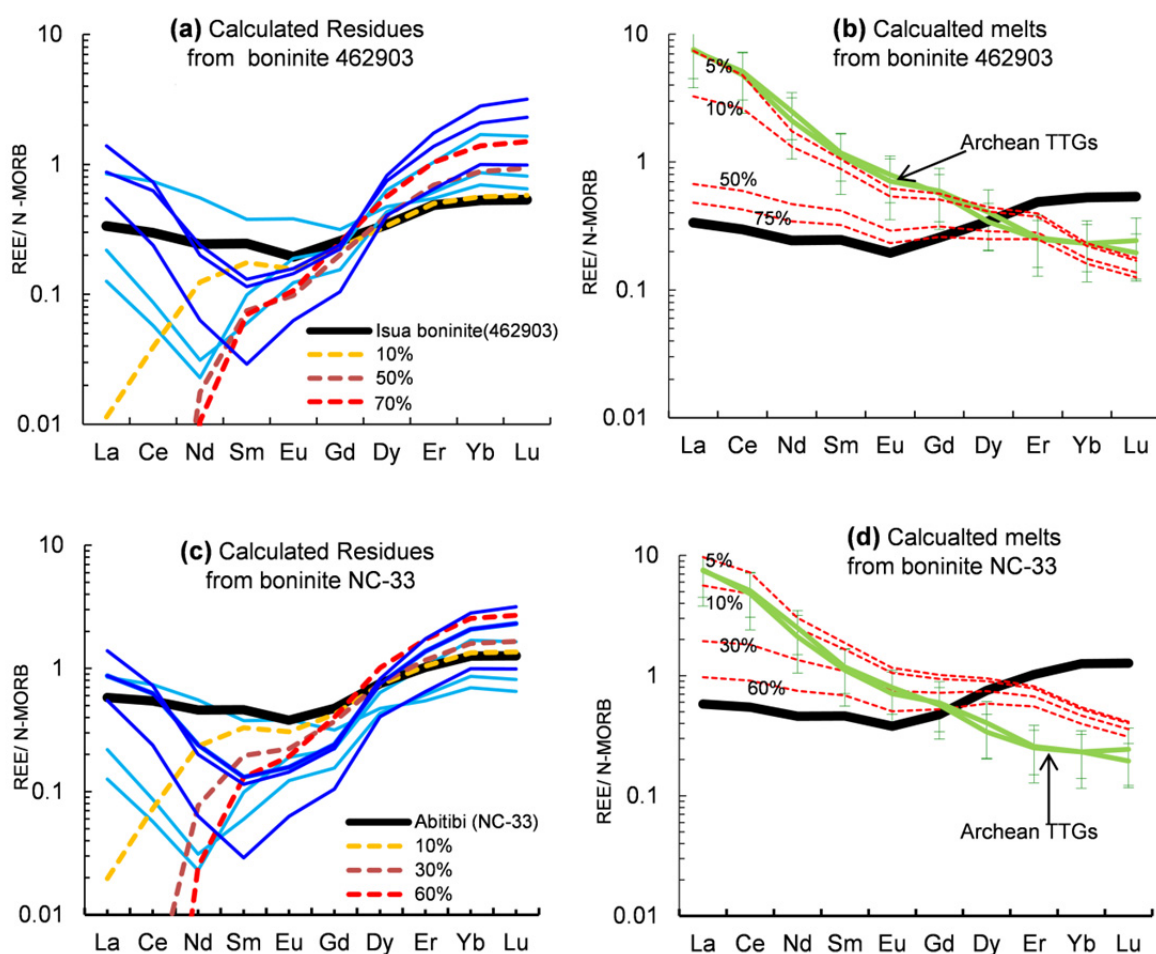


Fig.21 Results of nonmodal fractional partial melting calculation using two Archean boninitic rocks as starting compositions. The REE partition coefficients are from Green et al., (2000).The melting model is 60% cpx +40% garnet =100% melts. We use two boninites with different REE abundances as the starting compositions (Isua boninites (462903) from (Polat et al., 2002),and Abitibi boninite (Nc-33) from (Kerrich et al., 1998)).The result for Isua boninite (462903) are shown in diagram (a) for the residua compositions (colored dashed lines) of different degrees of partial melting of boninite 462903 (black line) and (b) for resulting melts. and a comparison with Archean TTGs (green lines). Diagrams (c) and (d) are residues and melt compositions for boninite NC-33.

6.2 Age of the Bellsbank eclogites

Age information potentially obtainable from eclogitic rocks from the mantle is the age of the origin of the protolith, the age of eclogitisation and possibly also the age(s) of subsequent partial melting and metasomatic events. In theory, protolith ages may be obtained from (reconstructed) bulk rock isochrons or from model ages. These ages may be close to the eclogitisation age if protolith emplacement is followed very shortly by subduction. Internal mineral isochrons (with or without the incorporation of the bulk rock isotope composition) could give the age of eclogitisation. Two-point grt-cpx isochrons could also give the age of eclogitisation but a control of these ages via a bulk rock composition is generally not feasible because of common contamination by the host kimberlite. Two-

point isochrons give at best minimum ages along a cooling path (see discussion in the following chapter). Bulk rock isochrones practically do not exist so far because a genetic link has to be established between the various types of eclogites. A successful attempt for such an approach is shown below. However, bulk rock errorchrons exist. Examples are errorchrons from eclogites from Newlands on the Kaapvaal craton which give limiting ages between 2.92 and 4.12 Ga (Menzies et al. 2003), a 2.9 Ga Re-Os errorchron age from Siberian eclogites (Pearson et al. 1995), a 2.77 Ga Sm-Nd errorchron from Roberts Victor (Jacob et al. 2005) and a 2.1 Ga Lu/Hf errorchron from Diavik on the Slave craton (Schmidberger et al. 2007). Examples for model ages are a 2.47 ± 0.2 Ga Pb-Pb model age from the Premier mine (Kramers 1979) and a 2.7 Ga Lu-Hf age from a clinopyroxene from Lac de Gras (Aulbach et al. 2007). Eclogitisation is probably reflected in a 2.7 Ga garnet growth isochron of one eclogite from Roberts Victor (Jagoutz et al. 1984), in a 2.7 Ga Pb-Pb geochron age from clinopyroxenes from Greenland (Tappe et al. 2010) and a 2.1 Ga Pb-Pb model age from clinopyroxenes from Diavik (Schmidberger et al. 2007). The eclogitic rocks from the Bellsbank diamond mine show very little to almost no chemical overprint of highly incompatible elements (compare Figs. 11 a,b) so that their original chemistry after melt extraction (groups A and B1 except for BE4) or from the protoliths (Groups A' and B2) is largely kept. The small degrees of enrichment affected only the LREE and not the middle to heavy REE and Hf. Most of the Nd and partly also Sm will therefore stem from the enriching agents and an enrichment age may be obtained from the Sm-Nd isotope system. We combined our own data with the Sm-Nd data of Neal et al. (1990) and Shervais, et al. (1988) and obtained a 2.08 ± 0.38 Ga errorchron with $\epsilon_{\text{Nd}} = +28$ (Fig. 22). We excluded the samples BE11 and BE2 from this correlation because they show practically no Nd enrichment in their trace element patterns (Fig. 11a,b). It is interesting to note that the 2.08 Ga age coincides with the age of the Bushveld Complex of 2.06 Ga (Walraven et al., 1990) on the other hand and with the range of ages between 1.75 to 2.1 Ga for the Kheis-Magondi belt (Beukes and Smit, 1987; Alterman and Höllich, 1991).

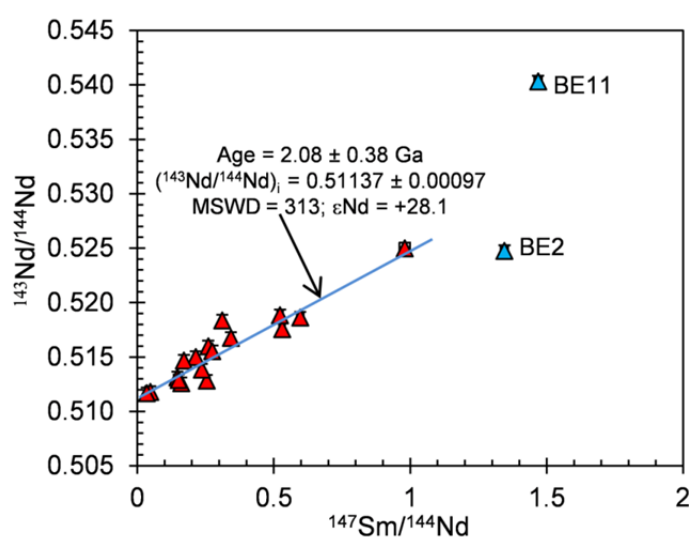


Fig. 22 Isochron diagram of bulk rock $^{143}\text{Nd}/^{144}\text{Nd}$ ratios against $^{147}\text{Sm}/^{144}\text{Nd}$ (own and literature data). The red triangles yield an errorchron age of 2.08 Ga with $\epsilon_{\text{Nd}} = +28$. The two samples (blue triangles) off that line are the those which practically do not show any enrichment in Nd and Sm.

6.2.1 Age of group A' and B2 eclogite

A common Sm-Nd isochron through the bulk rock isotopic compositions of all groups is permissible since enrichment occurred after the assembly and stabilization of the Kaapvaal craton. The Lu-Hf system, however, was practically not affected by this process and may therefore give information of the more original history of the rocks. We have suggested that the protoliths of groups A' and B2 probably are cogenetic and metamorphosed portions of a subducted oceanic crust. The reconstructed bulk rocks should therefore linearly align in an isochron diagram. It can be seen in Fig. 23 that three samples give an age of 4.12 ± 0.06 Ga with $\epsilon_{\text{Hf}} = 3 (\pm 7)$ i.e. within error the initial of the primitive mantle at that time, but sample BE1 lies off the supposed isochron. Such an old age is not directly matched by any crustal ages from the Kaapvaal craton (but see discussion below) or by Re-depletion ages from its lithospheric mantle. Only a Re-Os errorchron from Newlands eclogites yields the same age (Menzies et al, 2003)

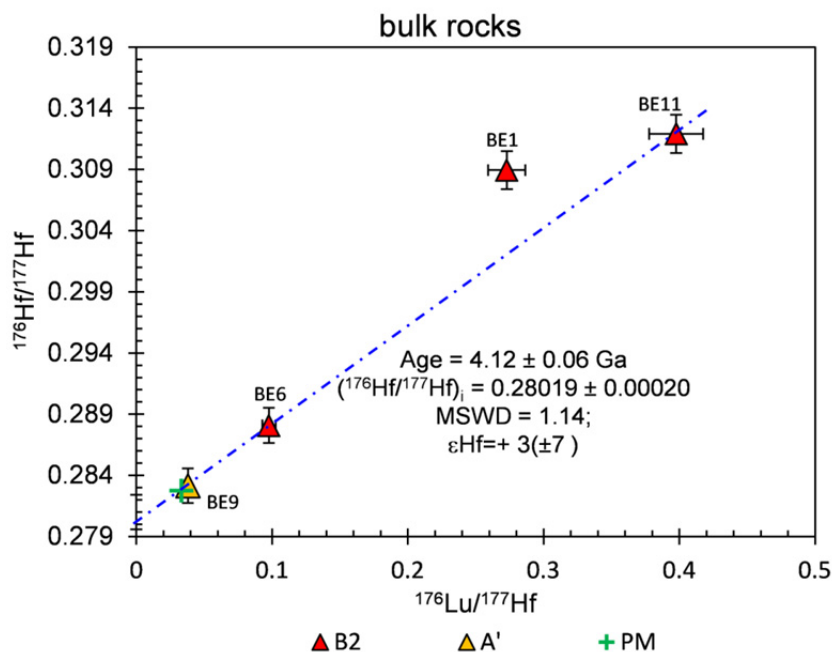


Fig. 23 Lu-Hf isochron diagram for calculated bulk rocks from group A' and B2 eclogites.

How reliable is then an age obtained from so few samples? The validity of such an age is increased, if the members of the isochron give an identical model age. This must be the case because otherwise the initial of the isochron is not that of the primitive mantle. We calculated model ages from the bulk rocks in the way as shown geometrically in Fig.24 with the results shown in Fig. 25. The group A' and the two B2 samples on the isochron give model ages around 4.1 Ga and the BE1 sample (which is off the isochron) gives a older than the earth age of 5.55 Ga. Sample BE11 (group B2) is the most convincing case for a meaningful and accurate model age. Its REE pattern is continuously depleted until Nd with no Hf anomaly which indicates that there was no Hf addition. Garnet and clinopyroxene have the same ϵ_{Hf} at the time of eruption (120 Ma) of around +1005 each and the bulk

rock has the same very radiogenic ϵ_{Hf} at 120 Ma. Such high values require a long-time evolution even with the relatively high $^{176}\text{Lu}/^{177}\text{Hf}$ of 0.398. Consequently, the Hf model age is 4.12 ± 0.29 Ga (Fig. 24b, 25a). Model ages from garnet alone are minimum ages but already this is 3.51 ± 0.06 Ga in this sample (Fig. 24b, 25b). The principles of how to judge the quality of a model calculation is shown schematically in Fig. 24a. Garnet and clinopyroxene are in isotopic equilibrium i.e. they and the bulk rock have identical isotope ratios since the origin of the protolith until the time of eruption (or when a closure temperature is reached – yellow circle in Fig. 24a). They then develop separately as shown as the yellow line for garnet and the green line for clinopyroxene. If the angle of intersect between the garnet resp. bulk rock evolution with the mantle evolution line is steep (large differences of the mother daughter and today's isotope ratios to the mantle) the error on the calculated model age is small. A test for an undisturbed development since the origin is the agreement or disagreement of the calculated isotope ratios of garnet and clinopyroxene at the time of the kimberlite eruption. High temperature from above the closure temperature samples like the A' and B2 samples (see discussion in next chapter) always show this. If, however, there was recent or subrecent contamination of the mineral phases by a metasomatic agent, or from the host kimberlite magma or if one mineral separate was not perfect, the isotope ratios will disagree. Everything is perfect for sample BE11 but not for samples BE6 and BE1. In sample BE6 clinopyroxene is disturbed which finds its expression in an artificially high 1.6 Ga two-point isochrone age. However, the contaminated cpx does not change the calculated bulk composition very much because garnet is dominant in this rock (80% Hf budget and more than 99% Lu budget are in garnet) and the cpx isotopic composition is not very different from garnet. The bulk composition would therefore still be part of the isochron. The garnet model age is 3.31 Ga, close to that of sample BE11. In sample BE1, which lies off the isochron, garnet is disturbed, indicated by younger than the eruption age two-point isochron (82 Ma). The garnet alone gives an old model age of 4.25 Ga and the bulk rock 5.55 Ga (Fig. 25a,b).

The group A' sample BE9 plots close to today's primitive mantle composition. The ϵ_{Hf} at 120 Ma is +13 in both garnet and cpx and the bulk rock is more radiogenic than the chondritic ratios at that time. This difference is probably due to the neglected presence of possible rutile in the calculation of the bulk Lu/Hf ratio. However the modal abundance of rutile will only be small and its effect on a calculated model age also small. The bulk rock model age of BE9 is 4.02 Ga (very similar to that of BE6 and BE11) but with a big uncertainty of ± 2.45 Ga since the $^{176}\text{Lu}/^{177}\text{Hf}$ ratio (0.0380) is very close to the primitive mantle value of 0.0332 (Fig. 24 c,d).

Despite the small number of samples we believe that the 4.12 Ga age is genuine and find geological support of this age. For the mantle, we find it only in a 4.1 Ga errorchron from eclogites from Newlands ((Menzie et al. 2003). But evidence for the existence of continental crust before 4.0 Ga is ubiquitous.

The oldest crustal zircon ages from the Barberton greenstone belt on the Kaapvaal craton is around 3.7 Ga (Kröner et al, 1996) and the Hf model ages with respect to a depleted mantle not quite reach 4 Ga. Zeh et al. (2012) report 4.08 ± 0.18 Ga Hf model ages for zircons from the 3.66 Ga with TTG gneisses in the Swaziland. U-Pb ages older than 4.0 Ga are known from Australia (Jack Hills; e.g.

Froude et al., 1983, Compston and Pidgeon, 1986.) and Canada (Acasta gneisses e.g. Bowring, et al., 1989, 1999.).

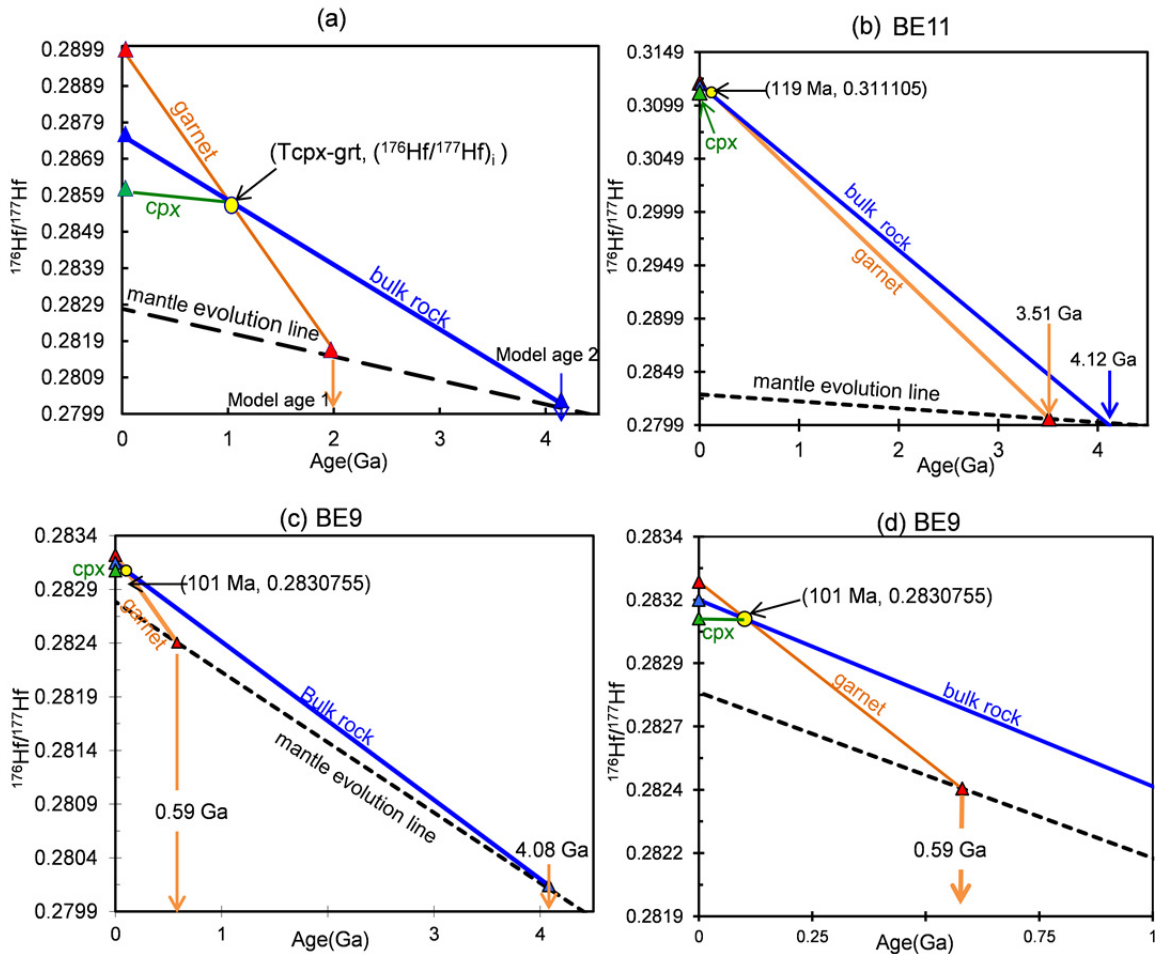


Fig.24 The Lu-Hf isotope evolution paths of eclogites with time. Diagram (a) shows the principle development of the Hf isotope ratios of a bulk rock (blue line), its garnet (yellow line), and its clinopyroxene (green line) and also the mantle evolution (dash line). Before eclogites reach the closure temperature of the Lu-Hf system, garnets and clinopyroxenes have the same $^{176}\text{Hf}/^{177}\text{Hf}$ ratios as the bulk rock. The closure ages can be derived from grt-cpx two point isochron ages. It may be a cooling age or the eruption age of the kimberlite. The yellow circle is the crossing point of of the three colored lines and represents the closure age t_{clos} . After t_{clos} , the Hf isotopes in garnets and clinopyroxenes develop according to the respective Lu/Hf ratios. The triangles at the age of zero in (a) are meant to be the measured $^{176}\text{Hf}/^{177}\text{Hf}$ ratios at t_0 for garnet and clinopyroxene, but the bulk rock $^{176}\text{Hf}/^{177}\text{Hf}$ value is calculated. In diagrams (b) and (c) show our actual measured isotope $^{176}\text{Hf}/^{177}\text{Hf}$ ratios of garnets and clinopyroxenes and calculated bulk rock based on their modal abundance. Diagram (a) shows results of sample BE11 and (b) shows results for sample BE9. The diagram (d) shows more detail information of diagram (c), from 1 Ga onwards in X axis and $^{176}\text{Hf}/^{177}\text{Hf}$ ratio of 0.28190 since. A Hf model age calculated from garnet alone is a minimum age (model age 1), while that of the bulk rock is the age of the protoliths (model age 2). Clinopyroxene alone generally will not intersect the mantle evolution line. If Hf is preferentially enriched in clinopyroxene, the calculated bulk rock Hf composition will be modified and yield a maximum age, commonly older than the earth. Garnet and bulk rock model give therefore the limiting values for the real age of an eclogite, resp. its protolith.

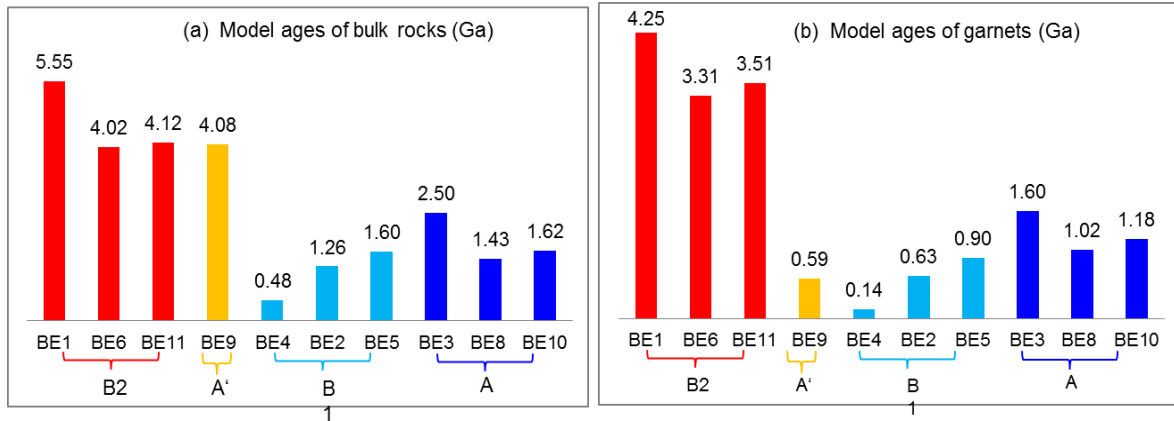


Fig.25 Model ages of bulk rocks (a) and model ages of garnets (b) Different groups present as bar with colors. The ages are noted on the top of the bars (in Ga). Sample names and group names are noted under the bars (group B2: red, group A': yellow, group B1: light blue, group B2: dark blue)

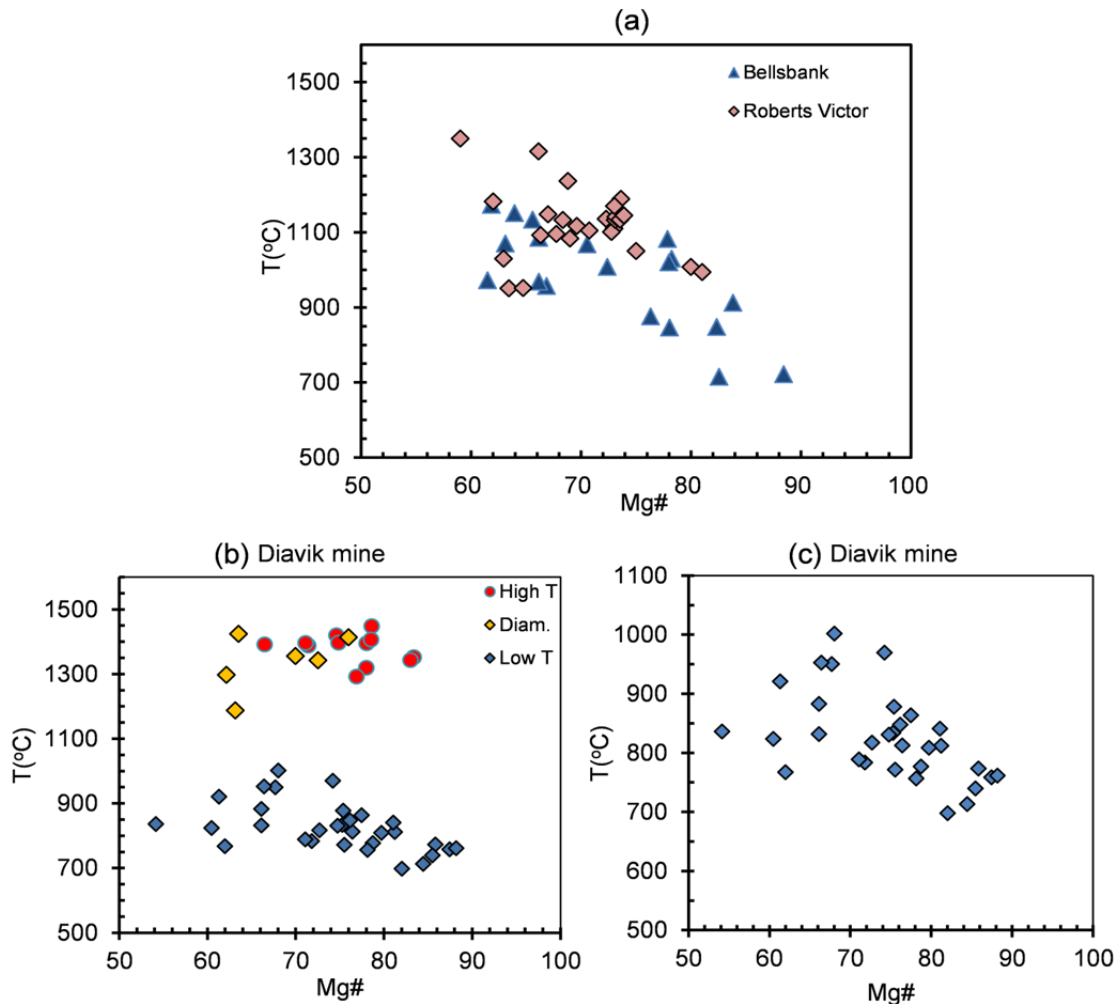


Fig. 26 a,b,c Correlation diagrams of Mg# with temperature for various eclogite localities. Diagram (a) shows the data for Bellsbank and Roberts Victor, diagram (b) all data from the Diavik mine, Slave craton of Schmidberger et al., (2007) and (c) only the lower temperature data. The eclogites show a negative correlation of the temperature of last equilibration with Mg#s from the Kaapvaal craton and the Slave craton.

6.2.2 Age of group A and B2 eclogites

The Hf isotopic compositions of group A and B1 are much more radiogenic than group A' and B1. The bulk ϵ_{Hf} varies from +13 to +9591 at 120 Ma. Strong negative HFSE anomalies indicate the potential presence of rutile in these rocks although it was not found. All samples have very young model ages from 0.48 to 2.50 Ga (Fig.25,a,b). They do not have any age meaning but are partly caused by the lack of information on rutile and also because the primitive mantle is not an appropriate reference for these with a complex petrologic history.

7. Summary, further aspects and thoughts

1. The Bellsbank kimberlites carried very different eclogitic lithologies as xenoliths to the Earth's surface. Four groups are distinguished based on their major, trace element and isotopic composition: High-CaO group B2 with flat HREE, low-MgO group B1 with highly fractionated HREE, group A' with highest-MgO and flat HREE and high-MgO group A with highly fractionated HREE.
2. Reconstructed bulk rock compositions of high-CaO group B2 and high-Mg group A' share many geochemical features with modern gabbroic rocks from mid oceanic ridge settings like Mg numbers, SiO₂, CaO, Al₂O₃ and Na₂O contents. Flat middle to heavy REE patterns, low REE contents and positive Eu anomalies of two group B2 eclogites are analogous to plagioclase-rich (cumulative) oceanic gabbros. One B2 eclogite has more elevated REE contents and may represent a melt composition. Group A' eclogites have close to primitive Mg numbers and also low and flat HREE patterns and may be former low -pressure Cpx- rich cumulates. The protoliths of groups A' and B2 are probably genetically linked in time and space.
3. Reconstructed high-MgO group A and low-MgO group B1 eclogites have similar trace-element patterns with remarkably steep positive slopes in their HREE patterns and extremely low and subchondritic Zr/Hf ratios. Subchondritic Zr/Hf ratios are features of magmas like boninites which are partial melting products of a previously depleted mantle. The difference of group A and B1 eclogites to Archean boninitic rock are the strongly fractionated REE patterns of the former and their very high HREE contents. This can be reconciled if these garnet pyroxenites were restites of partial melting of boninitic rocks after eclogitisation. The comparison in the major element compositions presented in Figs. 3 and 4 shows that groups A and B1 eclogites could be restites of partial melting of boninitic parental rocks in the generation of tonalitic melts.
4. The $\delta^{18}\text{O}$ values of the calculated bulk rocks vary from 2.63 to 4.95‰ which is lower than mantle value. Only one sample has 6.58‰ above the mantle. The low $\delta^{18}\text{O}$ values are explicable by low temperature seawater alteration of the precursor rocks and support a subduction origin of the Bellsbank eclogites studied here. A positive correlation between the

$\delta^{18}\text{O}$ and $(\text{Ce/Lu})_N$ ratios points to an increase of $\delta^{18}\text{O}$ concomitant with a metasomatic event especially since the most incompatible element enriched sample BE4 also has the highest $\delta^{18}\text{O}$.

5. All eclogites studied here can be related to basaltic and boninitic protoliths which were metamorphosed via subduction-like processes. The interesting and not easily explainable fact is that a) the group A and B1 garnet pyroxenites were derived from shallower depths but they are those, which we relate to boninitic precursors and which had experienced high degrees of partial melting, (Fig. 6) and b) the group A and B2 eclogites were derived from much greater depths but they are those which appeared to lost only a minimal melt fraction and are compositionally very similar to MORB lithologies. The compositional variation with depth (temperature) can be seen directly in Fig. 26 a, where Mg# is inversely correlated with temperature for Bellsbank but also Roberts Victor samples. It is also seen to a lesser extent for Diavik in Canada (Fig. 26 b,c) but not in Koidu (W-Africa; not shown here). A tentative explanation can be that partial melting of the eclogitic rocks occurred during the time of thermal relaxation of the subcratonic mantle after its assembly as a mixture of a hotter mantle into which cooler lithologies were subsucted. Partial melting occurred in the eclogitic lithologies because they melt at lower temperatures than surrounding peridotite (e.g. Yaxley and Green, 1998). Some of the partially molten eclogite portions may even uprise diapirically and eventually leave highly depleted restites at shallower depths. We may even go as far as postulating that the SCLM in the shallower part between the crust-mantle boundary and about 100 km consists of a much higher proportion of restitic eclogite than assumed so far. They could be the restites of partial melting in the generation of the ubiquitous TTG's found within the Archean crust. So instead of having eclogite within the Archean subcratonic mantle sinking into the deeper mantle or core-mantle boundary a substantial portion may remain neutrally buoyant within the above depth interval. Partial melting of eclogite makes the restite less dense and more similar to peridotite (Pertermann and Hirschmann, 2003). Their presence may not be picked up in seismic velocity profiles because of the size of the bodies. They are also not easily picked up in the xenolith or xenocryst inventory of the kimberlites because the sampling process seems to exempt this depth interval as is apparent from the depths of origin of most peridotite xenoliths suites.
6. This study presents the most extreme Hf and Nd isotopic ratios which were ever reported for silicate rocks with highest $\epsilon_{\text{Hf}} = +10452$ and highest $\epsilon_{\text{Nd}} = +540$. Because groups A and B2 samples have lost a large melt fraction in the garnet stability field, the Sm and Nd abundances are very low after partial melting. If such samples were subsequently reenriched their Sm and Nd abundances would stem mostly from the enrichment agent. An errorchron obtained from such samples gives an age of the $2.08 \pm 0.38\text{Ga}$ similar to the age of the Bushveld complex (2.06 Ga) and within the age range of the Kheis-Magondi belt. The metasomatic imprint onto the majority of the Bellsbank eclogites is very low and the Lu-Hf isotopic system seems not to

be affected by such a process. We therefore used the bulk rock Hf model ages and tried to constrain the age of formation of the protoliths from isochrons and model age calculations. Trace element abundances and patterns give information on genetic links and original rock compositions. From these considerations we find that groups A' and B are MORB-related, give a 4.12 Ga isochron age with an initial of a primitive mantle at that time and model ages of about 4.1 Ga. The two of their garnets also give reliable model ages of 3.51 and 3.31 Ga as minimum possible ages. The boninite-related eclogites A and B1 yield young to very young model ages including their garnets (Fig. 23). This may be partly due to the non-consideration of possible rutile but mostly reflects the complex genetic development of these rocks. The potential parental rocks to these garnet pyroxenites are boninites which are the products of an already depleted mantle. This mantle had already elevated Lu/Hf ratios (and developed higher $^{176}\text{Hf}/^{177}\text{Hf}$ ratios) before being partially molten again to generate the boninites. These continue to develop their $^{176}\text{Hf}/^{177}\text{Hf}$ ratios until being molten again in the eclogite stability field. A model age calculation will therefore always yield young ages when they are related to a primitive mantle.

Reference

- Allaz J., Maeder X., Vannay J.C., Steck A., 2005, Formation of aluminosilicate-bearing quartz veins in the Simano nappe (Central Alps): structural, thermobarometric and oxygen isotope constraints. *Schweizerische Mineralogische und Petrographische Mitteilungen* **85**, 191–214.
- Alterman W., Höllich I.W., 1991, Structural history of the southwestern corner of the Kaapvaal craton and the adjacent Namaqua realm: new observations and s reappraisal. *Precambrian Research* **52**, 133-166.
- Anhaeusser C.R., 2006, A reevaluation of Archean intracratonic terrane boundaries on the Kaapvaal Craton, South Africa: Collisional suture zones? *GSA Special Papers* **405**, 193-210.
- Armstrong R.A., Compston W., Retief, E.A., Williams I.S., and Welker H.J., 1990, Zircin ion microprobe bearing on the age and evolution of the Witwatersrand triad. *Precambrian Research* **53**, 243-266.
- Aulbach S., O'Reilly S.Y. and Pearson N.J., 2011, Constraints from eclogite and MARID xenoliths on origins of mantle Zr/Hf–Nb/Ta variability. *Contributions to Mineralogy and Petrology* **162**, 1047-1062.
- Aulbach S., Pearson N.J., O'Reilly S.Y. and Doyle BJ, 2007, Origins of xenolithic eclogites and pyroxenites from the central Slave Craton, Canada. *Journal of Petrology* **48**, 1843-1873.
- Aulbach S., Shirey S.B., Stachel T, Creighton S, Muehlenbachs K and Harris J.W., 2009, Multiple diamond formation episodes at the Kaapvaal craton margin: Re-Os of Jagersfontein sulfide inclusions. *Contributions to Mineralogy and Petrology* **127**, 525-540.
- Bach W., Alt J. C; Niu Y.L., Humphris S. E., Erzinger J. A. and Dick, Henry J.B., 2001, The geochemical consequences of late-stage low-grade alteration of lower ocean crust at the SW Indian Ridge: Results from ODP Hole 735B (Leg 176). *Geochimica Et Cosmochimica Acta* **65(19)**, 3267-3287.
- Barth M, Rudnick R.L, Horn I., McDonough W.F., Spicuzza M., Valley J.W. and Haggerty S.E., 2001, Geochemistry of xenolithic eclogites from West Africa, part I: a link between low MgO eclogites and Archean crust formation. *Geochimica Et Cosmochimica Acta* **65**,1499–1527.
- Barth M., Rudnick R.L., Horn .I, and McDonough W.F., Spicuzza M., Valley J.W. and Haggerty S.E., 2002, Geochemistry of xenolithic eclogites from West Africa, part II: origins of the high MgO eclogites. *Geochimica Et Cosmochimica Acta* **66**, 4325–4345.
- Beukes N.J., Smit C.A., 1987, New evidence for thrust faulting in Griqualand West South Africa: implications for stratigraphy and the age of red beds. *South African Journal of Geology* **90**, 378-387.
- Bennett S.L., Blundy J and Elliott T, 2004, The effect of sodium and titanium on crystal-melt partitioning of traceelements. *Geochimica Et Cosmochimica Acta* **68**, 2335–2347.
- Bizzarro M., Baker J.A., and Ulfbeck D., 2003, A new digestion and chemical separation technique for rapid and highly reproducible determination of Lu/Hf and Hf isotope ratios in geological materials by MC-ICPMS. *Geostandards Newsletter-the Journal of Geostandards and Geoanalysis* **27**, 133-145.
- Blichert-Toft J. and Albarede F.,1997, The Lu-Hf isotope geochemistry of chondrites and the evolution of the mantle-crust system. *Earth and Planetary Science Letters* **148**, 243-258.
- Bowring S.A., Williams I.S. and Compston W., 1989, 3.96 Ga gneisses from the Slave Province, Northwest Territories, Canada. *Geology* **17**, 971- 975
- Bowring S.A., Williams I.S. and Compston W., 1999, Priscoan (4.00±4.03 Ga) orthogneisses from northwestern Canada, *Contrib Mineral Petrol* **134**, 3-16.
- Caporuscio F.A. and SmythJ.R., 1990, Trace element crystal chemistry of mantle eclogites. *Contrib. Mineral. Petrol.* **105**, 550–561.
- Caro G., Bourdon B., Birck J.L. and Moorbath, S., 2006, High-precision ¹⁴²Nd/¹⁴⁴Nd measurements in terrestrial rocks: Constraints on the early differentiation of the Earth's mantle. *Geochimica Et Cosmochimica Acta* **70**, 164-191.
- Chu N.C., Taylor R.N., Chavagnac V., Nesbitt R.W., Boella R.M., Milton J.A., German C.R., Bayon G. and Burton K., 2002, Hf isotope ratio analysis using multi-collector inductively coupled plasma mass spectrometry: an evaluation of isobaric interference corrections. *Journal of Analytical Atomic Spectrometry* **17**, 1567-1574.

- Clement C.R., Dawson J.B., Geringer G.J., Gurney J.J., Hawthorne J.B., Krol L, Kleinjan L and Van Zyl A.A. ,1973, Guide for the Prst Peld excursion, First Int Kimberlite Conf.
- Cocker J.D., Griffin B.J. and Muehlenbachs K., 1982, Oxygen and carbon isotope evidence for sea-water–hydrothermal alteration of the Macquarie Island ophiolite Earth and Planetary Science Letters **61**, 112–122.
- Coleman R. G., Lrt D. E. Bnamv, L. B. and axo Bnalwoocr W. W.,1965, Eclogites and eclogites; their differences and similarities. Geol Soc. Ama. Bull **76**, 483-508.
- Compston W. and Pidgeon R.T., 1986, Jack Hills, a further occurrence of very old detrital zircons in Western Australia. Nature **321**, 766-769.
- Coplen, T. B. 1995, Discontinuance of SMOW and PDB. Nature **375**, 285.
- Mattey D., Lowry D. and Macpherson C.,1994, Oxygen isotope composition of mantle peridotite, Earth and Planetary Science Letters **128**, 231–241.
- de Wit, M.J., de Ronde, C.E.J., Tredoux, M., Roering, C., Hart, R.J., Armstrong, R.A., Green, R.W.E., Peberdy, E. and Hart, R.A., 1992, Formation of an Archaean continent. Nature **357**, 553-562.
- Deckart, K., Bertrand, H. and Liegeois, J.-P., 2005. Geochemistry and Sr, Nd, Pb isotopic composition of the Central Atlantic Magmatic Province (CAMP) in Guyana and Guinea. Lithos **82**, 289-314.
- DeWolf, C.P., Zeissler, C.J., Halliday, A.N., Mezger, K. and Essene, E.J., 1996, The role of inclusions in U-Pb and Sm-Nd garnet geochronology: Stepwise dissolution experiments and trace uranium mapping by fission track analysis. Geochimica Et Cosmochimica Acta **60**, 121-134.
- Eggins S.M., Woodhead J.D., Kinsley L.P.J., Mortimer G.E., Sylvester P., McCulloch M.T., Hergt J.M. and Handler M.R., 1997, A simple method for the precise determination of >40 trace elements in geological sample by ICPMS using enriched isotope internal standardization. Chemical Geology **134**, 311-326.
- Eglington, B.M. and Armstrong, R.A., 2004, The Kaapvaal Craton and adjacent orogens, southern Africa: a geochronological database and overview of the geological development of the craton S. Afr. J. Geol., **107**, 13-32.
- Ehrlich, S., Gavrieli, I., Dor, L.B. and Halicz, L., 2001, Direct high-precision measurements of the $^{87}\text{Sr}/^{86}\text{Sr}$ isotope ratio in natural water, carbonates and related materials by multiple collector inductively coupled plasma mass spectrometry (MC-ICP-MS). Journal of Analytical Atomic Spectrometry **16**, 1389–1392.
- Eiler M., 2001, Oxygen isotope variations of basaltic lavas and upper mantle rocks. in: J.W. Valley, D.R. Cole (Eds.), Stable Isotope Geochemistry, Reviews in Mineralogy and Geochemistry **43**, pp. 319– 364.
- Erzinger J., 1989, chemical alteration of oceanic crust. Geol. Rundsch **78**, 731–740.
- Froude D.O., Ireland T.R., Kinny P.D., Williams I.S., Compston W., Williams I.R. and Myers J.S. ,1983, Ion microprobe identification of 4,100±4,200 Myr-old terrestrial zircons. Nature, **304**, 616-618.
- Garden, P.B., Carlson, W.R., Shirey B.S. and Gurney J.J., 2003, Re-Os systematics of lithospheric peridotites and eclogites from the Bobbejaan and Bellsbank Dykes, Kaapvaal Craton. 8th International Kimberlite Conference.
- Green, T.H., Blundy, J.D., Adam, J. and Yaxley, G.M., 2000, SIMS determination of trace element partition coefficients between garnet, clinopyroxene and hydrous basaltic liquids at 2–7.5 GPa and 1080–1200 degrees C. Lithos **53(3–4)**, 165–187.
- Gonzaga R.G., Menzaies M.A., Thirlwall M. F. Jacob D. E. and Leroex A., 2010, Eclogites and Garnet Pyroxenites: Problems Resolving Provenance Using Lu-Hf, Sm-Nd and Rb-Sr Isotope Systems, Journal of Petrology, **51**, 513-535.
- Gregory R.T. and Taylor H.P. ,1981, An oxygen isotope profile in a section of the Cretaceous oceanic crust, Samail ophiolite, Oman: evidence for $\gamma^{18}\text{O}$ buffering of the oceans by deep (N5 km) seawater–hydrothermal circulation at mid-ocean ridges, J. Geophys. Res. **86**, 2737–2755.
- Griffin, W.L. and O'Reilly, S.Y., 2007, Cratonic lithospheric mantle: is anything subducted ? Episodes **30 (1)**, 43–53.
- Harris, J.W. and Gurney J.J., 1979, Inclusions in diamond. The properties of diamond, ed. J.E. Field, pp. 555-591, Academic Press, London.
- Hart S.R., Blusztajn J, Dick H.J.B., Meyer P.S. and Muehlenbachs K, 1999, The fingerprint of seawater circulation in a 500-meter section of ocean crust gabbros. Geochimica Et Cosmochimica Acta **63**, 4059–4080.

- Harte, B. and Kirkley, M. B., 1997, Partitioning of trace elements between clinopyroxene and garnet: Data from mantle eclogites. *Chemical Geology* **136**, 1-24.
- Hartnady, C.J.H., Joubert, P., Stowe, C.W., 1985, Proterozoic crustal evolution in southern Africa. *Episodes* **8**, 236-244.
- Hatton, C.J. and Gurney, J.J. 1987, Roberts Victor eclogites and their relation to the mantle. In: Nixon, P.H. (Ed.), *Mantle Xenoliths*. Wiley, London, pp. 453– 463.
- Heaman, L.M., Creaser, R.A., Cookenboo, H.O. and Chacko, T., 2006, Multi-stage modification of the Northern Slave mantle lithosphere: evidence from zircon- and diamond-bearing eclogite xenoliths entrained in Jericho kimberlite, Canada. *Journal of Petrology* **47**, 821–858.
- Huang J.X., Gréau Y., Griffin, W.L., O'Reilly, S.Y. and Pearson N. J., 2012, Multi-stage origin of Roberts Victor eclogites: Progressive metasomatism and its isotopic effects. *Lithos* **142–143**, 161–181.
- Humphris S.E., Alt J.A., Teagle A.H. and Honnorez J.J., 1998, Geochemical changes during hydrothermal alteration of basement in the stckwork beneath the active TAG hydrothermal mound. In *Proceedings of the ocean Drilling Program Scientific Results* (eds. P.M. Herzig, S.E. Humphris, D.J. Miller, and R.A. Zierenberg) **158**, 255-276.
- Ionov, D.A. and Weiss, D., 2002, Hf isotope composition of mantle peridotites: first results and inferences for the age and evolution of the lithospheric mantle. Abstract, 4th Int. Workshop on Orogenic Lherzolites and Mantle Processes, Samani, Japan, pp. 56-57.
- Jacob, D., Jagoutz, E., Lowry, D., Matthey, D., Kudrjavitseva, G., 1994, Diamondiferous eclogites from Siberia: remnants of Archean oceanic crust. *Geochimica Et Cosmochimica Acta* **58**, 5191– 5207.
- Jacob, D.E., Bizimis, M. and Salters, V.J.M., 2005, Lu/Hf and geochemical systematics of recycled ancient oceanic crust: evidence from Roberts Victor eclogites. *Contributions to Mineralogy and Petrology* **148 (6)**, 707–720.
- Jacob, D.E., Viljoen, K.S. and Grassineau, N.V., 2009, Eclogite xenoliths from Kimberley, South Africa - a case study of mantle metasomatism in eclogites. *Lithos* **112 (Suppl. 2)**, 1002–1013.
- Jacobs J, Pisarevsky S, Thomas RJ and Becker T, 2008, The Kalahari Craton during the assembly and dispersal of Rodinia. *Precambrian Research* **160**, 142–158.
- Jagoutz, E., Dawson, J.B., Hoernes, S., Spettel, B. and Wanke, H., 1984, Anorthositic oceanic crust in the Archean Earth. 15th Lunar Planet. Sci. Conf., pp. 395–396. Abs.
- Kerrick R, Wyman D, Fan J, Bleeker W., 1998, Boninite series: low-Ti tholeiite associations from the 2.7 Ga Abitibi greenstone belt. *Earth and Planetary Science Letters* **164**, 303–316.
- Klemme S., Blundy J. D., and Wood B. J., 2002, Experimental constraints on major and trace element partitioning during partial melting of eclogite. *Geochimica Et Cosmochimica Acta* **66**, 3109–3123.
- Kramers, J.D., 1979, Lead, uranium, strontium, potassium and rubidium in inclusion-bearing diamonds and mantle-derived xenoliths from Southern Africa. *Earth and Planetary Science Letters* **42**, 58–70.
- Kröner, A., Hegner, E., Wendt, J.I. and Byerly, G.R., 1996, The oldest part of the Barberton granulite-greenstone terrain, South Africa: evidence for 1213 crust formation at 3.5 and 3.7 Ga. *Precambrian Research* **1214** **78**, 105–124.
- Kusakabe M., Maruyama S., Nakamura T. and Yada T., 2004, CO₂ laser-BR_F₅ fluorination technique for analysis of three oxygen isotopes of rocks and minerals. *J. Mass Spectrom. Soc. Jpn.* **52**, 205–212.
- Lazarov, M., Brey, G.P. and Weyer, S., 2009, Time steps of depletion and enrichment in the Kaapvaal craton as recorded by subcalcic garnets from Finsch (SA). *Earth and Planetary Science Letters*, **279 (1-2)**, 1-10.
- Maboko, M.A.H. and Nakamura, E., 1995, Sm-Nd garnet ages from the Uluguru granulite complex of Eastern Tanzania: further evidence for post-metamorphic slow cooling in the Mozambique belt. *Precambrian Research* **74 (4)**, 195-202.
- MacGregor I.D. and Manton W.I., 1986, Roberts Victor eclogites: ancient oceanic crust. *J. Geophys. Res.* **91(B14)**, 14063-14079.
- Maier D.W., Arndt T.N., and Curl A.E., 2000, progressive crustal of the Bushveld Complex: Evidence from Nd isotopic analyses of the cumulate rocks. *Contrib Mineral Petrol* **140**, 312-327.
- Magaritz M and Taylor H.P., 1974, Oxygen and hydrogen isotope studies of serpentinization in Troodos Ophiolite complex, Cyprus, *Earth and Planetary Science Letters* **23**, 8-14.
- McDonough, W.F. and Sun, S.S., 1995, The composition of the Earth. *Chemical Geology* **120**, 223-253.

- Menzies, A.H., Carlson, R.W., Shirey, S.B., and Gurney, J.J., 1999, Re-Os systematics of Newlands peridotites xenoliths: implications for diamond and lithosphere formation. In: J.J. Gurney, J. L. G., M.D. Pascoe and S.H. Richardson, eds., Proceedings of the 7th International Kimberlite Conference, Red Roof Design, Cape Town, 566-573.
- Menzies A.H., Carlson R.W., Shirey, S.B. and Gurney, J.J., 2003, Re-Os systematics of diamond-bearing eclogites from the Newlands kimberlite. *Lithos* **71**, 323– 336.
- Münker, C., Weyer, S., Scherer, E. and Mezger, K., 2001, Separation of high field strength elements (Nb, Ta, Zr, Hf) and Lu from rock samples for MC-ICPMS measurements. G-cubed, 2, paper number 01GC000183.
- Neal C. R., Taylor A. L., Davidson P. J., Holden P., Halliday N. A., Nixon H. P., Paces B. J., Clayton R. N., and Mayeda K. T., 1990, Eclogites with oceanic crustal and mantle signatures from the Bellsbank kimberlite, South Africa, part 2: Sr, Nd, and O isotope geochemistry. *Earth and Planetary Science Letters* **99**, 362-379.
- Nikogosian, I. K. and Sobolev, A.V., 1997, Ion-microprobe analysis of melt inclusions in olivine: experience in estimating the olivine-melt partition coefficients of trace elements. *Geochemistry International* **35**, 119-126.
- O'Hara, M., 1969, The origin of eclogite and arie'gite nodules in basalt. *Geol. Mag.* **106**, 322– 330.
- O'Hara, M.J., Saunders, M.J. and Mercy, E.L.P., 1975, Garnet– peridotite, primary ultrabasic magma and eclogite; interpretation of upper mantle processes in kimberlite. *Phys. Chem. Earth* **9**, 571–604 (First international conference on kimberlites).
- O'Hara, M.J. and Yoder, H.S., 1967, Formation and fractionation of basic magmas at high pressure. *Scott. J. Geol.* **3**, 67–117.
- Pearson D. G. Davies G. R. and Nixon P. H., 1993, Geochemical Constraints on the Petrogenesis of Diamond Fades Pyroxenites from the Beni Bousera Peridotite Massif, North Morocco, *Journal of Petrology* **34**, 125-172.
- Pearce, N.J.G., Perkins, W.T., Westgate, J.A., Gorton, M.P., Jackson, S.E., Neal, C.R., Chenery, S.P., 1997, A compilation of new and published major and trace element data for the NIST SRM 610 and NIST SRM 612 glass reference materials. *Geostandards Newsletter* **21**, 115-144.
- Pearson, D.G. and Nowell, G.M., 2004. Re-Os and Lu-Hf Isotope Constraints on the Origin and Age of Pyroxenites from the Beni Bousera Peridotite Massif: Implications for Mixed Peridotite-Pyroxenite Mantle Sources. *Journal of Petrology* **45**, 439-455.
- Pearson, D.G., Shirey, S.B., Bulanova, G.P., Carlson, R.W. and Milledge, H.J., 1999, Re–Os isotope measurements of single sulfide inclusions in a Siberian diamond and its nitrogen aggregation systematics. *Geochimica Et Cosmochimica Acta* **63**, 703–711.
- Pearson, D.G., Shirey, S.B., Harris, J.W. and Carlson, R.W., 1998, A Re–Os isotope study of sulfide diamond inclusions from the Koffiefontein kimberlite, S. Africa: constraints on diamond crystallization ages and mantle Re–Os systematics. *Earth and Planetary Science Letters* **160**, 311-326.
- Pearson, D.G., Snyder, G.A., Shirey, S.B., Taylor, L.A., Carlson, R.W. and Sobolev, N.V., 1995, Archaean Re–Os age for Siberian eclogites and constraints on Archaean tectonics. *Nature* **374**, 711-713.
- Pertermann M. and Hirschmann M.M., 2003, Anhydrous partial melting experiments on MORB-like eclogite: Phase relations, phase compositions and mineral- melt partitioning of major elements at 2-3 Gpa. *Journal of Petrology* **44**, 2173-2201.
- Pin, C. and Zalduegui, J.F.S., 1997. Sequential separation of light rare-earth elements, thorium and uranium by miniaturized extraction chromatography: Application to isotopic analyses of silicate rocks. *Analytica Chimica Acta* **339**, 79-89.
- Polat A, Hofmann AW, Rosing M, 2002, Boninite-like volcanic rocks in the 3.7–3.8 Ga Isua greenstone belt, West Greenland: geochemical evidence for intra-oceanic subduction zone processes in the early earth. *Chemical Geology* **184**, 231–254.
- Polat, A. and Hofmann, A. W., 2003, Alteration and geochemical patterns in the 3.7–3.8 Ga Isua greenstone belt, West Greenland. *Precambrian Research* **126**, 197–218.
- Pollack, H. and Chapman, D., 1977, On the regional variation of heat flow, geotherms, and lithospheric thicknesses. *Tectonophysics* **38**, 279– 296.

- Presnall, D. C., Gudfinnsson, G. H. and Walter, M. J., 2002, .Generation of mid-ocean ridge basalts at pressures from 1 to 7 GPa. *Geochimica Et Cosmochimica Acta* **66**, 2073-090.
- Raczek I., Stoll B., Hofmann A.W. and Jochum K.P., 2001, High-precision trace element data for the USGS reference materials BCR-1, BCR-2, BHVO-1, BHVO-2,nAGV-1, AGV-2, DTS-1, DTS-2, GSP-1 and GSP-2 by ID-TIMS and MIC-SSMS. *Geostandards Newsletter: The Journal of Geostandards and Geoanalysis*, **25**, 77-86.
- Raczek, I., Jochum, K.and Hofmann, A., 2003. Neodymium and strontium isotope data for USGS reference materials BCR-1, BCR-2, BHVO-1, BHVO-2, AGV-1, AGV-2F GSP-1,GSP-2 and eight MPI-DING reference glasses. *Geostandards Newsletter—the Journal of Geostandards and Geoanalysis* **27 (2)**, 173–179.
- Rapp, R.P. and Watson, E.B., 1995, Dehydration melting of metabasalt at 8-32 kbar. Implications for continental growth and crust – mantle recycling. *Journal of Petrology* **36**, 891– 931.
- Richardson, S.H., Shirey, S.B., Harris, J.W.and Carlson, R.W., 2001. Archean subduction recorded by Re–Os isotopes in eclogitic sulfide inclusions in Kimberley diamonds. *Earth and Planetary Science Letters* **191**, 257–266.
- Rudnick, R.L., Eldridge, C.S. and Bulanova, G.P., 1993, Diamond growth history from in situ measurement of Pb and S isotopic compositions of sulphide inclusions. *Geology* **21**, 13–16.
- Rumble D. III and Hoering T. C, 1994, Analysis of oxygen and sulfur isotope ratios in oxide and sulfide minerals by spot heating with a carbon dioxide laser in a fluorine atmosphere. *Acc. Chem. Res.* **27**, 237–241.
- Schmickler, B., Jacob, D.E.and Foley, S.F., 2004, Eclogite xenoliths fromthe Kuruman kimberlites, South Africa: geochemical fingerprinting of deep subduction and cumulate processes. *Lithos* **75 (1–2)**, 173–207.
- Schmidberger S. S., Simonetti A. , Heaman M. L., Creaser A. R. and Whiteford S., 2007, Lu–Hf, in-situ Sr and Pb isotope and trace element systematics formantle eclogites from the Diavik diamond mine: Evidence forPaleoproterozoic subduction beneath the Slave craton, Canada, *Earth and Planetary Science Letters*, **254**, 55–68.
- Schmidberger, S.S., Simonetti, A., Francis, D. and Gariepy, C., 2002, Probing Archean lithosphere using the Lu–Hf isotope systematics of peridotite xenoliths from Somerset Island kimberlites, Canada. *Earth and Planetary Science Letters* **197**, 245-259.
- Schmitz, M.D., Bowring, S.A., de Wit, M.J.and Gartz, V., 2004, Subduction and terrane collision stabilize the western Kaapvaal craton tectosphere 2.9 billion years ago. *Earth and Planetary Science Letters* **222**, 363-376.
- Schoene, B., Dudas, F.O.L., Bowring, S.A. and de Wit, M. 2009, Sm–Nd isotopic mapping of lithospheric growth and stabilization in the easternKaapvaal craton. *Terra Nova* **21**, 219–228.
- Schulze, D.J., 1989. Constraints on the abundance of eclogite in the upper mantle. *J. Geophys. Res.* **94(B4)**, 4205–4212.
- Schulze, D.J., Valley, J.W.and Spicuzza, M., 2000, Coesite ecologies from the Roberts Victor kimberlite, South Africa. *Lithos* **54**, 23– 32.
- Sharp Z. D., 1990, A laser-based microanalytical method for the in situ determination of oxygen isotope ratios of silicates and oxides. *Geochimica Et Cosmochimica Acta* **54**, 1353–1357.
- Shervais J.W., Taylor L.A., G. Lugmair, R.N. Clayton, T.K. Mayeda and R. Korotev.,1988, Archean oceanic crust and the evolution of sub-continental mantle: Eclogites from southern Africa, southern Africa. *Geological Society of America Bulletin* **100**, 411-423.
- Shirey S.B., Richardson S.H.and Harris J.W., 2008, Mesoarchean to Mesoproterozoic Re–Os ages for sulfide inclusions in Orapa diamonds and implications for Kaapvaal-Zimbabwe craton development. In: Extended abstract of 9th international Kimberlite conference, A-0036.
- Smart, K.A., Heaman L. M., Chacko T. , Simonetti A., Kopylova M., Mah D., and Daniels D., 2009. The origin of high-MgO diamond eclogites from the Jericho Kimberlite, Canada. *Earth and Planetary Science Letters* **284(3–4)**, 527–537.
- Smit K.V, ShireyS.B., Richardson S.H. and Gurney J.J., 2010, Re–Os isotopic composition of peridotitic sulphide inclusionsin diamonds from Ellendale, Australia: Age constraints onKimberley cratonic lithosphere. *Geochimica Et Cosmochimica Acta* **74**, 3292–3306.

- Smith CB, 1983, Pb,Sr,Nd isotopic evidence for source of Southern Africa Cretaceous kimberlites. *Nature* **304**,51-54.
- Smith CB, Allsopp H.L., Kramers J.D., Hutchinson G. and Roddick J.C., 1985, Emplacement ages of Jurassic-Cretaceous South African kimberlites by the Rb-Sr method on phlogopite and whole-rock samples. *Trans Geol Soc S Afr.* **88**, 249-266.
- Smith C.B., Allsopp H.L., Kramers J.D., Hutchinson G. and Roddick, J.C., 1985, Emplacement ages of Jurassic-Cretaceous South African kimberlites by the Rb\Sr method on phlogopite and whole-rock samples. *Transactions of the Geological Society of South Africa* **88**, 249-266
- Smithies, R. H., Champion, D. C. and Sun, S.S., 2004, The case of Archaean boninites. *Contrib. Mineral. Petrol.* **147**, 705-721.
- Snyder, G.A., Jerde, E.A., Taylor, L.A., Halliday, A.N., Sobolev, V.N. and Sobolev, N.V., 1993, Nd and Sr isotopes from diamondiferous eclogites, Udachnaya kimberlite pipe, Yakutia, Siberia: evidence of differentiation in the early Earth? *Earth and Planetary Science Letters* **118**, 91-100
- Staudigel H., Davies G.R., Hart S.R. K.M. Marchant and Smith B.M.,1995, Large-scale isotopic Sr, Nd and O isotopic anatomy of altered oceanic crust—DSDP/ODP sites 417/418, *Earth and Planetary Science Letters* **130**, 169-185.
- Sun, S.S., McDonough, W.F., 1989, Chemical and isotopic systematics of oceanic basalts: implications for mantle composition and processes. In: Saunders, A.D., Norry, M.J. (eds.). *Magmatism in the Ocean Basins*. Oxford (United Kingdom), Blackwell Scientific Publications, Geological Society, **42** (Special Publications), 313-345.
- Tappe S., Smart A. K., Pearson D. G., Steenfelt A. and Simonetti An., 2011, Craton formation in Late Archean subduction zones revealed by first Greenland. *Geology* **39**,1103-1106.
- Tatsumi, Y., 1986. Formation of the volcanic front in subduction zones. *Geophysical Research Letters* **13**, 717-720.
- Taura, H., Yurimoto, H., Kurita, K. and Sueno, S.,1998, Pressure dependence on partition coefficients for trace elements between olivine and the coexisting melts. *Physics and Chemistry of Minerals* **25**, 469-484
- Taylor L.A. and Neal C.R., 1989, Eclogites with oceanic crustal and mantle signatures from the Bellsbank kimberlite, South Africa, Part 1: Mineralogy, petrography, and whole-rock chemistry, *J. Geol.* **97**, 551-567.
- Thirlwall, M.F., 1991, High precision multicollector isotope analysis of low levels of Nd as oxide. *Chemical Geology* **94**, 13-22.
- Thomas, R.J., von Veh, M.W. and McCourt, S., 1993, The tectonic evolution of southern Africa: an overview. *Journal of African Earth Sciences* **16**, 5-24.
- Valley J.W. Kitchen, N., Kohn M.J., Niendorf C.R and Spicuzza M.J., 1995, UWG-2, a garnet standard for oxygen isotope ratios: strategies for high precision and accuracy with laser heating, *Geochimica Et Cosmochimica Acta* **59**, 5223-5231.
- Viljoen K.S.,1995, Graphite- and diamond-bearing eclogite xenoliths from the Bellsbank kimberlites, Northern Cape, South Africa. *Contrib Mineral Petrol* **121**, 414- 423.
- Walraven, F., Armstrong, R.A., Kruger, K.J., 1990, A chronostratigraphic framework for the north central Kaapvaal Craton, the Bushveld Complex and the Vredefort Structure. *Tectonophysics* **171**, 23-48.
- Waight, T., Baker, J and Willigers, B.,2002. Rb isotope dilution analyses by MC-ICPMS using Zr to correct for mass fractionation: towards improved Rb-Sr geochronology? *Chemical Geology* **186**, 99-116.
- Wang Z.R., Bucholz C., Skinner B. , Shimizu N and Eiler J., 2011, Oxygen isotope constraints on the origin of high-Cr garnets from kimberlites. *Earth and Planetary Science Letters* **312**,337-347.
- Westerlund, K.J., Shirey, S.B., Richardson, S.H., Carlson, R.W., Gurney, J.J. and Harris, J.W., 2006, A subduction wedge origin for Paleoarchean peridotitic diamonds and harzburgites from the Panda kimberlite, Slave craton, evidence from Re-Os isotope systematics. *Contrib. Mineral. Petrol.* **152**, 275-294.
- Wittig, N., Baker, J.A., and Downes, H., 2007, U-Th-Pb and Lu-Hf isotopic constraints on the evolution of subcontinental lithospheric mantle, French Massif Central. *Geochimica Et Cosmochimica Acta* **71**, 1290-1311.
- Yaxley G: and Green D.H.,1998, Reactions between eclogites and peridotites:mantle refertilisation by subduction of oceanic crust. *Schweiz. mineral. Petrogr. Mitt.* **78**, 243-255.

Zeh A., Gerdes A. and Millonig L., 2011, Hafnium isotope record of the Ancient Gneiss Complex, Swaziland, southern Africa: evidence for Archaean crust–mantle formation and crust reworking between 3.66 and 2.73 Ga, *Journal of the Geological Society* **168**, 953–963.

Appendix

Tables A.1: Major element compositions and cation values in garnet and cpx of eclogites

Table A.1a: garnets

Table A.1b: cpx

Table A.1c: reconstructed bulk rocks

Table A.1a: Major and minor element compositions (**Table A.1a-1**) and structural formulae (**Table A.1a-2**) of garnets from eclogites from Bellsbank mine, obtained by EPMA. Values are in wt%. Three to five measurements were performed on each garnet depending on sample size. Relative errors are 1-2% for major elements. Since the variation of the data of each element on individual sample is always smaller than the relative errors. Only averages are shown here.

Table A.1a-1 Major-element compositions (wt%) and end-members (mol. prop.) of Bellsbank eclogitic garnets																		
group	sample	SiO ₂	Na ₂ O	K ₂ O	CaO	MnO	MgO	Cr ₂ O ₃	FeO ^{total}	Al ₂ O ₃	TiO ₂	P ₂ O ₅	NiO	Total	Mg#	Gross%	Pyr%	Alm%
B2	BE1	41.20	0.08	0.01	17.29	0.17	9.10	0.06	10.74	22.78	0.16	0.01	0.04	101.63	60	45	33	22
	BE6	41.81	0.06	0.00	12.14	0.18	11.98	0.25	12.63	22.94	0.15	0.02	0.02	102.06	63	31	43	25
	BE11	40.65	0.07	0.00	17.66	0.22	8.62	0.04	11.18	22.02	0.15	0.02	0.02	100.63	58	46	31	23
B1	BE2	41.03	0.03	0.50	8.74	0.42	11.69	0.06	17.09	22.70	0.08	0.01	0.00	101.85	55	23	42	35
	BE4	41.10	0.13	0.00	5.93	0.48	12.63	0.09	19.18	22.29	0.41	0.05	0.02	102.29	54	15	46	39
	BE5	41.57	0.04	0.00	9.19	0.40	12.86	0.10	14.96	22.71	0.13	0.01	0.01	101.96	61	24	46	30
A	BE3	42.69	0.02	0.01	7.47	0.29	17.88	0.23	9.56	23.63	0.03	0.01	0.00	101.80	77	19	62	19
	BE8	41.20	0.04	0.00	9.30	0.44	14.57	0.11	12.01	22.86	0.07	0.01	0.01	100.61	80	12	71	17
	BE10	41.80	0.03	0.01	7.85	0.42	15.95	0.18	11.59	22.63	0.06	0.01	0.00	100.53	71	20	57	23
A'	BE7	42.80	0.07	0.00	4.66	0.37	20.55	0.20	9.01	23.14	0.25	0.01	0.00	101.04	68	24	52	24
A'	BE9	42.31	0.04	0.01	4.43	0.49	18.44	0.22	12.20	22.67	0.13	0.07	0.03	101.03	73	11	65	24

Table A.1a-2 Cations of Bellsbank eclogitic garnets															
group	sample	Si	Na	K	Ca	Mn	Mg	Cr	Fe	Al	Ti	P	Ni	Total	
B2	BE1	3.01	0.01	0.00	1.35	0.01	0.99	0.00	0.66	1.96	0.01	0.00	0.00	8.01	
	BE6	3.01	0.01	0.00	0.94	0.01	1.29	0.01	0.76	1.95	0.01	0.00	0.00	8.00	
	BE11	3.01	0.01	0.00	1.40	0.01	0.95	0.00	0.69	1.92	0.01	0.00	0.00	8.02	
B1	BE2	3.00	0.00	0.00	0.69	0.03	1.28	0.00	1.05	1.96	0.00	0.00	0.00	8.01	
	BE4	3.00	0.02	0.00	0.46	0.03	1.38	0.01	1.17	1.92	0.02	0.00	0.00	8.02	
	BE5	3.01	0.01	0.000	0.71	0.02	1.39	0.01	0.91	1.94	0.01	0.00	0.00	8.01	
A	BE3	3.01	0.00	0.00	0.56	0.02	1.88	0.01	0.56	1.96	0.00	0.00	0.00	8.01	
	BE8	3.01	0.01	0.00	0.35	0.02	2.15	0.01	0.53	1.92	0.01	0.00	0.00	8.02	
	BE10	3.02	0.00	0.00	0.61	0.03	1.72	0.01	0.70	1.93	0.00	0.00	0.00	8.01	
A'	BE7	2.99	0.01	0.00	0.72	0.03	1.58	0.01	0.73	1.96	0.00	0.00	0.00	8.02	
A'	BE9	3.02	0.01	0.00	0.34	0.03	1.96	0.01	0.73	1.91	0.01	0.00	0.00	8.01	

Chapter 4: The origin of eclogites and garnet pyroxenites...

Table A.1b: Major and minor element compositions (**Table A.1b-1**) and structural formulae (**Table A.1b-2**) of cpx from eclogites from Bellsbank mine, obtained by EPMA. Values are in wt%. Three to five measurements were performed on each garnet depending on sample size. Relative errors are 1-2% for major elements. Since the variation of the data of each element on individual sample is always smaller than the relative errors, only averages are shown here.

Table A.1b-1 Major-element compositions (wt%) and end-members (mol. prop.) of Bellsbank eclogitic clinopyroxenes																				
group	sample	SiO ₂	Na ₂ O	K ₂ O	CaO	MnO	MgO	Cr ₂ O ₃	FeO ^{total}	Al ₂ O ₃	TiO ₂	P ₂ O ₅	NiO	Total	Mg#	Jd%	Wo%	Hy%	Al ^{IV}	Al ^{VI}
B2	BE1	56.56	9.01	0.01	10.18	0.00	5.98	0.06	1.42	16.93	0.19	0.00	0.17	100.51	88	63	19	18	0.04	0.65
	BE6	56.86	8.24	0.00	11.53	0.01	7.22	0.34	1.70	14.53	0.21	0.02	0.21	100.85	88	57	22	21	0.03	0.57
	BE11	55.93	9.17	0.00	9.88	0.01	5.85	0.04	1.57	17.16	0.14	0.00	0.09	99.84	87	64	19	18	0.05	0.66
B1	BE2	55.79	3.87	0.02	18.41	0.05	12.02	0.08	4.00	6.14	0.13	0.01	0.09	100.59	84	26	35	38	0.00	0.26
	BE4	55.73	4.47	0.03	15.99	0.07	11.40	0.07	6.01	6.32	0.50	0.02	0.03	100.62	77	29	31	40	0.00	0.27
	BE5	55.86	3.89	0.00	18.41	0.06	12.11	0.09	3.73	6.20	0.16	0.01	0.09	100.59	85	27	35	38	0.00	0.26
A	BE3	55.67	2.52	0.01	21.19	0.02	14.77	0.19	1.68	4.48	0.04	0.02	0.08	100.65	94	18	40	42	0.01	0.17
	BE8	55.15	2.43	0.00	21.12	0.05	14.74	0.11	2.33	4.18	0.12	0.01	0.07	100.30	92	16	41	43	0.02	0.16
	BE10	55.38	2.39	0.01	21.32	0.03	14.98	0.17	2.26	4.03	0.14	0.01	0.09	100.79	92	16	41	43	0.02	0.15
A'	BE7	55.46	2.48	0.02	19.34	0.09	16.04	0.28	2.72	3.53	0.21	0.02	0.05	100.23	91	16	37	47	0.01	0.14
A'	BE9	55.52	1.67	0.01	21.21	0.10	16.15	0.12	3.56	2.19	0.14	0.01	0.06	100.72	89	10	41	49	0.00	0.09

Jd: jadeite; Wo: Wollastonite Hy: Hypersthene

Table A.1b-2 Cations of Bellsbank eclogitic clinopyroxenes														
group	sample	Si	Na	K	Ca	Mn	Mg	Cr	Fe	Al	Ti	P	Ni	Total
B2	BE1	1.958	0.605	0.000	0.378	0.000	0.309	0.002	0.041	0.691	0.005	0.000	0.005	3.993
	BE6	1.974	0.554	0.000	0.429	0.000	0.373	0.009	0.049	0.595	0.006	0.001	0.006	3.995
	BE11	1.950	0.620	0.000	0.369	0.000	0.304	0.001	0.046	0.705	0.004	0.000	0.002	4.002
B1	BE2	1.997	0.269	0.001	0.706	0.002	0.641	0.002	0.120	0.259	0.004	0.000	0.003	4.003
	BE4	2.000	0.311	0.001	0.616	0.002	0.610	0.002	0.181	0.267	0.014	0.001	0.001	4.006
	BE5	1.997	0.269	0.000	0.705	0.002	0.645	0.003	0.111	0.261	0.004	0.000	0.003	4.001
A	BE3	1.985	0.175	0.000	0.810	0.001	0.785	0.005	0.050	0.189	0.001	0.001	0.002	4.003
	BE8	1.981	0.169	0.000	0.813	0.002	0.789	0.003	0.070	0.177	0.003	0.000	0.002	4.010
	BE10	1.981	0.166	0.000	0.817	0.001	0.799	0.005	0.068	0.170	0.004	0.000	0.002	4.011
A'	BE7	1.989	0.172	0.001	0.743	0.003	0.858	0.008	0.082	0.149	0.006	0.000	0.001	4.012
A'	BE9	1.997	0.117	0.000	0.818	0.003	0.866	0.003	0.107	0.093	0.004	0.000	0.002	4.009

Table A.1c Reconstructed bulk rocks compositions (wt%) with 20% error

group	sample	SiO ₂	Na ₂ O	K ₂ O	CaO	MnO	MgO	Cr ₂ O ₃	FeO ^{total}	Al ₂ O ₃	TiO ₂	P ₂ O ₅	NiO	Total	Mg#	model abundance (grt:cpx)	potential Rutile (vol%)
B2	BE1	45.04	2.31	0.01	15.51	0.13	8.32	0.06	8.41	21.32	0.16	0.01	0.07	101.35	64	75% : 25 %	
	BE6	45.57	2.10	0.00	11.98	0.13	10.79	0.27	9.89	20.83	0.17	0.02	0.07	101.76	66	75% : 25 %	
	BE11	44.47	2.34	0.00	15.72	0.17	7.93	0.04	8.77	20.80	0.15	0.01	0.04	100.43	62	75% : 25 %	
B1	BE2	48.41	1.95	0.26	13.58	0.24	11.85	0.07	10.54	14.42	0.11	0.01	0.04	101.22	67	50% : 50%	0.20
	BE5	48.72	1.96	0.00	13.80	0.23	12.48	0.10	9.34	14.45	0.14	0.01	0.05	101.28	71	50% : 50%	0.07
	BE4	48.41	2.30	0.02	10.96	0.28	12.01	0.08	12.59	14.30	0.46	0.04	0.02	101.45	63	50% : 50%	
A	BE3	47.88	1.02	0.01	12.95	0.18	16.63	0.21	6.40	15.97	0.03	0.01	0.03	101.34	82	60% : 40%	0.11
	BE8	46.78	1.00	0.00	14.03	0.28	14.63	0.11	8.14	15.39	0.09	0.01	0.04	100.49	76	60% : 40%	0.26
	BE10	47.23	0.98	0.01	13.23	0.27	15.56	0.17	7.85	15.19	0.09	0.01	0.03	100.63	78	60% : 40%	0.21
A'	BE7	47.86	1.03	0.01	10.53	0.26	18.74	0.23	6.49	15.29	0.23	0.02	0.02	100.72	84	60% : 40%	0.21
	BE9	47.59	0.69	0.01	11.14	0.33	17.52	0.18	8.74	14.48	0.13	0.04	0.04	100.91	78	60% : 40%	0.53

Tables A.2 trace element of garnets and cpx from Bellsbank eclogites

Table A.2a: garnet

Table A.2b: cpx

Table A.2c: in house garnet standard PN2b and BIR-1 Basalt glass

Table A.2a LA-ICP-MS analyses of trace element concentrations of **garnets** from Bellsbank eclogites Values (in ppm) are averages of several spot analyses. Abbreviations: No.–number of spot analyses; b.d.l.– below detection limit.

Table A.2a Trace-element compositions (ppm) of garnets											
group	B2	B2	B2	B1	B1	B1	A	A	A	A'	A'
sample	BB1	BB6	BE11	BB2	BB4	BB5	BB3	BE8	BE10	BE7	BE9
No.	7	10	7	11	10	9	9	6	7	6	7
Li	0.46	0.38	0.58	0.67	0.58	0.22	b.d.l.	0.14	0.15	0.14	0.19
Sc	22	17	49	64	47	67	64	161	127	89	134
V	280	116	258	196	132	182	185	249	185	136	122
Cr	311	1484	307	444	582	501	1450	844	1437	1691	1495
Mn	1495	1363	1807	3622	3865	3208	2672	3570	3147	3171	3778
Co	66	86	65	76	74	77	56	65	67	60	71
Ni	115	151	66	30	25	40	30	32	35	50	42
Ga	9	8	10	8	10	8	5	7	6	12	9
Rb	0.04	0.04	b.d.l.	0.07	0.06	0.04	0.07	0.03	0.02	b.d.l.	b.d.l.
Sr	0.17	0.09	0.08	0.05	0.57	0.03	0.03	0.12	0.07	0.26	0.19
Y	7.87	4.98	17.49	63.43	34.49	39.78	33.03	82.79	66.96	9.15	15.74
Zr	2.12	4.97	2.35	1.68	21.84	1.76	0.87	0.74	2.75	10.54	35.27
Nb	0.00	0.01	b.d.l.	0.01	0.08	0.02	0.13	0.23	0.17	0.28	0.23
Ba	0.01	b.d.l.	0.12	b.d.l.	b.d.l.	b.d.l.	b.d.l.	0.10	0.13	0.11	0.14
La	0.04	0.02	0.11	0.01	0.04	0.01	0.01	0.05	0.03	0.02	0.01
Ce	0.35	0.15	0.38	0.05	0.44	0.02	0.07	0.41	0.34	0.32	0.18
Pr	0.08	0.03	0.03	0.01	0.16	0.00	0.01	0.09	0.08	0.13	0.09
Nd	0.59	0.21	0.13	0.10	1.50	0.08	0.07	0.64	0.69	1.35	1.18
Sm	0.27	0.28	0.40	0.38	1.06	0.24	0.07	0.37	0.40	0.77	1.21
Eu	0.27	0.34	0.32	0.35	0.54	0.23	0.09	0.22	0.22	0.33	0.55
Gd	0.39	0.41	1.45	1.29	1.40	0.93	0.51	1.55	1.58	1.08	2.22
Tb	0.15	0.12	0.35	0.67	0.54	0.47	0.33	0.60	0.60	0.20	0.38
Dy	1.29	0.93	2.83	7.48	5.06	5.10	4.08	8.27	7.45	1.54	2.70
Ho	0.30	0.19	0.65	2.24	1.29	1.41	1.20	2.83	2.37	0.35	0.56
Er	0.91	0.55	2.03	8.43	4.27	4.95	4.41	11.85	9.36	1.11	1.63
Tm	0.14	0.08	0.32	1.51	0.68	0.82	0.77	2.23	1.65	0.17	0.23
Yb	1.07	0.64	2.18	13.08	5.27	6.66	6.45	18.21	13.48	1.25	1.62
Lu	0.14	0.08	0.35	1.93	0.75	0.95	0.97	3.10	2.26	0.19	0.25
Hf	0.05	0.10	0.11	0.03	0.31	0.05	0.04	0.03	0.06	0.15	0.38
Ta	0.00	b.d.l.	0.01	0.00	0.00	0.00	0.00	0.01	b.d.l.	0.02	0.02
Pb	0.00	0.01	0.23	0.01	0.01	0.01	0.01	0.44	0.18	0.50	0.90
Th	0.02	0.02	0.12	0.01	0.01	0.03	0.04	0.06	0.09	0.01	0.01
U	0.04	0.02	0.06	0.01	0.03	0.02	0.04	0.16	0.09	0.04	0.03

Table A.2b LA-ICP-MS analyses of trace element concentrations of **cpx** from Bellsbank eclogites Values (in ppm) are averages of several spot analyses. Abbreviations: No.–number of spot analyses; b.d.l.– below detection limit.

Table A.2b Trace-element compositions (ppm) of clinopyroxenes											
group	B2	B2	B2	B1	B1	B1	A	A	A	A'	A'
sample	BB1	BB6	BE11	BB2	BB4	BB5	BB3	BE8	BE10	BE7	BE9
No.	6	10	9	9	10	9	9	9	7	7	8
Li	11.44	10.00	27.37	8.20	2.80	2.45	0.85	1.13	1.28	0.54	0.86
Sc	9	10	10	30	26	27	18	35	30	24	34
V	670	443	1208	553	355	487	390	869	750	317	322
Cr	290	1798	572	368	445	366	866	653	1255	2318	1065
Mn	59	100	132	366	681	282	220	349	332	646	695
Co	15	21	29	34	34	32	18	27	28	24	35
Ni	938	1245	997	466	204	520	457	519	602	388	499
Ga	29	26	45	14	15	13	7	9	8	9	7
Rb	0.18	0.03	b.d.l.	0.06	b.d.l.	b.d.l.	b.d.l.	0.03	0.02	0.03	b.d.l.
Sr	9.52	12.51	8.00	16.94	253.72	20.72	45.45	112.02	76.38	323.16	419.36
Y	0.06	0.06	0.17	2.34	3.18	1.38	1.04	2.32	2.33	2.03	1.70
Zr	0.49	1.92	0.50	3.10	31.49	2.11	0.64	0.78	2.93	19.08	29.00
Nb	b.d.l.	0.01	b.d.l.	0.00	0.20	0.17	0.69	1.40	1.09	1.16	0.93
Ba	0.39	0.01	2.04	0.05	0.34	0.09	0.13	0.74	1.16	7.60	0.17
La	0.22	0.34	0.68	0.98	6.58	1.70	5.32	13.47	8.47	10.95	8.78
Ce	0.50	0.72	0.81	1.33	17.34	2.06	7.05	21.27	18.33	37.49	32.95
Pr	0.05	0.08	0.03	0.10	2.52	0.18	0.63	1.76	1.81	5.33	4.95
Nd	0.19	0.27	0.06	0.42	10.90	0.62	1.66	4.65	5.66	22.95	23.26
Sm	0.03	0.06	0.06	0.37	1.78	0.21	0.17	0.52	0.63	3.51	4.40
Eu	0.01	0.04	0.03	0.16	0.49	0.10	0.07	0.16	0.20	0.86	1.09
Gd	0.03	0.05	0.09	0.53	1.41	0.35	0.32	0.48	0.63	1.90	2.18
Tb	0.01	0.00	0.01	0.09	0.17	0.06	0.05	0.08	0.10	0.17	0.17
Dy	0.02	0.02	0.07	0.54	0.90	0.36	0.27	0.52	0.60	0.69	0.65
Ho	0.00	0.00	0.02	0.09	0.13	0.06	0.04	0.10	0.10	0.08	0.07
Er	0.02	0.01	0.02	0.20	0.27	0.11	0.08	0.23	0.20	0.16	0.12
Tm	0.00	0.00	0.01	0.02	0.03	0.01	0.01	0.03	0.02	0.02	0.01
Yb	0.01	0.00	0.01	0.13	0.16	0.07	0.05	0.14	0.12	0.08	0.05
Lu	0.00	0.00	0.01	0.01	0.02	0.01	0.01	0.02	0.01	0.01	0.01
Hf	0.06	0.16	0.10	0.24	1.54	0.18	0.07	0.08	0.21	0.63	1.02
Ta	b.d.l.	b.d.l.	0.02	b.d.l.	0.02	0.01	0.02	0.08	0.05	0.09	0.10
Pb	0.02	0.02	0.42	0.15	0.63	0.15	0.63	1.02	0.97	0.67	1.10
Th	0.02	0.03	0.10	0.09	0.12	0.34	0.90	0.92	0.85	0.19	0.26
U	0.00	0.00	0.01	0.01	0.02	0.01	0.09	0.18	0.14	0.05	0.06

Table A.2c LA-ICP-MS analyses of trace element concentrations of results on the international standard BIR Basalt glass and the in house garnet standard-PN2b. The trace-element data of BIR-1 from Eggins et al. (1997) is shown for comparison. Abbreviations: No. – number of analyses; b.d.l. – below detection limit.

Table A.2c Trace elements of BIR-1 Basalt glass and in house garnet standard- PN2b (in ppm)										
No.	35			54						
standard	PN2b	relative stdev(%)	std Err(%)	BIR-1 basalt glass standard	relative stdev(%)	std Err(%)	d.l. average(ppm)	Eggins et al. (1997)	USGS-84FLA - 02;1984	
		(1σ)	(1σ)		(1σ)	(1σ)		(ppm)	(ppm)	±(ppm)
Li	0.26	16	4.6	2.86	22	3.7	0.033	3.4	3.40	0.40
Sc	78	6	1.8	42	13	2.2	0.053	44	44	4
V	121	4	1.1	310	22	3.7	0.265	310	313	23
Cr	112	5	1.5	416	33	5.6	0.027	382	380	40
Mn	2910	6	1.7	1446	16	2.7	0.356	1417	1320	80
Co	71	4	1.2	51	18	3.0	0.052	52	51	3
Ni	41	5	1.4	159	22	3.8	0.09	166	166	16
Ga	6	3	0.9	13	19	3.2	0.047	16	16	2
Rb	0.029	32	8.9	0.181	30	5.2	0.009	0.24	1.00	0.90
Sr	0.28	27	7.6	108	11	1.8	0.026	110	108	14
Y	55.88	8	2.3	13	12	2.1	0.012	16.5	16	2
Zr	44.24	8	2.3	12.26	11	1.9	0.033	14.5	22	7
Nb	0.045	21	5.8	0.518	10	1.7	0.004	0.55	2.00	0.50
Ba	0.045			6.330	10	1.7	0.008	6.40	7.70	2.20
La	0.016	34	9.3	0.600	10	1.7	0.004	0.58	0.88	0.33
Ce	0.190	20	5.6	1.834	12	2.1	0.013	1.85	2.50	1.10
Pr	0.086	9	2.5	0.363	10	1.8	0.033	0.37	0.50	0.40
Nd	1.057	7	2.1	2.357	10	1.7	0.006	2.35	2.50	0.70
Sm	1.268	7	2.0	1.062	10	1.7	0.034	1.10	1.08	0.09
Eu	0.772	5	1.3	0.509	10	1.8	0.005	0.52	0.54	0.04
Gd	3.875	8	2.2	1.606	14	2.4	0.003	1.97	1.90	0.40
Tb	0.962	7	2.1	0.314	11	1.9	0.012	0.38	0.41	0.05
Dy	8.762	8	2.2	2.354	12	2.1	0.005	2.50	2.40	0.30
Ho	2.123	8	2.3	0.509	12	2.1	0.003	0.57	0.50	0.08
Er	6.680	8	2.2	1.512	12	2.1	0.005	1.70	1.80	0.30
Tm	0.982	9	2.5	0.222	13	2.2	0.008	0.27	0.27	0.07
Yb	6.562	8	2.3	1.590	12	2.0	0.009	1.60	1.70	0.19
Lu	0.926	10	2.6	0.227	13	2.3	0.01	0.25	0.26	0.04
Hf	0.838	10	2.9	0.486	13	2.3	0.007	0.56	0.58	0.06
Ta	0.005	36	10	0.037	12	2.0	0.007	0.04	0.06	0.04
Pb	0.922	215	60	4.043	84	14.5	0.005	3.20	3.20	0.80
Th	0.004	47	13	0.030	10	1.7	0.003	0.03	0.89	0.70
U	0.004	22	6	0.015	22	3.8	0.002	0.01	0.03	

Table A.3 Oxygen isotope data of garnet and cpx mineral separates of Bellsbank eclogites and the reconstructed bulk-rock compositions based on the mineral modal abundances

Table A.3 Oxygen isotope compositions of garnets, cpx and bulk rocks				
Group	sample	$\delta^{18}\text{O}$ (garnet)	$\delta^{18}\text{O}$ (cpx)	$\delta^{18}\text{O}$ (reconstured WR)
	BE1	3.46	4.57	3.74
B2	BE6	3.77	4.30	3.90
	BE11	2.50	2.99	2.63
A'	BE9	4.87	5.10	4.96
	BE2	2.73	3.34	3.04
B1	BE5	3.13	3.75	3.44
	BE4	6.75	6.40	6.58
	BE3	4.12	4.30	4.19
A	BE8	3.44	5.33	4.20
	BE10	3.98	4.50	4.19
		mean	std.error (2s)	
standard	UWG-2 Grt (n=8)	5.98	0.08	
standard	quartz L1 (n=3)	18.10	0.42	
	UWG-2 reference value	5.89-5.90		
	quartz L1 reference vale	18.15		

Tables A.4 Summary of two-point Lu-Hf and Sm-Nd isochrons, calculated Fe²⁺-Mg exchange Temperatures of Krogh88 and the estimated pressure by projecting to the local geothermal, and oxygen isotope ($\delta^{18}\text{O}$) of garnets and cpx and the corresponding whole rocks.

(The data includes new data from this study on Bellsbank eclogites and also combines the literature data from eclogites and garnets pyroxenites)

Tables A.4 Two-point Lu-Hf and Sm-Nd isochron ages , Temperatures and Pressure, $\delta^{18}\text{O}$										
location	eruption age(Ma)	group	sample	T [Krogh88](°C)	P(kb)	Lu-Hf age (Ma)	Sm-Nd age (Ma)	$\delta^{18}\text{O}$ -grt	$\delta^{18}\text{O}$ -cpx	$\delta^{18}\text{O}$ -WR
Bellsbank	120	B2	BE1	1151	61	104±1	434±6	3.46	4.57	3.7
Bellsbank	120	B2	BE6	1085	55	1549±14	596±6	3.77	4.3	3.9
Bellsbank	120	B2	BE11	1173	63	119±2	885±12	2.504	2.99	2.6
Bellsbank	120	B1	BE2	957	45	277±1	175±30	2.73	3.34	3.0
Bellsbank	120	B1	BE5	1068	53	348±1	110±1	3.13	3.75	3.4
Bellsbank	120	B1	BE4	1070	53	127±1	131±2	6.75	6.4	6.6
Bellsbank	120	A	BE3	848	38	779±2	516±62	4.12	4.3	4.2
Bellsbank	120	A	BE8	876	39	532±3	519±6	3.44	5.33	4.2
Bellsbank	120	A	BE10	846	38	552±3	292.1±4	3.98	4.5	4.2
Bellsbank	120	A'	BE9	912	42	116±3	1642±130	4.87	5.1	5.0
*Bellsbank	120	A	438-7	968	45		97±45	3.04		
*Bellsbank	120	A	438-2	972	45		33±8	3.42	3.25	3.31
*Bellsbank	120	A	437-1	715	30		287±96	5.02	5.25	5.11
*Bellsbank	120	A	437-2	722	30		355±10	3.25	3.42	3.31
*Bellsbank	120	B	2791-21	1134	58		671±18	2.8		
*Bellsbank	120	C	437-5	1008	48		1608±25	3.9		
*Bellsbank	120	C	437-7	1082	55		863±120	4.40		
*Bellsbank	120	C	2791-34	1020	49		767±23	4.3		
*Angola	80-100		Angola	966	40		584±14	6.07		
*Namibia	71		Deutsche Erde	1190	55		185±1	4.76	4.87	4.82
*Kao	89		KAO	819	40		264±6	4.12	4.72	4.34
*Diavik	55	Low-T	MX2	773	33	1411±11	1211±22			
*Diavik	55	Low-T	MX7	813	35	1469±8	1427±14			
*Diavik	55	Low-T	MX9	826	35	1104±6	380±7			
*Diavik	55	Low-T	MX15	755	32	1450±8	982±27			
*Diavik	55	Low-T	MX45	764	33	460±3	96±8			
*Roberts Victor	120		BD1191	1350	75	1402±7	903±5	3.27		
*Roberts Victor	120		DEJ5	1182	65	2230±13	1194±5	3.42		
*Roberts Victor	120		BD1175	1008	48	477±28	221±38	6.08		
*Roberts Victor	120		BD3699	1148	60	351±20	110±13	6.74		
*Roberts Victor	120		RV1	994	48	199±55	-2	6.87		
*Roberts Victor	120		HRV247	1050	51	226±62	146±14	6		
*Roberts Victor	120		R30	730		1953±13	963±42	4.53	4.79	4.66
*Roberts Victor	120		DEJ02	1315		227±47	245±25	5.97	5.84	5.905
*Roberts Victor	120		DEJ03	975		129±12	208±19	6.37	6.35	6.36
*Roberts Victor	120	Type IA	RV07/02	1117	57	150±40	109±29	4.95		
*Roberts Victor	120	Type IA	RV07/03	1316	80	118±32	89±26	7.29		
*Roberts Victor	120	Type IA	RV07/09b	1084	55	144±24	103±17			
*Roberts Victor	120	Type IA	RV07/13	1093	55	140±21	115±22	6.36		
*Roberts Victor	120	Type IA	RV07/20	1105	55	108±22	101±18	5.39		
*Roberts Victor	120	Type IA	RVF6	1030	50		146±8			

Chapter 4: The origin of eclogites and garnet pyroxenites...

*Roberts Victor	120	Type IA	RVF8	1096	55		236±23			
*Roberts Victor	120	Type IB	RV07/01	1110	55	112±32	92±15	6.69		
*Roberts Victor	120	Type IB	RV07/07	1136	60		102±16	4.22		
*Roberts Victor	120	Type IB	RV07/11	1101	55	144±36	58±17	5.56		
*Roberts Victor	120	Type IB	RV07/14	1133	60	128±29	113±42			
*Roberts Victor	120	Type IB	RV07/16	1189	65	127±36	101±17	4.13		
*Roberts Victor	120	Type IB	RV07/18	1141	60	145±52	96±43	6.18		
*Roberts Victor	120	Type IB	RV07/19	1170	62	115±30	93±11			
*Roberts Victor	120	Type IB	RV07/22	1134	60	158±35	127±35	5.85		
*Roberts Victor	120	Type IB	RV07/29b	1145	60	131±32	103±16			
*Roberts Victor	120	Type IB	HRV 247C	1133	60		140±13			
*Roberts Victor	120	Type IB	HRV 77bimin	1237	70	53±10	104±13			
*Roberts Victor	120	Type IB	RV07/17	1135		198±30	209±36	6.26		
*Roberts Victor	120	Type IIA	RV07/12	951	45	1282±100	831±52			
*Roberts Victor	120	Type IIA	RV73/12	952	45	764±94		3.52		
*Roberts Victor	120	Type IIB	RV07/08	1203	65	1148±120	792±75	3.91		
*Lovedale	74-130		2073	1050		161±3	76±3	5.9	6.11	
*Lovedale	74-130		2093	1300		120±1	89±2	8.4	8.6	
*Roodekraal	74-130		RDK1	1190		778±3	441±2	4.5	5	
*Bultfontein	84		B21	923		164±13	24±9	5.11	5.48	5.295
*Bultfontein	85		713	820		981±4	173±5			
*Malaita	44		RG01	1100		69±12	42±6	5.58	5.85	

Samples with * markers are from literature.

(*Roberts Victor data is from Jacob et al., 2005 and Huang et al., 2012; *Bellsbank data is from Shervias et al., 1989 and Taylor and Neal, 1990; **Roberts Victor, *Lovedale, *Roodekraal, *Roodekraal, *Bultfontein and *Malaita data is from Gonzaga et al., 2010; *Diavik data is from Schmidberger et al., 2007).

Tables A.5: Lu-Hf and Sm-Nd isotope compositions

Table A.5a: Lu-Hf isotope of garnets, cpx and reconstructed bulk rocks

Table A.5b: Sm-Nd isotope, garnets, cpx and reconstructed bulk rocks

Table A.5c: Lu-Hf isotope of in house garnet standard PN3b and BHVO-1 Basalt

Table A.5d: Sm-Nd isotope of in house garnet standard PN3b and BHVO-1 Basalt

Tables A.5a Lu-Hf isotope of garnets, cpx and reconstructed bulk rocks										
Group	model abundance	sample	$^{176}\text{Lu}/^{177}\text{Hf}$	$^{176}\text{Hf}/^{177}\text{Hf}$	2s	$\epsilon\text{Hf}(120\text{Ma})$	two-point isochron age (Ma)	initial of two-point isochron	ϵHf (two-point isochrone)	Model age (Ga)
	25%	BE1-cpx	0.00123	0.308528	3.1E-05	914				
	75%	BE1-Grt	0.35123	0.309064	3.1E-05	905				4.25 ± 0.21
B2		BE1-bulk	0.27291	0.308944		907	82±7	0.308525	930	5.55±0.61
	25%	BE6-cpx	0.00028	0.285076	2.9E-05	84				
	75%	BE6-Grt	0.12893	0.289001	2.9E-05	212				3.31 ± 0.17
B2		BE6-bulk	0.09766	0.288086		182	1610±18	0.285067	519	4.02 ± 0.63
	25%	BE11-cpx	0.00122	0.311108	3.1E-05	1004				
	75%	BE11-Grt	0.46126	0.312171	3.1E-05	1006				3.51 ± 0.18
B2		BE11-bulk	0.39766	0.311909		1002	119±5	0.311105	1031	4.12 ± 0.29
	40%	BE2-cpx	0.00775	0.333847	3.3E-05	1808				
	60%	BE2-Grt	7.74449	0.375527	3.8E-05	2669				0.63 ± 0.03
B1		BE2-bulk	2.12612	0.345102		2038	288±1	0.333805	1882	1.26 ± 0.31
	40%	BE5-cpx	0.00511	0.318911	3.2E-05	1280				
	60%	BE5-Grt	3.52273	0.342738	3.4E-05	1844				0.90 ± 0.05
B1		BE5-bulk	1.22176	0.327032		1470	362±2	0.318876	1371	1.6 ± 0.33
	40%	BE4-Cpx	0.00147	0.283142	2.8E-05	15				
	60%	BE4-Grt	0.20673	0.283230	2.8E-05	2				0.14 ± 0.01
B1		BE4-bulk	0.06004	0.283167		11	23±11	0.283141	18	0.48 ± 0.31
	40%	BE3-cpx	0.01059	0.349350	3.5E-05	2356				
	60%	BE3-Grt	4.40275	0.416237	4.2E-05	4374				1.6 ± 0.08
A		BE3-bulk	2.07361	0.380331		3288	810±4	0.349189	2	2.5 ± 0.45
	40%	BE8-cpx	0.02653	0.467093	4.7E-05	6520				
	60%	BE8-Grt	19.75638	0.671689	6.7E-05	12192				1.02 ± 0.05
A		BE8-bulk	10.92399	0.578323		9589	553±3	0.466817	6724	1.43 ± 0.19
	40%	BE10-cpx	0.00728	0.337252	3.4E-05	1929				
	60%	BE10-Grt	4.70616	0.387844	3.9E-05	3345				1.18 ± 0.06
A		BE10-bulk	1.85555	0.375372		3130	574±3	0.337174	2086	1.62 ± 0.31
	40%	BE9-cpx	0.00087	0.283077	2.8E-05	13				
	60%	BE9-Grt	0.07319	0.283239	2.8E-05	13				0.59 ± 0.03
A'		BE9-bulk	0.03801	0.283150		13	120±29	0.283075	37	4.08 ± 2.45

Table A.5b Sm-Nd isotope data of garnets, cpx and reconstructed bulk rocks										
Group	model abundance		$^{147}\text{Sm}/^{144}\text{Nd}$	$^{143}\text{Nd}/^{144}\text{Nd}$	2s	ϵNd (120Ma)	two-point isochron age (Ma)	initial at (two-point isochron)	ϵNd (two- point isochron)	Model age (Ga)
	25%	BE1-cpx	0.08098	0.51547	0.000052	57				
	75%	BE1-Grt	0.28013	0.51604	0.000052	65				6.10
B2		BE1-bulk	0.26010	0.51598		64	435 ± 55	0.51524	61.8	7.84
	25%	BE6-cpx	0.12002	0.51607	0.000052	68				
	75%	BE6-Grt	0.58067	0.51787	0.000052	96				2.07
B2		BE6-bulk	0.53071	0.51756		91	596 ± 24	0.51561	73	2.37
	25%	BE11-cpx	0.38030	0.53400	0.000053	414				
	75%	BE11-Grt	1.55799	0.54083	0.000054	529				3.13
B2		BE11-bulk	1.46830	0.54031		521	885 ± 15	0.53179	396.8	3.29
	40%	BE2-cpx	0.47375	0.52376	0.000052	213				
	60%	BE2-Grt	1.96027	0.52546	0.000053	223				1.11
B1		BE2-bulk	1.34527	0.52476		219	175 ± 78	0.52321	210.8	1.60
	40%	BE4-cpx	0.37277	0.51278	0.000051	0				
	60%	BE4-Grt	0.09571	0.51254	0.000051	0				0.12
B1		BE4-bulk	0.16094	0.51259		0	131 ± 39	0.51246	-0.2	0.19
	40%	BE5-cpx	0.90794	0.51862	0.000052	106				
	60%	BE5-Grt	0.22332	0.51861	0.000052	116				1.28
B1		BE5-bulk	0.59699	0.51863		111	2 ± 16	0.5186	116.5	2.27
	40%	BE3-cpx	0.05608	0.51323	0.000051	14				
	60%	BE3-Grt	0.33449	0.51417	0.000051	28				1.69
A		BE3-bulk	0.23639	0.51384		23	516 ± 39	0.51304	20.9	4.55
	40%	BE8-cpx	0.42477	0.51407	0.000051	24				
	60%	BE8-Grt	0.06416	0.51284	0.000051	6				0.96
A		BE8-bulk	0.14691	0.51312		10	519 ± 31	0.51263	12.8	-1.50
	40%	BE10-cpx	0.36736	0.51329	0.000051	10				
	60%	BE10-Grt	0.06780	0.51272	0.000051	4				0.59
A		BE10-bulk	0.15163	0.51288		5	292 ± 36	0.51259	7	-0.83
	40%	BE9-cpx	0.22454	0.51251	0.000051	-3				
	60%	BE9-Grt	0.26840	0.51298	0.000051	6				0.74
A'		BE9-bulk	0.25396	0.5128288		3	1642 ± 280	0.51009	-8	0.51

Tables A.5c Lu-Hf isotope data for repeated digestion of in house garnet standard (PN3b) (**Table A.5c-1**) and BHVO-1 Basalt (**Table A.5c-2**). Abbreviations: ID – isotope dilution; Laser- in situ measurement by Laser Ablation ICP-MS.

Table A.5c-1 Lu-Hf isotope data of in house garnets standard (PN3b)						
sample	$^{176}\text{Hf}/^{177}\text{Hf}$	$^{176}\text{Lu}/^{177}\text{Hf}$	ID-Lu [ppm]	ID-Hf [ppm]	laser-Lu [ppm]	laser-Hf [ppm]
PN3b-1	0.283022	0.089	0.49	0.79		
PN3b-2	0.283061	0.0901	0.51	0.81		
PN3b-3	0.283057	0.0883	0.48	0.76		
PN3b-4	0.283087	0.0897	0.42	0.67		
mean	0.283057	0.0893	0.48	0.76	0.52	0.77
std.Err (abs) (2 σ)	0.00002	0.0007				
std.Err (%) (2 σ)	0.007	0.8				

Table A.5c-2 Lu-Hf isotope data of BHVO-1 standard				
sample	$^{176}\text{Hf}/^{177}\text{Hf}$	$^{176}\text{Lu}/^{177}\text{Hf}$	ID-Lu [ppm]	ID-Hf [ppm]
BHVO-1-1	0.283095	0.00874	0.28	4.5
BHVO-1-2	0.28308	0.00876	0.3	4.9
BHVO-1-3	0.283126	0.00873	0.26	4.19
BHVO-1-4	0.283119	0.00872	0.28	4.5
BHVO-1-5	0.283098	0.0088	0.28	4.59
mean	0.283107	0.00875	0.28	4.53
std.Err(abs) (2 σ)	0.000013	0.00003		
std.Err(%) (2 σ)	0.005	0.33		
Blicher-Toft et al., 2001	0.283108 \pm 5	0.00876	0.29	4.48
Bizzarro et al., 2003	0.283108 \pm 8	0.00877		

Tables A.5d Sm-Nd isotope data for repeated digestion of in house garnet standard (PN3b) (**Table A.5d-1**) and BHVO-1 Basalt (**Table A.5d-2**). Abbreviations: ID – isotope dilution; Laser- in situ measurement by Laser Ablation ICP-MS.

Table A.5d-1 Sm-Nd isotope data of PN3b in house standard						
sample	$^{143}\text{Nd}/^{144}\text{Nd}$	$^{147}\text{Sm}/^{144}\text{Nd}$	ID-Sm (ppm)	ID-Nd (ppm)	laser-Sm (ppm)	laser-Nd (ppm)
PN3b-1	0.7196	0.512876	1.52	1.2		
PN3b-2	0.7227	0.512962	1.54	1.21		
PN3b-3	0.7198	0.512913	1.6	1.29		
PN3b-4	0.719	0.512913	1.51	1.19		
mean	0.7203	0.512916	1.54	1.22	1.53	1.17
std Err(abs) (2σ)	0.0016	0.000035				
std Err(%) (2σ)	0.23	0.00692				

Table A.5d-2 Sm-Nd isotope data of BHVO -1 standard				
sample	$^{143}\text{Nd}/^{144}\text{Nd}$	$^{147}\text{Sm}/^{144}\text{Nd}$	ID-Sm (ppm)	ID-Nd (ppm)
BHVO-1-1	0.512937	0.1482	6.4	25.5
BHVO-1-2	0.51292	0.1461	5.9	24.1
BHVO-1-3	0.512929	0.1467	5.9	24.6
BHVO-1-4	0.512971	0.1479	6.4	25.3
BHVO-1-5	0.512934	0.147	6.3	25.1
mean	0.512938	0.1472	6.2	24.9
std.Err(abs) (2σ)	0.000017	0.0008	0.2	0.4
std.Err(%) (2σ)	0.0034	0.54		
Raczek et al., 2003; 2001	0.512957 ± 8		6.2	25

Table A.6 Sr isotope compositions of cpx

(The Rb,Sr concentrations are from in situ analysis by laser ablation ICP-MS)

Table A.6 Sr isotope compositions of cpx							
Group	sample	Rb (ppm)	Sr (ppm)	$^{87}\text{Rb}/^{86}\text{Sr}$ (calculated)	$^{87}\text{Sr}/^{86}\text{Sr}$	internal error (2 S.D.)	ϵSr (at 120Ma)
B2	E1 cpx	0.177	10	0.0070	0.70951	0.000006	69
B2	E6 cpx	0.032	13	0.0081	0.70895	0.000005	61
B2	E11 cpx	b.d.l.	8		0.70838	0.000005	53
B1	E2 cpx	0.063	17	0.0108	0.71232	0.000006	108
B1	E5 cpx	b.d.l.	21		0.70581	0.000004	16
B1	E4 cpx	b.d.l.	254		0.70488	0.000002	3
A	E3 cpx	b.d.l.	45		0.70490	0.000066	3
A	E8 cpx	0.034	112	0.0009	0.70456	0.000007	-2
A	E10 cpx	0.024	76	0.0009	0.70440	0.000003	-4
A'	E9 cpx	b.d.l.	419		0.71228	0.000006	108
standard	SRM 987 (n=15)				0.71025	0.000016	
standard	BHVO-1				0.70343	0.000018	

Figs. A.1 Photos of eclogites



Sample BE1



Sample BE2



Sample BE3



Sample BE4



Sample BE5



Sample BE6



Sample BE7



Sample BE8



Sample BE9



Sample BE10



Sample BE11

Chapter 5

Mantle eclogites and garnet pyroxenites - the meaning of two-point isochrons, Sm-Nd and Lu-Hf closure temperatures and the cooling of the subcratonic mantle

1. Introduction

Bimineralic eclogites and garnet pyroxenites, make up a small but petrologically significant portion of the subcontinental lithospheric mantle (e.g. Sobolev, 1977; Schulze, 1989; Gurney et al., 1991). They were brought to the Earth's surface as xenoliths mostly by kimberlites through Archean crust and show a wide variability in chemical and isotopic composition (e.g. Taylor and Neal, 1989; Neal et al., 1990; Jacob et al., 2005; Aulbach et al., 2007; Schmidberger et al., 2007; Gonzaga et al., 2010; Huang et al., 2012). The variability is the result of multiple origins of their protoliths and potential chemical changes before and/or after eclogitisation. Two main models exist for their petrogenesis: (1) a mantle origin as high-pressure igneous precipitates from (ultra-)mafic melts within the lithosphere with subsequent metamorphic adjustment (e.g. O'Hara and Yoder, 1967; O'Hara, 1969; O'Hara et al., 1975; Hatton and Gurney, 1987; Caporuscio and Smyth, 1990; Griffin et al., 2007; Huang et al., 2012) (2) a subduction origin as metamorphosed products of oceanic crust (e.g. Helmstaedt and Doig, 1975; Jagoutz et al., 1984; MacGregor and Manton, 1986; Shervais et al., 1988; Taylor and Neal, 1989; Ireland et al., 1994; Jacob and Foley, 1999; Barth et al., 2001; Jacob et al., 2003, 2004, 2005; Aulbach et al., 2007; Schmidberger et al., 2007). Subsequently, they may have experienced metasomatism and/or partial melting (summarized by Jacob 2004) and may be parental to the Archean tonalite-trondjemite-granodiorite series (TTG's; e.g. Barth et al., 2001; Rapp et al., 1995). The characterization of these eclogitic materials, their petrogenesis, and their geologic ages will provide important constraints on the origin and development of the subcratonic lithosphere and also on diamond formation. Tantalizing questions are the nature of the protoliths, their age and the age of eclogitisation. Due to wide variability in petrological and geochemical character as a result of very different protoliths and differing subsequent history of metamorphism, melting and re-enrichment conclusive age constraints are difficult to obtain. Pioneering work offers Archean ages for eclogites, e.g. a 2.9 Ga Re-Os isochron age from Siberian eclogites (Pearson et al., 1995), around 2.7 Ga for eclogites from Roberts Victor (Kapaal craton) based on the Sm-Nd isotope system (Jagoutz et al., 1984; Jacob, et al. 2005) and ~2.5 Ga from Pb-Pb isotope systematics (Kramers, 1979). Similar late

Archean ages were obtained as in-situ Pb-Pb ages on cpx from eclogite xenoliths from a kimberlite in West Greenland (2.7 ± 0.3 Ga) (Tappe et al., 2011) and as a Hf model age for an eclogite cpx from Lac de Gras from the Slave Craton (Aulbach et al., 2007). However, a bulk rock isochron from eclogites from Diavik only yielded a Palaeoproterozoic age of < 2.1 Ga in agreement with in-situ Pb isotope data from their clinopyroxenes (Schmidberger et al., 2007). The majority of ages stem from two-point garnet-clinopyroxene isochrons which give a whole range of ages from Proterozoic to eruption age and to future age (e.g. Jacob et al., 2005; Schmidberger et al., 2007; Gonzaga et al., 2010) It is not possible to put a geologic meaning to this wide spread of ages. It was proposed previously that such ages either record the time of the emplacement of the kimberlite magma, or the age of the time of “frozen” mineral equilibrium or are a disequilibrium age in the form of future ages caused by metasomatism (e.g. Dodson, 1973; Jacob et al., 2004, 2005). The geological significance of two-point isochrones is still unknown.

In order to investigate this question further we studied 11 eclogites with exceptionally fresh garnets and clinopyroxenes for their major and trace elements and their Sm-Nd and Lu-Hf systematics. They were collected from the coarse grained concentrate of the Bellsbank diamond mine on the W-block of the Kaapvaal craton. This locality was chosen because of the reported freshness of the samples and because previous work from Shervais et al. (1988), Taylor and Neal (1989) and Neal et al. (1990) showed that the eclogites and garnet pyroxenites originate from a wide range of temperatures (and inferred pressures) from as low as 730°C up to 1200°C , that some samples have an extremely depleted character with very low incompatible trace element contents and with resultant extremely high Nd isotope ratios. The incompatible trace element depletion and high Nd isotope ratios indicate little metasomatic overprint and the wide range of conditions of origin may provide samples which stem from below and above the closure temperatures of the respective isotope systems. This may enable us to reach more definite conclusions on the meaning of two-point isochrones of mantle eclogites and garnet pyroxenites and also to obtain information on the thermal development of the lithospheric mantle.

2. The frame

The Earth's mantle is a huge metamorphic complex which undergoes permanent changes ruled by plate tectonics but which also has enclaves underneath Archean crust which is exempt from the convecting mantle since at least 2.5 Ga. This part has evolved towards a steady thermal state since it originated either by plume accretion (genetic model 1 – hot plume models; e.g. Boyd, 1989) or subduction in a broad sense (model 2 – subduction; Kesson and Ringwood, 1989). Model 2 is favoured by us because of various geochemical indicators in the peridotites and because of the presence of eclogites with low-pressure precursors (Stachel et al., 1998; Lazarov et al., 2009; Wittig et al., 2008; Shu et al., 2012 submitted to GCA). Cooling of the mantle after its assembly undoubtedly has to occur for model 1 but probably also for model 2 because of a possible faster recycling mechanism of the crust into the mantle and resulting processes and final stabilization in the Archean (Herzberg and Rudnick, 2012). Further cooling of an already stable subcratonic mantle may occur by

denudation. Under such circumstances, two point garnet-clinopyroxene isochrons from mantle xenoliths (peridotites or eclogites) should give either cooling ages or eruption ages depending on whether the mantle portion under consideration was below or above the closure temperature of a radiogenic system. A further kind of “age” is obtained if either of the two mineral phases is preferentially disturbed by a more recent event. The phase to be disturbed is generally cpx with the effect that artificially old ages are obtained.

Closure temperatures are dependent on composition, cooling rate, grain size and geometry (Dodson, 1986). A closure temperature is defined as a member of a temperature interval, where volume diffusion ceases upon cooling. For a mineral pair, it is determined by the mineral with the slower diffusion rate.

Principally, the closure temperature of a system at an assumed cooling rate can be determined from the diffusion properties of the element (or pair) in the constituent minerals and the geometric properties of the minerals (Dodson, 1986 and later work e.g. by Ganguly and Tirone, 1998, 2001). These principles with modifications were used e.g. by Bedini et al. (2004) to determine cooling rates for the lithospheric mantle. These authors estimate that the cooling rate for the Kaapvaal lithospheric mantle must lie between 40-105 °C/Ga. Irrespective of poorly known diffusion coefficients the assumed geometric mineral properties also contribute to the uncertainties in these estimates. One way to evaluate the closure temperature of an isotopic system for mineral pairs is to investigate similar rock types from similar geologic setting but various temperatures which cover the range from below and above the closure temperatures. The low temperature samples will develop and keep the isotopic gradient between minerals while the high temperature samples continue to be in isotopic mineral exchange and give identical ages, if no subrecent overprint occurs. In the slowly cooling subcratonic mantle it should be possible to obtain an estimate of the closure temperature from grt-cpx two-point ages. If a cooling model holds true for the mantle underneath the cratons, two point isochrons from the different isotopic systems should give different ages depending on the last equilibrium temperature and the closure temperatures of the isotopic systems. They should give an alignment of increasing ages (cooling ages) with decreasing temperatures below the closure temperature and kimberlite eruption age above. The intersect should be the closure temperature which should be a minimum for these very slowly cooling rocks. It should also be possible to estimate the cooling rate of the mantle from the difference in the closure temperatures and the temperature dependence of the cooling ages.

3. Analytical Methods

The major elements were analysed by EPMA (electron probe micro-analysis) in the wavelength-dispersive mode (WDS) with a JEOL JXA 8900RL at the University of Frankfurt with an acceleration voltage of 15 kV, a beam current of 20 nA and a spot size of 3 µm. Each sample was analyzed by 3-15 spots (depending on the grain size) to test for compositional homogeneity. In clinopyroxenes with spongy rims, only the fresh cores were analyzed. The integration time for peak and back ground measurements varied between 10s to 30s depending on the elements. Standards were natural minerals and pure oxides and metals. The ZAF algorithm was used for matrix correction.

The trace elements were analyzed by Laser ablation ICP MS using a New Wave Research LUV213TM 161 ultraviolet Nd-YAG laser coupled with a Finnigan Element 2 at the Goethe University in Frankfurt. The laser was used at a pulse frequency of 10 Hz and an energy pulse of 0.6 -0.8 mJ (corresponding to 60%-80% laser power) with spot sizes of 60-95 μm . NIST 612 glass was used as a calibration standard. USGS BIR-1 glass concentrations from Eggins et al., 1997) was the external and Ca from microprobe analysis of the minerals the internal standard. BIR-1 glass and one in-house garnet standard (PN2b) were measured several times within each sequence. The raw data were processed on-line using the GLITTER software.

For the analysis of the Lu/Hf and Sm/Nd isotopic systems the crushed mineral grains were first leached at room temperature in 6 M HCl or HNO_3 in an ultrasonic bath for about half an hour. The dried down fragments were hand-picked to optical purity and, if necessary, the acid ultrasonication repeated and the grains re-picked. Finally, 30 to 150 mg of garnet separates were ultrasonicated with MQ H_2O and dried prior to spiking with ^{176}Lu - ^{180}Hf and ^{149}Sm - ^{150}Nd tracers before dissolution. Our total procedural Hf blank measured for our methods were from 25 ± 5 pg for repeat measurements by isotope dilution (ID) ICP MS, which is necessary for measurement of the very low Hf concentrations. For those samples with Hf lower than 5 ng, blank corrections were carefully applied. Our total procedural Lu blank were from 5 ± 2 pg. The isotope ratios were analysed in a static mode with a multi collector ICP-MS (Finnigan Neptune). The sample amounts of Hf were always more than 3 ng. With our instrumental set up we are able to measure such low concentrations of Hf (3 ng result in a signal of ~ 90 mV on 176Hf) with a precision of around 1ϵ (on $^{176}\text{Hf}/^{177}\text{Hf}$). Repeated measurements of the Hf standard JMC475 produced $^{176}\text{Hf}/^{177}\text{Hf}$ of 0.282153 ± 0.000014 (2s), which is in good agreement with the literature (Blichert-Toft et al. 1997; Chu et al. 2002). Replicate digestion and analysis of BHVO-1 gave $^{176}\text{Hf}/^{177}\text{Hf} = 0.283107 \pm 0.000013$ (2s) which is in good agreement with the values reported by Blichert-Toft et al. 2001 and Bizzarro et al. 2003. Nd-isotope and Sm-ID measurements were also performed by MC ICP-MS. The Nd aliquots always contained more than 20 ng Nd. Such amounts could be measured with a precision of better than 0.5ϵ as determined by replicate standard measurements. Procedure blanks were lower than 70 pg for Nd and 25 pg for Sm. Repeated measurements of Nd isotope standards yielded $^{143}\text{Nd}/^{144}\text{Nd} = 0.511725 \pm 0.000068$ (2s) for Merck Nd_2O_3 and 0.5119538 ± 0.000026 for Ames-Nd. This is in good agreement with literature values (Deckart et al. 2005; Caro et al. 2006). Replicate digestion and analysis of BHVO-1 yielded $^{143}\text{Nd}/^{144}\text{Nd} = 0.512938 \pm 0.000017$ (2s). Uncertainties of Lu-Hf and Sm-Nd ratios and isotope compositions are based on replicate BHVO-1 standard solutions measurements are within 2ϵ for $^{176}\text{Hf}/^{177}\text{Hf}$ and $^{143}\text{Nd}/^{144}\text{Nd}$, and 0.33% for $^{176}\text{Lu}/^{177}\text{Hf}$ and 0.54% for $^{147}\text{Sm}/^{144}\text{Nd}$.

4. Sample description, chemical composition of garnet and cpx and geothermobarometry

4.1 Sample description

Eleven eclogite xenoliths with 3-6 cm in diameter from the coarse grained concentrate of the Bellsbank diamond mine were studied here. The primary minerals, garnet and clinopyroxene, are exceptionally fresh with less than 10% alteration products which are restricted to the grain boundaries and cracks. Most samples have secondary spongy rims of cpx around primary cpx cores. Altered areas are composed of fine grained phlogopite, serpentine, calcite and some microcrystalline material with dark and brownish colors. Grain sizes of garnets and clinopyroxenes range between 5 and 7 mm. All but one sample texturally belong to type II eclogites, as defined by MacGregor and Carter (1970) except sample (BE4) which is a type I eclogite.

In hand specimen, group A eclogites (3 samples) show pinkish garnets and light green clinopyroxenes. The modal abundances are somewhere between 50%:50% to 60%:40%. Group B1 eclogites (3 samples) appear similar to group A but garnets are more orangy and clinopyroxenes dark green. Also, relatively large phlogopites (plates of up to 4 mm) exist which appear primary. Group B2 eclogites (3 samples) have pale-orange garnets, buff-green clinopyroxenes (75:25) and two have kyanite and one corundum. The clinopyroxenes are most strongly altered at their rims compared to the other eclogite types. The two group A' eclogites have large and roundish orange garnets embedded in a matrix of irregular, smaller pale-green clinopyroxenes.

4.2 Major element mineral composition

Garnets and the original cores of the clinopyroxenes (inside the spongy rims) are extremely homogeneous in their major elements in each sample. There is no core-to-rim or inter-grain compositional variation. However, there is a considerable compositional range between the samples which confirms the range found by Shervais et al. (1988) and Taylor and Neal (1989) as shown in Figs.1 a,b. Average compositions are given in **Tables A.1** in the appendix in chapter 4.

Garnets plot in the fields A and B in the eclogite nomenclature scheme of Coleman et al. (1965). A larger number of the samples has relatively low grossular contents, but ranges from pyrope-rich to almandine-rich compositions, From there they extend to grossular-rich compositions (Fig. 1a). The latter are kyanite and corundum bearing. Cr₂O₃ contents range from 0.06 to 0.25 wt%, TiO₂ from 0.1 to 0.4 wt% and MnO from 0.2 (high T) to 0.5 wt% (low T).

Clinopyroxenes have a corresponding wide compositional variability as shown in Fig. 1b in a negative correlation of Na₂O versus MgO as an expression of the wide range of the jadeite component in these eclogites and garnet pyroxenites. The Cr₂O₃ contents vary from 0.06 to 0.34 wt%, TiO₂ from 0.04 to 0.5 wt% and MnO 0.1 to 0.03 wt%.

This compositional variability, the petrography, the trace elements and the isotopic compositions (see below) led us to introduce four subgroups A, A', B1 and B2: (1) group A' eclogites have highest MgO and lowest Na₂O (2) group A eclogites high MgO and low Na₂O (3) group B1 eclogites low MgO, highest FeO and intermediate Na₂O and (4) group B2 eclogites highest CaO and highest Na₂O (plus kyanite, or corundum).

Group B2 with their jadeitic clinopyroxenes are real eclogites, groups A and A' are garnet pyroxenites and group B1 are transitional.

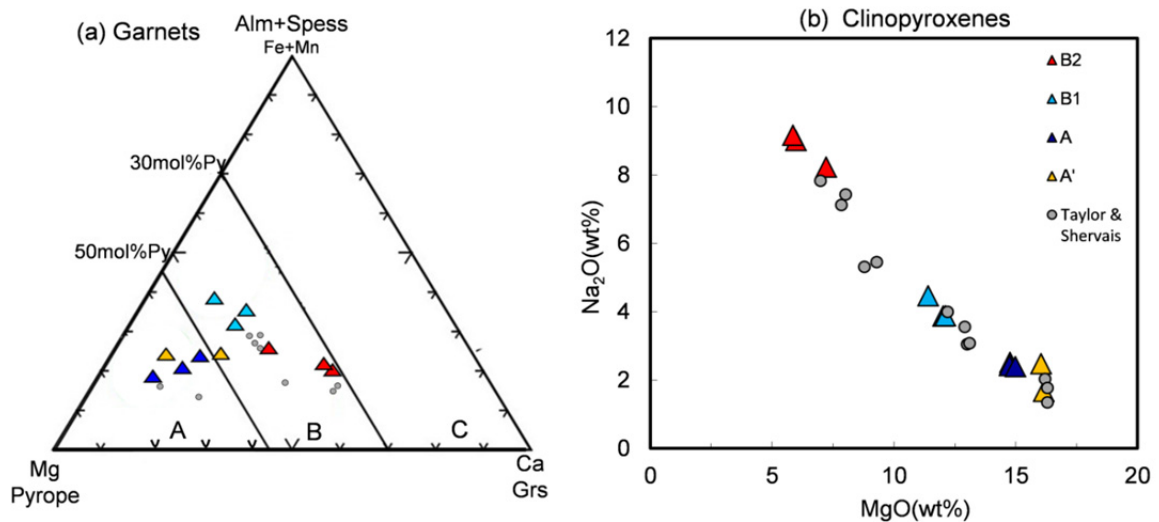


Fig.1 a,b Major element composition of garnets and clinopyroxenes. The small grey dots are data from previous work from Bellsbank (Taylor and Neal, 1989 and Shervais et al., 1988).

4.3 Garnet-clinopyroxene geothermobarometry

Only the original clinopyroxene cores were combined with the garnet compositions to estimate temperatures with the Fe²⁺-Mg exchange thermometer between garnet and clinopyroxene in the version of Krogh (1988). Uncertainties in the use of this thermometer are the influence of the possible presence of Fe³⁺ and, related to this, the presence of excessive amounts of an acmite (NaFe³⁺Si₂O₆) component. Purwin et al., (2012), accepted for publication in Contributions to Mineralogy and Petrology) showed experimentally in a Na-free system that the influence of Fe³⁺ for this thermometer is negligible because of a partition coefficient of about one for Fe³⁺ between garnet and clinopyroxene. Sodium potentially has an influence if it is incorporated into cpx as an acmite component. However, we find from Moessbauer spectroscopy (unpublished data) that Fe³⁺ is very low. Also, Al is high enough in our clinopyroxenes that all Na present can be incorporated as a jadeite component.

Temperatures were calculated by projecting the Krogh (1988) K_D's onto a 38 mW/m² conductive geothermal gradient (Chapman and Pollack, 1977) in an iterative way with the help of the inhouse PTEXL spreadsheet in the version provided by T. Stachel. This gradient is suggested to be valid for Bellsbank (Garden et al., 8th International Kimberlite Conference) and is similar to Newlands, which is situated 30km to the southeast (Menzies et al., 1999). The results of calculated temperatures

of crystallization together with the estimated pressures are presented in Table.1 and shown in Fig. 2. Group B2 give the highest temperatures between 1050-1150°C and 5.5-6.5 GPa and group A the lowest around 825°C at 3.5-4.0 GPa. Groups B1 and A' give intermediate temperatures between 850-1000°C at intermediate pressures between 4.2-5.2 GPa.

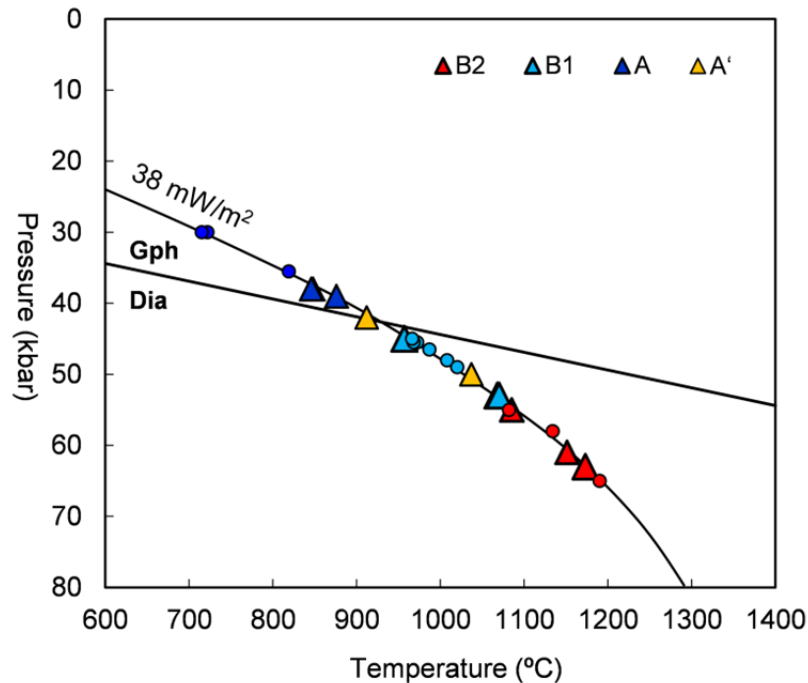


Fig.2 Temperatures were calculated according to Krogh (1988) by projecting it in an iterative onto the 38 mW/m² conductive geothermal gradient of Chapman and Pollack (1977). Triangles with various colors present data of various groups from this study and the small grey dots are data from previous study (Taylor and Neal, 1989 and Shervais et al., 1988).

4.4 Trace elements

Trace elements are reported in the previous chapter 4. We only show the range of the primitive mantle (McDonough and Sun, 1995) normalized REE + Zr and Hf patterns of the four groups A+ B1 and A'+B2 in Fig. 3. Garnets from groups A and B1 have extremely fractionated REE patterns with very high HREE and very low LREE and Zr+Hf. The REE patterns in the corresponding clinopyroxenes slope oppositely whereby the LREE are overabundant compared to the MREE and HREE. A' and B2 garnets have low REE abundances, flat MREE and HREE and are depleted in LREE. The corresponding cpx REE patterns also slope negatively, but B2 clinopyroxenes have the lowest and A' clinopyroxenes the highest REE abundances. Nevertheless, the partitioning of the REE between garnet and clinopyroxene appears to be in equilibrium as indicated by the coincidence of the slopes of the REE partition coefficients between our rocks and published experimental results (e.g. Green et al. 2002). The range of partition coefficients of REE exceeds the experimental range by far and appears to be almost solely a function of the jadeite component in cpx and far less of P and T (not shown). The Lu/Hf ratios in the garnets (and of calculated bulk rocks) of groups A and B1 are very

high which lead to a fast growth of the $^{176}\text{Hf}/^{177}\text{Hf}$ ratio. Two of the B2 samples have positive Eu anomalies in both garnet and clinopyroxene.

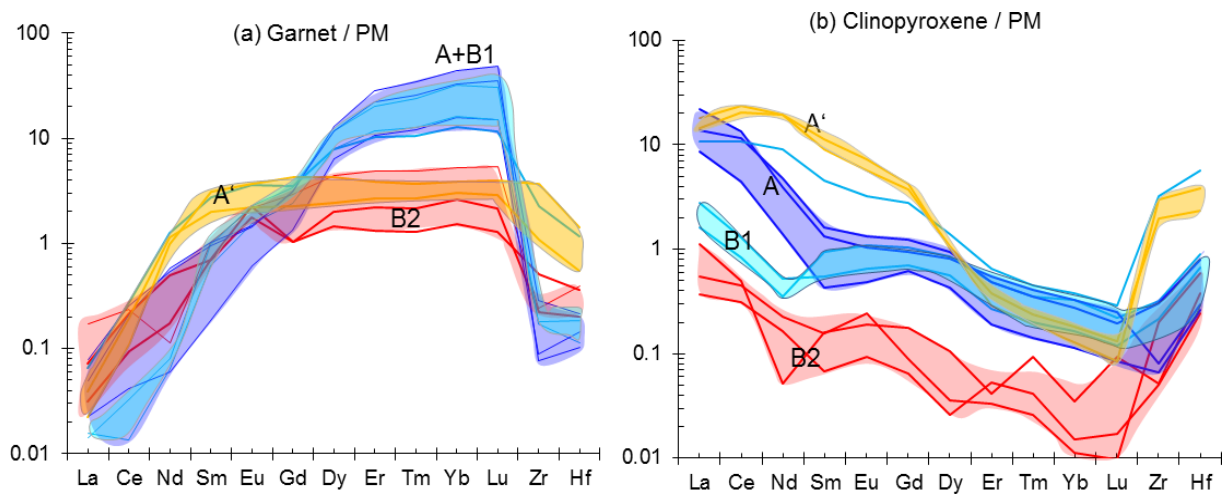


Fig.3 Primitive mantle (McDonough & Sun, 1995) normalized trace element patterns + Zr and Hf of (a) garnets and (b) clinopyroxenes from Bellsbank eclogites. The colored bands highlight the range of each of the four types which were distinguished from their petrography and major and trace element abundances. The REE patterns indicate similarities between groups A (dark blue shaded) and B1 (light blue shaded) and groups B2 (red shaded in red) and A' (yellow shaded).

5. Isotopic results

The Sm-Nd, Lu-Hf and Sr isotope ratios were determined in ten of the eleven samples analyzed for major and trace elements. The Lu-Hf and Sm-Ns isotope data is shown in table A.4 in chapter 4. The Sm-Nd and Lu-Hf two-point isochron ages are shown in table 1(below) together with variable literature data.

5.1 The Sm-Nd isotope system

The results (including ϵNd values corrected back to the time of kimberlite eruption at 120 Ma ago) are given in **Table A.5b in chapter 4** and shown in isochron diagrams in Figs.4 a,b. Because the $^{143}\text{Nd}/^{144}\text{Nd}$ ratios have an extreme range, the figure is split into two for clarity reasons. Coexisting garnets and clinopyroxenes are connected by tie lines and calculated two-point isochron ages are given for each sample. The ages vary from the eruption age of the Bellsbank fissures (≈ 120 Ma) up to 1.6 Ga. The lower temperature samples generally give ages older than the eruption ages (up to 885 Ma) and the higher temperature samples give ages closer to eruption age except one high-T group A' sample (BE9) with 1.6 Ga. The Nd-isotope ratios of all samples are high to very high compared to the present-day primitive or depleted mantle as already noted in the work of Taylor and Neal (1990). On

average, group B2 eclogites (red triangles in Fig. 4a) have the most radiogenic Nd isotope ratios. Sample BE11 has the most extreme values with $\epsilon\text{Nd} = +550$ in garnet and $\epsilon\text{Nd} = +417$ in clinopyroxene (today's ϵNd in N-MORB's is around 10). Group B1 samples (light blue triangles) also can have very high Nd isotopic ratios like sample BE2 with $\epsilon\text{Nd} = +250$ in garnet and $\epsilon\text{Nd} = +217$ in clinopyroxene. The group A garnet pyroxenites (dark blue triangles) have much less radiogenic Nd with $\epsilon\text{Nd} +12$ in cpx and ϵNd of +30 in garnet as the highest in this group. Group A' garnet pyroxenites (yellow triangles) are the least radiogenic with $\epsilon\text{Nd} = +7$ in garnet and -2 in cpx.

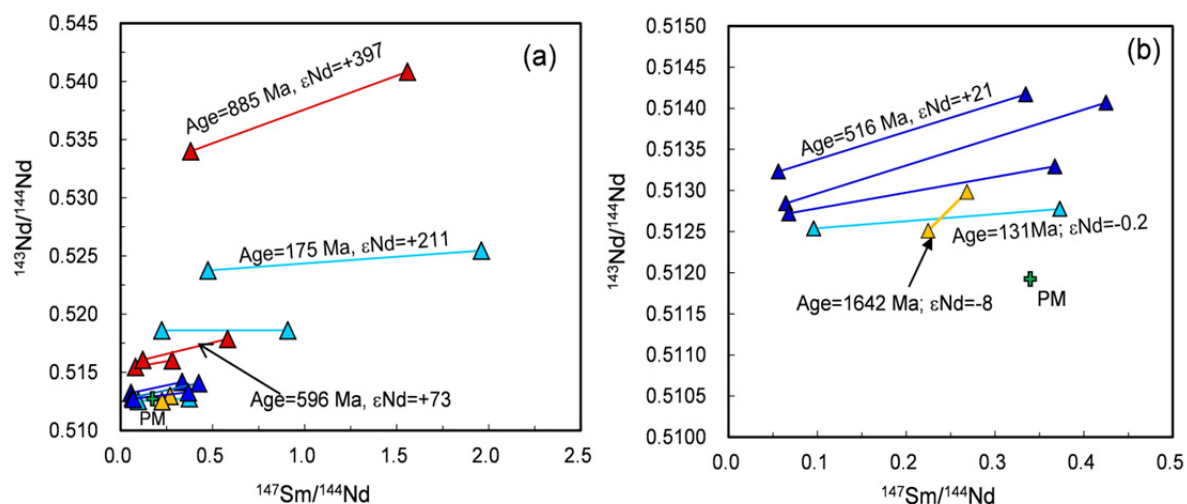


Fig.4a,b. The results of the Sm-Nd isotope measurements plotted into isochron diagrams. Coexisting clinopyroxenes and garnets are connected by tie-lines and two-point isochrone ages were calculated from them. Ages together with the initial ϵNd are given for some of them. The green cross presents as the present-day primitive mantle value. Fig.4.b is a blow-up Fig.4.a.

5.2 The Lu-Hf isotope system

The results (including ϵHf values corrected back to the time of kimberlite eruption at 120 Ma ago) are given in **Table A.5a in chapter 4** and shown in isochron diagrams in Figs. 5 a, b. The differences between the various groups are more apparent in the Lu-Hf than in the Sm-Nd isotope system. Overall, young and close to kimberlite eruption ages are obtained from the higher temperature eclogites and older than eruption ages are gained from the low-T samples, group A and B1 from 288 Ma to 810 Ma. Only sample BE4 from group B1 with a high temperature of 1033 °C gives a too young age of $23 \pm 1\text{Ma}$. The younger age from sample BE4 can result from later enrichment of Hf which observed in both garnet and clinopyroxene. This age may present a mixed information of Hf isotope between the original bulk rock and the enrichment agent. Two of the group B2 samples give eruption age, $\sim 120\text{Ma}$, while sample BE6 gives a significantly older age of 1.6Ga but still with a high initial ϵHf of +519. Group A' eclogite BE9 yields an eruption age of 120Ma. The Hf isotope compositions of all samples are very high to extreme. The BE 8 sample has the most extreme values of + 13754 in garnet, and +6518 in cpx, to our knowledge the highest value reported for eclogites. The group A garnet

pyroxenites have the highest ϵ_{Hf} values, followed by the two low-temperature B1 samples and the by B2 eclogites. The A' and the one high-T B1 sample (enriched, BE4) have lowest ϵ_{Hf} as for ϵ_{Nd} values.

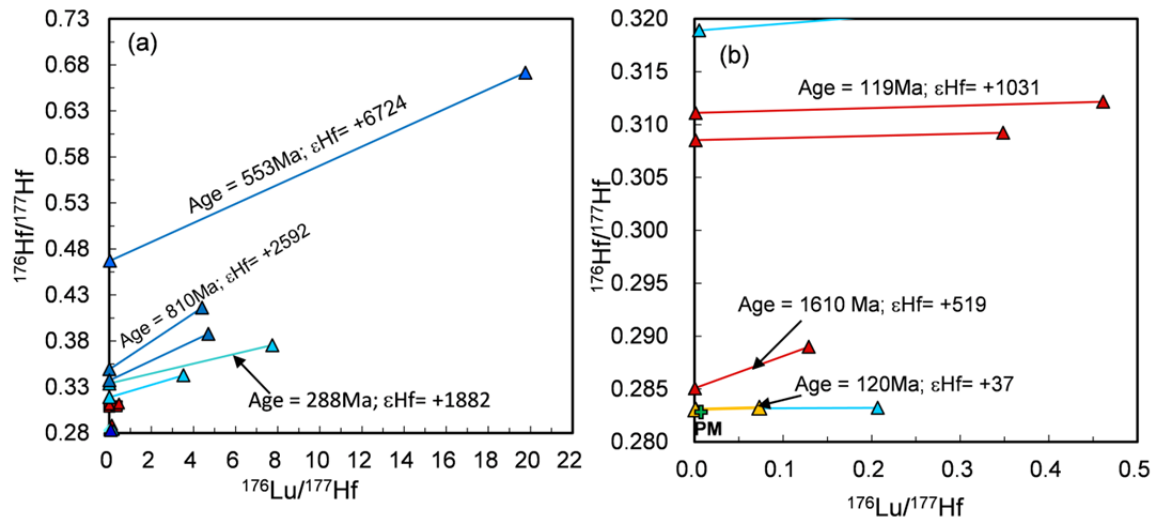


Fig. 5 a,b. The Lu-Hf two-point isochrone ages from Bellsbank eclogites and garnet pyroxenites. The green cross presents as the present-day primitive mantle value. Fig.5.b is the more detail of part of Fig.5.a (scale from X axis: 0-0.5, Y axis: 0.280 - 0.320)

Location	eruption age(Ma)	type(group)	sample	T [Krogh88](°C)	P(kb)	Lu-Hf age (Ma)	Sm-Nd age (Ma)
Bellsbank	120	B2	BE1	1151	61	104±1	434±6
Bellsbank	120	B2	BE6	1085	55	1549±14	596±92
Bellsbank	120	B2	BE11	1173	63	119±2	885±12
Bellsbank	120	B1	BE2	957	45	277±1	175±30
Bellsbank	120	B1	BE5	1068	53	348±1	110±1
Bellsbank	120	B1	BE4	1070	53	127±1	131±2
Bellsbank	120	A	BE3	848	38	779±2	516±62
Bellsbank	120	A	BE8	876	39	532±2	519±6
Bellsbank	120	A	BE10	846	38	552±1	292±4
Bellsbank	120	A'	BE9	912	42	116±3	1642±130
*Bellsbank	120	A	438-7	968	45		97±45
*Bellsbank	120	A	438-2	972	45		33±8
*Bellsbank	120	A	437-1	715	30		287±96
*Bellsbank	120	A	437-2	722	30		355±10
*Bellsbank	120	B	2791-21	1134	58		671±18
*Bellsbank	120	C	437-5	1008	48		1608±25
*Bellsbank	120	C	437-7	1082	55		863±110
*Bellsbank	120	C	2791-34	1020	49		767±23
*Diavik	55	Low-T	MX2	773	33	1411±11	1211±22
*Diavik	55	Low-T	MX7	813	35	1469±8	1427±14
*Diavik	55	Low-T	MX9	826	35	1104±6	380±7
*Diavik	55	Low-T	MX15	755	32	1450±8	785±27
*Diavik	55	Low-T	MX45	764	33	460±3	96±8

Table 1 continued							
Location	Eruption age(Ma)	Type /Group	Sample	T [Krogh88](°C)	P(kb)	Lu-Hf age (Ma)	Sm-Nd age (Ma)
*Roberts Victor	120	Type II	BD1191	1350	75	1402±7	903±5
*Roberts Victor	120	Type II	DEJ5	1182	65	2230±13	1194±5
*Roberts Victor	120	Type I	BD1175	1008	48	477±28	221±38
*Roberts Victor	120	Type I	BD3699	1148	60	351±120	110±13
*Roberts Victor	120	Type I	RV1	994	48	199±55	-0.9
*Roberts Victor	120	Type I	HRV247	1050	51	226±62	146±14
**Roberts Victor	120	Type II	R30	730	31	1953±13	963±42
**Roberts Victor	120	Type II	DEJ02	1315	85	227±47	245±25
**Roberts Victor	120	Type II	DEJ03	975	46	129±12	208±19
*Roberts Victor	120	Type I	RV07/02	1117	57	150±40	109±29
*Roberts Victor	120	Type I	RV07/03	1316	80	118±32	89±26
*Roberts Victor	120	Type I	RV07/09b	1084	55	144±24	103±17
*Roberts Victor	120	Type I	RV07/13	1093	55	140±21	115±22
*Roberts Victor	120	Type I	RV07/20	1105	55	108±1	101±18
*Roberts Victor	120	Type I	RVF6	1030	50		148±8
*Roberts Victor	120	Type I	RVF8	1096	55		236±23
*Roberts Victor	120	Type I	RV07/01	1110	55	112±32	92±15
*Roberts Victor	120	Type I	RV07/07	1136	60		102±16
*Roberts Victor	120	Type I	RV07/11	1101	55	144±36	58±17
*Roberts Victor	120	Type I	RV07/14	1133	60	128±29	113±42
*Roberts Victor	120	Type I	RV07/16	1189	65	127±36	101±17
*Roberts Victor	120	Type I	RV07/18	1141	60	145±52	96±43
*Roberts Victor	120	Type I	RV07/19	1170	62	115±30	93±11
*Roberts Victor	120	Type I	RV07/22	1134	60	158±35	127±35
*Roberts Victor	120	Type I	RV07/29b	1145	60	131±22	103±16
*Roberts Victor	120	Type I	HRV 247C	1133	60		140±13
*Roberts Victor	120	Type I	HRV 77bimin	1237	70	52.5±9.9	104±13
*Roberts Victor	120	Type I	RV07/17	1135	59	198±30	209±36
*Roberts Victor	120	Type II	RV07/12	951	45	1282±100	831±52
*Roberts Victor	120	Type II	RV73/12	952	45	764±94	
*Roberts Victor	120	Type II	RV07/08	1203	65	1148±120	792±25
*Lovedale	74-130		2073	1050	52	161±3	76±3
*Lovedale	74-130		2093	1300	80	120±1	89±3
*Roodekraal	74-130		RDK1	1190	65	778±3	441±2
*Roodekraal	84		B21	923	42	164±13	24±9
*Bultfontein	84		B21	923	42	164±13	24±9
*Bultfontein	85		713	820	36	981±4	173±5
*Malaita	44		RG01	1100	56	69±11.7	42±6

Table 1 The two-point Lu-Hf and Sm-Nd isochrone ages from the Bellsbank eclogites from this study and the data from the literature (with *) from various localities. (*Roberts Victor data is from Jacob et al., 2005 and Huang et al., 2012; *Bellsbank data is from Shervias et al.,1989 and Taylor and Neal,1990; **Roberts Victor,*Lovedale,*Roodekraal,*Roodekraal, *Bultfontein and *Malaita data is from Gonzaga et al., 2010; *Diavik data is from Schmidberger et al., 2007).

6. Discussion

6.1 The meaning of the two-point isochrones and closure temperatures

The origin of the eclogites and garnet pyroxenites is discussed in the previous chapter 4. The kyanite or corundum bearing eclogites (group B2) are interpreted as plagioclase-rich cumulates from basaltic precursors based on their flat HREE patterns, their very low HREE contents and their positive Eu-anomalies. The group A' garnet pyroxenites have flat HREE patterns with an increase in the LREE and abundances similar to MORB. Group A and B1 garnet pyroxenites are interpreted as restites of melting of boninite-like precursors. Our small sample set with simple garnet-cpx assemblies consists of very diversified lithologies which appear to be correlated with their depth of origin (see Fig. 2) and the age of the Lu-Hf two-point isochrones (Fig.6). The ages decrease with increasing temperature up to about 900°C from whereon they are roughly constant. This is not visible for the Sm-Nd two-point isochron ages from our data alone (Fig.7). They also give old ages below 900°C and eruption ages above but also very old ages at these temperatures. What then is the meaning of two-point isochrones from rocks which were residing in a mantle which supposedly was in a steady-state since at least 2.5 Ga?

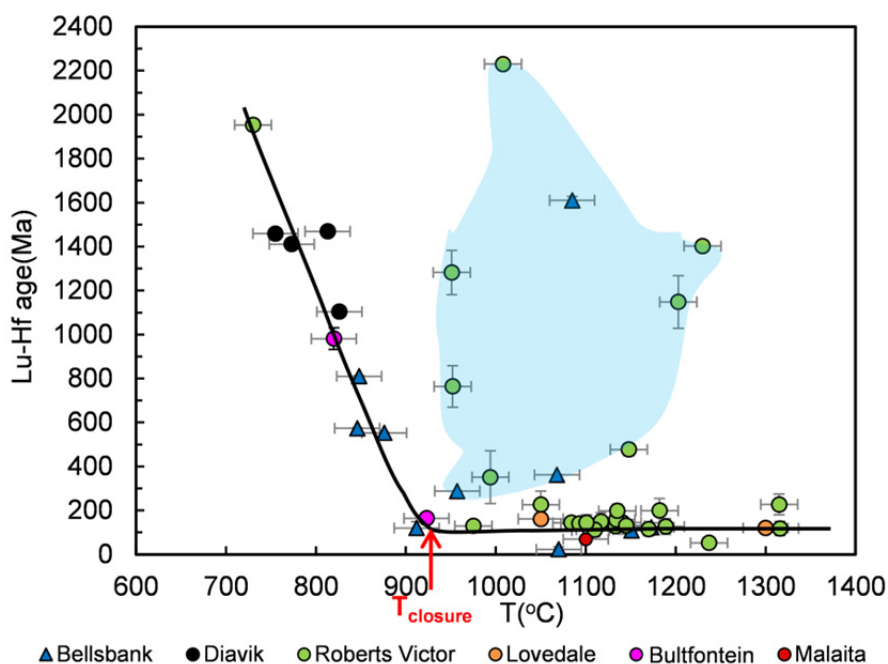


Fig.6 Correlation of Lu-Hf two point isochrone ages and the calculated temperature of our samples and sample from the literature. One population of low-T samples show ages decreases with increasing temperature until 920 °C followed by a substantial number of samples which give constant ages close to the eruption age at higher temperatures as indicated by the black line. We propose a closure temperature for the Lu-Hf system around 920 °C at the bend of the black line (indicated by the red arrow). The field shaded by blue comprises high-T samples with old, but meaningless ages which were probably caused by a recent preferred enrichment of clinopyroxene. The different symbols with various colors are samples from various localities (see legend). Data are from Schmidberger et al. (2007; Diavik); Jacob et al. (2005) and Huang et al. (2012; Roberts Victor), Lovedale, Bultfontein and Malaita (summarized by Gonzaga et al, 2007).

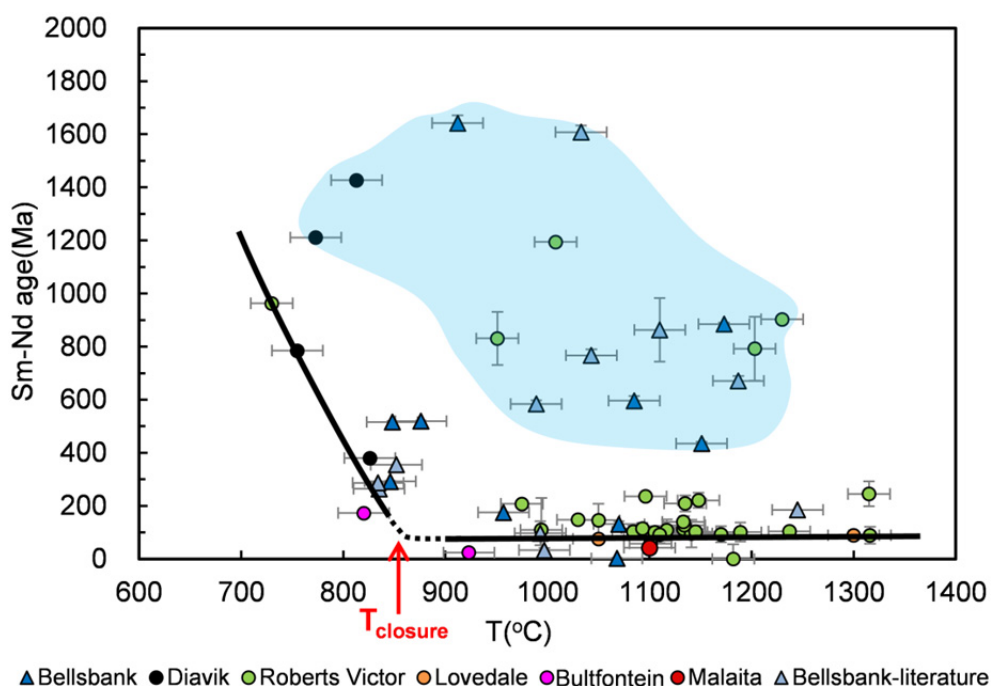


Fig.7 Correlation of Sm-Nd two point isochron ages and the calculated temperature of our samples and sample from the literature. One population of low-T samples show ages decreases with increasing temperatures until around 840 °C followed by a substantial number of samples which give constant ages close to eruption age with increasing temperatures, as indicated by the black line. Consequently, we propose the closure temperature for the Sm-Nd system around 840 °C at the bend of the black line (indicated by the red arrow). The field shaded by blue comprises of high-T samples with old but meaningless ages probably due to recent preferred enrichment of clinopyroxene. See legend for the symbols. Bellsbank: Taylor and Neal, 1990 and Shervais et al.1988; Diavik: Schimderberg et al. (2007); Roberts Victor: Jacob et al. (2005) and Huang et al. (2012); Lovedale, Bultfontein and Malaita from a compilation by Gonzaga et al. (2007)

We have compiled our own new data for Lu-Hf and Sm-Nd for Bellsbank eclogites and garnet pyroxenites with data from the literature (Fig.6, 7). Complete isotope data sets with major element compositions exist from Diavik in Canada (Schmidberger et al., 2007), Malaita from the Solomon Islands (Gonzaga et al, 2010), Roberts Victor, Lovedale and Bultfontein in South Africa (Jacob et al., 2005, Gonzaga et al, 2010 and Huang et al., 2012) and from Bellsbank (Shervais et al., 1988 and Taylor and Neal, 1990). We have recalculated the P,T-conditions of origin in the same way as for our samples and have also used a 38 mW/m² conductive continental geothermal gradient. It can be seen best for Lu-Hf that an envelope is formed around a cloud of young to old ages with an oblique low temperature limb below about 920°C (840°C for Sm-Nd) and, above these temperatures, a line which corresponds to the kimberlite eruption ages (around 120 Ma for the south African occurrences; Fig. 6,7). We consider these temperatures at the intersects as closure temperatures of the respective isotope systems and interpret the ages along the low temperature limbs as cooling ages. The samples with kimberlite eruption ages were in continuous equilibrium above the closure temperature until the time of eruption. All other old ages from high-T samples are artificial due to a preferred and relatively recent disturbance of clinopyroxene and possibly also due to difficulties of obtaining clean enough cpx

separates (symbols within the blue shaded areas in Fig.6,7). It is also important to note, that the Lu-Hf ages are almost always older than the Sm-Nd ages for individual samples (Fig. 8) which supports the findings of a higher closure temperature for the Lu-Hf system than for the Sm-Nd system.

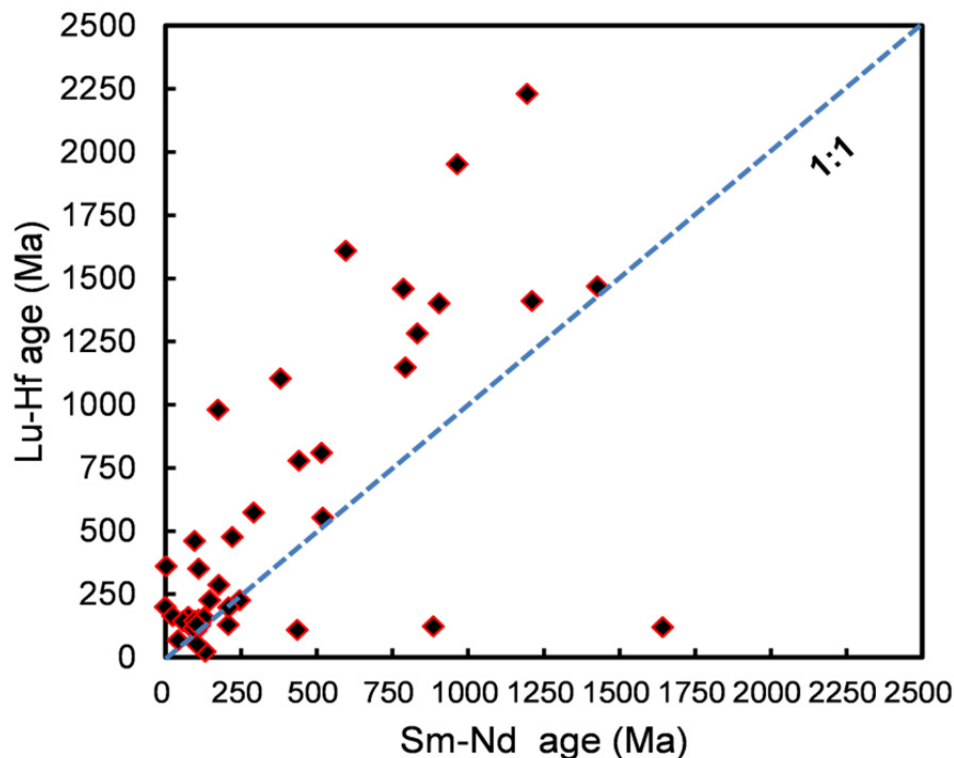


Fig.8 Diagram of Sm-Nd two-point isochrones against Lu-Hf two-point isochron ages from this study and existing literature data. The black dashed line is the 1:1 correlation line.

6.2 Constraints on the cooling of the subcratonic mantle- inference from the two isotopic systems

The difference for each sample in the cooling ages of the two isotopic systems can be used to make deductions about the cooling of the subcratonic mantle from the Proterozoic until today. We assume in a first step that Archean cratons and their mantle were a stable assembly since 2.5 Ga and that the depth from which the eclogites were derived by the kimberlites is the same as 2.5 Ga ago. If we take, e.g. sample RV30 with a 2 Ga Lu-Hf and a 0.96 Ga Sm-Nd cooling age and a present day temperature of around 700 °C along a 38 mW/m² geothermal gradient (Table1 and Fig. 9) we must deduce that its temperature was 920 °C two Ga ago (the closure temperature for the Lu-Hf system) and 840 °C (the closure temperature for Sm-Nd) 1 Ga ago, i.e. that this part of the mantle cooled by ~80°C within 1 Ga. We can extend this approach to three further samples along the cooling limbs in Figs. 6.7 and plot them into Fig.9 (where they are shown with their respective cooling ages noted next to them). If we then superimpose the conductive geothermal gradients as given by Chapman and Pollack (1977) onto these points, we find that the 2 Ga age point lies on the 46 mW/m² geothermal

gradient, the ~1 Ga age points close to 42 mW/m² and that with an eruption age for Sm-Nd on the 38 mW/m. From this, we infer that the subcratonic mantle cooled since 2 Ga from a geothermal gradient corresponding to 46 mW/m² to 38 mW/m² 120 Ma ago. By using the age differences for Lu-Hf and Sm-Nd of each sample and the difference between the closure temperatures, we derive cooling rates between 80 to 110 °C/Ga. This range is consistent with estimates by Michaut et al. (2007) based on considerations of the heat production by radiogenic elements in a depleted mantle and an Archean crust and the heat decay by conduction in a depleted mantle. These cooling rates are also within the 40–105 °C/Ga range deduced by Bedini et al., (2004) from model calculations for garnet peridotites from southern Africa on the basis of assumed grain sizes, initial thermal conditions at the time of oldest Re-depletion ages and garnet Sm–Nd ages.

Since when, from which thermal regime and why is the subcratonic lithospheric mantle cooling? Age constraints for the Kaapvaal W-Block are the oldest Re-depletion ages of up to 3.2 Ga (Menzies et al., 1999) for the mantle, 3.1 Ga for the crust and the oldest cooling age of 2 Ga for the Roberts Victor garnet pyroxenite RV30. The latter is a firm age but also only a minimum age for eclogites and garnet pyroxenites from southern Africa, The ages for the protolith may be obtained from model ages for the Lu-Hf system. Yet they depend on the validity of the assumption of a primitive Earth mantle as a reference and on the grt:cpx ratios which are used for calculating bulk rocks. We can show from trace element abundances (Shu et al., 2012) that group A' and B2 garnet pyroxenites resp, eclogites are chemically little changed metamorphic equivalents of MORB lithologies and will yield reliable model ages. Three of four of the A' and B2 samples give Lu-Hf model ages around 4.1 Ga ages (see also previous chapter 4). Model ages from their garnets are minimum ages and reach up to 3.5 Ga, We therefore argue that these samples are the witnesses of the oldest processes in the subcratonic mantle where they were metamorphosed in the eclogite facies.

A subduction (-like) process will bring the water-rich and cooler slabs into a hotter mantle. Thermal equilibration will first lead to devolatilisation and partial melting in the slab and the surrounding mantle with effective heat loss during this process. In a scenario where a plume model is applied for the formation of the subcratonic mantle thermal equilibration is basically by cooling. Michaut et al, (2007) states that, independent of the initial conditions of formation of the mantle, the initial thermal conditions in the Archean are out of equilibrium. It will take about 1 Ga to reach a stable thermal state of the lithospheric mantle which may be a period in the time span between 4.1 and 2.5 Ga. The cooling recorded in the eclogites and garnet pyroxenites reflects the state after thermal equilibration.

The study of eclogites and garnet pyroxenites from the mantle may contribute to the ongoing discussion of closure temperature in metamorphic rocks. The mantle rocks have the advantage over crustal eclogites that minerals are mostly unzoned, that they have very rarely inclusions like zircon or monazite and generally were at stable or very slowly changing P, T conditions for a very long time period. Closure temperatures derived from them should therefore be the minimal possible temperatures. Most metamorphic processes (except in the granulite and hornfels facies) take place at lower temperatures and cooling rates in the crust are much faster than in the mantle. Both Sm-Nd and Lu-Hf ages from grt-cpx pairs or different growth generations of garnet therefore must report ages of

progressive metamorphism. However, Sm-Nd ages are mostly younger than Lu-Hf ages (e.g. Schmidt et al., 2008). The younger ages generally were interpreted as retrogressed ages in agreement with the faster diffusion rates of the Sm-Nd compared to the Lu-Hf couple. The high closure temperatures for both systems derived in this study disagree with this interpretation but support the model of Skora et al. (2005, 2006). They interpret the age difference as reflecting prolonged growth of zoned garnets which incorporate the REE differentially (Lu maxima in the cores and Nd maxima further along towards the rims). Both ages are then ages of progressive metamorphism.

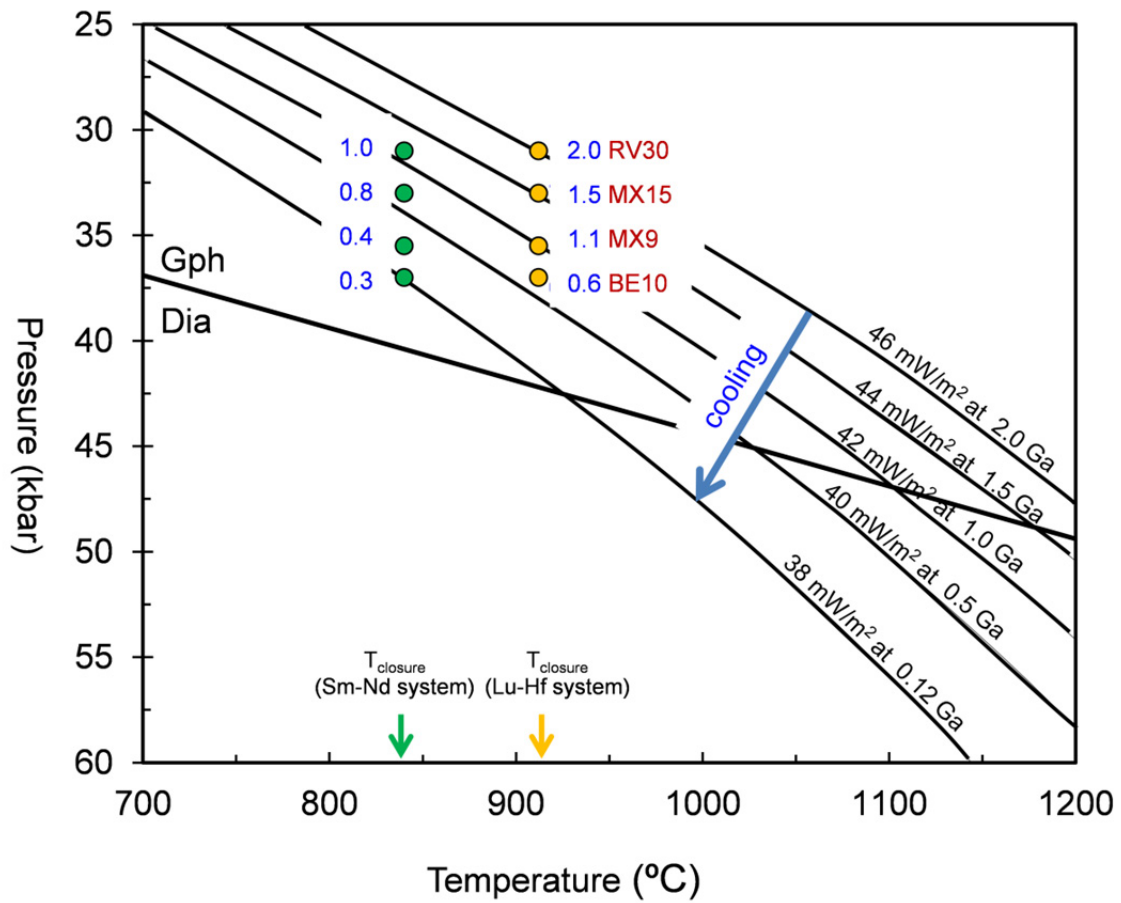


Fig.9 The cooling of the subcratonic mantle since the Proterozoic. The cooling corresponds to a decrease of a geothermal gradient from 46 mW/m² at around 2 Ga to 38 mW/m² at 120 Ma ago and a cooling rate between 80 to 110 °C/Ga).

References

- Aulbach S., Pearson N.J., O'Reilly S.Y. and Doyle B.J., 2007, Origins of xenolithic eclogites and pyroxenites from the central Slave Craton. Canada. *Journal of Petrology* **48**, 1843-1873.
- Barth M., Rudnick R.L., Horn I., McDonough W.F., Spicuzza M., Valley J.W. and Haggerty S.E., 2001, Geochemistry of xenolithic eclogites from West Africa, part I: a link between low MgO eclogites and Archean crust formation. *Geochim Cosmochim Acta* **65**, 1499–1527.
- Bedini, R.M. Blichert-Toft, J., Boyet, and M. Albarede; F., 2004, Isotopic constraints on the cooling of the continental lithosphere. *Earth Planet. Sci. Lett.* **223**, 99–111.
- Boyd, F.R., 1989, Compositional distinction between oceanic and cratonic lithosphere. *Earth Planet. Sci. Lett.* **96**, 15–26.
- Caporuscio, F.A. and Smyth, J.R., 1990, Trace element crystal chemistry of mantle eclogites. *Contrib. Mineral. Petrol.* **105**, 550–561.
- Chapman, D.S., Pollack H.N., 1977, Regional geotherms and lithospheric thicknesses. *Geology* **5**, 265-268.
- Coleman, R.G., Lee, D.E., Beatty, L.B., Brannock, W.W., 1965. Eclogites and eclogites: their differences and similarities. *Geol. Soc. Amer. Bull.* **76**, 483–508.
- Dodson M.H., 1986, Cooling profile in cooling system. *Materials Science Forum Vol.7*, pp 145-154.
- Dodson M.H., 1973, Closure temperature in cooling Geochronological and petrological systems. *Contrib. Mineral. Petrol.* **40**, 259–274.
- Ganguly J., Tirone M., and ig, R. L., 1998, Diffusion Kinetics of Samarium and Neodymium in Garnet, and a Method for Determining Cooling Rates of Rocks, DOI: *Science* **281**, 805.
- Ganguly J. and Tirone, 2001, Relationship between cooling rate and cooling age of a mineral: Theory and applications to meteorites. *Meteoritics & Planetary Science* **36**, 167-175.
- Garden, P.B., Carlson, W.R., Shirey B.S. and Gurney J.J., 2003, Re-Os systematics of lithospheric peridotites and eclogites from the Bobbejaan and Bellsbank Dykes, Kaapvaal Craton. 8th International Kimberlite Conference.
- Gonzaga R.G., Menzies M.A., Thirlwall M. F., Jacob D. E., and Leroex A., 2010, Eclogites and Garnet Pyroxenites: Problems Resolving Provenance Using Lu-Hf, Sm-Nd and Rb-Sr Isotope Systems. *Journal of Petrology* **51**, 513-535.
- Green, T.H., Blundy, J.D., Adam, J. and Yaxley, G.M., 2000, SIMS determination of trace element partition coefficients between garnet, clinopyroxene and hydrous basaltic liquids at 2–7.5 GPa and 1080–1200 °C. *Lithos* **53 (3–4)**, 165–187.
- Griffin, W.L. and O'Reilly, S.Y., 2007, Cratonic lithospheric mantle: is anything subducted? *Episodes* **30 (1)**, 43–53.
- Gurney, J.J., Moore, R.O., Otter, M.L., Kirkley, M.B., Hops, J.J. and McCandless, T.E., 1991, Southern African kimberlites and their xenoliths. In: Kampunzu, A.B., Luballa, R.T. (Eds.), *Magmatism in Extensional Structural Settings*. Springer, pp. 495–536.
- Hatton, C.J. and Gurney, J.J., 1987. Roberts Victor eclogites and their relation to the mantle. In: Nixon, P.H. (Ed.), *Mantle Xenoliths*. Wiley, London, pp. 453–463.
- Helmstaedt, H. and Doig, R., 1975, Eclogite nodules from kimberlite pipes in the Colorado plateau—samples of subducted Franciscan type oceanic lithosphere. *Phys. Chem. Earth* **9**, 95–111 (First international conference on kimberlites).
- Herzberg, C. and Rudnick, R.L., 2012, Formation of cratonic lithosphere: An integrated thermal and petrological model. *Lithos*, doi:10.1016/j.lithos.
- Huang J.X., Gréau Y., Griffin, W.L., O'Reilly, S.Y. and Pearson N. J., 2012, Multi-stage origin of Roberts Victor eclogites: Progressive metasomatism and its isotopic effects. *Lithos*, **142–143**, 161-181.
- Ireland, T.R., Rudnick, R.L. and Spetsius, Z., 1994, Trace elements in diamond inclusions reveal links to Archean granites. *Earth Planet. Sci. Lett.*, **128**, 199–213.
- Jacob, D.E., Bizimis, M. and Salters, V.J.M., 2005, Lu/Hf and geochemical systematics of recycled ancient oceanic crust: evidence from Roberts Victor eclogites. *Contrib. Mineral. Petrol.* **148 (6)**, 707–720.
- Jacob, D.E. and Foley, S.F., 1999, Evidence for Archean ocean crust with low high field strength element signature from diamondiferous eclogite xenoliths. *Lithos* **48**, 317–336.
- Jacob, D.E., Schmickler, B. and Schulze, D.J., 2003, Trace element geochemistry of coesite-bearing eclogites from the Roberts Victor kimberlite, Kaapvaal craton. *Lithos* **71**, 337–351.

- Jacob, D.E., 2004, Nature and origin of eclogite xenoliths from kimberlites. *Lithos* **77**, 295–316.
- Jagoutz, E., Dawson, J.B., Hoernes, S., Spettel, B. and Wanke, H., 1984, Anorthositic oceanic crust in the Archean Earth. 15th Lunar Planet. Sci. Conf., pp. 395–396. Abs.
- Kesson, S.E. and Ringwood, A.E., 1989, Slab-mantle interactions 2. The formation of diamonds. *Chemical Geology* **78**, 97-118.
- Kramers, J.D., 1979, Lead, uranium, strontium, potassium and rubidium in inclusion-bearing diamonds and mantle-derived xenoliths from Southern Africa. *Earth Planet. Sci. Lett.* **42**, 58–70.
- Krogh, E.J., 1988, The garnet-clinopyroxene Fe-Mg geothermometer – A reinterpretation of existing experimental data. *Contrib. Mineral. Petrol.* **99**, 44-48.
- Lazarov, M., Brey G.B. and Weyer S. (2009) Time steps of depletion and enrichment in the Kaapvaal craton as recorded by subcalcic garnets from Finsch (SA). *Earth Planet. Sci. Lett.* **27**, 1–10.
- MacGregor, I.D. and Manton, W.I., 1986, Roberts Victor eclogites: ancient oceanic crust. *J. Geophys. Res.* **91** (B14), 14063-14079.
- MacGregor, I.D. and Carter, J.L., 1970, The chemistry of clinopyroxenes and garnets of eclogite and peridotite xenoliths from the Roberts Victor mine, South Africa. *Phys. Earth Planet. Inter.* **3**, 391–397.
- McDonough, W. F. & Sun, S.-S., 1995, The composition of the Earth. *Chemical Geology* **120**, 223-253.
- Menzies, A.H., Carlson, R.W., Shirey, S.B., and Gurney, J.J., 1999, Re-Os systematics of Newlands peridotite xenoliths: implications for diamond and lithosphere formation. In: J.J. Gurney, J. L. G., M.D. Pascoe and S.H. Richardson, eds., *Proceedings of the 7th International Kimberlite Conference*, Red Roof Design, Cape Town, 566-573.
- Michaut, C. and Jaupart C., 2007, Secular cooling and thermal structure of continental lithosphere. *Earth Planet. Sci. Lett.* **257**, 83–96.
- Neal C. R., Taylor A. L., Davidson P. J., Holden P., Halliday N. A., Nixon H. P., Paces B. J., Clayton R. N., and Mayeda K. T., 1990, Eclogites with oceanic crustal and mantle signatures from the Bellsbank kimberlite, South Africa, part 2: Sr, Nd, and O isotope geochemistry. *Earth Planet. Sci. Lett.* **99**, 362-379.
- O'Hara, M.J. and Yoder, H.S., 1967, Formation and fractionation of basic magmas at high pressure. *Scott. J. Geol.* **3**, 67–117.
- O'Hara, M., 1969, The origin of eclogite and aegirite nodules in basalt. *Geol. Mag.* **106**, 322–330.
- O'Hara, M.J., Saunders, M.J., Mercy, E.L.P., 1975, Garnet–peridotite, primary ultrabasic magma and eclogite; interpretation of upper mantle processes in kimberlite. *Phys. Chem. Earth* **9**, 571–604 (First international conference on kimberlites).
- Pearson, D.G., Snyder, G.A., Shirey, S.B., Taylor, L.A., Carlson, R.W. and Sobolev, N.V., 1995, Archaean Re–Os age for Siberian eclogites and constraints on Archaean tectonics. *Nature* **374**, 711-713.
- Purwin H., Lauterbach S., Brey G.P., Woodland B.A., Kleebe, H.J., 2012, An experimental study of the Fe oxidation states in garnet and clinopyroxene as a function of temperature in the system CaO-FeO-Fe₂O₃-MgO-Al₂O₃-SiO₂: implications for garnet-clinopyroxene geothermometry, Accepted by *Contributions to Mineralogy and Petrology*.
- Rapp, R.P. and Watson, E.B., 1995, Dehydration melting of metabasalt at 8-32 kbar. Implications for continental growth and crust – mantle recycling. *Journal of Petrology* **36**, 891–931.
- Schmidberger S. S., Simonetti A., Heaman M. L., Creaser A. R. and Whiteford S., 2007, Lu–Hf, in-situ Sr and Pb isotope and trace element systematics for mantle eclogites from the Diavik diamond mine: Evidence for Paleoproterozoic subduction beneath the Slave craton, Canada. *Earth Planet. Sci. Lett.* **254**, 55–68.
- Schmidt, A., Weyer, S., Mezger, K., Xiao, Y., Hoefs, J. and Brey, G.P., 2008, Rapid eclogitisation of the Dabie-Sulu UHP terrane? Constraints from Lu-Hf chronology. *Earth Planet. Sci. Lett.* **273**, 203-213.
- Schulze, D.J., 1989, Constraints on the abundance of eclogite in the upper mantle. *J. Geophys. Res.* **94** (B4), 4205–4212.
- Shervais J.W., Taylor L.A., G. Lugmair, R.N. Clayton, T.K. Mayeda and R. Korotev., 1988, Archean oceanic crust and the evolution of sub-continental mantle: Eclogites from southern Africa, southern Africa. *Geological Society of America Bulletin* **100**, 411-423.
- Shu et al., 2012, Geochronological and geochemical constraints on the formation and evolution of the mantle underneath the Kaapvaal craton: Lu-Hf and Sm-Nd systematics of subcalcic garnets from highly depleted peridotites submitted to *Geochim Cosmochim Acta*.
- Skora S, Mahlen N, Baumgartner LP, Johnson C, and Pilet S., 2005, Garnet zoning pattern, growth mechanisms and the development of Lu-depleted halos in eclogites. *Suppl Geochim Cosmochim Acta* **69**(10), A403.

- Skora S., Baumgartner L. P., Mahlen J. N., Johnson M. C., Pilet Sebastien and Hellebrand. E., 2006, Diffusion-limited REE uptake by eclogite garnets and its consequences for Lu–Hf and Sm–Nd geochronology. *Contrib Mineral Petrol* **152**, 703–720.
- Sobolev, N.V., 1977, Deep-seated inclusions in kimberlites and the problem of the composition of the upper mantle. American Geophysical Union, Washington, DC. 279 pp.
- Stachel, T., Viljoen, K.S., Brey, G.P. and Harris, J.W., 1998, Metasomatic processes in lherzolitic and harzburgitic domains of diamondiferous lithospheric mantle: REE in garnets from xenoliths and inclusions in diamonds. *Earth Planet. Sci. Lett.* **159**, 1-12.
- Tappe S., Smart A. K., Pearson D. G., Steenfelt A. and Simonetti An., 2011, Craton formation in Late Archean subduction zones revealed by first Greenland eclogites. *Geology*, **39**, 1103-1106.
- Taylor L.A. and Neal C.R., 1989, Eclogites with oceanic crustal and mantle signatures from the Bellsbank kimberlite, South Africa, Part 1: Mineralogy, petrography, and whole-rock chemistry, *J. Geol.* **97**, 551-567.
- Wittig, N., Pearson, D.G., Webb, M., Ottley, C.J., Irvine, G.J., Kopylova, M., Jensen, S.M. and Nowell, G.M., 2008, Origin of cratonic lithospheric mantle roots: A geochemical study of peridotites from the North Atlantic Craton, West Greenland. *Earth Planet. Sci. Lett.* **274**, 24.

Chapter 6

Future perspectives

1. Perspectives for eclogite studies

A substantial amount of work has been carried out on mantle eclogite from various cratons worldwide like the Kaapvaal, Slave and Siberian craton. However, the information is still sketchy and more work is needed from localities and with a wider range of analytical methods. A big unknown is still when and where the mantle began to differentiate by partial melting to generate the basaltic components and when plate tectonics was initiated. By applying combined major, trace element and isotope studies different aspects and processes in the long history of these rocks may reconstructed, for which a particular isotope system or combination of methods is especially suited, With the combined Lu-Hf and Sm-Nd isotope systems we may distinguish multiple events which may be correlated with the early tectonomagmatic evolution of the craton. The Lu-Hf system apparently allows us to look further back in the history of a rock than the Sm-Nd system.

In this study, we come to the conclusion that the four different types of eclogite and garnet pyroxenites from Bellsbank have a subduction origin. The diversity of the chemical and isotopic compositions of these rocks reflects the nature of the subducted material and also the chemical modifications via subduction-related processes, such as dehydration and melt loss. The subducted basaltic components from the deep mantle with surface derived protolith signatures can be used to investigate the early plate tectonic processes. When the plate tectonic process started is still a hot debate. The most pristine eclogites in this study give an early Archean age of around 4.1 Ga from a bulk rock isochron (Fig.1, a repeat of Fig.23 in chapter 4) and the model ages of the isochron members and a 3.51 Ga garnet model which is a minimum age for such rocks as discussed in chapter 4. Such an age from eclogites with a deep mantle origin is not only that of the basaltic protolith but also of the time of some the subduction type process which brings the protolith into the deep Earth. An isochron consisting of only three members is still not a very strong argument for making very far reaching conclusions concerning the whole Earth's history. But the results seen in Fig.1 are very encouraging. Future work should therefore concentrate on such samples for which major and trace elements of the constituent minerals indicate that they have largely preserved their original identity and which appear to be co-genetic. Such samples are available to us from Bellsbank and further work is planned.

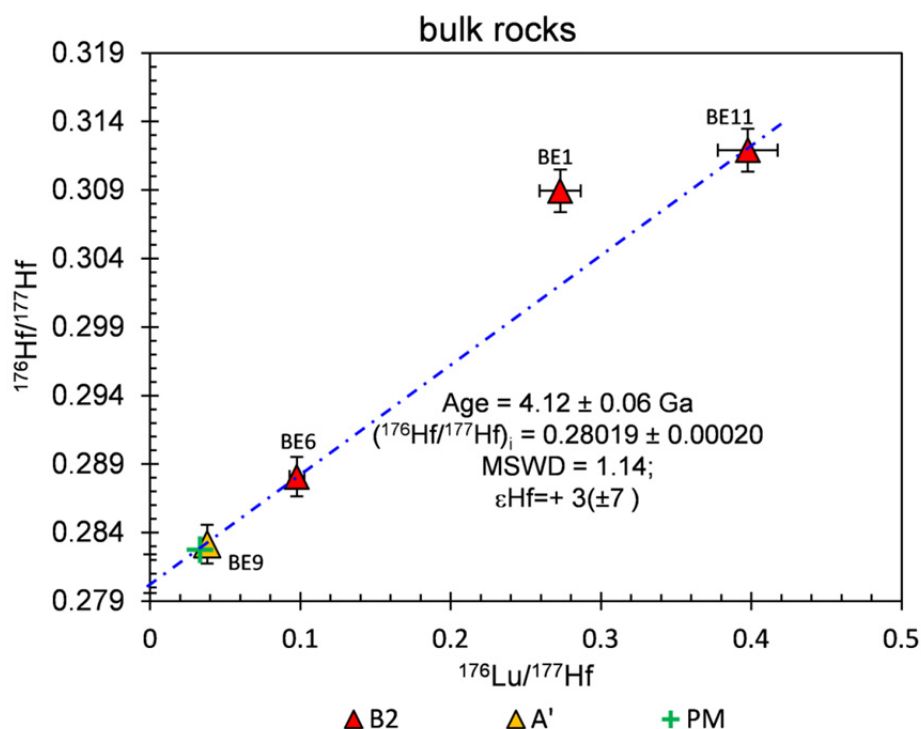


Fig.1 Lu-Hf isochron diagram for the whole rocks calculated by the garnet-clinopyroxene compositions. The genetically MORB-subducted group A' (yellow triangle) and B2 (red triangles) eclogites plot around the 4.1 Ga reference line ($\epsilon\text{Hf} = 0$). The green cross is the present-day primitive mantle composition.

We use the same methods for group A and B1 eclogites and garnet pyroxenites to obtain age information. These rocks which we assume to be of boninitic origin have experienced a more complex history, especially the loss of melt by high degrees of partial melting. The bulk rocks of these groups and their garnets give younger (maximum = 2.5 Ga) to very much younger model ages (minimum = 140 Ma). Despite these common properties and other chemical similarities they do not plot along an isochron like rock suites do when they are co-genetic. Taking the two groups separately results in two "isochrons", with the young age of 1.2 Ga, but extremely high ϵHf (+ 1839 for group A and +743 for B1; see Fig. 2). Even if 1.2 Ga would be a valid age, it would have to be interpreted as dating a partial melting event. The high ϵHf then still tells us that the protoliths are very old. Samples similar to A and B1 seem to occur in many eclogite localities (e.g. Roberts Victor, Koidu), but their incompatible trace element contents are mostly much more elevated and similar to sample BE4 from Bellsbank from group B1. The elevated incompatible element contents will blur the more original history of the rocks. The hope is that a larger data set of Bellsbank samples or similar samples from other localities (already available from a recent collection campaign) will enable us to clarify genetic relationships between the groups.

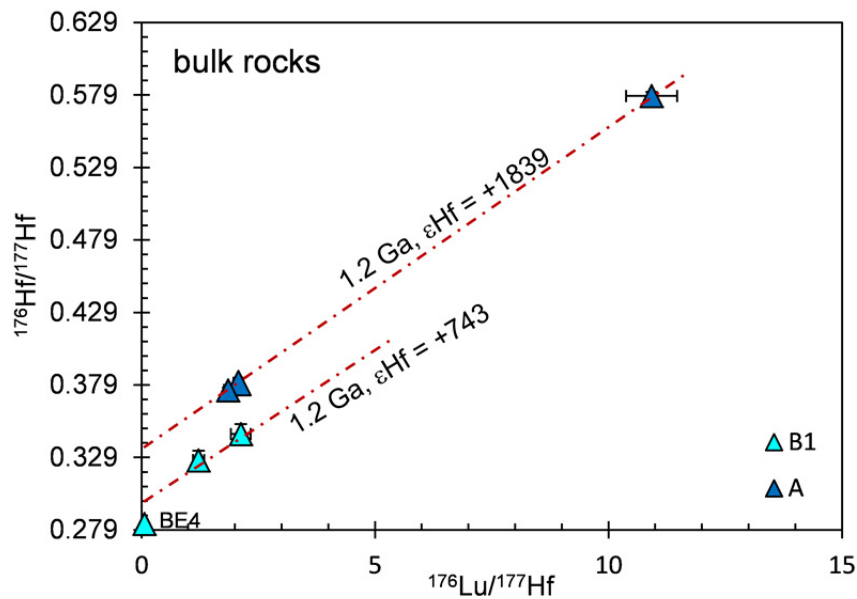


Fig.2 Lu-Hf isochron diagram for the whole rock samples from Bellsbank calculated from their garnet-clinopyroxene compositions. Lines fitted through the three A samples and two of the B1 samples give 1.2 Ga each. The highly incompatible trace element enriched sample BE4 plot separately.

2. Closure temperatures for Lu/Hf and Sm/Nd in peridotite and cooling of the mantle

A major proportion obtained for mantle eclogites are grt-cpx two-point isochrons whose meaning is, however, doubtful. It was possible from our work on the eclogites from Bellsbank and from literature data to attach a meaning to these ages. We found that they are cooling ages below the closure temperatures of the isotopic systems (~ 920 °C for the Lu-Hf system and ~ 840 °C for the Sm-Nd system) and kimberlite eruption ages above these temperatures. If they give older ages at these temperatures they are meaningless because of preferred contamination of the clinopyroxenes. To place our deductions on a firmer ground these studies have to be continued with low temperature samples. Such samples are available from Bellsbank and Roberts Victor from southern Africa but seem to occur in greater number at Diavik in Canada.

Similar to eclogites it should be possible to obtain information on closure temperatures in clinopyroxene-bearing garnet peridotites. We tested these prospects with available literature data, i.e. with published two-point isochrones from Finsch (Lazarov et al., 2012) and from the Gibeon province (Luchs et al., 2012; under review in Precambrian Research) and with measured whole rock-garnet two-point isochrones from the Somerset islands (Schmidberger et al., 2001). As seen in Figs. 3 and 4 the closure temperatures for the peridotitic system seem to be higher than for eclogitic systems. The reason for such a difference may not lie in very much different volume diffusivities in eclogitic and peridotitic systems but rather in the fact that in eclogites, garnets and clinopyroxenes are always touching whereas in peridotites, they swim in a matrix of olivine and orthopyroxene. An exciting

prospect is that information on the cooling of the mantle could be obtained from two independent and very different systems. We have estimated cooling rates somewhere between 80 – 110°C per Ga from the eclogites. Garnet peridotites should give the same results.

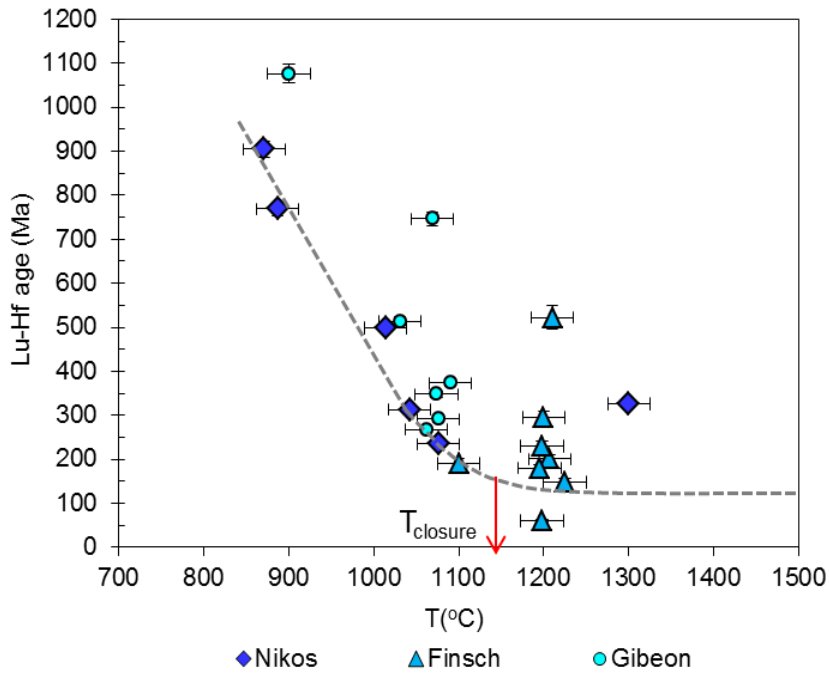


Fig.3 Correlation of calculated temperatures and the two-point Lu/Hf ages of peridotites from Nikos (Somerset island; bulk rock - garnet), Finsch (Kaapvaal craton; grt - cpx) and Gibeon Townsland in Namibia (grt-cpx). The Nikos kimberlite eruption age is 100 Ma, that of the Finsch kimberlite 120 Ma and of the Gibeon kimberlites 71Ma.

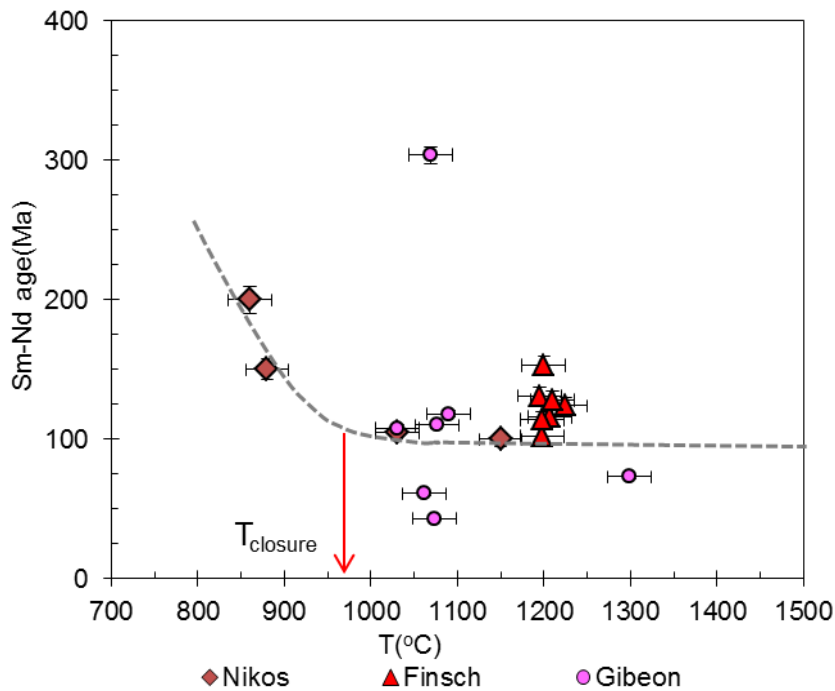


Fig.4 Correlation of calculated temperatures and the two-point Sm/Nd ages of peridotites from Nikos (Somerset Island; bulk rock - garnet), Finsch (Kaapvaal craton; grt - cpx) and Gibeon Townsland in Namibia (grt-cpx). The Nikos kimberlite eruption age is 100 Ma, that of the Finsch kimberlite 120 Ma and of the Gibeon kimberlites 71Ma.

3. A note on mineral separation and contamination

The big advantage of having a LA ICP MS system for trace element analysis available and performing isotope dilution is, that information can be obtained especially on the quality of the mechanical mineral separation, the quality of the blank and of the probability of contamination from the host rocks.

We have made the following observations: From figures 5 to 8, it can be deduced that the Sm/Nd system is more easily contaminated than the Lu/Hf system and more easily in clinopyroxene than in garnet. The reasons for this lie in the facts that the abundances of Sm and Nd are much higher than of Lu and Hf in the potential contaminant, the kimberlite host rock and that clinopyroxenes have cleavages which make it more “accessible” for the contaminant than garnet with no cleavage. We use for our column chemistry we use the identical portion of the mineral separates to elute the Sm and Nd and Lu and Hf. The very low concentrations of Hf require large amounts of samples (especially garnet), sometimes up to 150 mg, in order to obtain the lowest Hf contents (around 5 ng in 1 ml 2% HNO₃) necessary for the isotope measurement. The clinopyroxenes have much higher Hf concentrations of Hf, so that only much smaller mineral separates are needed. Therefore, the comparison of the isotope dilution and in situ data is much better than for garnets (compare Figs. 6 and 8). On the other hand, Lu-Hf is very consistent for clinopyroxenes and garnet (compare Figs. 5 and 7). It is therefore advisable for future work, to use two different mineral portions for Sm/Nd and Lu/Hf. Only very low amounts of sample are required for the Sm/Nd wet chemistry, which lowers the danger of having contaminated sample grains in the separates and which also allows the use of less acid which will lower the blank. Lu and Hf with their much lower abundances require larger sample amounts but the danger of contamination from kimberlite is much lower than for Sm and Nd.

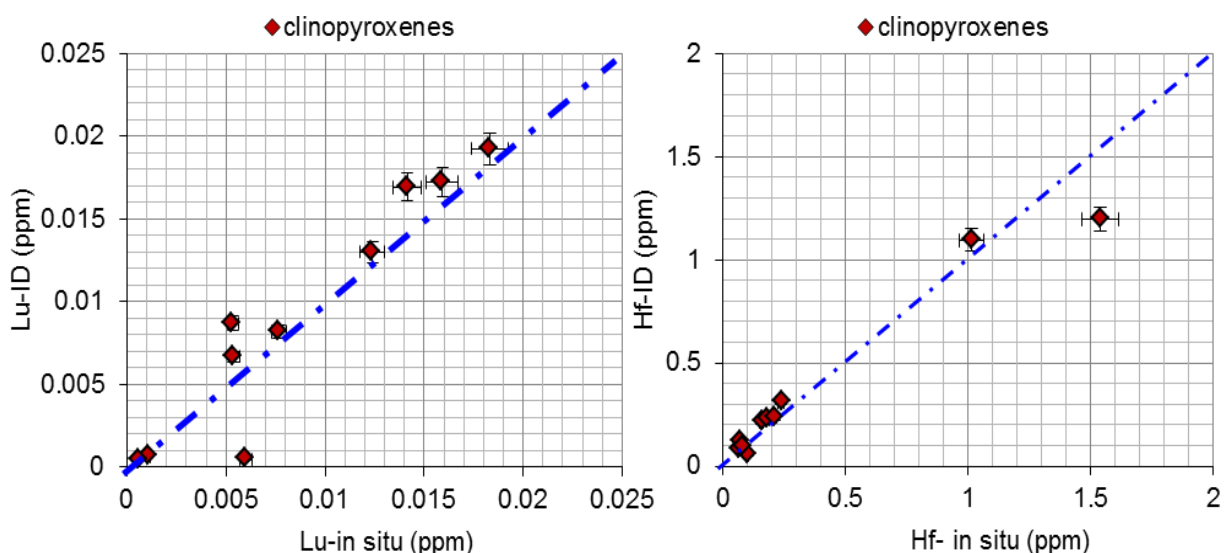


Fig.5 The comparison of Lu and Hf isotope dilution data with the in situ analysis of clinopyroxenes from eclogites.

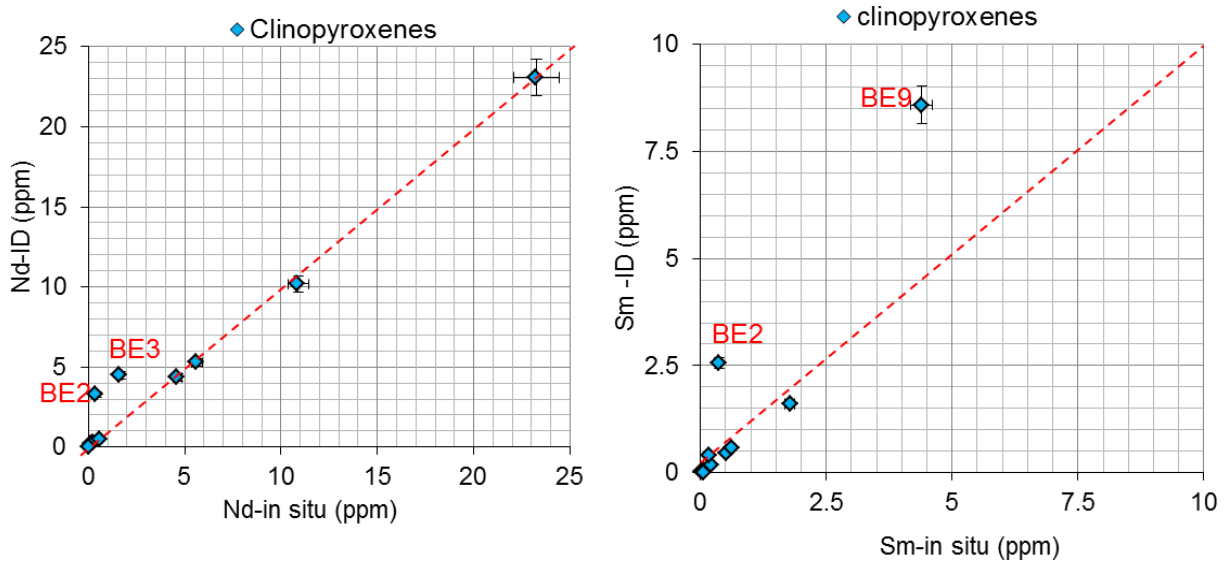


Fig.6 The comparison of Nd and Sm isotope dilution data with the in situ analysis of clinopyroxenes from eclogites.

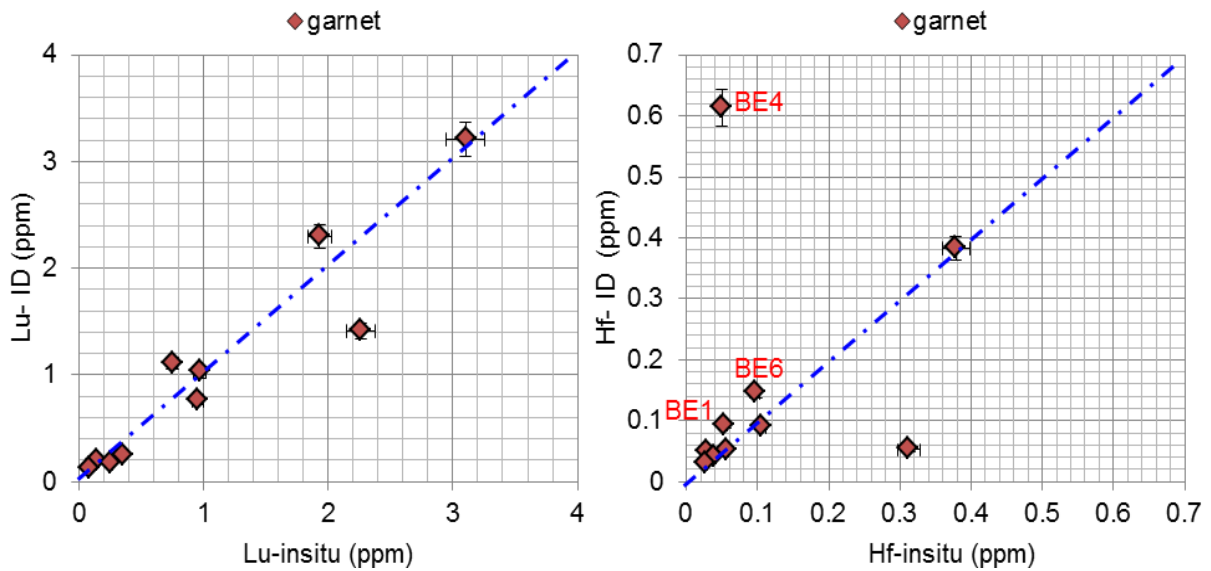


Fig.7 The comparison of Lu and Hf isotope dilution data with the in situ analysis of garnets from eclogites.

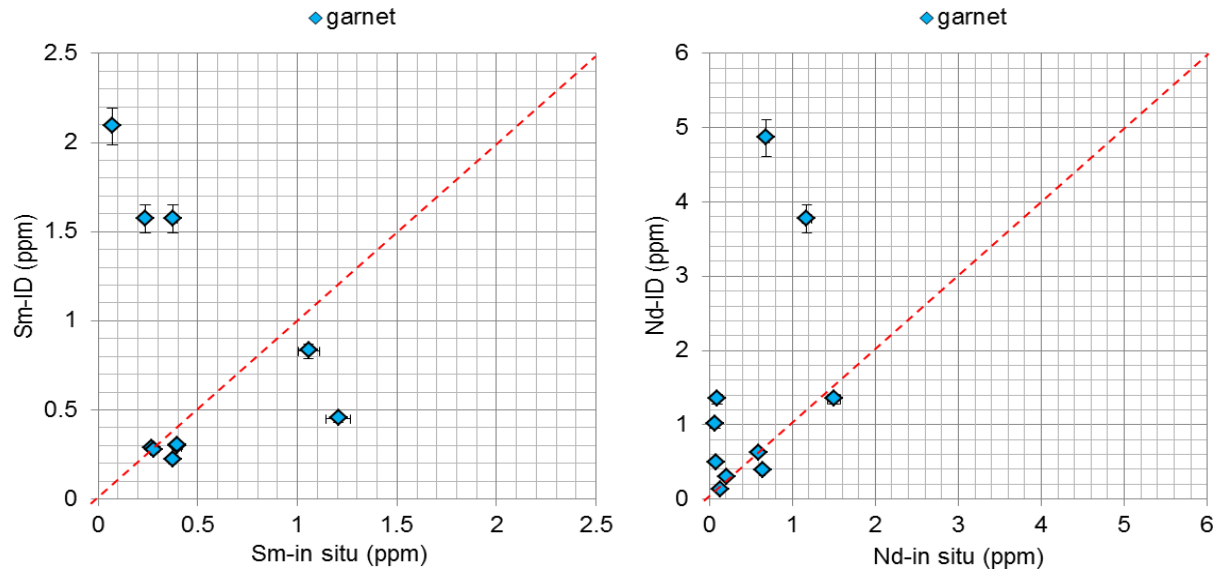


Fig.8 The comparison of Sm and Nd isotope dilution data with the in situ analysis of garnets from eclogites.

Acknowledgements

I was eager and nervous to start a new life in Germany four years ago as it was my first time abroad. I had no idea what was going to be. Eventually, it was really wonderful experience studying in Goethe University, and living in Frankfurt. It comes the end of my PhD. I would like to thank you all who support and help me in the last four years.

First of all, I would like to thank my M.S. advisor Prof.Zhao Zhidan for encouraging me to start this journey in Frankfurt and for continuous support and encouragement ever since.

My PhD journey started with the excellent trip to South Africa (to collect samples for my PhD project) with Jeff Harris and Gerhard Brey. Jeff was a fantastic company in the field through his local knowledge, advice, discussions and social skills. I could never image that two professors were crawling on the hot ,dirty ground (more than 40°C) in the concentration dumps from different diamond mines in South Africa to look for garnets for my project.

My PhD supervisor, Gerhard Brey, provides the extraordinary environment to all his PhD students. We all agreed he is intelligent, enthusiastic, caring, encouraging, very funny and also very messy (just take a look of his office). He is also very honest and told us what we need to hear. I thank him let me grow and develop my way of doing research, spent time discuss with me. Many thanks for spending hours to polish the English of my thesis and also for the German translation of the “Zusammenfassung”. Working with him is very enjoyable experience. It makes me think doing research is the dreaming career.

I am very grateful for continuous help and support from my colleagues. Marina Lazarov and Stefan Weyer generously passed their Lab knowledge and skills to me at the beginning of my PhD. Heidi Hoefer, Axel Gerdes and Michael Seitz continuously offered support and help from the labs during my measurements. Many thanks to Axel, He is always very patient to teach me how to perform measurement on Laser Ablation and MC ICP MS, and on chromatographic procedures and also passed on the zircon knowledge to me a bit. His knowledge on machines and on how to perform efficiently accurate measurements impresses me. I also thank F. Kneissl, A. Neumann, J. Schastok, J. Heliosch, Jennifer Stepler, Linda Marco, Melanie and Susi for helping with sample preparation, like providing thin and thick sections, acids. And I am also thankful to Thomas Kautz for his help with arragneing computer and softwares. Thanks for Heidi and Gerhard, I could discover that I got the lyme disease which I had no ideas about. They helped me to pass those most difficult time. Without their help, I can not imagine how I will be now.

Especial thanks to my wonderful office roommate Michael Seitz, his wife Sabine and his mother Maria, they provide me the nicest environment in Frankfurt and make me feel comfortable to stay in

Acknowledgements

Germany. Sharing holiday time with them was one of the most wonderful moments in my life. I also thank Mahdi Ghobadi and Timo Luchs for a nice brotherhood under Gerhard's supervision.

Evelyn Wendt, Svenja Lubs and Bana Hoy are the nicest persons, always helping with the complex document stuff for the administration because of my poor German.

It will be forever a wonderful memory that all people here in the institute are being so nice, Alan Woodland, Kevin Klimm, Sabine Klein, Anna Wagner, Beverley Tkalcec, Sascha Staubach and Nadia Knapp and Purwin Horst. And Aleksandra Stojic, Bibi Förster and Chen Xiwen are being such good companies in the institute. It is a joy to see Andrei Giris and Vadim Bulatov during their visiting.

Also importantly, our grill machine has to be thanked for its hard working Wednesdays in each summer to provide sufficient sausages and steaks for almost 30 people.

During my PhD, I benefitted a lot through discussion. I enjoy discussions with Gerhard, Axel Gerdes, Sonja Aulbach and Armin Zeh through these years. I will never forget David Green, Barry Dawson, Greg Yaxley and Jeff Harris showing interests on my project and spending time discussing with me during their short visits in Frankfurt. Al Hoffman also provided very good suggestions in discussions about the cooling of the mantle. I appreciate very much that Greg Yaxley spent time to go through the manuscript which is now submitted to GCA. His encouragement on the English really keeps me going. Thomas Stachel kindly provided the newest version of PTEXL program and gave suggestions on processing more accurate P-T calculation.

My project was supported by the Deutsche Forschungsgemeinschaft (BR 1012/33-1). Jim Davidson from Petra Diamonds made the access to the Bellsbank diamond mine possible and Steve West from DiamondCorp did the same for the Lace mine. Thanks to both of them since my PhD would not have been possible without the valuable samples I collected from these localities. Jock Robey was the other important contact person in South Africa for me. With his connections he gained us access to Roberts Victor, the Boshof road dump and the dump reworking facility at the DeBeers mine in Kimberley. His enthusiasm about our subjects is overwhelming.

In the end, I have to mention my old friends from China and my family. They constantly sent care and love to me which was a strong driving force. Thanks to my home country for the scholarship from China Scholarship Council which offered me the opportunity to study abroad.

CURRICULUM VITAE

November, 2012

CONTACT ADDRESS

Qiao SHU

Institut fuer Geowissenschaften
Facheinheit Mineralogie - Petrologie und Geochemie
Altenhoferallee 1
D-60438; Frankfurt am Main, Germany

Tel: ++49 (0)69 798-40136

Fax: ++49 (0)69 798-40121

Email: shu@em.uni-frankfurt.de



PERSONAL INFORMATION

Nationality: People's Republic of China

Birthday: 8 October, 1983

Place of Birth: Lanxi, Zhejiang Province, P.R. China

EDUCATION

2008/09- present: PhD study at the Mineralogy Department at the Goethe University in Frankfurt am Main, Germany.

Project title: *"The formation and the geochemical and thermal evolution of the lithospheric mantle beneath the Kaapvaal craton recorded by subcalcic garnets from harzburgites and by pristine eclogites and garnet-pyroxenites".*

Supervisor: Prof. Gerhard. P. Brey PhD, Dr.h.c.

2006/09-2008/09: MSc program at Faculty of geology at China University of Geosciences, Beijing.

Project involved: *Geochemistry and its significance of the volcanic rocks from Nianbo formation of Linzizong Group in the Cuoqin area, Tibet.*

Research orientation: *Chemical and isotopic analysis of the igneous rocks from the Nianbo formation (around 58Ma) as tracers for the source region and their genesis*

Supervisor: Prof. Dr. Zhidan Zhao

2002/09-2006/07: Bachelor, graduated from Faculty of Geology at China University of Geosciences, Beijing.

Thesis: Sedimentary microfacies analysis on the lower part of the Qingshankou Group in the western part of the Talaha area in the north part of Songliao Basin, China

Supervisor: Prof. Dr. Renchen Xin

PROFESSIONAL SKILL FOR LABORATORY WORK

1. Microscopy
2. XRF and EPMA for major elements analysis
3. Applying laser Ablation Inductively-Coupled Plasma Mass Spectrometer (ICP-MS) for analyzing trace elements on silicate minerals
4. Applying Multi Collector-ICP-MS for isotope analyzing
5. Wet chemical separation for Lu-Hf; Sm-Nd, Rb-Sr and Li for isotopic measurement
6. Skills for maintaining the clean lab: e.g. Acids distillation, Spike Calibration, preparation for wet chemistry

FIELD-WORK TRAINING DURING UNDERGRADUATE STUDY

Summer 2003: Geological cognitive internship on in Beidaihe, China (2 weeks)

Summer 2004: Geological mapping internship in Zhoukoudian, China (5 weeks)

Summer 2005: Description and classification of sedimentary rocks from the drill core in Daqing Oilfield, China (2 weeks)

FIELD-WORK EXPERIENCE

August 2007: Collecting volcanic rocks (rhyolite, perlite, Trachyte, Debris lava, and Tuff) in Cuoqing area, south Gangdies Belt, Lhasa block, Tibet (3 weeks)

April 2009: Collecting mantle xenoliths and xenocrysts (garnets) from diamond mines in the Kaapvaal craton (South Africa) for my PhD project (2 weeks)

TEACHING AND WORKING EXPERIENCE

2007-2008: Three semesters teaching assistant of the undergraduate student courses, "Crystal Optics and Rock-forming Minerals and Petrology" (teaching hand specimens and thin section microscopic observation skill, including igneous, sedimentary and metamorphic rocks)

2006-2008: working part time at the Geological Museum of China, Beijing

Project: Building the searchable database for the National digital geological Museum of China

AWARDED GRANTS

2002/09-2003/09: minor award of University Scholarship (1st semester); the third-class award of University Scholarship (2nd semester)

2003/09-2004/09: minor award of University Scholarship (3rd semester); the major award of University Scholarship (4th semester)

2004/09-2005/09: minor award of University Scholarship (5th semester); the third-class award of University Scholarship (6th semester)

2005/09-2006/09: minor award of University Scholarship (7th semester); the major award of University Scholarship (8th semester)

2007: CNPC (China national petroleum corporation) Scholarship

2010/07: Goldschmidt 2010 Travel Grant (Knoxville, Tennessee, USA)

2012/02: Financial Assistance from the 10th Kimberlite Conference

2008/09 -2012/03: National Scholarship of China for my PhD study in Germany.

2012/04-present: funded by the Deutsche Forschungsgemeinschaft

LIST OF PUBLICATIONS

SHU Qiao, XIN Ren-chen, and ZHANG Wie, 2008, Sedimentary microfacies in the lower part of the Qingshankou Formation in the Talin Hiag region, northern Songliao Basin. *Sedimentary Geology and Tethyan Geology*, 28(2).

ZHANG Wei, CHEN Maohong, YE Huishou, LIU Jun, SHU Qiao, 2008, The Geological Features and Evolution of Metallogenic Tectonics of the Ore Bearing Quartz Veins at Hukeng Tungsten Deposit , Jiangxi Province. *Acta Geologica Sinica*, 82(11):1531-1539.

Shu Q. Brey G.P., Gerdes A. and Hoefler H.,2012, Geochronological and geochemical constraints on the formation and evolution of the mantle underneath the Kaapvaal craton: Lu-Hf and Sm-Nd systematics of subcalcic garnets from highly depleted peridotites. Submitted to GCA. Under review.

ABSTRACTS AT INTERNATIONAL CONFERENCES

Shu Q., Brey G and Aulbach S, 2010, History of Lithospheric Mantle beneath Western Kaapvaal Craton: Signatures from Subcalcic Garnets, *Geochimica et Cosmochimica Acta*, 74(11), 957.

Brey G.P, Becker H, Lazarov M and Shu Q., 2010, Final Depletion of the Kaapvaal Cratonic Root: Lu-Hf Versus Re-Os Dating of Garnet Peridotites from the Finsch Mine (South Africa), *Geochimica et Cosmochimica Acta*, 74(11)-122.

Shu Q. and Brey G, 2011, Ultra-Depleted Eclogites: Residues of TTG Melting. *Mineralogical Magazine*, 75(3), 1866.

Qiao Shu., Gerhard Brey, Sonja Aulbach, 2011, Subcalcic garnets in the lithospheric mantle: witnesses of multiple depletion, subduction and reenrichment. International Conference on Craton Formation and Destruction, Beijing (ICCFD).

Shu Q., Brey G.P, Gerdes A; Hoefler H.E, 2012, Ultra-depleted eclogites: residues of TTG melting, 10th International Kimberlite Conference, Abstract Reg No. 10IKC-288.

Brey G, Luchs T, Shu Q., Lazarov M, Becker H, 2012, Combined trace element, Sm-Nd, Lu-Hf- and Re-Os studies constrain the age, origin and the development of the Kaapvaal subcratonic mantle, Long abstract.